Optical coherence tomography shape analysis and retinal disease

By

Stewart Lake

MB ChB (Hons), BMedSci, FRCOphth (UK), FRANZCO

Thesis
Submitted to Flinders University
for the degree of

Doctor of Philosophy

College of Science and Engineering
13 July 2022

Table of Contents

List of figures

List of Tables

Abstract

Optical coherence tomography (OCT) has evolved over a period of 30 years from an interesting research tool to a ubiquitous method of imaging the eye in clinical practice, now considered essential in the management of corneal, glaucoma, neuro-ophthalmic and retinal disease. Without it, the transformation of the management of medical retinal diseases (macular degeneration and diabetes) through the use of anti-vascular endothelial growth factors would have been difficult and far more complex for both patient and physician. This thesis emerged from the observation that OCT retinal shape differs between eyes, particularly with increasing myopia, leading to the question as to whether there was useful information to be learned from the retinal contour.

Both magnetic resonance imaging and more recently the OCT have already been used to analyse the shape of the posterior segment of the eye. The objectives of this thesis are to more widely explore retinal shape measured with spectral domain OCT. OCT samples an area smaller than the retinal entirety, and combined images may alter shape information, so local retinal shape is used. While many papers have described the retinal curvature of myopic eyes, here the irregularity in retinal contour is employed as a sign, describing its distribution across both the posterior and mid-peripheral retina. This irregularity is then correlated with axial length, the primary determinant of myopia. This thesis further advances the understanding of retinal shape by examining the relationship between irregularity and posterior vitreous detachment (PVD), retinal tears and retinal detachment. Using discriminant analysis, a machine learning algorithm suitable for small-medium sized datasets, evidence is found for differences in retinal irregularity between eyes that can be used to classify retinal detachment and PVD eyes. Between eye and within eye observations over time suggest these differences do not arise from the PVD event or surgery, nor are they directly associated with chorio-retinal scarring from the use of therapeutic laser. During the course of this work, swept source OCT became available. Images collected with the swept source OCT confirm the utility of retinal irregularity features as a tool for classification.

The novel shape analysis described here requires only data easily available in the clinic, and has the potential to provide quick, high resolution, cost effective local shape information relevant to eye health. As a result of this work, it is now known that quantification of peripheral retinal irregularity with OCT is not only possible but useful. Retinal irregularity is a biomarker that relates to myopia, and may improve the ability to predict retinal detachment, which opens the possibility that vision loss may be preventable in at risk eyes.

Declaration

I certify that this thesis does not incorporate without acknowledgment any material previously submitted for a degree or diploma in any university; and that to the best of my knowledge and belief it does not contain any material previously published or written by another person except where due reference is made in the text.

9 March 2022

Acknowledgements

The start of the work leading to the writing of this thesis was at least for me a rapid process, but there were several reasons and parties involved. A casual comment I made to Professor Doug Coster led to him arranging a meeting specifically to encourage me to undertake some structured research, so he has my thanks for getting things started. He both recommended I speak to and recommended me to Professor Keryn Williams. Her suggestions were that I both undertake a higher degree, and that if I was going to do something I should pick something big. This led to a meeting with Professor Karen Reynolds who became my principal supervisor and asked Keryn and Associate Professor Murk Bottema to co-supervise me. I am aware of the privilege it has been to have these three remarkable people as supervisors. I cannot thank them enough.

I would like to thank Associate Professor Richard Mills and Professor Jamie Craig for their encouragement. Creating an atmosphere that fosters research in a busy hospital clinic takes extra work and there was never any wavering in their support for me. Professor Justine Smith's quiet and thoughtful input has been invaluable. Mary Durban, Jochen Straub, Gerd Klose, and Matthew Everett of Zeiss have all been very generous with their knowledge and time. Deb Sullivan in the Department of Ophthalmology always knew what was needed to progress grant applications and navigate the University bureaucracy. Tyra Lange created the invaluable A2.m function to speed image analysis. My wife, Caroline, has been very forgiving of weekends, nights, and holidays spent hunched over a laptop. I am grateful to Doctors Wilson Wong, Weng Onn Chan, Bobak Bahrami, and in particular Dr Ayub Qassim, for referring on to me patients suitable for imaging. Dr Yen Harn Yew was volunteered to help with Section 3.1.1. Tanya, Hayley, Lisa and Molly at the Flinders Eye Clinic reception and all the reception staff at Eyemedics were very helpful in organising times for potential participants to attend. Angela Chappell and Carly Emerson took many of the photographs used as illustrations in this work and were patient when I took control of the OCT at all times of the day. Pawel Skuza of Flinders University provided helpful statistical advice where required.

Finally, I need to thank the hundreds of patients and volunteers who have turned up at the Eye clinic to have their pupils dilated and retina imaged. In these busy and sometimes troubled times they have been willing to surrender their time to help, for no personal gain. Without their generosity nothing would happen. Being witness to both the fear and courage some of them have displayed as they face the experience of retinal detachment surgery was a significant driver for this work. It would be a terrible thing to leave them dealing with the same challenges at the end of my career that they faced at the beginning.

Thesis outcomes

Publications arising directly from this thesis

Lake SR, Bottema MJ, Williams KA, Reynolds KJ. Optical coherence tomography retinal irregularity-based classification of retinal detachment and posterior vitreous detachment eyes. Submitted to Medical Physics, May 2021.

Lake S, Bottema M, Williams K, Reynolds K. Correlation between optical coherence tomography retinal shape irregularity and axial length. PLoS ONE (2019); 14(12). https://doi.org/10.1371/journal.pone.0227207

Presentations related to this thesis

Lake S, Williams K, Bottema M, Reynolds K. Merging retinal optical coherence tomography images in three dimensions. IOVS June 2021;62(8):1783.

Lake SR, Bottema MJ, Williams KA, Reynolds KJ. Toward a test for retinal detachment: machine learning and retinal shape. Paper on demand, American Society of Retinal Specialists annual meeting, July 2020. https://beta.asrs.org/user/abstract/91a8ac87-778c-4720-9bc7-88d849bdbab4

Lange T, Lake SR, Reynolds KJ, Bottema MJ. Automated computational diagnosis of peripheral retinal pathology in optical coherence tomography (OCT) scans using graph theory. Presented at Digital Image Computing: techniques and Applications (DICTA), Melbourne, 2020. https://www.dicta2020.org/wp-content/uploads/2020/09/87_CameraReady.pdf

Lake S, Bottema M, Williams K, Reynolds K. Macular Shape in Eyes with and without A Posterior Vitreous Detachment. Presented at APOIS Inaugural meeting, Singapore. 17-19 January 2020.

Lake S, Bottema M, Williams K, Reynolds K. Optical coherence tomography shape analysis describes myopic retinal shape. IOVS 2019; 60(9): 142.

Retinal OCT statistical shape analysis. Oral presentation at ANZSRS Retinal satellite meeting, RANZCO 50th Annual Scientific Congress, Adelaide, November 2018.

List of Abbreviations

2D	two dimensions / two dimensional
3D	three dimensions / three dimensional
A	anterior
ARM	age related maculopathy
.bin	(a file format)
BMO	Bruch's membrane opening
CCD	charge-coupled device
CSR	central serous retinopathy
CT	computed tomography
C_v	coefficient of variation
FE	fellow eye
GABA	gamma aminobutyric acid
HD	high definition
ICC	intra-class correlation
IQR	interquartile range
.img/IMG	(a file format)
I	inferior
IT	infero-temporal
K	curvature
kHz	kilohertz
LED	light emitting diode
LVW	Livewire
Mac	macula
MH	macular hole
MHz	megahertz
mm	millimetres
µm	micrometres
µW	microwatts
MRI	magnetic resonance imaging

mW	milliwatts
N	nasal
NAD	no abnormality detected
nm	nanometres
Ny	Nyquist frequency
OAG	open angle glaucoma
OCT	optical coherence tomography
OCTA	OCT angiography
OHRB	outer highly reflective band
OHT	ocular hypertension
P	posterior
PVD	posterior vitreous detachment
rmsa	root means squared anomaly
(R)RD	(rhegmatogenous) retinal detachment
RPE	retinal pigment epithelium
RT	retinal tear
RVO	retinal vein occlusion
S	superior
SARS-Cov-2	severe acute respiratory syndrome coronavirus 2
SD OCT	spectral domain
SD	standard deviation
SLD	super-luminescent diode
SLO/LSO	scanning laser ophthalmoscope
SS OCT	swept source OCT
ST	supero-temporal
STARD	standards for reporting of diagnostic accuracy
STM	permission authority
SVM	support vector machines
T	temporal
.tif(f)	tagged image file format
WHO	World Health Organisation

Chapter 1. Introduction

Over the last 30 years optical coherence tomography (OCT) has revolutionised the understanding and management of ophthalmic disease. Its ease of use, accessibility and low cost have enabled identification and regular monitoring of some of the anatomical correlates of visual impairment, particularly with diseases of the optic nerve, neurosensory retina, and choroid. Awareness of OCT reliability, combined with the volume of information produced, has led to the development of multiple tools for the quantitative analysis of retinal structure as a guide to disease management[1]. More recently, some attention has been paid to the shape or contour of the macula[2], with retinal shape usually represented by the path that the high signal intensity retinal pigment epithelium takes across the OCT B scans.

Myopia is expected to produce a global epidemic of visual impairment by 2050[3]. Myopia is associated with an increased eye size and an increasingly abnormal eye shape with greater refractive error. Myopic eye shape was initially investigated with magnetic resonance imaging (MRI) of the whole eye[4], but OCT has also been shown to be of use in analysing myopic pathology with regard to both retinal shape[2] as well as neurosensory retinal degeneration[5]. Most OCT-based research has focussed on the macula and its diseases. OCT measured macular curvature has been reported for myopic traction maculopathy[6], degenerative myopic retinopathy[7,8], and dome shaped maculopathy[9], with these reports fitting retinal shape to a best fit curve, and consequently discarding any shape differences between the retinal contour and that curve. Extra-macular OCT has been used to describe features of the peripheral retina in isolated peripheral retinal images[10,11]. Larger optical sections have been created through the merging of separate scans[12]. However, OCT analysis of the shape of extra-macular areas has not been reported.

This thesis examines macular and mid-peripheral retinal shape with the OCT, and its relationship to disease. As OCT samples retina within a defined space, only local retinal shape is measured. A particular and unique focus of this work is consideration of the retinal irregularity rather than just the general curvature of any retinal sample.

The remainder of this introductory Chapter 1 reviews the anatomy of the retina (Section 1.1.1), then describes the diseases studied in this work, specifically myopia, posterior vitreous detachment (PVD), retinal tears and retinal detachment, and macular holes (Section 1.1.2). Retinal detachment is a sight threatening retinal emergency associated with myopia[13]. The retinal breaks that cause retinal detachment arise in the peripheral retina, away from areas normally imaged in clinical practice, and the mid-peripheral retina is another focus of this thesis. After a brief review of retinal imaging modalities (Section 1.2.1), OCT is described in greater detail (Sections 1.2.2 and 1.2.3). Prior work in posterior segment retinal shape analysis is reviewed in Section 1.2.4, followed by a brief review of image processing methods relevant to this work (Sections 1.2.5-1.2.7).

Chapter 2 describes the image capture (Section 2.1) and analysis (Section 2.2) methods common to Chapters 3-6.

Chapter 3 explores the reliability of shape measurement with OCT (Section 3.1), and tests whether merging OCT images would enable analysis of larger features (Section 3.2). The ability to quantify gaze position might provide an external frame of reference for non-macula retinal images, and Section 3.3 looks at the measurement of gaze position during OCT image capture of non-macular retina. Section 3.4 describes the variation in retinal shape across retina that can be imaged with an unmodified commercially available OCT. The relationship between shape and myopia is reported in Chapter 4. While many papers have described retinal curvature differences in larger eyes, here the irregularity in retinal contour is employed as a sign, and correlated with axial length, the primary determinant of myopia.

Chapter 5 explores the link between shape and disease. Section 5.1 investigates whether macular shape is changed by PVD, through the comparison of groups with and without a PVD, and comparison of macular shape before and after macular hole surgery or spontaneous PVD. Section 5.2 uses discriminant analysis to train a classifier to distinguish between retinal detachment and PVD eyes using shape features. As a desirable outcome would be a tool to identify eyes at risk of retinal detachment before PVD occurs or vision is lost, further analyses are performed to check whether factors such as chorio-retinal scarring

from surgery, or the occurrence of PVD itself alter shape. The relationship between shape and retinal detachment is further tested with swept source OCT in Chapter 6.

The goal of optometric and ophthalmic care is to prevent vision loss and control visual impairment. Identifying more eyes at risk of retinal detachment would further those goals. The specific aim and objectives of this thesis are presented in Section 1.3. It is hoped that this work has made some progress toward reducing the burden that patients experience from retinal detachment.

1.1.1 Anatomy

The retina

The neurosensory retina receives an image focused by anterior ocular structures, performs the first processing of this image, and transmits visual information to the brain via the optic nerve. The retina lies on the retinal pigment epithelium (RPE), is bound anteriorly by the ora serrata, and extends posteriorly from this across the posterior pole, covering 72% of the interior of the eye (Figure 1.1.1)[14]. The outermost retinal layer, comprising the photoreceptor rods and cones, interdigitates with the apical processes of the RPE. Retinal attachment is maintained by a combination of hydrostatic force, and viscoelastic adhesion[15]. Net fluid flux from anterior to posterior in the eye, generated by active transport of electrolytes by the RPE cells and subsequent osmotic flow, provides a hydrostatic force. The viscous interphotoreceptor matrix, a material that lies between photoreceptor and RPE cells, may also create some adhesion (Figure 1.1.2)[16]. Retinal thickness varies from 300 μm in the peri-foveal region to 80 μm in the periphery[15,17]. A typical 23 mm axial length eye is estimated to have a total retinal area[18] of 1094 mm^2.

Retinal pigment epithelium

The RPE is a monocellular layer that protects and provides nutrition to the outer retina, including the photoreceptor cells. The RPE does this by maintaining the blood-retinal barrier, transporting nutrients and waste products to and from the rods and cones,

managing retinoid metabolism, and phagocytosing redundant outer segments[17]. The RPE-Bruch membrane complex thickness is approximately 22 μm in healthy eyes, but this varies by location, and by how much of the interdigitations with the photoreceptors are included[19]. These apical processes consist of microvilli, thought to maximise the surface area for transepithelial transport, and photoreceptor sheaths that cap the retinal outer segments. The RPE cells are 10-14 μm thick at the macula, then become flatter and wider (up to 60 μm across at the ora) more peripherally[17]. Measured by optical coherence tomography (OCT), the RPE signal layer is up to 40 μm thick, and forms the major part of the outer highly reflective band, which has the highest intensity signal in normal retina.

Vitreous

The vitreous gel fills the space between the retina posteriorly, and the lens, lens zonules, and ciliary body anteriorly[20]. A mixture of water, sodium hyaluronate, and collagens, it has an outer collagenous cortex over the retina that merges with the vitreous base anteriorly. The central vitreous is more liquid[21].

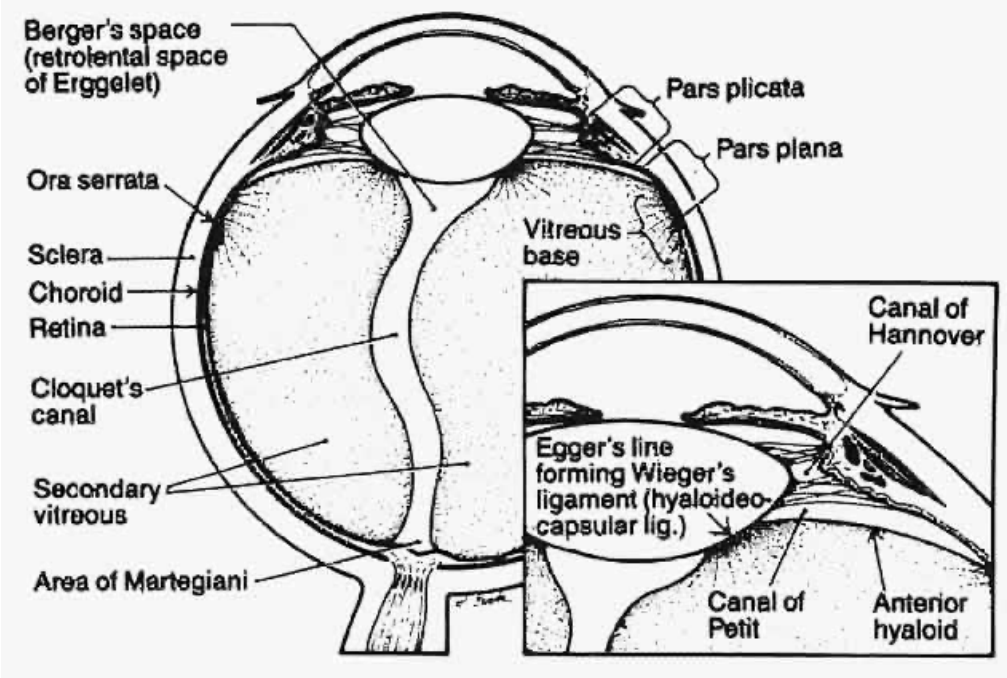

Figure 1.1.1. Anatomy of the eye. Anatomy of the relationships between the retina, vitreous, and vitreous base. The vitreous base lies under the ora serrata, extending (in adult life) anteriorly over the pars plana, and posteriorly over the anterior retina[22]. (This figure published under STM automatic permission guidelines, from Wilkinson & Rice, Michel's Retinal Detachment, Mosby, 1997, Copyright 1997).

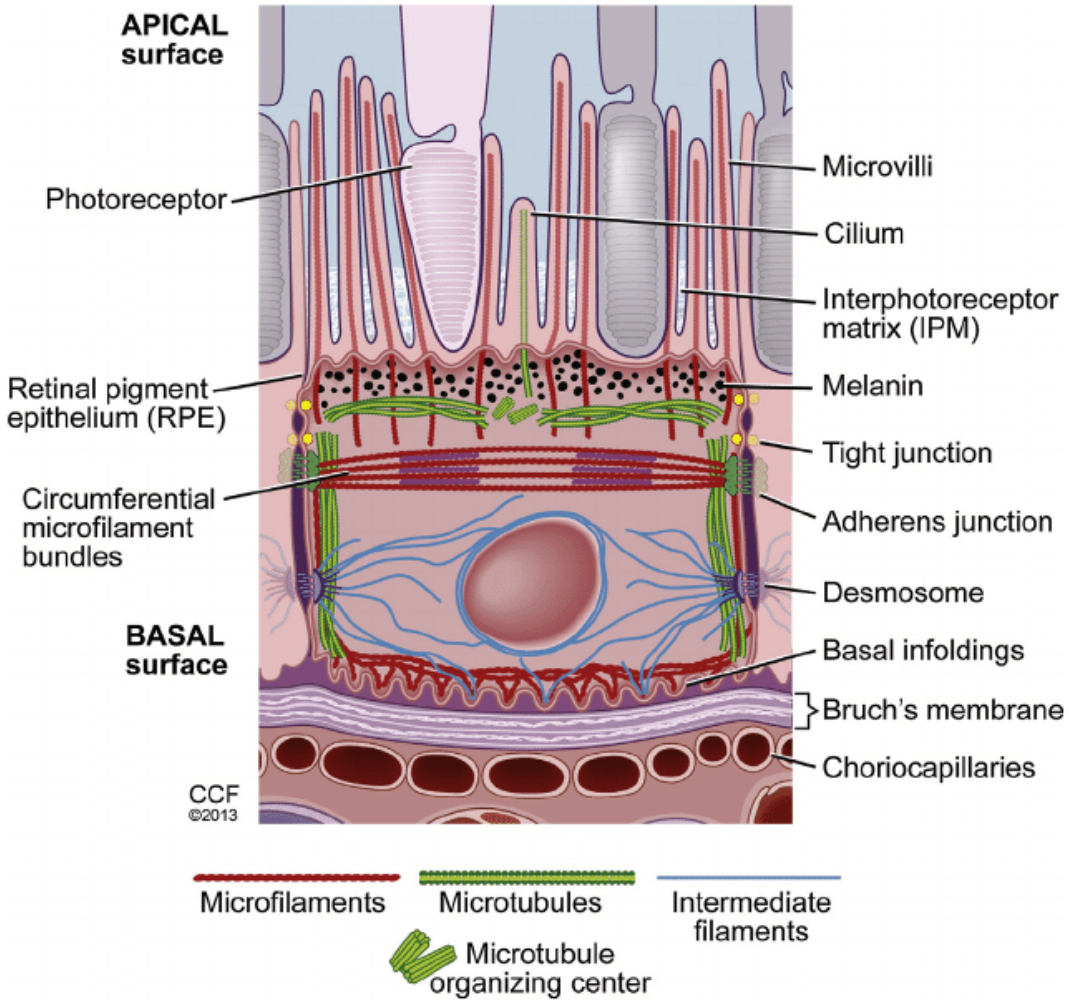

Figure 1.1.2. Retinal pigment epithelium. Diagram of the relationship between the retina, and retinal pigment epithelium. Light comes from the front of the eye, which is above the image. (This figure published under STM automatic permission guidelines from Bonilha VL, Retinal pigment epithelium (RPE) cytoskeleton in vivo and in vitro. Experimental Eye Research. 2014 Sep 1; 126: 38-45. Copyright Elsevier 2013).

The vitreous base is a firm connection between the retina and the vitreous cortex that straddles the ora serrata, the anterior limit of the retina. The posterior extent of the vitreous base sits at the ora at birth, and remains *roughly* parallel to the ora through life as it grows posteriorly, further in men than women, and nasally further than temporally. This means the posterior border of the vitreous base approaches coronal concentricity in later life. Posterior vitreous base extension occurs from synthesis of new vitreous collagen from vitreous hyalocytes[21]. In adults it sits 1.00 - 3.68 mm from the ora, with a mean extent 1.32-1.79 mm varying by quadrant of the eye[23]. The posterior face of the vitreous base is

sharpest in those with a posterior vitreous detachment (PVD)[24].

Vitreous collagen is predominantly type II, with IX next most common, and V/XI making up most of the rest[23]. Cortical collagen is oriented roughly parallel with the retinal surface. Vitreous collagen fibres are long, uniform and unbranched. At the vitreous base the fibres pass through the inner limiting membrane perpendicularly, to merge with fibrils on the cellular side[23], forming a firm and unbreakable adhesion.

1.1.2. Vitreo-retinal pathology

Posterior vitreous detachment

Progressive vitreous liquefaction, starting as early as four years of age, is accompanied by weakening of adhesion between the posterior vitreous face and inner limiting membrane of the retina[23]. PVD, the separation of the posterior hyaloid from the retina, occurs when the liquid vitreous enters the retro-hyaloid space through a defect in the weakened cortex. PVD increases in prevalence from the age of 40, with a diagnosis of PVD reported to be present in 50% at 50 years old and 65% of those aged 65 as determined by clinical examination[25], then in 80% of 80 year olds[26,27]. PVD occurs earlier in myopes, a median of 10 years earlier overall, but at an increasingly younger age the more myopic the eye[28,29]. Histological correlation with clinical diagnosis of PVD suggests that the true incidence may be lower, with many clinically suspected cases of complete vitreous separation in fact being a vitreo-schisis, or splitting of the vitreous cortex, with the outermost vitreous layer remaining attached to the retina[30]. Separation is not an "all or nothing" event[31]: incomplete PVD, the separation from posterior pole structures such as the optic disc or fovea, with persistent attachment elsewhere, can be visualized with spectral domain OCT[25,32]. OCT has increasingly been used to analyse and diagnose PVD[33]. Incomplete PVD decreases in prevalence through later adult life, as complete posterior vitreous detachment occurs[25,31]. For this work, a PVD was defined as documented separation of the posterior hyaloid face from optic disc, macula, and surrounding posterior pole structures[34], with a history of typical symptoms.

The majority of PVDs are benign, producing irritating “floaters” in vision from the shadow cast on the retinal surface by opaque aggregates of collagen fibrils and glial tissue within the detached mobile cortex. The further from the retina they lie, the smaller the area of the cone of shadow to produce symptoms, although smaller pupils will produce a longer penumbra and increase symptoms[21]. Photopsias (“flashing lights”) may occur at the time of separation and are thought to arise from mechanical irritation of the retina[35]. Photopsias that persist after the acute posterior vitreous detachment are typically seen in the temporal visual field in low light conditions. They are thought to arise from the mobile vitreous cortex, swinging from the vitreous base in the fluid-filled vitreous cavity[36].

Macular holes

Macular holes are round, full-thickness neurosensory retinal defects centred on the fovea, the thinnest part of the posterior retina that is the structure responsible for the central and greatest acuity vision[37]. They are thought to arise from predominantly antero-posterior vitreo-macular traction arising during the period of incomplete PVD[38]. Peri-foveal posterior hyaloid separation with persistent attachment at the fovea leads to a full thickness defect with radial then tangential displacement of the retinal tissue. Developing in the sixth to eighth decades of life, idiopathic macular holes are thought to be associated with failure of posterior vitreous detachment formation[12]. Presenting with a sub-acute blurring of vision, untreated over three quarters will progress to vision loss severe enough to meet the WHO criteria for blindness[39,40].

More common in females than males, most idiopathic macular holes respond very well to surgical intervention within 6 months of onset. Vitrectomy with induction of posterior hyaloid face detachment and peeling of the inner limiting membrane of the retina has an anatomical success rate over 90%[41,42]. The procedure is thought to produce hole closure by removing the centripetal force through PVD induction. Removing the inner limiting membrane and associated residual vitreous cortex on the retinal surface removes the tangential traction from the posterior hyaloid face and takes away the most inelastic retinal layer, enabling the retinal tissues displaced laterally during hole formation to migrate back to their origin[43].

Retinal tears

In a minority of cases, the PVD involves a more traumatic separation, with retinal tears produced where an abnormally tight point of adhesion lifts the retina at, or posterior to, the vitreous base[35]. The true prevalence of these complicated or "traumatic" PVD is difficult to determine: many patients either do not present for review or are managed in primary ophthalmic care. The reported incidence of retinal tears varies from 0.59% to 27% in different studies, depending upon what population has been sampled [44]. In one series of acute PVDs presenting to an ophthalmology unit, 8.2% had a retinal tear, with a wide variation in incidence in other case series of up to 47%, presumably reflecting varying referral patterns[35].

Once flow from liquid vitreous into the sub-retinal space overwhelms the ability of the RPE to remove fluid, retinal detachment occurs. Not all retinal tears lead to retinal detachments, with the hypothesis being that the retinal pigment epithelial pump maintains retinal apposition in some cases[45,46]. Straatsma[47] found an incidence of retinal tears at autopsy of 3.3% of patients (1.9% of eyes), similar to Foos' finding of retinal tears in 2% of autopsy eyes[48]. Martin Sanchez & Roldan Pallares[49] found a prevalence of 3% retinal tears in myopic eyes, unrelated to severity of myopia or age. Westfall et al[50] found 8% of acute symptomatic PVD eyes (which excludes all those who do not present to eye health care) had a retinal tear, whereas the combined incidence of retinal tear and detachment in those presenting to healthcare with PVD-related symptoms was reported as 14%[51]. A more recent estimate is that just over half of retinal tears produced by an acute PVD will produce a retinal detachment[35]. Acute symptomatic retinal tears are thought to have the highest risk of progression to retinal detachment, particularly in the older population in whom posterior vitreous detachment has occurred (and caused the symptoms). The incidence of retinal detachment, the end result of progressive, untreated retinal tears that will lead to visual loss, is approximately 1:10,000 per annum[52]. This is close to the estimated lifetime risk of 1%[13]. Van der Put et al[53] found annual incidence of retinal detachment of 18.2 per 100 000, with a peak at 52.5 years. Wong et al[54] found an overall incidence of 10.5 per 100 000, with different incidences in different ethnicities in Singapore, but did not address possible

differences in refractive error between groups as a source of the difference. Together, these suggest that retinal tears are 2-3 times more common than retinal detachment.

Treatment of retinal tears

Retinal tears without retinal detachment can be treated by using laser photocoagulation or cryopexy to create a firm chorio-retinal adhesion (essentially a scar) and prevent retinal detachment[14]. Once retinal separation from the RPE occurs, surgery is required[35].

Retinal detachment

Acute PVD is a common, often annoying, but benign event in the aging eye. In a minority it is complicated by retinal tear formation which, if untreated, can lead to retinal detachment and vision loss even with effective surgical care. The time period between acute PVD involving a retinal tear and development of retinal detachment varies, and may be hours or weeks depending on conditions within the eye. Once detached, outer retinal cells including the photoreceptor cells that lose contact with the RPE cells that maintain their function, cease working and undergo apoptotic cell death[55]. The result is severe loss of vision from the area of retina affected, and is not entirely reversible even with appropriate surgery[56]. In approximately half of eyes presenting with retinal detachment, the macula has separated from the underlying RPE cells ("macula off"), and nearly all of these will be left with some permanent visual impairment affecting central vision[53].

Approximately 6-34% of individuals with a retinal detachment in one eye will develop a retinal detachment in the fellow eye[57–61]. There is no test to predict eyes at risk of retinal detachment. Myopia is known to be a risk for retinal detachment, with the size of the risk varying with degree of myopia[62] consistent with the risk being related to the size of the eye[13,63]. Although lattice degeneration is seen more commonly in eyes with a complicated PVD, most eyes with lattice degeneration do not develop a retinal detachment, so prophylactic treatment is rarely indicated[46,64,65,66]. Those with known high risk of retinal detachment, including type 1 Stickler syndrome[67] and the fellow eyes of giant retinal tears[68], do benefit from prophylactic retinal laser[69].

Incidence of retinal detachment compared to PVD

The true relative incidence of retinal detachment and posterior vitreous detachment in the population is difficult to determine, as many uncomplicated PVDs will either not present to healthcare or be rapidly assessed by primary healthcare. The relative incidence of PVD and retinal detachment has been estimated from the literature in different ways. Of those presenting to medical eye care with new-onset floaters, with or without photopsia, it was estimated that 14% would have a retinal tear or detachment requiring treatment[35,51,70,71], a ratio of approximately 6:1.

An estimation of the relative probability for the wider population incidence can loosely be made based upon independently reported incidence of the two groups. The incidence of retinal detachment has been reported as between 1: 8 000 – 10 000 individuals per annum in several reports[52,57,59], including those of comparable populations to this study. The prevalence of PVD has been reported at 57% in subjects over 85 years[72] beyond which it was assumed further posterior vitreous detachment events are uncommon. Assuming no difference in mortality linked to PVD development or retinal detachment, this equates to a ratio of approximately 50:1.

Myopia

The refractive state of the eye is largely determined by the combination of anterior corneal curvature (which provides the majority of the refractive power of the eye) and axial length. Emmetropia is the state where parallel incident light rays are brought to a focus at the retina. Hyperopia, or hypermetropia, is the state where the focal point of parallel light rays lies posterior to the retina. In myopia parallel incident light rays are brought to a focal point anterior to the retinal surface, leading to a blurred image[73]. While myopia can occur from an increased focal power of the anterior ocular structures (in particular the cornea, but also the lens of the eye), most myopic eyes exhibit a greater axial length than do emmetropic eyes. Most of the axial growth that produces myopia happens in the second decade of life. However axial length can increase in myopia even in the middle years: this increase is greater in larger, more myopic eyes[74]. Posterior segment eye shape (in particular retinal shape) affects ocular pathology and leads to visual impairment in other ways than just

refractive error. Lattice degeneration, retinal tears and retinal detachment are more common in larger, myopic eyes[52]. Severe, or pathological myopia, has various definitions, usually related to the increased eye size at which pathological chorio-retinal changes[75], particularly typical patchy chorio-retinal atrophy, develop[76]. Frisina et al[77] related posterior staphyloma type to both ocular shape observed on MRI and OCT profile, and chorio-retinal atrophy. This is more common once refractive error is less than -6.00 dioptres, or axial length greater than 26.5 mm[78]. However, myopic retinopathy becomes more prevalent after the fifth decade of life[76], meaning larger eyes in early life are less likely to show chorio-retinal pathological changes[79]. Posterior staphylomata that developed after the fifth decade of life produced a temporally distorted globe shape associated with visual field defects (Figure 1.1.3)[4]. Simulations of retinal haemodynamics found that pathological alterations in eye shape equivalent to myopia adversely affect the retinal vascular circulation[80].

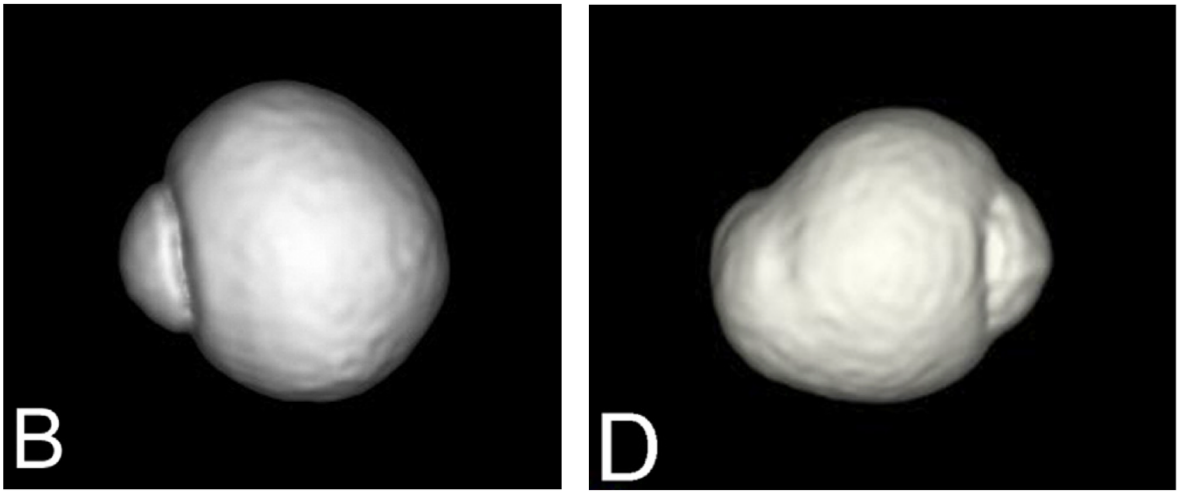

Figure 1.1.3. MRI globe reconstructions. Nasal view of MRI reconstructions of an emmetropic eye (labelled B, looking to the left), and a myopic eye (labelled D, looking to the right). The myopic eye has a posterior staphyloma, posteriorly, in the left of the image. Both images demonstrate artefactual "dimpling" of the surface from the reconstruction algorithms, as well as the asymmetric shape of the posterior segment. (This figure published under STM automatic permission guidelines from Moriyama M, Ohno-Matsui K, Hayashi K, Shimada N, Yoshida T, Tokoro T, Morita I. Topographic analyses of shape of eyes with pathologic myopia by high-resolution three-dimensional magnetic resonance imaging. Ophthalmology. 2011 Aug 1;118(8):1626-37. Copyright 2011, American Academy of Ophthalmology).

Prevalence of myopia

Myopia is becoming a public health issue in many parts of the world, predicted to increase and affect up to 46%, or four billion people by 2050[3] . The Beijing Eye Study found 77% of 18-year-old school students had myopia, with 5% having high axial myopia of less than -8.00 dioptres[81]. The same study found 20% of university students had high axial myopia. In Seoul, 96.5% of 19 year old men are myopic[82]. In comparison, the Blue Mountains Eye Study in Australia found only 2.7% of adults 40 years and over had myopia less than -5.00 dioptres[83], and 2.4% of adults over 40 in a rural population in China were similarly myopic[84]. This suggests that myopia is particularly increasing in prevalence in younger, urban populations[85].

In Australia, the 2005 report, "Eye Health in Australia" estimated 15-20% of the adult population was myopic[86]. However, an increase has not been documented in Australian primary schools to date, with a myopia prevalence of 13% amongst a representative primary school population in Queensland, and a lower incidence in European Caucasian children than East Asian[87,88].

Genome wide association studies have identified loci in severe myopia relate to genes expressed in the sclera, retina, and retinal pigment epithelium[89]. Genes for myopia have been identified in Stickler syndrome (COL2A1 and COL11A1), type VI Ehlers-Danlos syndrome (lysyl-protocollagen hydroxylase), and Marfan syndrome (fibrillin)[90].

Myopisation and its effects

Eye shape affects focus at different retinal eccentricity, and it has been suggested this may influence eye growth and final refractive error at maturity[91]: local feedback from peripheral defocus may modulate eye growth. Demonstration that visual feedback influences growth of the eye and consequent axial myopia was first demonstrated in macaque monkeys[92], and is seen in visual deprivation from visual pathway opacities – both experimentally induced[93] and in clinical observation[94]. Relative peripheral ametropia (in particular, hyperopic defocus in myopic eyes) has been hypothesized as a drive for eye growth and myopia progression. Experimental models have produced results supporting this hypothesis: marmosets fitted with bifocal contact lenses that induce relative peripheral hyperopia developed axial

myopia[95].

Clark et al[96] summarised techniques of peripheral refraction and determination of retinal shape across the posterior 30 degrees of retina, and discussed the hypothesis that relative peripheral hyperopia leads to myopic progression. They combined spectral domain OCT-determined retinal curvature, peripheral refraction measured by an auto-refractor, and partial coherence interferometry to measure axial length. Increased curvature was found in myopic eyes 5° from fixation, closer to fixation than other studies, and consistent with a more prolate shape. This study demonstrated the utility of OCT in analysing retinal shape in its relation to refractive states.

For defocus to influence eye growth and myopia progression, a signal must pass between the visual pathway and the sclera. The proposed mechanism of scleral remodelling to allow eye growth in myopia is a local retino-choroidal signal that activates scleral fibroblasts and myofibroblasts. Although the exact mechanism remains unclear[97], there is some evidence that retinal dopamine release inhibits myopic progression[98]. Dopamine, insulin, glucagon, and GABA agonists and antagonists have been shown to influence choroidal and scleral growth[90].

The tissue of origin of myopisation has been hypothesised to be Bruch's membrane[5]. Jonas, Ohno-Matsui & Panda-Jonas noted that the distances between the foveola and Bruch's membrane opening (BMO) near the optic disc (which itself does enlarge), and distance between the superior and inferior temporal arcades, do not correlate with axial length. Hence the macular Bruch's membrane does not enlarge with axial length. The BMO shifts temporally in myopia, contributing to the increased peripapillary gamma zone (the gap between the margin of the optic disc and edge of Bruch's membrane). Sclera and choroid thin post equatorially with increasing axial length, whereas Bruch's membrane does not. The absence of an increase in choroidal and scleral volume with axial length suggested enlarging eyes rearrange these tissues rather than grow more tissue. The RPE cells enlarge with increasing axial length[99]. Posterior RPE cell density and retinal thickness do not reduce with increasing axial length, whereas they do in the peripheral retina. Jonas & Ohno-Matsui hypothesise that the efferent process of myopisation is Bruch's membrane production at

the equator, reducing RPE density here, with thinning of the posterior choroid by compression or stretch through increased Bruch's membrane area, while neurosensory macula, RPE and Bruch's membrane structures are preserved.

1.2.1. Imaging the eye (non-OCT)

Eye size: axial length

Axial length is the standard clinical assessment of the size of an eye. Measured as the distance from the corneal apex at the front of the eye to the fovea at the back, it is usually measured by partial coherence interferometry or ultrasound A scans. Along with corneal curvature it describes the refractive status of the eye. Most commonly measured prior to cataract surgery, it is the primary determinant of myopic refractive error. Myopic eyes tend to be larger than emmetropic eyes, which are themselves typically larger than hyperopic eyes. With an increased interest in myopia control, axial length is recognised as an ideal metric for assessing the effect of interventions on prevention of myopic progression[100].

Fundoscopy and photography

The first recorded visualisation of the retina *in vivo* occurred in 1704 when Jean Mery noted that he could see the retinal blood vessels of (live) cats immersed in water[101]. More practically, Purkinje developed an ophthalmoscope in 1823, which was re-invented by von Helmholtz in 1851[102]. Gullstrand's development of the science of ophthalmoscopy (for which he won the 1911 Nobel prize) led to the construction of the first fundus camera in 1925[103].

Retinal photography (Figure 1.2.1) and fluorescein angiography (fluorescent dye assisted imaging with the use of filters, Figure 1.2.2) remained the primary retinal imaging technique up to the development of the OCT in 1991. They provide a two-dimensional view of the translucent retinal tissue and blood vessels overlying the retinal pigment epithelium and choroid.

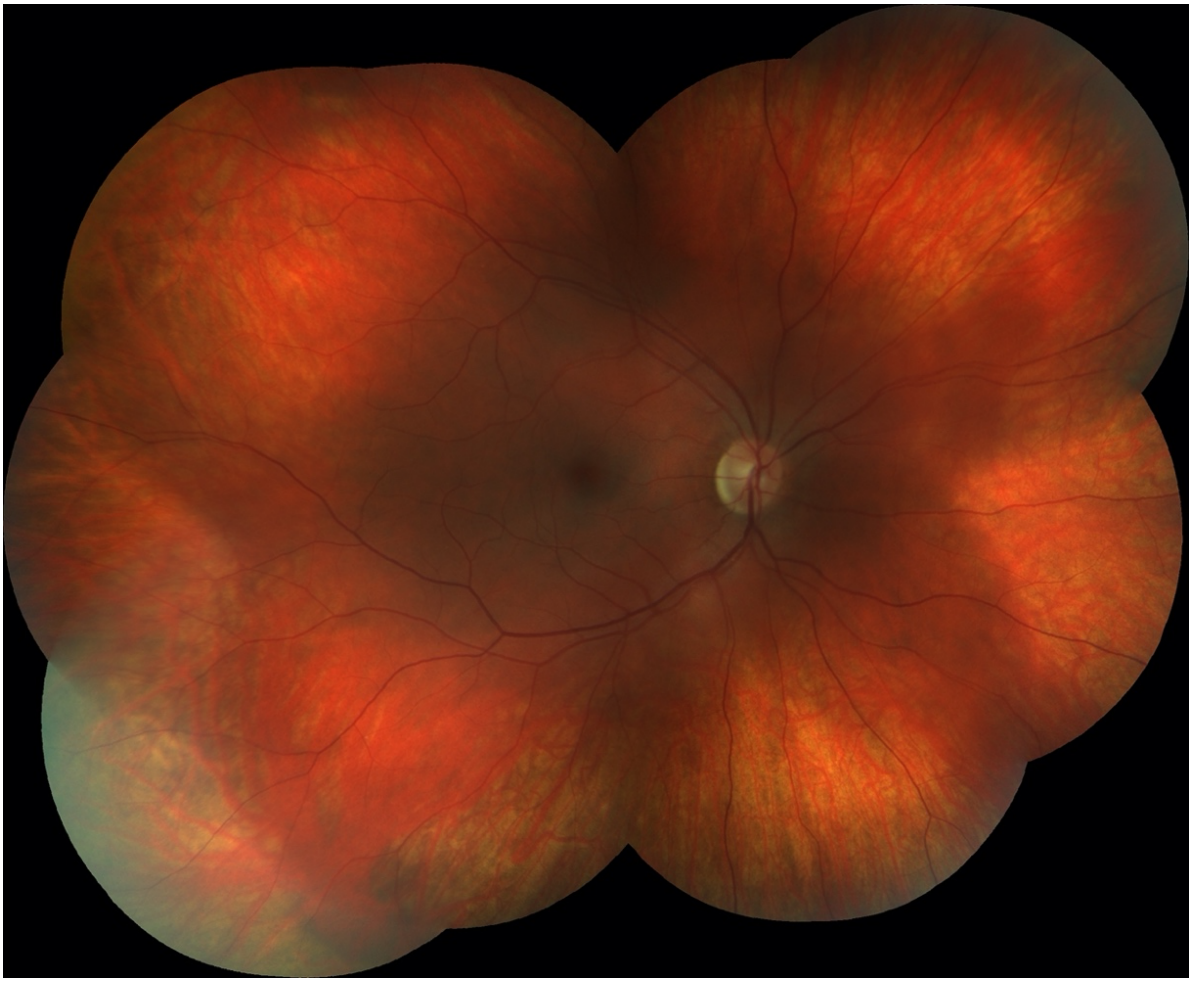

Figure 1.2.1. Fundus photography. Colour fundus photograph of a right eye. The image is a montage of ten separate fundus photographs. This is a normal eye.

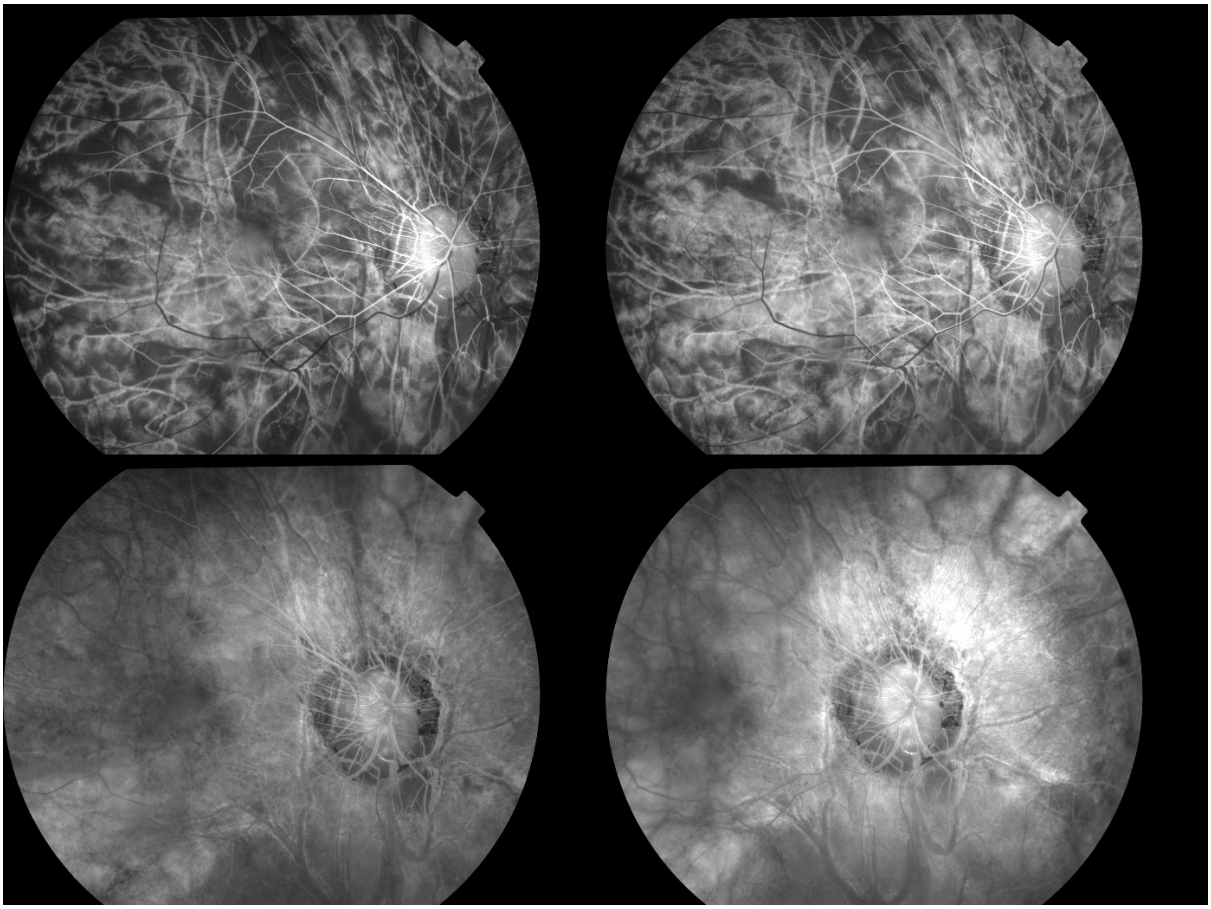

Figure 1.2.2. Fluorescein angiography. Images from a highly myopic eye. Both retinal and choroidal circulations are seen, the former the white lines emerging from the optic nerve head, right of centre in all four images.

Early three dimensional images were provided through stereo fundus photography[104], and the scanning laser ophthalmoscope provided some depth information, but only with a resolution of 100 μm, which is of limited utility for retina with a tissue thickness 150-250 μm[105].

Ultrasound

While OCT can provide high axial resolution, ultrasound has greater tissue penetration with lower resolution (Figure 1.2.3). Ultrasound requires different probes for anterior and posterior chamber examination, with the posterior chamber typically imaged with a 10 MHz probe. A 10 MHz ultrasound has a resolution of up to of 150 μm, but eye movement artefact and loss of detail of anterior ocular structures limit its accuracy. At 50-80 MHz, ultrasound can resolve down to 20 μm, but only penetrates tissue to a depth of 3 mm, and is useful in examining the anterior chamber[106,107]. Colour Doppler ultrasound can show dynamic retinal blood flow[108,109]. Ultrasound is performed by placing the probe either on the open, anaesthetized eye, or through a closed eyelid. Both involve contact, which may exert some pressure and distort the globe. Despite its availability, ultrasound has been little used in quantifying posterior segment shape, probably because it can be time consuming, uncomfortable, requires a skilled operator, and differences between technicians may limit accuracy[110].

Figure 1.2.3. Ocular ultrasound. This eye has a closed funnel retinal detachment following trauma. The optic nerve is at the bottom of the image. The retina rises near vertically from the optic nerve head then reflects toward the vitreous base, due to extensive proliferative vitreo-retinopathy. This eye is blind.

Magnetic resonance imaging (MRI) and computed tomography

MRI can image the entire eye (reviewed by Nayak, Desai & Maheshwari[111], Figure 1.1.3). The high water content of vitreous gives it a low T1 signal that contrasts well with the relatively hyper-intense uveal signal, which also enhances with contrast. On T2, the bright vitreous signal obscures surrounding tissues. Surface coils may be placed on the eye for higher spatial resolution, but the signal remains sensitive to eye movement artefact. Standard investigations have a pixel size of 1 mm, but can be improved to 500 μm with higher Tesla scanners[112].

While MRI has been considered the gold standard in posterior globe curvature estimation, its resolution is too low to measure many of the features observed with OCT[110,113]. Gradient field non-linearities produce pincushion-like radial distortions requiring some calibration and correction. Magnetic field inhomogeneities may influence the imaging of the eye which has comparatively large variation in magnetic susceptibility in different tissues. As a result,

precise subject positioning is required, and difficulties in achieving this, as well as its cost, can limit its widespread use for research[110]. Computed tomography (CT) has slightly better intraocular resolution (500-1000 μm) with faster scan times reducing motion artefact. This greater resolution leads to its use for stereotactic interventions[114]. CT imparts a not insignificant dose of radiation to the eye and sensitive crystalline lens[106], which limits its use for research imaging.

Peripheral retinal imaging (non-OCT)

Conventional fundus imaging typically covers 35-55°, centred on, or close to the posterior pole. With the eye turned away from the camera, peripheral fields can be captured with range and image quality dependent upon pupil dilation and optical factors. Wider field (non OCT) peripheral retinal imaging includes colour photography (the RetCam, Clarity Medical Systems, Pleasanton, CA, Figure 1.2.4), and wide field scanning laser ophthalmoscopes such as the Optos (Optos plc, Dunfermline, UK, Figure 1.2.5), both of which have the facility to add retinal angiography. The RetCam can reach 120°, and the Optos up to 200° field of view, with a lower range superiorly and inferiorly[115]. Witmer & Kiss[116] concluded that imaging the ora requires a 230° field of view (imaging the equator requires a 180° field when the image is centred on the posterior pole). The distortion of the retinal field in a wide-field photograph is similar to the Mercator projection on a map of the world, both representing a three dimensional spherical surface with a two dimensional image[117]. The peripheral areas are magnified and distorted compared to the posterior pole. Conversion for the distortion of area can be performed[118].

Nomenclature standardisation of descriptive terms for imaging of different retinal structures has been established[119]. This separates retinal areas into the posterior pole, mid-periphery (or widefield) and far-periphery (ultra-widefield).

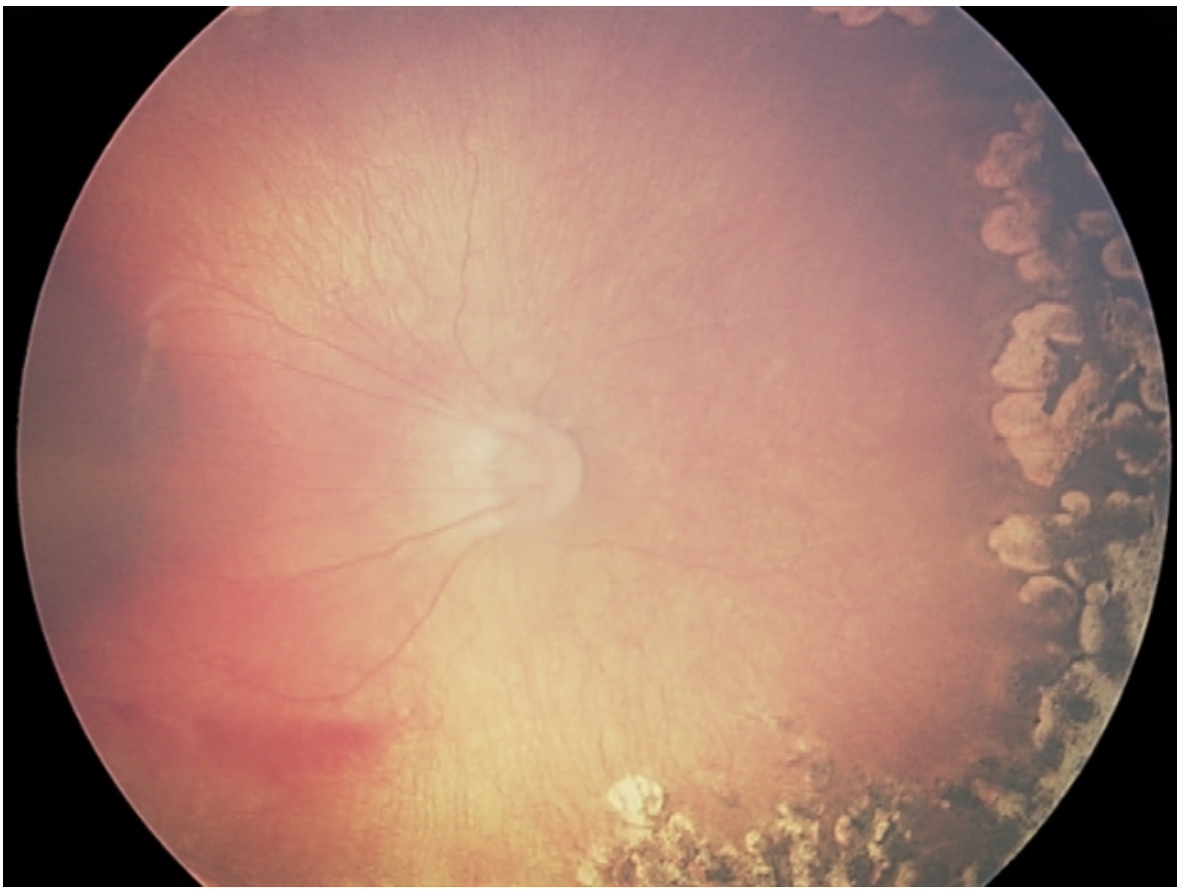

Figure 1.2.4. Widefield retinal photography, RetCam. Image shows the right eye of a neonate who has had laser treatment for retinopathy of prematurity. This is a review image taken weeks after the laser treatment. Laser scars are seen on the right of the image. The temporal retinal vessels (to the left in the image) are straightened due to traction from temporal peripheral pre-retinal fibrosis.

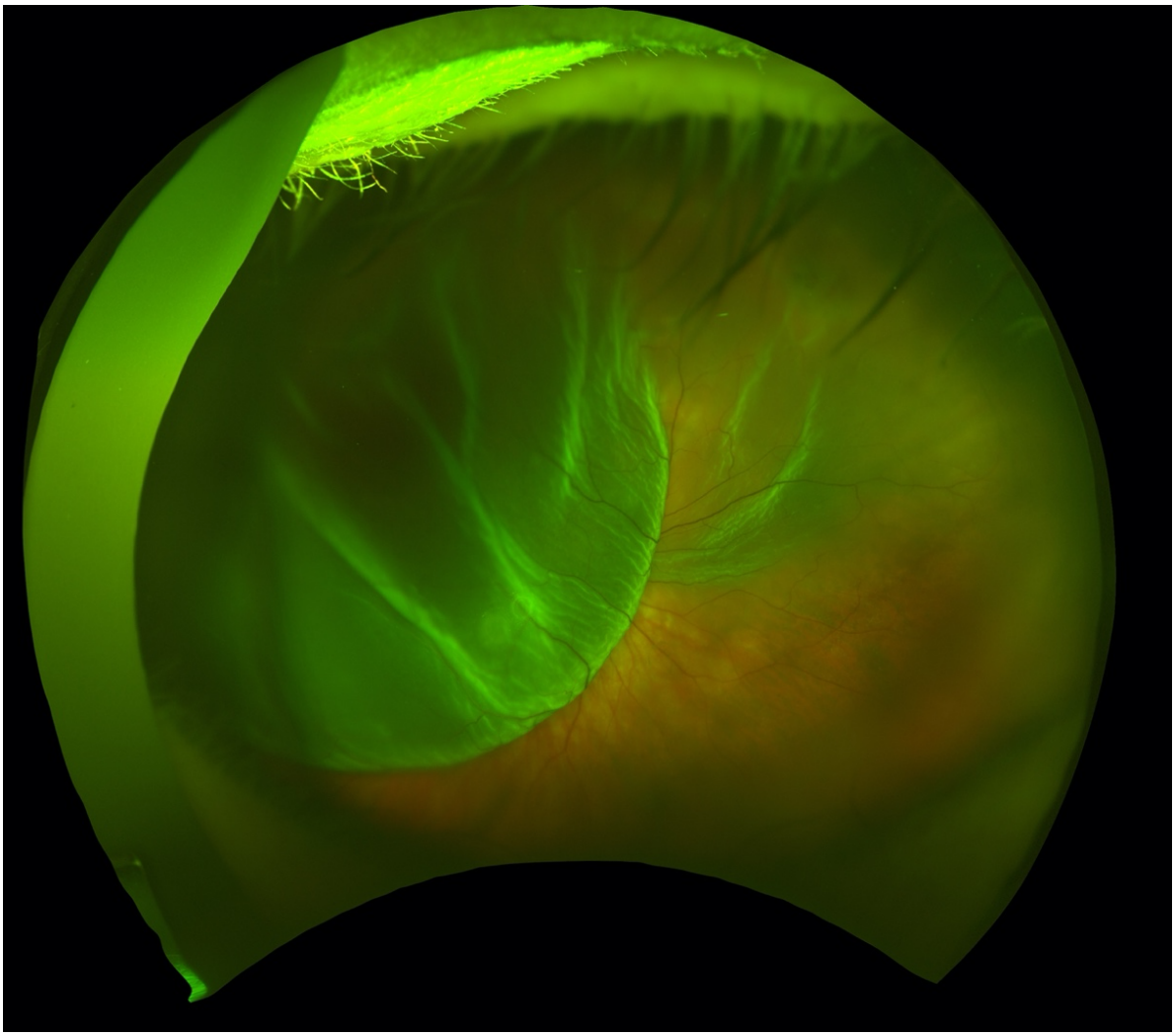

Figure 1.2.5. Optos wide field fundus image of a right retinal detachment. Taken with the Optos scanning laser ophthalmoscope. The false colour image enhances colour differences: detached retina appears green, above, as it transmits less of the orange light from the underlying retinal pigment epithelium. In reality the retinal tissue has a grey appearance.

1.2.2. Optical coherence tomography

OCT is widely used in ophthalmology to image the retina and optic nerve head[7,91,120]. A Michelson interferometer, spectral domain OCT uses low coherence interferometry with frequency domain signal separation via a diffraction grating to provide image resolution comparable to histological (microscopic) samples. Axial resolution theoretically approaches 2 μm, with transverse resolution 15 μm[91,121] providing image definition greater than ultrasound or magnetic resonance imaging. Yet OCT captures images rapidly, non-invasively, and repeatedly, with minimal patient inconvenience and no risk. Energy incident upon the eye is minimal: power is less than 1.5 mW at the cornea. Most clinical images are taken of the posterior pole – the macula and disc, where the common pathologies of glaucoma, diabetes and macular degeneration can be seen. Zeiss Cirrus OCT machines, one of the most common machines used in ophthalmic practice in Australia, can capture from 27 000 – 68 000 individual A scans per second, and swept source OCT can capture up to 200 000 A scans per second.

OCT imaging of the retina was first reported by Huang[122], with images of tissue samples of the retina and coronary artery. *In vivo* ocular imaging was reported in 1994[123]. Early commercial OCTs involved moving the reference mirror to image each voxel and complete the A scan (time domain OCT), which limited acquisition speed and have largely been replaced by spectral domain OCT (SD OCT). In this, a broad bandwidth superluminescent diode (SLD) light source is used, and the returning signal split into component frequencies by a grating and received by a charge-coupled device containing photo-detectors with varying frequency sensitivity, allowing different wavelengths to provide signal from different tissue depths. This results in much faster A scan generation. This rapid signal generation has permitted fast scanning speeds to capture multiple parallel B scans for three-dimensional tissue assays (Figure 1.2.6). Swept source OCTs (SS OCT) use a tuneable laser of varying wavelength to further increase imaging speed.

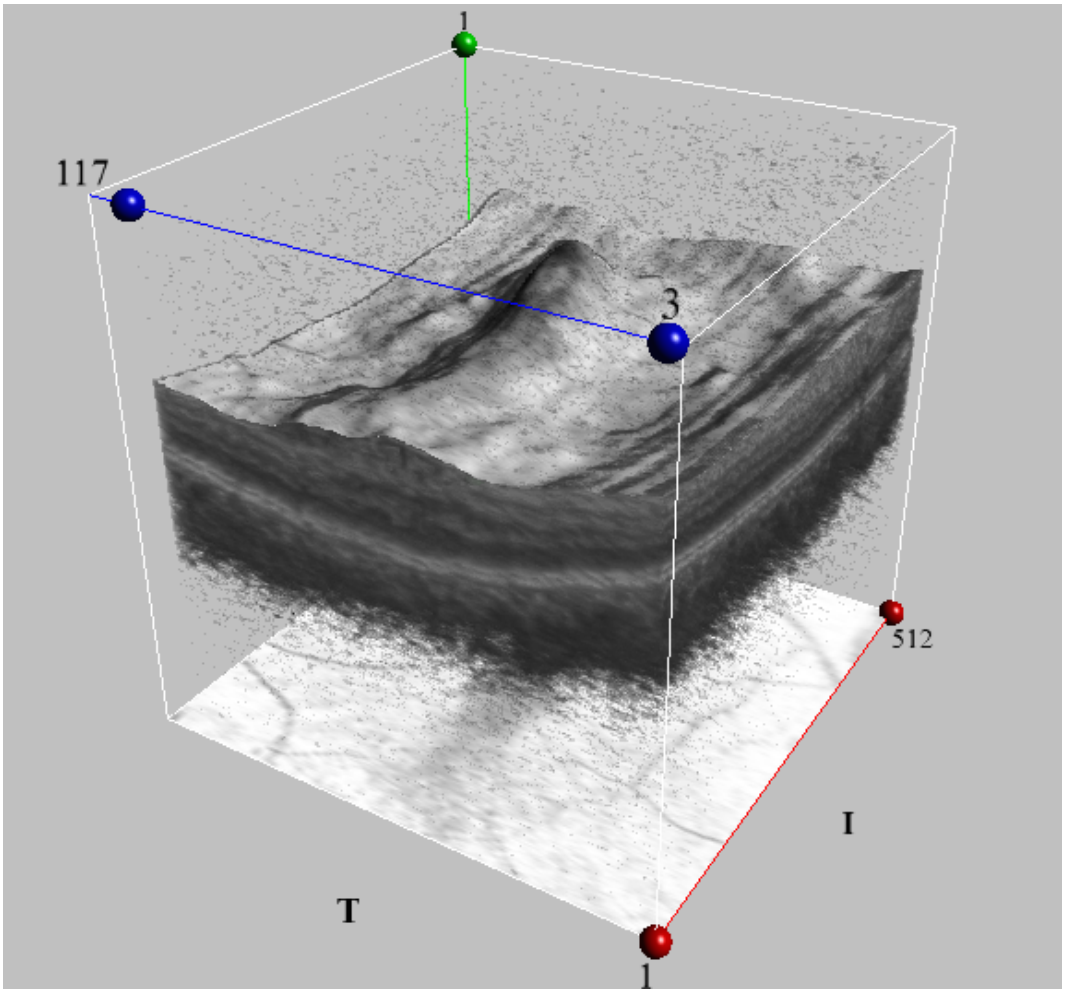

Figure 1.2.6. 3D OCT image. Three-dimensional reconstruction of retinal tissue. The scanning laser ophthalmoscope image of the area is projected beneath the OCT cube. The image is formed from 512 A scans arranged side by side in the direction given by the red line, and letter I. This forms a single B scan. Then, 128 B scans are aligned in parallel up the blue line, letter T. The retinal surface is toward the top, and the paler layer in the middle of the OCT cube represents the retinal pigment epithelium and ellipsoid layers.

Retinal OCT is oriented from the point of view of the examiner: the *x*-axis horizontal left to right, *y*-axis vertically inferior to superior, and *z*-axis antero-posterior. A B scan image is constructed from multiple A scans (a single antero-posterior assay) aligned in parallel. The image voxels are anisotropic. Lateral (*x*-axis) resolution is affected by the optical factors of the camera and the eye, and is approximately 15 μm with the Zeiss Cirrus. *y*-axis resolution is determined by the interval between each B scan: the vertical angular displacement between each image. In the Zeiss Cirrus macular cube protocol this is 45 μm. The interval between scans and consequent *y*-axis resolution is larger with other scan algorithms, with

the HD21 raster scan spacing adjustable between 50-500 μm. The axial (*z*-axis) resolution is as low as 2 μm reflecting the high sensitivity of interferometry.

The Zeiss Cirrus OCT has a camera to image the external eye, and a separate camera (a scanning laser ophthalmoscope) for imaging the fundus, with field of view of 36° lateral width, and 26° vertical height. The light source is a superluminescent diode for interferometry with a centre optical frequency of 840 nm. The area scanned by the standard OCT cube within the camera field covers approximately 20° of retina, or 6 mm horizontally.

Schmitt[124] described the physics behind the OCT. Waves are coherent if they are of the same frequency and have a constant phase difference. The coherence length is the length of a wave along which (a specified degree of) coherence is maintained, and is proportional to the square of the mean wavelength, and inversely proportional to the bandwidth. A laser has a coherence length of meters, but the use of a superluminescent diode with a broader bandwidth reduces this to micrometres. The broader the bandwidth, the better the axial resolution. Other factors affecting coherence length include the speed of light and refractive index of the media. In OCT literature, coherence length is given as

$$L = 0.44 \frac{\lambda_0^2}{\Delta\lambda}$$

where λ_0 is the centre optical frequency, and $\Delta\lambda$ the bandwidth of the light source. Thus, for a near infrared 840 nm wavelength superluminescent diode with a bandwidth of 100 nm the coherence length is 2-3 μm, however adjustment for the absorption and refractive index of water reduces the useful bandwidth and hence resolution of the OCT to around 10 μm.

The broader the emission bandwidth, the better the resolution and contrast, as long as chromatic aberration and mismatch between reference and sample beams remains low[124]. Near infrared light of 840 nm provides good tissue penetration, is safe and non-irritating to the subject. Voxel signal intensity is represented on a grey-scale or converted to a colour map via a look-up table, with red equal to white (high reflectance) and blue replacing lower intensity (darker) pixels.

OCT is now widely used for vitreo-macular interface disorders, diabetes, macular degeneration, and glaucoma[125]. Interferometry produces high axial resolution, but the lower transverse resolution comes from the limits set by the entire optical pathway (instrument and eye) affecting the spot size on the target tissue. This can be increased with pupil dilation, and is decreased by defocus (refractive error) and higher order aberrations. Swept source OCTs can provide greater resolution, use a longer wavelength improving tissue penetration, and generate signal even faster to allow fast repeatable scans of any point to detect motion via phase and amplitude shift of signal. Such motion in the retina is usually from blood flow, which has led to the development of OCT angiography[126,127]. OCT retinal oximetry may be possible[128].

OCT image processing

The standard image output from commercial OCTs has undergone considerable processing for presentation and to enable accurate and repeatable segmentation for analysis of disease states. The processes vary by device and manufacturer, but the first step in image production from data is pre-processing: A scans are normalized (the signal intensity in each A scan balanced to match adjacent scans) and previously were flattened (aligned) by intensity and spatial position (usually by the outer highly reflective band and inner limiting membrane – the two highest intensity layers in the signal), to transform the data into a common space (Figure 1.2.7)[129]. Flattening in lower frequency scans allowed (posterior) *z*-axis truncation to reduce file size[130], and segmentation by surface layers to provide a consistent shape for visualization other segments[131–133]. Segmentation involves the distinction of up to 27 separate retinal layers by boundary classification – the consistent sudden changes in signal intensity[120].

The outer highly reflective band consists of photoreceptor cells, RPE, Bruch's membrane, and choroid, that can be separated into three highly reflective interfaces, presumed to be the ellipsoid layer, RPE, and Bruch's membrane[134]. This high signal layer was often used as the reference line to be flattened for segmentation.

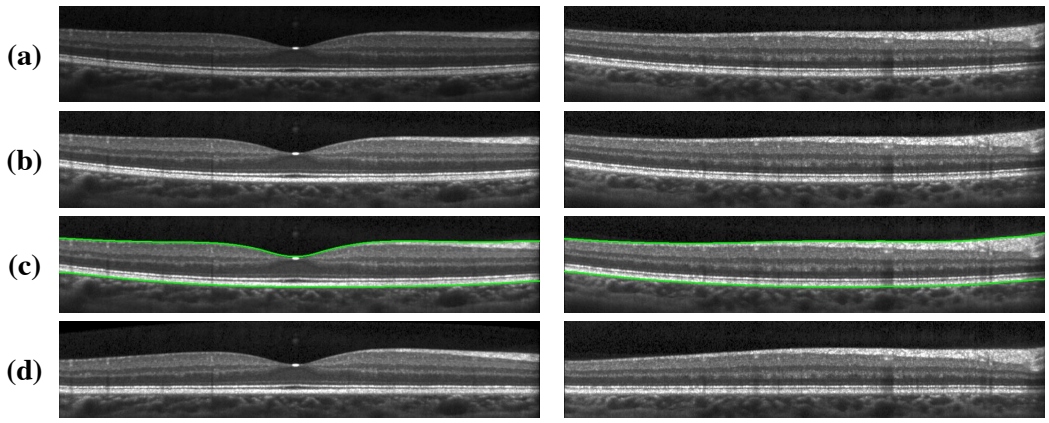

Figure 1.2.7. Pre-processing OCT flattening. The outer highly reflective band (brightest white horizontal line) shows pre-processing effects. In (b), the signal intensity is normalized along the line. (c) shows identification of retinal boundaries, which are flattened in (d). (Reprinted with permission from Lang et al (2013), © The Optical Society).

OCT image artifacts

OCT images require correction for the distortion effects produced by the geometry of the scanning beam (distance between source and subject, fan scanning, oblique scan effects), motion errors (eye and head movement), and differences in refraction.

Axial length effects

OCT curvature values need to be corrected for OCT image acquisition artifacts. Variation in axial length has the greatest impact on errors in retinal curvature estimation with the OCT, with tilt and eye position less significant. Correction for this has been performed by pre-calculating the error induced by axial length differences using ray-tracing models[135], or through more complex combined anterior and posterior OCT imaging for true individual eye optical effects[136]. As well as axial length, alterations in device-to-eye distance alters measured retinal shape[137], so correct head and eye alignment during imaging is important. More difficult to correct for are optical pathway distortions arising from the beam passing through different parts of the peripheral cornea and lens on a pathway at an angle to the visual axis. The aberrations and distortions resulting from this are indeterminate, variable, and therefore difficult to correct. However, the absolute size of these effects is small[138].

Eye motion artifact

Eye motion induced artifacts can be reduced by multiple scan signal averaging, or eye tracking with the use of a scanning laser ophthalmoscope to maintain alignment with target tissue[120]. The capture speed for a single B scan is fast enough with SD OCT that very little motion artifact occurs. However, the reconstructed B scan at 90° to the fast scan direction (created by extracting all A scans with a constant x coordinate from multiple parallel B scans) does display "rippling" from micro-saccades, blinks, and other eye movements. This can be reduced by autocorrelation that aligns stacks of frames: each frame is used as a template to align the next frame in the series[139]. Both axial flattening from this auto-correlation, and eye movement artifact correction, can be performed by scanning twice, with the fast scan direction rotated by 90 degrees from the horizontal to vertical direction. The fast acquired data from one scan orientation can be used to correct movement artefact in the slow scan direction of the other. The faster scanning speeds of newer devices reduce the requirement for correction for eye movements[140,141]. Fast scan direction B scans may show "tilt" due to paraxial imaging off the optical axis of the eye (oblique scans, see below)[131,142].

Fan scanning errors

While A scans are collected in an arc originating from the signal source, they are presented as a square B scan (Figure 1.2.8). The result is the A scans at the margins in any B scan are displaced and represented posterior to their actual sample position. When operating the Cirrus OCT, the technician identifies the pupil plane to acquire the image. This allows the OCT to set the reference path length as the pupil plane to retina distance. The effective point of rotation differs for the vertical and horizontal fans with the former 1.65 mm anterior to the posterior. Axial displacement of the eye from the scanner (resulting from not positioning the eye so the reference path length starts at the pupil plane) leads to bending of retinal structures. The error in image position relative to object is given by:

$$E^{\mathrm{l}} = \left(r_0 + \frac{z}{n}\right) \sin\alpha$$

$$E^{\mathrm{a}} = \left(r_0 + \frac{z}{n}\right) \cos\alpha - r_0.$$

where E^{l} is the lateral displacement of the image point from its true location, E^{a} the axial displacement of the image, r_0 = reference path length, z = the movement of the scanner

from r_0, with n= 1.38, the refractive index of retina, and from anterior to posterior the retinal thickness averages 250 μm. At the null angle $\propto$, E^a = z/n, and E^1 is zero[143]. For the standard Cirrus scan, $\propto = 10$ degrees for a macular cube with a 6 mm line scan (half the 20° scan area). The result of this fan scanning distortion is that objects perpendicular to the scan axis (with a constant true *z*-axis position) would "frown", or droop in the image. At the lateral locations on a 6 mm macular cube, the axial displacement is approximately 186 μm if r_0 = 24. Therefore, careful head positioning is required for accurate retinal assessment. Lateral displacement error (E^1) is around 4 μm, and so is below the limit of resolution for the OCT.

Fan scanning errors can be corrected *post hoc* using knowledge of the beam geometry, but this is dependent upon the beam passing through the centre of the pupil and knowledge of the reference point displacement (Figure 1.2.8). With earlier devices, axial (*z*-axis) displacement of the eye, bringing the reference point away from the pupil plane, led to this bending of image due to the path length variation in some OCT machines[139]. The Zeiss Cirrus OCT only acquires a retinal signal when axially positioned so the reference point is at the pupil plane, avoiding these axial positioning bending errors. While this effect of differences in the axial position of the eye influencing shape are reduced by focussing the image of the external eye during scanning, as well as accounting for variation in the axial length of the eye, the fact that A scans are acquired in an arc and converted to a rectangular output image will reduce the measured curvature. This is a feature of the machine consistent across all images, and is not corrected in this work. Any *x*-axis, or *y*-axis displacement of the beam from the centre of the pupil will lead to oblique scanning tilt errors, discussed below.

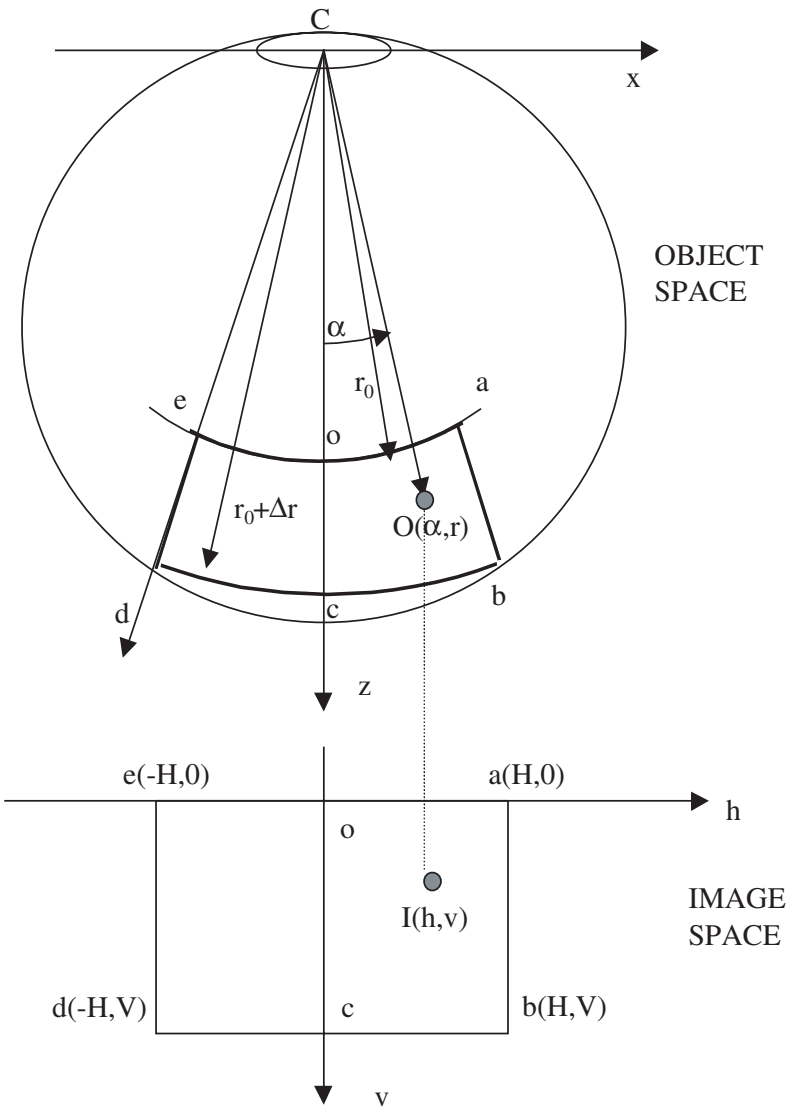

Figure 1.2.8. Fan-shaped OCT A scan acquisition converted to a rectangular B scan image. Fan scanning errors result when a signal acquired in an arc from a point source emitter is converted to output presented in a rectangular form. Arcs ae, and bd, in the upper image, are presented in the image as flattened lines. This results in lateral and posterior displacement of each point in the output. The reference plane (x) is shown here through the middle of the lens. In fact, with the Zeiss Cirrus OCT the horizontal scanning reference point is set at the pupil plane of the subject. The vertical pivot is from a point 1.65 mm anterior to the horizontal. (From Podoleanu et al (2004), © Institute of Physics and Engineering in Medicine. Reproduced by permission of IOP Publishing. All rights reserved).

Oblique scanning induced errors

Oblique scanning (imaging the retina off the optical axis) alters the reference path length across the width of the B scan: retina contralateral to the entry point will be further away from the OCT source, and displayed as such. This leads to the retinal image tilted toward or away from the observer in a manner unrelated to its true position (Figure 1.2.9). While accurate and consistent A scans are obtained within each B scan, each different pupil entry point used when scanning peripheral retina will have differing obliquity, producing different tilt[142].

Flattening

In pre-processing, flattening, in particular, is unhelpful when determining retinal shape and contour (Figure 1.2.7). While reversal of flattening can be performed with the use of ray diagrams, at least for the posterior pole[137], fortunately this is not required for Zeiss Cirrus data. With this OCT device, conversion of a fan scanned image to rectangular/cuboidal output is performed by aligning the A scans, with the reference path length equivalent to the pupil to retina distance. No extra flattening is performed, so reversal of this step is not necessary for Cirrus output.

Refractive index effects

Varying refractive indices of intraocular tissues, including the retina, lead to the distortion of the RPE line under the foveal dip: under the (thinner) fovea, the RPE will appear elevated (by about 2.1 μm) due to less travel distance through retina with its different refractive index to vitreous[143]. These errors are at the limit of resolution for the OCT, and have little impact on the measured location of the RPE, which has a thickness of 20-40 μm.

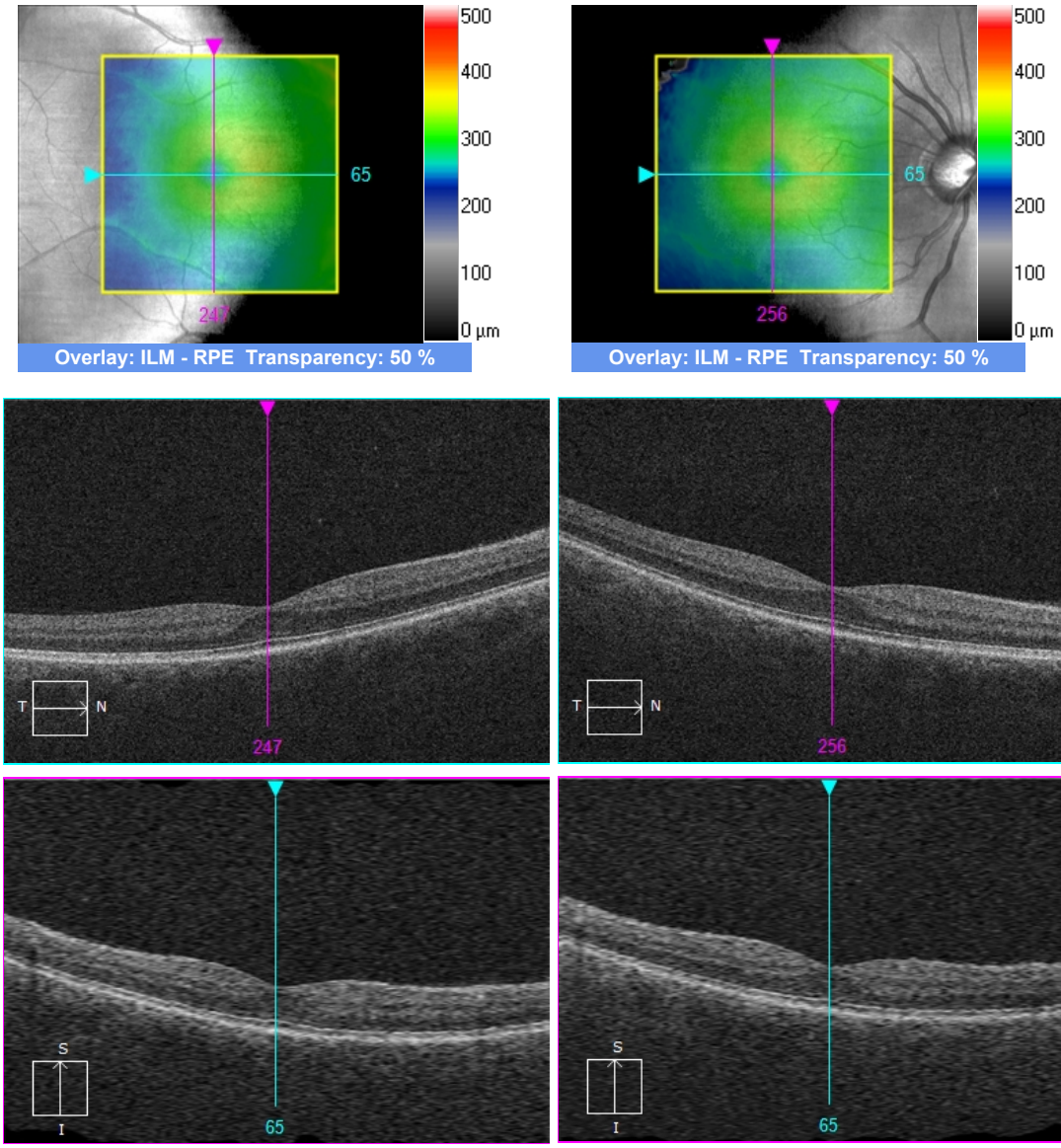

Figure 1.2.9. Oblique scanning-induced image tilt. These two macular cube scans were centred on the same point of the same right eye but captured off axis. The images on the left are taken through the nasal (right) side of the pupil, and the scans on the right taken through the temporal (left) side of the pupil. In the horizontal scan (middle image on each side), the part of the macula contralateral to the scanner is further away, so it is displaced posteriorly in the image. The lower OCT image is vertical, and unaffected, as the scanner has been moved left to right only.

Vignetting

Loss of signal intensity in the peripheral A scans from an image arises from reduced scatter and leads to reduced contrast and reduced ability to identify retinal structures. In these areas, only the higher intensity signals can be reliably identified, but position and shape are not affected.

Scatter

Scattering refers to the redirection of light from interaction in the transmitting medium (effectively the entire eye). Other than back-scatter and wide angle scatter (which deflect the light away and reduce signal), low angle forward scatter that still passes through the temporal coherence gate reduces resolution and contrast, while wide angle scatter reduces contrast but not resolution. Speckle is a noise feature present in all narrow band imaging systems, including OCT. Speckle arises from random back-scatter and forward propagation delay from forward scatter contributing to the returning beam signal. These image effects do not alter the location of image compared to object and so do not affect measurement of shape[124]. Noise reduction occurs during acquisition and processing, with methods including multiple signal averaging, and signal intensity correction between A scans.

1.2.3. Peripheral retinal OCT imaging

A standard OCT line scan extends 6-9 mm across the posterior pole of the eye. The term "wide field OCT" has been used to describe the use of faster (newer) OCT systems to acquire a line scan of 9-12 mm length[144], although this term is now reserved for peripheral retinal images beyond a 50° field of view[10]. The larger B scan widths have been used to extend the range of image acquisition, which has improved the OCT imaging of non–posterior pole retinal anatomy. Techniques employed to extend the range further toward the retinal periphery include asking the subject to look away from the OCT scan axis (eccentric fixation), which brings peripheral retina into the field of view[145]; and the use of condensing lenses (similar to those used for indirect ophthalmoscopy) to widen the field of view by increasing the angular range of the imaging light source[144,146,147].

Eccentric fixation for peripheral retinal imaging has been used to describe the OCT features of peripheral retinal pathologies. Kothari et al[148] used unmodified spectral domain and time domain OCT this way to image peripheral retinal features including lattice and pavingstone degeneration in 36 eyes. These are single scan samples of peripheral retinal anatomy, with each image discrete and isolated from the larger retinal picture. Choudhry et al[10] et al used the term "ultra-wide field" to describe OCT images captured at 200° from the posterior pole, adding dioptric power within the (unmodified) OCT system to bring focus forward as the distance to the anterior retina decreased from the posterior pole. Pichi et al[145] reported peripheral retinal OCT findings in healthy eyes, and those with macular degeneration, retinitis pigmentosa, and central serous retinopathy. Carrai et al[149] reported peripheral retinal OCT in 40 eyes with central serous retinopathy. The images presented in these reports were montages of individual OCT B scans, combined using Adobe Photoshop (San Jose, CA) to link the macula and eccentric retina. These works did not look at retinal shape, but described the vitreo-retinal features identified within the scan window.

Mori et al[12,150] used the Heidelberg Spectralis OCT with eccentric fixation to capture peripheral images and describe the changes within the retinal layers. In particular, they described the reduction in ganglion cell layer thickness in the retinal periphery. Images were again stitched together with Adobe Photoshop. The merging technique involved aligning OCTs by rotating the peripheral scans to fit the curve of the retinal pigment epithelium seen in the macular scan. They did not adjust images for curvature artifact, and perhaps as a result found the peripheral retinal image appeared flattened. The same group used stitching to compile wide field of view OCT images in another report on the vitreo-retinal interface changes seen in differing stages of macular hole. While this did not consider retinal shape, it was an interesting attempt to relate vision threatening disease to peripheral vitreo-retinal morphology seen with the OCT[12].

Reports on wider field OCT with the use of condensing lenses include one series of 27 eyes, with a purpose built wide field of view swept source OCT with indirect lenses (20 dioptre and 40 dioptre) used to achieve a 20 x 20 mm, or 80° field of view, in a single scan, without requiring eye movements or image stitching[146]. This field of view was centred on the

posterior pole, and it is the image size reduction from the condensing lens that widens the area of coverage of the OCT scan. Similarly, the use of the 20 dioptre condensing lens has been demonstrated to increase the field of view to 1.45 – 1.65 with SD OCT[144] and 1.64 – 1.67 with swept source OCT devices[151]. This magnifies the voxel and reduces resolution, as well as increasing the complexity of the optics of the system, which can make image acquisition more challenging.

Peripheral retinal imaging introduces extra factors that interfere with the quality of imaging obtained. Oblique scanning[142] has little effect on retinal image curvature[135] but does reduce the image resolution through a range of factors, including: vignetting (loss of sampling beam intensity at the edge of the pupil, or due to suboptimal axial position); increased aberrations and reduced backscatter at an increased angle of incidence[152] to the curved retinal surface; curved retina taking the imaged tissue beyond the focal range; and loss of sensitivity as the image transitions posteriorly away from the OCT systems zero-delay plane. With the eye movements required for eccentric retinal images, induced vignetting is particularly noticeable in affecting the quality of the retinal image[153]. Despite the lower intensity signal resulting from these effects, the high intensity signal from the retinal pigment epithelium remains apparent, a useful feature considering retinal shape analysis is dependent on this line.

1.2.4. Posterior segment and retinal shape analysis

The eye is neither a perfect sphere nor even an ideal ellipsoid. Magnetic resonance imaging (MRI) has been employed to investigate both globe and retinal shape. Studies of human eye shape with a range of refractive errors generally show myopic eyes are further from an ideal sphere than emmetropic eyes, with a tendency to be prolate (the shape of an ellipse rotated about its major axis) rather than oblate (an ellipse rotated about its minor axis)[154]. MRI data has also been used to validate OCT derived shape information, which has added more granular detail.

Beenakker[112] used MRI to generate a topographic map of the posterior 30 degrees of the retina, reporting the topography as the distance of any retinal point from the lens centre. These results were in close agreement with partial coherence interferometry. They found an increasingly prolate form to the posterior 30° of the eye with increasing myopia. This study did not seek to investigate retinal shape features other than relative curvature.

Thinner sclera is seen posterior to the equator in myopic eyes compared to emmetropic eyes[78], and there was some thought that the growth of the eye in myopia is purely an axial elongation. That this is not necessarily the case was confirmed by Atchison et al[155], who calculated ellipsoid best fits for eye shape of 21 emmetropic and 66 myopic eyes. The model of eye shape was generated with measurements of retinal curvature from just one transverse axial (horizontal) and one sagittal (vertical) MRI section per eye, using a surface coil and an LED fixation target to minimize eye movement and improve resolution. The ellipsoids were tilted around the vertical axis by approximately 11° in all eyes, consistent with peripheral refraction asymmetry in the horizontal visual field. Increased myopia was associated with a much greater increase in the axial semi-diameter than horizontal or vertical semi-diameter, although the myopic eyes were bigger in all dimensions compared to the emmetropic eyes. Myopic eye growth was neither simply an equatorial elongation (where the size of the eye at the equator is unchanged as axial length increases) nor a uniform global growth (even expansion of eye size in all dimensions), but had different expansion in different meridians. Myopic eyes were larger axially (anterior to posterior) more than vertically, and vertically more than horizontally (left to right). In emmetropes the different axes had less variation in size, and the antero-posterior axis remained the largest. The study did not look at local differences in individual eyes, nor the effects of eye size on different disease states. MRI retino-choroidal thickness decreased at the equator in myopic eyes, although this change was small (0.014 mm per dioptre) and well below MRI resolution[155].

Another group reconstructed the three dimensional form of the eye from a three Tesla MRI scanner[156]. This enabled determination of variation from sphericity, and confirmed nasal-temporal asymmetry, with the temporal hemisphere of the eye more bulbous (Figure 1.2.10, in particular sub-images (c), (f), and (g)). MRI determined axial length was on average

0.41 mm greater than the same measure determined by partial coherence interferometry with the IOLMaster (Carl Zeiss AG, Germany). This difference was considered significant. They attributed this difference to the MRI voxel resolution, although it is not clear in the report whether the posterior margin of the calculated globe included sclera, or only uveal tissue. The paper did not relate eye shape to the presence of retinal pathology.

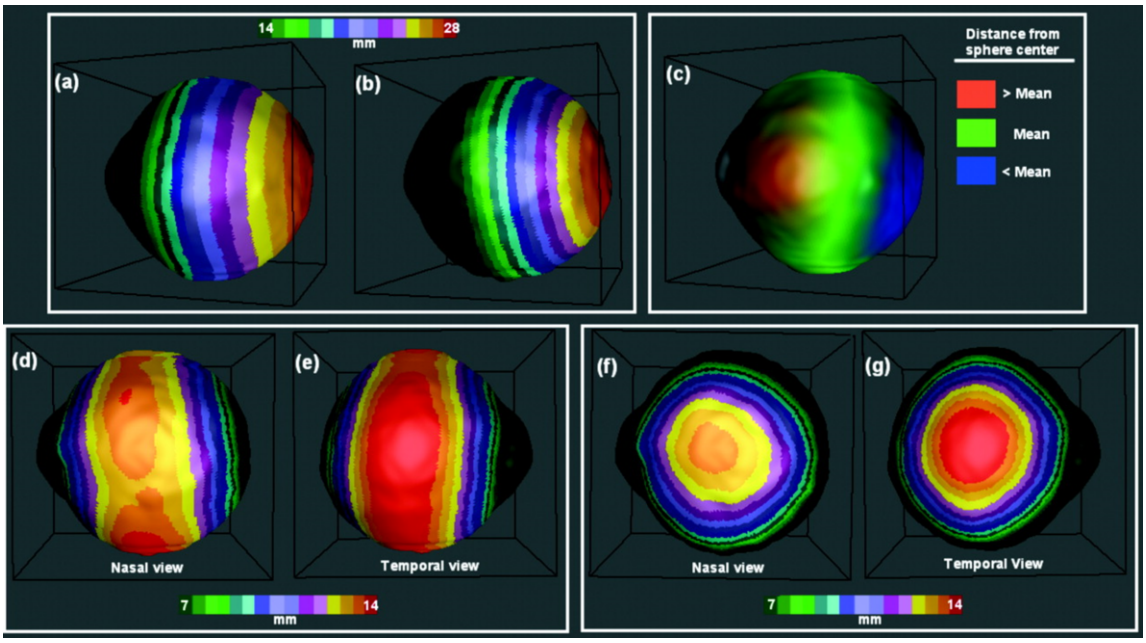

Figure 1.2.10. MRI globe surface topography. Reconstruction of a right eye. (a) The total (Pythagorean) distance from the corneal pole; (b) axial distance from the same point. (c) Deviation from sphericity, with colours representing differences from the mean radius of the best-fit sphere to the posterior portion of the eye model, not including the anterior chamber. The posterior pole of the eye has a smaller radius than the mean best fit sphere, implying an oblate shape. (d–g) The distance from the longitudinal axis of the eye, with (d) and (e) showing total distance from the axis, and (f) and (g) showing only the horizontal distance component (i.e., the distance from a vertical plane incorporating the visual axis). The bottom panels demonstrate a clear asymmetry in this eye, with the eye more bulbous in the temporal direction. In (a) to (f) the cornea is to the left. In (g) the cornea is to the right[156]. Reproduced with permission, copyright of the Association for Research in Vision and Ophthalmology, 2006.

Shimada[157] use wide angle ultrasonography to compare retinal detachment eyes to a sample of eyes without retinal detachment. The retinal detachment eyes had both a greater axial length and a larger horizontal (but not vertical) diameter than non-retinal detachment eyes. Selection criteria of the non-retinal detachment eyes was not reported, in particular whether they had experienced a PVD. One interpretation of their result is simply that longer eyes are also wider.

The use of OCT in the analysis of abnormal retinal contour in myopia has concentrated on the posterior pole, and in particular the extremes seen with myopic posterior staphyloma, due to its consistent landmarks (the fovea and optic disc), ease of imaging, and known clinical significance. A link has been established between the shape of posterior staphyloma and the myopic retinal complications of atrophy and myopic traction maculopathy[4,6,158,159,160]. Miyake et al[158] reported on the use of OCT to determine the contour of the posterior pole in myopic staphyloma, relating OCT defined retinal contour to disease. They took 12 radial OCT B scans, centred around the fovea, of 182 myopic eyes, and described the local radius of curvature along these line scans. The curvature along these lines was plotted at 1 μm intervals in a colour topography map, similar to that used in corneal topography. Using this, fundus shape was related to the observed chorio-retinal changes. In particular, higher curvatures and greater point to point curvature variance was associated with chorio-retinal atrophy. Moderate curvature and moderate point to point curvature variance was associated with myopic retinoschisis; and lower curvature and point to point variance associated with myopic choroidal neovascular membranes.

Scleral shape has been associated with myopic retino-choroidal lesions, including chorio-retinal degeneration and myopic retinal schisis[7,8,161]. Dome-shaped maculopathy is a well-recognised pathology of myopic eyes with subretinal fluid without choroidal neovascularisation, reduced vision and a convex inward ridge shaped deformation of retinal shape within a posterior staphyloma[9,162,163]. The aetiology has been attributed to uneven paracentral scleral thinning leading to variable scleral rigidity[164]. Wakazono et al[6] used the custom software Retinaview (Canon Inc., Tokyo, Japan) to examine posterior scleral curvature, and found curvature changes between 3 mm and 6 mm from the fovea were associated with myopic traction maculopathy.

Other authors have explored the shape of structures seen in OCT other than retinal shape as defined by the contour of the retinal pigment epithelium. Scheibe et al[165] developed a model to describe and analyse the shape of the normal foveal (inner) surface in three dimensions using the Heidelberg Spectralis OCT (Heidelberg Engineering Co, Heidelberg, Germany). Ruiz-Medrano et al[166] described the shape of the posterior choroido-scleral (not retinal) interface. They concluded that both normal variants of concave and S-shape contours were associated with focal choroidal thinning. Guimaraes et al[167] used spectral domain OCT to reconstruct the retinal vasculature in 3D. Ohno-Matsui et al[7] described the shape of posterior scleral curvature with swept source OCT in highly myopic eyes.

Posterior pole shape has been quantified by measurements of its curvature and how this relates to disease. Macular curvature, quantified by the mean, standard deviation, and range of curvature, has been shown to differ between myopic eyes with and without a staphyloma, where the former had a greater range and standard deviation but lower average local curvature. This lower curvature related to the longer axial length observed in staphylomatous eyes[2]. In contrast Numa et al[168] measured the mean and variance of macular curvature in a Japanese population. Both values were significantly greater in the presence of diagnosed staphyloma by fundus photography and OCT, and these measurements were sufficient in themselves to diagnose staphyloma. Curvature was significantly correlated with axial length (ρ = 0.480, $p < 0.005$). McNabb et al[113,136] used graph theory to segment retina after rough manual segmentation, and estimated curvature determined by fitting a circle to the corrected OCT segmentation. Using an OCT that provided anterior and posterior images simultaneously, they used the anterior OCT images to correct the distortions in the posterior retinal curvature arising from anterior segment effects on the beam pathway. These were validated via comparison with MRI determined retinal curvature. The process was used to create retinal topographic maps of the posterior pole[169]. Eyes with papilloedema were flattened nasally, and myopic eyes with staphyloma had a greater variation in macular curvature compared to normal.

Peripheral refraction has also been used to estimate retinal curvature. This tends to under-

estimate retinal curvature, particularly with increasingly myopic eyes, compared to the more accurate corrected OCT curvature measurements[96,170]. Peripheral refraction also requires dedicated hardware and only produces limited results at defined points[110]. Tabernero & Schaeffel[171] designed a scanning infra-red photo-retinoscope to measure peripheral refraction 45° from fixation along the horizontal meridian, potentially providing a greater sensitivity to local variations in refractive path length than obtained with MRI. The peripheral myopic eye was "bumpier" than an emmetropic eye, requiring a higher order polynomial to match data than that for emmetropic eyes. They attributed this to loss of scleral rigidity, leading to increasingly irregular eyeball shape in myopia, as is seen with MRI reports[7,156], and the formation of staphyloma.

Kuo et al[110] compared MRI and OCT measured radius of curvature of the posterior pole. Fifty-two subjects who had undergone MRI and OCT were taken from the Singapore Epidemiology of Eye Disease (SEED) project. Coronal MRI slices of 1 mm voxel resolution of right eyes were segmented, and the posterior segment oriented around a visual axis defined as 3.5 degrees off the optical axis drawn through the apices of the anterior corneal, anterior lens and posterior lens surfaces. This was to align the MRI images with the axis of the OCT. The retinal pigment epithelial layer was segmented within a standard 6 x 6 mm macular cube, with OCT distortions corrected by an optical model in OpticStudio Standard (Zemax, Kirkland, USA). Both MRI and OCT showed a trend for eyes becoming more prolate as myopia increased. OCT and MRI agreed as to form (oblate versus prolate) in 47 of the 52 eyes. OCT categorized 5 eyes as prolate that MRI classified as oblate. The authors considered MRI as the gold standard, despite MRI having the more limited resolution of 1 mm. They used only a single OCT field to define curvature, with no "stitching" of adjacent images to widen the area investigated.

Much of the quantitative analysis of OCT retinal contour has been on the best fit curve to the retinal pigment epithelium, often but not always called retinal curvature. Kuo et al[110] calculated the radius of curvature from the spherical solution to the general quadric equation fit to the retinal pigment epithelium. As most solutions from the OCT image using the general conic equation produce a hyperboloid form, and minor differences in scan position can lead to widely diverging results due to programmatic approximations of infinite

series, correction by a reflection of the posterior shape anteriorly at the distance of the axial length was made to restrict the solution to an ellipsoid. The asphericity of this ellipsoid was quantified by $R_x^2/R_z^2 - 1$, with R the radii of curvature perpendicular to each other. They found the resulting distortion-corrected OCT measurements of curvature and asphericity had an individually important if overall non-significant difference from MRI measurements of curvature.

Swept source OCT macular shape was described using curvature calculated from 17 points 1 mm apart using cubic spline interpolation curve fitting to three, 4 mm sections: one central and one on each side from a 16 mm B scan. The peri-macular curvature was greater than macular curvature in both horizontal and vertical scans, with no difference found between vertical and horizontal central macular curvature. The retinal pigment epithelial curvature was found to be affected by the underlying choroidal and scleral tissues[172].

Non – curvature metric retinal shape analysis

Differences between baseline retinal curvature and the actual retinal shape have been used to identify the drusen induced "bumps" in the RPE line in age-related macular degeneration[173–176]. The best fit curve was taken from both second order[174,176] and the average of multiple 5th order[173] polynomials calculated from a random selection of points taken from the RPE layer. The difference between this and the true contour was explored to identify a threshold irregularity above which pathological change were likely to be present.

Kafieh[177] used image processing tools to identify the RPE, and from that distinguish abnormal retina from normal through what they label as curvature. This is a different property from the retinal curvature quantified in other papers above, and in this work, and is more like the concept labelled irregularity in this thesis.

Shape features in other disease

Focal choroidal excavation is a localised outpouching of the retinal pigment epithelium line found rarely in macular OCT scans (Figure 1.2.11)[178]. As focal choroidal excavation has been reported to both follow and precede choroidal neovascularisation, it is unclear what process is occurring in these eye[179–183]. One hypothesis is that it arises from choroidal fibrosis

drawing inner retinal structures outward. It may be a feature of pachychoroid spectrum disease, characterised by other OCT features including thickened outer choroid, RPE and neurosensory retinal changes.

Differentiation between optic nerve drusen, an apparent swelling of the optic disc due to anterior migration of calcified hyaloid bodies within the optic nerve that in most has little effect on vision, from papilloedema, a neuro-ophthalmic emergency arising from raised intra-cranial pressure can be a difficult clinical decision to make. The OCT has been demonstrated to provide useful information. Both show alterations in the disc contour, with the disc drusen themselves often visible on OCT. Reported retinal contour differences are an 'A' pattern to the peri-papillary Bruch's membrane – RPE complex seen in papilloedema[184] as compared to a 'V' pattern seen with optic nerve drusen[185].

Shape has also been shown to affect the assessment of disease severity. Variation in retinal curvature, particularly nasal to the optic disc, has been found to affect the ability to detect the pathological nerve fibre layer abnormalities used to monitor for glaucoma[186].

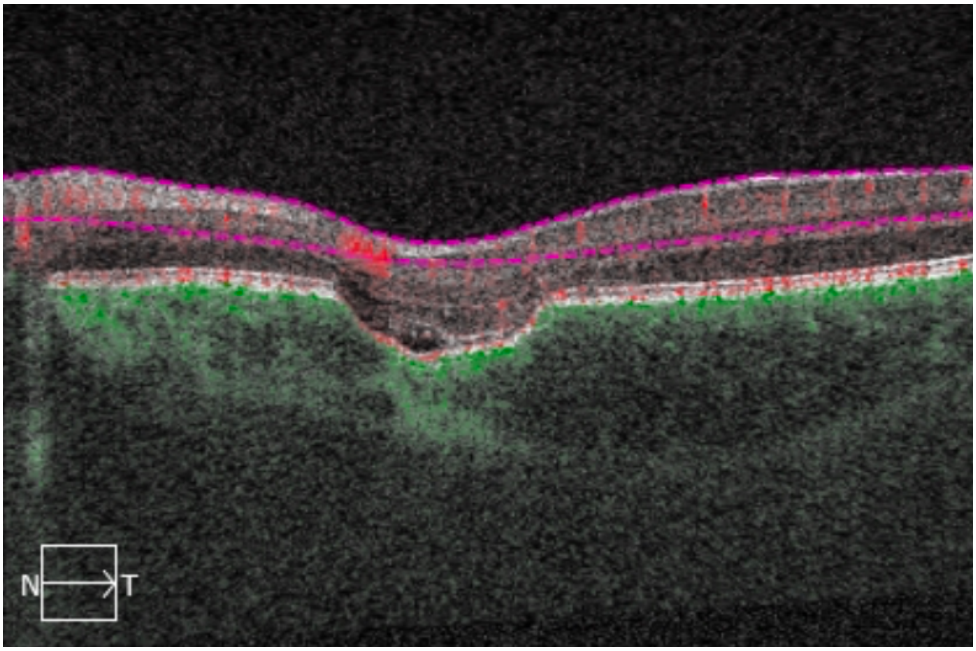

Figure 1.2.11. Focal choroidal excavation. OCT angiogram B scan from a 15 year old girl who presented with choroidal neovascularisation. The local concavity seen in the RPE contour (just left of centre) has been hypothesised to occur from fibrosis and contraction of choroidal tissue. This has been observed to appear both before and after choroidal neovascular membrane formation.

Summary
Research on posterior segment shape has increasingly used the OCT due to its ability to image the retina in a fast, accurate and reliable manner. Compared to MRI, OCT has superior resolution, with the disadvantage of only sampling a portion of retina in a single scan. Imaging beyond the posterior pole has been performed with both eccentric fixation and the use of condensing lenses. Posterior pole shape differences have already been explored in relation to myopia and its complications, macular degeneration, optic disc drusen, and focal choroidal excavation.

1.2.5. Gaze direction analysis

An anterior segment image of the eye is taken at the time of OCT imaging with the Zeiss Cirrus OCT. Stored in the iris.bin image in the OCT .img exported data package, it is a 480 x 640 pixel image of the external eye taken at the end of the OCT scanning. This provides some information on gaze direction that may be useful in identifying which area of the retina has been imaged. The corneal light reflex is not helpful for determining gaze orientation when OCT imaging is being performed, as the light reflexes are complicated by multiple sources within the room, or absent due to low light levels. When not obscured by the eyelids, the iris and pupil are easily seen.

There has been considerable work in gaze direction analysis across different settings that can be divided into the laboratory environment and "real world" settings, often with the aim of assessing and improving an individual's interaction with the environment, including human-machine interface tasks. Most methods for this use either the light reflex from the corneal surface, or the pupil shape. Laboratory based methods to assess gaze direction include reflectance differences between sclera and anterior segment structures[187,188], detection of Purkinje images in the near -infra-red reflected from anterior chamber structures (ISCAN device[189]), and electro-oculography, which assesses the potential difference between the anterior and posterior structures of the eye[190].

Open environment gaze determination frequently takes the form of image analysis, often focussed on detection of pupil location[191], either through passive image analysis, or active near infra-red light illumination and detection of response[192]. These often use a Hough transform[193] to identify the circular margin of the pupil[194]. Gaze estimation "in the wild" needs first to identify the eye in an image, either by characteristic image patterns (appearance based) or model based detection of local features around the eye, a process that has been improved through machine learning[195] and deep learning techniques[196,197]. One example of open environment infrared reflectance, requiring what were described as special glasses but in fact resemble more the anglerfish illium, performed gaze detection using a dynamic assessment of pupil shape, size, and position[188].

Analysis of gaze position during OCT image acquisition falls between these situations. In this work, gaze position analysis broadly resembles the laboratory based situation rather than the complex open world challenges[198], as it is performed in a closed environment, with a specific single image taken for each position of interest, and a label for each image reflecting where the subject was being asked to look. The latter is important, as pupil shape alone cannot distinguish between upgaze and downgaze, left and right gaze. In this work (Chapter 3), all that is required is measurement of the pupil ellipse from an external eye image of generally good quality. The total numbers were small enough for manual segmentation of the pupil to suffice.

1.2.6. Machine learning

Statistical shape analysis is a discipline that quantifies shape features independent of image orientation, translation, or scale. A numerical description of shape enables feature analysis and comparison of multiple samples. With a large number of potential variables of unknown significance, machine learning is an ideal tool to explore this field. Machine learning involves the development of algorithms, created from sample observations, that can then provide information about new observations. Models are defined using a training set of observations, in which each observation is described by the same set of variables (also

known as attributes, features, predictors, or dimensions). The training set may be supervised, in which the observations used to create the algorithms have labels, or unsupervised, in which case data mining is performed to identify new classes. Statistical or probabilistic methods may be combined with Boolean logic and conditional probability to improve learning from labelled examples. Machine learning can identify complex patterns or trends within the data that may not be otherwise apparent[199].

One possible advantage of machine learning is the ability to input a larger number of potential variables, reducing but not eliminating the element of potential bias in variable selection compared to more traditional statistical techniques. With supervised machine learning, this can be interpreted as the testing of a hypothesis that the classifier attempts to answer: "does x, y, and z predict A?" and is a process similar to more traditional experiments with a narrow or well-defined focus. In contrast, unsupervised learning asks, "what do x, y, and z reveal?" The latter has been subject to some criticism, with the concern that spurious associations may be created, and unintended bias may be introduced, leading to erroneous conclusions[200]. Riley[201] breaks these issues into three:

Inappropriate data splitting: while data samples may be separated into training and testing sets randomly, they may not have a random distribution with different weighting over time. For example, diagnostic rigor may improve over the course of the study (or deteriorate).

Hidden variables: the data set used in the study may include information such as "meta-data", details about where or when the information was taken, which may skew the distribution of diagnoses in the sample.

Mistaking the objective: the desired outcome may differ from the outcome created with the settings used to generate the algorithm, particularly with regard to the cost of errors. Additionally, for some early labels used in screening for disease, expert opinion may differ as to the significance of any particular state.

Steps in the machine learning process

Feature selection

Feature, predictor, variable, or dimensionality reduction may be performed by eliminating factors with little or no predictive value (stepwise backward reduction). In some cases, additional attributes may reduce the performance of the classifier through overfitting[202]. The reverse approach of stepwise addition, involves starting with the single most useful feature, then sequentially adding further features (based on the size of their contribution to the model) until no further gains in accuracy are made. Feature transformation (such as principal component analysis) can be used to create new variables from a combination of features.

Classifier generation

The majority of the samples in a data set are usually used to train the algorithm to the problem. This may be 2/3 to 90% of the entire sample. Ideally the data set should have many more observations than dimensions to avoid overfitting, with a sample to feature ratio variously suggested as 5:1[203], 10:1[204] or $\log_{10}(N)$ features, where N is the number of samples[205]. With a random selection of samples taken to train the classifier, re-iterations of the training process may create different classifiers with different predictive results. Larger differences between models created with different selections from the same set imply a skew in the data set leading to poor utility. The robustness of the classifier can be tested by multiple iterations of classifier generation and comparison of results via *k*-fold cross validation. This involves splitting the training set by randomly allocating each observation to one of *k* folds. A classifier is then trained on the data from $k - 1$ folds and tested on the remaining fold. The process is repeated *k* times, each time with a different fold left out for testing. Each of the *k* classifiers will be distinct from each other, but if the data are uniform, they should be similar to one another. The consistency of the model is reflected in the size of the standard deviation of the *k* models error rate. As the observations are allocated randomly the estimation of the variance can be improved by repeating the cross-validation multiple times[206]. The number of folds used for cross validation can be varied by the number of observations, and may be five, ten, or in the case of “leave one out” equal to the size of

the dataset. In practice, the 5- or 10-fold cross validation has been reported to be effective, assuming sample size is sufficient[206,207].

Confirmation of algorithm utility

Algorithms created with a training set of data are then tested with an independent set of observations taken from the same population, to confirm their predictive value. An ideal classifier would give all the samples within a group the same label, with a different label for each separate group. Results can be presented in a confusion matrix (Table 1.2.1).

Table 1.2.1. Ideal classifier performance.

Category	Label 1	Label 2
Group 1	all group 1 samples	no group 1 samples
Group 2	no group 2 samples	all group 2 samples.

Algorithm selection

The "no free lunch" hypothesis states that no single algorithm is best for all data sets[208]. The choice of classifier depends principally on the type of data studied, as well as the size of the dataset, including whether the variables (and labels) are continuous or categorical data. Different types of classifier include:

1. Logic based. Decision trees partition groups by a series of branching nodes, with a test at each node to divide the observation into groups based on a single variable analysis. These work well with discrete and categorical data.

2. Perceptrons. A perceptron is a binary linear classifier. This provides weights or bias to its input layer (typically a vector of variables) to classify the observation into (usually one of two) possible outputs. Perceptrons are the building block of multi-layer neural networks.

3. Statistical models generate the probability that any observation has a particular label. This includes linear and quadratic discriminant analysis. Bayesian networks and maximum

entropy are also statistical approaches. Discriminant analysis creates a classification function for each group from weighted combinations of features that maximise the separation of groups. *K* nearest neighbours classify a sample based on the *K* nearest neighbours to establish boundaries between training groups. In contrast to linear discriminant analysis, these may have arbitrarily complex boundaries between groups, with the result that small changes in the data may alter local boundaries significantly[209].

4. Support vector machines (SVMs) find the hyperplane that best separate classes based on maximising the observation free margin between the classes. In many cases there will be no hyperplane to separate the groups, in which case transformation of the feature space into a space with a greater number of dimensions, using kernel functions, will allow group separation. SVMs work well with continuous data, and larger dimension data sets, as the solution requires only the identification of the points on or near the hyperplane.

Classifier types 3 and 4 are not "black box" systems, and the decision-making processes are more transparent than methods 1 and 2, although the latter methods can be interrogated by alterations in the dataset.

Discriminant analysis

Discriminant analysis is a computationally efficient supervised machine learning algorithm. Its aim is to convert the multiple variables taken from each observation that are used to classify them into their different groups, and convert these to a single dimension that maximises the separation of class means while minimising the within-class scatter. This can be stated as, and found by, solving for the direction of the new dimension vector v in

$$J(v) = \frac{(\tilde{\mu}_1 - \tilde{\mu}_2)^2}{\tilde{s}_1^2 + \tilde{s}_2^2}$$

where μ and s are respectively mean and scatter for classes 1 and 2 in the new dimension (which are unknown before training). This can be demonstrated to be equivalent to

$$J(v) = \frac{v^t S_B v}{v^t S_W v}$$

where S_B is the between class scatter matrix before projection, and S_W the sum of the within class scatter matrices also before projection, therefore both these values are known from

the dataset. This is the Rayleigh quotient which by differentiation with respect to v and setting $J(v) = 0$ converts to a solvable eigenvalue problem.

From labelled multivariate samples, discriminant analysis generates functions to determine the probability that any new sample will belong to any particular group (Figure 1.2.12). It maximises the separation of the groups by applying weights to each of the variables (also known as features, predictors, or attributes) used to describe each sample, according to the utility of that variable in discriminating between labelled groups. The success of the model (in terms of stability, or robustness) is reflected in the standard deviation of the accuracy of subgroup classifiers created from cross-validation of the training set[210,211]. Discriminant analysis was developed for Gaussian data, but remains a robust method when this condition is not met. All machine learning algorithms perform better with larger data sets.

Machine learning in ophthalmology

There has been a rapid escalation in the use of machine learning in ophthalmology[212,213,214] , so that an understanding of its use, performance and limitations is needed by general clinicians as well as specialists[215]. Lemm[206] provides good illustrations and simple mathematical descriptions of classification. OCT images have been extensively used as data for machine learning, due to their ease of acquisition, wide availability, and high resolution. Macular disease detection classifiers analyse images for the presence of intraretinal fluid as a feature, either within B scans or through the alteration in retinal thickness[216,217], or use deep learning techniques on larger datasets[218,219]. Machine learning with OCT images has been used for automated diagnosis of macular degeneration and diabetic macular oedema[176].

Multiple classifiers were used to test 38 features to detect glaucoma with the OCT[220]. The best result was obtained with 8 parameters using a support vector machine. A similar approach was used to find which classifier best identified glaucoma from standard automated perimetry[221]. The authors selected a high specificity arguing that because the prevalence of glaucoma is low and progression slow, the cost of a false positive is greater than that of a false negative. The classifiers performed as well as glaucoma experts. Other approaches include the use of linear discriminant analysis on nerve fibre layer thickness and

Bruch's membrane opening size from OCT images to diagnose glaucoma[222]. Discriminant analysis has also been used to differentiate between glaucomatous and non-glaucomatous eyes using Fourier transformation of retinal nerve fibre layer measurements[223].

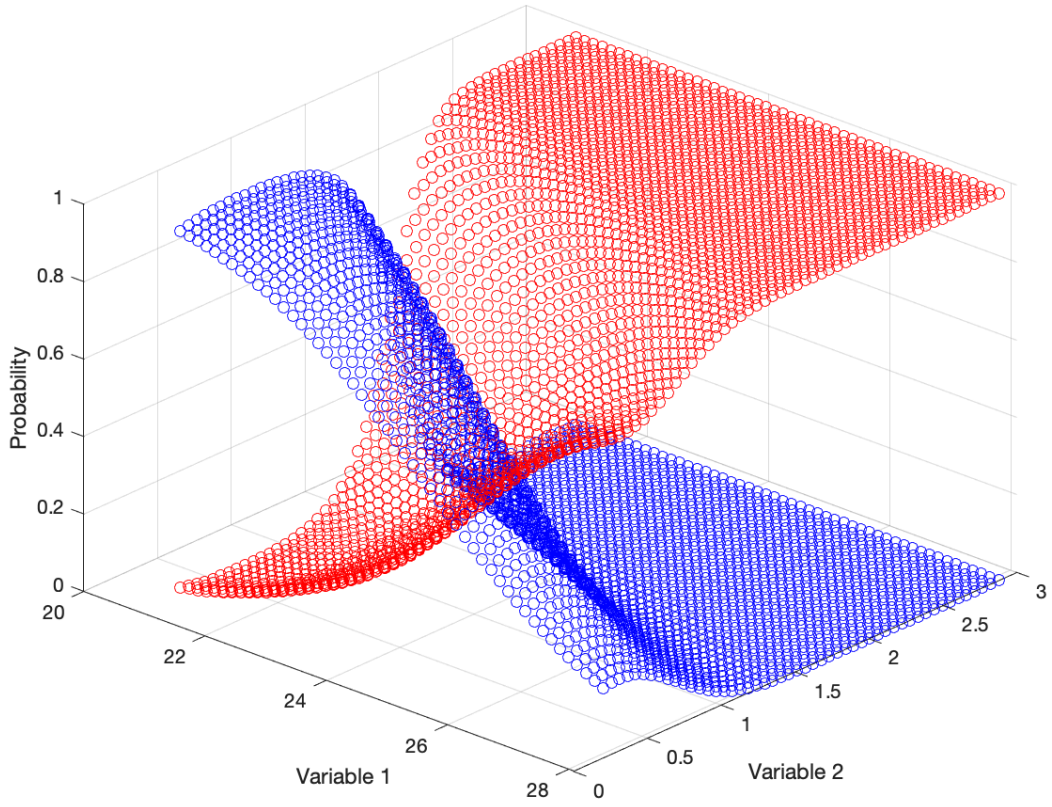

Figure 1.2.12. Illustration of a two-variable discriminant analysis classifier. Two variables were used to generate a classifier with two possible outcomes, with the results shown by the red and blue surfaces. For any combination of the two variables, discriminant analysis calculates the results of two quadratic equations, one for label 1 (blue), and one for label 2 (red). The result of each equation is the probability that an eye with that combination of features will belong to the red or blue group, and is plotted on the *z*-axis. The classifier allocates any sample to the group that has the highest probability with given inputs. As there are only two possible outcomes (labels) the sum of probabilities for the red and blue labels always adds up to 1. The probability any sample belongs to the red group becomes more likely with increased variable 1 and 2 values. At lower values of variables 1 and 2, the probability that an eye belongs to the blue group increases (top left of image), and the blue surface rises above the red.

1.2.7. Fourier transformation

The Fourier transform allows manipulation (analysis through both deconstruction and synthesis) of a signal, on the understanding that any continuous signal can be recreated from or separated into multiple sine waves of varying frequency, phase and amplitude (Figure 1.2.13). Fourier analysis enables image processing, mathematical data manipulation, and elimination of unwanted frequencies, such as noise, within a signal.

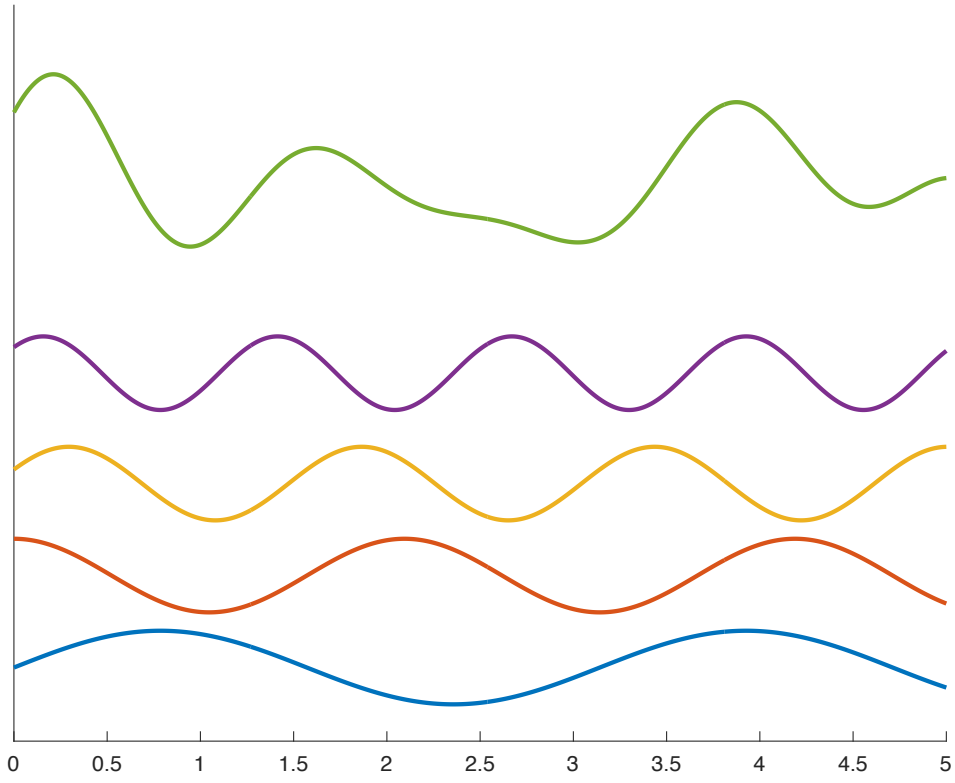

Figure 1.2.13. Fourier analysis. The apparently irregular topmost (green) line is the sum of the lower four sine waves (where each line has its own *y = 0*). The ability to express an irregular continuous (theoretically infinite) line as the sum of regular sine waves of varying amplitude and frequency allows numerical analysis of complex data.

Briefly, Fourier's revelation was that any point *x* on the vibrating string of an instrument is displaced by an amplitude whose function depends on its position on the string and time, and is the sum of the possible standing waves of the string of wavelength λ:

$$A(x) = \sum_{n=1}^{\infty} b_n \sin\left(2\pi \frac{x}{\lambda_n}\right)$$

and if not fixed at each end

$$A(x) = \sum_{n=1}^{\infty} a_n \cos\left(2\pi \frac{x}{\lambda_n}\right) + \sum_{n=1}^{\infty} b_n \sin\left(2\pi \frac{x}{\lambda_n}\right).$$

With Euler's formula

$$e^{i\theta} = \cos\theta + i\sin\theta$$

the Fourier series becomes

$$A(x) = \sum_{n=0}^{\infty} c_n e^{-i\left(2\pi \frac{x}{\lambda_n}\right)}.$$

The Fourier transform is a description of a continuous signal by its component frequencies, with any signal consisting of the total of all constituent frequencies whose relative contribution to the signal is determined by the set of weightings *X*:

$$x(t) = \int_{-\infty}^{+\infty} X(\omega) e^{i\omega t}\, d\omega.$$

For a series with discrete sampled values such as pixels, this is determined by the discrete Fourier transform[224]:

$$Y_j = \sum_{k=0}^{n-1} y_k e^{-i2\pi \frac{jk}{n}}$$

1.3. Aims and objectives

There is a need to identify a sign that can predict which eyes are at risk of retinal detachment. If this were found, it could be used to explore the ability of treatment to prevent vision loss from this disease, which currently requires emergency surgery to control. Larger myopic eyes are known to be at increased risk of retinal detachment. MRI has demonstrated that myopic eyes have increased irregularity compared to emmetropic eyes. OCT has become widely available in optometric and ophthalmological practice and images the eye on a smaller scale with smaller sample volume than MRI. OCT has already been used to examine both the structure of the posterior segment as well as document changes in macular curvature with short-sightedness.

The overall aim of this work is to look for features that may allow identification of eyes at risk of retinal detachment through the quantitative analysis of retinal shape. The specific objectives chosen to achieve this aim were:

- to investigate whether retinal shape can reliably be assessed with OCT;
- to explore the utility of OCT in assessing retinal shape in myopic eyes; and
- to develop a test based on retinal shape that can identify retinal detachment eyes as a step toward identifying eyes at risk of retinal detachment before vision is lost.

Chapter 2. Technical considerations/materials & methods

Introduction

This thesis presents work on the process and utility of retinal shape analysis as it relates to myopia, PVD, macular hole, retinal tear and retinal detachment. While the studies discussed in Chapters 3 – 6 vary in subject selection and specific image analysis, this chapter presents the general methods of data acquisition, analysis, and interpretation that they have in common. Comparison of a large numbers of retinal shape samples requires their quantification. This is achieved here through their observation in the frequency domain, enabling the comparison of multiple samples through statistical analysis.

The process of participant recruitment, the OCT image settings (scan size, spacing, and orientation), and areas of retina sampled are described, along with the key terms used to describe the OCT scans and the retinal shape (Section 2.1). The fundamental steps of image analysis are reported including image extraction and retinal shape identification. This is followed by the description of the process of shape analysis, including calculation of curvature and the Fourier transformation of the irregularity (Section 2.2). The objective is the measurement of each scans shape features in a manner that is consistent while accounting for variation in retinal image sample size and orientation. Finally, common statistical methods are mentioned.

Human research ethics committees and participant recruitment

The study was undertaken with Southern Adelaide Clinical Human Research Ethics Committee approval, in accordance with the Declaration of Helsinki. Site specific approval was subsequently obtained for Flinders Medical Centre, and Eyemedics, Adelaide. Approval was also obtained from the Royal Australian and New Zealand College of Ophthalmologists ethics committee. As well as the retinal and emergency ophthalmology clinics of Flinders Medical Centre and Eyemedics, some patients were referred by retinal specialists at the Royal Adelaide Hospital and Pennington Eye Clinic, Adelaide. All participants were examined by a retinal specialist (SL).

Participant information and consent forms are shown in Appendix A. After written informed consent, eyes were dilated with one drop of tropicamide 1% (Bausch & Lomb, Chatswood, Australia), and where greater mydriasis required one drop of phenylephrine 2.5% (Bausch & Lomb, Chatswood, Australia). The image identifiers used create de-identified data, with each eye identified by one letter followed by two-to-four numbers. The first digit is an even number for a right eye, and an odd number for left eyes.

2.1. OCT image parameters

OCT energy/optics/acquisition time

All spectral domain OCTs were taken with the Zeiss Cirrus HD-OCT 5000 (Carl Zeiss Meditec AG, Germany). The imaging beam light source is an 840 nm superluminescent diode, with a nominal 600 +/- 60 µW at the cornea. OCT cube acquisition times were 2 – 9 seconds.

Swept source OCT images were taken with a Zeiss Plex Elite 200 kHz OCT. This used a tunable laser with a sweep range of 980 – 1120 nm, centred between 1040 – 1060 nm, delivering a nominal 4.5 mW at the cornea.

Line scanning ophthalmoscope images for both spectral domain and swept source devices used a 750 nm superluminescent diode with less than 1.5 mW incident on the cornea, a field of view of 36° wide and 30° height, and resolution of 25 µm. Iris images were taken with an infrared LED CCD camera at a wavelength of 700 nm.

Slice thickness/interval

Spectral domain OCT

Throughout this thesis the term B scan applies to a single retinal OCT image, and the term cube refers to a set of B scans acquired together using a standard clinical protocol, even when the B scans do not form a cubic shape when re-assembled relative to one another. All these B scans are multiple pass composite images, which control for within B scan axial

artefacts arising from subject movement[225]. A summary of cube protocols is provided in Table 2.1.

Spectral domain OCT – retinal survey

The most commonly used spectral domain cube protocol was the HD 21, taking 21 parallel 9 mm B scans separated by 0.4 mm.

Spectral domain OCT – radial macular cubes

Studies examining macular shape used the HD radial cube, which consists of 12 radially oriented 6 mm B scans, with each B scan rotated 15° to the next around a central point (Figure 2.1). HD radial B scans were acquired in an identical pattern whether a right or left eye, which means the scan number oriented supero-temporal to infero-nasal in the right eye is supero-nasal to infero-temporal in the left eye. To correct this, left eye scans were reallocated to match right eye scans (Table 2.2).

Table 2.1. Description of OCT cube protocols

Name	B scan orientation	No. B scans per cube	B scan spacing	B scan width (pixels)	B scan width (mm)	B scan depth (pixels)	B scan depth (mm)	comment
Spectral domain OCT								
HD 21	Horizontal	21	0.4 mm	1024	9	1024	2	
HD radial	radial	12	15 degrees	1024	6	1024	2	Centred on fovea via fixation
Swept source OCT								
UHD spotlight	Perpendicular to gaze direction	1	-	2047	16	3072	6	
Angio	horizontal	500	(0.018 mm)	500	9	1536	3	

Table 2.2. Radial scans: left and right scan correspondence.

Right eye	-1	-12	-11	-10	-9	-8	7	-6	-5	-4	-3	-2
Left eye	1	2	3	4	5	6	7	8	9	10	11	12

A negative means the direction of scanned was reversed to match contralateral scan orientation, although this has no effect on calculation of curvature or irregularity.

Swept source OCT

Swept source OCT cubes used included 9 x 9 mm Angio cubes, with 500 pixels in both *x* and *y* directions and a 3 mm long, 1536 pixel A scan size. The UHD spotlight consisted of a single B scan 16 mm (2047 pixels) wide and 6 mm (3072 pixels) deep (Table 2.1).

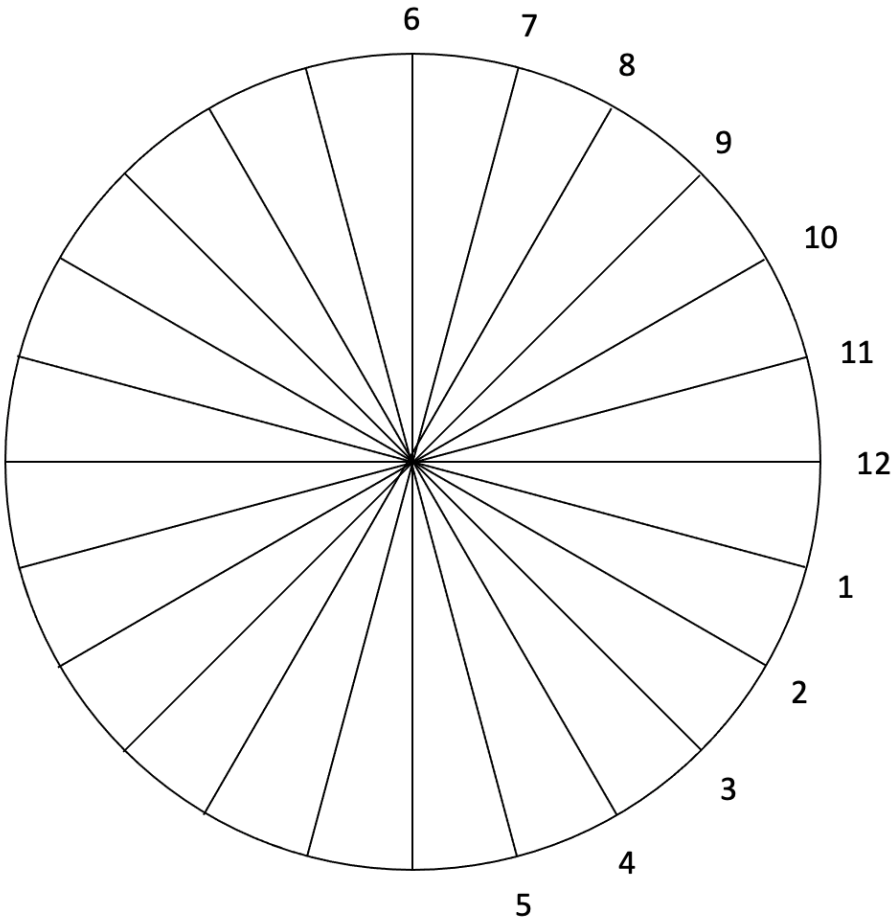

Figure 2.1. Radial B scan key. Orientation of radial HD B scans used for macular shape analysis, each scan consisting of a diameter rotated around a centre point, which for all images in this work was centred on the fovea. The numbers index the B scans and are used to identify scan position (Chapter 5.1.1). These do not correspond to the pdf output labels produced in the Cirrus reports.

Pixel size

Spectral domain device manual quoted axial resolution is 5 µm in tissue, with 15 µm transverse resolution. However, SD OCT image sizes were analysed in metric length (millimetres) converted from pixels using the reported B scan width of 9 mm and depth 2 mm. The spectral domain B scans used in this study were 1024 x 1024 pixels. The UHD spotlight swept source B scans were reported to be 16 mm wide with 6 mm deep A scans, with pixel dimensions of 2047 wide by 3072 deep. OCT angiogram image sizes were reported as 9 mm by 9 mm by 3 mm deep, with pixel dimensions of 500 by 500 by 1536 deep.

Orientation

Unless otherwise specified, all SD OCT scans were taken with a horizontal orientation for consistency within and between eyes and to maximise the sampled retinal area in each cube. Changing scan orientation from the horizontal would reduce the area imaged in a single cube as B scan length drops to 6 mm, and potentially increase variation in sampling between eyes.

Within the B scan, the lateral direction was the *x*-axis, and the axial direction the *z*-axis. The *y*-axis was perpendicular to these two, which was the vertical direction along which parallel B scans were arranged in the HD21 cube.

Sampled retinal area

Retina was imaged with standard OCT cube protocols and no intermediate lenses added between subject and device[144,146,151]. According to the standardised nomenclature for retinal imaging, this equates to the posterior pole and mid-peripheral retina[119].

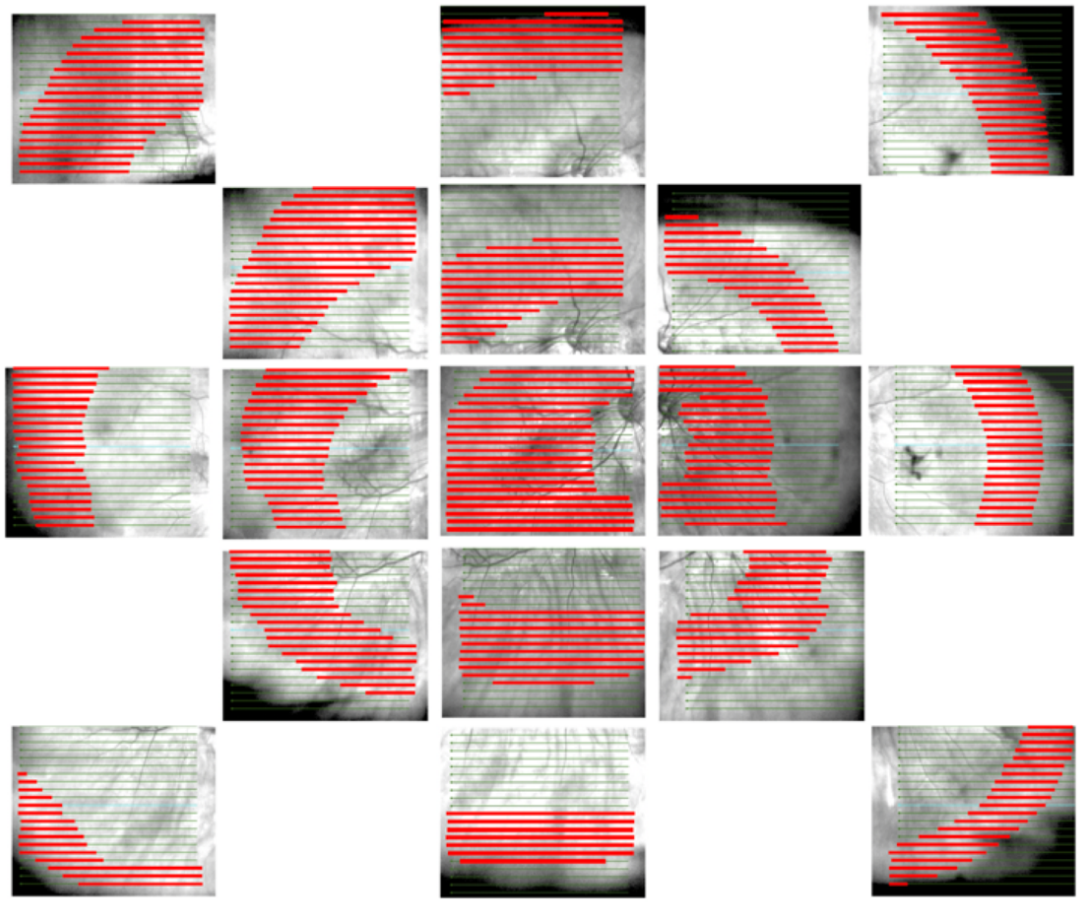

Figure 2.2. Example of retinal sampling. Exploded retinal map from a highly myopic eye (axial length 28.25 mm) illustrating areas imaged with the OCT. Each horizontal line marks the location of a B scan. The OCT cube samples a volume with a depth of 2 mm, and as the retina curves antero-posteriorly through the cube, it is only seen in the section of each B scan highlighted in red. It is the posterior staphyloma in this eye that leads to loss of retinal image capture inferior to the optic disc. The OCT will sample wider areas in non-myopic eyes. Fourier transform moduli were corrected to compensate for different retinal image lengths in different B scans (function `AnnotSLO`).

Cube locations/ Data capture

HD21 line scans were obtained, with 9 mm horizontal scans and 0.4 mm line spacing. Starting at the macula, cubes were obtained by asking the participant to look in different directions and sample retina from the macula to as far peripheral as possible. In the extreme gazes the scanning laser ophthalmoscopic retinal image blacks out in some eyes

(no view) but a B scan may still be obtained, with the RPE high intensity signal visible even in areas of vignetting.

Multiple OCT cubes were taken asking the participant to look in different directions, to enable image acquisition from different parts of the posterior hemisphere of the retina. Montages of the scanning laser ophthalmoscope images were constructed to illustrate the area sampled (Figure 2.2). Due to the curvature of the eye, the retinal image is seen in different antero-posterior locations within the parallel B scans of an OCT cube. With increasing obliquity, this means with some OCT cubes the retinal image disappears anteriorly or posteriorly out of the image acquisition area. As a result, retinal image data are incomplete across the area visible in the scanning laser ophthalmoscope images. Rescanning the same area with the acquisition volume moved anteriorly or posteriorly can image missed areas in a separate cube.

The first cube was taken with the participant looking directly toward the OCT fixation point (the macular cube). Subsequent OCT cubes were taken in 8 positions of gaze: superiorly, inferiorly, horizontally to the left and right, up and right, up and left, down and right, and down and left (Figure 2.3). Ideally 2 OCT cubes were taken in each direction of gaze, one at the edge of the macular cube, and the second more peripheral. Each of these locations was considered a “region” for image feature analysis. Cubes were allocated to regions on the basis of information recorded at time of image capture and examination of the retinal image taken simultaneous to the OCT. Only one cube per region per eye was used for analysis (Table 2.3).

5		3		17
	4	2	16	
7	6	1	14	15
	8	10	12	
9		11		13

Figure 2.3. OCT cubes retinal region key. Representation of a right eye, showing the numeric region identifier of OCT cubes used in this study. The macula is region 1. Compare to Figure 2.2.

Table 2.3. Tabular list of regions with their numeric identifier.

Region number	Region description
1	Macula
2	Posterior superior
3	Anterior superior
4	Posterior supero-temporal
5	Anterior supero-temporal
6	Posterior temporal
7	Anterior temporal
8	Posterior infero-temporal
9	Anterior infero-temporal
10	Posterior inferior
11	Anterior inferior
12	Posterior infero-nasal
13	Anterior infero-nasal
14	Posterior nasal
15	Anterior nasal
16	Posterior supero-nasal
17	Anterior supero-nasal

2.2. Image analysis

Analysis was performed with functions written in MATLAB (The MathWorks, Inc., Natick, MA) for this study. Function names are given in each section where used and identified by `Courier` font. The script of each function is given in Appendix C.

Image segmentation

Livewire[226] is a free-to-download add on to Fiji/ImageJ, a health science image processing suite developed by the National Institute of Health[227]. This uses graph theory, identifying the least cost path from one pixel to the next to define the borders of regions of interest for image segmentation. Livewire will follow (with observer input) high intensity lines such as the ellipsoid layer or retinal pigment epithelium on the OCT. From this, the *x,z* coordinates of points along the line were saved, so that properties of the geometry of the line can be studied.

Data extraction

Raw .img data files were exported from the OCT device with the IMG export facility. These were converted to tagged image file format (tiff) with ImageJ or MATLAB, and in each B scan the retinal shape was traced using the Livewire plugin macro for ImageJ. The retinal shape was represented by the retinal pigment epithelial line or outer highly reflective band in all but the macular scans. Macular shape information was taken from the ellipsoid line, as this high intensity line was more reliably tracked with Livewire, and is parallel to (and therefore has the same shape as) the retinal pigment epithelial line in the images acquired (Figure 2.4). The line region of interest was saved as a text file of pixel coordinates. The data for each eye were stored within a folder for each cube, within which were subfolders consisting of up to 21 text files containing the *x,z* coordinate of the retinal pigment epithelium from each B scan. The retinal shape data consisted of two columns, representing the *x* (lateral) and *z* (axial) coordinates for each pixel representing the retinal shape in the B scan. This coordinate information was converted from pixels to physical length in millimetres for analysis.

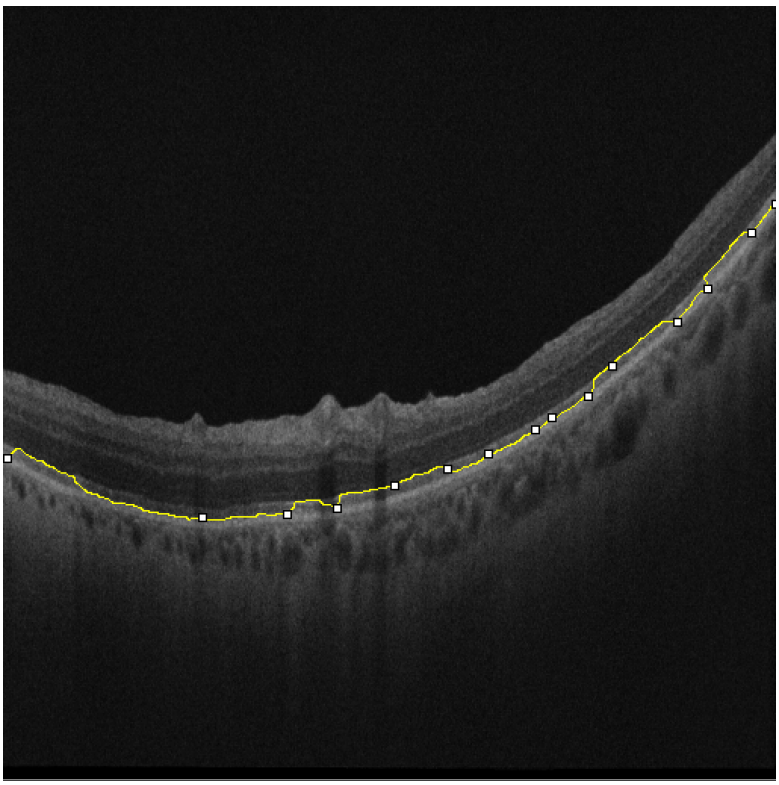

Figure 2.4. Inconsistent retinal shape identification. OCT image of macular tissue with a highly reflective ellipsoid layer distinct from the RPE line. If attempts were made to follow the retinal pigment epithelium line in macular tissue with a high intensity ellipsoid layer, the two parallel high intensity signals confuse the Livewire least cost pathway algorithm leading to jumps in the contour pathway. This was avoided by taking shape from the ellipsoid layer, which parallels the RPE line and has high enough signal to entrain Livewire without jumps.

Shape metrics

For analysis, the B scan retinal shape information was separated into two components: a base curve, and the difference between the retinal shape and base curve, called the irregularity (Figure 2.5).

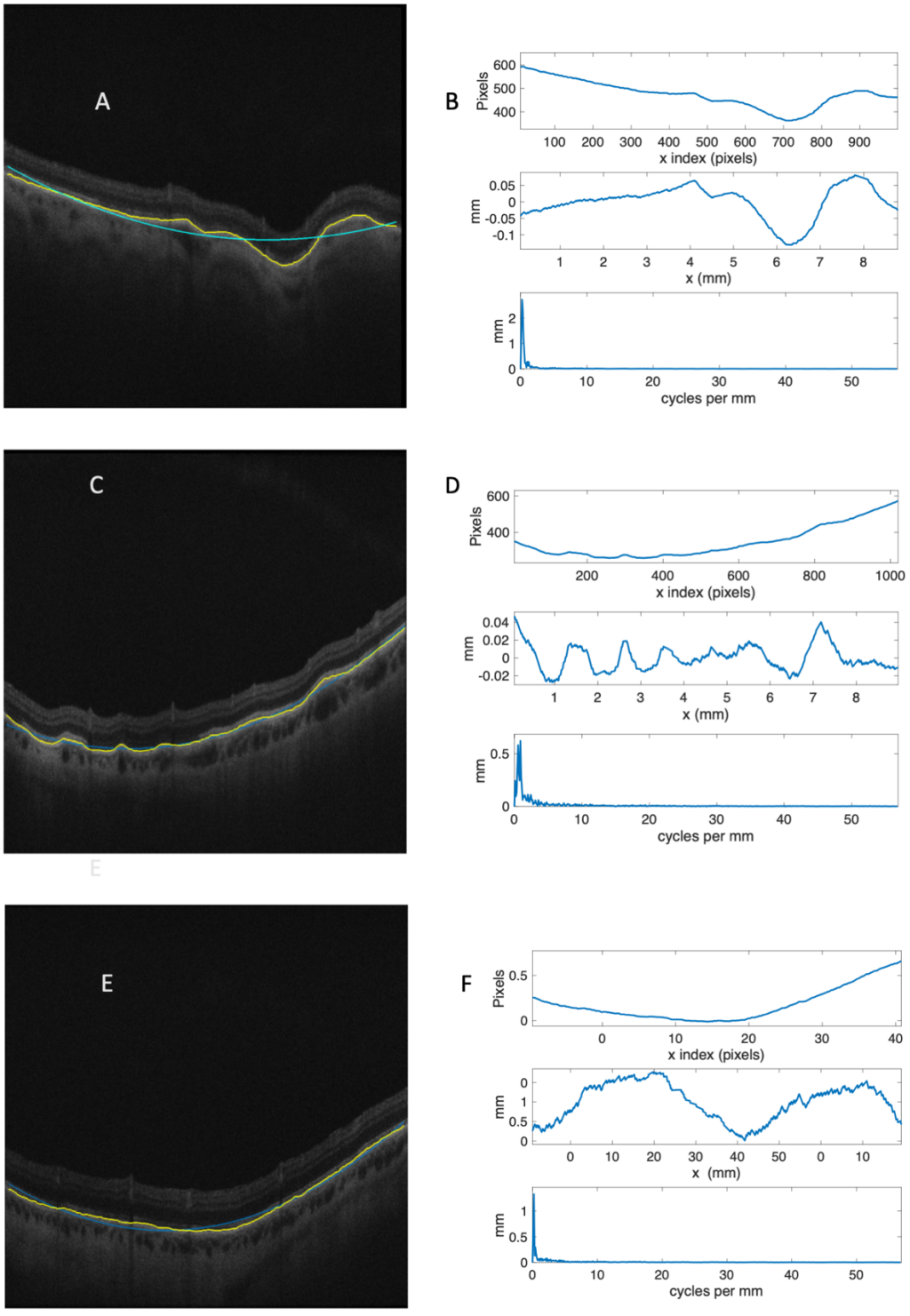

Figure 2.5. Retinal shape analysis. Retinal shape was taken from the contour of the retinal pigment epithelium in OCT B scans. Figures A, C, & E: the retinal contour is highlighted in yellow in the B scan images, and this contour is used for shape analysis. The quadratic best fit curve is superimposed in blue on the OCT images. Figures B, D, & F present the Fourier analysis of OCTs A, C, and E respectively. The B scan retinal contour is plotted in the uppermost panel of B, D, F. The middle panel in B, D, and F present the residual after the best-fit quadratic curve has been subtracted, with the Fourier transform of the residual in the lowermost. There is very little shape information at higher frequencies in the frequency domain.

Curvature

Conic equations can be used to derive the radii of conic shapes that reflect the base curve of the retinal shape. Most retinal images on OCT are either elliptical or hyperbolic in form[110]. The latter are counter-intuitive in having an imaginary radius as well as a real one, but mathematically this is not problematic. The principal disadvantage in conic sections is that the derivation of the radii from the general conic equation coefficients is not a robust process. Solving for the radius of curvature of a retinal image is a poorly constrained problem, due to the retina within the B scan comprising too small and localised a sample arc of the larger conic shape. Minor changes in retinal position or orientation leads to wide variation in the solution for the radii, making it an unreliable method for analysis.

Instead, a parabolic second order polynomial equation was used to describe the best fit curve to the B scan. To account for shape information within the best-fit quadratic that was subtracted from the retinal shape prior to Fourier transformation, the curvature at the vertex of the best-fit curve was recorded for each B scan (hereafter curvature). Curvature was derived geometrically rather than optically, and was used to differentiate OCT shape from other measurements in vision science (such as corneal shape) that use its inverse, the radius of curvature. This approach has been used in most analyses of retinal shape[110,136,137]. Curvature has the intuitive advantage that as its magnitude increases, the shape of the curve becomes more acute.

Using the simple quadratic curve formula $z = ax^2+bx+c$, the x-coordinate of the vertex of this is found at $-b/2a$.

Hence the z coordinate of the vertex $z_v = a.(b^2/4a^2) – b^2/2a + c$

or $z_v = -b^2/4a + c$.

Curvature is given by:

$$R = \frac{\frac{d^2z}{dx^2}}{\left[1+\left(\frac{dz}{dx}\right)^2\right]^{\frac{3}{2}}}.$$

As $dz/dx = 2ax + b$ and $d^2z/dx^2 = 2a$

$$R = \frac{2a}{[4a^2x^2 + 4abx + b^2 + 1]^{\frac{3}{2}}}.$$

Inserting $x=-b/2a$ to find the curvature at the vertex, then $R=2a$.

The best-fit quadratic was generated by the `polyfit` function in MATLAB and subtracted from the retinal contour line (Figure 2.5). This was done to avoid contamination of the Fourier transform (aliasing) of the retinal irregularity by mismatches at the endpoints of the signal. An example of the scanning laser ophthalmoscopic image of the OCT cube warped onto the B scan shape information is shown in Figure 2.6, with the best fit curves superimposed in red.

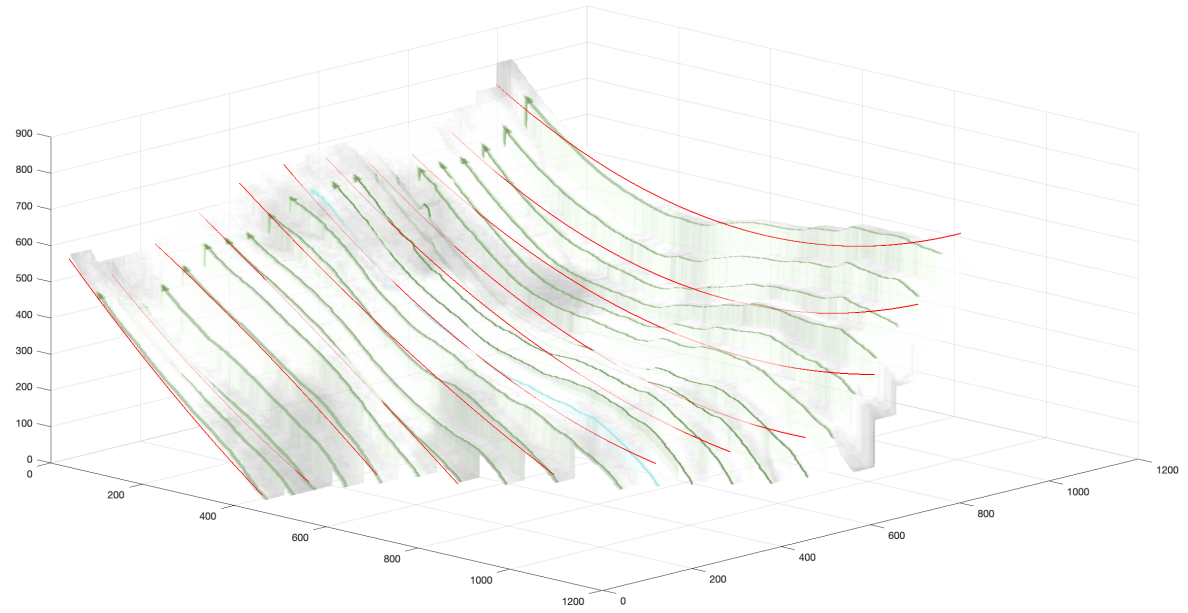

Figure 2.6. Retinal shape, 3D OCT cube. OCT cube retinal shape re-created from the B scan retinal pigment epithelium shape. The scanning laser ophthalmoscope image has been imposed on the surface, with the position of each B scan marked by the green and blue lines. The best fit curve to every second B scan is superimposed in red. Axes are in pixels.

Correction for OCT imaging artifacts

Image capture with OCT is subject to the distortions discussed in Section 1.2.2 "OCT image artifacts". The OCT devices used in this thesis (Zeiss spectral domain OCT Cirrus and swept source OCT Plex Elite) compensate for the effects of eye motion through multiple pass composite images, correct for the distance between light source and the anterior segment of the eye through focussing the external eye image during scanning, and do not perform pre-image processing flattening. Refractive index effects, vignetting, and scatter do not affect the retinal contour studied here. The conversion from an acquired arc of A scans to a rectangular output leads to some flattening of the retina across all images and was not corrected here.

As the distance from the reference point of the OCT at the pupil and the retina affect measured retinal curvature[137], correction for this was performed. OCT retinal curvature was corrected using the axial length induced error correction from Steidle & Straub[135]. They reported the correction required according to variation in axial length, and kindly provided by personal communication their measured values in 1 mm increments between 20 and 28 mm (Table 2.4), that were only reported in graphical form in print. To determine the exact correction value for any axial length (which is routinely given to 1/100th of a mm), a goodness-of-fit calculation was performed for linear, second and third order polynomial lines fit to the data. The differences between the empirical and best fit curve values for each 1 mm increment were calculated for each order polynomial. This was lowest for the second order polynomial, so this was used to correct curvature for each scan. Correction factors were provided for eyes with integer axial length 21 – 28 mm, so within and beyond this range, the actual correction value was calculated from the second order polynomial fit to the available data. For correction, curvature was converted to radius of curvature, the appropriate correction value deducted, and curvature recalculated.

The median curvature for a single cube reflected the typical curvature within the volume of that cube. The interquartile range of curvature for a single cube was the interquartile range of the curvatures of the B scans within that cube. This represented the degree to which curvature changes across the area of the cube from top to bottom, and not the spread of

observations from a single sample. For an entire eye, the interquartile range of curvature represented the range of values within the eye. Some B scans had negative curvature (convex into the eye), for instance at the edge of staphyloma.

Irregularity

The second component of the image for analysis is the residual values left after the base curve is subtracted from the retinal pigment epithelial line. Examples of these are shown in Figure 2.5. With the base curve removed from the retinal line, the residuals resemble a noisy, roughly horizontal signal.

Table 2.4. Axial length induced error in OCT curvature.

Axial Length	Retinal Radius of Curvature	Induced Error
20	17.34	3.94
21	16.30	2.90
22	15.29	1.89
23	14.32	0.92
24	13.40	0.00
25	12.53	-0.87
26	11.72	-1.68
27	10.97	-2.43
28	10.28	-3.12

All values in mm. Data reproduced with the permission of Dr Jochen Straub[135].

Fourier transformation

A Fourier transformation was performed on the residual. This irregularity consisted of vectors of x- and z- axis coordinate data. To prepare these data for analysis, where there were duplicate values of x, a single z value was attached to this x value equal to the mean of the z values recorded for the duplicate x values. Gaps in the sequence of x values (from A scans where the retinal image was obscured) were filled by linear interpolation. If the signal (length of the x vector) was less than 1024 points long, then the signal was padded by zeros to equal 1024. If the signal was more than 1024 points long, the ends were cut to limit the length to 1024. The discrete Fourier transform of the z values was computed and since z was a signal of length 1024, the modulus for the Fourier transform was defined on 512 evenly

spaced frequency values in the range 0 to Ny (Nyquist frequency). The moduli of the Fourier transform of the 30 lowest frequency bins constituted the output vector representing the shape of the B scan. Higher frequency information was discarded as noise.

Correcting for the differences in retinal length in B scans

A set of scanning laser ophthalmoscope images from OCT cubes of one eye is shown in Figure 2.2. Due to the curvature of the eye, in some regions the retina passes obliquely through the rectangular B scan window, and the retinal image does not always cross the entire width of the B scan, nor does the retina appear in all B scans in a cube. The moduli for each frequency bin were corrected for the length of the signal (the adjusted length of the retina in the B scan) to allow comparison of images of different size, as not all retinal images in peripheral retina extend from one side of the B scan to the other (Figure 2.2). This results in all irregularity values in the frequency domain being measured in mm^2 per mm of retina imaged, or simply mm.

Anomaly

The anomaly was defined as the difference in B scan irregularity from the average B scan irregularity, with units the same as the irregularity, of mm^2 per mm, or mm. Anomaly was calculated as follows.

All cubes sampled from all the eyes used in any chapter were included, and the Fourier spectrum of each B scan irregularity determined. The eyes were distributed into five folds in the following manner, to ensure that there was an even distribution of axial lengths and diagnoses between each fold. Eyes were sorted separately for each diagnostic group by axial length and any eyes with no axial length measurement excluded from further analysis. The `randperm` function was used to randomly allocate eyes in each group into 5 folds by generating consecutive sets of random numbers from 1-5 equal to the number of eyes included. Numbers in each fold were non-equal when the sample was not divisible equally by five, when the remaining *n* samples were randomly placed into *n* groups. For eyes in each fold an average B scan irregularity was calculated from all the images in the other 4 folds, equivalent to 80% of the entire sample. For all-of-eye features, B scans from all regions were used to create the average value.

As an example, consider 53 retinal detachment and 61 PVD eye spectral domain OCT scans used for classifier development in Chapter 5. Across the five folds, mean B scan irregularity coefficient of variation was 0.0099, suggesting consistency between folds. This consistency in mean B scan irregularity was used to simplify anomaly calculation as more eyes were included in this study. For ongoing recruitment of eyes in Chapter 5, the average anomaly of the five folds detemined from the initial dataset in Section 5.2 was used.

Shape feature terminology

The difference between the retinal shape and its best-fit quadratic curve was represented by values taken from the Fourier transform of the retinal irregularity. Table 2.5 summarises the terms used to describe shape features. The first (total anomaly) was the sum of the absolute difference between the 30 lowest frequency bin moduli of a scan and the average irregularity values of the same frequency bins. The second variable was the largest single frequency bin difference in any B scan compared to average bin values (peak anomaly (Figure 2.7)). The third was the root mean square of the difference between the scan bin moduli and the average normal bin values, named rmsa. These variables reflected the difference of any B scan from the average B scan in its control group. More irregular retinal shapes that correspond poorly to a quadratic curve had greater total anomaly, peak anomaly, and rmsa. The interquartile range of total anomaly, peak anomaly and curvature was used to describe the spread of values within each eye, region, or cube.

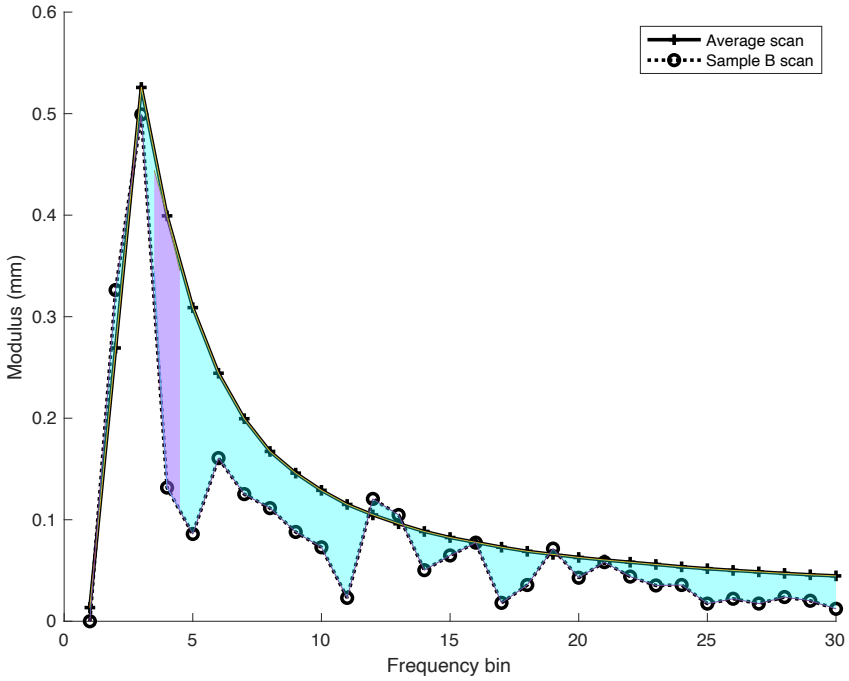

Figure 2.7. Illustration of features: total anomaly and peak anomaly. The average frequency bin value for all B scans is illustrated by the solid line. The coloured shaded areas (cyan and lilac) represent total anomaly for the sample B scan (dotted line). Peak anomaly is the bin value with the largest difference from the average, and is illustrated by the lilac shaded area.

Table 2.5. Description of shape terms.

Quantity	Description	Units	Comment
Retinal shape	Path of the retinal pigment epithelium across an OCT B scan		
Curvature	The vertex curvature of the best fit quadratic curve fit to the retinal shape	mm^{-1}	
Irregularity	Residual shape after best fit curve removed, usually referring to this within the frequency domain	mm	Unless specified, refers to bins 1-30 only
Total anomaly	Difference between a B scan irregularity and the average B scan irregularity in the frequency domain	mm	A measure of irregularity
Anomaly spectrum	The distribution of total anomaly across the frequency bins	mm	
Peak anomaly	The modulus of the largest frequency bin in the anomaly spectrum	mm	

All values taken from bins 1-30. All values corrected for sampled retinal length, making the anomaly units mm^2 per mm, hence mm. Section 5.2 determined which specific [region, bin] anomaly values were to be used for classification. This may or may not be the peak anomaly.

Statistics

All-of-eye and regional median and interquartile range features (total anomaly, peak anomaly, root mean square anomaly, and curvature) were correlated to axial length by Spearman's rank correlation with 95% confidence intervals calculated with Fisher's z-transformation[228]. Bonferroni-Holm correction for multiple comparisons was performed with α = 0.05. Eyes that were scanned twice were compared by the Wilcoxon signed rank sum test.

Test-retest reliability of shape metrics was explored with Bland Altman plots, with classifier performance assessed by sensitivity and specificity, and stability by the standard deviation of the success rates in five-fold cross validation of the training set. The two-sample *t*-test

was used to check for similarity between groups, and the paired *t*-test for where comparison was for change of state in individual eyes. Classifier output was reported in a confusion matrix, with specificity and sensitivity the key measures. A two-tailed Fisher's exact test was performed on the model confusion matrices and classification label correspondence to test the probability of non-random distribution.

Chapter 3. Validation and exploration of the limits of methodology

Introduction

This aim of this chapter is to investigate whether and how information taken from OCT images can be relied upon to assess retinal shape, and describe that retinal shape across the posterior retina.

The Australian Therapeutic Goods Administration requires medical imaging devices to provide accurate, precise and stable measurements (Medical Devices Essential Principles Checklist[229]). Commercial OCT machines such as the Cirrus have documented reliability in segmentation and volume determination of retina and surrounding tissues[230]. In other words, test-retest measurements are consistent. Shape is not a metric normally measured or quantified in standard OCT analyses, although if it were to vary substantially, the consistency of retinal volume estimation and segmentation would be compromised.

In section 3.1, two aspects of determining the reliability of OCT retinal shape analysis are considered: first, that the retinal contour produced by the operator of Livewire in ImageJ is consistent if repeated by a different operator measuring the same image; and second, that repeat OCTs of the same retina have the same shape, assuming no change in the retina itself. As long as retinal shape itself does not vary over time, any variation in these measurements would suggest a reliability issue.

In Section 3.2, overlapping swept source OCT cubes are reconstructed in three dimensions and merged via two different methods to explore the utility and limitations of composite images for retinal shape analysis. OCT provides high resolution, cross-sectional, two dimensional retinal images, and images taken in parallel have been used to reconstruct local retinal shape from these sections in three dimensions. OCT is capable of sampling a limited area of retina in a single image. Wider field images have become available with developing technologies including swept source OCT, as well as through the merging in series of individual B scans in two dimensions. Merging swept source OCT images in three

dimensions (3D) has not previously been reported. Should merged images retain accurate shape information, it may be possible to consider larger scale shape features measured from the composite images. Conversely, if errors are introduced from the merger, information taken from composite data cannot be relied upon.

Section 3.3 explores the use of the external eye image taken at time of OCT imaging to determine whether gaze direction analysis could help in describing which area of retina is being imaged. OCT cubes sample a retinal area with multiple parallel lines with the measurement of shape used here taken from the most irregular scan within the cube. This sampling method compensates for some differences in eye position, but gaze position analysis is explored to determine whether it can provide further evidence of which area of retina has been sampled where landmarks such as retinal vessel anatomy vary. This section analyses the elliptical eccentricity of the pupil margin imaged when the OCT is taken to assess how far, and in which direction, the eye is turning.

The ability to quantify shape enables comparison of a large volume of samples. The OCT only samples retina locally rather than globally. Section 3.4 describes how locally sampled retinal shape varies as a quantity by the area of retina imaged. Section 3.5 presents the conclusions and discusses the significance and limitations of Sections 3.1-4.

Published work

The contents of Section 3.4 have been published in "Correlation between optical coherence tomography retinal shape irregularity and axial length. (Lake S, Bottema M, Williams K, Reynolds K. PLoS ONE (2019); 14(12). https://doi.org/10.1371/journal.pone.0227207). My contributions to this paper included data collection and analysis (90%), writing and editing (85%), and research design (25%). My co-authors contributed equally to research design (25% each); proof reading, revision of and guidance on writing the papers (5% each); and instruction and advice on data analysis (10%).

3.1. Reliability

Aim

The aim of this section was to assess the reliability of OCT measured retinal shape. First, a visual inspection of the correspondence of shape in repeat scans taken from oblique angles is presented. Then, repeated retinal measurement from a set of scans using the graph theory-based Livewire tool are compared. Thirdly, the consistency of retinal shape measured with Livewire is assessed by comparing the results of the same images segmented by two different observers. Finally, repeat images of the same retina are compared to test whether they have the same shape.

Visual inspection

Repeat imaging of the same retinal sample and visual inspection of these scans confirmed good correspondence between one image and its repeat (Figure 3.1.1). Figure 3.1.2 illustrates peripheral retinal features that were imaged at two separate sittings. Visually, there was good correspondence between the images despite variation in position within the scan window – there are rotational and translational differences between images of similar retinal areas. Each OCT cube is in its own coordinate system, and can be rotated and translated compared to other images of the same or different eyes[142]. Analysis of shape depends on features that are independent of rotation, translation or scaling. Orientation independent information on shape is required to compare images of the same area of retina taken from differing angles.

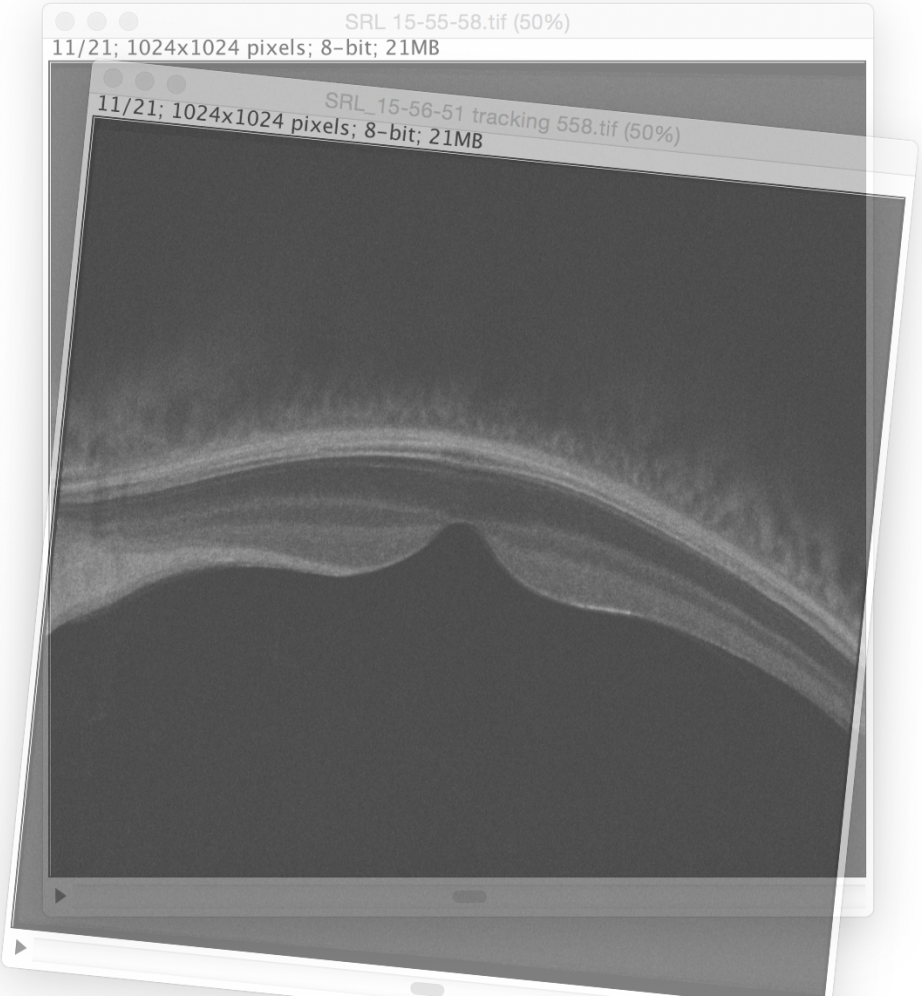

Figure 3.1.1. Macular shape consistency. Two B scans from the same eye taken consecutively, one through the nasal side of the pupil, and the second the temporal side. This rotates the image around a vertically oriented axis, and has been called oblique scanning[142]. Despite image rotation, superimposing one image on the other made it clear the retinal shape was unchanged.

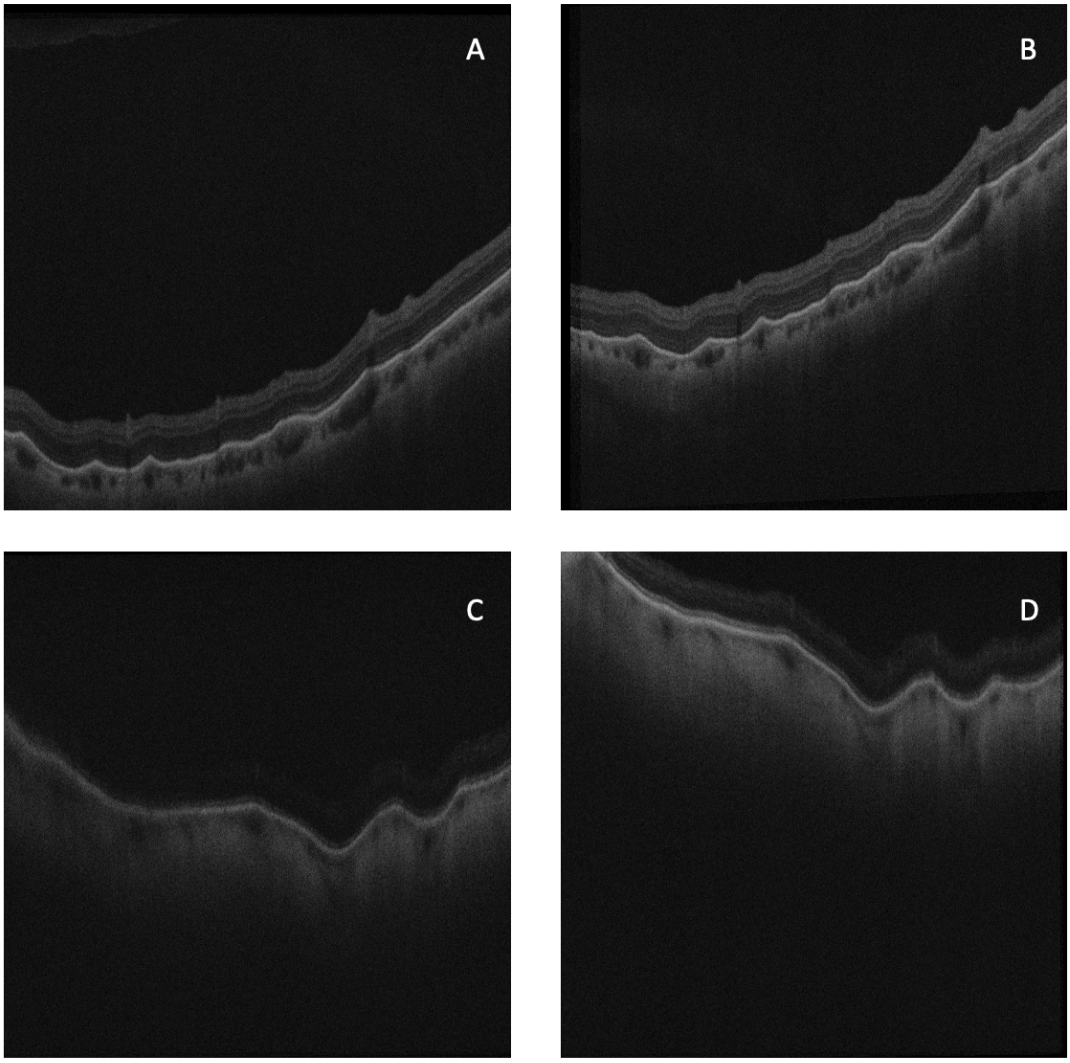

Figure 3.1.2. Shape consistency. Repeat OCT images of inferior retina from two different eyes (A & B, and C & D), with the second set of images (B & D) taken weeks after the first set (A & B). While the retina was translated and rotated from one image to the next, there was persistence of shape features.

3.1.1 One eye measured by two different operators

To ascertain that the Livewire RPE contour identification process was reliable and user independent, retinal shape from OCT cubes of one eye were measured twice with the ImageJ Livewire plug by two independent observers.

Methods

The OCT cubes from a retinal survey of a single eye were used. This was the right eye of a 54 year old man with axial length 24.70 mm, with no pathology other than minor peripheral lattice degeneration. There were 345 B scans with retina present from 18 HD21 cubes (one from each of the 17 regions (Figure 2.3 and Table 2.3) with an 18th cube not classified). All images were taken at a single sitting on 17 February 2017.

To address small variations in the start and finish points that each operator used to capture retinal contour, alignment of vectors was performed by checking that the two observers had matching initial *x*-index in each *x*-coordinate vector (lateral pixel position). Where there was a mismatch, the longer *x*-vector was truncated to match the shorter.

Statistical methods

Comparison of the two sets of retinal shape was made through the root mean square difference between the two *z*-coordinate vectors. Then, to address any systematic error, one *z*-vector from each pair of scans was translated by the mean difference between the two *z*-vectors (in case one measurement was taken from a different retinal layer compared to the other, changing the axial position without changing the shape information). The root mean square error between the translated vector and its pair was calculated. Median and interquartile range of curvature and irregularity were also determined from the two sets of measurements and compared by a Wilcoxon sign rank test (`RetestLVWrmse`).

Results

The number of B scans extracted from each cube was the same in each test. Mean root mean square error (standard deviation) was 3.06 +/- 3.95 pixels. After correcting for average shift (i.e., deduct the average difference between the two), mean root mean square error was 1.28 +/- 1.49 pixels, a difference of less than two pixels. Results of the comparison of curvature and irregularity metrics derived from each assay are shown in Table 3.1.1.

Table 3.1.1. Between observer shape measurement correspondence.

Shape feature	Examiner 1 Mean +/- SD	Examiner 2 Mean +/- SD	*p*-value
K	0.034 +/- 0.015	0.035 +/- 0.015	0.93
IQR *K*	0.013 +/- 0.016	0.012 +/- 0.016	0.94
irregularity	2.54 +/- 1.06	2.60 +/- 1.05	0.89
IQR irregularity	1.39 +/- 0.52	1.38 +/- 0.62	0.96

Comparison of the two Livewire measurements of retinal shape from 18 cubes from a single eye. Cube values were compared by two-sample *t*-test (column 4). *K* = curvature, IQR = interquartile range, SD = standard deviation. Units: *K*: mm^{-1}, irregularity: mm.

Conclusion

Retinal shape did not significantly differ when measure by two different observers with Livewire.

3.1.2 Sample eyes measured multiple times on different occasions

Methods

This study re-imaged the same areas of retina multiple times, to test whether the shape metrics were consistent between observations (Figure 3.1.3). Five eyes, described in Table 3.1.2, had HD radial macular cubes taken repeatedly. Images were acquired between October 2019 and March 2021. Their shape information was described by the measurements of curvature and total irregularity.

Statistical analysis

The reliability of measurements taken from multiple repeat images was assessed using intra-class correlation coefficients (ICC) of metrics taken from repeated sampling of maculae[231]. Intra-class correlation coefficients range from 0 to 1 with the value of one indicating identity. Functions used were `icc` and `icc21` from MATLAB File exchange[232,233]. Measurements were tested with intra-class correlation using a two way random effects

model with a single rater assessment (to determine how useful a single test would be) requiring absolute agreement (implying no bias between measurements)[234].

Results

Table 3.1.2 summarises the eyes imaged with repeat macular HD radial cubes centred by fixation. Intra-class correlation is shown in Table 3.1.2 for the 12 B scans in each cube described by curvature and total irregularity (24 values per eye, column 5), and then the B scan irregularity spectrum (360 values – 30 bins for each of the 12 B scans, column 6).

Table 3.1.2. Description of eyes with repeat macular imaging.

Eye	Number of cubes	Time interval: first – last scan	Reason for attending	ICC (2,1) K and total irregularity	ICC (2,1) irregularity
L2 01	9	Single session	Volunteer	0.9934	0.9839
L1 02	9	Single session	Myopia assessment	0.9485	0.9353
L1 03	7	6 months	Myopia, vitreo-macular traction in fellow eye	0.9879	0.9762
L2 04	8	17 months	Retinal vein occlusion, fellow eye	0.9854	0.9811
L1 05	5	10 months	Myopic macular disease in fellow eye	0.9714	0.9436

Number of cubes = the number of macula OCT cubes taken of each eye. Each cube consists of 12 radially oriented B scans, centred on the fovea. ICC = intra-class correlation coefficients, K = curvature.

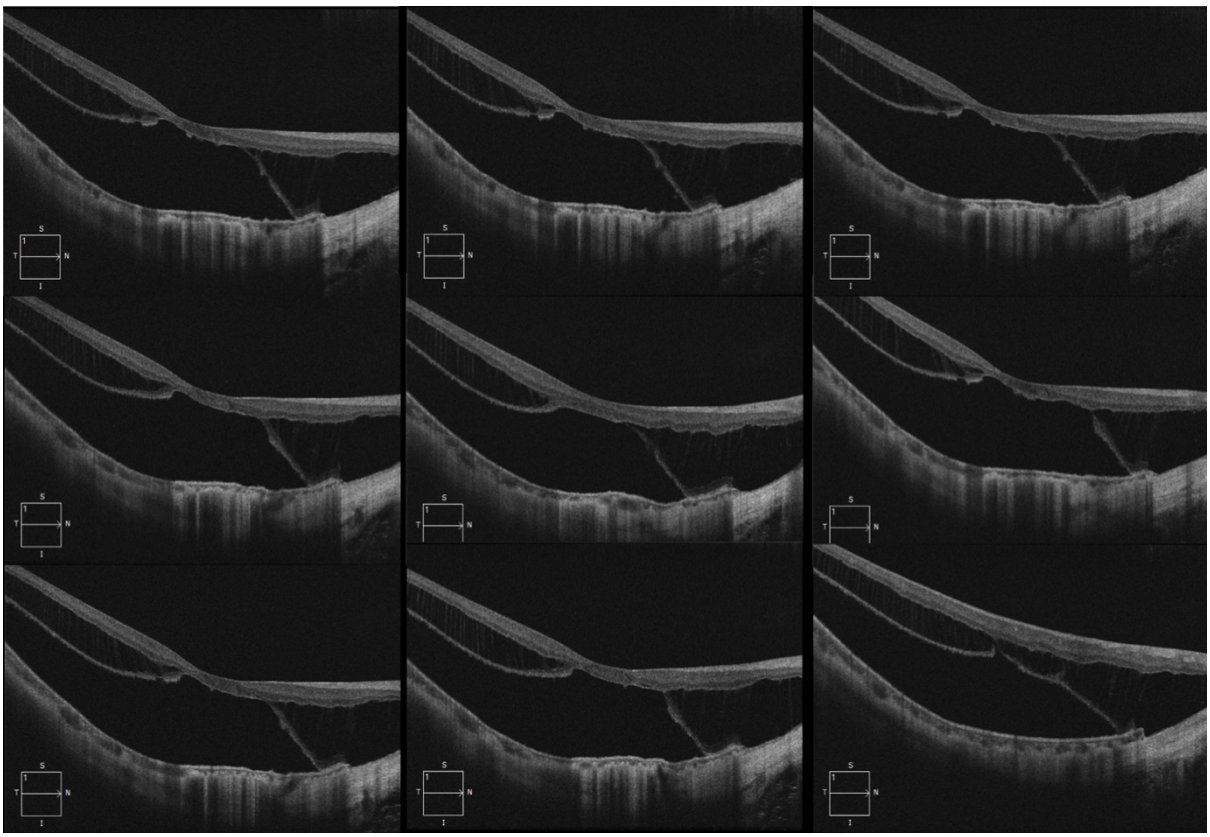

Figure 3.1.3. Repeat macular imaging, myopic eye. Single B scans from nine HD-radial cubes taken consecutively from the same macula. This was a highly myopic eye with a macular schisis and poor vision. This should increase the magnitude of shape features due to greater curvature and greater irregularity compared to an emmetropic eye, as well as increase the risk of poor alignment from one cube to the next due to poor fixation. Subtle differences in anatomy can be seen from one scan to the next. Despite this, intra-class correlation was high (> 0.9), and comparable to the intra-class correlation of a non-myopic eye.

Conclusion

The measures of curvature, irregularity, and the frequency distribution of the irregularity were consistent between repeated HD-radial scans. These assessments of the reliability of retinal shape measurements taken from OCT images confirm that shape can be reliably assessed with OCT. Further tests of reliability are reported for the performance of a classifier using shape in sections 5.2 and 5.3.

3.2. Merging OCT cubes

Individual OCT images have been shown to be a reliable method of measuring retinal shape, with spectral domain OCT sampling a limited area of retina of length 9 mm. Analysis of larger scale shape features requires the joining together of adjacent or overlapping scans, involving potentially three dimensions of translation and three dimensions of rotation. Here, this process was performed to assess whether the resulting composite images were reliable enough for shape analysis.

Aim

The aim was to assess whether fusing images preserved retinal shape in a way that might enable larger scale features to be extracted.

Methods

Subjects

Pairs of overlapping OCTs were taken from five eyes of five human volunteers. Subjects are described in Table 3.2.1. Images were taken between September 2020 and May 2021.

Table 3.2.1. Subject eyes for merging OCT cubes.

Eye	Side	Axial length (mm)	Pathology	Cube locations
SS 0028	L	23.74	PVD	Macula & ST to disc
SS 0066	L	24.06	Retinal tear	Macula & IT to disc
SS 0067	L	26.54	FE to RD	Macula & ST to disc
SS 0082	R	25.27	RD	Macula & temporal to macula
SS 0102	R	24.78	Stickler syndrome	(a) ST to disc & superior (b) superior & far ST

L = Left eye, R = Right eye, FE = fellow eye, RD = retinal detachment, ST = supero-temporal, IT = infero-temporal.

Overlapping pairs of 9 x 9 mm SS OCT cubes were taken. The scanning laser ophthalmoscope images were adjusted to pixel dimensions of 500 x 600 to correspond to the B scan pixel dimensions. Twenty five B scans were sampled from each cube by `CretiffSScube`, starting at B scan 10, and sampling 25 B scans out of the 500 at 20 B scan intervals, finishing at B scan 490. These were used to reconstruct local retinal shape within the area covered by the scanning laser ophthalmoscope. For each eye, three pairs of corresponding points were identified in the scanning laser ophthalmoscope images from each pair of cubes. The reconstructed 3D images were merged via two different methods, both using a rigid transformation to preserve shape features. In the first method, two sequential axis-angle rotations were performed to align the three points, using a function written for this process in MATLAB. To validate these results, a second method using a single axis-angle rotation using a quaternion was performed. The quaternion was generated from the same three corresponding points in the two cubes using an open-access function from MATLAB File Exchange.

Steps

The z index was corrected to be the same scale as x and y, by

$$z_c = \frac{z.sf}{sfz}$$

where *sf* = 500 pixels/9 mm, and *sfz* = 1536 pixels/3 mm for the swept source 9 x 9 mm Angio cubes.

Method 1, sequential axis-angle rotation

First, three matching points were identified from the scanning laser ophthalmoscope images: I1: *a, b, c* from the macular cube, and I2: *x, y, z* from the overlapping eccentric cube. These points were from small-scale high-contrast margins, such as the edge of the optic disc, or the branching or intersection of blood vessels.

Step 1:
translate I2 to I1: *x* moved to *a*

y & *z* become y_2 & z_2

b & *c* unmoved

Step 2:
Rotate so y_2 is coincident with *b*, by rotating I2 by angle ε, where

$$\varepsilon = \arctan(\|b \times y_2\| / b \cdot y_2)$$

around the axis perpendicular to plane y_2ab: axis $= b \times y_2$

z_2 becomes z_2'

Step 3:
A second rotation to bring z_2' (previously *z* then z_2) to *c*: by angle δ. This would move y_2 off *b* if performed around the axis perpendicular to $z_2'ac$. Therefore, rotation was around axis *ab*, which required finding point *p* on *ab* where *zp* and *zc* were normal to *ab*.
Assume distance $|az_2'| = |ac|$ (as *c* and z_2' are the same point in the eye seen in rotated images), angle *bac* = angle baz_2', which is the angle between 2 vectors, θ:

$$\theta = \arctan(\|ba \times az_2'\| / ba \cdot az_2').$$

To get these vectors, subtract *a* from *b*, and a from z_2'.
As

$$\|ap\| = \|az_2'\| * \cos(\theta)$$

and the coordinates of *p* are:

$$p = a + \|ap\| * \widehat{ab}$$

where $\widehat{ab}$ is the unit vector of ab, calculated by: `(b-a)./norm(b-a)`

Method 2, rotation via calculation of a quaternion

The second composite image was merged from the two OCT cubes using a single rotation with a quaternion. This was calculated from the same three corresponding pixels in the two images as above, using function `absor` from MATLAB File Exchange[235].

Statistical analysis

The mean and standard deviation of the disparity in *z*-axis coordinates from the overlapping A scans in each composite image was determined. Comparison of the performance of the sequential axis-angle and the quaternion rotations was made via a paired *t*-test of this

disparity from all sets of eyes. Image manipulation and analysis were performed with `mergeSLO3DSSa` and `mergeSLO3DPt2SSa`.

Results

Sample composite images from these eyes are shown in Figures 3.2.1 – 3.2.3.

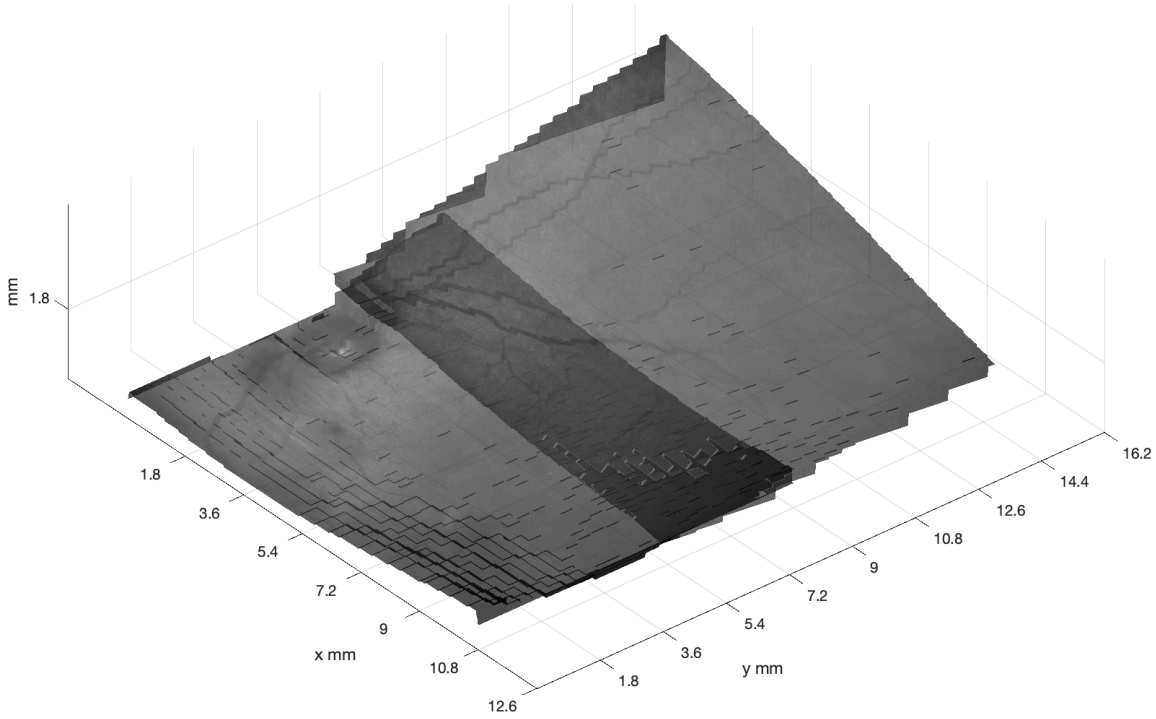

Figure 3.2.1. Merged cubes: a healthy eye with a "normal" shape. Quaternion method.

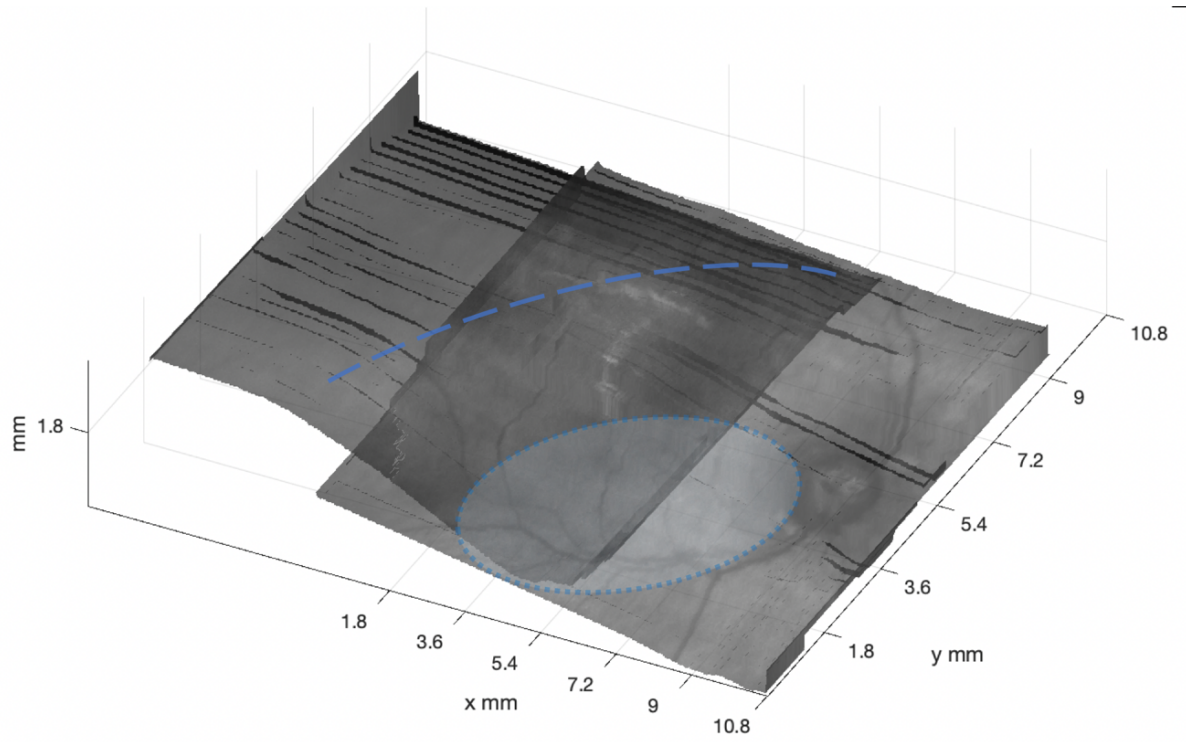

Figure 3.2.2. Merged cubes: myopic eye post retinal detachment repair. The shallow posterior staphyloma visible inferior to the disc and macula (dotted oval line) is demarcated by a ridge (dashed arc) superior and temporal to the macula. The combined OCT image reveals the plateau supero-temporally, emphasizing the nature of the ridge (axial length 25.27 mm, axis angle method).

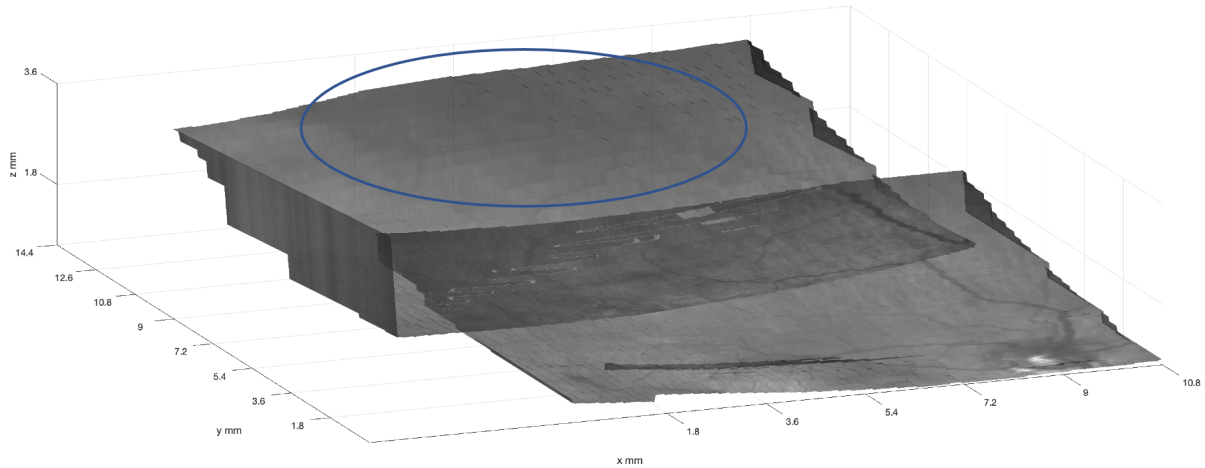

Figure 3.2.3. Merged cubes: Stickler syndrome. 29 year old female with Stickler syndrome who had a retinal detachment repair via vitrectomy. In the cube superior to the macula an inward swelling is seen (blue oval). There is some mismatch in alignment with the superior cube retinal surface rolled anti-clockwise relative to the macular cube (quaternion method).

Mean disparity in A scan (z-axis) position

Across all merged images:

Mean (+/- standard deviation) disparity, sequential axis-angle method: 30.37 +/- 20.32 pixels

Mean disparity, quaternion rotation method: 34.14 +/- 23.99 pixels

Considering all A scans where retinal image was superimposed, the axial difference (*z*-axis) in retinal position between the two cubes ranged from -97 to 79 (sequential axis angle method) and -103 to 25 (quaternion method). This was large enough to have an impact on observed retinal shape. The difference in performance between the two methods was statistically significant (two-sample *t*-test, $p<0.005$)[236], implying the sequential axis angle method was slightly more accurate by a mean of 3.77 pixels (confidence interval 3.70 – 3.83). However, as this was in the *z*-axis where 1536 pixels = 3 mm, this average disparity difference between the two methods was very small (3.77 pixels = 0.007 mm), and is practically unimportant.

Conclusion

Although each rotation on average induced small errors, the sequential rotation axis angle method performed statistically better than the single rotation quaternion method. The difference between the two methods was small and would have little effect on qualitative analysis. However, the range of A scan z-axis position disparity with both methods was large enough that without further image manipulation, quantitative retinal shape analysis could not be performed. Merged OCT images provided a good qualitative description, or illustration, of wide field retinal shape in three dimensions.

3.3. Gaze direction analysis

This section aimed to determine whether analysis of gaze position, determined from the orientation and shape of the pupil in anterior segment images taken at time of OCT image capture, was helpful in quantifying which area of retina was being imaged. This was to explore whether cubes from different eyes that were qualitatively given the same region were consistently sampling the same retinal area. Two experiments were performed to see if gaze direction analysis were helpful in challenging the findings of Section 5.2 and Chapter 6 of this thesis. Firstly, anterior segment images were analysed from swept source OCT cubes captured when subjects were asked to look in uncomplicated, easily comprehensible directions: up, down, left, and right, as well as straight ahead. These were analysed to describe and detect variations both between and within the defined gaze positions. Secondly, an analysis was performed comparing the anterior segment images taken from the two retinal regions used by the classifier in Section 5.2: superior, and supero-temporal. The specific objective of this section was to assess how distinct these two gaze positions were.

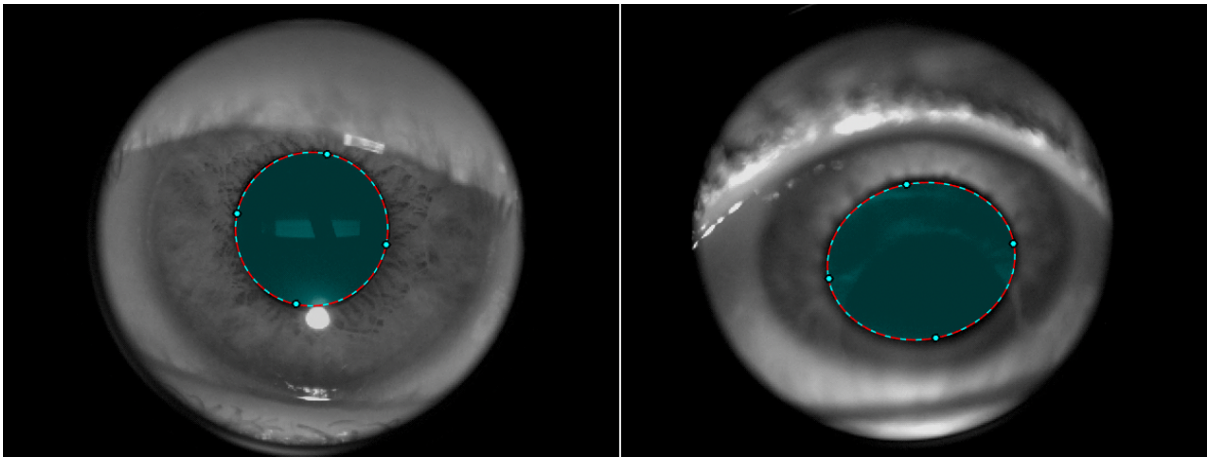

Figure 3.3.1. Sample pupil shape ellipses. The inner margin of the pupil was identified using the MATLAB `roi.ellipse` function. The semi-axes lengths, aspect ratio, rotation, and centre point were recorded for analysis. Note the gaze direction in the right image can be perceived as looking up or down. Gaze orientation labelling is performed from the eye position known at time of image capture (the image on the right is in fact looking up, which can be inferred from the presence of sclera visible at 6 o'clock, inferior to the iris).

Gaze position was quantified by analysing two measurements taken from the shape of the pupil margin (Figure 3.3.1, Table 3.3.1): the direction in which the eye was looking (gaze direction, the angle of rotation of the pupil ellipse); and how far the eye looked away from straight ahead (gaze excursion, angle α). For this study, the observations for right eyes were mirrored to match the gaze direction of the left eyes.

Methods

The external eye images were 640 x 480 pixel size, and reconstructed using `CretiffSS`. From these images the pupil shape was determined using the `ellipse.roi` function, and their aspect ratio and rotation angle were used to compare position (`Pupilanalysis`, `PupilanalysisSS`, and `PupilanalysisSD2`).

The eye may move forward or backward between successive OCT image captures. In particular, there is a tendency to tilt the head upward in upgaze, taking the head and eye away from the OCT. This was minimised by asking the participant to keep their forehead against a fixed headrest. To correct for this, the size of the axes of the eccentric pupil were corrected by comparing the major axis in eccentric gaze (the larger axis perpendicular to gaze direction) to the eye's average axis size in the primary position. This average was used to correct for elliptical pupils in the primary position and the fact that the major axis in primary position may be at a different orientation to the major axis when looking away. For example, if when looking straight ahead the axes are at 0 and 90°, neither will correspond to the major axis when looking up to the right, which may be 45° to the horizontal (Figure 3.3.2). Therefore, corrected MiAxE = (AvAxC/MaAxE)*MiAxE, where MiAxE = minor axis length in excursion, MaAxE = major axis length in excursion, and AvAxC = average of the pupil margin ellipse axes lengths looking straight ahead (when imaging the macula).

Table 3.3.1. Description of terms used to describe the gaze position of the eye.

Term	Description	Assessed by
Gaze position	The direction the subject was asked to look in (region – see Table 2.3)	Instruction to subject
Gaze direction	The direction actually taken (“where”)	Pupil margin ellipse rotation
Gaze excursion	How far the eye moved from the primary position (“How far”)	Pupil margin ellipse eccentricity, angle α,

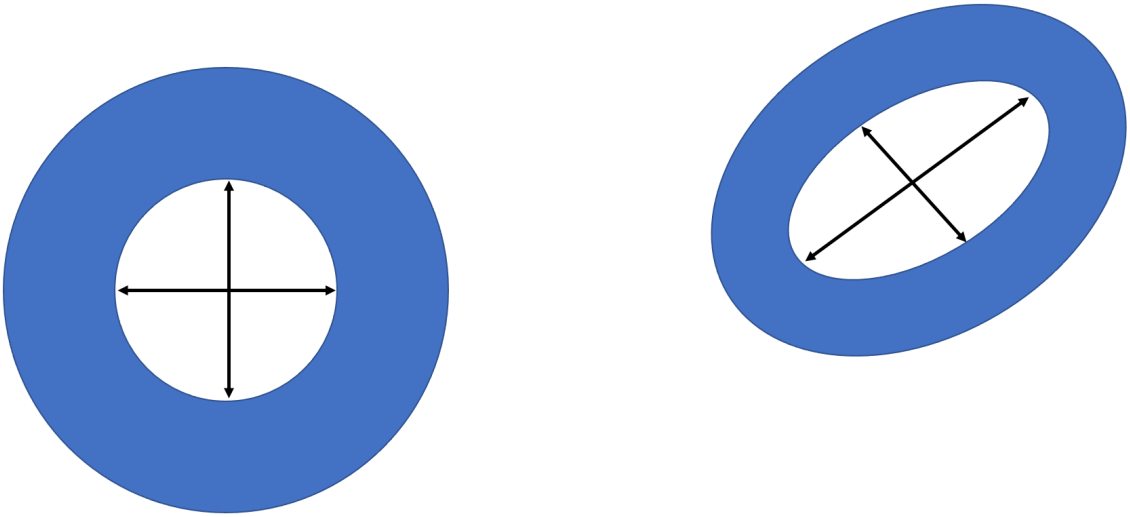

Figure 3.3.2. Pupil assessment. Eccentricity was the ratio of the largest diameter divided by the smallest diameter. Looking ahead for macular imaging (left image), this was close to 1.0. When looking away, such as up and to the right (right image), eccentricity increases, and the axes rotate. The rotation of the axes reflects where the eye is looking (gaze direction), and the ellipse eccentricity how far from straight ahead gaze direction has changed (measure by angle α).

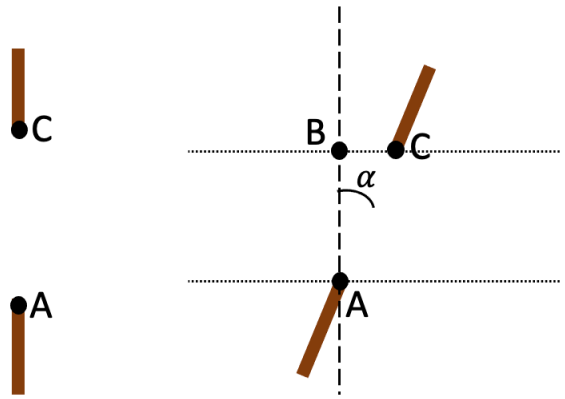

Figure 3.3.3. Iris and pupil diameter shown in cross section, with the eye looking to the left. Size of pupil diameter AC (left) in the primary position becomes AB when the pupil plane deviates from the vertical in upgaze (right) by angle α.

An eccentric pupil has "reclined" by angle α = arccos(|AB|/|AC|). This angle reflects the angle the eye has deviated from straight ahead (Figure 3.3.3). Here it was called gaze excursion angle, to distinguish it from the rotation of the pupil ellipse which reflects gaze direction.

3.3.1 Horizontal and vertical gaze positions (swept source OCT images)

This analysis explored whether gaze direction and excursion angles varied as expected: consistent within, but with differences between, the different gaze positions.

Subjects

Analysis was performed on 415 external eye images taken with 415 B scans from 94 eyes of 48 participants imaged between July and November 2020.

Results

Macular cube gaze position

All scans were taken with the subject asked to look at the internal fixation point on the OCT, to image the macula centred upon the fovea. As a result, excursion angle was 0 (arccos(1)).

Mean gaze direction = 6.93°, with a standard deviation 63.83° reflecting variation in pupil orientation between eyes.

Peripheral gaze positions

Table 3.3.2 presents the mean +/- standard deviation gaze direction and gaze excursion angles for the four gaze positions up, down, temporal, and nasal. On average, subjects looked slightly above the horizon on nasal and temporal gaze positions, and laterally away from their midline with vertical gaze positions. Gaze excursion angle was on average less for upgaze than downgaze, and equal for nasal and temporal gaze positions.

Table 3.3.2. Mean gaze direction and excursion for cardinal gaze positions.

Gaze position	Where/direction (SD)	How far/excursion (SD)
Up	3.01 (27.18)	26.83 (10.47)
Down	-5.90 (9.46)	37.61 (10.40)
Temporal	-6.03 (18.06)	32.94 (8.85)
Nasal	3.90 (24.04)	31.12 (10.33)

The gaze direction angle is relative to the horizon (lateral gaze positions) and vertical meridian (for up and down gaze), positive values in a clockwise direction, as for a left eye. All measurements in degrees. SD = standard deviation

Between-eye distribution of gaze position

Figure 3.3.4 illustrates the gaze direction and excursion angles for gaze positions up, down, nasal, and temporal.

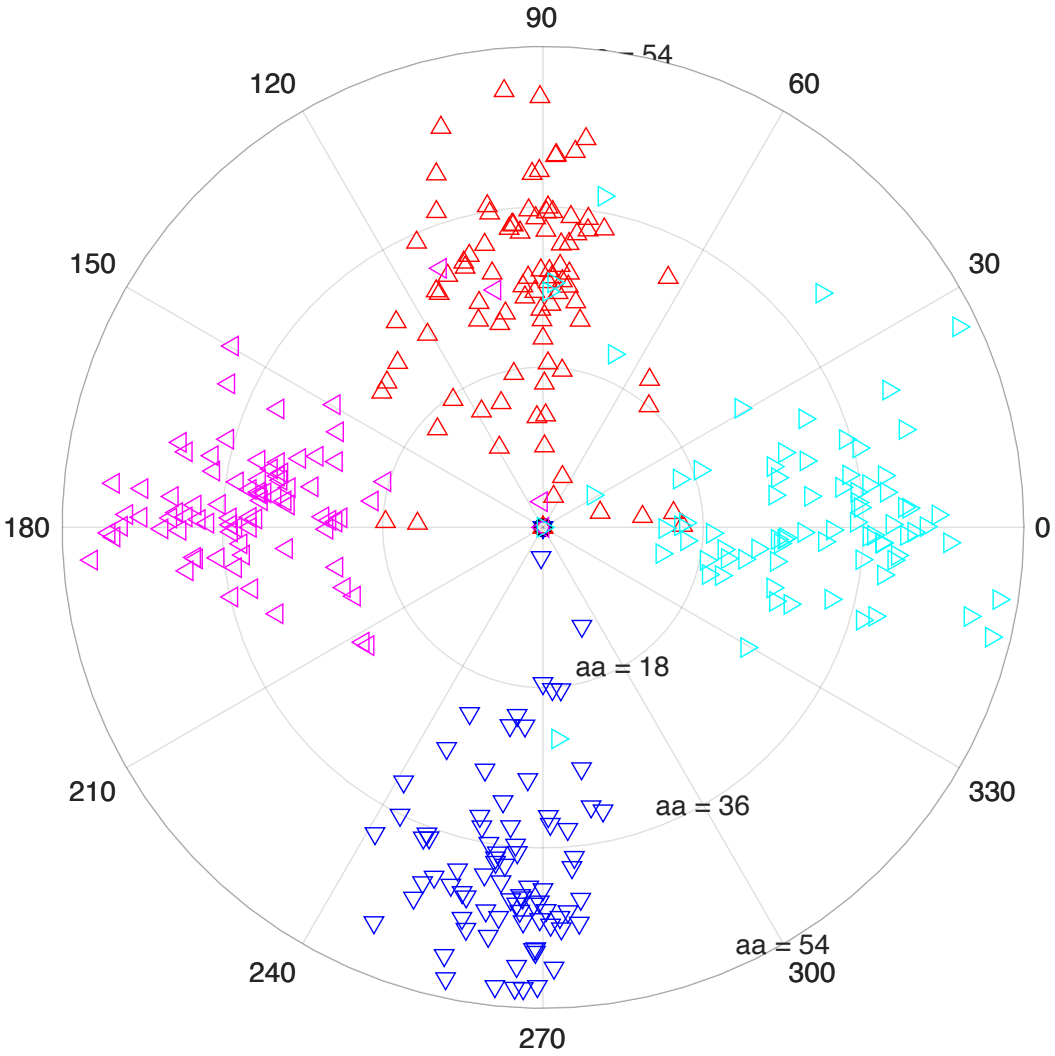

Figure 3.3.4. Gaze position analysis. Gaze direction and excursion angle for gaze positions up (red), down (blue), temporal (magenta) and nasal (cyan). Gaze excursion angle is represented by the displacement from the centre (radius), and gaze direction is represented by the polar angle. The pupil ellipse shape does not differentiate between eyes looking in diametrically opposite directions (that is, up was not distinguishable from down when assessed by pupil shape alone). Gaze position was recorded at time of imaging, and opposing gaze positions have been separated here by 180° for clarity.

3.3.2 Comparison of superior and supero-temporal gaze position

Results

Subjects

The three gaze positions “macula”, “superior” and “supero-temporal” were analysed from the external eye pictures taken during SD OCT imaging of eighty-eight eyes. In twenty of the 264 images it was not possible to measure the shape of the pupil due to poor image quality. Twelve of these were from the superior gaze position, and eight from the superior-temporal position.

Gaze position

The average pupil margin elliptical eccentricity for macular scans was 1.08, lower than that of the eccentric gaze positions (1.14 for superior, and 1.33 for supero-temporal). Mean gaze direction was 14.8° nasal to the vertical for the superior gaze position (Table 3.3.3), and 49.2° anti-clockwise from the positive *x*-axis, supero-temporal gaze. Mean gaze excursion angle was less for the superior gaze position (25.5°) than the supero-temporal gaze position (39.1°).

The displacement of the pupil centre from the image centre (Table 3.3.3) alters the relationship between gaze position and location of retina imaged. Furthermore, during image capture the OCT reticle can be moved around the observed retinal area in three dimensions, further complicating the relationship between gaze position and imaged retinal area.

Table 3.3.3. Mean gaze direction and excursion for superior and supero-temporal gaze positions.

	Mean (SD) gaze direction (degrees)	Mean gaze excursion angle (degrees)	Pupil displacement from image centre (pixels)	Direction pupil displacement
Macula	1.2		19	-22.42
Superior	14.8 (37.6)	25.5 (10.7)	36	-23.48
Supero-temporal	49.2 (30.8)	39.1 (10.3)	32	-25.85

SD = standard deviation.

Within-gaze position variability

Figure 3.3.5 illustrates gaze excursion and gaze direction for superior and supero-temporal gaze positions. More than half (45 out of 79 supero-temporal gaze images measured) of the supero-temporal gaze position images had an excursion angle greater than 40°, with a gaze direction between 40-80°. In contrast, the superior gaze position tended to be directed slightly more to the nasal than temporal direction, with a lower gaze excursion.

The eye with a superior gaze position zero excursion (at the centre of the polar plot Figure 3.3.5) is shown in Figure 3.3.6. This was a vertically oval pupil where upgaze reduced the elliptical shape.

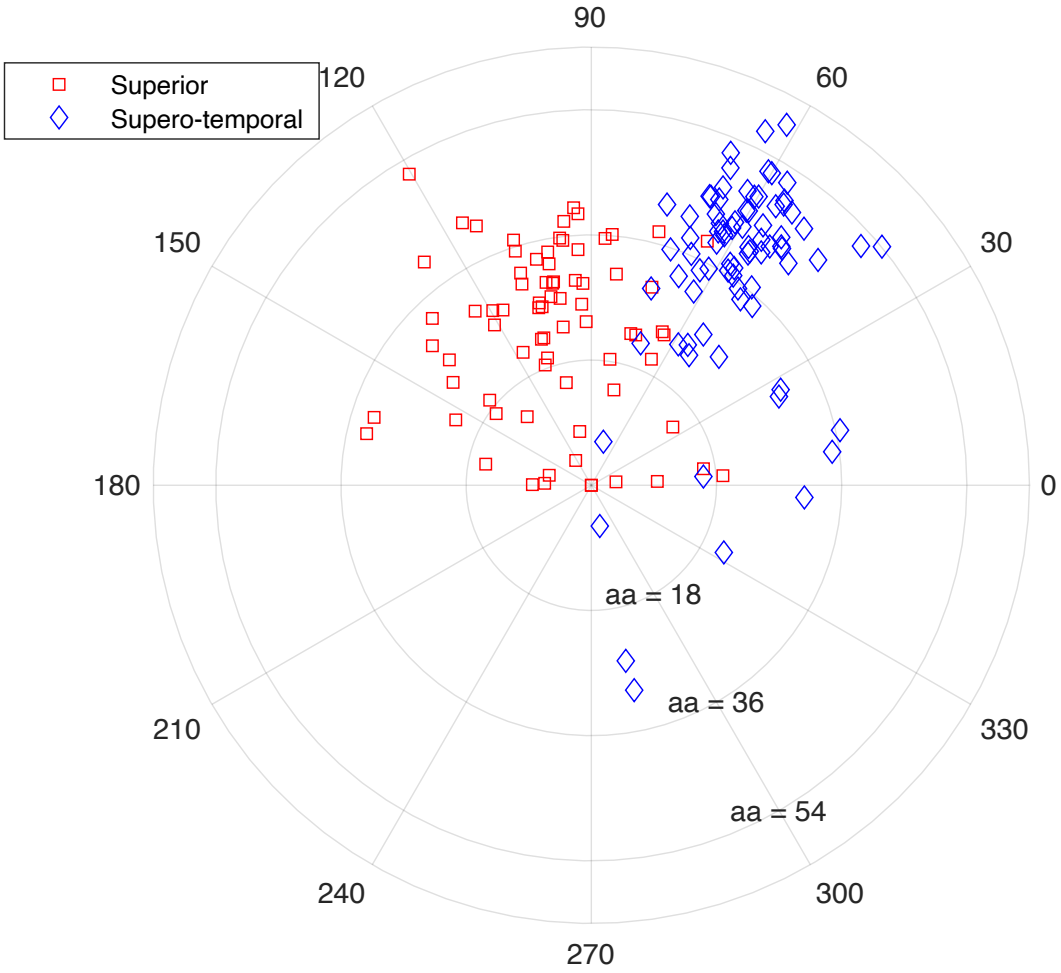

Figure 3.3.5. Superior and supero-temporal gaze position analysis. Gaze direction (polar angle) and gaze excursion (radius aa, in degrees) for superior and supero-temporal gaze positions. The nasal direction is at the polar angle 180°.

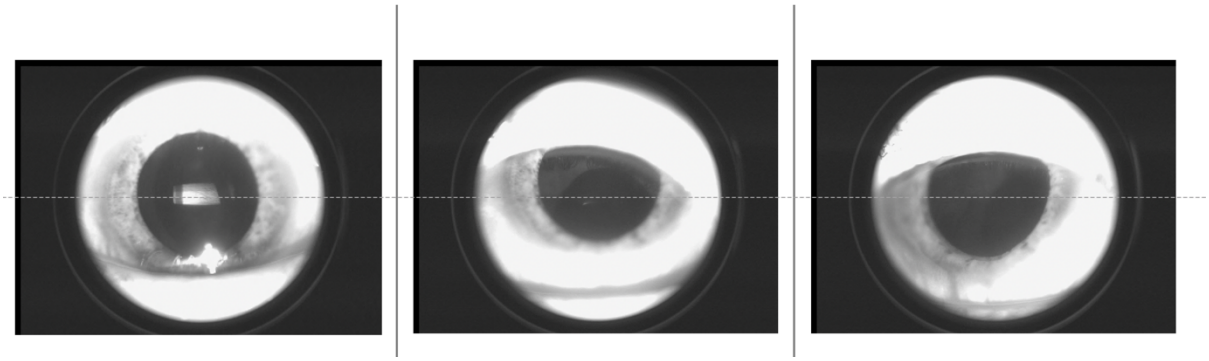

Figure 3.3.6. External eye images. This eye was identified as having zero gaze excursion in upgaze in Figure 3.3.5. The vertically oval pupil in forward gaze (left image) was foreshortened in upgaze to a more circular shape, confounding the analysis of position. Note also in the supero-temporal position (right image) optical distortions from the cornea magnify the iris width to the left of the pupil and shorten the iris (lower right) which may affect observed pupil shape.

Differentiation between gaze positions within individual eyes

To determine to what degree the superior and supero-temporal gaze positions were sampling different areas from the same retina, Figure 3.3.7 presents each eye according to the difference between superior and supero-temporal gaze position by where (direction) and how far (excursion) they looked. Points close to the origin identify eyes where there was little difference between gaze position for the two images in a single eye (close to zero difference in gaze direction and gaze excursion between the two positions). The participant closest to the origin (R289) did show little difference between the anterior segment pupil images across the two gaze positions (Figure 3.3.8).

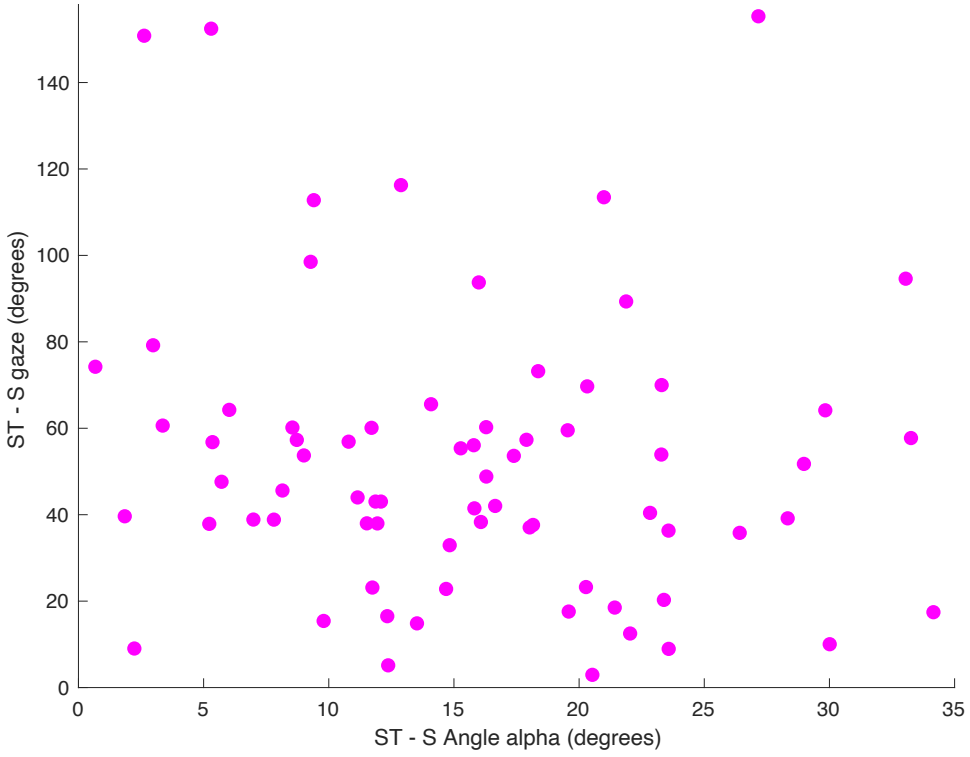

Figure 3.3.7. Within-eye gaze position differences. Each point represents one individual eye, with the x-axis representing the difference in excursion angle for that eye between superior and supero-temporal regions, and the y-axis the difference in superior and supero-temporal gaze direction. The three uppermost points with gaze direction difference greater than 140° had oval pupils that confounded the gaze position analysis. Points close to the origin are from eyes with little apparent difference between the two gaze positions (see Figure 3.3.8).

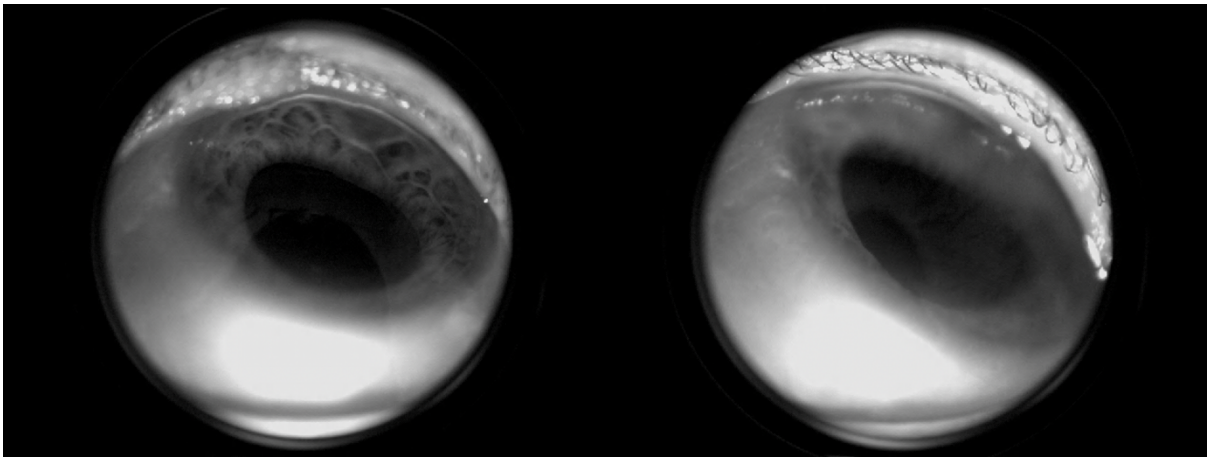

Figure 3.3.8. Gaze position. Eye R289, the closest subject to the origin in Figure 3.3.7. Superior gaze (left) differs little from supero-temporal gaze (right). This retinal tear eye was labelled "2" by the classifier in Chapter 5, equivalent to the retinal detachment classification. This label would likely have arisen from the magnitude of a single region anomaly value alone (see discussion, Section 5.2).

Influence of age on upgaze excursion

Aging is known to lead to a deterioration in eye movement tasks including smooth pursuit eye movements and saccadic responses[237]. To explore whether age affected the gaze position during OCT imaging, the correlation between age and both upgaze and downgaze was performed (Figure 3.3.9). The effect size of age on gaze excursion was low, but significant for upgaze ($r^2 = 0.029$, $\rho = -0.24$, $p = 0.02$) and not downgaze ($r^2 = 0.017$, $\rho = 0.11$, $p = 0.32$).

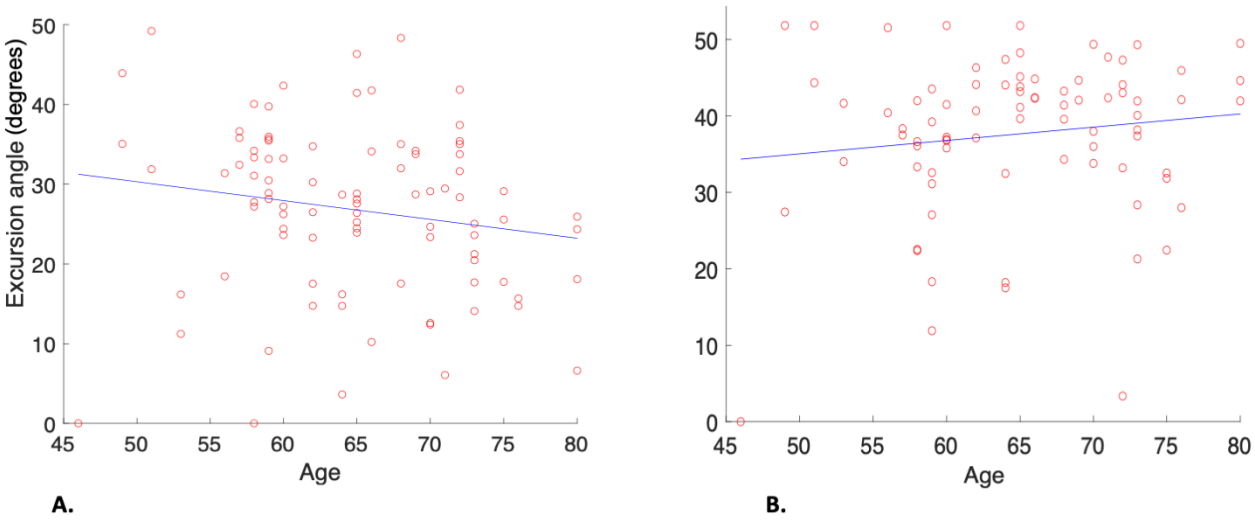

Figure 3.3.9. Effect of age on gaze excursion for upgaze and downgaze. Effect size was small (upgaze, figure A, left, $r^2 = 0.029$, downgaze figure B, right, $r^2 = 0.017$), and only significant for upgaze. The low effect size may be due to the effects of aging only becoming apparent in the oldest participants: note the reduction in eyes looking more than 30° upwards after 70 years.

Conclusion

Based on analysis of pupil shape, gaze excursion differed between gaze positions in a manner consistent with the known direction of action of the extra-ocular muscles. There was less variation between eyes in gaze excursion than in gaze direction. Gaze position analysis could identify a lack of difference between different gaze positions in an individual eye. However, there are significant issues with this technique that limit its usefulness and the conclusions that can be made. Between eye comparisons of position were limited by factors including a non-circular pupil, and from optical effects of observing anterior segment structures through the peripheral cornea (Figures 3.3.6 & 3.3.8)[238]. Relating gaze position to retinal area imaged was further complicated by variation in the position of the imaging beam to the pupil, and the ability to vary the OCT reticle position within the OCT window. Therefore it was concluded that this gaze position analysis has limited value in quantifying the location of sampled retinal area, and this method did not contribute to later chapters of this thesis.

3.4. Description of posterior pole and mid-peripheral retinal shape

This section describes the variation in local retinal shape across the eye. First, the distribution of the magnitude of total anomaly across the entire set of scans is described. Then, the curvature and anomaly from each region is reported.

Methods

Subjects

Seventy eyes of 70 participants were recruited from ophthalmology clinics in South Australia between October 2016 and August 2019. Their reason for attending the clinic were new onset floaters (51 eyes, all with posterior vitreous detachment), optometric initiated review for retinal assessment of myopic eyes (16 eyes), ocular hypertension (one eye, no structural or posterior segment abnormality), and previous retinal detachment or retinal tear in the contralateral eye (two eyes, both with posterior vitreous detachment but no retinal pathology). Myopic maculopathy was present in 13 participants: 3 with a tessellated fundus (category 1 in the International photographic classification of myopic maculopathy[239]), 4 with diffuse chorio-retinal atrophy (category 2), and 6 with patchy choroidal atrophy (category 3). Participant age range was 33–83 years (median 62 years), with axial length from 21.11–36.88 mm (median 24.52 mm). There were 40 right eyes, and 30 left eyes; 37 were female, 33 male.

A retinal OCT survey was performed for each eye, and B scan retinal curvature and anomaly were determined as described in Chapter 2. Results are described by the distribution of anomaly values across all scans, and by the median and interquartile range of anomaly values and curvature across the different regions of the eye (`XvalMYPVDbyALmm`).

Results

Distribution of magnitude of irregularity

The distribution of the size of total anomaly is illustrated by a histogram in Figure 3.4.1. B scan examples from total anomaly values of 5, 10, 20, and 35 mm are presented in Figure

3.4.2. The majority of eyes had low anomaly values, reflecting a good correspondence of retinal shape to a parabola.

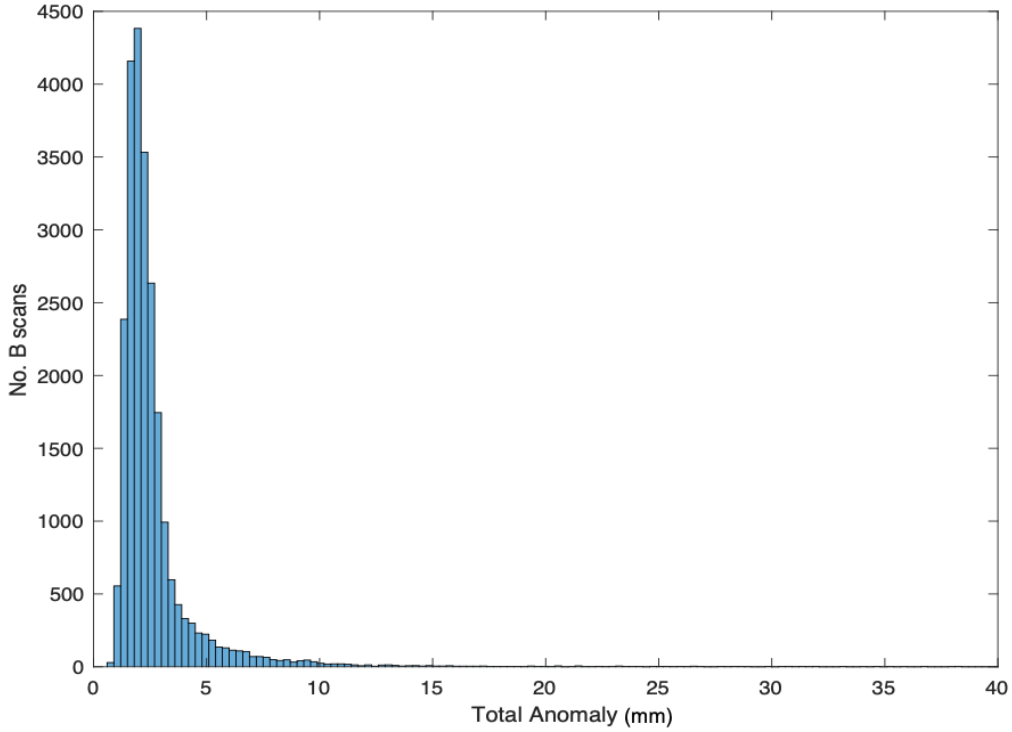

Figure 3.4.1. Distribution of total anomaly, all B scans. The number of B scans for each total anomaly value is shown. 94% of B scans had a total anomaly less than 5 mm. Median B scan total anomaly was 2.14 mm. Units of anomaly: mm.

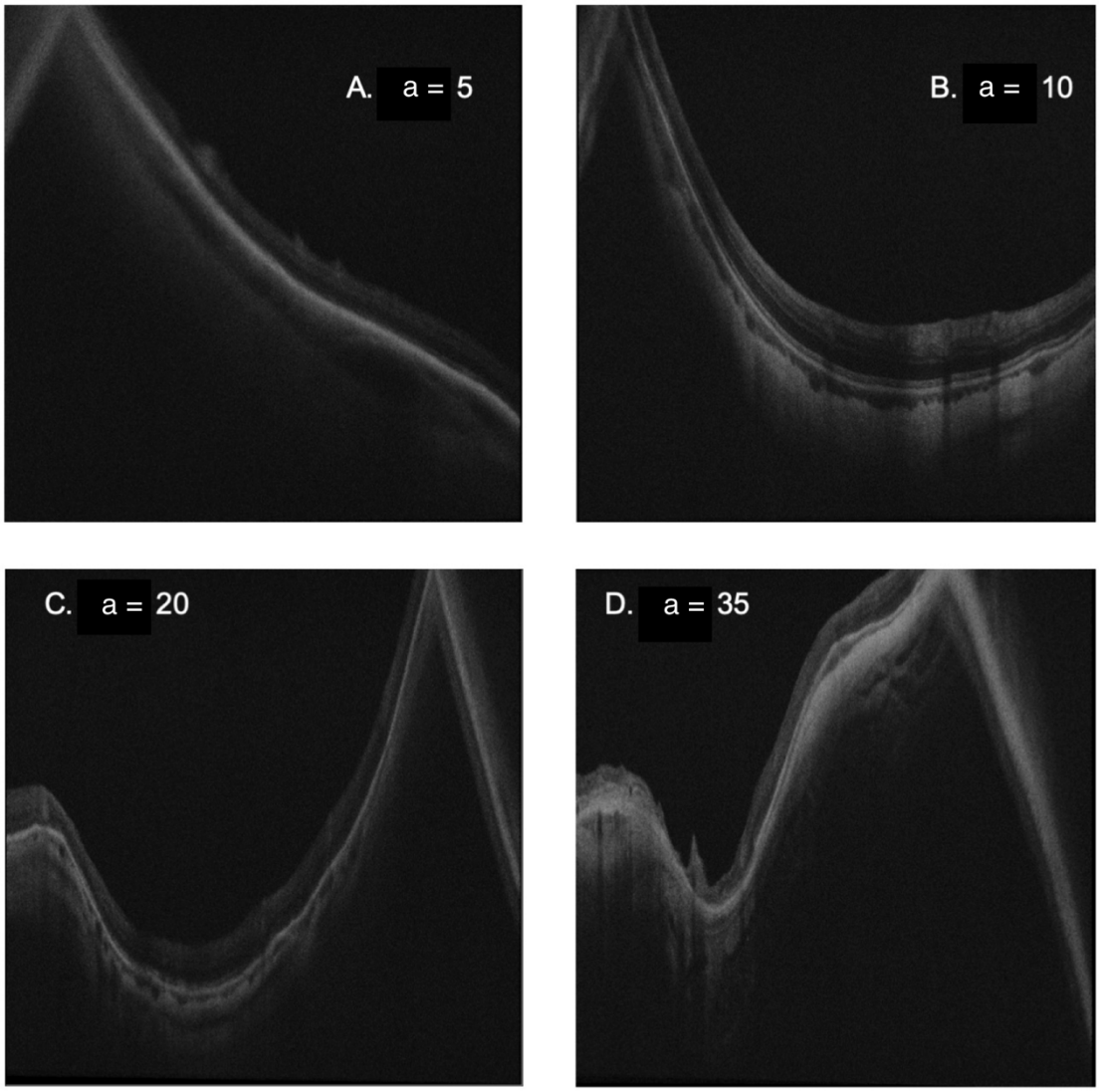

Figure 3.4.2. Sample B scans by total anomaly value. Representative B scans with total anomaly 5 mm (A), 10 mm (B), 20 mm (C), and 35 mm (D) are presented. All feature values were corrected for the retinal width in the B scan, to allow comparison between images (the anomaly value units are in fact mm^2 per mm of retinal length). Retinal mirror artefacts (to the left side in images A & B, and the right side of C & D) were ignored. a = total anomaly.

The magnitude of irregularity in different regions is shown in Fig 3.4.3a. Regional median total anomaly, peak anomaly value, root mean square anomaly, and curvature values are presented in Table 3.4.1. The anterior inferior regions had the greatest irregularity, followed by the macula. This means these regions had the most irregular retinal contour that

corresponded least with a best-fit quadratic curve. To investigate whether this distribution was particular to this group, the same measurements for a different set of eyes (retinal detachment eyes) were examined (Fig 3.4.3b). This second set of eyes exhibited a very similar distribution in retinal irregularity.

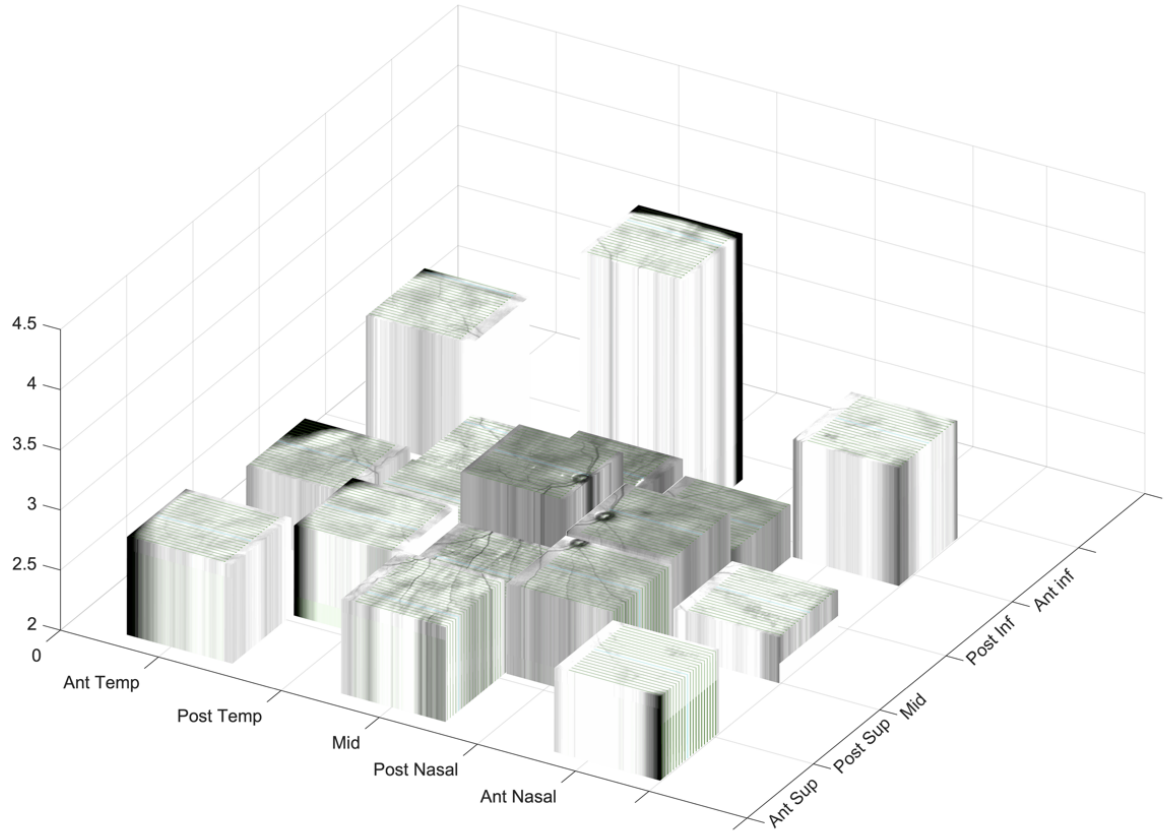

Figure 3.4.3a. Retinal OCT shape irregularity in different regions of the eye. Graphical representation of the magnitude of irregularity (the sum of the first 30 frequency bins of the Fourier transformation of B scan shape) in different regions of the eye, viewed from a viewpoint supero-nasal to the eye (looking down on a left eye from a point above the medial end of the eyebrow). The vertical axis scale is in mm, so the taller the column the greater the irregularity. The anterior inferior and macular regions were the most irregular locations.

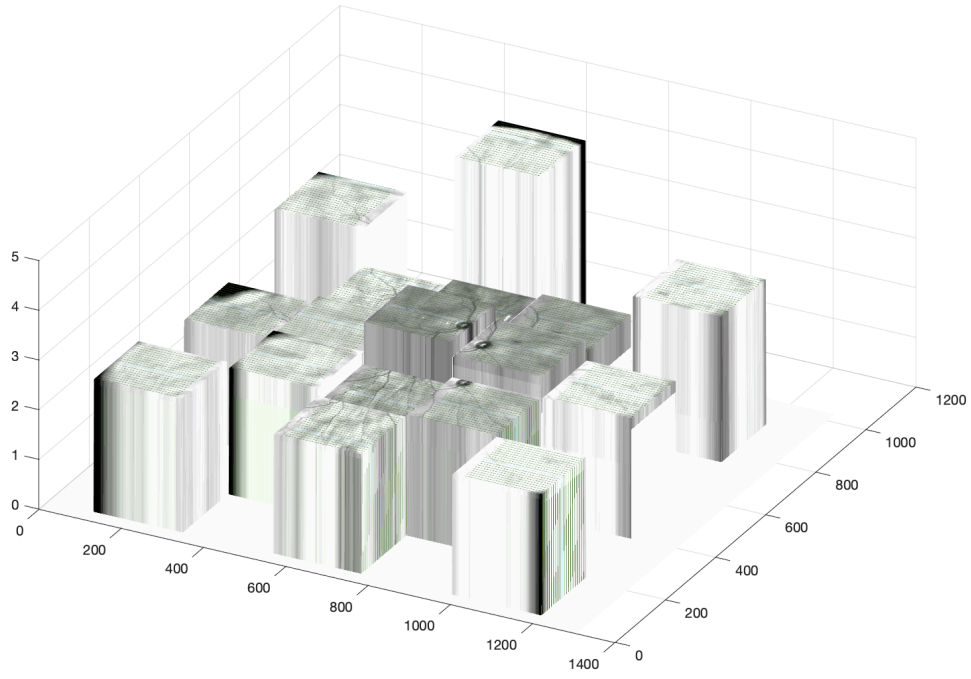

Figure 3.4.3b. Retinal irregularity distribution (2). This is the same presentation of median retinal shape irregularity as in Figure 3.4.3a, but for a different set of eyes. These eyes had all experienced retinal detachment, and surgical repair via vitrectomy. The distribution of irregularity across the eye was very similar to Fig. 3.4.3a, suggesting this pattern of regional variation is common.

Table 3.4.1. Regional shape median and interquartile range values.

Region	Median total anomaly	Median peak anomaly	Median rmsa	Median *K*	IQR total anomaly	IQR peak anomaly	IQR rmsa	IQR *K*
1	2.445	0.515	0.139	0.026	1.511	0.368	0.087	0.020
2	1.838	0.387	0.108	0.026	1.043	0.275	0.068	0.018
3	1.910	0.417	0.114	0.018	1.160	0.289	0.077	0.025
4	1.813	0.400	0.109	0.028	0.927	0.284	0.064	0.023
5	2.235	0.327	0.109	0.036	1.050	0.168	0.062	0.027
6	1.681	0.341	0.093	0.032	0.886	0.242	0.056	0.021
7	2.018	0.257	0.090	0.039	0.819	0.094	0.039	0.028
8	1.671	0.349	0.095	0.031	0.803	0.207	0.050	0.025
9	2.170	0.327	0.107	0.031	0.884	0.159	0.056	0.032
10	1.906	0.404	0.109	0.032	1.131	0.297	0.078	0.019
11	3.017	0.727	0.188	0.031	1.814	0.387	0.117	0.026
12	1.766	0.337	0.096	0.034	0.819	0.211	0.052	0.018
13	2.310	0.402	0.121	0.029	1.200	0.169	0.072	0.024
14	1.989	0.382	0.108	0.036	0.958	0.263	0.063	0.021
15	1.760	0.211	0.079	0.028	0.763	0.136	0.041	0.025
16	1.962	0.401	0.109	0.027	1.027	0.280	0.064	0.019
17	2.078	0.372	0.108	0.026	1.028	0.175	0.062	0.025

The regions with the largest values (the macula and anterior inferior regions) were more irregular than regions with smaller values. Descriptors total anomaly, peak anomaly, and rmsa describe the variation in irregularity seen in B scans within a region, compared to the average B scan irregularity within the same region. Median total anomaly = region median absolute difference from the average region value. Median peak anomaly = median largest single frequency bin difference from the region average. rmsa = root mean square difference between each B scan and the average bin value. *K* = curvature at the vertex of the best-fit curve to the retinal shape. Units are mm for total anomaly, peak anomaly, and rmsa, and units are mm^{-1} for *K*. For the region identifiers key, see Table 2.2.

Distribution of higher anomaly B scans around the eye (MYPVDFrBsgtThr)

The proportion of B scans with total anomaly greater than 5 mm in each region is shown in Tables 3.4.2, 3.4.3 and Figure 3.4.4. Consistent with the distribution seen in Figures 3.4.3, the inferior regions had the most high-anomaly scans.

Table 3.4.2. Fraction of B scans in each region with total anomaly > 5 mm.

	Temporal		Midline		Nasal
Superior	0.067		0.035		0.066
		0.062	0.042	0.066	
Midline	0.053	0.052	0.106	0.066	0.022
		0.039	0.048	0.061	
Inferior	0.035		0.110		0.082

Overall, 5.9% of B scans had total anomaly > 5 mm. Data presented as for a right eye, with the macula central, temporal regions to the left. Excludes B scans with no retinal image.

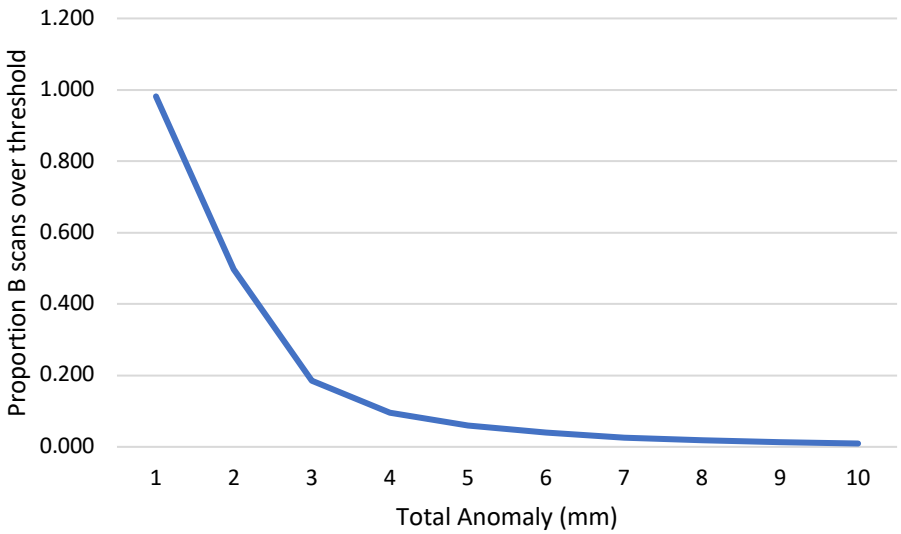

Figure 3.4.4. Proportion of B scans over total anomaly threshold. The x-axis displays the anomaly value, the y-axis the proportion of all B scans that exceed that anomaly value. This is a graphical illustration of the bottom row of Table 3.4.3.

Table 3.4.3. Fraction of B scans (with retinal image) over anomaly threshold, by region.

	Threshold (mm)									
Region	**1**	**2**	**3**	**4**	**5**	**6**	**7**	**8**	**9**	**10**
Mac	0.986	0.692	0.330	0.142	0.106	0.082	0.066	*0.053*	0.043	0.036
PS	0.934	0.416	0.133	*0.067*	0.042	0.027	0.020	0.016	0.013	0.011
AS	0.968	0.460	0.154	*0.066*	0.035	0.017	0.006	0.001	0.000	0.000
PST	0.974	0.395	0.144	0.093	*0.062*	0.040	0.023	0.010	0.006	0.004
AST	1.000	0.662	0.234	0.115	*0.067*	0.041	0.025	0.017	0.009	0.006
PT	0.965	0.324	0.107	0.073	*0.052*	0.038	0.029	0.021	0.013	0.010
AT	0.998	0.513	0.145	0.077	*0.053*	0.042	0.035	0.026	0.024	0.020
PIT	0.959	0.320	0.112	*0.065*	0.039	0.026	0.018	0.013	0.008	0.004
AIT	0.998	0.600	0.174	*0.063*	0.035	0.029	0.020	0.020	0.018	0.013
PI	0.972	0.449	0.169	*0.086*	0.048	0.026	0.019	0.012	0.008	0.005
AI	1.000	0.830	0.505	0.264	0.110	*0.074*	0.040	0.025	0.015	0.010
PIN	0.988	0.370	0.129	0.084	*0.061*	0.045	0.032	0.022	0.015	0.009
AIN	0.999	0.654	0.257	0.122	0.082	*0.053*	0.030	0.023	0.013	0.007
PN	0.991	0.495	0.166	0.099	*0.066*	0.044	0.028	0.017	0.009	0.005
AN	0.976	0.350	0.109	*0.050*	0.022	0.010	0.005	0.003	0.001	0.000
PSN	0.984	0.478	0.173	0.104	*0.066*	0.041	0.025	0.014	0.011	0.008
ASN	0.998	0.540	0.186	0.105	*0.066*	0.042	0.024	0.014	0.010	0.007
Mean	**0.982**	**0.497**	**0.185**	**0.096**	***0.059***	**0.040**	**0.026**	**0.018**	**0.013**	**0.009**

The threshold (shown in the column headings) at which the fraction of scans in each region was greater than 0.05 is italicised in blue: more irregular regions have this value further to the right. This indicates how many scans in any region have elevated anomaly values, reflecting increased irregularity compared to the average scan. Key: Mac = macula, A = anterior, P = posterior, I = inferior, N = nasal, S = superior, T = temporal.

Conclusion

Most B scan retinal contours corresponded closely to a parabola described by a quadratic equation. In 94% of B scans the size of residual shape after removal of the best fit curve was of low value, having a total anomaly value less than 5 mm. Furthermore, the irregularity sampled in this way differed in different areas, with the inferior retina the most irregular

both in magnitude and number of higher anomaly scans. The anterior inferior region had the greatest average irregularity, and the greatest total anomaly. The macular region had more B scans with a total anomaly higher than 5 mm, suggesting this area had a moderately increased anomaly, which is likely to be due to the adjacent optic disc.

3.5. Conclusions and discussion

Reliability

The aim of this section was to determine if repeated measurements taken from the same OCTs produced the same or similar results in retinal shape metrics, and whether repeat OCTs from an eye produced the same result each time. Both re-measurement of the same images by different operators, and re-imaging the same retina multiple times produced consistent results. This was unsurprising. The Livewire tool, based on graph theory, has been extensively used in biomedical image analysis. Contemporary OCT devices also have scanning rates fast enough that many of the image artefacts seen with slower (time-domain) devices are not apparent. All the B scan images used in this work were multiple-pass composite images constructed from A scans repeated 4-8 (spectral domain) to 100 times (swept source). This speed and duplication eliminated potential eye and head motion artifact which would have led to a registration failure and loss of the composite image. These images were all from a retinal survey of one eye. This does not test whether measurement reliability varies between different eyes, but does assess reliability across the varied retinal presentations seen in the different regions (see Figure 3.4.3). Both observers were ophthalmologists used to examining OCT images. This work cannot eliminate the possibility that other observers may not be as consistent. However, minimal instruction and no supervision was performed of observer 2, suggesting familiarity with OCT images was an acceptable standard.

Most statistical tests are designed to determine whether a difference is present and not necessarily able to prove identity. The statistical non-significant difference between the measurements taken here should be considered less important than the high degree of similarity between the repeat measurements.

Merging OCT cubes

Although the average magnitude of induced error was low with both rotation methods, quantitative analyses of composite images will have limited benefit without further image processing, as these combinations of unmodified images revealed differences in retinal position in the overlapping areas which would affect measured retinal shape. For this reason, further analyses in this thesis were directed to local retinal shape features found within individual B scans.

Gaze position analysis

Knowledge of where an eye was looking at the time of imaging might enable identification of the part of the retina imaged. If gaze position were quantifiable, it would define which part of the eye had been imaged and allocated to any particular region and ensure consistent sampling between eyes. With a lack of consistent between-eye internal landmarks once away from the optic disc and fovea, this section explored the use of the external eye image as an indication of eye position. Results were mixed. There were differences on average when comparing different gaze positions. However, there was significant within-gaze position variation in terms of the direction of gaze and how far in that direction different eyes had travelled.

Section 3.3.1 explored the gaze position from iris images used the swept source OCT. Four cardinal directions of gaze were assessed: up, down left and right, and as these instructions are simple to understand it might have been expected that differences between individuals would be low. This analysis was performed as these gaze directions are more intuitively comprehensible to a participant – it is easier to consistently “look up” than “look up to the right”, so analysis of these gaze positions removed some subjectivity and assessed the method itself. The second section analysed the superior and supero-temporal gaze positions used by the classifier in Section 5.2. The method used here cannot determine the direction of the gaze of the eye from the image alone: pupil shape with supero-temporal gaze may appear identical to the infero-nasal gaze position.

For this analysis to be helpful in evaluating what part of retina was imaged with the OCT, the assumptions included that the pupil eccentricity when imaging the macula should be close to 1 (a round pupil); and that the beam pathway passes through the centre of the pupil. If these were correct, then confirmation that the same retina was being sampled in different eyes would arise from finding that the gaze excursion angle was similar across eyes for any single gaze direction; that the gaze direction should be similar across eyes for any gaze position; and that the macula position should have the narrowest range of gaze direction, noticeably different from the gaze positions looking away. Except for the final point, none of these factors were strictly true, limiting the usefulness of this approach.

The eye does not gimbal around a fixed origin, but moves more like a horse's head controlled by reins. There is therefore no direct link between the measured gaze position from examination of the pupil shape and the area of retina imaged with OCT. Eye movement control varies between individuals[240] and is influenced by many factors including age[241], which affect upgaze more severely than other directions[242], as well as vestibular dysfunction[243], and neurological disease[244,245].

This analysis ignores any torsion around z-axis (roll), and neglects optical effects from an off-centre path through the cornea, which has been shown to magnify anterior segment features along the gaze direction axis and will have greater effects with increasingly eccentric gaze[246]. This might seem to favour a reduction in measured eccentricity, but as this effect increases toward the distal edge of the cornea, the iris may be widened distally, leading to a reduction in apparent pupil width and increase in measured pupil eccentricity (Figure 3.3.8). This method ignores any shift in the pupil centre relative to the visual axis with changes in pupil size[247]. However, as all eyes in the study were dilated this effect should not be significant.

Further limitations to the method include the fact that some ellipse matching to the pupil, particularly as gaze diverts further away, was on an arc of the pupil margin only, rather than the full pupil margin, due to eyelid and peripheral cornea interfering with visualisation. In some cases, it was not possible to identify enough of the pupil for analysis.

The OCT beam pathway was always horizontal, and when the eye is looking away, the imaging beam completes a chord rather than a diameter across the eye. In addition, any displacement of the imaging beam pathway from the pupil centre affects the area of retina imaged. Moving the reticle off the pupil centre images more peripheral retina if displaced in the direction of gaze, and images more posterior retina if moved opposite to the direction of gaze. This loosens the link between the observed gaze position and the area of retina sampled. Further analysis could compensate for the off-centre image acquisition seen here (Table 3.3.3) to better assess the significance of variation in gaze direction and excursion between eyes for any gaze position. However, it should be noted that the retina was sampled with 21 parallel B scans with SD OCT, and each imaged region was defined by the highest anomaly B scan out of the 21 B scans per cube. This vertical sampling spread further reduces the impact the variation in gaze position would have on inter-eye comparison.

The superior rectus muscle has a mixed elevation and intorsion action from looking straight ahead, but a pure elevation action in lateral gaze. Looking directly upward is a more complex composite movement for the eye than looking up and out. Therefore, it was not surprising that participants generally looked further from the primary position when looking supero-temporally than superiorly.

If the eye looked equally up and out when looking supero-temporal the rotation angle would be expected to be 45°. As it was 49°, this suggests a gaze position only marginally more superior than supero-temporal. The average difference between gaze directions for superior and supero-temporal gaze positions was 35°, a good separation. The superior gaze position was always imaged before the supero-temporal, so the slight nasal displacement of the former was not related to the subject deliberately looking away from the supero-temporal position. The nasal trend may arise from the operator subconsciously and pre-emptively seeking to differentiate the superior position from the supero-temporal.

Comparing which part of the retina has been imaged in different eyes from the retinal image itself is limited by a lack of defined landmarks once in the mid-periphery and away from the optic disc and fovea. Choroidal pigmentation and retinal vessels and their branches

vary between individuals in their appearance and location. The more recognisable vascular landmarks (such as first, second, and third order branching points) may vary in their absolute position relative to one another and there are uncertainties around the variable growth of the eye: whether it is a characterised by generalised inflation, variable regional stretch, or even addition of new tissue landmarks. The axial length (distance from image focal point and retina) will also slightly influence image size from optical effects.

Retinal imaging in this work was performed without strictly defined points of fixation for the subject. For gaze excursions for the two superior and supero-temporal regions analysed here, participants were asked to look up as far as possible, with the gaze direction "straight up", or "up to the right/left", in all cases guided by the operator observing the participant's position. The scanning laser ophthalmoscope retinal image was useful in confirming the position of the peri-macular cube relative to the posterior pole, and was useful in modifying gaze position – to ensure it was away from but adjacent to the macula. The position of the more eccentric mid-peripheral cubes studied here could broadly be confirmed by the visualisation of more distal retinal vasculature, as well as through sighting the participants gaze position by looking at the subject around the OCT machine. While the gaze excursion would be expected to vary from person to person, in these eyes it varied less than the gaze direction, although analysis of both was limited by the factors mentioned above.

Retinal shape distribution

Sections 3.1-3.3 provide confidence that OCT sampled retinal shape measurements can be relied upon to assess local shape features, although each image should be considered separately for analysis and does not provide information about larger-scale or generalised information about retinal shape. Section 3.4 used this approach to describe the variation in curvature and irregularity across the posterior pole and mid-peripheral retina. This found that irregularity was greatest inferiorly. The irregularity at the macula relates to posterior staphyloma development in myopic eyes, but may also be linked to the adjacent optic disc influencing local anatomy.

The lower average irregularity in the nasal and temporal regions compared to inferiorly may reflect real differences in irregularity in these regions. However, it should be acknowledged that these regions with lower average irregularity were sampled longitudinally, while the upper and lower regions were sampled transversely, which may have contributed to the difference. There may be differences in retinal shape arising from this different orientation: if the more midline horizontal regions (temporal and nasal) were imaged perpendicular to the visual axis (a vertical scan) irregularity in these regions might be higher (and the reverse might be true for the superior and inferior regions). This was not possible with the spectral domain OCT. Only horizontally oriented B scans can be 9 mm in length (although that has changed with more recent OCT devices).

Local retinal shape was sampled with OCT by multiple passes of the superluminescent diode light source. This irregularity suggests growth of posterior eye tissues is non-uniform with irregular expansion[5]. If so, this also implies that once away from the distinct landmarks of the fovea and optic nerve, exact correspondence of sampled retinal area from one eye to the next is not just technically difficult but meaningless. Similar, rather than identical, areas can be sampled for comparison.

Summary

This chapter demonstrated that OCT can be relied upon to measure *local* retinal shape. The mismatch seen in combined images introduced errors, so each scan needs to be analysed individually, with shape information reflecting local, within-scan features. Gaze position analysis had enough confounding factors in the method that it was not helpful in describing retinal regions, and the significance of the identified variation in gaze position is reduced when analysing shape as each region is described by the maximum anomaly in any single B scan out of 21 scans in each cube sampling each region. Retinal shape varied around the eye in a consistent manner, with the inferior retinal areas the most irregular.

Chapter 4. The correlation between retinal shape irregularity and axial length

Introduction

Multiple sources have identified an increase in the incidence of myopia within populations over time, an increase projected to reach epidemic proportions through the first half of this century[3]. An inconvenience for many, the more severe forms of myopia carry with them a significant risk of visual impairment particularly in the later years[248]. The causes of visual impairment include myopic maculopathy, glaucoma, inability to access visual aids (a common cause of admission to blind schools in the developing world[249,250]), and retinal detachment[13].

Axial length is the primary determinant for most myopia[100], and highly myopic eyes are known to have an increased incidence of staphyloma and globe shape irregularities on the scale documented by MRI, and visible with OCT[168]. OCT retinal shape sampling might be assumed to show increased irregularity with increasing axial length, but the sampling scale is smaller than MRI, with a width of 9 mm and maximum depth of 2 mm for spectral domain OCT, so that irregularity observed with MRI may not relate to OCT irregularity, and vice versa. Any correlation between the larger scale shape features of myopia documented with MRI and smaller scale features observed with OCT is uncertain.

Reported work with MRI has focussed on the most extreme examples of myopia[158,251]. What has not been demonstrated is whether irregular globe shape only appears above a threshold of eye size, or changes in a continuous manner. If the former were the case, irregularity might be absent or minimal in hyperopic eyes and appear only in larger globes. This would imply that the regional irregularity noted in Section 3.4 originated from the subset of larger eyes alone.

The aim of this study is to determine whether there is a correlation between retinal irregularity and axial length.

Published work

The contents of Chapter 4 have been published in "Correlation between optical coherence tomography retinal shape irregularity and axial length. (Lake S, Bottema M, Williams K, Reynolds K. PLoS ONE (2019); 14(12). https://doi.org/10.1371/journal.pone.0227207). My contributions to this paper included data collection and analysis (90%), writing and editing (85%), and research design (25%). My co-authors contributed equally to research design (25% each); proof reading, revision of and guidance on writing the papers (5% each); and instruction and advice on data analysis (10%).

Null Hypothesis

That OCT measured retinal irregularity has no correlation with axial length.

Methods

Subjects

The eyes included in this study (n = 70) were the same sample analysed in a previous section, the regional distribution of irregularity (Chapter 3.4, Table 4.1).

Statistical analysis

All-of-eye and regional median and interquartile range of total anomaly, peak anomaly, root mean square anomaly, and curvature were determined as described in Chapter 2, and correlated to axial length by Spearman's rank correlation (`XvalMYPVDbyALmm`, `MYPVDALregXvalmm`, `MYPVDALstatsmm`, `MYPVDallBSdatamm`, and `MYPVDALregstatsmmKc`). The 95% confidence intervals were calculated with Fisher's z-transformation:

95% confidence intervals = tanh (arctanh (r) ±1.96/√(n−3)).

Bonferroni-Holm correction for multiple comparisons was performed with α = 0.05 (`BHcorrmmALK`).

Results

Correlation between all-of-eye shape variables and axial length

Collating both regional and all-of-eye measures, the lowest *p*-value required for significance using Bonferroni-Holm correction for multiple comparisons with $\alpha = 0.05$ was 0.00046. After correction, there was significant positive correlation with axial length for 36 metrics. These included the all-of-eye values median total anomaly ($\rho = 0.66$), peak anomaly ($\rho = 0.61$), and root mean square anomaly ($\rho = 0.67$). No correlation was seen between all-of-eye median curvature and axial length ($\rho = 0.11$). Interquartile range total anomaly ($\rho = 0.60$), interquartile range root mean square anomaly ($\rho = 0.48$), and interquartile range of curvature ($\rho = 0.61$) also correlated with axial length. Full results for all-of-eye variables are shown in Table 4.2 and Figure 4.1. Correlation was repeated with the largest eye (axial length 36.88 mm) removed in case this eye was skewing the results, with almost identical results, as the non-parametric analysis uses rank order, not absolute variable size.

Table 4.1. Participant demographics.

	Median	**Range**
Age	62	33-83
Axial length	24.52	21.11 – 36.88
Sex	33 male, 37 female	
Laterality	40 right, 30 left	
Ethnicity	Caucasian	67
	Filipino	1
	Chinese	1
	Black American	1

Seventy eyes from 70 participants. Age in years, axial length in mm.

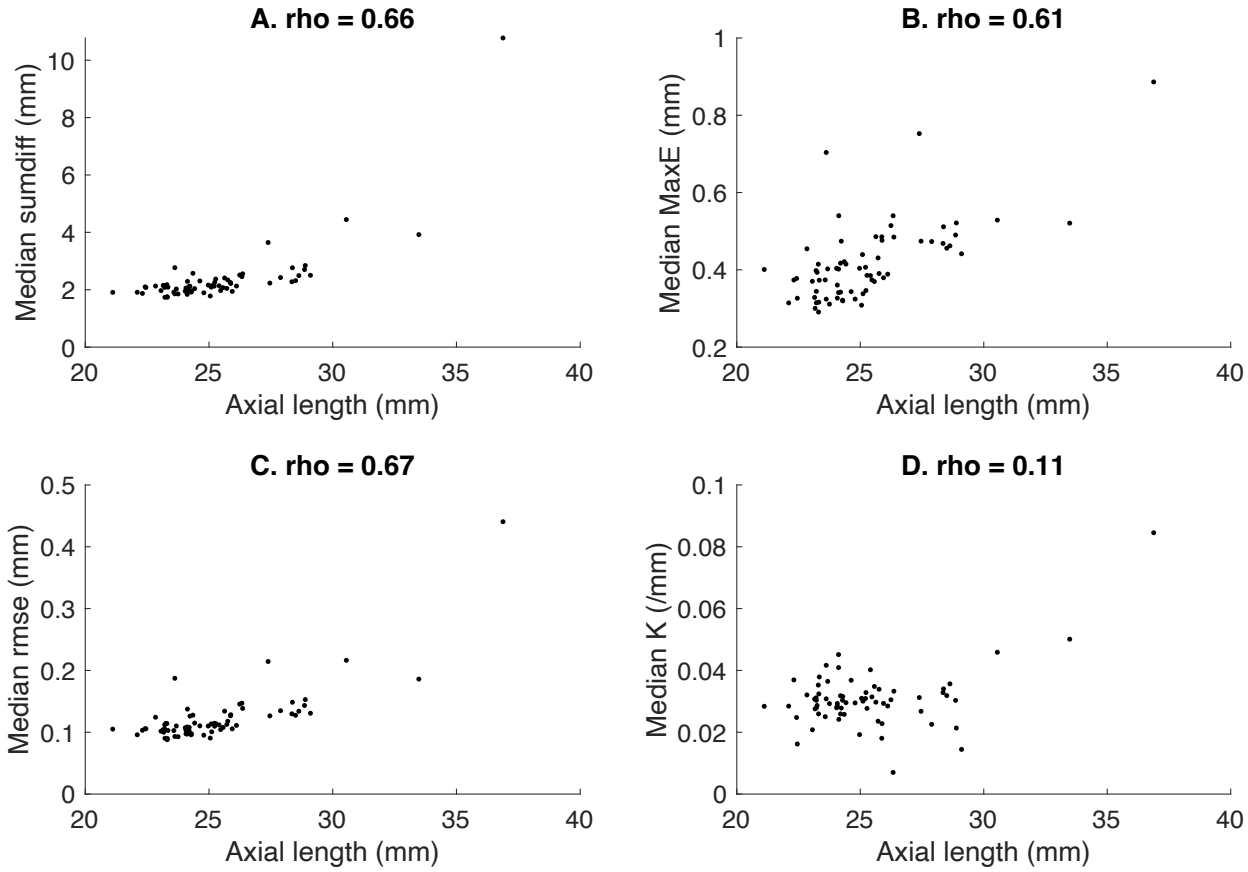

Figure 4.1. The correlation between retinal shape metrics and axial length. Scatter plots of whole-of-eye features median total anomaly (A), median peak anomaly (B), median root mean square anomaly (C), and median curvature (D) plotted against axial length. Spearman's rank correlation ρ is shown for each and was significant for A-C (see Table 4.2).

Table 4.2a. Spearman's rank correlation between shape metrics and axial length.

Correlation ρ	median total anomaly (95% CI)	median peak anomaly (95% CI)	median rmsa (95% CI)	median K (95% CI)
All of eye	**0.66 (0.49 – 0.77)**	**0.61 (0.46 – 0.75)**	**0.67 (0.52 – 0.78)**	0.11 (-0.14 – 0.32)
Macula	**0.52 (0.34 – 0.68)**	**0.50 (0.32 – 0.67)**	**0.50 (0.33 – 0.67)**	0.32 (0.10 – 0.53)
Posterior superior	**0.47 (0.24 – 0.62)**	**0.46 (0.20 – 0.59)**	**0.49 (0.25 – 0.63)**	0.16 (-0.16 – 0.31)
Anterior superior	0.42 (0.19 – 0.60)	0.35 (0.11 – 0.55)	0.41 (0.19 – 0.60)	0.17 (-0.16 – 0.33)
Posterior ST	0.33 (0.07 – 0.52)	0.32 (0.08 – 0.53)	0.35 (0.11 – 0.55)	-0.22 (-0.45 – 0.02)
Anterior ST	0.08 (-0.15 – 0.34)	0.11 (-0.15 – 0.34)	0.08 (-0.12 – 0.37)	-0.02 (-0.26 – 0.23)
Posterior temporal	**0.44 (0.21 – 0.61)**	0.34 (0.17 – 0.59)	0.38 (0.22 – 0.62)	-0.18 (-0.37 – 0.12)
Anterior temporal	0.09 (-0.16 – 0.33)	0.31 (0.10 – 0.54)	0.21 (-0.01 – 0.46)	0.11 (-0.18 – 0.32)
Posterior IT	**0.48 (0.24 – 0.64)**	0.37 (0.14 – 0.57)	0.42 (0.19 – 0.61)	-0.38 (-0.50 - -0.04)
Anterior IT	0.28 (-0.03 – 0.44)	0.29 (0.06 – 0.51)	0.34 (0.04 – 0.49)	-0.30 (-0.49 - -0.03)
Posterior inferior	**0.56 (0.38 – 0.70)**	**0.49 (0.30 – 0.66)**	**0.49 (0.30 – 0.66)**	0.32 (0.15 – 0.56)
Anterior inferior	0.20 (-0.04 – 0.42)	0.10 (-0.14 – 0.33)	0.17 (-0.09 – 0.38)	0.03 (-0.21 – 0.27)
Posterior IN	**0.47 (0.27 – 0.65)**	0.41 (0.19 – 0.59)	**0.45 (0.25 – 0.63)**	0.13 (-0.11 – 0.36)
Anterior IN	0.35 (0.13 – 0.56)	0.29 (0.09 – 0.53)	0.29 (0.01 – 0.47)	-0.15 (-0.44 – 0.02)
Posterior nasal	0.35 (0.10 – 0.53)	0.30 (0.06 – 0.51)	0.35 (0.09 – 0.53)	0.21 (-0.09 – 0.39)
Anterior nasal	0.14 (-0.08 – 0.40)	0.05 (-0.22 – 0.27)	0.14 (-0.13 – 0.36)	-0.09 (-0.35 – 0.13)
Posterior SN	0.41 (0.18 – 0.58)	**0.44 (0.21 – 0.60)**	0.41 (0.18 – 0.58)	0.11 (-0.18 – 0.30)
Anterior SN	**0.61 (0.44 – 0.75)**	**0.47 (0.31 – 0.68)**	**0.59 (0.44 – 0.75)**	-0.17 (-0.43 – 0.05)

Tables 4.2a & b. Spearman's rank correlation ρ between axial length and median and interquartile range total anomaly, peak anomaly, rmsa, and curvature. Values significant after Bonferroni-Holm correction for multiple comparison are highlighted in bold, and for all these values $p < 0.001$. Correlation between irregularity measures (median total anomaly, peak anomaly, and rmsa) and axial length was greater at the macula and adjacent cubes than in more anterior cubes. Interquartile range of curvature (IQR K) correlated with axial length in most nasal regions. rmsa = root mean square anomaly, IQR = interquartile range, ST = supero-temporal, IT = infero-temporal, IN = infero-nasal, SN = supero-nasal.

Table 4.2b. Correlation between interquartile range of shape metrics and axial length.

Correlation ρ	IQR total anomaly (95% CI)	IQR peak anomaly (95% CI)	IQR rmsa (95% CI)	IQR K (95% CI)
All of eye	**0.60 (0.41 – 0.72)**	0.06 (-0.18 – 0.29)	**0.48 (0.28 – 0.64)**	**0.61 (0.44 – 0.74)**
Macula	**0.47 (0.26 - 0.63)**	**0.53 (0.34 – 0.68)**	**0.52 (0.26 – 0.63)**	**0.44 (0.26 – 0.63)**
Posterior superior	0.25 (0.01 – 0.46)	0.24 (0.03 – 0.47)	0.26 (0.03 – 0.47)	0.20 (-0.01 – 0.44)
Anterior superior	0.33 (0.11 – 0.55)	0.34 (0.17 – 0.59)	0.37 (0.14 – 0.57)	0.11 (-0.20 – 0.29)
Posterior ST	0.16 (-0.09 – 0.40)	0.11 (-0.20 – 0.30)	0.13 (-0.15 – 0.34)	0.34 (0.09 – 0.54)
Anterior ST	0.00 (-0.20 – 0.29)	-0.06 (-0.22 – 0.27)	-0.06 (-0.24 – 0.25)	0.07 (-0.20 – 0.29)
Posterior temporal	**0.44 (0.22 – 0.62)**	0.13 (-0.11 – 0.38)	0.28 (0.09 – 0.53)	**0.47 (0.24 – 0.64)**
Anterior temporal	0.33 (0.09 – 0.53)	0.12 (-0.27 – 0.22)	0.21 (-0.06 – 0.42)	0.23 (0.00 – 0.47)
Posterior IT	0.41 (0.19 – 0.60)	0.10 (-0.23 – 0.27)	0.20 (-0.09 – 0.40)	0.31 (0.03 – 0.49)
Anterior IT	0.29 (0.05 – 0.51)	0.16 (-0.10 – 0.38)	0.28 (0.02 – 0.48)	**0.47 (0.26 – 0.65)**
Posterior inferior	**0.48 (0.27 – 0.64)**	0.32 (0.08 – 0.51)	0.29 (0.08 – 0.51)	0.35 (0.12 – 0.54)
Anterior inferior	0.04 (-0.20 – 0.28)	-0.16 (-0.34 – 0.14)	-0.12 (-0.33 – 0.14)	0.31 (0.05 – 0.50)
Posterior IN	0.37 (0.13 – 0.55)	0.08 (-0.18 – 0.30)	0.26 (-0.01 – 0.45)	**0.45 (0.26 – 0.64)**
Anterior IN	0.29 (0.05 – 0.49)	0.08 (-0.19 – 0.29)	0.18 (-0.05 – 0.42)	0.20 (-0.07 – 0.40)
Posterior nasal	0.27 (0.01 – 0.46)	0.14 (-0.17 – 0.32)	0.20 (-0.08 – 0.39)	**0.57 (0.36 – 0.70)**
Anterior nasal	0.39 (0.15 – 0.57)	-0.06 (-0.27 – 0.22)	0.16 (-0.12 – 0.36)	**0.45 (0.23 – 0.62)**
Posterior SN	0.25 (0.00 – 0.45)	0.15 (-0.13 – 0.34)	0.20 (-0.04 – 0.42)	**0.58 (0.40 – 0.72)**
Anterior SN	**0.52 (0.32 – 0.68)**	0.04 (-0.19 – 0.30)	0.37 (0.15 – 0.57)	0.43 (0.24 – 0.64)

See Table 4.2a for explanatory footnotes.

Correlation between regional measurements and axial length

Correlation between regional irregularity and axial length was strongest in the macula and posterior extra-macular cubes as measured by median total anomaly, peak anomaly, and root mean square anomaly. Interquartile range of curvature correlated with axial length in most nasal regions (Table 4.2b).

Discussion

This method provides a quantitative description of the deformation of the retinal contour that arises in relation to the size of the eye. The null hypothesis can be confidently rejected. Overall, retinal shape irregularity increased with axial length, even as local curvature did

not. This correlation was strongest at the macula and regions adjacent to it. This suggests that the irregularity relates to growth or expansion of the eye that occurs at or around the posterior pole.

The ability to quantify OCT retinal shape allows comparison of multiple scans within and between eyes. Median and interquartile range are conservative choices of metrics to represent retinal shape, which limit the impact of outlying values on the analysis. The shape descriptors derived from the Fourier transformation and best-fit curvature are unaffected by position and orientation of the retinal image within the B scan. Some distortions of retinal contour occur during OCT image capture, most significantly due to axial length, so correction of curvature for axial length-induced artefact was performed[135,143]. Optical distortions from anterior chamber structures may alter retinal topography[113]. Both tilt of the eye and lateral decentration have little effect on retinal geometry in OCT, although they reduce the size of retinal arc sampled [135,138]. The speed of A scan acquisition and the use of composite B scans preserves real information on retinal shape within the OCT image. Just as the pattern on an embossed leather belt is recognisably the same whether it is held straight or flexed, so the information within the Fourier transformation of retinal irregularity reflects real retinal features.

Participant eyes were included in this study if they were found to have no abnormality on examination (other than the myopic retinal changes described in the Methods, Chapter 3.4), as the purpose was to explore and describe retinal shape features in non-pathological eyes. This analysis does not identify the cause of retinal irregularity. The reason for the progression is uncertain. Some of the irregularity was likely to be related to staphylomata. The suggestion that the tissue driving myopic eye growth is Bruch's membrane[5] raises the possibility that "overproduction" of this layer leads to tissue redundancy and "wrinkling", at least in the transverse orientation of these scans. Alternatively, it may more directly relate to alterations in choroidal thickness or sclera: the irregular contour seen in dome-shaped maculopathy has been reported to be due to variations in scleral thickness leading to alterations in scleral rigidity[252]. Spectral domain OCT does not have sufficient resolution at depth to discriminate between these possibilities, particularly in mid-peripheral retina where signal strength is reduced. Imaging with swept source OCT may clarify this further.

The measurements presented here confirm impressions gathered from visual inspection of B scans in different parts of the eye. Irregularity, measured by Fourier analysis of the residual, increased with axial length at and around the macula. Interquartile range of curvature correlated with axial length at the macula and in most nasal regions, so these areas had a wider range of curvatures as axial length increased. The shape metrics of the anterior inferior and infero-nasal regions had no correlation to axial length. The inferior regions exhibited the most irregular retinal contour on OCT, irrespective of axial length (the images in Figure 3.1.2 are from inferior retinal regions). The uniformly high irregularity of shape in these regions may have masked any correlation between axial length and shape.

The correlation between shape features and axial length agrees with the known irregularity of the eye at a larger scale seen with increasing myopia on MRI. This correlation could therefore be anticipated from clinical and MRI observations of globe shape, but has not previously been described with the resolution of the OCT. As the OCT has much greater resolution than MRI, retinal shape features reported here are so small that MRI images are unlikely to be able to confirm or refute the measurements taken with the OCT. In myopic eyes, the macula can be abnormal in shape with highly curved concave sections from staphylomata. Posterior non-macular cubes in myopic eyes image the margins of staphylomata and have negative curvature (convex inwards), and OCT cubes anterior to this often display a straight retinal contour. These factors reduce median curvature values in myopic eyes while increasing the range of curvature values and explain why median curvature does not correlate with axial length while interquartile range of curvature does, particularly in nasal regions.

Measurement of variation in local curvature and the Fourier analysis of differences between OCT retinal contour and the best-fit curvature provide a measure of regional variation in shape. Although macular curvature analysis has been reported before[2,136,158,168], this is the first work to systematically describe and quantify the residual, or difference between measured curvature and actual retinal contour, and extends the analysis to the mid-peripheral retina. This mid-peripheral shape is also in agreement with an estimation of peripheral retinal contour from peripheral refraction[171]. Local curvature cannot be

extrapolated to represent the shape of the posterior segment as a whole. In summary, retinal OCT shape irregularity increased along with the axial length of the eye.

Chapter 5. Development of a classifier to identify retinal detachment eyes

With retinal shape irregularity shown to correlate with axial length, the known major risk factor for retinal detachment, this chapter explores whether retinal shape can help identify eyes that have experienced a retinal detachment. As noted in the introduction, there is a real clinical need to identify these eyes before vision is lost. The aim of this chapter is to explore the ability of a classifier trained on retinal shape features to identify eyes that have had a retinal detachment in a *post hoc* group of PVD and retinal detachment eyes.

For such a classifier to be useful in predicting disease before PVD has occurred, the effects on shape of the intervening events between the *ex ante* pre-PVD state and the post-PVD and post retinal detachment states need to be explored: does the PVD itself, the retinal tear, or the treatment events for retinal detachment (vitrectomy, and laser) influence retinal shape? These are explored and are presented in sections of this chapter as follows:

Section 5.1 explores the effects of PVD on macular shape in three ways: a cross-sectional comparison of retinal irregularity and curvature in a group of eyes that have had a PVD compared to a group of eyes that have not; a longitudinal comparison of macular shape in eyes before and after surgery for macular hole, where PVD is surgically induced as part of the clinical care; and a longitudinal analysis of macular shape in eyes that have been opportunistically imaged before and after spontaneous PVD.

Section 5.2 trains and tests a classifier on eyes that have had either a PVD, or a retinal detachment repaired by vitrectomy, with the aim of separating retinal detachment eyes from the entire sample. The classifier is further tested with a group of eyes that have had treatment for a retinal tear without retinal detachment.

Section 5.3 looks at the change in shape metrics from retinal OCT surveys in eyes that have been imaged both before PVD, then after PVD (3 eyes), or after surgery for PVD related retinal detachment (2 eyes).

Section 5.4 presents an analysis of whether the presence of visible scarring produced by therapeutic retinal laser treatment visible in the OCT images alters the performance of

the classifier trained in Section 5.2. Also reported is whether the classifier performance is influenced by the location of the retinal tears within the eye, in particular whether the presence of superior or supero-temporal retinal breaks improved its success rate.

Published work

Part of the contents of Sections 5.2 and 5.3 have been submitted as a paper to Medical Physics, titled “Optical coherence tomography retinal irregularity-based classification of retinal detachment and posterior vitreous detachment eyes.” Authors Lake SR, Bottema MJ, Williams KA, Reynolds KJ. The paper differs in that the results in this thesis consist of a larger dataset than those in the publication. My contributions to that paper included data collection and analysis (90%), writing and editing (85%), and research design (25%). My co-authors contributed equally to research design (25% each); proof reading, revision of and guidance on writing the papers (5% each); and instruction and advice on data analysis (10%).

5.1. The effect of posterior vitreous detachment on macular shape

Introduction

Were image analysis to be used to predict PVD-related vision threatening events such as retinal detachment prior to the occurrence of PVD, one would need to know what effect PVD itself has on retinal shape. Were PVD to alter retinal shape, prediction based on evidence taken after the event would be less likely to help decision-making based on shape measurements taken before PVD. Conversely, an absence of shape change with PVD would suggest that information acquired from eyes post-PVD could be used to interpret the significance of pre-PVD retinal shape.

The fovea is a consistent landmark in all non-pathological eyes. It is the source of the highest acuity vision, and being located at the posterior pole, it is easy to image with the OCT in a cooperative subject in whom no media opacities are present. The ability of subjects to fixate with the fovea, its anatomical consistency, and the facility of many OCT machines to register an image to allow repeat examination of the same site allows fast, easy, and reproducible image capture. Along with the optic disc, the macula is the most commonly imaged part of the eye, so that sample images are widely available. As a landmark, it also facilitates comparison of shape between eyes.

PVD may occur at any time within the age range 55 – 85 years, and the time of occurrence of PVD is unpredictable in any individual[27,28]. This makes it difficult to obtain a large volume of longitudinal information regarding whether PVD leads to change in shape within a single eye. While many individuals present to eye health practitioners with a new onset PVD, pre-PVD image capture from these eyes relies on chance encounters with patients assessed ideally for fellow eye co-morbidity to record macular OCTs before and after PVD. This makes comparison of retinal OCT images pre- and post- PVD for any single eye an opportunistic event.

The largest dataset in this section presents a cross-sectional analysis of macular shape, performed by comparing the maculae of a group of eyes that have had a PVD to the maculae of those that have not. This cross-sectional analysis looked for differences between

the two groups, rather than differences within individual eyes over time. The hypothesis was that there would be no difference in macular shape comparing eyes with a PVD to eyes without a PVD. Analysis of this is presented in Section 5.1.1.

One situation where the time of posterior hyaloid separation is known is with idiopathic full thickness macular holes, a visually symptomatic pathology associated with an attached posterior hyaloid that is treated by surgically inducing a PVD. This procedure provides an opportunity to document pre-operative shape (when no PVD is present), and compare this to the shape after the surgically induced PVD. All these eyes were routinely imaged both before and after surgery to diagnose the macular hole and assess the success of surgery. This provides some longitudinal data on shape change from PVD, albeit with a surgically induced event rather than a natural one. The objective was to investigate whether shape metrics differ between pre-operative and post-operative states. Analysis of these eyes is presented in Section 5.1.2.

To test whether spontaneous PVD produced shape changes at the macula, a comparison of HD radial OCT images was performed from subjects who had been imaged prior to PVD, then imaged again after PVD had occurred. This has the advantage of a longitudinal analysis of eyes, investigating the effects on shape of “natural” or spontaneous PVD, but with the disadvantage that recruitment was more difficult with a lower number of samples as a result. Analysis of these eyes is presented in section 5.1.3.

Aim

Section 5.1 explores whether macular shape is affected by PVD.

Common methods

The OCT imaging protocol for this study was different from others in this chapter, with a single HD radial cube acquiring 12 radially oriented B scans of 6 mm, all centred at the fovea. Retinal shape was taken as the high intensity ellipsoid layer traced using the Livewire plug in for ImageJ.

Retinal shape was analysed with the combination of best fit curvature and total irregularity after the best fit curve was deducted from the retinal shape (`MHFEPVxzcomp`, and `prepostMHcomp`). Magnitude of irregularity was calculated in the frequency domain as the sum of the first thirty frequency bin moduli. Curvature was corrected for axial length induced artifact. There were twelve curvature and twelve irregularity values per macula cube. To manage the nested data structure, the shape of each eye was analysed with mean and range of curvature and mean and range of irregularity[253]. This is analogous to analysis of corneal shape which is summarised by average dioptric power and astigmatism (the difference between maximum and minimum power).

5.1.1. Cross-sectional comparison of macular shape between eyes with and eyes without a PVD

Methods

Participants were recruited from the retinal clinics of Flinders Medical Centre and Eyemedics, Adelaide between July and December 2019. If they required OCT imaging as part of their normal clinical care they were approached and after informed consent macular OCT images were taken for this study.

Posterior vitreous detachment was diagnosed when both symptoms and examination were consistent with a PVD, with an absence of any visible posterior hyaloid seen on the OCT at the macula or the disc (Figure 5.1.1). The latter was confirmed with extra imaging across the disc where not clear within the standard length 6 mm radial scans.

No PVD was diagnosed by the presence of hyaloid attached to any posterior pole structure seen within the B scan, optic disc or macula. This included eyes where vitreo-macular separation was apparent within the macular OCT but attachment was still seen to the optic disc on a wider or adjacent scan.

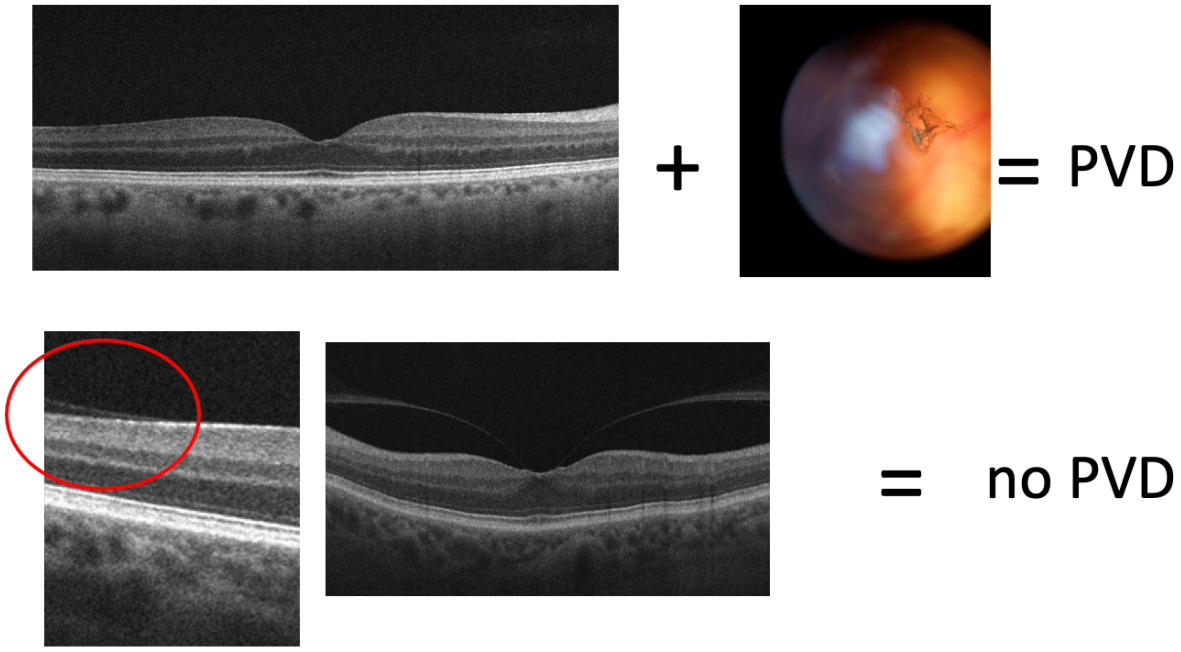

Figure 5.1.1. OCT appearance of eyes with a PVD (top) and without PVD (bottom). The upper row (PVD eyes) has no visible posterior hyaloid membrane seen in the OCT (left) with a visibly detached posterior hyaloid seen on clinical examination (colour fundus photograph, right). The lower row OCTs (no PVD) illustrate posterior hyaloid still attached to the macula, with either minimal separation (red ellipse, lower left), or perifoveal separation (lower right). All analyses in this work considered PVD to have occurred when the posterior hyaloid face was documented to have completely separated from both optic disc and macula.

Statistical analysis

Difference between these groups was assesssed by a two-sample *t*-test, with significance set at $p \leq 0.05$.

Results

Participant reasons for attending clinic are shown in Table 5.1.1. Participant demographics are shown in Table 5.1.2. There were 51 eyes without and 49 eyes with a PVD. B scan shape features are shown individually (not clustered by eye) in Figure 5.1.2.

Table 5.1.1. Participant reasons for attending clinic.

Reason for attending	Number no-PVD eyes	Number PVD eyes
PVD		34
Retinal detachment, FE	9	3
Macular hole, FE	6	
PVD, FE	5	1
Review for diabetes	5	2
Post op cataract surgery, FE	4	1
OAG/OHT	4	2
CSR, FE	3	
Epiretinal membrane, FE	2	4
Retinal tear, FE	3	
Retinal vein occlusion, FE	2	
ARM	1	2
cataract	2	
Choroidal naevus	1	
Healthy eye	1	
Iritis	1	
Lattice degeneration	1	
Macular microaneurysm, FE	1	
Total	51	49

Key: ARM = age related maculopathy, CSR = central serous retinopathy, FE = fellow eye (the pathology listed was in the other eye, with no abnormality in the eye included), OAG = open angle glaucoma, OHT = ocular hypertension, PVD = posterior vitreous detachment, RVO = retinal vein occlusion.

Table 5.1.2. Participant demographics.

	No PVD (+/- SD)	PVD (+/- SD)	*p*-value (*t*-test)
Mean age (years)	64.8 +/- 8.82	66.2 +/- 8.19	0.40
Mean axial length (mm)	23.89 +/- 1.02	24.29 +/- 1.48	0.18
Mean K (mm^{-1})	*0.0238 +/- 0.014*	*0.027 +/- 0.021*	*0.005**
Mean residual (mm)	*2.480 +/- 1.113*	*3.341 +/-2.525*	*< 0.005**

* Significance of these values should be treated with caution, as this involves single level analysis of nested data. See main text.

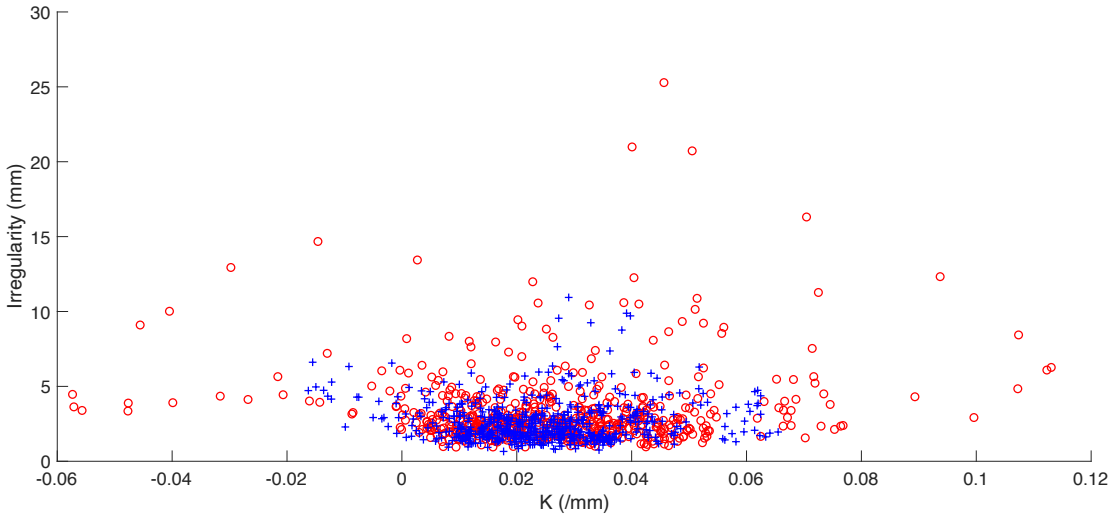

Figure 5.1.2. Scatter plot of irregularity and curvature. Each point represents a single B scan. Red circles are from PVD eyes, and blue crosses from eyes with no PVD. There was a greater spread of values for curvature and irregularity from B scans of eyes with a PVD. However, analysis of this requires accounting for the nested nature of the data – that 12 scans belong to each eye[254].

Comparison of group shape features

Both range of curvature and range of irregularity differed significantly between the two groups (mean range of curvature difference between groups = 0.0088 mm^{-1}, p= 0.0028, 95% confidence intervals for difference between groups 0.0145 – 0.0031 mm^{-1}. Mean range irregularity difference = 1.114 mm, p = 0.043, 95% confidence interval of difference

between groups 0.0373 – 2.190 mm). Examples of maculae with high and low curvature ranges are shown in Figure 5.1.3.

Mean irregularity was significantly greater in PVD eyes (mean difference = 0.7643 mm, p = 0.0018, 95% confidence intervals 0.135-1.394 mm). Mean curvature was not different between the no PVD and PVD groups (mean difference = 0.0025 mm^{-1}, p = 0.43, 95% confidence intervals -0.0088 – -0.0038 mm^{-1}, Table 5.1.3).

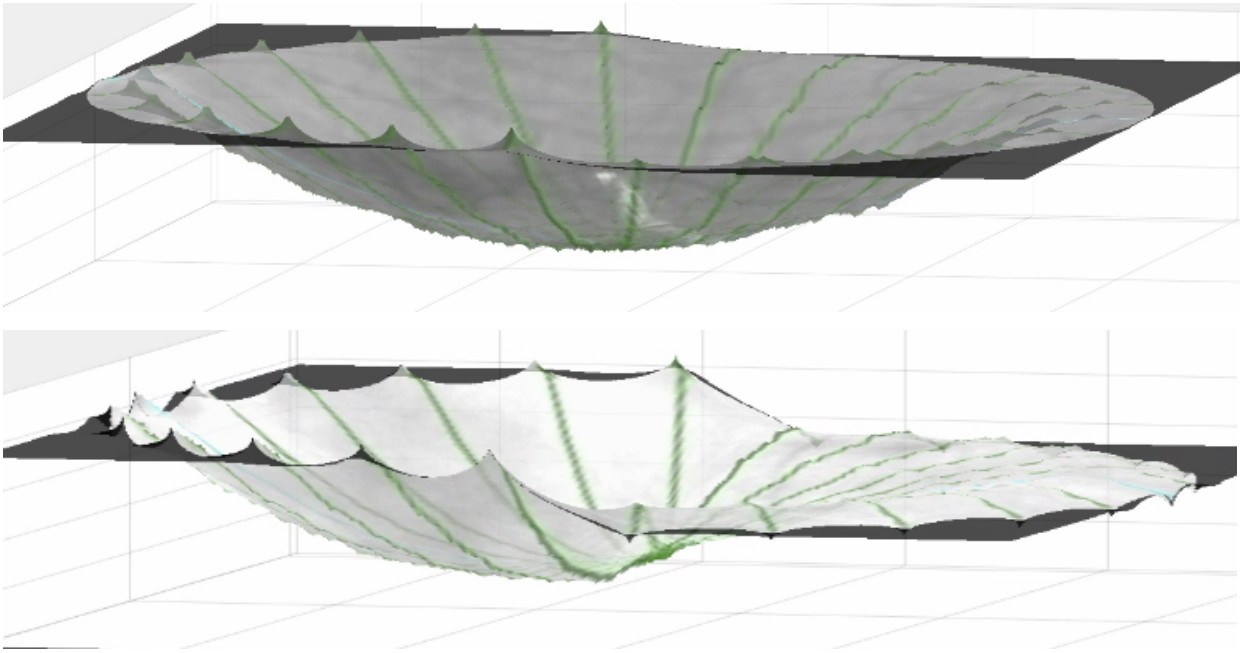

Figure 5.1.3. Three-dimensional reconstruction of maculae. A narrow range of macular curvature (top), and a wide range of macular curvature (bottom, myopic eye). The sides of the square tiles on the surface plane below the maculae are 1.2 mm. The tiles on the walls are 0.05 mm high.

Table 5.1.3. Comparison of macular curvature and irregularity in eyes with and without a PVD.

	Mean *K*	Range *K*	Mean irregularity	Range irregularity
No PVD	0.0243 +/- 0.0128	0.0156 +/-0.0071	2.577 +/- 1.091	2.370 +/- 1.417
After PVD	0.0268 +/- 0.0185	0.0244 +/- 0.0192	3.341 +/- 1.974	3.484 +/- 3.594
***p*-value**	0.43	0.0028	0.018	0.043

p-values determined with a two-sample *t*-test. K = curvature, SD = standard deviation. Units for curvature are mm^{-1}, and mm for irregularity.

Location of maxima and minima

Orientation of the B scan with the maximum curvature differed between PVD and no PVD eyes (maximal curvature scan orientation: PVD eyes 5.06 (anticlockwise of vertical), no PVD eyes 6.33 (clockwise of vertical), $p = 0.041$, see Figure 2.1). This significant value likely reflects the discrete nature of the B scan orientation variables (indices 1-12) and the small sample sizes, rather than a true shift in maximum curvature orientation. There were no other significant differences in B scan distribution of maximal and minimum curvature or irregularity between eyes with and without a PVD (two-sample *t*-tests, *p*-values = 0.21-0.95). Maximum and minimum curvature and irregularity did occur in all B scan orientations, but minimum curvature was most commonly in the horizontal meridian scan (Figure 5.1.4). The maximum curvatures were approximately orthogonal to the minimum, with a separation in maximum and minimum curvature of 60-120° (4-8 scans) in 88%, and 75-105° in 57%.

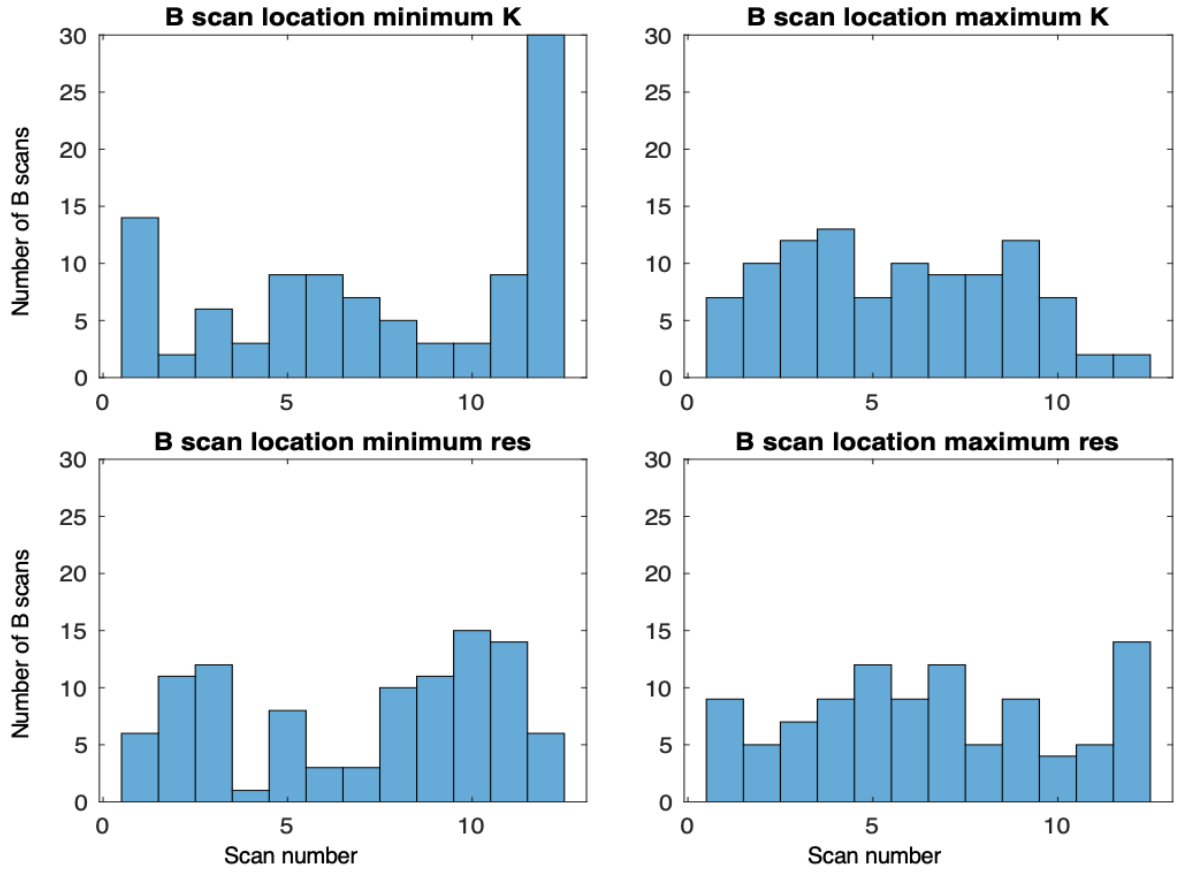

Figure 5.1.4. Location of maximum and minimum curvature and irregularity. Eyes with and without a PVD combined. The notable feature here was the minimum curvature was most commonly seen in the horizontal meridian (B scans 12, and 1). Scan 12 is the horizontal meridian B scan.

Conclusion

PVD eyes had greater average irregularity, and greater range of irregularity and curvature than eyes without a PVD. There was no significant difference in axial length or age between the two groups, suggesting these were not likely to be confounding factors.

5.1.2 Macular shape before and after macular hole repair

Methods

Participants attending retinal clinics in South Australia with an idiopathic full thickness macular hole between February 2019 and May 2021 were invited to participate. Radial HD OCTs centred in the fovea were taken prior to surgery, and the same scan protocol repeated after surgery once the intra-ocular gas had cleared and the macula was visualised (Figure

5.1.5). Intra-ocular gas typically takes up to 2 months to disperse and allow imaging of the macula after surgery, and post-operative imaging was performed as soon as possible after this within the clinical setting.

Macular hole eyes by definition have a break in the ellipsoid layer due to the hole in the per-operative images, and in the post-operative images if surgery was unsuccessful or structural recovery poor. For this zone, to stay parallel with the retinal contour, the retinal shape was taken as a line parallel to the retinal pigment epithelial layer/Bruch's membrane highly reflective band and continuous with the edges of the ellipsoid layer.

Statistical analysis

Comparison of pre- and post- operative observations was performed with a paired *t*-test. Two-sample *t*-tests were performed to compare the pre-operative macular hole shape to the sample of eyes with no PVD and no macular hole, to investigate whether the presence of the macular hole had affected shape. For all tests significance was set at $p \leq 0.05$.

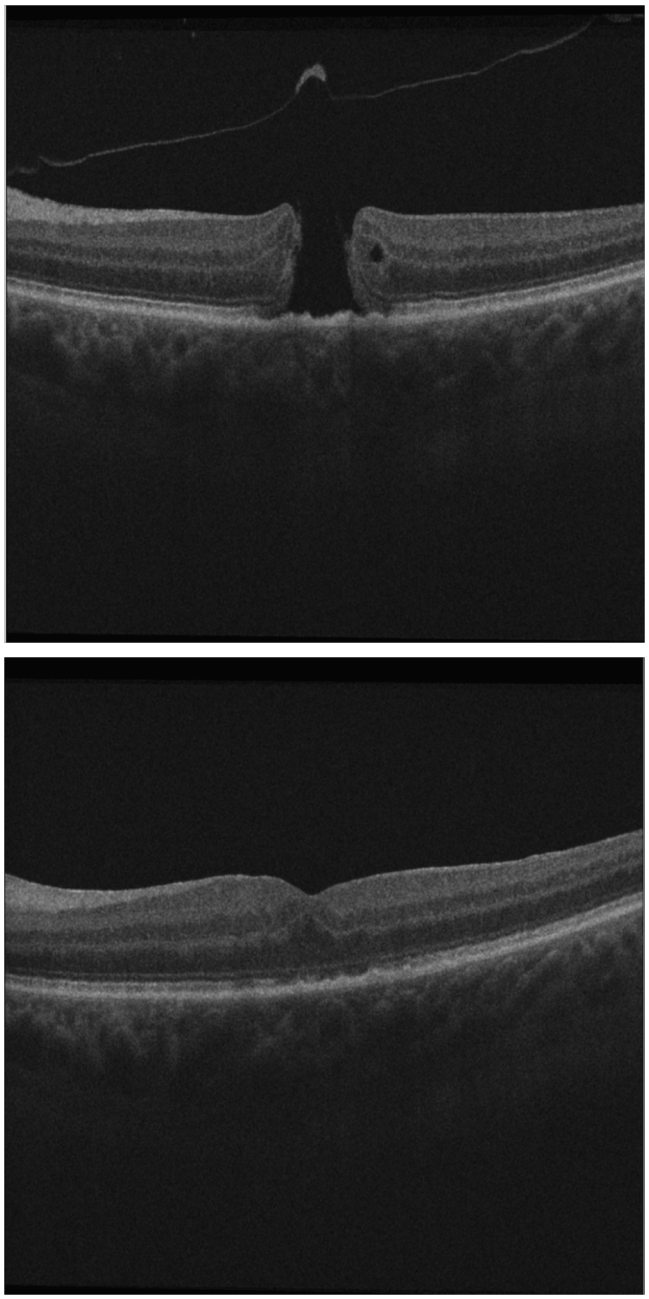

Figure 5.1.5. Macular hole prior to surgery (top), and after surgical closure (bottom).

Results

Twenty seven eyes were imaged before and after surgery: ten right eyes, seventeen left eyes, eighteen female, nine male, with average age 70 (range 56-90) years and axial length 23.87 (22.01 – 30.24) mm. Twenty three eyes were surgical successes (hole closure) with a single procedure, with one eye (a highly myopic eye) a success after a second procedure. Individual B scan curvature and irregularity distribution are shown in Figure 5.1.6.

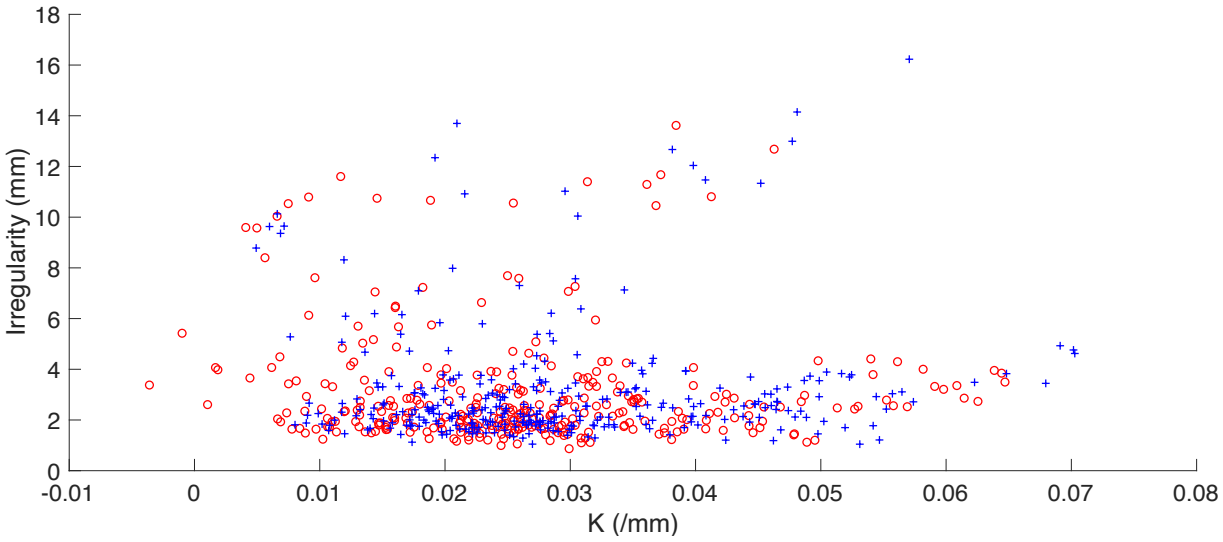

Figure 5.1.6. Scatter plot of B scan irregularity and curvature, macular hole eyes. Each point represents a B scan from pre-operative eyes (blue crosses), or post-operative eyes (red circles).

There was no difference in range of curvature or irregularity, pre- versus post- operation (mean difference in range of curvature between groups = 0.0006 mm^{-1}, $p_K = 0.24$. Mean difference in range of irregularity between groups = 0.0083 mm, $p_{irr} = 0.96$, two-sample *t*-tests, Figures 5.1.7 and 5.1.8).

There was a statistically significant difference between mean curvature pre-operation and mean curvature post-operation (difference between groups = 0.0025 mm^{-1}, $p_K = 0.04$), with no difference in mean irregularity pre- to post- operation (difference between groups = 0.089 mm, $p_{res} = 0.25$).

Comparing macular mean and range of curvature and irregularity between pre-operative macular hole eyes and 45 eyes without a macular hole with no PVD (eyes from the cross-sectional group in section 5.1.1, above): there was no significant difference between macular hole eye shape before surgery and the macular shape of eyes without a PVD. Difference in the mean irregularity between these groups was neither statistically significant when the highly myopic macular hole eye was included ($p = 0.058$), or excluded ($p = 0.16$, Table 5.1.4).

Table 5.1.4. Comparison between pre-operative and post-operative macular curvature and irregularity for macular hole eyes.

	Mean *K*	Range *K*	Mean irregularity	Range irregularity
MH	0.029 +/- 0.011	0.016 +/- 0.0076	3.17 +/- 2.18 [2.82*]	2.45 +/- 1.80
Post op MH	0.026 +/- 0.012	0.016 +/- 0.0082	3.08 +/- 2.04	2.46 +/- 1.82
***p*-value**	0.04	0.24	0.25	0.96
no PVD	0.024	0.0150	2.48	2.31
***p*-value**	0.10	0.61	0.058 [0.16*]	0.68

The first three rows report the comparison of pre-operative macular shape to post-operative macular shape in eyes with a full-thickness macular hole. The lower two rows provide information on a sample of eyes without a PVD and their comparison to the pre-operative macula hole images (bottom row). The "no PVD" group (n = 45) differs slightly from that presented in Section 5.1.1: the latter included 6 fellow eyes from participants with a macular hole which were removed from this analysis. * Indicates mean pre-operative irregularity and *p*-value excluding one highly myopic macular hole eye (axial length 30.24 mm). K = curvature, MH = macular hole. Units for curvature are mm^{-1}, and mm for irregularity.

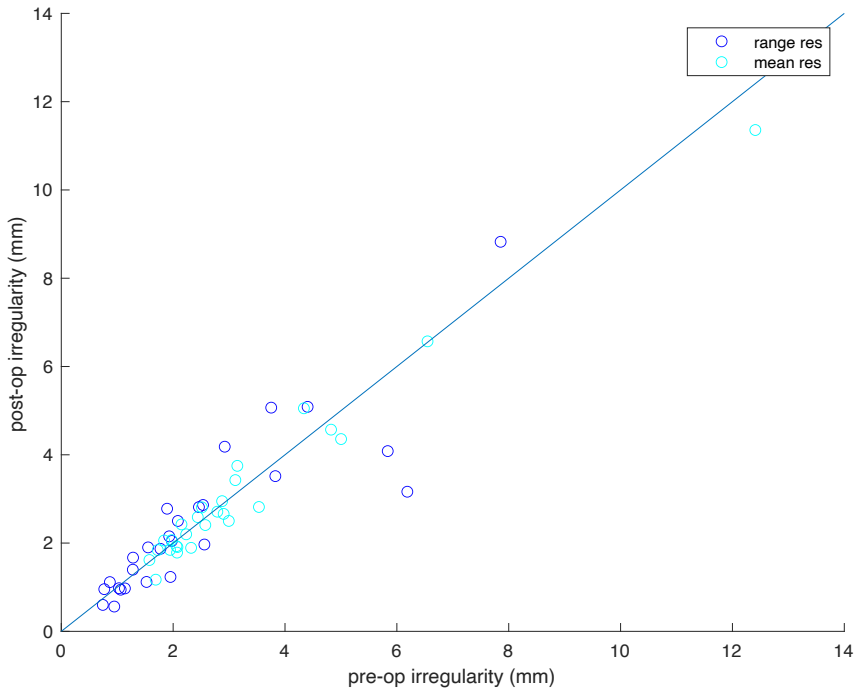

Figure 5.1.7. Pre-operative and post-operative macular hole irregularity. There was no difference in irregularity between the pre-operative and post-operative state for these eyes (Table 5.1.5).

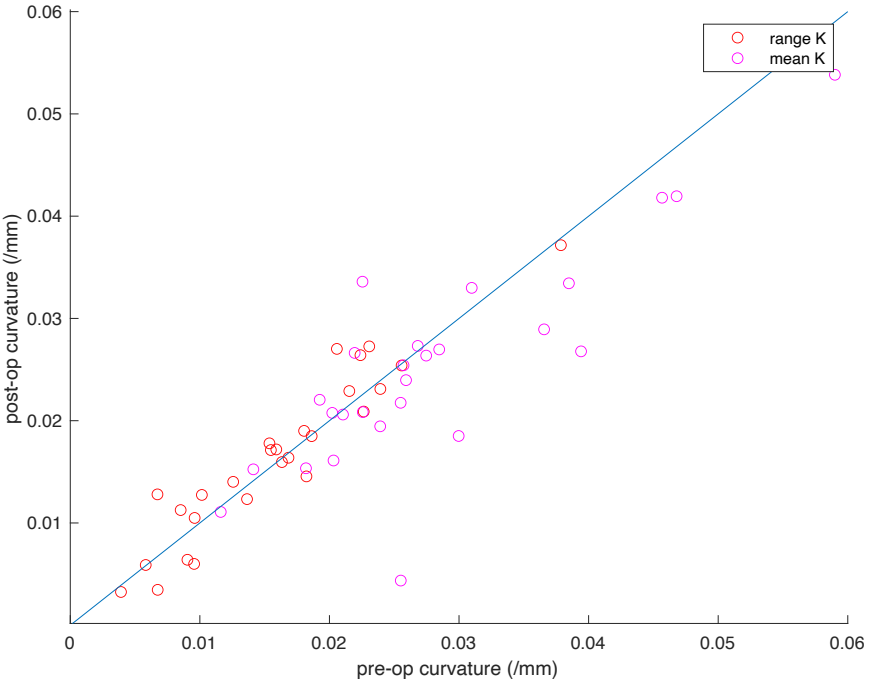

Figure 5.1.8. Curvature before and after surgery for macular hole. Scatter plot of post-operative mean and range of curvature against pre-operative mean and range of curvature for macular hole eyes, with the pre-op = post-op line drawn in blue. There was a statistically significant difference between mean curvature pre-op and mean curvature post-op (difference between groups = 0.0025 mm^{-1}, $p_K = 0.04$), but no difference in range of curvature pre- versus post- operation (mean difference in range curvature between groups = 0.0006 mm^{-1}, $p_K = 0.24$). K = curvature.

Location of maximum and minimum shape metrics

The locations of the maximum and minimum values of curvature and irregularity are shown in Figure 5.1.9. There was no difference in the orientation of maximum and minimum curvature and irregularity comparing pre-operation to post-operation macular hole eyes (p_k = 0.73, p_{res} = 0.41). In 50% of cubes the maximum and minimum curvature and in 37% of cubes (n = 20) the maximum and minimum irregularity were 5-7 scans apart (90° +/- one scan separated by 15°), making the maxima and minima approximately perpendicular to each other. In 60% of cubes irregularity and in 72% of cubes curvature were 4-8 scans (60-120°) apart.

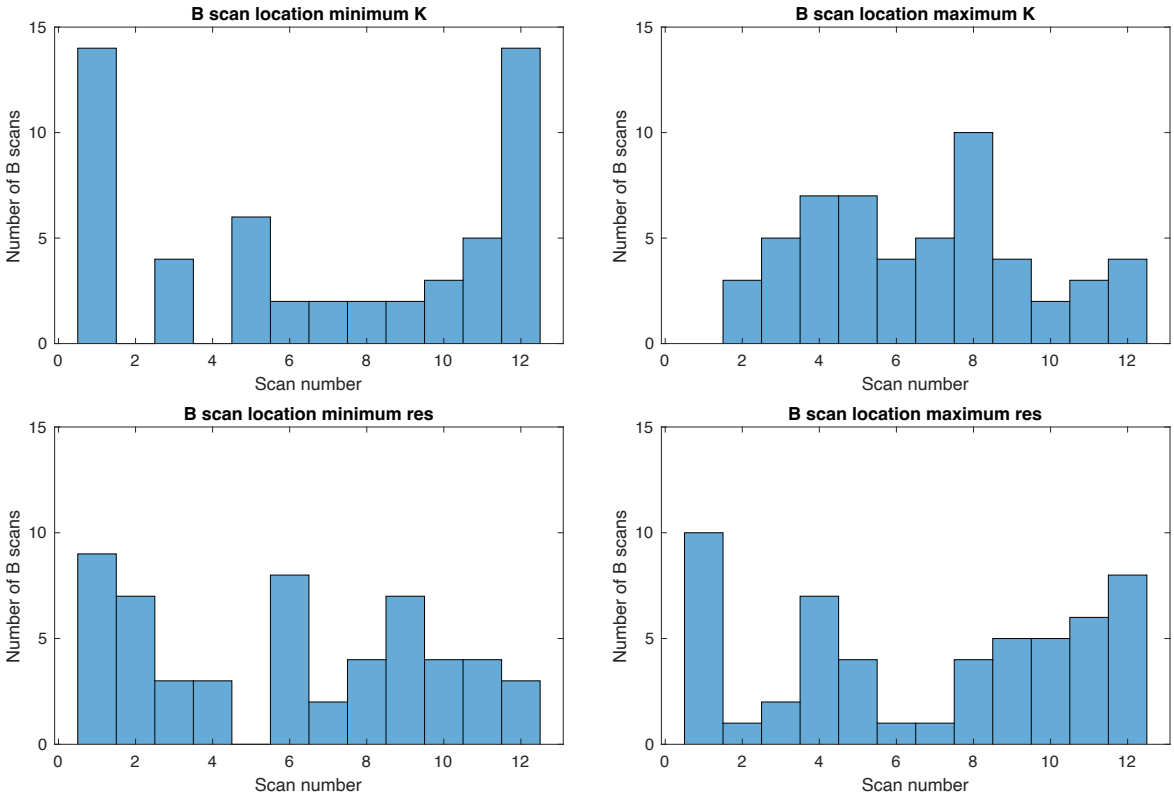

Figure 5.1.9. Shape metric location, macular holes. Histograms of the location of the maximum and minimum curvature and irregularity values of all the macular hole radial scans. The most notable finding is again that the minimum curvature was most commonly seen in the horizontally oriented scans (1 and 12, top left chart). K = curvature, res = irregularity. See Figure 2.1 for the scan number key.

Conclusions

The only difference in retinal shape found in comparing eyes before and after macular hole surgery involving posterior hyaloid detachment was a larger mean curvature found before

surgery compared to after surgery. It is possible, then, that surgery or PVD leads to a small reduction in the curvature of the macular shape. There was no significant difference between eyes with a macular hole before surgery and eyes without a PVD but no macular hole. This suggests there was nothing unique in shape in macular hole eyes, and that the radial and tangential traction from the posterior hyaloid face hypothesised to cause macular holes does not affect shape.

5.1.3 Macular shape before and after PVD

Methods

Eyes were imaged in retinal clinics at Flinders Medical Centre or Eyemedics, Adelaide. Participants were recruited if they attended with a new onset PVD where the eye had already had HD radial macular scans performed at a previous visit as part of normal clinical care.

Statistical analysis

Comparison of before and after PVD observations was performed with a paired *t*-test, with significance set at $p \leq 0.05$.

Results

Eighteen eyes were identified and imaged between December 2019 and February 2022: eight right, ten left eyes, described in Table 5.1.5.

There was no difference overall in mean and range of curvature and irregularity, comparing macular scans before and after PVD (Table 5.1.6), with little within-eye change in irregularity (Figure 5.1.10) or curvature (Figure 5.1.11).

Table 5.1.5. Eyes imaged before and after PVD.

Eye	Age	Interval between images (months)	Reason for initial attendance
V1 60	71	2	diabetic eye disease
V2 61	62	8	eye check - NAD
V1 62	76	11	fellow eye macular hole
V1 63	70	2	cataract
V1 64	69	4	ARM
V2 65	71	6	cataract
V2 66	66	9	fellow eye to retinal detachment
V2 67	52	11	Retinal tear fellow eye
V2 68	63	2	PVD other eye
V1 69	69	3	diabetic eye disease
V2 70	74	19	Fellow eye VMT
V2 71	60	2	fellow eye to retinal detachment
V2 72	56	20	Glaucoma review
V1 73	75	12	Glaucoma review
V2 74	70	17	Glaucoma review
V2 75	73	14	Post cataract surgery
V1 76	69	4	ARM
V1 77	75	10	Fellow eye to cataract surgery

NAD = no abnormality detected, ARM = age-related maculopathy, VMT = vitreo-macular traction. Age is at time of first examination in years.

Table 5.1.6. Comparison of macular curvature and irregularity from eyes before and after PVD.

	Mean K	Range K	Mean irregularity	Range irregularity
Pre-PVD	0.020 +/- 0.017	0.019 +/- 0.011	3.81 +/- 2.27	3.35 +/- 2.14
Post PVD	0.020 +/- 0.019	0.020 +/- 0.011	3.81 +/- 2.04	3.51 +/- 2.28
***p*-value**	0.92	0.83	0.92	0.07

K = curvature, SD = standard deviation. Units for curvature are mm^{-1}, and mm for irregularity.

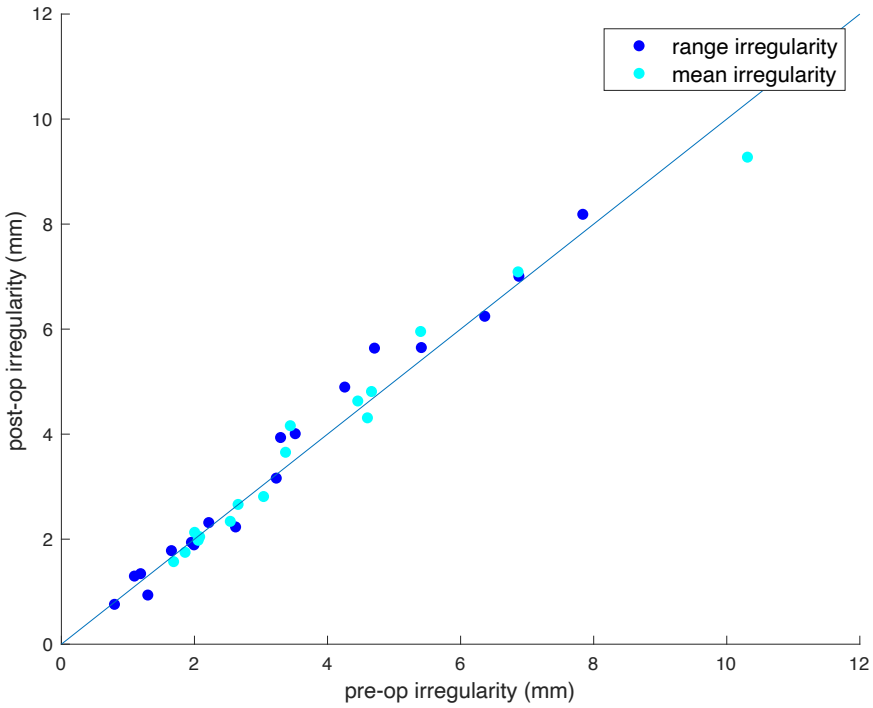

Figure 5.1.10. Macular irregularity before and after PVD. There was no significant difference in macular irregularity in these eyes imaged before and after spontaneous PVD, with the line of no change drawn in blue. (Table 5.1.6).

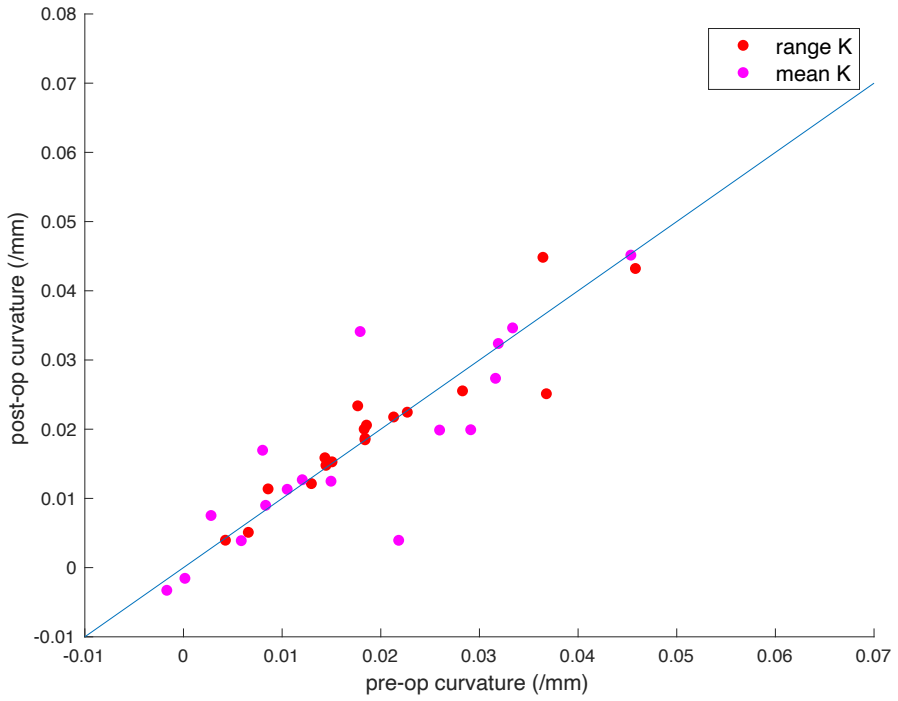

Figure 5.1.11. Macular curvature before and after PVD. Scatter plot of mean and range of curvature before and after spontaneous PVD, with the line of no change drawn in blue. K = curvature.

Conclusion
There was no difference in the shape metrics of macular scans in these eyes, when comparing images taken before PVD to after PVD. This result particularly differs from the findings of cross-sectional analysis comparing eyes with a PVD to those without, presented in Section 5.1.1. Irregularity was high in this group, most likely due to a mixed pathology including age related maculopathy with the presence of drusen.

The maxima and minima were evenly distributed around the 12 radial B scans except for the minimum curvature, which was again most commonly seen in the horizontally oriented scan. This is the scan orientation most commonly examined in clinical practice, and the flattest overall. The separation of maximum and minimum curvature was "regular", or approximately perpendicular to each other, in more than half of the eyes.

Discussion

The third cohort, that of eyes imaged both before and after spontaneous PVD, found no difference in macular shape metrics from development of PVD, despite having some heterogeneity in comorbidities. While perhaps high quality data in terms of no (potentially confounding) surgical intervention and a paired sample, this was from the smallest sample of the three groups. Section 5.1.2 provided data that the only intra-eye change in shape metrics after surgically induced PVD and macular hole closure was a reduction in curvature after surgery. While cataract surgical incisions alter corneal curvature, incisions for vitrectomy are smaller and far from the posterior pole, and are known not to alter refraction and hence have little effect on the (more proximal) corneal shape[255,256]. It therefore seems improbable that the vitrectomy itself influences posterior curvature or irregularity. The cross-sectional data (comparing eyes with a PVD to eyes without) in Section 5.1.1 had the largest sample size and found differences in mean irregularity and range of curvature and irregularity – essentially the opposite of the macular hole group.

The coefficient of variation of all these parameters was high: 0.42 – 1.03 for irregularity, and 0.44 – 1.02 for curvature. A power calculation, based on α = 0.05 with an 80% chance of

detecting a difference between the two groups from Section 5.1.1 (PVD and no PVD eyes) requires 210 eyes to detect a real difference for irregularity, and 1720 eyes for curvature. Using the pre- and post- operative macular hole data finds 746 eyes for curvature and 16,640 for irregularity would be required to detect a difference between the groups. For the eighteen eyes in 5.1.3 (before and after PVD), 554 822 samples would be required for curvature and 28 028 758 eyes for irregularity to detect a difference. The large sample size required to detect a difference suggests the effect of PVD on curvature and irregularity is small, and that the significant findings in these analyses were spurious[257]. The shape differences seen in the cross-sectional group (Section 5.1.1) most likely reflect inter-eye variation in metrics rather than actual PVD effects (see Figure 5.1.12). It is concluded that PVD has little effect on macular curvature, and even less effect on irregularity.

The fellow eyes from participants who had experienced a retinal detachment in one eye have been imaged as part of this project, and five individuals to date have re-presented with a PVD or retinal detachment and volunteered for repeat imaging. The comparison of these eyes is described in section 5.3, which provides further information about the effects of PVD (and surgery for retinal detachment) on shape.

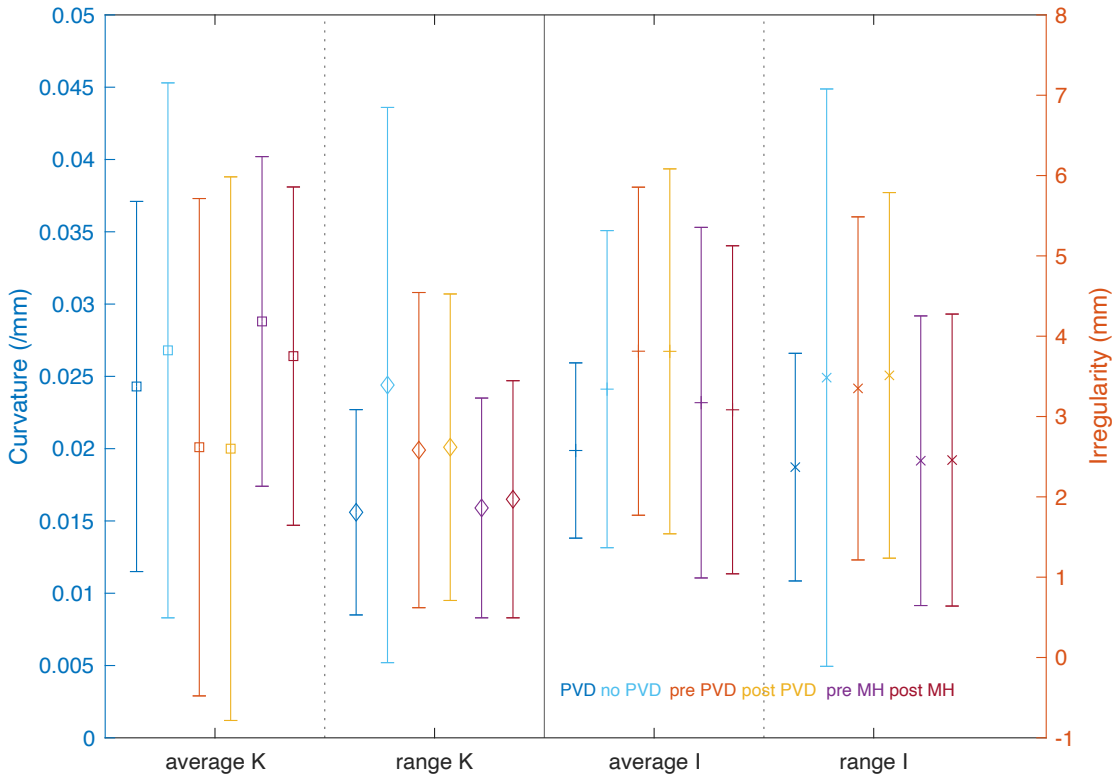

Figure 5.1.12. Summary of macular shape features. The average and range of curvature (left axis) and irregularity (right axis), for the six groups (identified by coloured names along the bottom of the chart) compared in sections 5.1.1-3, with +/- one standard deviation error bars for each value. For each comparison pair the measures were similar, with wide error bars confirming there was insufficient power for conclusions to be drawn. K = curvature, mm^{-1}, I = irregularity, mm.

5.2. Classification of retinal detachment and PVD eyes using shape

Introduction

Retinal shape irregularity and axial length both correlate with increasing myopia. Myopia itself is a major risk factor for development of retinal detachment after PVD, but axial length alone is not specific enough to predict retinal detachment. This section investigates whether a combination of these retinal shape features and axial length can differentiate between retinal detachment and PVD. If this is possible, and if PVD itself does not alter retinal shape, then it may be possible to predict retinal detachment before the PVD has occurred.

This section compared regional retinal shape in OCT images of eyes that have had a retinal detachment with those that have had PVD. The comparison was used to identify features to train a machine learning classifier (using quadratic discriminant analysis) to discriminate between retinal detachment and PVD eyes. The classifier was generated with a training set of eyes that had either experienced a retinal detachment or an uncomplicated PVD. The models were then tested with a separate validation set of PVD and retinal detachment eyes from the same sample. Although this chapter does not describe a fully developed test for retinal detachment, results are presented that comply with the recommendations of the STARD initiative reporting standards for studies of tests of diagnostic accuracy[258]. As there is no test for retinal detachment, there is no reference test available for comparison of effectiveness[259].

An agnostic approach to feature selection was used, looking for maximal points of difference in the anomaly spectrum between retinal detachment and PVD eyes in the feature identification set to use as algorithm predictors.

Aim

The aim of this section was to develop a classifier that can separate eyes that have had a retinal detachment from eyes that have experienced a PVD.

Methods

Retinal breaks are not uniformly distributed around the retinal periphery, but more commonly found superiorly and temporally[260]. Retinal irregularity has a different pattern of distribution, with the greatest value found inferiorly. To explore if irregularity in different areas of the eye differs in retinal detachment and PVD eyes, the approach used was to explore the average B scan anomaly spectrum and select as features those points in individual region spectra that had the greatest difference between retinal detachment and PVD eyes, without prior assumptions as to where or what these should be. The first step was to explore the distribution of anomaly within the retinal detachment and PVD eyes. The aim was to review all the anomaly data to identify areas of larger difference between the two groups that might be useful for training a classifier.

Subjects

Participants were recruited from ophthalmology clinics in South Australia between October 2016 and February 2021. Three groups were collected; eyes that had had an uncomplicated acute symptomatic PVD confirmed by a retinal specialist, eyes that had undergone vitrectomy without scleral buckling for rhegmatogenous retinal detachment, and eyes that had laser retinopexy to treat a PVD related tear without retinal detachment. Retinal tear eyes were maintained as a distinct group from retinal detachment eyes due to their different clinical presentation. The reasoning behind this is presented in the discussion. Only one eye from any participant was used for training or testing.

Classifier development

The process of image acquisition and feature generation was as described in the methods in Chapter 2. B scan anomaly spectra, curvature, age, and axial length were taken from PVD and retinal detachment eyes. Forty of the PVD eyes were also used in the description of the distribution of irregularity and to investigate the correlation between axial length and shape irregularity (Chapters 3 and 4).

Classifier development progressed through a feature selection – training – testing process. Feature identification was performed with the training set of eyes, with a separate validation set preserved for testing (`Regdescr`, `Regdescre3D`). Once the best features were selected, the classifier was trained, then tested with the validation set of eyes (`BSspec`). The training set consisting of 45 PVD and 35 retinal detachment eyes, which was approximately two-thirds of the initial sample of eyes. Ongoing recruitment of subjects enlarged the testing sets. The classifier was further tested with retinal tear eyes as an independent validation set. Five-fold cross-validation of the classifier was performed with the same training set of 80 eyes, using a test fold of 20% on classifiers generated by 80%, and run 100 times to determine the standard deviation of the model success rate (`ClsXval`).

Statistical analysis

The two-sample *t*-test was used to check for similarity between group demographics. Model performance is presented in a 3 x 2 table, with a two-tailed Fisher's exact test used to test the probability of non-random distribution of classification between retinal detachment and PVD groups. Accuracy was defined as number of PVD eyes labelled '1' plus the number of retinal detachment eyes labelled '2' divided by the total number of eyes.

Single variable models

Axial length was the most successful single variable classifier, with larger axial length known to increase the risk of retinal detachment. To test whether axial length alone was sufficient to enable classification of eyes, a single variable classifier using axial length was tested for sensitivity and specificity in identifying retinal detachment eyes.

Test reliability

A subset of eyes was imaged twice with no change in their ocular status, and each imaging set tested independently. This was to explore the stability of classification with repeat imaging. While it could be concluded from Chapter 3 that shape analysis is reliable, it was noted that variations in gaze direction (Section 3.3) potentially introduced some variability, at least between individuals. Furthermore, even with an individual following gaze

instructions consistently, movement of the sampling cube window antero-posteriorly might alter the area of retina sampled (see Methods – cube locations, Figures 2.2 and 2.3).

Group weighting

Weighting the probability of allocating a label to an observation can be done by altering the prior probability allocated to each group. By default, this is set to the relative number of each group in the training set, and is found and changed within the classifier by altering the '`Prior`' input to the classifier `fitcdiscr` in MATLAB. For example, if both groups were equally common, weighting would be [0.50 0.50]. Weighting for optimal classifier performance was explored using the training set, before testing with the validation set. Prior probability was evaluated across the range [1-Wt Wt] for [PVD RD] with Wt = 0.01 – 0.99 in increments of 0.01 (`CreROCTS`).

Results

Demographics

Ninety-seven eyes of individuals who had presented with an acute symptomatic PVD were recruited after examination by a retinal specialist. A second group of 99 eyes had undergone vitrectomy for a PVD-associated retinal detachment without scleral buckling. There were 68 eyes in the retinal tear group. There were 134 right eyes, 130 left eyes, with 159 male participants and 105 females. Participant demographics are presented in Table 5.2.1, and mean age and axial length of the groups are presented in Table 5.2.2. Eyes that had suffered a retinal detachment had a significantly longer mean axial length than PVD eyes, and were from significantly younger individuals. The mean axial length of eyes with a retinal tear was shorter than for the retinal detachment group eyes, but longer than for eyes with PVD, with no difference in age.

Table 5.2.1. Participant demographics.

	Sex		Laterality		Ethnicity*
	M	F	R	L	
PVD	50	47	50	47	Black American (1)
Retinal detachment	72	27	51	48	South Asian (1)
Retinal tear	37	31	33	35	South Asian (1)

* Only non-Caucasian ethnicities listed. All ethnicities self-reported.

Table 5.2.2. Subject demographics (study variables).

		Age - years (+/-SD)	AL - mm (+/-SD)
PVD	Training set (n=45)	64.5 +/- 6.6	24.08 +/- 1.10
	Test set (n=52)	66.2 +/-5.1	24.36 +/- 1.24
	All (n=97)	65.3* +/- 5.9	24.23† +/- 1.18
Retinal detachment	Training set (n=35)	63.1 +/- 7.4	25.10 +/- 0.98
	Test set (n=64)	61.4 +/- 9.5	25.09 +/- 1.33
	All (n=99)	62.1* +/- 8.8	25.09† +/- 1.21
Retinal tear	All (n=68)	64.1‡§ +/- 6.2	24.62$^{\|\|\#}$ +/- 1.28

Mean age and axial length (AL) for the three groups, subdivided where appropriate into training set and validation set. Age is in years, with axial length in millimetres. Comparison of all retinal detachment eyes to all PVD eyes: * age: p=0.0027, † axial length: p<0.005 (0.00000115). RT eyes to all PVD eyes. ‡Age: p = 0.18, $^{\|\|}$ axial length: p = 0.04. RT eyes to all retinal detachment eyes. §Age: p = 0.09, $^{\#}$ axial length: p = 0.01 (two sample t-test). RT = retinal tear eyes, PVD = posterior vitreous detachment eyes, SD = standard deviation.

Feature exploration: higher magnitude anomaly values

As noted in Chapter 3, the majority of B scans exhibit very low irregularity, and this pattern was repeated in the B scans in these eyes (Figures 5.2.1 & 5.2.2). This will significantly influence any average values taken from areas of the eye. Initial analysis was therefore focused on B scans with total anomaly over a threshold determined by the observed

distribution. To explore the irregularity of the eye for feature selection, only B scans with total anomaly > 5 mm were used for feature selection, although all scans were used for training and testing.

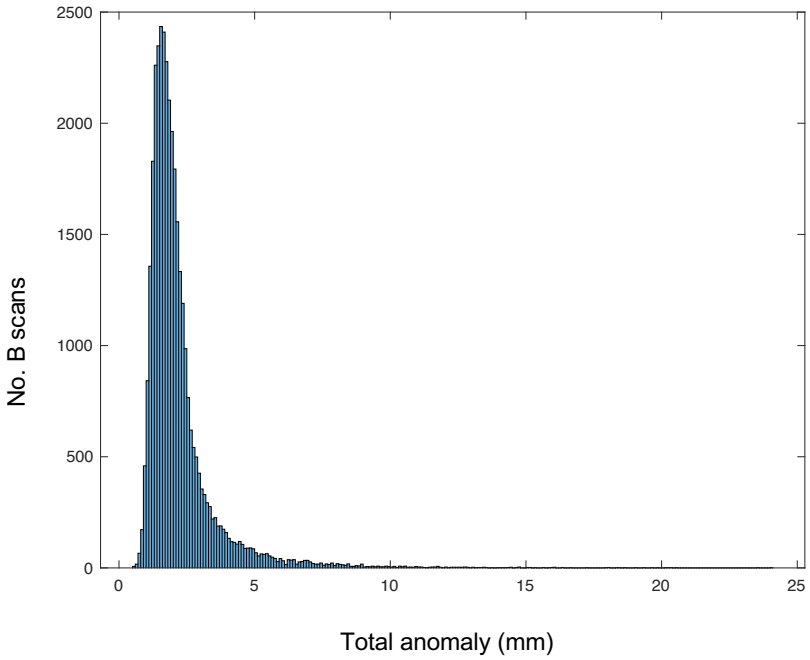

Figure 5.2.1. Histogram of the distribution of B scans by total anomaly value. Only 3.4% of B scans had total anomaly > 5 mm, and 35.7% had total anomaly > 2 mm. These data are from the retinal detachment and PVD group eyes in this section. *x*-axis is B scan total anomaly (mm), *y*-axis number of B scans with that anomaly.

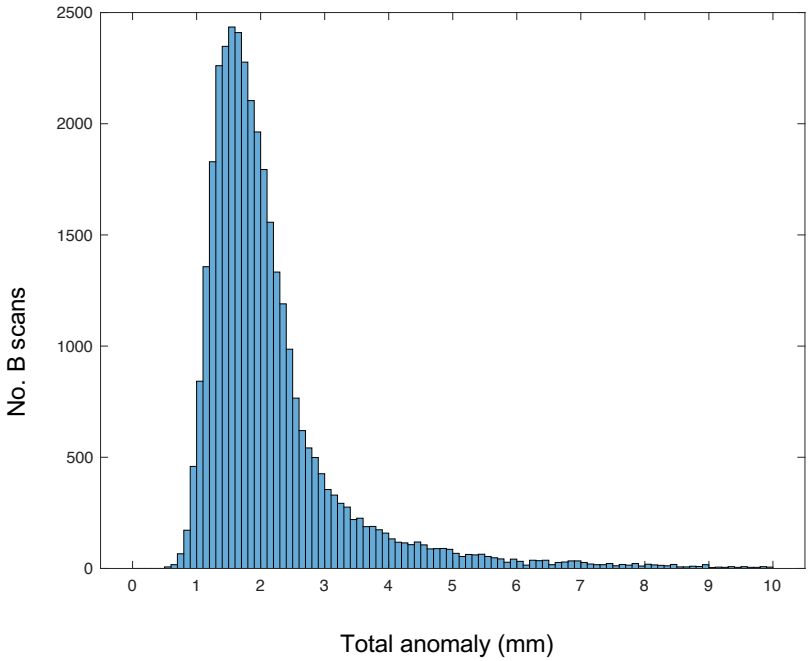

Figure 5.2.2. B scan anomaly distribution. The same histogram in Fig 5.2.1 limiting the *x*-axis to total anomaly 0-10 mm to illustrate distribution at these lower values. *x*-axis is total anomaly (mm), *y*-axis number of B scans with that anomaly.

Figure 5.2.3 below presents the histogram of the bin indices of *peak* anomaly (the frequency bin location in each scan with the greatest anomaly) for B scans from retinal detachment and PVD eyes with total anomaly > 5 mm. Peak anomaly shows very little difference in distribution between diagnostic groups across the B scan spectra, except for a slight increase in higher bin/frequencies for peak anomaly for retinal detachment eyes.

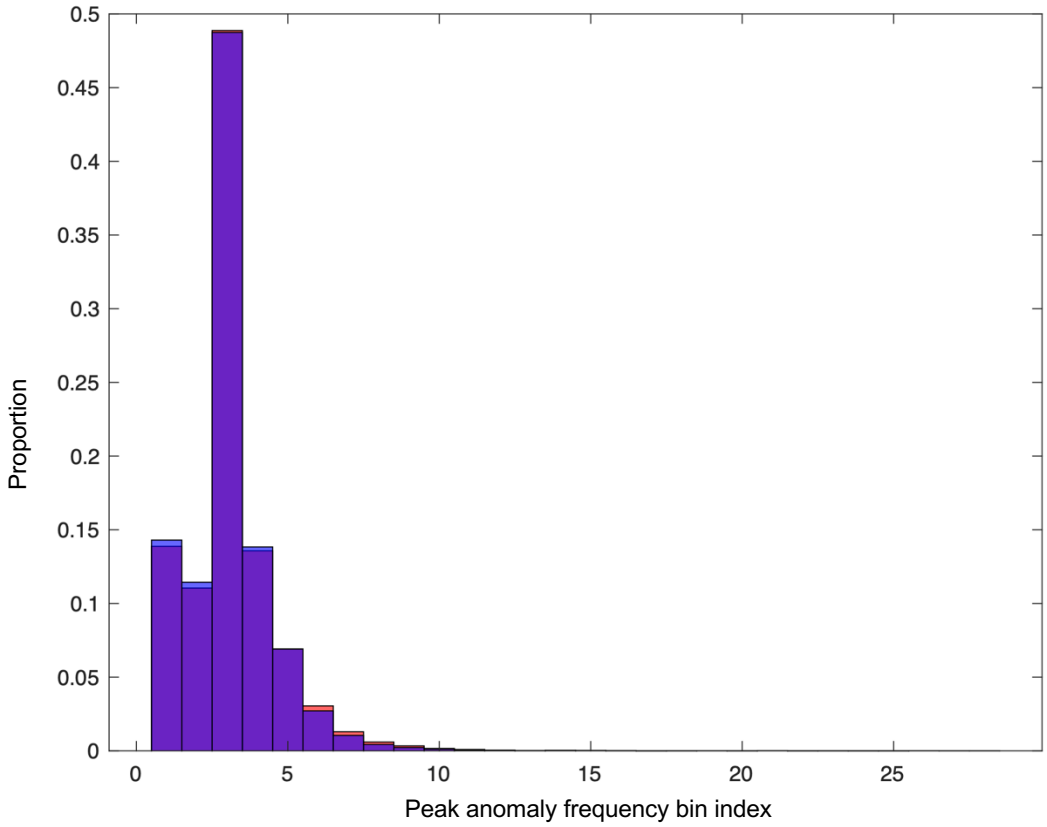

Figure 5.2.3. Peak anomaly indices. Histogram of the bin index location of the largest single frequency bin (peak anomaly) for retinal detachment and PVD eye B scans. This includes all B scans from all regions. The *y*-axis is normalised to compare the distribution of peak anomaly between the two groups. There was very little difference between the groups, and in both diagnostic groups peak anomaly was most commonly in bin 3. PVD eyes shown in blue, retinal detachment eyes in red: the purple colour arises from the overlap of the two.

Figure 5.2.4 presents the regional distribution of frequency bin indices of peak anomaly (the bin location of peak anomaly within the eye, a breakdown of Figure 5.2.3 into individual

regions) for retinal detachment and PVD groups, with again little difference. From these two figures it can be concluded that peak anomaly varies little between the two groups.

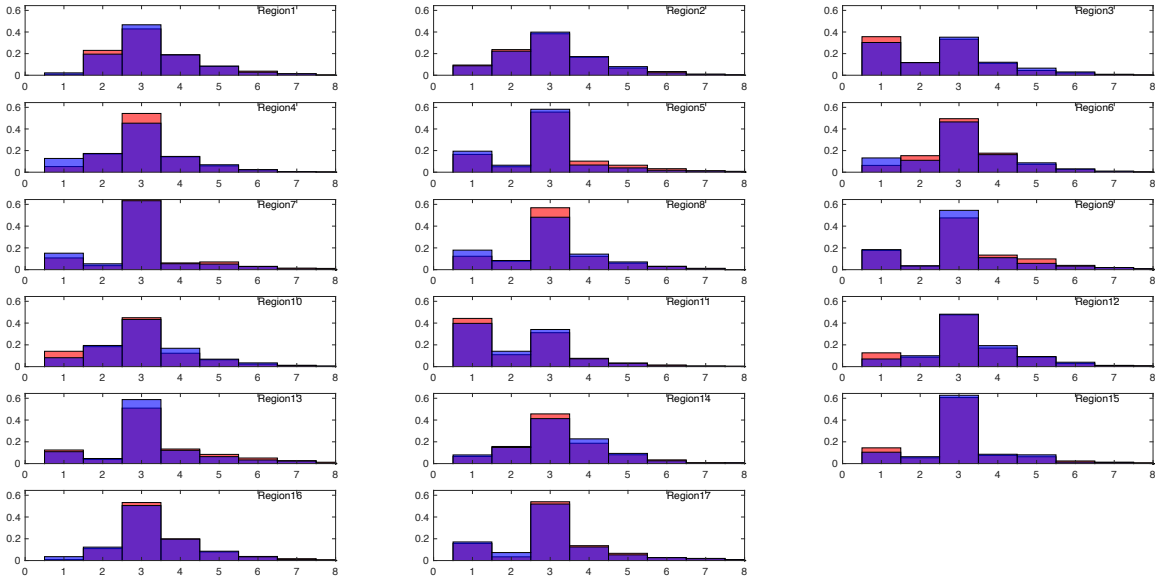

Figure 5.2.4. Peak anomaly bin index distribution by region. While there are some differences in distribution between regions there is little difference between retinal detachment and PVD groups. PVD in blue, retinal detachment in red, the purple colour comes from the overlap of the two.

The number of B scans by region that have total anomaly greater than 5 mm for retinal detachment eyes were (shown as for a right eye: the macular region is positioned centrally in bold type, and the supero-temporal region the top-left number):

253		403		213
	124	119	27	
156	79	**50**	105	175
	145	168	157	
228		618		246.

And for PVD:

292		389		254
	189	111	62	
207	181	**50**	134	139
	241	98	96	
268		615		224

For all gaze directions there were more B scans with greater anomaly in the distal regions compared to the proximal regions.

All-of-eye B scans, with anomaly > 5 mm

The average normalised all-of-eye anomaly bin distribution for retinal detachment and PVD eyes is shown in Figure 5.2.5, with larger differences seen in bins 1-6, and the largest difference in bin 2.

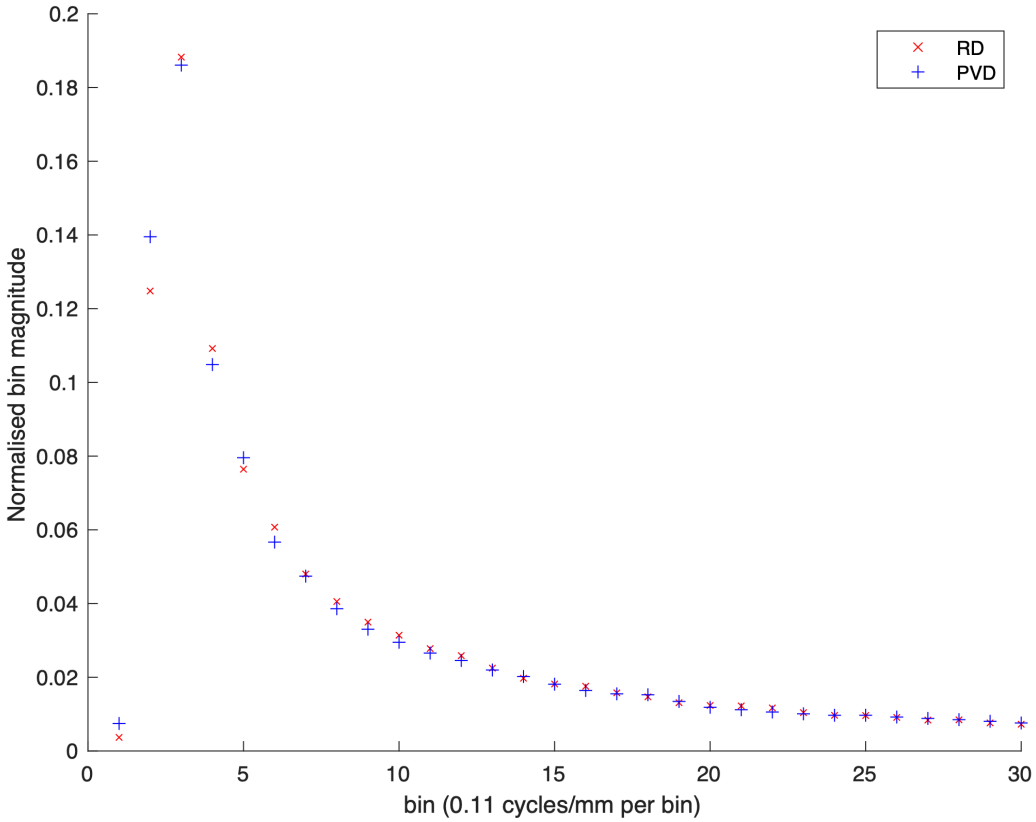

Figure 5.2.5. Mean normalised anomaly spectrum. The average anomaly spectrum of retinal detachment and PVD eyes is shown, including only B scans where total anomaly > 5 mm. RD = retinal detachment.

The non-normalised (absolute bin difference from the average B scan value) distribution is shown in Figure 5.2.6.

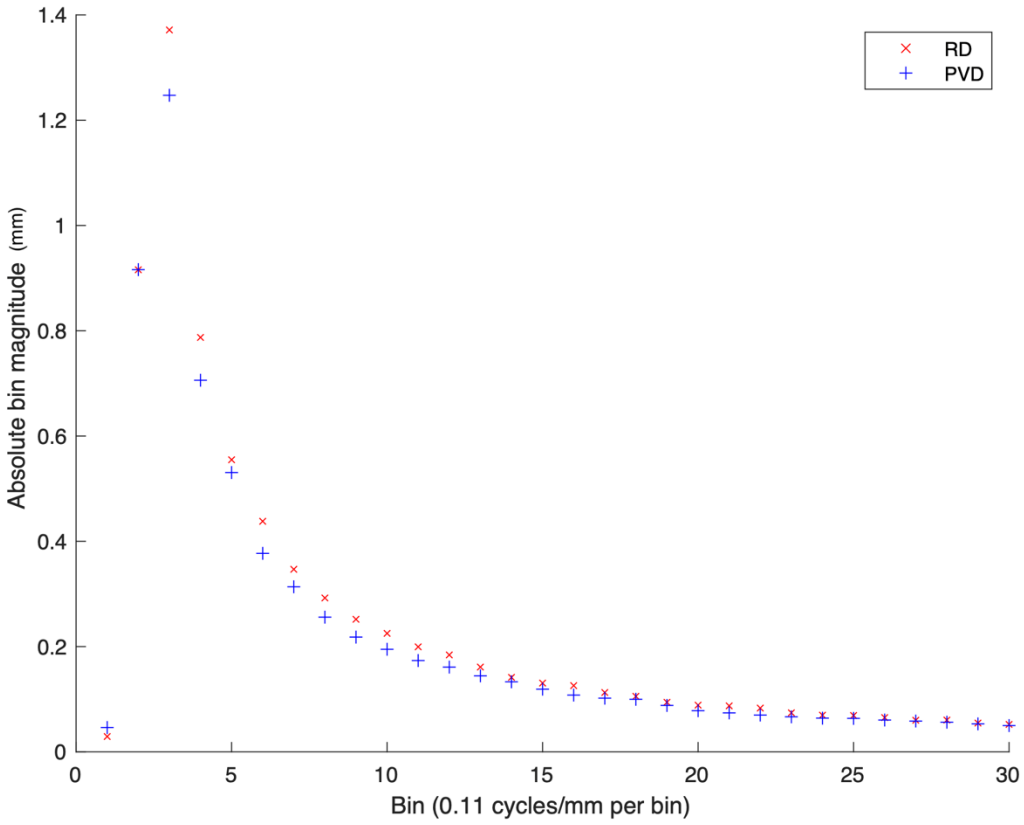

Figure 5.2.6. Mean anomaly spectrum of retinal detachment and PVD eyes. Retinal detachment (RD) eyes have a greater average anomaly than PVD eyes, with the largest differences in bins 3, 4, and 6. Includes only B scans where total anomaly > 5 mm.

From the above, it can be seen the number of larger total anomaly scans (Figures 5.2.1 & 5.2.2) was similar to the group of eyes analysed in Chapters 3.4 & 4 (Figure 3.14), with most B scans having total anomaly < 5 mm. The distribution around the eye of higher total anomaly scans was similar in the retinal detachment and PVD groups. The bin index of maximum anomaly was similar between retinal detachment and PVD eyes (Figures 5.2.3 & 5.2.4). However, differences were apparent between the groups within the anomaly spectrum (Figures 5.2.5 & 5.2.6). These differences were explored for feature selection.

Feature identification

Features were identified from regions using only B scans with total anomaly > 5 mm, by looking for regional differences between retinal detachment and PVD group average anomaly spectra.

Regional differences, anomaly > 5 mm

Regional normalised (total anomaly =1) anomaly spectra for retinal detachment and PVD eyes are shown in Figure 5.2.7. The figure is repeated, with unified axes ranges and bins 11-30 removed to concentrate on the information in bins 1 - 10 (Figure 5.2.8).

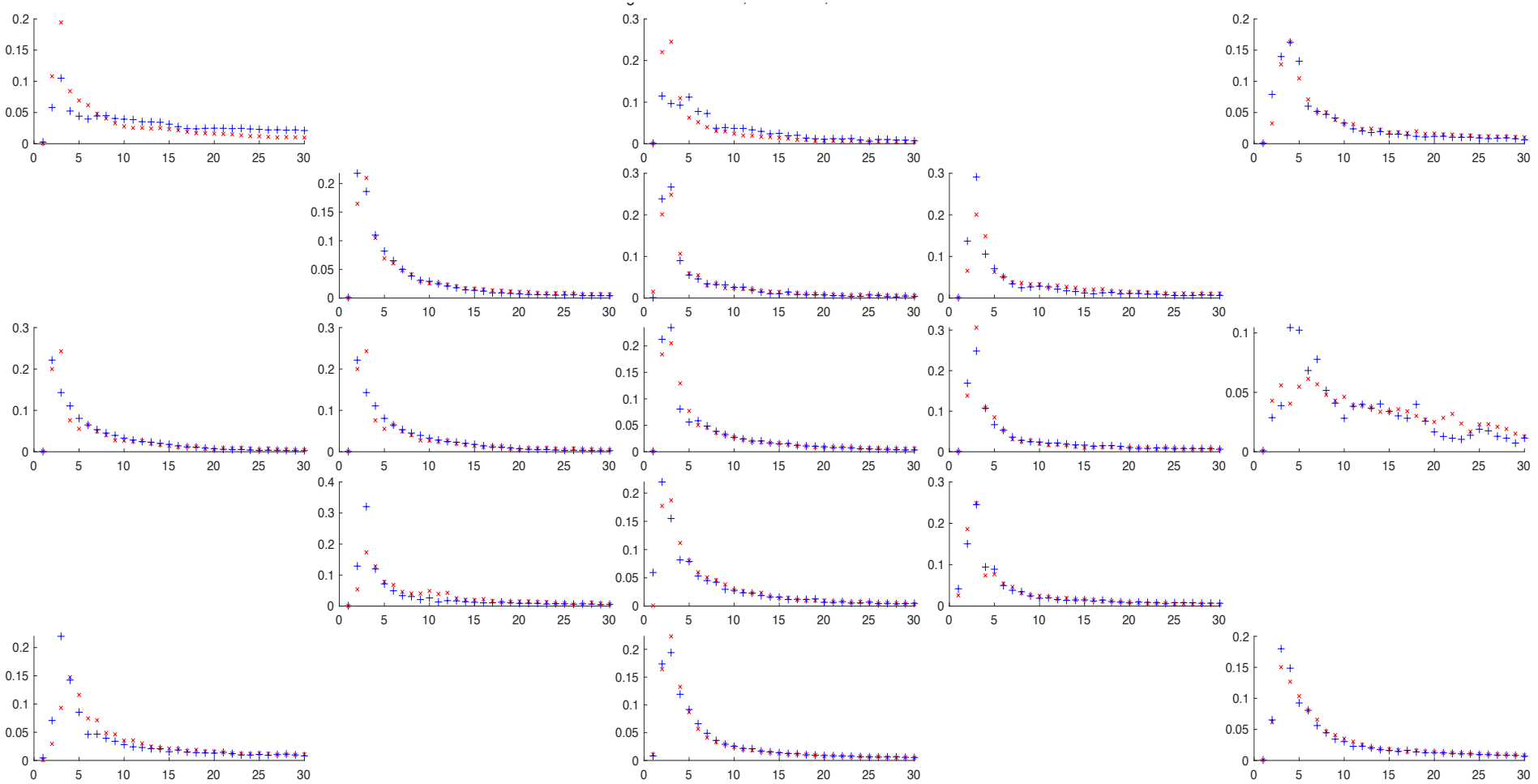

Figure 5.2.7. Mean normalised region anomaly spectra. Regions are shown as for a right eye, so the central subplot is the macula, and the top left subplot the distal supero-temporal region. Retinal detachment eyes (red) and PVD eyes (blue), including only B scans with total anomaly > 5 mm. The *x*-axes identify bin numbers, and the *y*-axes the normalised anomaly distribution.

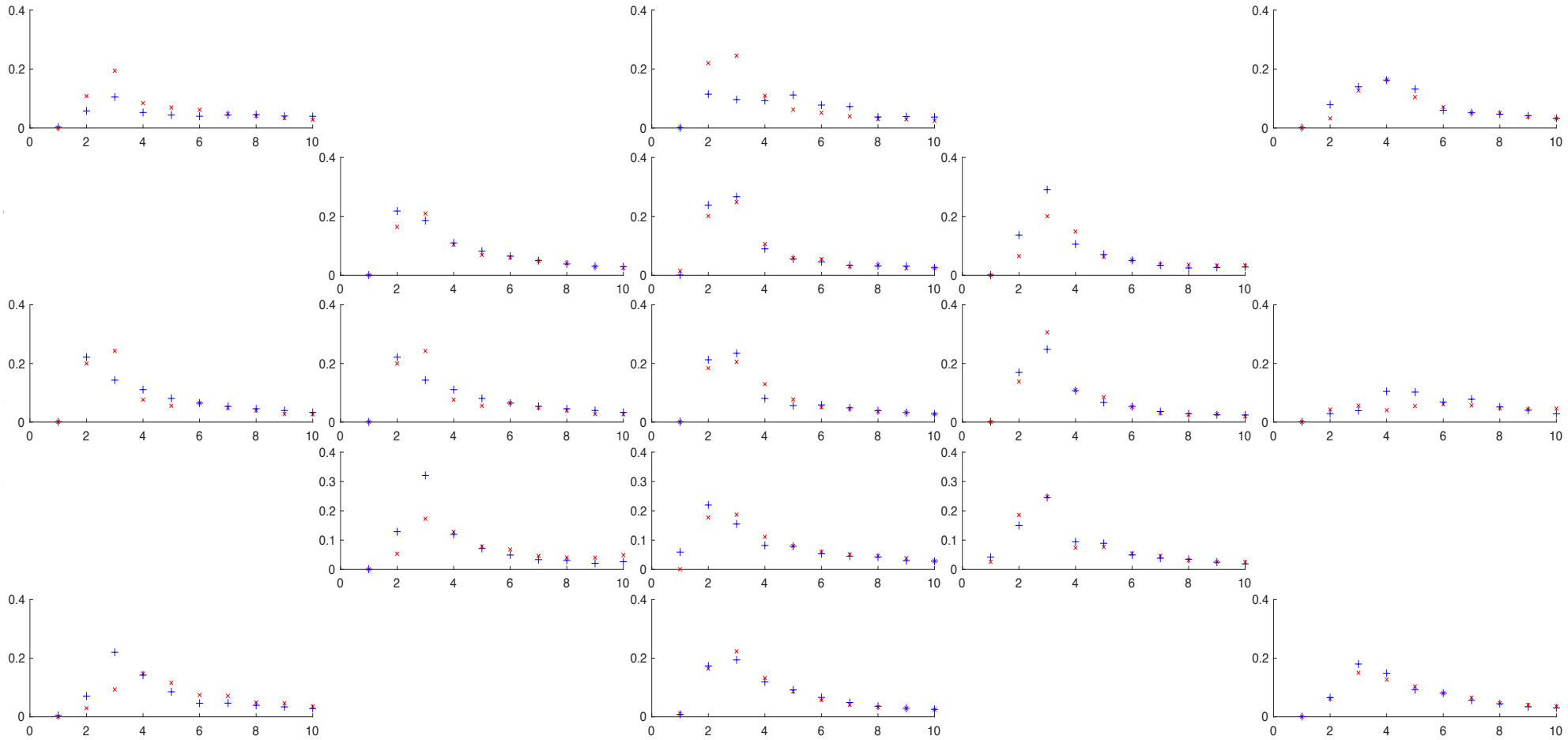

Figure 5.2.8. Mean normalised region anomaly spectra. The same data as shown in Figure 5.2.7, with only bins 1-10 included and *y*-axis ranges standardised for comparison. Retinal detachment eyes (red) & PVD eyes (blue). The *x*-axes are frequency bin number, and the *y*-axes anomaly values (with total anomaly set to 1).

Feature selection and reduction

The four largest regional differences in anomaly all came from bins 2 and 3, and were in regions 3 (distal superior), 8 and 9 (proximal and distal IT) for both normalised and absolute bin amplitudes. The next largest region differences were 4 and 5 (both supero-temporal) for absolute magnitudes, and 6 (proximal nasal) and 16 (proximal supero-nasal) for normalised distributions. The largest differences between the normalised region anomaly spectra for retinal detachment and PVD eyes were taken to narrow the number of potential features (from the 30 bins x 17 regions) before formal selection for classification. As there was some overlap between cubes sampling proximal and distal regions in the same direction (such as regions 8 and 9), only one region from the same direction (for example, either 8 or 9) was included as a source for a potential feature. Distal regions have more over-threshold (total anomaly > 5 mm) B scans than proximal regions (p154, above), so if two regions in the same direction exhibited a similar difference between the groups, the more distal was preferred. This narrowed the potential features to be used for classification to those shown in Table 5.2.3. Axial length was included as a feature, as it is known to affect both irregularity and retinal detachment risk. These anomaly features (identified using coordinates [region, bin]) were used to develop a discriminant model using as metrics the [region, bin] moduli with the greatest differences between the retinal detachment and PVD groups.

Table 5.2.3. Features explored for selection.

Region	Bin	Identifier
3	3	[3, 3]
9	3	[9, 3]
3	2	[3, 2]
6	2	[6, 2]
16	3	[16, 3]
5	3	[5, 3]
-	-	Axial length

Region refers to retinal location (Table 2.3). Bin refers to the frequency domain bin number. These features were selected as they had the largest difference between retinal detachment and PVD eyes in the normalised anomaly spectra.

Training

Using only anomaly > 5 mm B scan data for training was unsuccessful as the data were too sparse: the number of B scans with anomaly > 5 mm were too small to populate the classifier predictors with 3-5 variables. This remained the case even after lowering the anomaly threshold to 2 mm. Therefore, feature selection was performed on B scans with anomaly > 5 mm as above, but the training set included any scan with an arbitrary low threshold set as total anomaly > 0.01 mm to include all scans. All models were created using the same training set of eyes, starting with all seven variables in Table 5.2.3 and proceeding with a progressive reduction in number, exploring all possible combinations of features. The average performance for each number of features is presented in Table 5.2.4. Accuracy was higher with more variables, but classifiers with more than 3 features were rejected due to the size of the dataset. Within the three-variable classifiers, the most specific high-accuracy feature set was using features [3, 2], [5, 3], and axial length. This had a specificity of 0.89, sensitivity of 0.50, and accuracy of 0.70. Age was tested as a possible feature and did not improve classification.

Table 5.2.4. Classifier performance with progressive reduction in features.

No. variables	Specificity	Sensitivity	Accuracy
7	0.853	0.636	0.746
6	0.869	0.571	0.723
5	0.883	0.501	0.698
4	0.860	0.453	0.665
3	0.827	0.413	0.630
2	0.800	0.389	0.607

Specificity, sensitivity, and accuracy are the average classifier performance with the number of variables identified in column 1. All models were created using the same training set eyes.

Axial length single variable classification performance

As axial length is known to relate to risk of retinal detachment, its performance as a single variable was explored. Performance using axial length depended on the threshold axial length chosen to separate PVD and retinal detachment: at a specificity of 75%, sensitivity was less than 5%, and with a sensitivity of 40% specificity was only 34%.

Classifier cross-validation

Five-fold cross validation of the three variable classifier was performed to assess model stability. The training set eyes were divided into five folds with axial length stratified random allocation between the folds. Models were created with four of the folds and success rate tested with the fifth fold. This was repeated 20 times to produce 100 model success rates. Average success rate was 0.694, with a standard deviation of the success rates of 0.088 across the 100 models.

Group weighting

Figure 5.2.9 shows the training set sensitivity and specificity with different class weightings. The accuracy is shown in orange. Prophylactic retinal laser photocoagulation therapy has a poorly quantified but low risk of side effects (see Chapter 7: Discussion). In the situation with potentially an uncorroborated test for retinal detachment, a high specificity is more desirable than overall accuracy, especially when the disease state is much less common than the non-pathological one. For this reason, weighting was selected to attain the highest sensitivity with a specificity greater than 90%.

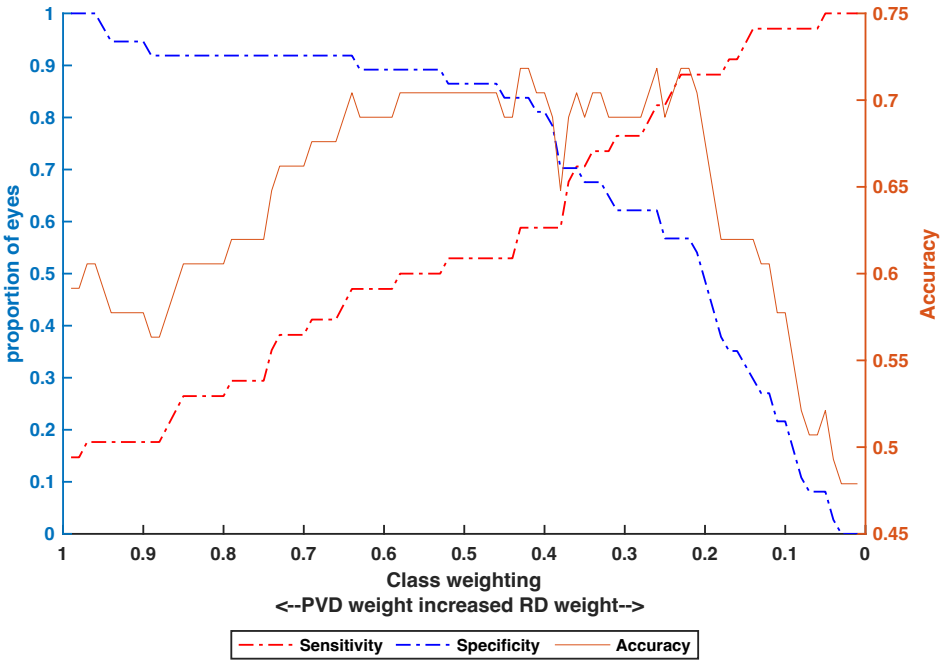

Figure 5.2.9. Classifier training set performance by class weighting. Weighting at *x = 0.5* is PVD: retinal detachment 0.5:0.5 (no class weighting). Weighting increases to the left to favour PVD up to 0.99:0.01, and to the right to favour retinal detachment up to 0.01:0.99. Optimal weighting was selected at x = 0.64, with a PVD: retinal detachment weighting of 0.64:0.36 for the greatest sensitivity while maintaining specificity over 90%.

Classifier performance – validation sets

With the test set of eyes, the classifier identified 23 out of 64 retinal detachment eyes (35%), with a specificity of 84%. A receiver operating characteristic curve was created from the test set eyes, with 95% confidence intervals generated through 5000 bootstrap replicas (Figure 5.2.10). Area under the curve was 0.75 (95% confidence intervals 0.58-0.85). Retinal tear eyes were employed as an independent validation set for the same classifier, conscious of the fact they have a different clinical presentation from retinal detachment eyes and may not be exactly the same condition. Out of the 68 retinal tear eyes, the classifier gave 16 (24%) the predicted retinal detachment label (Table 5.2.5).

The average values of both classifier shape features were smaller for the retinal tear than retinal detachment groups: mean (standard deviation) region 3 bin 2 anomaly was 0.80 +/- 0.62 mm for retinal detachment eyes, and 0.61 +/- 0.38 mm for retinal tear eyes. For region 5 bin 3 anomaly was 1.25 +/- 0.96 mm for retinal detachment eyes, and 0.94 +/- 0.59 mm for retinal tear eyes. Group axial length values are presented in Table 5.2.2.

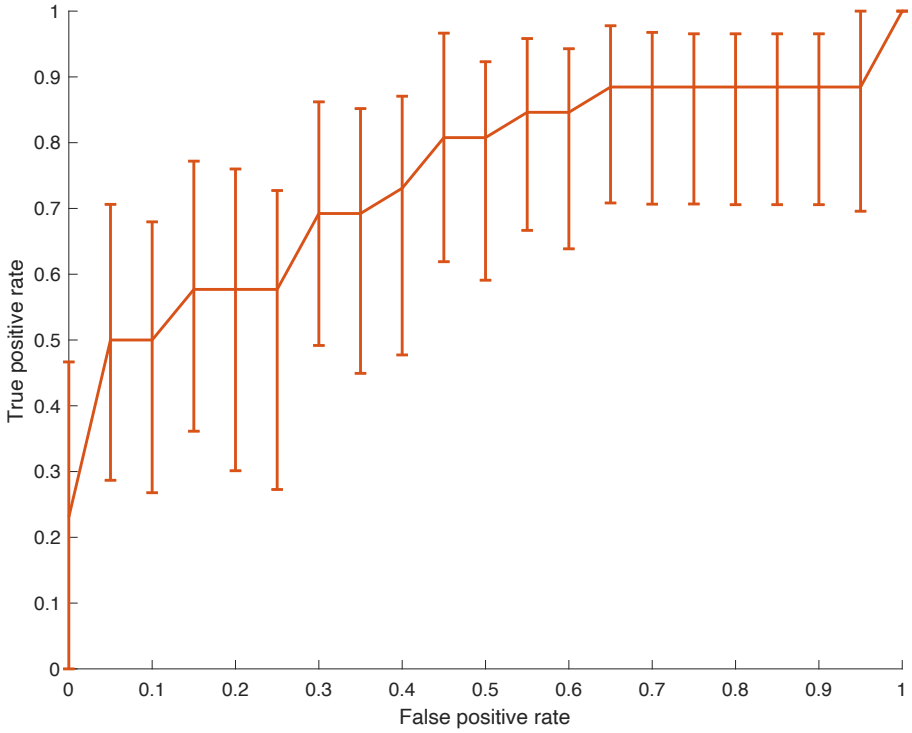

Figure 5.2.10. Receiver operating characteristic curve. Representing the classifier performance on the test set eyes, with 95% confidence intervals generated from 5000 bootstrap replicas. Area under the curve = 0.75 (95% confidence intervals 0.58-0.85).

Table 5.2.5. Test set results.

Category:	Label 1	Label 2	Total
PVD	*44*	*8*	52
RD	*41*	*23*	64
RT	52	16	68
Total	137	47	184

Performance of the three-variable classifier on the test set of retinal detachment and PVD eyes. The classifier had a sensitivity = 35%, and specificity = 84%, for identifying retinal detachment eyes. Fisher's exact two-tailed test, comparing PVD and RD distribution (numbers in italics) p = 0.019. Label 1 is classifier predicted class PVD, and label 2 classifier predicted retinal detachment. The retinal tear eyes are reported in the bottom row as an independent validation set, and were preserved as a distinct category but tested with the same classifier due to their distinct clinical presentation but similar pathology. PVD = posterior vitreous detachment, RD = retinal detachment, RT = retinal tear eyes.

Classification reliability

To test whether classification changed when eyes were re-imaged, patients who had been imaged once and who subsequently attended retinal clinics for normal clinical care were approached, and if they agreed were scanned again. For all repeat examinations, only distal superior and supero-temporal retinal regions were imaged. OCT cubes were taken using the same instructions as for the first imaging session: "look straight up", and "look up to your right/left". No reference was made to the initial OCTs to assess consistency of retinal imaging. Thirty-three eyes were re-imaged and analysed an average of 14 +/- 16 months apart (three PVD, 13 retinal detachment, 4 retinal tear, and 13 "fellow eyes"). For twenty-three of these eyes the classifier predicted PVD, and in ten eyes the classifier predicted retinal detachment. Thirty-two of the thirty-three eyes received the same classification from each imaging session, confirming that repeated images from the same eye produce the same classification results. One eye, a fellow eye without a PVD imaged 24 months apart, changed from PVD to retinal detachment classification without any change in clinical condition.

What do these B scans look like?

Sample B scans used by the classifier to correctly label retinal detachment eyes are shown in Figure 5.2.11 accompanied by the wavelengths of the feature frequency bins used in classification.

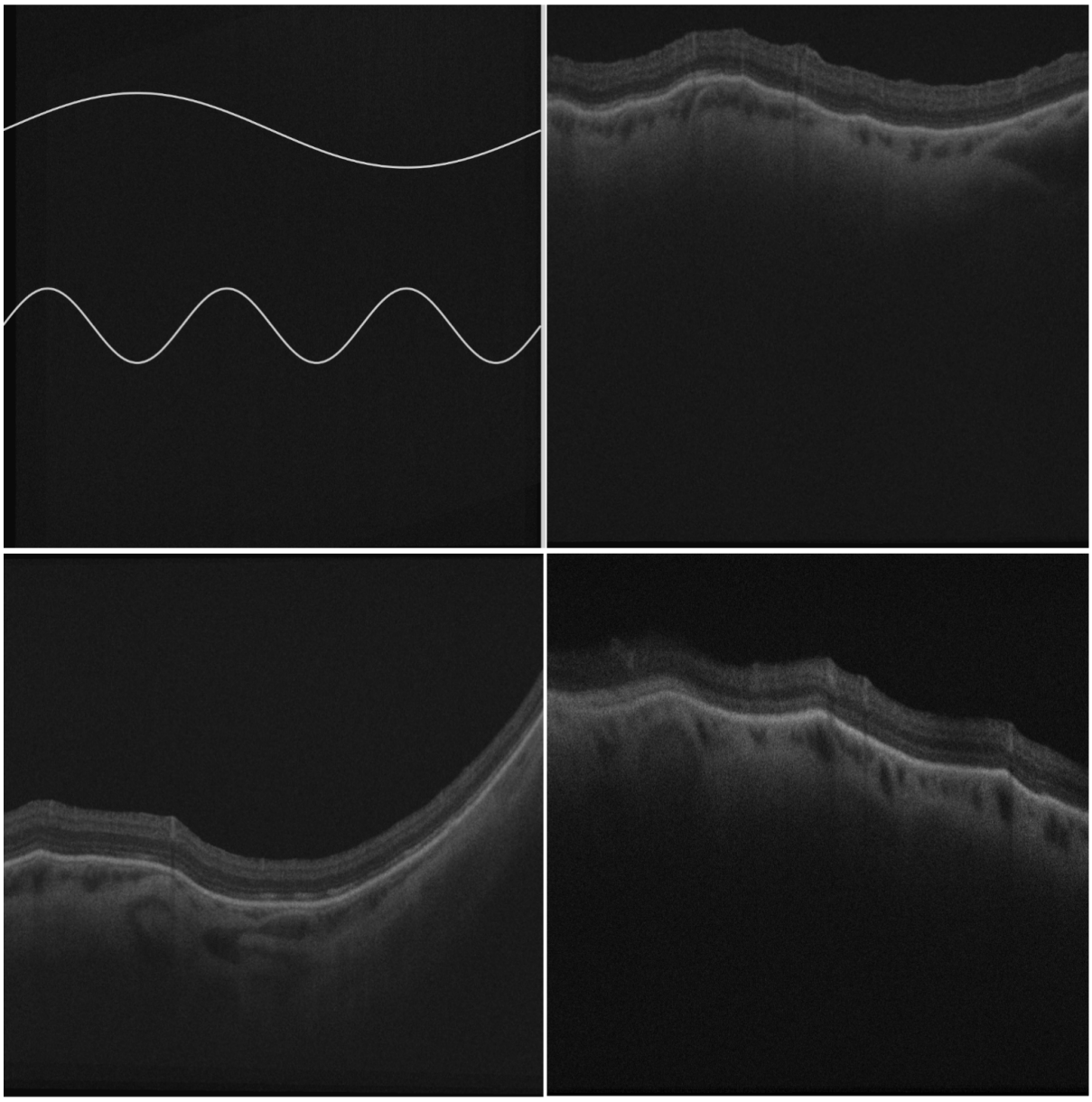

Figure 5.2.11. Shape features used in classification. The sine waves (top left) illustrate the two frequency bins used as classifier features. For comparison, three irregular B scans are shown from eyes correctly identified by the classifier as having had a retinal detachment.

Classifier space image construction

The decision surface in the three-variable classifier space (created by `CreClsImg`) is shown in Figure 5.2.12. The limits for the figure axes are the minimum and maximum values of each variable within the entire sample set (Table 5.2.6).

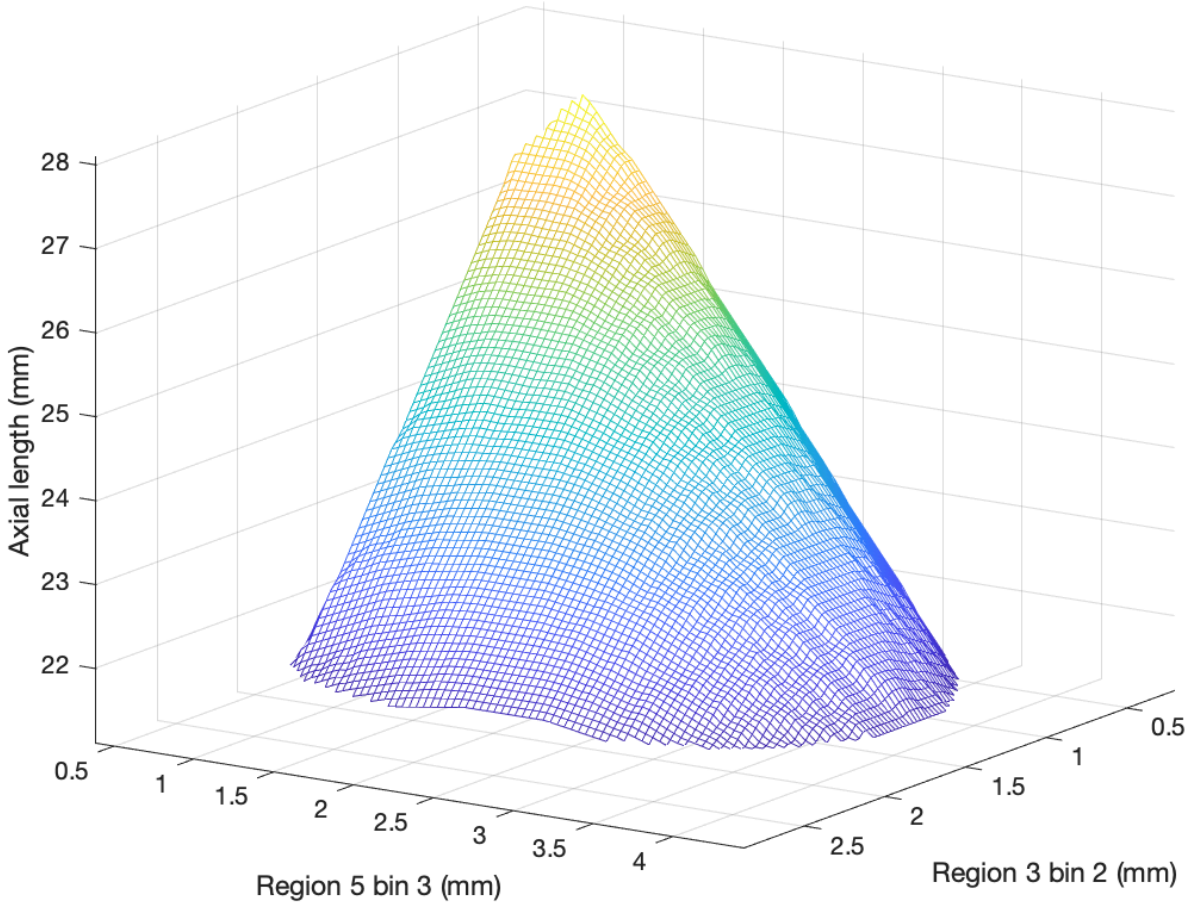

Figure 5.2.12. Illustration of the three-variable classifier decision surface. PVD eyes lie within the classifier space demarcated by the `meshgrid` cone. The risk of retinal detachment increased as shape feature values increased (Region 3 - bin 2, region 5 - bin 3, and axial length). Note the PVD volume is smaller than the retinal detachment volume in this space. This does not imply retinal detachment is more common. Eyes were not evenly distributed within this space with the majority having lower values in region 3 and region 5 anomaly and were concentrated within the conic section. The irregular (scalloped) margin at the base of the cone facing the Region 5 axis is an artifact of the image construction (`CreClsImg`).

Table 5.2.6. Range of feature values.

	Region 3 (mm)	Region 5 (mm)	Axial length (mm)
Minimum	0.20	0.39	21.11
Maximum	2.88	4.45	28.09

Includes all eyes from both training and testing sets.

Development and evaluation of a research test for ongoing prediction

Introduction

Section 5.2 identified shape features of retina that can identify a proportion of retinal detachment eyes from a mixed group of those and PVD eyes. The test has shown ability to identify eyes after they have had surgery for retinal detachment. Before use as a clinical test, it would need to be confirmed that it can identify eyes that will develop a retinal detachment before the PVD has occurred. As the risk of retinal detachment in any group varies from 1% (general population) to up to 20% (fellow eyes to retinal detachment eyes that do not have a PVD), a large number of eyes would need to be imaged to collect prospective data on classifier performance at identifying eyes at risk. While OCT image capture is quick, painless, and safe for the participant, imaging 17 regions of the eye was time consuming, which challenged workflow during regular clinic hours. The segmentation of seventeen or more OCT cubes was also time consuming and labour intensive. Processing a retinal survey used for the initial cohort of eyes in Section 5 took 3-5 hours, impractical for a point of care or large-scale research test. Time efficiency is important.

The task of performing OCT retinal surveys for a large number of eyes, most of which will never have a problem (and likely not attend an eye clinic) to prospectively evaluate classifier performance was logistically challenging. In addition, social distancing precautions were introduced in Australia in March 2020 to reduce the spread of SARS-Cov-2[261]. As a consequence of this, research participant visits were restricted where possible to interactions simultaneous to normal clinical care[262]. The outcome of Section 5.2.1, that the information required comes from axial length and just two mid-peripheral OCT cubes, was fortunate for further study. The three variable classifier model needed only OCT cubes from

regions 3 (superior), region 5 (supero-temporal), and axial length. Further testing of this classifier was undertaken with participants imaged using this reduced protocol. With only two cubes required, the processing time was reduced to less than 30 minutes.

Tyra Lange developed a shape analysis function named A2 for segmenting retinal OCT using graph theory and Dijkstra's algorithm as part of her dissertation for Engineering Honours at Flinders University[263]. The objective was to create a freestanding function that allowed any user to take OCT image files as input and receive a classification output. Like Livewire, this used graph theory. However, the use of Livewire/ImageJ requires some skill; it requires operator input to trace the path of the retinal pigment epithelium and place "anchor points", whereas the purpose-built algorithm identified the retinal shape with less operator input. Trials of A2 suggested it was faster and simpler to use, but had the disadvantage that as written, errors in path selection could not be corrected. In particular, contour was created across any OCT image, even if no retina was within the B scan, or the retinal image was an inverted, defocused retinal signal from mirror artifact.

This section reports on the utility of Tyra Lange's A2 function in identifying retinal detachment eyes. First, the ability to select only accurate segmentation was added to the function. Then, comparison of the relative performance of Livewire and A2 was undertaken. Differences in classification and speed of use of the two methods was evaluated.

Aim

To develop an algorithm that can take retinal OCT image files, analyse shape and produce a classification fast enough to be practical as a clinical test.

Methods

Subjects

51 eyes from 31 participants were included. 28 eyes had a diagnostic category, and 23 eyes were part of the predictive study of classifier performance with no confirmed diagnosis yet ("fellow eyes"). A summary of the steps in processing OCT images with both methods is shown in Table 5.2.7.

Table 5.2.7. Description of steps involved in two retinal OCT classification methods.

Procedure	A2FFT	A2FFT time to perform	LVW	LVW time to perform
Participant recruitment, consent, OCT imaging & axial length measurement, documentation: same for each method. Not included in analysis				
.img to .tif conversion	Performed by A2FFT	Seconds. Included	Manually to 30 May 2020, then by function	< 1 minute. Not included
Shape identification	A2FFT. User marks start and end point each B scan	Minutes. Included	Livewire/ImageJ. User traces contour from start to finish, marking intermediate points	Minutes. Included
File saving	Done by A2FFT	Trivial. Included	Manually	Trivial. Included
Classification	Done by A2FFT	Seconds. included	Separate function	Seconds. Not included

Included/not included = whether time taken for this step was included in time analysis.
A2FFT = function using graph theory for retinal contour identification. User identifies start and end point on each B scan of correctly identified retinal contour, or rejects B scan with no relevant information.
LVW = Livewire/ImageJ contour identification. User traces retina contour with start, finish, and intermediate marker points, the number of these depending on the complexity of the retinal shape.

Method 1: ImageJ/Livewire

For the Livewire analysis arm, tiff files were created from the OCT .img files, retinal shape captured with Livewire, images converted to the frequency domain and classification performed using the classifier developed in Section 5.2.

Method 2: A2FFT.

Script A2 was incorporated into function A2FFT. This was built around Tyra Lange's function. This program required user input of an eye identification code, axial length, and the full file name of the raw .img OCT image files, with these files present in the working directory or current folder in the MATLAB window. Starting with the region 3 cube, a tiff file

was created from the .img file, and each B scan presented in a new window with the retinal contour marked by a green line. The A2 output (the RPE delineated in green on the B scan) was presented to the operator who selected the start and endpoints of retinal shape. Due to inclusion of errors such as mirror artefact image, inner retinal border identification, and even absence of any retina all misleading contour identification, this manual step was necessary to select the start and end point correctly. `A2FFT` then truncated the retinal contour by the selected start and end points. This allowed removal of mirror artifact or B scan areas empty of information.

To facilitate rapid error free selection, start and end points were taken only from the *x*-index the user selects. Requiring a match between user selected retinal extent and the retinal shape in both *x* and *z* axes might generate errors unless the exact pixel on the retinal contour line was selected.

Once all 42 B scans from regions 3 and 5 were segmented, the three variable classifier was loaded, and anomaly calculated relative to the average B scan irregularity from all five folds of the classifier training sets. Mean coefficient of variation (C_v) for all 30 bins from the five average B scans was 0.0099 (range 0.0063 – 0.0585), confirming low variation between folds in average B scan value. The largest value (C_v = 0.0585) was for bin 1, and bin 2 the second largest with C_v = 0.0166. With axial length information input, the eyes were tested, and a result reported in the MATLAB command window with the optimised weighting.

Comparison of the speed of the two methods was performed in a retrospective manner. Time for each method was calculated using the final modification time in the file metadata, identified by the `dir` function in MATLAB. For Livewire, this was the total time between the first and last textfile created for each of the two OCT cubes that stored the contour information. This time included only time taken to extract shape information. For `A2FFT`, the time between creation of the first tiff image file to the time of the last image analysis datafile saved was used. This time period included conversion of .img file to .tif format, extraction of shape information with operator input, as well as classification (Table 5.2.6). For both methods, outlying time values arose from breaks in user activity. These were

known to be not related to the method itself, so any time durations greater than 30 minutes were removed.

Statistical analysis

Performance of the two methods of shape analysis were compared by classification as well as time taken for each process. Times for each method were compared by two-sample *t*-tests.

Results

Label attribution with A2FFT and LVW differed in two out of 51 eyes analysed. Both of these eyes were part of the predictive study, with no ground truth to identify which method was correct.

Time to perform analyses

There were 46 LVW eye and 50 A2 eye time periods within the range 0-30 minutes. Mean +/- standard deviation processing times were significantly shorter with A2FFT compared to Livewire use times (A2FFT = 524 +/- 62 seconds, LVW = 814 +/- 223 seconds, two-sample *t*-test, $p < 0.0005$ ($p = 5.52 \times 10^{-14}$)). In all but 4 of 45 eyes for which times from both methods are available, processing time was faster with A2FFT than LVW. Histograms of the time to perform analyses are shown for Livewire (LVW, figure 5.2.13), and A2 methods (A2FFT, figure 5.2.14).

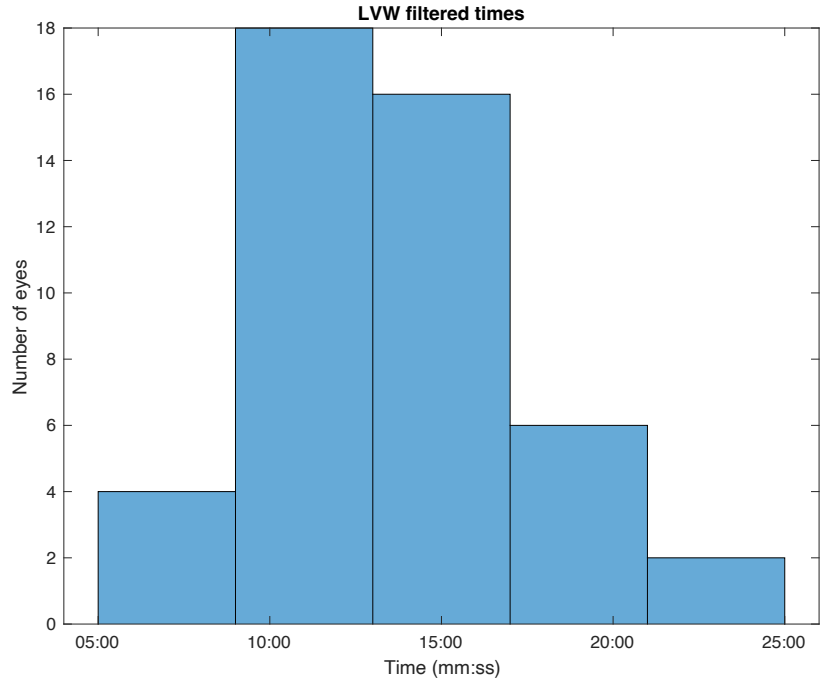

Figure 5.2.13. Curated Livewire image processing times. Excludes eyes where processing took more than 30 minutes.

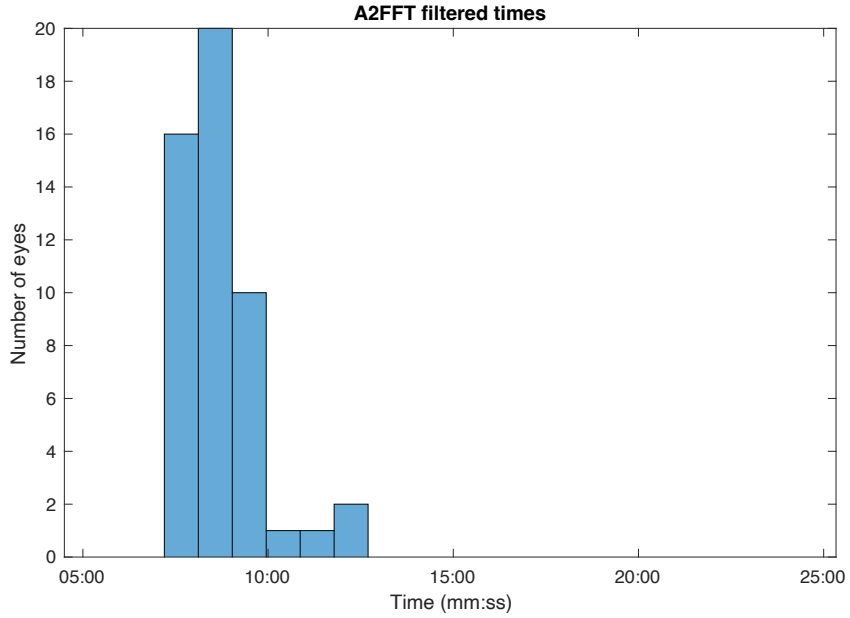

Figure 5.2.14. Processing times using `A2FFT`.

Conclusions

5.2 classifier development

A useful model to predict eyes at risk of retinal detachment should have a high specificity to avoid misclassifying eyes at no risk being labelled as at risk of retinal detachment, combined

with an ability to identify eyes that will develop a retinal detachment. The classifier described here had a reassuringly high specificity of 84%, with a sensitivity 35%. The high specificity within the validation set means that an eye with label 2 is highly likely to have a retinal detachment. This test has low sensitivity, so a label 1 result does not indicate no retinal detachment.

Classification of the retinal tear group had a sensitivity lower than the retinal detachment group itself. Retinal tear eyes had on average smaller anomaly feature values than retinal detachment eyes, and these differences between retinal tear and detachment eyes reduced classifier performance with the retinal tear eyes.

Classification was stable with re-imaging. This is in agreement with the results from the five eyes reported in section 5.3, where classification was unaffected by PVD or retinal detachment repair.

Conclusion: ongoing test development

Obtaining a classification result was faster using `A2FFT` compared to Livewire. `A2FFT` was also easier for the operator to perform, requiring less patience for contour identification. This method was preferred for ongoing classification.

Discussion - research test development

With broad retinal area imaging and analysis time consuming, the ability to streamline the process using retinal imaging from two areas and improved analysis times enables rapid participant recruitment and faster processing. This enabled ongoing and even prospective sampling of a larger number of eyes potentially at risk. In addition, with streamlined image capture it became more acceptable to more participants to have both eyes imaged, with the result that more eyes with identified diagnostic categories were available for testing the classifier.

Processing time with Livewire/ImageJ included only the time taken for shape identification, and did not include the time for identifying the contour in the first B scan in each cube (as

the start time was when the first B scan data was saved), whereas the A2FFT time included all B scans, classification time, and conversion of .img format image data files to tiff files. Despite these processing differences favouring the use of Livewire, it was found to take significantly longer. The time difference of almost 5 minutes per eye was enough to bring the test closer to a practical point of care test in clinical practice. As well as taking less time, user required input was simplified with the `A2FFT` algorithm. The faster process was therefore easier to perform, further increasing its acceptability.

While it is not surprising that a purpose-built algorithm would perform better than a general use biomedical image analysis tool, this was a significant development in enabling classification to be performed on a greater number of eyes. `A2FFT` enabled more eyes to be imaged in clinical time, with faster results. As a result, it was possible to recruit many more eyes for prospective evaluation of the classifier. The need to incorporate the process within routine patient essential clinical encounters was particularly important during the second half of 2020, when the SARS-Cov-2 pandemic required social interaction and the restriction of healthcare activity and hospital encounters to only those essential for patient care.

Discussion - classifier development

To develop the classifier, variables were selected from the training set anomaly spectra that had the largest difference between retinal detachment and PVD eyes, without preconceptions about what might be important. Then, using those variables as predictors, a model was constructed to discriminate between the two groups. When exploring cube regional spectra, including all the samples would result in values being heavily influenced by the majority of low magnitude anomaly B scans (Figure 5.2.1). Identifying predictors of interest from the differences between retinal detachment and PVD eyes in scans where the total anomaly was above a certain threshold, but using all the data for model construction, helped identify features to develop the classification function. The groups presented in this work were of moderate size, and the use of the majority of the sample for feature selection as well as training was an efficient use of data[205].

Discriminant analysis was chosen as it is a classifier suitable for smaller sample sizes. An early model (not presented here) used features from the overall survey metrics used to describe eyes in Chapters 3.4 and 4, which were found to vary both across the eye and with axial length, which is known to correlate with risk of retinal detachment. Fortunately, this was unsuccessful and the regional bin feature classifier successful, as testing an eye using OCT cube surveys across all regions would be much more time consuming and difficult to replicate in clinical practice. If the better performance was seen in classification from whole of eye metrics such as median metric values, the entire eye would require imaging for a test result to be reached. With the three variable ([3, 2], [5, 3], and axial length) classifier, only two OCT cubes were needed to perform the test. This time saving advantage was exploited to continue patient recruitment and extend the validation set.

The significant shape features from bins 2 and 3 equate to wavelengths of 3 – 9 mm. As this is the longest feature size within the 9 mm B scan window, the question arises as to whether even longer-wavelength (lower frequency) features would improve classification. This can only be tested with larger OCT images such as are available with swept source OCT, and is explored in Chapter 6.

It is possible that there was some overlap between OCT cubes of superior and supero-temporal retina. The criticism may be raised that classification was affected by imaging the same retina twice, or that incorrect attribution of cubes to regions will alter results, as the anomaly threshold in the classifier for the supero-temporal region (around 3.5 mm) was greater than that for the superior region 3 (around 2 mm, although both vary with axial length). However, the frequency bin used from the two regions differs, so the variable from each region samples a different shape feature. The significant feature from the supero-temporal region was of a shorter wavelength than superior region. This may relate to the shorter sample length of retina in the supero-temporal region B scans due to oblique imaging. Furthermore, the classification space illustrated in Figures 5.2.12 and 5.2.15 reveals that the quadratic classifier required an elevated feature value in an “or” rather than an “and” fashion to change label. In other words, one high value shape feature is enough to switch classification from one label to the other, with the impact of the second shape

feature magnitude less important than it would be were the classification boundary a linear discriminant and not a conic section.

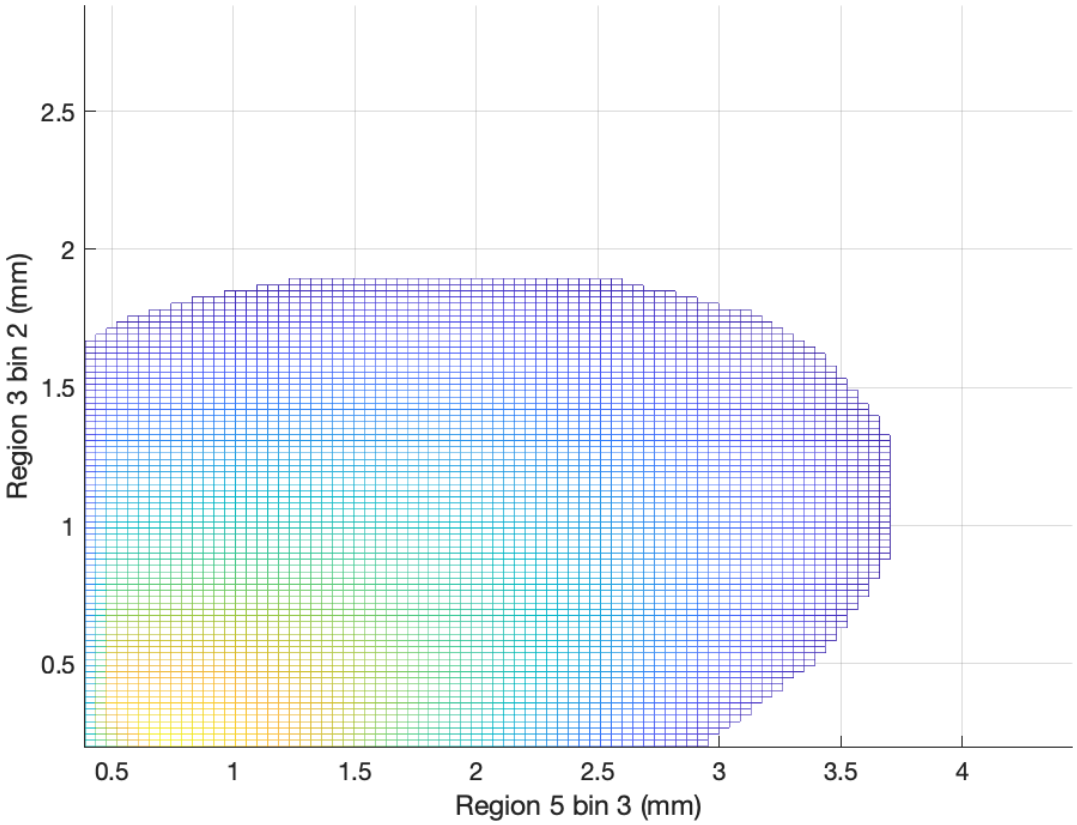

Figure 5.2.15. Classifier space (from Figure 5.2.12) viewed along the z-axis. The area equivalent to PVD is displayed by the coloured mesh. As either variable increases (along each axis), they pass a threshold where classification switches label. This threshold is not sensitive to changes in the alternate variable.

While clinicians do often not have a deep understanding of Fourier analysis, the conversion of the shape metric description from frequency to wavelength and their presentation on OCT images in Figure 5.2.11 attempts to illustrate what is being used by the classifier. This does not imply that prediction can be performed by visual inspection of OCTs, and the illustrated amplitude of the wavelengths does not relate to the threshold feature magnitude. Sample OCTs from correctly identified retinal detachment eyes are shown for illustrative purposes only. In performing analysis of validation set eyes, SL examined every B scan to confirm correct retinal shape segmentation. During this process, user prediction of

classifier outcome was inevitable, and as it turned out, often wrong. This was likely related to difficulties in assessing the magnitude of the significant shape features and whether they reached the required threshold (or not).

The retinal tear group were tested with a two-class classifier rather than treated as a third class, as current concepts in ophthalmology consider acute symptomatic retinal tear eyes to have the same pathology but with a different presentation compared to retinal detachment eyes. Prior to PVD occurrence there are only two possible outcomes when vitreous separation occurs: uncomplicated (no retinal tear), or PVD complicated by a retinal tear that without timely presentation to healthcare may lead to retinal detachment. The ultimate aim of the classifier is to identify eyes at risk of vision loss before emergency care is required, including both retinal tear and detachment eyes. Separation was maintained between retinal tear and retinal detachment eyes to preserve a clean data set, create a second validation set, and to explore feature differences between the retinal tear and detachment eyes that might provide evidence as to why some patients are able to present at an earlier stage of the disease than others. This revealed that the retinal tear group variables were intermediate in size between PVD and retinal detachment groups in terms of shape as well as axial length. The implications of this may be:

that the retinal tear group was heterogeneous, including eyes that will progress to retinal detachment as well as eyes that will not. This mix leads to lower anomaly values and lower classifier sensitivity.

that the lower feature size (axial length, and/or anomaly) in the retinal tear group delays progression to retinal detachment giving these subjects time to present to healthcare.

or that vitrectomy increased irregularity, producing the larger values seen in the retinal detachment group.

The reasons to test retinal tear eyes were:

to test the validity of the model with an independent data set.

to investigate whether the model was effective in a group that had not had surgery.

A criticism of the discriminant ability of the classifier might be that the model is detecting shape differences that arise from surgery (vitrectomy), and therefore that shape differences have no ability to identify eyes at risk of retinal detachment prior to PVD. The average B scan for this analysis was taken from the original PVD/retinal detachment group, with no retinal tear eyes, so the retinal tear eyes may reflect a different population (pathological group) from those of the training set eyes. Retinal tear without detachment may be a distinct pathological entity, which the model was not designed to identify. Not all retinal tears lead to retinal detachment. Clinical consensus considers that all acute symptomatic PVD associated retinal tears need intervention with laser photocoagulation or cryopexy to seal the tear and prevent retinal detachment developing, with evidence for the need to intervene with asymptomatic breaks currently lacking[264]. If this retinal tear sample reflects a more stable eye configuration than eyes that will develop retinal detachment, and the model detects only eyes that are likely to progress to detachment, then sensitivity in the retinal tear group will be reduced proportionately to the subset that will detach. If this were the case, while sensitivity would be reduced, the classifier would have the additional benefit of detecting higher risk eyes. There are likely to be multiple pathways to PVD associated retinal detachment. As well as bulk flow through retinal breaks overwhelming the ability of the RPE pump to maintain retinal attachment, delayed retinal detachment may occur from retinal pigment epithelial migration into the pre-retinal space, leading to fibroglial proliferation and inner retinal contraction increasing the separation/detachment force. All the retinal tear group eyes here were selected if they presented with an acute, symptomatic, PVD-related retinal tear, which is believed to be the group most at risk of progressing to acute retinal detachment.

The difference in mean axial length between the retinal detachment and PVD groups was not unexpected, as larger eyes are at greater risk of retinal detachment[265]. Axial length was the most successful single variable discriminant model, confirming the link between axial length and the risk of retinal detachment, but was not sufficient on its own to classify eyes accurately (for an axial length classifier with a specificity of 75%, sensitivity was less than 5%, and with a sensitivity of 40% specificity was only 34%), and did not account for the effectiveness of the entire model. The fact that age had no discriminant utility reflected the

narrow range of the sample population, but suggests that PVD occurring early or later does not affect the risk of retinal detachment occurring.

All groups had a PVD, but only the retinal detachment group had a vitrectomy as well as a retinal detachment. All vitrectomies were with 23-gauge instruments, with no scleral buckle. Vitrectomy or laser treatment may have had indirect effects on shape that can explain the differences between the two groups. Surgery may alter the irregularity of the posterior hemisphere of the eye as measured with this method, but this seems unlikely as vitrectomy has not been shown to alter the corneal shape even though that lies much closer to the surgical incisions[255,256]. Laser retinopexy was visible on some OCT B scans in the retinal detachment cohort. The impact of these factors is considered in the Section 5.4.

5.3. The effect of PVD and retinal detachment on retinal survey shape features

Introduction

As PVD may occur anytime over a 20-30 year period in the middle years of life, imaging someone before and after PVD for research relies on good fortune that the affected individual is imaged prior to any problem, then re-presents after PVD occurs and that the event occurs within the time span of the project. Fortuitously, this occurred with five participants who had OCT retinal surveys of their fellow eyes after a retinal detachment in the contralateral eye. Three eyes were enrolled then re-presented with an acute PVD without any retinal breaks. A further two eyes were imaged prior to PVD and subsequently progressed to retinal detachment. One was labelled 1 (PVD), and the other 2 (retinal detachment) by the classifier prior to retinal detachment. Both subsequently underwent vitrectomy to repair retinal detachment with good outcomes. All were approached and asked for permission to re-image their eyes to compare pre- and post-operative shape and provide some insight into how wider retinal shape features changed with hyaloid separation and surgery.

Here, the variation in shape between initial and subsequent examination was explored with the use of Bland Altman plots, with limits of agreement set by the re-imaging of eight eyes that had experienced no change in their ocular status.

Aim

The aim of this section was to assess whether retinal shape was changed by either PVD or vitrectomy for retinal detachment.

Methods

Subjects

Subject details are presented in Table 5.3.1. The images were taken using the same survey protocol of one macular and 16 mid-peripheral cubes, with no reference to the first imaging set taken when imaging the second time (Figures 5.3.1 & 5.3.2). Allocation of cubes to

retinal regions, and processing of image data was undertaken as described in the Section 2.2 and performed independently for each imaging session.

Table 5.3.1. Subjects with OCT retinal surveys before and after PVD or retinal detachment.

Imaged Eye/ Pathology	Axial length (mm)	FE Pathology	Interval between imaging sessions
PVD:			
Q129/S121	23.01	RD	30 months
S113/S125	22.65	PVD	7 months
S210/S410	26.06	RD	17 months
RD:			
R294/S223	24.56	RD	8 months
R276/S224	26.72	RD	13 months

FE pathology = fellow eye condition leading to clinical examination and imaging. RD = retinal detachment.

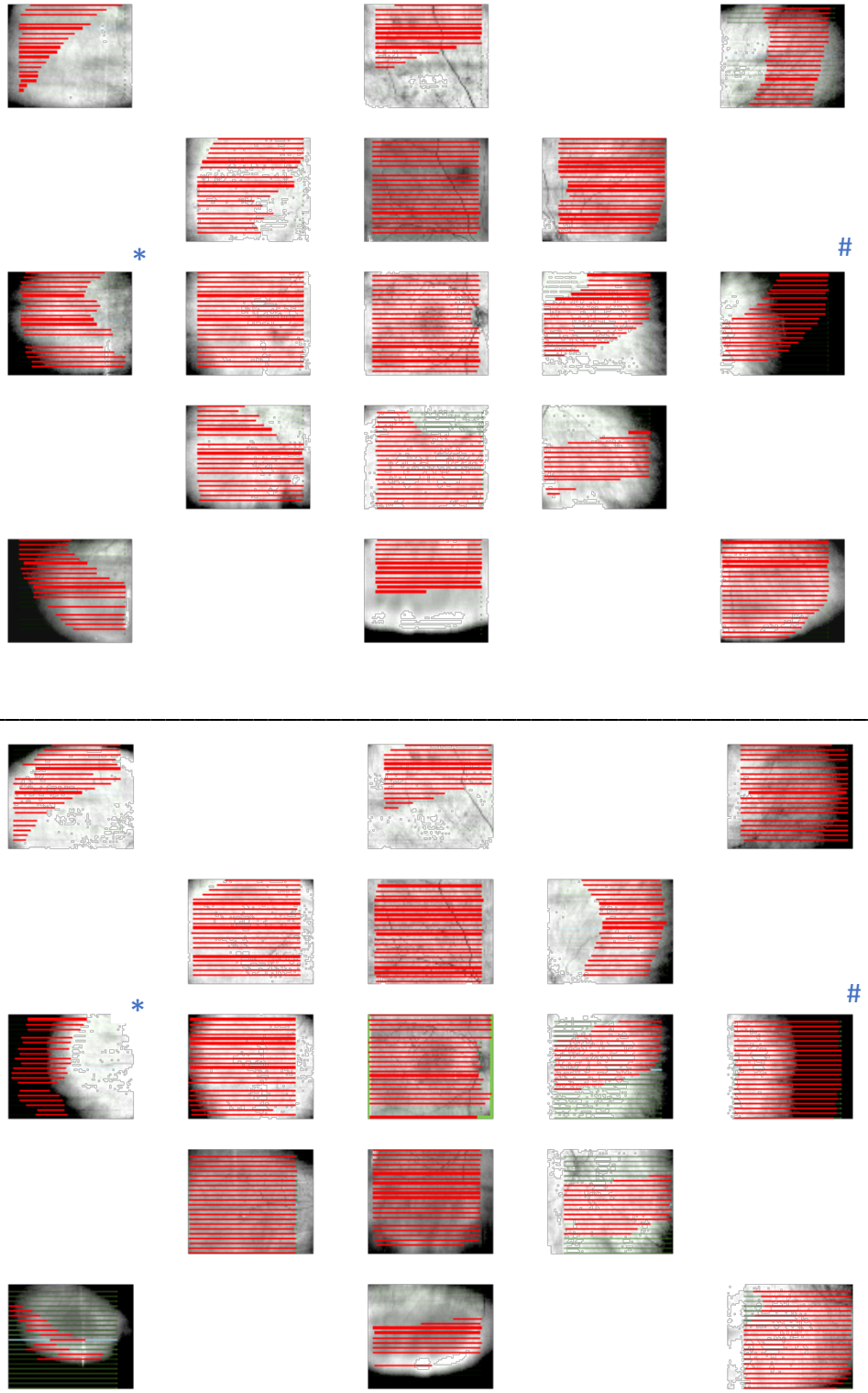

Figure 5.3.1. SLO maps of a PVD eye. Q129/S121, respectively before (top) and after (bottom) PVD. The black and white SLO images identify the areas of retina sampled, with the horizontal red bars indicating the segments of each B scan where retinal image was observed. As the B scan window depth is only 2 mm and the retina is curved, with increasingly peripheral scans a shorter length of retina was sampled. Correspondence between the two sittings was close, but with some differences (seen in cubes marked by blue asterisk and hash). SLO = scanning laser ophthalmoscopy (`AnnotSLO`).

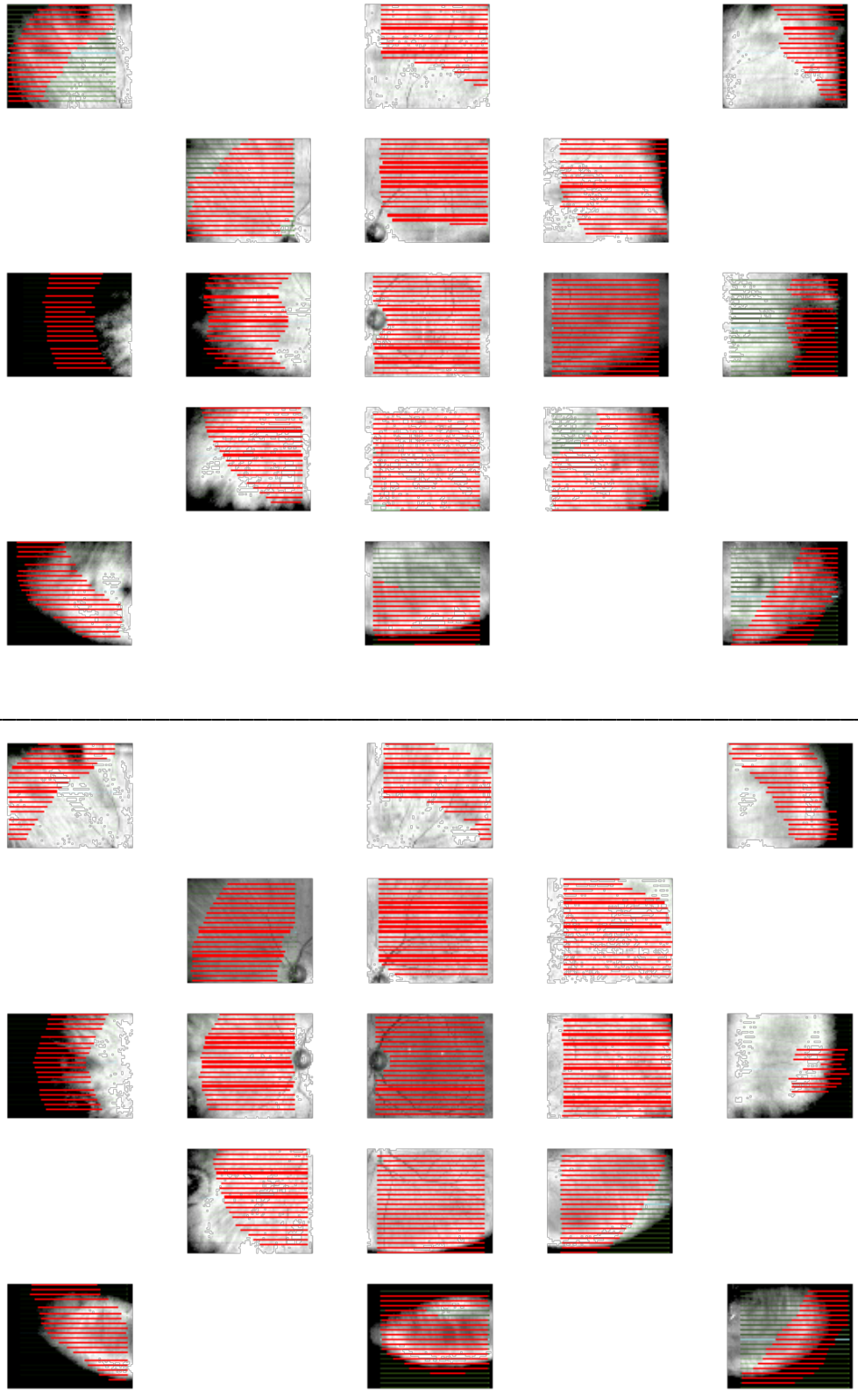

Figure 5.3.2. OCT cube maps before PVD and after retinal detachment repair. Comparison can be made between the areas imaged in the two sessions, with the upper set prior to PVD and the lower set taken following vitrectomy for retinal detachment. The differences in sampled area between the two sessions were small, as seen by comparing the red lines highlighting where retina was imaged in each scan.

Bland Altman plots

The repeat eye anomaly values were determined relative to an average B scan irregularity taken from the set of eyes used to assess the correlation of irregularity with axial length (Chapter 4). For the Bland Altman analysis (`Comprep`, `comprepBA`), the metrics assessed were the maximum regional anomaly values, as used in the retinal classifier created in Section 5.2, but included all frequency bins from 2-20 for all regions 1-17. Bins 1 and 21-30 were excluded as they were of such low magnitude that their variation would most likely reflect signal noise, and not reflect variation in shape between corresponding images. A $\log_2$ Bland Altman plot of the observations was created,

$$S(x,y) = \left(\frac{\log_2 A_1 + \log_2 A_2}{2}, \log_2 A_1 - \log_2 A_2\right)$$

as a comparison of the ratio of the measurements was preferable using the $\log_2$ difference for the *y*-axis as feature magnitude may vary substantially between bins[266].

Control eyes

The Bland Altman plot does not set the threshold for what is acceptable variation in test-retest performance. Following convention, the use of +/- 1.96 standard deviations was used here. These limits of agreement were generated using eight eyes that were imaged twice in the same manner, without any change in their ocular status. The details of these eyes are presented in the Table 5.3.2. These eight eyes were re-examined on separate days.

Table 5.3.2. Eyes imaged twice with no change in ocular status between examinations.

ID	Side	Interval between exams	Age at first exam	Diagnosis	Axial length
P 123	R	13 months	62	Volunteer – retinoschisis	23.47
Q 228	L	4 months	33	Volunteer – no pathology	22.91
P 216	L	22 months	45	Myope – no pathology	26.11
Q 296	L	4 months	73	Retinal detachment	27.19
R 151	R	6 weeks	33	Myope – no pathology	25.94
R 207	L	5 months	65	Retinal tear	24.07
R 150	R	1 day	33	Volunteer – no pathology	23.92
R 164	R	6 weeks	28	Myope – no pathology	27.21

Age in years. Axial length in mm.

Results

The Bland Altman plots for the eyes that experienced PVD are shown in Figures 5.3.3 – 5.3.5, and for retinal detachment in Figures 5.3.6 & 5.3.7. Exploration of those points outside the limits of agreement found only one that was in lower frequency bins 2 and 3 from the superior and supero-temporal retina used for classification, in the second retinal detachment eye (Figure 5.3.7). Most outliers were in higher frequency bins, except for region 15 (distal nasal) in the first PVD eye Q129 (marked by the blue hash in Figure 5.3.1), and to a lesser degree region 7 (distal temporal, blue star, same Figure) in the same eye, where both cubes had clearly sampled a different retinal region at each sitting. Figure 5.3.8 presents all the values outside limits of agreement for the second retinal detachment eye (Figure 5.3.7), which had both the largest anomaly values and the most number of points outside the limits of agreement. Most of these outliers were from low amplitude regions of the anomaly spectrum, consistent with measurement variation from 'noise'.

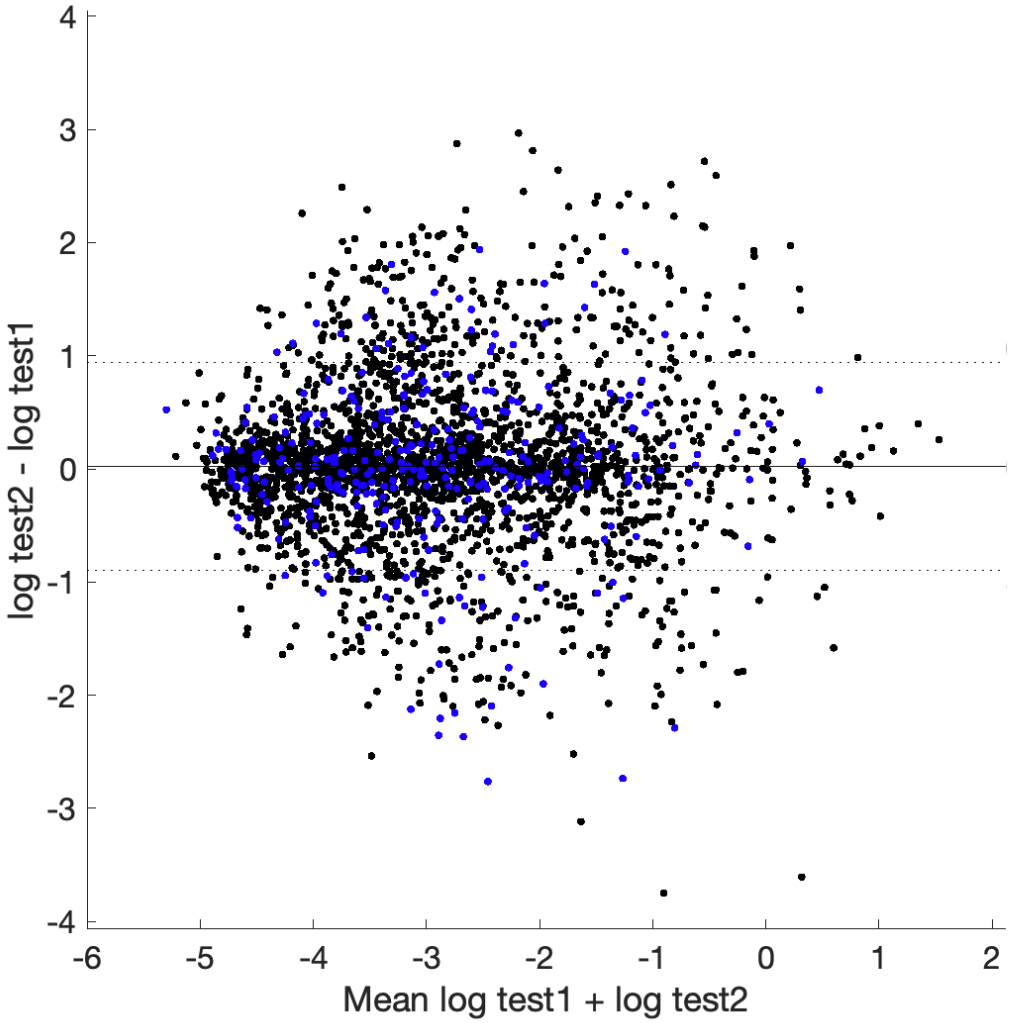

Figure 5.3.3. Bland Altman plot, eye imaged before and after PVD (Q129/S121). The anomaly variation from pre- to post- PVD (in blue) is compared with the anomaly variation of eight eyes imaged twice with no change in ocular status (imaged in black). Each point represents one of bins 2-20 from the anomaly spectrum for each of the 17 regions. Only frequency bins 2-20 were included, as the size of anomaly outside this range is small and variation likely to be reflect noise. This is a $\log_2$ Bland Altman plot, so $\log_2 A_2 - \log_2 A_1$ is plotted against $(A_2 + A_1)/2$, where A_1 and A_2 are anomaly bin values 2-20 from regions 1-17.

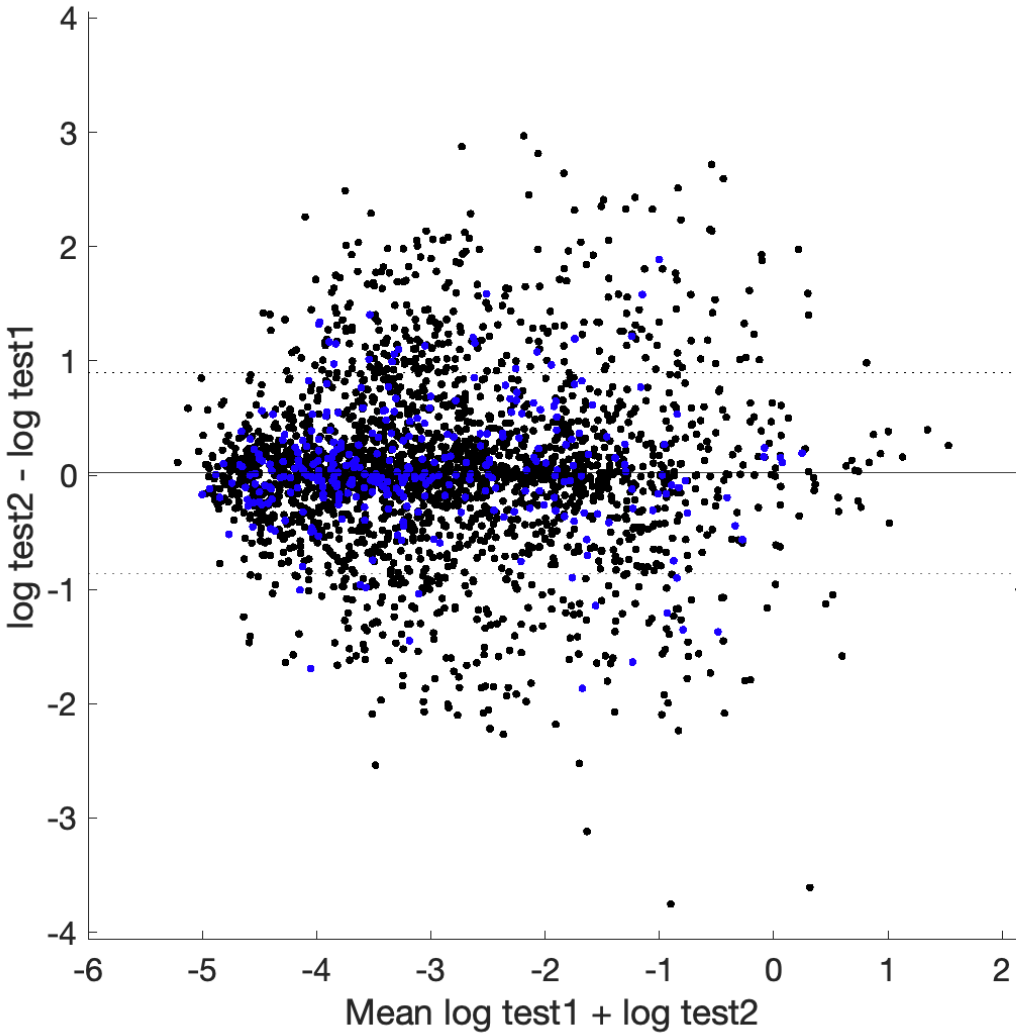

Figure 5.3.4. Bland Altman plot, eye imaged before and after PVD. Eye (S113/S125) imaged before and after PVD (blue points), with limits of agreement set by the control eyes (black points).

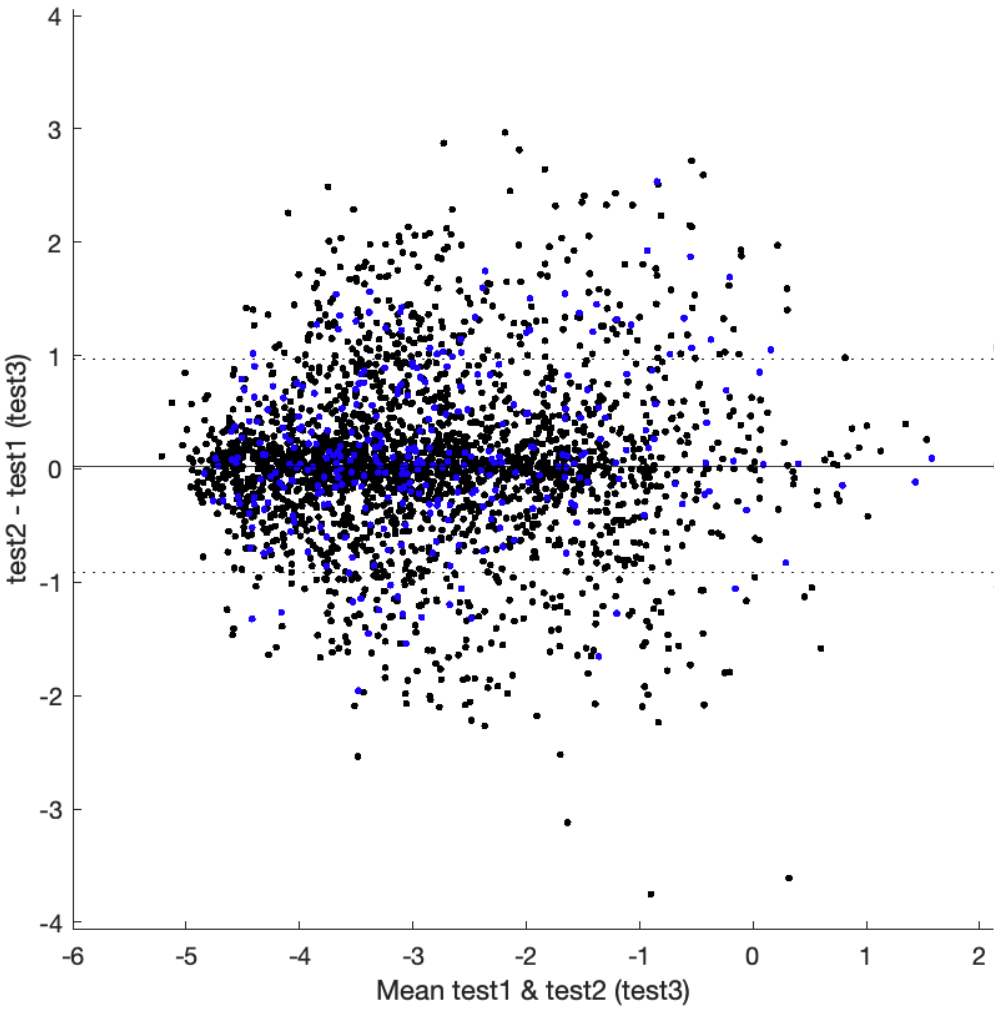

Figure 5.3.5. Bland Altman plot, eye imaged before and after PVD. Comparison of two imaging sessions (in blue) for eye S210/S410, before and after PVD.

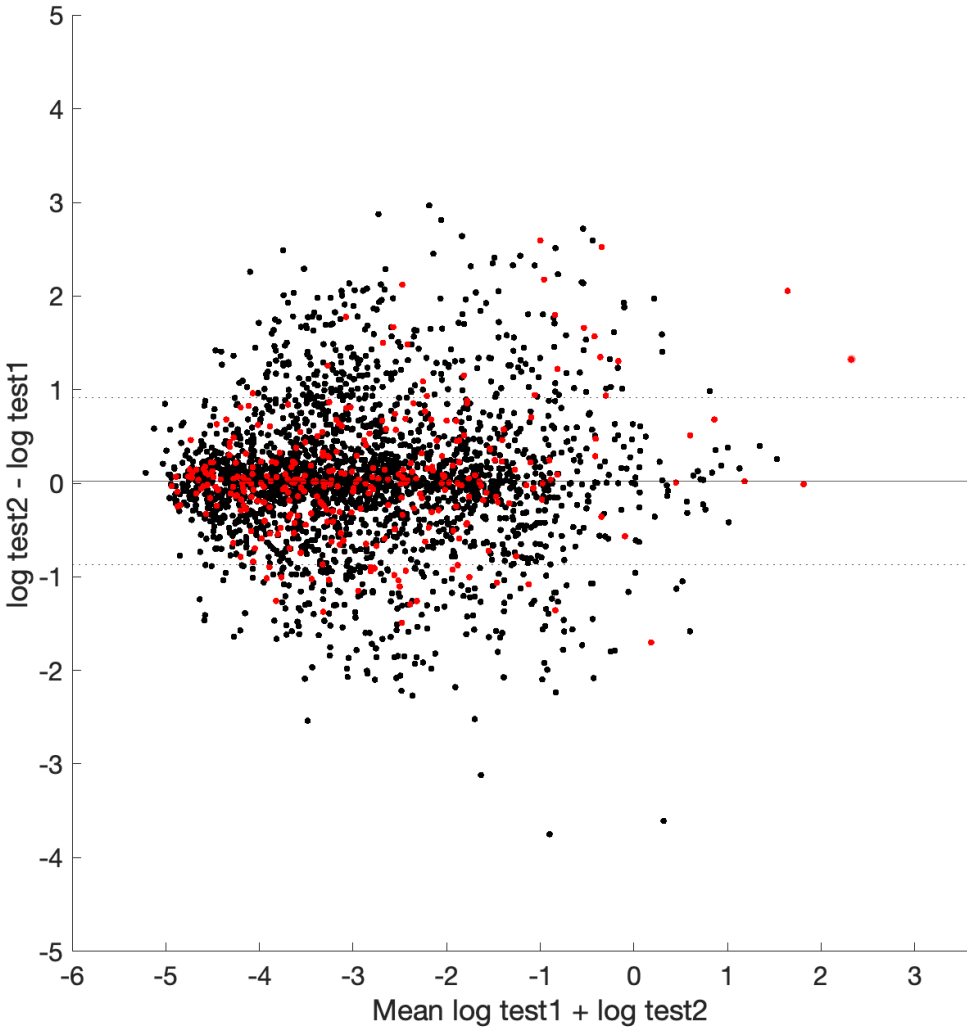

Figure 5.3.6. Bland Altman plot, retinal detachment eye (R294/S223) anomaly variation between before-PVD and after-vitrectomy for retinal detachment (plotted in red). Control eyes plotted in black.

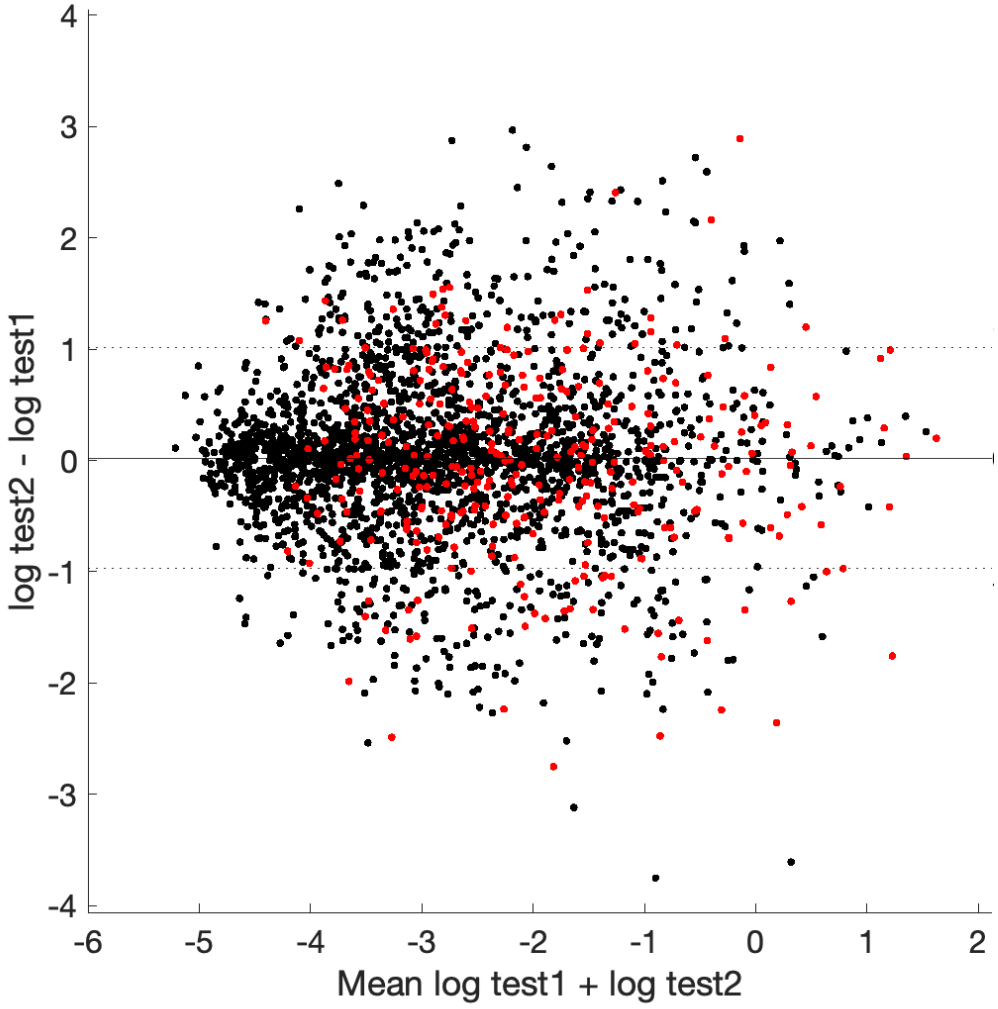

Figure 5.3.7. Bland Altman plot, second retinal detachment eye. This eye was imaged before PVD and after vitrectomy for retinal detachment (R276/S224).

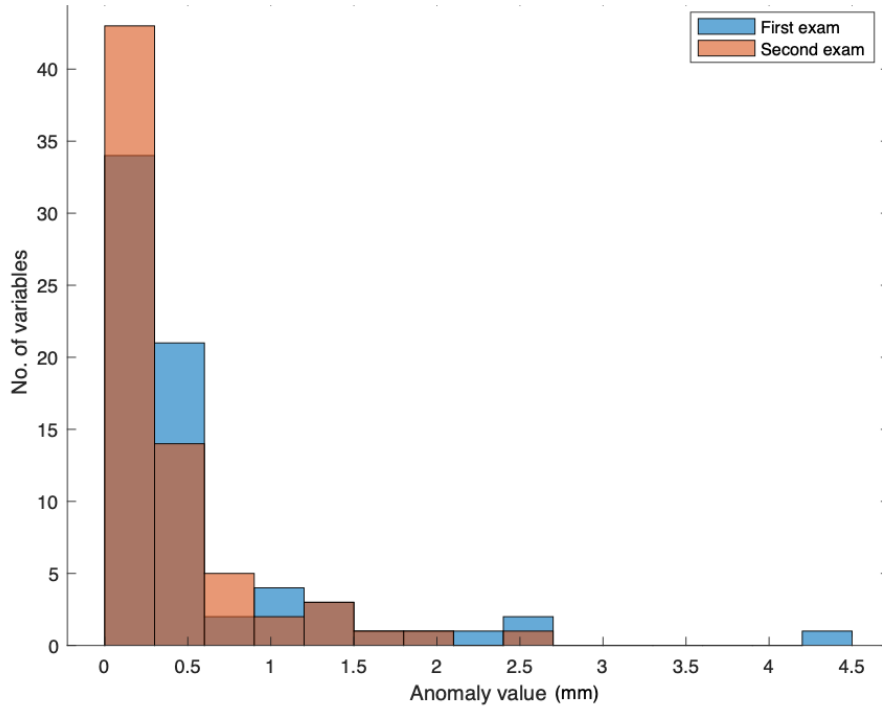

Figure 5.3.8. Histogram of anomaly bin values outside limits of agreement. The *y*-axis gives the number of variables (bin moduli) at each anomaly bin value indicated by the *x*-axis where their test-retest difference was outside the limits of agreement set by the test-retest examination of eyes with no change in state (Table 5.3.2). Most of these anomaly values are of very small magnitude, so that small variations will lead to breaching the limits of agreement without any change in classifier performance. The darker brown colour arises from the lighter brown and blue overlap. This is eye R276/S224 (Figure 5.3.7)

Conclusion

The test-retest variability was low comparing before and after PVD, and comparable to eyes imaged twice with no change in ocular status. Correspondence between before PVD and after PVD related retinal detachment repair anomaly values was also good, with a low number of variations in higher anomaly values. Anomaly measurements appear to be stable despite PVD and retinal surgery in these eyes. Most metrics from these eyes were within limits of agreement (+/- 1.96 standard deviations from the mean) set by eyes imaged twice without change in state, and all but one of the [region, bin] anomaly values used in the classifier in these eyes was within the limits of agreement. In consequence of this, there was no change in the classification label for any of these eyes imaged twice. With all imaging, however, it is important to sample the correct tissue. The hypothesis that PVD or vitrectomy for retinal detachment alters retinal shape could not be confirmed.

Discussion

With the horizontal peripheral retinal B scans from HD 21 cubes separated by 0.4 mm, it is unlikely repeat scans will always image the exact same retinal tissue, both from variation in gaze position and changes in the position of the OCT scans within the imaging viewfinder. Macular scans can use the Cirrus facility to align repeat images, but this is more problematic with eccentric images relying on participant eye movements to visualise an area where the retinal landmarks may be indistinct and the retinal image of poor quality. With repeat imaging of these eyes, the same process was undertaken both times, with subjects asked to look in set directions (up, up to the right, etc.), but with no attempt to match the second imaging set to the first. This might result in some variation in the area of retina imaged for any region. Furthermore, the area imaged by the OCT within the visualised region can vary: in the x- and y- axis directly by moving the OCT reticle, as well as x- and y- axis variation from z-axis displacement sampling a separate zone within the cubic window. As quantification of shape through Fourier analysis is very sensitive, some variation in output as a result of these differences was to be expected. The question was, does the small alteration in area of examination significantly alter the measurements, and does this alteration alter classification? From the five eyes examined here, the answer seems to be no.

5.4. The effects of laser and retinal break location on classification

Introduction

All retinal tear and detachment eyes used in training and testing the classifier had received laser photocoagulation to seal retinal breaks, either as a stand-alone intervention or during vitrectomy. Laser therapy disrupts the outer retina and retinal pigment epithelium, and may damage the choroid, by way of producing chorio-retinal adhesion and to prevent sub-retinal fluid migration. These effects may both alter retinal shape as well as the identification of the retinal contour. Where the latter factor applied (retino-choroidal scarring leading to loss of the retinal pigment epithelium landmark) contour tracking was terminated, i.e., no shape information was taken. However, it is also possible that the effects of laser therapy influence the surrounding retinal shape. Not all eyes will have visible laser within the regions imaged with OCT. The retinal tears may be in a different region of the eye from the superior and supero-temporal, or located more peripherally to the area that was imaged. To investigate whether laser within the OCT images was influencing classification, the classification of eyes with and without visible laser was compared.

A related question was whether the presence of the retinal breaks themselves in the regions considered by the classifier affected performance. The classifier used only shape information from superior and supero-temporal retina, and it is notable that those locations are the most common site of retinal break formation[260]. It might be the case that the classifier preferentially detected the most common pathology (superior and supero-temporal breaks) and neglected retinal breaks arising elsewhere. This was explored by looking at the category labels applied where the breaks were in superior and supero-temporal retina compared to labelling of eyes where the retinal breaks occurred elsewhere.

Aim

This section aimed to answer two queries regarding two factors that may influence the classification of retinal detachment and PVD eyes through OCT measured retinal shape. If either of these factors influence classification, then the test will be less successful at predicting retinal detachment prior to PVD occurring. The first was whether chorio-retinal laser scarring visible in OCT images was influencing classification. The second was whether

location of the retinal break in the superior and supero-temporal retinal improved classifier performance.

Methods

The effect of laser

Laser was considered present for this analysis if chorio-retinal scarring was seen on the OCT images, or if the chorio-retinal scarring was visible in the retinal image taken at time of image capture, even if not present within the (smaller) area of retina sampled by OCT.

Subjects

This analysis was performed with 132 validation set retinal tear and detachment eyes.

Statistical analysis

Fisher's exact test was used to test for non-random distribution of visible laser between the classifier labels.

Location of retinal break

Subjects

Retinal break locations were taken from the clinical notes and record of treatment. The presence of visible retinal breaks or laser in the OCT image was not required for this analysis. Where breaks were in multiple locations, eyes were included in the superior/supero-temporal group if any of the breaks were present within those regions. Eyes were included in the "other" group only if no breaks were present superiorly or supero-temporally.

All 89 eyes with information on retinal break position from the validation dataset up to T1 123 (12 April 2021) were included.

Fisher's exact test was used to test for non-random distribution of label attribution comparing eyes with any retinal breaks in the superior and supero-temporal regions compared to eyes with only retinal breaks elsewhere.

Results

Effect of visible laser

82 (62%) had no laser scars in the OCT cubes used for classification, with the laser either anterior to the region imaged or in a different part of the eye. Distribution of visible laser by classification is shown in Table 5.4.1. Of the thirty nine eyes labelled '2' (23 retinal detachment and 16 retinal tear), 26 (66 %) had no laser marks identifiable within the OCT images (Fisher's exact test, p = 0.56), suggesting that laser made no difference to classification.

Table 5.4.1. Relationship between classification label, and the presence of laser induced scarring in regions 3 & 5.

	Laser reaction present S/ST retinal area	
Category label	**Yes (laser marks present)**	**No (laser not present)**
1	37	56
2	13	26

Total: 132 eyes. S = superior, ST = supero-temporal regions.

Effect of retinal break location

Distribution of retinal break location by classification label is shown in Table 5.4.2. Fisher's exact test applied to this table found no significant difference between groups (p = 0.75), suggesting that location of tear(s) had no impact on classification for retinal detachment and retinal tear eyes.

Table 5.4.2. Relationship between classification label, and the presence of retinal breaks in regions 3 or 5.

	Retinal break present S/ST retinal area?	
Category label	**No (not present S/ST)**	**Yes (break(s) present S/ST)**
1	11	45
2	5	15

Total: 76 eyes. S = superior, ST = supero-temporal regions.

Conclusion and Discussion

Neither visible laser scarring in OCT images, nor location of retinal break in the superior or supero-temporal retina significantly influenced classification of retinal detachment or retinal tear eyes. Were they to do so, it could be expected that attempted classification prior to PVD would be less successful. Based on the distributions in Tables 5.4.1 and 5.4.2, 320 eyes would be required to have sufficient power to confirm or refute the hypotheses that location of retinal break or the presence of visible laser have no effect on classification.

SL examined all B scans and noticed no pattern in retinal shape adjacent to chorio-retinal laser scars, although eyes were not imaged prior to laser, and it was possible that shape change in adjacent retina did occur. Identifying retinal shape with graph theory algorithms can be complicated by significant chorio-retinal scarring, which produces deeper higher intensity pixels. As a result, segments of scarred retina in OCT were often cut from retinal shape extraction and information from that part of the retina excluded, with fewer samples taken from eyes with laser reaction. This might reduce rather than increase the sensitivity of classification, so it is possible that a combination of these factors (laser increasing irregularity but reducing retinal sampling) produced the absence of any observed effect.

Chapter 6. Swept source OCT and retinal shape

Introduction

Chapters 3.4, 4, and 5 have explored the use of SD OCT in analysing retinal shape. Over the last decade, the swept source OCT has emerged as a new imaging modality with its own unique properties. SD OCT scan rates of 65 000 A scans per second can be exceeded by swept source devices, which may achieve up to 200 000 A scans captured per second[267,268]. Swept source OCT uses a tuneable laser to replace the SD OCT super-luminescent diode as the sampling light source, with the returning light from the object captured by a dual-balanced photodetector[269]. This laser has a wavelength centred at 1060 nm, longer than the SD OCT light source, which has the disadvantage of reducing its minimum theoretical axial resolution, although the fast resampling combined with image processing can offset this to produce results similar to SD OCT[270]. The advantages of swept source OCT are a faster image capture rate and lower sensitivity roll off with increasing tissue penetration which provides greater image quality across the depth of tissue[166,172]. This has improved OCT angiography[271–273], as well as enabled longer and wider retinal sampling in a single B scan[274,275].

The larger B scan image size makes the swept source OCT of interest for retinal shape analysis. Chapter 5 identified the useful shape features for classification of retinal detachment eyes had a wavelength between 3 – 9 mm, the latter being the maximum width of the B scan window (Figure 5.2.10). This raises the possibility that larger shape features captured by a wider B scan may improve classification performance.

Furthermore, the maximal scan width of 9 mm obtainable with SD OCT is only available in horizontal orientation (newer SD OCT devices released after swept source OCT became available can obtain both increased B scan widths of 12 mm as well as rotate the orientation away from the horizontal). The Zeiss Plex Elite swept source OCT has a maximum sample length of 16 mm which can be oriented to any angle. Section 3.4 found greater irregularity in inferior and superior retinal areas compared to temporal and nasal areas (Figure 3.4.3). As all scans were obtained in the horizontal orientation, this means the temporal and nasal scans are oriented roughly parallel with the optical axis of the eye, and the superior and

inferior scans perpendicular. Irregularity may be equally great in the horizontal meridian as in the superior or inferior when imaged with coronal sections; swept source OCT can investigate retinal shape in this direction.

This chapter reports the analysis of retinal shape measurements with swept source OCT, to investigate whether it can increase the understanding of retinal shape and its relationship to PVD, retinal tear, and retinal detachment.

As in Chapter 5, there are many more potential predictors than samples. For this reason, selection of optimum and elimination of unhelpful features is required. Ridge, Least Absolute Shrinkage Selector Operator (LASSO), and elastic net are regularization methods to reduce overfitting a model to its training data and improve its performance in validation sets. They reduce within feature variance at the expense of increased feature bias. Ridge reduction will not eliminate features whereas LASSO will, making the latter suitable for predictor selection. As a result, LASSO performs better than ridge regularisation where many of the predictors do not influence model performance (have little or no predictive value). Elastic net as a compromise between ridge and LASSO has the advantage in dealing better with correlated predictors[276].

Aims

To compare retinal shape taken with the swept source OCT to that taken with SD OCT. Furthermore, to investigate whether the larger features and different image orientations made possible with swept source OCT improved classification of retinal detachment eyes.

Methods

Subjects

Participants were recruited as in Chapter 5, from out-patient clinics at Flinders Medical Centre, Eyemedics, and the Royal Adelaide Hospital, South Australia. All were imaged between July 2020 and January 2022 at Flinders Medical Centre using a Zeiss swept source Plex Elite OCT. Eyes were imaged from individuals who had experienced either a PVD, retinal tear, or retinal detachment.

Swept source OCT images were taken with the UHD 1 Spotlight 200 kHz scan, a single 16 mm (2047 pixels) wide by 6 mm (3072 pixels) deep composite image created from 100 repetitions of the B scan (Figure 6.1). Here, five images were taken from each eye. The first macula image was followed by images taken with the participant looking up, down, left, and right. The left and right scans were oriented vertically, at 90 degrees to the horizonal, with the scans taken looking up and down parallel to the horizon. If the scan position is moved too peripherally, the retina may be lost by intrusion of the pupil margin or other opacities into the field of view. OCT image scan capture was performed at the most extreme eccentricity where retina could still be visualised across the full 16 mm B scan window (Figure 6.1). The 6 mm deep scan ensured all but the most irregular (highly myopic) eyes were able to be imaged across the full width of the scan window.

Correlation with axial length

Spearman's rank correlation was performed between axial length and average anomaly, anomaly for each region, and age, for all eyes and by diagnostic group.

Image processing

The process of image analysis was similar to that described in the methods for SD OCT images (Chapter 2), with programs written specifically for this study in MATLAB. All retinal shape information was extracted from the OCT images using the programs `CretiffSS` and `SSA2FFT` (Appendix C), which used the purpose-built graph theory algorithm developed by Tyra Lange (Section 5.2, Development and evaluation of a research test for ingoing prediction). The identified retinal contour had the best fit curve removed, and then a fast Fourier transformation of the irregularity left after removal of best fit curvature was performed. Anomaly values were calculated by comparing each scan irregularity to the average irregularity of 80% of the PVD eye sample, with the average irregularity determined from scans distributed randomly into five-folds in an axial length stratified manner. A feature vector was created for each eye consisting of the first 30 bins from the anomaly spectrum for each of the four directions of gaze (in order up, down, temporal, nasal), the best fit curvatures to the retinal contour for each region in the same order, and then the

axial length of the eye and the participants age, to create 126 potential predictors (`SStabFFT` and `SStabana`).

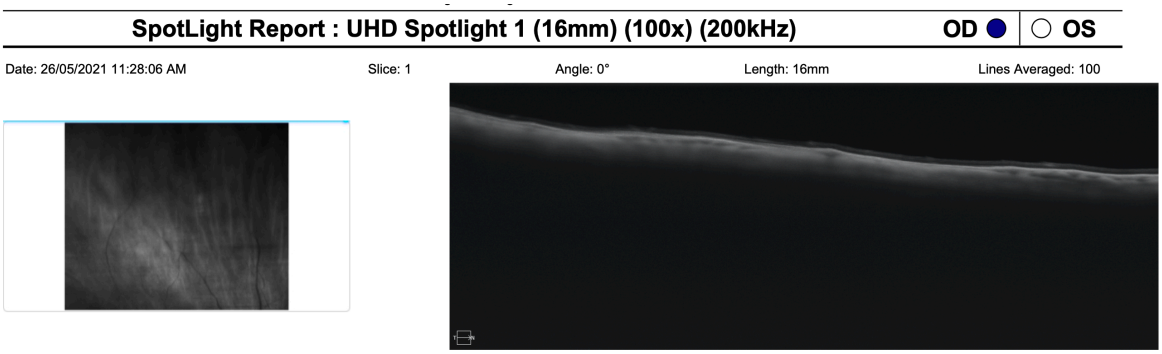

Figure 6.1. Sample swept source OCT image output. The blue line at the top of the retinal image (left) identifies what part of the retina is imaged by the OCT (seen on the right). As shown here, the retina imaged by OCT could be outside the area imaged by the scanning laser ophthalmoscope.

Feature selection

Eyes were split into training and testing sets, and feature selection performed with the training set prior to testing (`SSTrTst`). Univariate and multivariate feature selection approaches were explored. The regularisation methods LASSO and elastic net were used to identify potential feature combinations. Both LASSO and elastic net input variables were scaled to a mean of 0 with variance of 1 with elastic net $\alpha = 0.5$, and ten-fold cross-validation to identify potential features. Maximum relevance – minimum redundancy[277], the absolute difference between retinal detachment and PVD anomaly values, neighbourhood component analysis, rank importance of predictors using the ReliefF algorithm, and univariate feature ranking via Chi-squared tests and regression testing to determine whether each predictor was independent of the response variable was performed. For these latter six methods a table was constructed listing the most importance predictors identified by each method (Table 6.2).

Once a reduced feature set was obtained, all possible combinations of these were explored with quadratic discriminant analysis to identify the classifiers with three or fewer predictors with the highest sensitivity for a specificity greater than 0.90 within the training set. After

optimisation of group weighting to again maximise sensitivity for specificity greater than 0.90, classifier performance with the test set was determined. These specificity thresholds were selected to reduce the number of false positives (identifying a PVD eye as one with a retinal detachment).

Results

Subjects

Participant demographics and the number of eyes in each group and are reported in Table 6.1. Subjects with a retinal detachment were younger and had larger eyes than those who experienced PVD. Those who experienced a retinal tear had eyes with shorter axial length than those who presented with a retinal detachment.

Table 6.1. Participant demographics.

Group	Number of eyes	Age (SD)	Axial length
PVD	77	65.3 (6.1)	24.41 (1.10)
Retinal detachment	64	62.6 (8.5)*	25.10 (1.10)**
Retinal tear	51	64.1 (6.5)	24.41 (1.12)***

* Age, $p = 0.04$; **axial length, $p < 0.005$, comparing PVD to retinal detachment. *** axial length differed between retinal tear and retinal detachment eyes, $p = 0.001$, with no other difference between retinal tear eyes and the other groups. Two-sample *t*-tests, SD = standard deviation. Age in years, axial length in mm.

Within-eye distribution of irregularity

Irregularity was greatest in the inferior retina. Irregularity in the coronal-oriented temporal and nasal scans was slightly less than the superior irregularity (Figure 6.2).

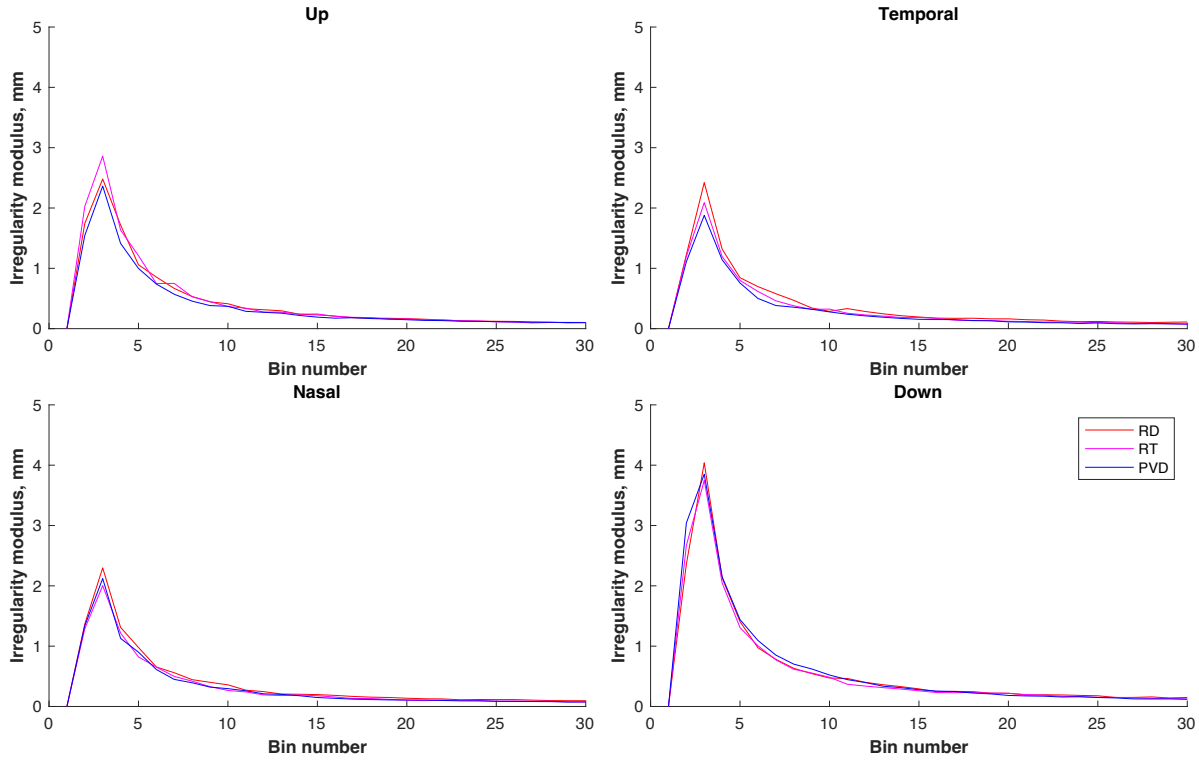

Figure 6.2. Regional irregularity, swept source OCT. Average irregularity was greater in the inferior retina for all diagnostic groups. PVD eyes (blue), retinal detachment eyes (red), retinal tear eyes (pink). Up = superior retina, down = inferior retina.

Correlation of irregularity with axial length

Axial length correlated weakly with the average total anomaly of all eyes (p = 0.02, ρ = 0.17), and average total anomaly for the PVD group alone (p = 0.04, ρ = 0.23), but not with average anomaly of retinal detachment or retinal tear eye groups. Within the four individual regions, axial length correlated weakly with the total anomaly from superior (p = 0.05, ρ = 0.14) and inferior (p = 0.015, ρ = 0.18) retina. In individual diagnostic groups this correlation only persisted for PVD eyes (superior retina, p = 0.08, ρ = 0.20; inferior retina, p = 0.03, ρ = 0.24) and not with retinal detachment or retinal tear eyes.

Feature selection

Elastic net regularisation identified a group of six predictors, with feature vector indices [4; 36; 79; 83; 86; 125] and mean squared error 0.22; and LASSO a group of three predictors [4; 83; 125] with mean squared error 0.24. The top six candidate features from the other feature reduction methods are shown in Table 6.2. There are 22 different features in this

table. As all the elastic net regularisation features are within the top five rows of Table 6.2, these six features were further explored through training set classifier performance.

Table 6.2. Six best candidate features.

Abs (RD – PVD)/PVD	MRMR	ReliefF	Neighbourhood component analysis	Chi2	F-test
4 U4	4 U4	125 AxL	33 D3	4 U4	4 U4
80 T20	125 AxL	126 Age	32 D2	36 D6	36 D6
86 T26	32 D2	4 U4	34 D4	125 AxL	125 AxL
79 T19	89 T29	36 D6	4 U4	95 N9	95 N9
83 T23	124 Tbfc	39 D9	2 U2	31 D1	31 D1
90 T30	122 Dbfc	21 U21	126 Age	28 U28	115 N25

Each column reports in order the 1st to 6th best candidate features for each selection method. Column 1: the absolute difference between average retinal detachment and PVD eye feature value, divided by the magnitude of the PVD feature value. MRMR = maximum relevance minimum redundancy. Relieff = predictor importance ranked through algorithmic variable weighting that rewards common dependencies, based on the categories of the 10 nearest neighbours. Chi2 = variable selection through *p*-values from Chi-squared tests of variable and diagnosis. F-test = predictor ranking via *F*-test *p*-value. The first column is an unsupervised method, the others are supervised filter methods. Each candidate feature is identified by a number reflecting its position in the feature vector, as well as by key. Key: U, D, T, N = up, down, temporal, and nasal anomaly bin regions, with the accompanying number equal to bin number, bfc = best fit curvature, AxL = axial length.

Training set classifier performance

All possible combinations of 1 – 6 features from the six feature candidates were identified and used to train quadratic discriminant classifiers. The four classifiers with the highest sensitivity for specificity with the training set are shown in Table 6.3. The classifier generated from features 4 (fourth bin from the superior retinal scan), 83, and 86 (respectively bins 23 and 26 from the temporal retinal scan) was selected for use. Five-fold cross validation of the classifier using training set eyes repeated 20 times had an average success rate = 0.66, with the standard deviation of the success rates = 0.07. Table 6.4 presents the confusion matrix including subsequently recruited validation set eyes. Initial receiver operating characteristic curve generated by 5000 bootstrap replicas had an inverse sigmoid or logit shape suggesting the predictor had a non-linear (U-shaped) relationship

with outcome[278]. This was corrected by centring the classifier output to its median value, leading to an area under the curve = 0.74 (95% confidence intervals 0.59 – 0.85, Figure 6.3).

Table 6.3. Classifier performance.

	Training set eyes		Test set eyes		
Features	**Specificity**	**Sensitivity**	**Specificity**	**Sensitivity (RD)**	**Sensitivity (RT)**
[4,79,86]	0.912	0.366	0.95	0.36	0.41
[4,83,86]	0.912	0.390	0.90	0.50	0.35
[79,83,125]	0.912	0.488	0.90	0.45	0.24
[79,86,125]	0.930	0.366	0.90	0.45	0.25

Training then testing set performance for four quadratic discriminant analysis classifiers. The classifier in the second row is described further in Table 6.4 and Figure 6.3. For this model, cross validation of the mean success rate of the training set = 0.66, with standard deviation of the success rates = 0.07. RD = retinal detachment, RT = retinal tear.

Table 6.4. Confusion matrix for swept source OCT classifier.

	Label 1	**Label 2**	**Total**
PVD	26	5	31
Retinal detachment	13	12	25
Total	39	17	56

Numbers represent eyes from the combination of the initial and extended validation set eyes. This classifier was the second line in Table 6.3. Sensitivity = 0.48, specificity = 0.84, Fishers exact test, p = 0.018.

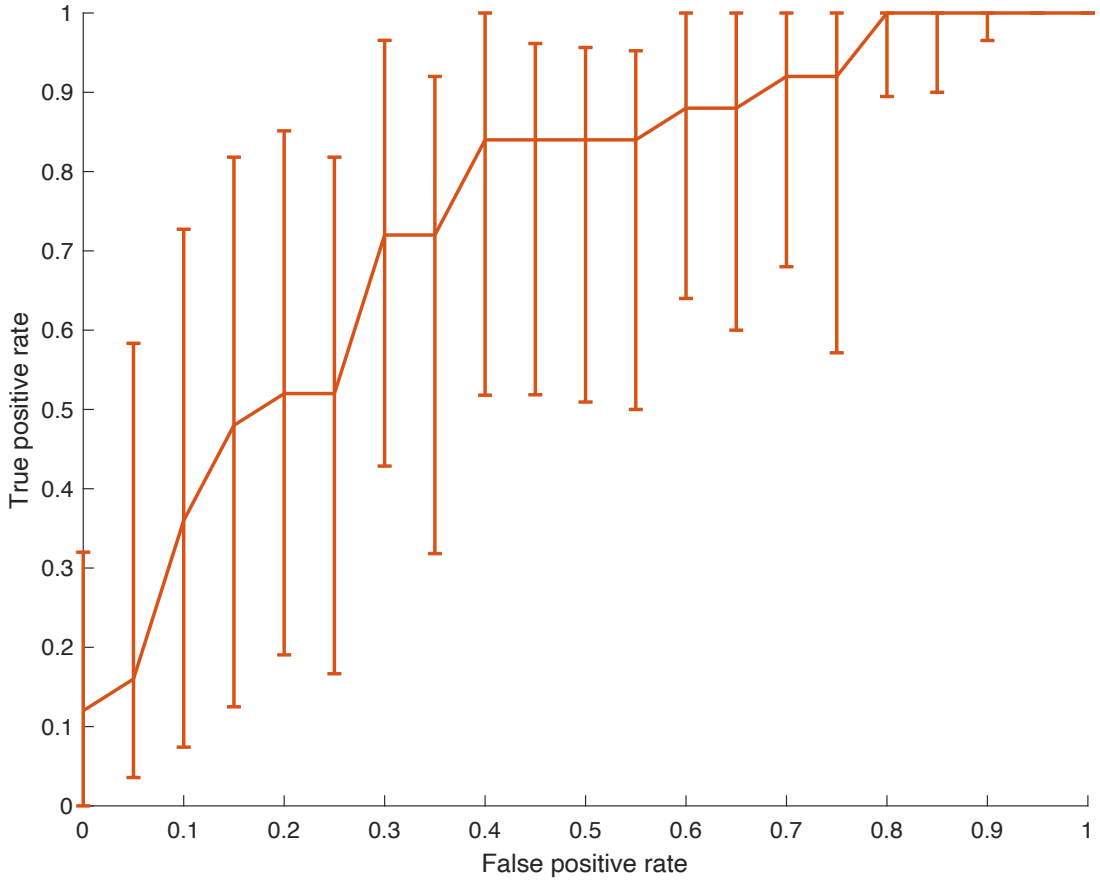

Figure 6.3. Receiver operating characteristic curve. The vertical bars represent the 95% confidence intervals, generated by 5000 bootstrap replicas. Classifier output centred to the median. Area under the curve = 0.74 (95% confidence intervals 0.59 – 0.85), generated with `SSneweyetest`.

Conclusions and discussion

Shape feature distribution within-eye and between eyes of different size

The swept source OCT became available during the course of this study. The increased B scan size and variability of B scan orientation enabled exploration of shape in a manner complementary to that of SD OCT. Swept source OCT retinal irregularity exhibits an irregularity distribution similar to SD OCT irregularity (Section 3.4), being greatest in inferior retina. Nasal and temporal retinal irregularity with swept source OCT was sampled vertically, orthogonal to SD OCT. In this orientation, irregularity in these regions was of a similar magnitude to superior retina, suggesting the lower magnitude irregularity seen in SD OCT (Figure 3.4.3) related more to the horizontal scan orientation rather than to regional

differences between superior and inferior retina and temporal and nasal retina. This supports the hypothesis that mid-peripheral irregularity is greater when measured coronally compared to transversely.

Swept source OCT shape correlated with axial length in eyes with a PVD. The lack of correlation between axial length and shape in retinal tear and detachment eyes, along with the slightly greater average irregularity in these eyes suggests that these eyes are simply more irregular regardless of size.

Features

PVD eyes alone were used to create the average B scan irregularity, so the average B scan reflected the most common diagnostic group. If further classifiers were to be developed, it would be undesirable to use varying proportions of a mixture of pathologies for each to generate an average scan. Candidate feature selection was performed with both an average B scan from the PVD eyes and then repeated with an average B scan from PVD and retinal detachment eyes combined and produced the same feature sets (Table 6.2), confirming this distinction was minimal for this dataset.

Feature selection took as potential features the shape anomaly and best fit curve from four peripheral regions, eye axial length and subject age. From 126 possible features, reduction to candidate features was explored by two methods: regularisation with LASSO and elastic net, looking for combinations of features; and features taken from maximum relevance – minimum redundancy, neighbourhood component analysis, ReliefF algorithms, *F*-test/Chi-squared for feature – response dependence, and the average difference between retinal detachment and PVD features divided by the PVD feature value. Results from these approaches produced similar candidate features.

Of the six candidate features selected by elastic net and used to train classifiers, two were consistent with or expected from the results from the SD OCT classifier: 4 (upper region longer wavelengths), and 125 (axial length). One predictor, 36 was from the consistently more irregular inferior region. The three remaining features were comparatively higher

frequencies from the temporal region. Temporal and nasal retina was imaged in a vertical orientation with the swept source OCT, which was not performed with SD OCT.

The best three-variable model had a sensitivity and specificity in the validation set similar to the training set. The three features used were bins 4 (superior retina), 23 and 26 (temporal retina). With a bin width of 0.0625 cycles mm^{-1}, these are 0.25 cycles mm^{-1} (a 4 mm feature wavelength superiorly), 1.44 cycles mm^{-1} (a 0.69 mm feature wavelength temporally), and 1.62 cycles mm^{-1} (a 0.61 mm feature wavelength temporally). The first (bin 4, superior retina) parallels the useful shape features identified with SD OCT. The useful temporal features are almost an order of magnitude smaller. This may relate to the temporal scans coming from more anterior retina than the superior scans (Figure 3.3.4 and Table 3.3.2).

Classifier

Four classifiers were tested (Table 6.3), with two including a lower frequency superior retinal anomaly (which was used in the SD OCT classifier, Chapter 5) and two including axial length. These were tested as both the other features in each model and their training set performances were all similar to each other. They were tested to see whether the superior retinal anomaly or axial length proved more important in classification. Perhaps surprisingly in the context of prior knowledge of the association between myopia and retinal detachment, the superior retinal shape feature had greater utility than axial length. None of the best performing classifiers included both axial length and the upper region fourth anomaly bin, which would be a combination similar to the SD OCT classifier. The lowest frequency features that were sampled with swept source OCT but not SD OCT were not utilised in these classifiers, suggesting that larger B scan size is not critical when sampling shape to classify retinal detachment and PVD eyes.

The swept source OCT classifier performed slightly better in both sensitivity and specificity than the SD OCT classifier. This used one shape feature that was and two shape features that were not sampled by SD OCT in Chapter 5. Newer SD OCT devices are likely to be able to image this retinal anomaly in the temporal region. This swept source OCT data provides further support to the concept that retinal shape differs between eyes that have experienced a retinal detachment and those that have experienced a PVD. It does not

identify whether this pattern of shape features precede retinal detachment. Prospective data will be required to demonstrate whether these features are present prior to retinal detachment occurring.

Chapter 7. Discussion

Thesis overview

The aims of this thesis were to explore whether new information could be extracted from retinal OCT, specifically the shape of the retinal contour as represented by the retinal pigment epithelium. In particular, the objective was to investigate the relationship between retinal shape and myopia and retinal detachment. Similar work exploring posterior segment shape in myopia has previously been performed both with MRI for globe shape, and OCT, focussed on the macula. While shape has been used to identify disease, this has been largely in a qualitative manner for conditions such as dome-shaped maculopathy, focal choroidal excavation, and optic nerve head swelling. Most of the prior work in myopia has been focussed on the larger eyes with the greatest differences in shape. Imaging artefact effects on observed shape are recognisable, and either small (oblique scanning, defocus) or correctable (the effect of axial length on curvature)[135]. The key developments of this thesis are the extension of shape analysis to identify eyes with retinal detachment, the analysis of shape across a continuum of eye sizes and consequent refractive errors, and the systematic use of quantitative OCT retinal shape analysis beyond the macula. Much (but not all) of the prior work has been on the best fit curvature to retinal shape. This work has demonstrated that retinal irregularity is a useful property worthy of analysis.

OCT irregularity increased with increasing eye size represented by axial length in a manner similar to the increased globe irregularity seen with increasing myopia in MRI. This is the first identification of this irregularity in peripheral retina[279]. This provides some reassurance that what has been measured is consistent with prior knowledge of myopic eye shape. The discovery that irregularity consistently differs in magnitude in different regions of the eye, with inferior areas more irregular, is a novel finding.

The age range of the subjects in Chapter 5 was narrow, confined to those had experienced PVD in at least one eye, usually in the middle years of life. The pathology of myopia progresses throughout life, and therefore it is possible that irregularity itself will increase over time. Shape anomaly increased in one eye re-tested over two years without experiencing PVD, altering its classification from “PVD” to “retinal detachment”. If this

increase in anomaly over time is repeated in other eyes, it will limit the useful classification period for retinal detachment from decades or years to years or months, particularly in eyes with anomaly values close to the classification thresholds (Figure 5.2.12).

A shape analysis discriminator will be of clinical utility if it can identify eyes at risk of retinal detachment prior to the development of PVD, to direct counselling or even administer prophylactic retinal laser to reduce the risk of vision loss from retinal detachment. The classifier developed in Chapter 5 was able to identify with high specificity some (but not all) retinal detachment eyes from a sample of retinal detachment and PVD eyes. If the same classifier has the same specificity in eyes that have not undergone PVD, a positive test outcome will indicate future risk of retinal detachment. While sensitivity is low, this is preferable to a low specificity which would potentially expose eyes with low risk of retinal detachment to unnecessary intervention[221], and this is the first report of any method that can distinguish between retinal detachment and PVD eyes with the OCT. Specificity is more important here than success rate (assuming the test has some sensitivity). Without external verification, a clinical test should avoid a false positive that might expose a non-pathological eye to intervention.

Gaze position analysis

There were noticeable differences in gaze positions during imaging between different individuals. The OCT cube protocol used for Chapters 4 and 5 consisted of 21 parallel B scans over 8 mm of vertical range, with classification based upon the most irregular scan within that sample. As a result, the exact location of any scan used in different eyes varied between individuals, reducing the link between gaze position and retinal shape information. This variation is a sampling issue but does not invalidate the consideration of regional variation in irregularity or classification between eyes.

There is evidence that each individual has an “oculomotor signature”, or consistent quantitative performance in ocular smooth pursuit and saccadic eye movements[240]. This individual gaze consistency may contribute to the consistency in within-eye shape analysis, both in regional shape metrics (as seen in Bland Altman plots) and in the classification result

when individual eyes were re-imaged. The finding here that the upgaze eye position maintained for imaging declines with age and is on average less than other directions of gaze is consistent with other measurements of eye movements but has not been reported before.

Retinal tears

Patients with retinal tears experience both a different presentation and management for a pathological process that is very similar if not necessarily identical to retinal detachment. This is not simply due to a longer interval between onset of symptoms and presentation to health care, as many individuals develop a retinal detachment within hours of symptoms while many retinal tears present weeks after symptomatic floaters. The axial length of eyes that experienced retinal tear without retinal detachment was longer than the axial length of PVD eyes, and both were shorter than the axial length of retinal detachment eyes. This, while not unexpected, has not been reported before, and it may be the smaller size (or lower shape anomaly) of the eye slows the development of retinal detachment, giving the subject time to access health care before neurosensory retinal separation. Not all symptomatic retinal tears lead to retinal detachment, and the non-inevitability of retinal detachment after retinal tear may be related to the difference in axial length, although with a large overlap in axial length range between the groups it is unlikely to be clinically helpful.

Impact of imaging protocols on this work

Retinal shape consistency over time (similar features are identified over an interval of months) and space (adjacent images, either in parallel or series, show consistency and evolution of shape feature rather than incoherent changes) was reassuring. The bulk of this work was performed with a Zeiss Cirrus 5000 spectral domain OCT, with a maximum image size of 9 mm horizontally oriented B scans. The standard horizontally oriented HD21 protocol chosen for this study was used to maximise the area sampled in a single cube, but does not provide any information on retinal shape in the perpendicular direction. Alteration of the orientation of the B scan in the spectral domain OCT window reduces the size of area covered to a 6 mm scan length, and complicates the comparison between cubes taken at different positions in different eyes, as it is difficult to maintain the scan orientation perpendicular to the gaze direction when knowledge of that gaze direction is imprecise. As a

result, different information is being considered in scans of the lateral (temporal and nasal) retina, where scans are oriented along the sagittal axis, to the information taken from the superior and inferior retina, where scan orientation is transverse or coronal. The parallel B scans in the HD21 cube protocol are not aligned in the *z*-axis direction, nor corrected for *y*-axis rotation, meaning each must be considered independently and shape information from the vertical (*y*-axis) direction cannot be examined. The decision to limit analysis to horizontal scans proved justified by the finding that the useful classification features came from the lower frequency features, which would have been missed were smaller 6 mm OCT cubes used. The alignment of the parallel scans in the *z*-axis with 6 mm cube protocol would have allowed some shape information from the perpendicular to be considered.

There is continuous improvement in technology for imaging the eye. During the period this thesis was undertaken the length of B scans available in commercially available devices increased from 9 mm to 16 mm within a single scan. The vertical scan window extent (*y*-axis) increased from 8 mm to 12 mm. One of the reasons this became possible was the increase in the depth (*z*-axis) range from 2 mm to 3 mm with spectral domain, and up to 6 mm with swept source OCT. The greater depth is required to usefully widen the field of view, as otherwise (without altering the *z*-axis position mid-scan, which would complicate analysis of shape) the curvature of the retina in a wider scan would take it outside the field of view.

Current technology limits what area of the retina can be examined. The regions covered in this work are from the posterior hemisphere extending anteriorly toward the posterior extent of the vitreous base. This enabled imaging of retinal tears and extended beyond the boundary of most myopic posterior staphylomata. Newer imaging devices have extended anteriorly what retina can be visualised[11,280] but these were not available for this work, with products discontinued internationally without becoming available in Australia. Swept source OCT provides better image resolution across the entire depth of the B scan than spectral domain OCT, which may improve understanding of the tissue origin of shape features. The larger swept source OCT cube protocols provide information from both the horizontal and vertical direction simultaneously. Consistent A scan sampling in the *x*- and *y*- axis orientations will improve the understanding of shape in the different dimensions.

The base curve of the retina was quantified by a quadratic or parabolic curve. Parabolic estimation of the base curve provides a straightforward single variable assessment of the retinal contour. It has the advantage of limiting the number of variables needed to describe the base curve to one: the vertex curvature of the parabola. A wider selection of curve solutions from all possible conic sections (as opposed to only parabolic solutions) would be expected to lead to a closer fit. This could describe the retinal base curve with 2 variables: the radii of curvature derived from the general conic equation. However, initial work during this thesis found that minor changes in orientation or sampled arc of the retina within the OCT image led to large changes in the solution to the radius of curvature from the general conic equation, making this approach unreliable. The alternative to deriving the conic radii is to use all the constants from the conic equation, replacing one variable with six that are less intuitive and no more robust to variation in orientation than the parabola.

While OCT retinal shape values quantified in this work were consistent with repeat imaging, measurement is influenced by factors other than the retina itself, including the optics of light transmission from source to object and back. Most but not all imaging artifacts discussed in the Introduction (Section 1.2.2) have little impact on the information studied in this thesis. Those that do can affect the assessment of base curvature. As a result, the quantities reported here for curvature reflect not the true local curvature of the eye, but the curvature influenced by the examination method. Furthermore, it should again be emphasised that local curvature has little relationship to broader retinal curvature as the OCT samples only a small and localised arc. B scan retinal shape here is therefore a property to compare to other B scans for comparison and classification. Different approaches to shape analysis and different imaging devices (OCT or other imaging tools) may produce different results.

Machine learning

This thesis differs in two important ways from many reports that have used machine learning techniques in ophthalmology[215]. Firstly, this is not an assessment of the potential for machine learning to be able to predict a disease that can be currently predicted by a human operator. Rather, it has used the techniques of machine learning to identify a novel

image-based feature that may become a diagnostic sign for retinal detachment. Secondly, the use of machine learning rather than deep learning techniques, while required by the lower sample size studied here compared to most, but not all, published deep learning papers[214,281], has the advantage of avoiding one of the hazards of "black box" algorithms in that the source of classification here is clear, even if the reason for the association between shape and pathology is at present uncertain. This promotes an understanding of the association between retinal shape and retinal detachment, opens further avenues for investigation[282], and gives more confidence in what may be considered unusual results[283].

Aetiology of irregularity

The retinal shape was measured with the eye turned away from the primary position. This work does not distinguish shape features that are gaze position independent from those that are induced by eccentric gaze. The features used here may be independent of eye position or arise from eccentric gaze due to localised variations in tissue flexibility. Imaging eccentric retinal shape with an OCT imaging beam that can alter its incident angle while the eye remains in the primary position might answer this question. Hoang[279] and others[284] have explored the shape changes produced from eye movements in highly myopic eyes (axial length 27-39 mm) with MRI. These were most apparent in downgaze with a measurement (the length and volume of an axially oriented cylinder within the vitreous chamber) that relates to changes in macula shape and position relative to the corneal limbal plane. The "corrugations" in retinal shape in the superior and inferior retinal periphery measured in this thesis are parallel to the direction of gaze and muscle action, and are therefore not arising from direct muscle-contraction induced globe compression. Ghosh[284] found a small increase in axial length on downgaze, and it may be that this axial lengthening is producing irregularity through secondary concentric contraction. Even if these features are gaze dependant, they remain a clinical sign related to myopia and retinal detachment.

Association between irregularity and myopia

The cause of the irregularity in myopia is not known. It may arise with staphyloma development, but irregularity in inferior retinal areas was present in eyes without known staphyloma, and is at a smaller scale than MRI shape features. The irregularity may come from underlying scleral changes[7,285], or from alteration in the choroid[286]. Quality of retinal

image falls in peripheral areas and at the posterior areas of the B scan due to scatter and loss of resolution, limiting the information that can be extracted about structures posterior to the retinal pigment epithelium. Dome shaped maculopathy, a convex intrusion of the macula in myopic eyes, is one example of regional irregularity-associated pathology. While this entity was not addressed in this work, hypotheses for the abnormal shape in these eyes include relative scleral thinning at the margins of the dome[164] measured with extended depth imaging OCT. Confidence in this finding was gained with the use of swept source OCT which improved scleral image definition and found the same increased scleral thickness under the dome compared to the surrounding regions, with no change in external scleral contour[252,287]. In contrast, Gaucher[9] hypothesised local choroidal thickening was the cause of dome-shaped maculopathy. Further hypotheses include localised hypotony, and altered vitreo-retinal traction, both within the staphyloma[288]. These mechanisms are unlikely to produce the shape irregularity seen in this work in eyes that are post vitrectomy and PVD eyes where no vitreous attachment remains. Regions of proliferative vitreoretinopathy seen in complex retinal detachment and traction retinal detachment eyes of diabetics are known to alter the contour of the inner retinal surface without alteration in retinal pigment epithelium shape[289,290], suggesting inner retinal structures do not have a significant effect on retinal contour.

Association between irregularity and retinal detachment

While the pathology of retinal tears is found at the posterior margin of the vitreous base at or around the equator, MRI imaging of globe shape finds most globe irregularity occurs in the posterior hemisphere. With the established link between axial length, myopia, and retinal detachment, the question arises as to the cause of the link between these, and the cause of the association between retinal OCT shape irregularity and retinal detachment. It is unlikely that the shape feature differences directly lead to retinal tear formation, but more likely that an underlying property of the eye causes both increased shape irregularity and promotes retinal tear formation.

Without any adaptative growth in the coronal size of the eye, Poisson's effect means that axial enlargement may lead to compression wrinkles perpendicular to globe elongation[291]. This may explain the increased irregularity seen in the longer retinal detachment eyes

compared to PVD eyes, with the inhomogeneity of the eye and its surroundings causing different wrinkle sizes in different locations[291,292]. The link between local irregularity differences and retinal detachment may relate to regional variation in the enlargement of Bruch's membrane.

Possible causes of this association include:
(a) That the association between retinal irregularity and retinal detachment relates to the growth of Bruch's membrane in the equatorial region of the eye[5,293]. Retinal breaks occurring with PVD are associated with localised posterior extension of the posterior margin of the vitreous base (Figure 7.1), which may relate to variation in axial expansion of the equatorial retina. The transverse irregularity documented in this work may similarly arise from Bruch's membrane expansion, but in the coronal dimension. If this is the cause of the association it would explain why the significant shape features are the lowest frequencies, representing a passive compression due to constraints on expansion in the coronal plane. It would also explain the relative insignificance of negative curvature, the convex inward shape seen in some regions in the eyes that might be expected to be pathological in what should be a broadly ellipsoid eyeball. If the relationship between irregular eye shape and eye size arises from excess growth in the area of Bruch's membrane, whether it flexes inward or out, subject to regional pressures, is unimportant. Small segments of the posterior margin of the vitreous base are drawn posteriorly with myopisation, either in continuity with or separated from the continuous vitreous base. These posterior points of firm vitreo-retinal attachment are put under extra mechanical strain when PVD occurs up to the vitreous base, leading to hole or tear formation. The relationship between retinal tear formation and irregularity is in this hypothesis an association arising from growth of the Bruch's membrane simultaneously exceeding the coronal size of the spheroid in which it is confined, leading to "wrinkles" in the sagittal plane, and axial expansion drawing local segments of vitreous base posteriorly, producing retinal tears when PVD occurs.

(b) Myopia and retinal detachment have both been associated with multiple gene loci related to collagen[294,295]. The alteration in connective tissue behaviour from collagen variation in these eyes may affect scleral integrity, leading to both small scale changes in scleral rigidity producing shape irregularity, as well as abnormal vitreo-retinal attachment.

(c) Variation in scleral strength leading to localised weakening and increased irregularity. These 'micro-staphylomas' alter the interaction between vitreous and retina, changing the strength of vitreo-retinal adhesion. In areas of posterior extension of the vitreous base, this leads to retinal tear formation when PVD occurs.

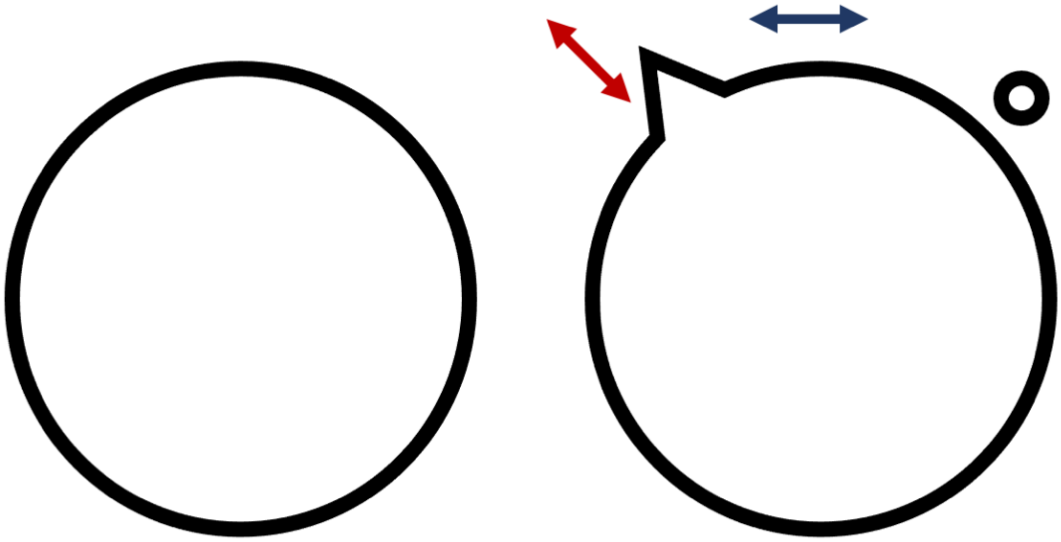

Figure 7.1. Schematic of the posterior margin of the vitreous base. Seen from within the eye looking forward, a non-pathological posterior vitreous base margin is shown on the left. The risk of retinal tear formation may arise from irregular expansion of the equatorial Bruch's membrane (red arrow, right image), with associated localised posterior extension of the posterior margin of the vitreous base. The classifier detects these eyes by identifying coronal expansion of Bruch's membrane (blue arrow). This is compressed due to limited globe growth in this dimension, leading to retinal contour irregularity.

Prevention of retinal detachment

Current literature supports the effectiveness of prophylactic 360° laser to the retinal equator in preventing vision loss from retinal detachment[67,296,297]. The issue with preventing retinal detachment, then, is not how but who (with a high degree of certainty) to treat. As no test is infallible and no treatment without risk, an understanding of the hazards of intervention is needed to assess the potential benefits. Were a test with imperfect specificity in identifying eyes at risk of retinal detachment to be developed, the question

arises as to what risks from prophylactic therapy would be acceptable. A Cochrane review reported the risk from 360° equatorial retinal laser prophylaxis ranged from 0 to 3.8%[298]. They reported side effects of retinal laser:

"include refractive errors, raised intraocular pressure, anterior segment ischaemia, cataract, anterior and/or posterior uveitis, cystoid macular oedema, epiretinal membrane, retinal breaks and diplopia. Although some of these are likely to be the result of the prophylactic interventions (refractive errors, anterior segment ischaemia, uveitis, cystoid macular oedema, epiretinal membrane and diplopia), others may be coincidental (cataract) or related to the underlying disorder (retinal breaks).[298]"

Of these complications, epiretinal membrane development at the macular (epi-macular membrane) is the most common adverse effect of retinal laser to cause permanent visual impairment. Retinal laser therapy is routinely used to treat ischaemic retinopathy in diabetes[299–301], retinal vein occlusion[302], and uveitis[303], to demarcate retinal breaks to prevent retinal detachment, and to treat retinal vascular leak in diabetes. Retinal laser prophylaxis has been used in young children with congenital peripheral retinal non-perfusion diseases (such as retinopathy of prematurity[304–307], familial exudative vitreo-retinopathy[308], incontinentia pigmentii[309], and Coats' disease[310]) as well as type 1 Stickler disease[67] and the fellow eyes of giant retinal tears. All these conditions are known to have a risk of epi-macular membrane formation with subsequent visual impairment, and as all these pathologies can themselves produce epi-macular membrane, it is unclear how much of the morbidity is due to the disease and how much is iatrogenic.

Epi-macular membrane after laser for retinal tears

Studies on laser treatment for retinal tears report a range of epiretinal membrane development frequency of 0 – 40% (with 23-2000 eyes or patients in each study). The highest incidence of 40% is from one study of 50 eyes[311,312]. Another study reported epi-macular membrane formation in 14% of eyes following the use of laser photocoagulation to treat a retinal break, compared to 10% of untreated retinal breaks found to develop epiretinal membrane, with no significant change in visual acuity [313]. The largest study, of

2000 eyes, reported an incidence of 0.2%[314], with greater laser energy use thought to contribute to the risk. Pollack[65] performed 360° circumferential prophylactic laser in 53 eyes with extensive lattice, retinal breaks, and other risk factors for retinal detachment. Two eyes developed retinal detachment, and 3.8% (2 eyes) developed epiretinal membrane not requiring surgery. Blackorby[315] performed a chart review looking for coding for retinal laser use with later diagnostic coding for ERM. In this series, 2.9% (48 of 1655 eyes) developed epi-macular membrane after an average interval of 12 months, with five requiring surgery. Govan[316] found a complication rate of 13.2% in 106 eyes treated with laser for "risk of retinal detachment": three eyes developed anterior uveitis, three eyes cystoid macular oedema (post cataract extraction), one a dilated pupil, two cataract, and one each of vitreous haemorrhage, retinal haemorrhage, choroidal haemorrhage, and epiretinal membrane (0.9% each).

Stickler syndrome prophylaxis & ERM

Fincham[67] (2014) and Ang[69] report no cases of epiretinal membrane following cryotherapy for prophylaxis against retinal detachment in Type 1 Stickler syndrome.

Giant retinal tear prophylaxis & epiretinal membrane

Both Wolfensberger[296] and Ripandelli[297] reported no epiretinal membrane development in their series of prophylactic retinal laser therapy to the fellow eyes of individuals who had experienced a giant retinal tear in one eye. Other reports on prophylaxis for giant retinal tears do not provide any data on epiretinal membrane development[317–319].

Summary

Epiretinal membrane may occur in 0 – 40% of eyes following retinal laser. While some authors relate the risk of occurrence to the amount of laser energy applied, this is unsupported across the range of papers considered here. Notably the case series that consider prophylaxis in eyes with no neurosensory retinal break at time of treatment[67,296,297] found no epiretinal membrane development. The difference may arise from the mixed aetiology of epiretinal membrane, with some developing from laminocyte proliferation after disruption of the posterior vitreous cortex, and others involving retinal pigment epithelium

cells after retinal tear formation[320]. Retinal pigment epithelial cell migration into the pre-retinal space contributes to epiretinal membrane formation, which is unlikely to occur with an intact retina. In the absence of a retinal break the cellular mix to generate surface retinal changes is more sparse, reducing the impact of pathological changes and clinical disease manifestation. This provides some indication that retinal laser photocoagulation itself has a low risk of producing epiretinal membrane in healthy eyes, and may be an acceptable treatment should a test for retinal detachment be developed.

Conclusion

Retinal shape irregularity can be measured with the OCT. This irregularity has a consistent variation across different regions of the eye, and increases with increasing axial length. There is a need to develop methods to reduce the vision loss that over 50% of individuals with retinal detachment experience. While vitreo-retinal surgery has experienced significant technological advances in the last 50 years that have improved both the patient experience and outcomes[321–323] prevention has been proven better than cure where at-risk eyes are identifiable. This thesis provides evidence that the crucial step of identifying who as at risk may be achievable for more patients through the analysis of retinal irregularity with OCT.

List of Appendices

```
CretiffSS
SSA2FFT
SStabFFT
SStabana
SSTrTst
SSneweyetest
```

Appendix A. Participant information and consent form

Flinders UNIVERSITY

Government of South Australia
SA Health

Participant Information Sheet/Consent Form

Central Adelaide Local Health Network

Title	*Optical Coherence Tomography (OCT) retinal topography*
Short Title	*OCT retinal topography*
Protocol Number	31.17
Coordinating Principal Investigator	*Dr Stewart Lake*
Associate Investigator(s)	*Prof. Karen Reynolds, Prof Keryn Williams, A/Prof Murk Bottema*
Location	*Flinders Medical Centre*

Part 1 What does my participation involve?

1 Introduction

You are invited to take part in this research project, *Optical coherence tomography (OCT) retinal topography*. This is because you have had drops to examine your eye (for your out-patient appointment), and we can clearly see your peripheral retina on examination. The research project is aiming to investigate whether the OCT scan can provide useful information about the contour, or shape, of the retina.

This Participant Information Sheet/Consent Form tells you about the research project. It explains the tests and research involved. Knowing what is involved will help you decide if you want to take part in the research.

Please read this information carefully. Ask questions about anything that you don't understand or want to know more about. Before deciding whether or not to take part, you might want to talk about it with a relative, friend or local doctor.

Participation in this research is voluntary. If you don't wish to take part, you don't have to. You will receive the best possible care whether or not you take part.

If you decide you want to take part in the research project, you will be asked to sign the consent section. By signing it you are telling us that you:
• Understand what you have read
• Consent to take part in the research project
• Consent to the use of your personal and health information as described.

You will be given a copy of this Participant Information and Consent Form to keep.

2 What is the purpose of this research?

While the eye is roughly spherical, it is known that the shape varies from person to person, with short-sighted people generally having larger, more irregularly shaped eyes than long-sighted people. The aim of the study is to see if reliable information on the shape of the retina can be gained from using OCT.

OCT is routinely used to image the posterior retina (the macula), but has not been routinely used to study peripheral retinal shape, or contour. If accurate contour information can be taken, it may be useful in the study of the development and effects of refractive errors, such as short-sightedness.

This research has been initiated by the study doctor, Dr Stewart Lake. The results of this research may be used by Dr Lake to obtain a doctorate in Biomedical Engineering.

3 What does participation in this research involve?

OCT uses near-infrared light (light that is close to the visible spectrum) to obtain highly detailed images of the retina. The instrument looks like a computer with a large built in camera. It has a chin rest on which you place your head while the scan takes place. One scan takes a few seconds, during which you may see some green and red lines while looking into the lens of the camera. A single scan covers approximately 4% of the retina (the light sensitive layer at the back of the eye).

Several scans of different parts of your eye will be taken, so that later analysis can investigate differences in shape between and within eyes, and the relationship between different areas. We will not be scanning your entire eye, but a small region as a sample to explore image analysis and reconstruction.

Before taking part, you will need to sign the consent form, below. Then Dr Lake will take you to the OCT machine. While the scans are being taken, you will be asked to look in different directions to help us see your retina. The number of scans will vary depending on how easy it is to see the retina. After the OCT scans are performed we may ask to take colour photographs of your retina to position the scans within your eye, or use a similar machine to measure the length of your eye.

The study takes place in a single visit. Once the test is completed no further study tests are required. No additional medications or tests are required.

This research project has been designed to make sure the researchers interpret the results in a fair and appropriate way and avoids study doctors or participants jumping to conclusions.

There are no costs associated with participating in this research project, nor will you be paid.

5 Other relevant information about the research project

For this study we plan to examine participants at Flinders Medical Centre. These may include healthy participants, as well as those who are short-sighted, long-sighted, or have had problems with their peripheral retina, such as retinal tears.

6 Do I have to take part in this research project?

Participation in any research project is voluntary. If you do not wish to take part, you do not have to. If you decide to take part and later change your mind, you are free to withdraw from the project at any stage.

If you do decide to take part, you will be given this Participant Information and Consent Form to sign and you will be given a copy to keep.

Your decision whether to take part or not to take part, or to take part and then withdraw, will not affect your routine treatment, your relationship with those treating you or your relationship with Flinders Medical Centre.

7 What are the alternatives to participation?

You do not have to take part in this research project to receive treatment at this hospital.

8 What are the possible benefits of taking part?

There will be no benefit to you from your participation in this research, however possible benefits may include an improved understanding of the shape of the eye that may help us better understand some retinal diseases.

9 What are the possible risks and disadvantages of taking part?

The dilating drops you have been given for your out-patient appointment will make your eyesight blurry for 2-3 hours. You should not drive during this period.

You may be asked to look up, out, or to the side to take the pictures. This can be a little uncomfortable but usually settles within minutes.

Should the images find any abnormality in your retina, the specialist will tell you and explain its significance. If any treatment is required for these abnormalities, the possible options will be discussed and should you decide to have treatment it will be performed either at Flinders Medical Centre or the Royal Adelaide Hospital, without cost to you.

This study does not involve exposure to ionising radiation.

10 What will happen to my test samples?

No blood or tissue tests are required, and no sample of your tissue will be taken.

13 What if I withdraw from this research project?

You can withdraw at any time simply by telling the investigator you do not wish to take part.

If you do withdraw your consent during the research project, the study doctor and relevant study staff will not collect additional personal information from you, although personal information already collected will be retained to ensure that the results of the research project can be measured properly and to comply with law. You should be aware that data collected by the sponsor up to the time you withdraw will form part of the research project

results. If you do not want them to do this, you must tell them before you join the research project

Part 2 How is the research project being conducted?

16 What will happen to information about me?

By signing the consent form you consent to the study doctor and relevant research staff collecting and using personal information about you for the research project. Any information obtained in connection with this research project that can identify you will remain confidential. The data will be stored on the OCT machine database, as part of your medical record. Sample data for analysis will be copied to portable hard drives for transfer to the Flinders University College of Science & Engineering for analysis. This data will be identifiable by a study code number. Your information will only be used for the purpose of this research project and it will only be disclosed with your permission, except as required by law.

Information about you may be obtained from your health records held at Flinders Medical Centre for the purpose of this research. By signing the consent form you agree to the research team accessing health records if they are relevant to your participation in this research project.

Your health records and any information obtained during the research project are subject to inspection for the purpose of verifying the procedures and the data. This review may be done by relevant authorities, the institution relevant to this Participant Information Sheet, Flinders University, or as required by law. By signing the Consent Form, you authorise release of, or access to, this confidential information to the relevant research personnel and regulatory authorities as noted above.

It is anticipated that the results of this research project will be published and/or presented in a variety of forums. In any publication and/or presentation, information will be provided in such a way that you cannot be identified, except with your permission.

Information about your participation in this research project will be recorded in your health record, on the OCT database itself.

In accordance with relevant Australian and/or South Australian privacy and other relevant laws, you have the right to request access to the information collected and stored by the research team about you. You also have the right to request that any information with which you disagree be corrected. Please contact the research team member named at the end of this document if you would like to access your information.

Any information obtained for the purpose of this research project that can identify you will be treated as confidential and securely stored. It will be disclosed only with your permission, or as required by law. Should this study lead to larger studies on retinal shape, we may wish to include your data in such. However, for this to occur, we will contact you to obtain consent for this additional use.

17 Complaints and compensation

If you suffer any injuries or complications as a result of this research project, you should contact the study team as soon as possible and you will be assisted with arranging appropriate medical treatment. If you are eligible for Medicare, you can receive any medical

treatment required to treat the injury or complication, free of charge, as a public patient in any Australian public hospital.

18 Who is organising and funding the research?

This research project is being conducted by Dr Stewart Lake.

No member of the research team will receive a personal financial benefit from your involvement in this research project (other than their ordinary wages).

19 Who has reviewed the research project?

All research in Australia involving humans is reviewed by an independent group of people called a Human Research Ethics Committee (HREC). The ethical aspects of this research project have been approved by the HREC of the Southern Adelaide Clinical Human Research Ethics Committee. This project will be carried out according to the *National Statement on Ethical Conduct in Human Research (2007)*. This statement has been developed to protect the interests of people who agree to participate in human research studies.

20 Further information and who to contact

The person you may need to contact will depend on the nature of your query.
If you want any further information concerning this project or if you have any medical problems which may be related to your involvement in the project (for example, any side effects), you can contact the principal study doctor Dr Stewart Lake on 8204 4252, or any of the following people:

Clinical contact person

Position	*The Ophthalmology Registrar (available 24 hours)*
Telephone	*8204 5511*

For matters relating to research at the site at which you are participating, the details of the local site complaints person are:

Complaints contact person

Position	*Director, Office for Research*
Telephone	*8204 6453*
Email	*Health.SALHNofficeforresearch@sa.gov.au*

If you have any complaints about any aspect of the project, the way it is being conducted or any questions about being a research participant in general, then you may contact:

Reviewing HREC approving this research and HREC Executive Officer details

Reviewing HREC name	*Southern Adelaide Clinical*
Position	HREC Executive Officer
Telephone	*8204 6453*
Email	*Health.SALHNofficeforresearch@sa.gov.au*

Local HREC Office contact (Single Site -Research Governance Officer)

Position	*Research Governance Officer*
Telephone	*8204 6453*
Email	*Health.SALHNofficeforresearch@sa.gov.au*

Consent Form - *Adult providing own consent*

Title	*Optical coherence tomography retinal topography*
Short Title	*OCT retinal topography*
Protocol Number	31.17
Coordinating Principal Investigator	*Dr Stewart Lake*
Associate Investigator(s)	*Prof. Karen Reynolds, Prof Keryn Williams, A/Prof Murk Bottema*
Location	*Flinders Medical Centre*

Declaration by Participant

I have read the Participant Information Sheet or someone has read it to me in a language that I understand.

I understand the purposes, procedures and risks of the research described in the project.

I have had an opportunity to ask questions and I am satisfied with the answers I have received.

I freely agree to participate in this research project as described and understand that I am free to withdraw at any time during the project without affecting my future health care.

I understand that I will be given a signed copy of this document to keep.

Name of Participant (please print) _____

Signature _____ Date _____

Declaration by Study Doctor/Senior Researcher†

I have given a verbal explanation of the research project, its procedures and risks and I believe that the participant has understood that explanation.

Name of Study Doctor/
Senior Researcher† (please print) _____

Signature _____ Date _____

† A senior member of the research team must provide the explanation of, and information concerning, the research project.

Note: All parties signing the consent section must date their own signature.

Form for Withdrawal of Participation - *Adult providing own consent*

Title	*Optical Coherence tomography retinal topography*
Short Title	*OCT retinal topography*
Protocol Number	*31.17*
Coordinating Principal Investigator	*Dr Stewart Lake*
Associate Investigator(s)	*Prof. Karen Reynolds, Prof Keryn Williams, A/Prof Murk Bottema*
Location	*Flinders Medical Centre*

Declaration by Participant

I wish to withdraw from participation in the above research project and understand that such withdrawal will not affect my routine treatment, my relationship with those treating me, or my relationship with *Flinders Medical Centre*

Name of Participant (please print) _____

Signature _____ Date _____

In the event that the participant's decision to withdraw is communicated verbally, the Study Doctor/Senior Researcher will need to provide a description of the circumstances below.

Declaration by Study Doctor/Senior Researcher†

I have given a verbal explanation of the implications of withdrawal from the research project and I believe that the participant has understood that explanation.

Name of Study Doctor/
Senior Researcher† (please print) _____

Signature _____ Date _____

† A senior member of the research team must provide the explanation of and information concerning withdrawal from the research project.

Note: All parties signing the consent section must date their own signature.

Appendix B. Note on data file format used in MATLAB functions

Fourier transform data for Chapters 3, 4 and 5 were stored in MATLAB workspace FFTconcat. These arrays were accessed by many of the functions analysing shape given in Appendix C. Within this workspace, a separate array held shape information for each diagnosis (for example: RD, RT, PVD, MH, FE, each with suffix Fb), with each eye's information in a separate row. Relevant columns were

4 axial length and age

5 identifiers for all cubes taken

6 cube identifiers for regions 1-17, in order

10 all eye B scan spectra, in an array frequency bins (1-30) x B scans (1-21) x cubes (in the same order as column 5 vector)

11 Regional cube spectra. A vector of cells identified by the cells in column 6, each cell containing a single cube B scan spectra (bin (1-30) x B scans (1-21)).

Other columns held information developed during analysis iteration and were not used in any of the processes described by this work.

Appendix C. MATLAB functions written for this thesis

Chapter 3.

Image reliability

1. RetestLVWrmse

```
%compare curvature & FFT for retest MP
%CHANGE: line 8 % 210, plus figure labels
%takes data from MP xz and xy and calculates FFT and K
%plus median, var, and iqr sum bins
%plus median, iqr, and variance K
%CHANGE: for accurate data, uncomment 427-428,432-433
%load MH data
str1 = '/Users/stewartlake/Documents/Retinalcontour/data validity/MP - livewire
check/MP repeat xy/';
cd (str1);

MHinfo = dir;
MHinfo = MHinfo(~ismember({MHinfo.name},{'.','..','.DS_Store'}));
MHnames = {MHinfo.name};

MHNum = size (MHnames,2);%number MP cubes
MHcubeFFTvec = cell(1,MHNum);%One eye per cell %each cell 30 bins x 12 B scans
MHbfccoeff = cell(1,MHNum);
MHK = cell(1,MHNum); % best fit curve vertex curvature.One eye per cell
MHID = cell(1,MHNum);
MHside = zeros(1,MHNum);
MedKMH = zeros(1,MHNum); %median MH K
IqrKMH = zeros(1,MHNum);%iqr MH K
VarKMH = zeros(1,MHNum);% variance MH K
MedFMH = zeros(1,MHNum);% median FFT bins 1-30
IqrFMH = zeros(1,MHNum);%iqr FFT bins
VarFMH = zeros(1,MHNum);%variance FFT bins
x2=cell(MHNum,21);
z2=cell(MHNum,21);

%generate data for MP cubes
for CurFol=1:MHNum

    MHnam = MHnames {1,CurFol}(1:5);%cube ID
    MHside = MHnames {1,CurFol}(2);%eye laterality (not needed)
    MHprefix = MHnames {1,CurFol}(1:2);%first two characters for textfile str
    %open cube of data
    nowFolderMH=MHnames{1,CurFol};

    cd (nowFolderMH);%open cube xz data folder

    %get directory of textfile (B scan) names
    MHdinfo = dir;
    MHnames_cell = {MHdinfo.name};
%gives a matrix called names_cell where each column has a filename
%then:
    outMH=regexp(MHnames_cell,'\d+','match');
    outMH=str2double(cat(1,outMH{:}));
%gives a matrix called out in which each row has a number from an original filename
%these are in column 2 if text file header has a number, column 1 if it
%doesn't.

%script alpha. takes a cube of data and
%Puts x and z coordinate values into an array (myData), each cell a line of data.
%Then separates this into arrays for x, and z.
    numFiles = size(outMH, 1);%number of B scans in cube
    startRow = 1;
    endRow = inf;
    myData = cell(1,numFiles);
    ximp = cell (1, numFiles);%this cubes x data
    zimp = cell (1, numFiles);%this cubes Z data
    cubeFFT = zeros (30, numFiles);
```

```
    Cubefreq = zeros (30, numFiles);
    MHKurv = zeros (numFiles,1);

    fileName = cell(1);

    zedres = zeros(1024,numFiles);
    Quadcoeffs = zeros(3, numFiles);
    VecLen1 = zeros (1, numFiles);


     for fileNum = 1:numFiles %work through B scan xz txt files
            Bscanline = outMH(fileNum,end);
            %This loop is for a single cube
            fileName =[];
            fileName1 = sprintf('-%04d.txt',Bscanline);
            fileName = [MHprefix fileName1];
            myData{Bscanline} = importfile(fileName,startRow,endRow);

            ximp{Bscanline}=myData{Bscanline}(:,1);
            zimp{Bscanline}=myData{Bscanline}(:,2);



            %now format x and z for FFT
            x=table2cell(ximp{Bscanline});
            z=table2cell(zimp{Bscanline});
            x2{CurFol,Bscanline}=cell2mat(x);
            z2{CurFol,Bscanline}=cell2mat(z);

            L = length (z2{CurFol,Bscanline});

            [FFTz,freq] =
FFTforOCT_R3mm(x2{CurFol,Bscanline},z2{CurFol,Bscanline});%mac hole FFT script
            VecLen1(fileNum) = length(z2{CurFol,Bscanline});%vector length(FFT
already corrected)

            %create matrix of residuals
            zVlen = size (z2{CurFol,Bscanline});
            zedres(1:zVlen,fileNum) = z2{CurFol,Bscanline};
            %zedres = zedres(1:1024,fileNum);

            %save quadratic coefficients
            sf = 1024/9;% 6 mm scan length
            xmm{Bscanline} = x2{CurFol,Bscanline}/sf;%convert to mm
            sfz = 1024/2;
            ZMM{Bscanline} = z2{CurFol,Bscanline}/sfz;
            p{Bscanline} = polyfit(xmm{Bscanline},ZMM{Bscanline},2);%
            Quadcoeffs (1,Bscanline) = p{Bscanline}(1);
            Quadcoeffs (2,Bscanline) = p{Bscanline}(2);
            Quadcoeffs (3,Bscanline) = p{Bscanline}(3);

            %put FFTz, freq into matrix, one column per B scan
            cubeFFT(1:30,Bscanline) = FFTz(1:30,1);
            %cubeFFT(1:30,fileNum)=cubeFFT(1:30,fileNum)/VecLen(fileNuM);
            Cubefreq(1:30,Bscanline) = freq(1:30)';

            MHKurv(Bscanline) = 2* (Quadcoeffs(1,Bscanline));%unrotated K


            %this section (155 - 176)creates rotated BFCvK

%p1 is the best fit line to the curve, to determine rotation angle
MHp1{Bscanline} = polyfit(xmm{Bscanline},ZMM{Bscanline},1);%first element p1 is
gradient

%rotate that line to the horizontal
angleA(Bscanline) = -atan(MHp1{Bscanline}(1));%angle for rotation

%rotate the curve by the same angle
```

```
%rotation matrix
R = [cos(angleA(Bscanline)) -sin(angleA(Bscanline)); sin(angleA(Bscanline))
cos(angleA(Bscanline))];

MHRotCd{Bscanline} = (cat(2,xmm{Bscanline},ZMM{Bscanline}))';%combine x & z in one
array
MHOdisp{Bscanline}(1) = mean(nonzeros(MHRotCd{Bscanline}(1,:)));
MHOdisp{Bscanline}(2) = mean(nonzeros(MHRotCd{Bscanline}(2,:)));
MHRotCd{Bscanline} = MHRotCd{Bscanline} - MHOdisp{Bscanline}';%move to origin for
rotation

MHRotCd{Bscanline} = R*MHRotCd{Bscanline};%rotated coordinates
MHRotCd{Bscanline} = MHRotCd{Bscanline} + MHOdisp{Bscanline}';%translate to
original position
MHRotp2{Bscanline} = polyfit(MHRotCd{Bscanline}(1,:),MHRotCd{Bscanline}(2,:),2);
MHRotKurv(Bscanline) = 2* MHRotp2{Bscanline}(1);%rotated BFCvK


     end

        cubeFFT(cubeFFT==0) = NaN;%30 rows for bins, 12 columns for B scans
        MHcubeFFTvec{CurFol} = cubeFFT;%each cell 30 bins x 12 B scans
        MedFMH(CurFol) = median (sum(cubeFFT));
        IqrFMH(CurFol) = iqr (sum(cubeFFT));
        VarFMH(CurFol) = var (sum(cubeFFT));

        MHbfccoeff{CurFol} = Quadcoeffs;

        MedKMH(CurFol) = median (MHKurv);
        IqrKMH(CurFol) = iqr (MHKurv);
        VarKMH(CurFol) = var (MHKurv);
        MHK{CurFol} = MHKurv;

        MHRotK{CurFol} = MHRotKurv;
        MedKMHRot(CurFol) = median (MHRotKurv);
        IqrKMHRot(CurFol) = iqr (MHRotKurv);
        VarKMHRot(CurFol) = var (MHRotKurv);

        cd ../

        MHID{CurFol} = MHnam(4:5);
        %nowSide = MHIID(nowMHID,str2double(MHside)+1);
        MHside(CurFol) = MHnam(2);
end



%load PV data (PVD eyes)
str1 = '/Users/stewartlake/Documents/Retinalcontour/data validity/MP - livewire
check/MP xz/';
cd (str1);

PVinfo = dir;
PVinfo = PVinfo(~ismember({PVinfo.name},{'.','..','.DS_Store'}));
PVnames = {PVinfo.name};

PVNum = size (PVnames,2);%number MP cubes
PVcubeFFTvec = cell(1,PVNum);%PVD FFT data
PVbfccoeff = cell(1,PVNum);
PVK = cell(1,PVNum);% best fit curve vertex curvature
PVID = cell(1,PVNum);
PVside = zeros(1,PVNum);
MedKPV = zeros(1,PVNum); %median MH K
IqrKPV = zeros(1,PVNum);%iqr MH K
VarKPV = zeros(1,PVNum);% variance MH K
MedFPV = zeros(1,PVNum);% median FFT bins 1-30
IqrFPV = zeros(1,PVNum);%iqr FFT bins
VarFPV = zeros(1,PVNum);%variance FFT bins
x1=cell(PVNum,21);
z1=cell(PVNum,21);
```

```
%generate data for MP cubes 2
for CurFol=1:PVNum

    PVnam = PVnames {1,CurFol}(1:5);%eye ID
    PVside = PVnames {1,CurFol}(2);%eye laterality
    PVprefix = PVnames {1,CurFol}(1:2);%first two characters for textfile str
    %open cube of data
    nowFolderPV=PVnames{1,CurFol};

    cd (nowFolderPV);%open cube xz data folder

    %get directory of textfile (B scan) names
    PVdinfo = dir;
    PVnames_cell = {PVdinfo.name};
%gives a matrix called names_cell where each column has a filename
%then:
    outPV=regexp(PVnames_cell,'\d+','match');
    outPV=str2double(cat(1,outPV{:}));
%gives a matrix called out in which each row has a number from an original filename
%these are in column 2 if text file header has a number, column 1 if it
%doesn't.

%script alpha. takes a cube of data and
%Puts x and z coordinate values into an array (myData), each cell a line of data.
%Then separates this into arrays for x, and z.
    numFiles = size(outPV, 1);%number of B scans in cube
    startRow = 1;
    endRow = inf;
    myData = cell(1,numFiles);
    ximp = cell (1, numFiles);%this cubes x data
    zimp = cell (1, numFiles);%this cubes Z data
    cubeFFT = zeros (30, numFiles);
    Cubefreq = zeros (30, numFiles);
    PVKurv = zeros (numFiles,1);

    fileName = cell(1);

    zedres = zeros(1024,numFiles);
    Quadcoeffs = zeros(3, numFiles);
    VecLen2 = zeros (1, numFiles);


     for fileNum = 1:numFiles %work through B scan xz txt files
            Bscanline = outPV(fileNum,end);
            %This loop is for a single cube
            fileName =[];
            fileName1 = sprintf('-%04d.txt',Bscanline);
            fileName = [PVprefix fileName1];
            myData{Bscanline} = importfile(fileName,startRow,endRow);

            ximp{Bscanline}=myData{Bscanline}(:,1);
            zimp{Bscanline}=myData{Bscanline}(:,2);



            %now format x and z for FFT
            x=table2cell(ximp{Bscanline});
            z=table2cell(zimp{Bscanline});
            x1{CurFol,Bscanline}=cell2mat(x);
            z1{CurFol,Bscanline}=cell2mat(z);

            L = length (z1{CurFol,Bscanline});

            [FFTz,freq] =
FFTforOCT_R3mm(x1{CurFol,Bscanline},z1{CurFol,Bscanline});%mac hole FFT script
            VecLen2(CurFol,Bscanline) = length(z1{CurFol,Bscanline});%vector
length(FFT already corrected)

            %create matrix of residuals
```

```
            zVlen = size (z1{CurFol,Bscanline});
            zedres(1:zVlen,fileNum) = z1{CurFol,Bscanline};
            %zedres = zedres(1:1024,fileNum);

            %save quadratic coefficients
            sf = 1024/9;% 6 mm scan length
            xmm{Bscanline} = x1{CurFol,Bscanline}/sf;
            sfz = 1024/2;
            ZMM{Bscanline} = z1{CurFol,Bscanline}/sfz;
            p{Bscanline} = polyfit(xmm{Bscanline},ZMM{Bscanline},2);%
            Quadcoeffs (1,Bscanline) = p{Bscanline}(1);
            Quadcoeffs (2,Bscanline) = p{Bscanline}(2);
            Quadcoeffs (3,Bscanline) = p{Bscanline}(3);

            %put FFTz, freq into matrix, one column per B scan
            cubeFFT(1:30,Bscanline) = FFTz(1:30,1);
            %cubeFFT(1:30,fileNum)=cubeFFT(1:30,fileNum)/VecLen(fileNuM);
            Cubefreq(1:30,Bscanline) = freq(1:30)';

            PVKurv(Bscanline) = 2* (Quadcoeffs(1,Bscanline));%unrotated K

%this section (356 - 377)creates rotated BFCvK

%p1 is the best fit line to the curve
p1{Bscanline} = polyfit(xmm{Bscanline},ZMM{Bscanline},1);%first element p1 is
gradient

%rotate that line to the horizontal
angleA(Bscanline) = -atan(p1{Bscanline}(1));%angle for rotation

%rotate the curve by the same angle

%rotation matrix
R = [cos(angleA(Bscanline)) -sin(angleA(Bscanline)); sin(angleA(Bscanline))
cos(angleA(Bscanline))];

PVRotCd{Bscanline} = (cat(2,xmm{Bscanline},ZMM{Bscanline}))';%combine x & z in one
array
PVOdisp{Bscanline}(1) = mean(nonzeros(PVRotCd{Bscanline}(1,:)));
PVOdisp{Bscanline}(2) = mean(nonzeros(PVRotCd{Bscanline}(2,:)));
PVRotCd{Bscanline} = PVRotCd{Bscanline} - PVOdisp{Bscanline}';%move to origin for
rotation

PVRotCd{Bscanline} = R*PVRotCd{Bscanline};%rotated coordinates
PVRotCd{Bscanline} = PVRotCd{Bscanline} + PVOdisp{Bscanline}';%translate to
original position
PVRotp2{Bscanline} = polyfit(PVRotCd{Bscanline}(1,:),PVRotCd{Bscanline}(2,:),2);
PVRotKurv(Bscanline) = 2* PVRotp2{Bscanline}(1);%rotated BFCvK


      end
         cubeFFT(cubeFFT==0) = NaN;
         PVcubeFFTvec{CurFol} = cubeFFT;
         MedFPV(CurFol) = median (sum(cubeFFT));
         IqrFPV(CurFol) = iqr (sum(cubeFFT));
         VarFPV(CurFol) = var (sum(cubeFFT));
         PVbfccoeff{CurFol} = Quadcoeffs;
         PVK{CurFol} = PVKurv;
         MedKPV(CurFol) = median (PVKurv);
         IqrKPV(CurFol) = iqr (PVKurv);
         VarKPV(CurFol) = var (PVKurv);

         PVRotK{CurFol} = PVRotKurv;
         MedKPVRot(CurFol) = median (PVRotKurv);
         IqrKPVRot(CurFol) = iqr (PVRotKurv);
         VarKPVRot(CurFol) = var (PVRotKurv);


         cd ../
```

```
        PVID{CurFol} = PVnam(4:5);
        %nowSide = PVIID(nowPVID,str2double(PVside)+1);
        PVside(CurFol) = PVnam(2);
end




%stat tests for difference between groups: one tailed Mann Whitney
[pFI,hIF] = ranksum(IqrFPV,IqrFMH);
[pKI,hIK] = ranksum(IqrKPV,IqrKMH);
[pVF,hVF] = ranksum(VarFPV,VarFMH);
[pVK,hVK] = ranksum(VarKPV,VarKMH);
[pMF,hMF] = ranksum(MedFPV,MedFMH);
[pMK,hMK] = ranksum(MedKPV,MedKMH);

[pKrotI,hIKrot] = ranksum(IqrKPVRot,IqrKMHRot);%for rotated BFCvK
[pVKrot,hVKrot] = ranksum(VarKPVRot,VarKMHRot);
[pMKrot,hMKrot] = ranksum(MedKPVRot,MedKMHRot);


%match z vector from each livewire & determine rmse
%find common x
MP1a = x1(:);
MP2a = x2(:);
MP1a(100)=[];%removes mismatched txt files (doesnt explain why?)
MP2a(334) = [];%see end of function
MP1 = MP1a(~cellfun('isempty',MP1a));
MP2 = MP2a(~cellfun('isempty',MP2a));

MPz1a = z1(:);
MPz1a(100)=[];
MPz2a = z2(:);
MPz2a(334)=[];
MPz1 = MPz1a(~cellfun('isempty',MPz1a));
MPz2 = MPz2a(~cellfun('isempty',MPz2a));

match2 = cell(length(MP2),1);
match1 = cell(length(MP2),1);
lengthvec = cell(length(MP2),1);
rmse = zeros(length(MP2),1);
rmsecorr = zeros(length(MP2),1);
answ=cell(2,1);

for NumBS = 1:length(MP2)

answ{1}=find(MP2{NumBS}==MP1{NumBS}(1),1);
answ{2}=find(MP1{NumBS}==MP2{NumBS}(1),1);

if (~(isempty(answ{2})))

    lengthvec{NumBS} = min(length(MP1{NumBS}),length(MP2{NumBS}));
    match1{NumBS} = MPz1{NumBS}(answ{2}:lengthvec{NumBS});
    match2{NumBS} = MPz2{NumBS}(1:lengthvec{NumBS}-(answ{2}-1));


elseif (~(isempty(answ{1})))

    lengthvec{NumBS} = min(length(MP1{NumBS}),length(MP2{NumBS}));
    match1{NumBS} = MPz1{NumBS}(1:lengthvec{NumBS}-(answ{1}-1));
    match2{NumBS} = MPz2{NumBS}(answ{1}:lengthvec{NumBS});


else
    lengthvec{NumBS} = min(length(MP1{NumBS}),length(MP2{NumBS}));
    match1{NumBS} = MPz1{NumBS}(1:lengthvec{NumBS});
    match2{NumBS} = MPz2{NumBS}(1:lengthvec{NumBS});
```

```
end

rmse(NumBS) = sqrt(sum((match1{NumBS} - match2{NumBS}).^2)/lengthvec{NumBS});
meandiff = mean(match1{NumBS} - match2{NumBS});
rmsecorr(NumBS) = sqrt(sum(((match1{NumBS}-meandiff) -
match2{NumBS}).^2)/lengthvec{NumBS});
%vector of rmse for all B scans in series
end


MnBsrmse = mean(rmse);
MnBsrmsecorr = mean(rmsecorr);
SDBsrmse = std(rmse);
SDBsrmsecorr = std(rmsecorr);


%signrank all the FTR/K for each assay in a single vector
for Ec=1:18

    SUMFFTMH{Ec} = sum(MHcubeFFTvec{Ec});
    SUMFFTPV{Ec} = sum(PVcubeFFTvec{Ec});

    KallMH{Ec} = 2*MHbfccoeff{Ec}(1,:);
    KallPV{Ec} = 2*PVbfccoeff{Ec}(1,:);

end

SUMFFTMH = [SUMFFTMH{:}];%vector of all B scan FTR30
SUMFFTPV = [SUMFFTPV{:}];
KallMH = [KallMH{:}];%vector of all B scan Ks
KallPV = [KallPV{:}];

[pFsum,hFsum] = ranksum(SUMFFTMH,SUMFFTPV);
[pKall,hKall] = ranksum(KallMH,KallPV);


%{
%scatter plot variance of K and FFT,MH v PV, rotated K
dx=0.000001;%label displacement
dy=0.1;
figure
hold on
scatter(VarKMHRot,VarFMH,[],'r')
%text(VarKMH +dx,VarFMH + dy,MHID);
scatter(VarKPVRot, VarFPV,[],'b')
%text(VarKPV +dx,VarFPV + dy,PVID);
title('MPYHY v MPSL cube rotated K v FFT variance');
xlabel('Krot var');
ylabel('FFT var');

%scatter plot variance of K and FFT,MH v PV
dx=0.000001;%label displacement
dy=0.1;
figure
hold on
scatter(VarKMH,VarFMH,[],'r')
%text(VarKMH +dx,VarFMH + dy,MHID);
scatter(VarKPV, VarFPV,[],'b')
%text(VarKPV +dx,VarFPV + dy,PVID);
title('MPYHY v MPSL cube K and FFT variance');
xlabel('K var');
ylabel('FFT var');

%scatter plot median K v FFT
figure
dx2=0.005;
dy2=0.1;
hold on
scatter(MedKMH,MedFMH,[],'r')
%text(MedKMH +dx2,MedFMH + dy2,MHID);
```

```
scatter(MedKPV, MedFPV,[],'b')
%text(MedKPV +dx2,MedFPV + dy2,PVID);
title('MPYHY v MPSL cube median K and FFT');
xlabel('K med');
ylabel('FFT med');

%scatter plot iqr K & FFT
figure
dx3=0.0001;
dy3=0.1;
hold on
scatter(IqrKMH,IqrFMH,[],'r')
%text(IqrKMH +dx3,IqrFMH + dy3,MHID);
scatter(IqrKPV, IqrFPV,[],'b')
%text(IqrKPV +dx3,IqrFPV + dy3,PVID);
title('MPYHY v MPSL cube iqr K and FFT');
xlabel('iqr K');
ylabel('iqr FFT');
%}
save ('/Users/stewartlake/Documents/Retinalcontour/data validity/MP - livewire
check/sgnrkrmse');
```

Merging 3D cubes

1. mergeSLO3DSSa

```
%SLO3Dcontour added to this
%create 3D surf plot cube (with BFC added)
%CHANGE:
%CHANGE: Cubename1, & Cubename2, lines 9/13
%CHANGE:
%CHANGE: create SLO images of both first, in location as per line 66 & 149
%corrected for SLO FoV 36 x 30 see guidance lines 70-71
clear
Cubename1 = 'SSa 0102 11-43-46';%'SSa 0067 14-23-57';%'SSa 0066 11-28-46';%macula
Eyename1 = Cubename1(1:8);
Eyeprefix1 = Cubename1(1:3);

Cubename2 = 'SSa 0102 11-44-29';%'SSa 0067 14-25-53';%eccentric
Eyename2 = Cubename2(1:8);
Eyeprefix2 = Cubename2(1:3);
%%
xzdir1= ['/Users/stewartlake/Documents/SS OCT eyes/' Eyename1 '/' Eyename1 ' xz/'
Cubename1 ' xz/'];
cd(xzdir1);
dinfo = dir;
    names_cell = {dinfo.name};
%gives a matrix called names_cell where each column has a filename
%then:
    out1=regexp(names_cell,'\d+','match');
    out1=str2double(cat(1,out1{:}));
%gives a matrix called out in which each row has a number from an original filename
%these are in column 2 if text file header has a number, column 1 if it
%doesn't.

%script alpha. takes a cube of data and
%Puts x and z coordinate values into an array (myData), each cell a line of data.
%Then separates this into arrays for x, and z.
    numFiles = size(out1, 1);
    startRow = 1;
    endRow = inf;
    myData = cell(1,numFiles);
    ximp = cell (1, numFiles);
    zimp = cell (1, numFiles);

    fileName = cell(1);
```

```
     for fileNum = 1:numFiles
            Bscanline = out1(fileNum,end);
            %This loop is for a single cube
            fileName =[];
            fileName = sprintf('-%04d.txt',Bscanline);
            fileName = [Eyeprefix1 fileName];
            myData{Bscanline} = importfile(fileName,startRow,endRow);

            ximp{Bscanline}=myData{Bscanline}(:,1);
            zimp{Bscanline}=myData{Bscanline}(:,2);



     end

     sf = 500/9;
sfz = 1536/3;
for BFC=1:numFiles
    NowBS = out1(BFC,end);
xmm{NowBS} = ximp{1,NowBS}.VarName1;
ZMM{NowBS} = zimp{1,NowBS}.VarName2;
p2{NowBS} = polyfit(xmm{NowBS},ZMM{NowBS},2);%unused
end

SLOpicname1 = ['/Users/stewartlake/Documents/SS OCT eyes/' Eyename1 '/' Eyename1 '
lslo/' Cubename1 '.png'];
SLOpic1 = imread(SLOpicname1);

%SLO FoV 36x30,lines 72,92,162,180,101, 190 from [500 500] to [500 600]
% & lines 101 190 from ximp2{1,Site2}.VarName1+1 to
floor(ximp2{1,Site2}.VarName1)*1.2+1
SLOpicMrNsize1 = imresize(SLOpic1,[500 600]);%pixel dimensions of B scans
IMGcontour1 = zeros(500,600);

 %put height into IMGcountour for surf
 for Site = 1:numFiles
     if ~isempty(ximp{1,Site})%only if there is B scan data here
         %LineWidth=LongI1(GaP1(Site+1))-LongI1(GaP1(Site)+1)+1;%width of green
lines
         %ThickZ1 = (repmat(zimp{1,Site}.VarName2',LineWidth,1))/4.5;%repeat z to
match line width
         ThickZ1 = fliplr(zimp{1,Site}.VarName2');%fliplr
         ThickZ1 = ThickZ1*sf/sfz;%converts to x index dimension size
         ColI1 = floor(ximp{1,Site}.VarName1*1.2)+1;
         IMGcontour1((((numFiles+1)-Site)*20)-10,ColI1)=ThickZ1;
           %the 26-Site places higher index B scans at the top of the image
     end
 end

 IMGcontour1(IMGcontour1==0)=NaN;


I1 = floor(fillmissing(IMGcontour1,'previous',1,'EndValues','nearest'));
I1 = floor(fillmissing(I1,'previous',2,'EndValues','nearest'));
%%
 %now generate second image contour map

xzdir2= ['/Users/stewartlake/Documents/SS OCT eyes/' Eyename2 '/' Eyename2 ' xz/'
Cubename2 ' xz/'];
cd(xzdir2);
dinfo2 = dir;
    names_cell2 = {dinfo2.name};
%gives a matrix called names_cell where each column has a filename
%then:
    out2=regexp(names_cell2,'\d+','match');
    out2=str2double(cat(1,out2{:}));
%gives a matrix called out in which each row has a number from an original filename
%these are in column 2 if text file header has a number, column 1 if it
```

```
%doesn't.

%script alpha. takes a cube of data and
%Puts x and z coordinate values into an array (myData), each cell a line of data.
%Then separates this into arrays for x, and z.
    numFiles2 = size(out2, 1);
    startRow = 1;
    endRow = inf;
    myData = cell(1,numFiles2);
    ximp2 = cell (1, numFiles2);
    zimp2 = cell (1, numFiles2);

    fileName = cell(1);


     for fileNum2 = 1:numFiles2
            Bscanline2 = out2(fileNum2,end);
            %This loop is for a single cube
            fileName =[];
            fileName = sprintf('-%04d.txt',Bscanline2);
            fileName = [Eyeprefix2 fileName];
            myData{Bscanline2} = importfile(fileName,startRow,endRow);

            ximp2{Bscanline2}=myData{Bscanline2}(:,1);
            zimp2{Bscanline2}=myData{Bscanline2}(:,2);

    NowBS2 = out2(fileNum2,end);
    xmm2{NowBS2} = ximp2{1,NowBS2}.VarName1;
    ZMM2{NowBS2} = zimp2{1,NowBS2}.VarName2;
    p22{NowBS2} = polyfit(xmm2{NowBS2},ZMM2{NowBS2},2);%unused
end

SLOpicname2 = ['/Users/stewartlake/Documents/SS OCT eyes/' Eyename2 '/' Eyename2 '
lslo/' Cubename2 '.png'];
SLOpic2 = imread(SLOpicname2);

%SLOpicMr2 = SLOpic2(end:-1:1,end:-1:1,:);

SLOpicMrNsize2 = imresize(SLOpic2,[500 600]);
IMGcontour2 = zeros(500,600);

 %put height into IMGcountour for surf
 for Site2 = 1:numFiles2
     if ~isempty(ximp2{1,Site2})%only if there is B scan data here
         %LineWidth=LongI2(GaP2(Site2+1))-LongI2(GaP2(Site2)+1)+1;%width of green
lines
         %ThickZ2 = (repmat(zimp2{1,Site2}.VarName2',LineWidth,1))/4.5;%repeat z to
match line width

%IMGcontour2(LongI2(GaP2(Site2)+1):LongI2(GaP2(Site2+1)),ximp2{1,Site2}.VarName1+1)
=ThickZ2;
         ThickZ2 = fliplr(zimp2{1,Site2}.VarName2');%fliplr
         ThickZ2 = ThickZ2*sf/sfz;
         ColI2=[];
         ColI2 = floor(ximp2{1,Site2}.VarName1*1.2)+1;
         IMGcontour2((((numFiles2+1)-Site2)*20)-10,ColI2)=ThickZ2;

     end
 end

 IMGcontour2(IMGcontour2==0)=NaN;


I2 = floor(fillmissing(IMGcontour2,'previous','EndValues','nearest'));
I2 = floor(fillmissing(I2,'previous',2,'EndValues','nearest'));

%%
 %create surf plot
%for first image
Imi1f = figure;
```

```
%[XX,MaP]=rgb2ind(SLOpicMrNsize1,256);
colormap(gray)
CubeHtmap=surf(I1,SLOpicMrNsize1,'FaceColor','texturemap','EdgeColor','none','CData
Mapping','direct','FaceAlpha',0.7,'FaceLighting','gouraud');
view(2);
%pbaspect([9 9 3]);%not needed - z converted to x scale in ThickZ1

Imi2f = figure;
%[XX2,MaP2]=rgb2ind(SLOpicMrNsize2,256);
colormap(gray)
CubeHtmap2=surf(I2,SLOpicMrNsize2,'FaceColor','texturemap','EdgeColor','none','CDat
aMapping','direct','FaceAlpha',0.7,'FaceLighting','gouraud');
view(2);
%pbaspect([9 9 3]);

%rest is for Pt2
%find three matching points looking at SLO map - I1: a,b,c & I2: x,y,z
%I2 = I2 + (a-x);%translate to match two points

%bring both to origin
%I2orgn = I2 - a;
%I1orgn = I1 - a;
```

2. mergeSLO3DPt2SSa

```
%mergeSLO3DPt2SSa from mergeSLO3DPt2v2 12 october 2020
%runs from data created by mergeSLO3DSSa.m
% MergeSLO3DSSa has created two 3D images, and displayed their SLO maps in 2D
%from those, select 3 matching points: a,b,c (I1 - host), and x,y,z (I2)
%enter the x,y coords in these matrices - leave z zero
%correct for Fov SLO 36 x 30 lines 42, e/d/+/1 lines 113 & 159
%%
%create surfaces
%I1 & I2 created with mergeSLO3D
a = zeros(3,1,1);%SSan0028 at the major ST vessel
b = zeros(3,1,1);%at the disc
c = zeros(3,1,1);%bv near the fovea
x = zeros(3,1,1);
y = zeros(3,1,1);
z = zeros(3,1,1);
%{
a(1) = 479;%SSa 0028;square SLO:56;Note (1) is y, (2) is x
a(2) = 265;%328;
b(1) = 330;%220;
b(2) = 69;%477;
c(1) = 387;%191;
c(2) = 426;%326;
x(1) = 174;%58;
x(2) = 272;%36;
y(1) = 38;%228;
y(2) = 72;%175;
z(1) = 77;%196;
z(2) = 431;%23;
%}
%{
a(1) = 88;%SSa 0066;Note (1) is y, (2) is x
a(2) = 126;% major xing
c(1) = 38;%
c(2) = 429;%minor branching ST
b(1) = 222;%disc
b(2) = 44;%
x(1) = 342;%
x(2) = 137;%;
z(1) = 301;%
z(2) = 440;%
y(1) = 495;%
y(2) = 41;

a(1) = 367;%SSa 0067;Note (1) is y, (2) is x, 14-23-57, 14-25-53
```

```
a(2) = 561;%  ST branch
b(1) = 329;%disc
b(2) = 91;%
c(1) = 488;%sup
c(2) = 235;%
x(1) = 111;%
x(2) = 557;%;
y(1) = 68;%
y(2) = 87;%
z(1) = 226;%
z(2) = 232;

a(1) = 168;%SSa 0082;Note (1) is y, (2) is x
a(2) = 25;%  ST branch
b(1) = 381;%disc
b(2) = 120;%
c(1) = 365;%sup
c(2) = 333;%
x(1) = 112;%
x(2) = 276;%;
y(1) = 324;%
y(2) = 362;%
z(1) = 324;%
z(2) = 576;

a(1) = 105;%SSa 0102;Note (1) is y, (2) is x
a(2) = 133;%  cubes 11-44-29 &
b(1) = 301;%
b(2) = 335;%
c(1) = 371;%
c(2) = 196;%
x(1) = 34;% cube 11-46-1
x(2) = 377;%;
y(1) = 247;%
y(2) = 561;%
z(1) = 298;%
z(2) = 418;
%}
a(1) = 387;%SSa 0102;Note (1) is y, (2) is x
a(2) = 494;%  cubes 11-43-46 &
b(1) = 250;%
b(2) = 330;%
c(1) = 415;%
c(2) = 120;%
x(1) = 177;% cube 11-44-29
x(2) = 560;%;
y(1) = 31;%
y(2) = 404;%
z(1) = 187;%
z(2) = 189;

a(3) = I1(a(1),a(2));%identifies z value from the 3D reconstruction of the
b(3) = I1(b(1),b(2));%B scans in mergeSLO3D - I1/2 where row=y,col=x
c(3) = I1(c(1),c(2));
x(3) = I2(x(1),x(2));
y(3) = I2(y(1),y(2));
z(3) = I2(z(1),z(2));

%scatter3(Imi1f,[a(1); b(1); c(1)],[a(2); b(2); c(2)],[a(3); b(3); c(3)]);
%scatter3(Imi2f,[x(1); y(1); z(1)],[x(2); y(2); z(2)],[x(3); y(3); z(3)]);

%create x and Y for I1 & I2
I2x=1:600;%not 500
I2x=repmat(I2x, 500,1);
%I2y=flipud(I2x');%try with y origin at the top - works better
I2y = (1:500)';
I2y = (repmat(I2y,1,600));
I1x=I2x;
I1y=I2y;
```

```
I2 = cat(3,I2y(1:500,:), I2x(1:500,:), I2);%500 x 600
I1 = cat(3,I1y(1:500,:), I1x(1:500,:), I1);%sheeets y,x,z



%%
%Translation

%move x to a
I22 = I2 - permute((x-a),[3 2 1]);%translate I2 to I1 to match two points (x to a)

y2= y - (x-a); %this moves y to translated location x on a (I2 on I1)
z2= z - (x-a);


%%
%create second surf image to rotate to I1 space
%note created after translation (I22)
I2surf = surf(I22(:,:,2),I22(:,:,1),
I22(:,:,3),SLOpicMrNsize2,'FaceColor','texturemap','EdgeColor','none','CDataMapping
','direct','FaceAlpha',0.7);
%2 & 1 reversed here as surf uses (x,y,z) while I2 are (y,x,z)

%%
%first rotation - y (now y2) to b. Subtract a to get vectors ab/ay2 not
0b/0y2Angle:
Epsilon = atan2d(norm(cross(b-a,y2-a)),dot(b-a,y2-a));%angle in degrees
%And the axis of rotation is
Axby = cross(b-a,y2-a);
Origin = a;

rotate(I2surf, Axby, Epsilon,Origin);
%

%Determine new z (z2prime) after first translation (z2) then rotation
%This uses AxelRot:
%Matt J (2020). 3D Rotation about Shifted Axis
%(https://www.mathworks.com/matlabcentral/fileexchange/30864-3d-rotation-about-
shifted-axis)
%MATLAB Central File Exchange. Retrieved September 24, 2020.

[z2prime,~,~]=AxelRot(z2,Epsilon,Axby,Origin);


%%
%Second rotation: z to c (now z2prime to c)
%{
%using axis angle here rotates y2 off b.
Delta=atan2d(norm(cross(c,z2prime)),dot(c,z2prime));
Axcz = cross(c,z2prime);
Originpr=a;
%}

%Need to make second rotation z2' to c around axis ab

%determine vectors ab (bvec) and az2' (z2pvec)
bvec = b-a;
z2pvec = z2prime-a;
%angle between these, theta
theta = atan2d(norm(cross(bvec,z2pvec)),dot(bvec,z2pvec));

%find p, where pz2' & pc are normal to ab (assumes |pz2'| = |pc|)
%lenap = |az2'|*cos(theta)
az2plen = sqrt((a(1) - z2prime(1)).^2 + (a(2) - z2prime(2)).^2 + (a(3) -
z2prime(3)).^2);
lenap = az2plen*cosd(theta);% as theta < 90 degrees

%point p is at a + lenap*unit vector ab(== (b-a)./norm(b-a))
p=a+lenap*((b-a)./norm(b-a));
```

```
%now second rotation, rotate z2' to c around axis ab at point p
Axab = b-a;

%angle delta = cpz2'
Delta = atan2d(norm(cross(z2prime-p,c-p)),dot(z2prime-p,c-p));
Originpr=p;


rotate(I2surf, Axab, Delta, Originpr);


%add surf I1
%axes(Imi2)
hold on
CubeHtmap=surf(I1(:,:,2),I1(:,:,1),I1(:,:,3),SLOpicMrNsize1,'FaceColor','texturemap
','EdgeColor','none','CDataMapping','direct','FaceAlpha',0.7,'FaceLighting','gourau
d');
%CubeHtmap=surf(I1(:,:,1),I1(:,:,2),I1(:,:,3),XX,'FaceColor','flat','FaceAlpha',0.7
);
%pbaspect([9 8 2]);
view(-64,14) %display image in 3D view
title('SSa 0102 axis angle v2, angles epsilon+, delta+, SLO FoV corrected');
%change axes values
set(gca,'XTick',[100 200 300 400 500 600 700 800 900] );
set(gca,'YTick',[100 200 300 400 500 600 700 800 900] );
set(gca,'zTick',[100 200 300] );
set(gca,'XTickLabel',[1.8 3.6 5.4 7.2 9 10.8 12.6 14.4 16.2] );
set(gca,'YTickLabel',[1.8 3.6 5.4 7.2 9 10.8 12.6 14.4 16.2] );
set(gca,'ZTickLabel',[1.8 3.6 5.4] );
xlabel('x mm');
ylabel('y mm');
zlabel('mm');
%%


%find matching x,y corrrdinates in I1 and moved I2, determine average
%displacement in z axis
rotXaxan=I2surf.XData;
rotYaxan = I2surf.YData;
rotZaxan = I2surf.ZData;

I22v = cat(2,rotYaxan(:),rotXaxan(:),rotZaxan(:));
%[I22prv,~,~]=AxelRot(I22v,Epsilon,Axby,Origin);
%[I22Dprv,~,~]=AxelRot(I22prv,Delta,Axab,Originpr);
I22Dprv = round(I22v);
I1v = reshape(I1,[],3);
OlapAxAn = ismembertol(I1v(:,1:2),I22Dprv(:,1:2),1/600,'ByRows',true);

DisparityAxAn = I1v(OlapAxAn,3)-I22Dprv(OlapAxAn,3);

MnDispAxAn = mean(abs(DisparityAxAn));
SDDispAxAn = std(abs(DisparityAxAn));


%%
%quaternion merging

Ac = [a(2) b(2) c(2); a(1) b(1) c(1);a(3) b(3) c(3)];
Bc = [x(2) y(2) z(2); x(1) y(1) z(1);x(3) y(3) z(3)];

[regParams,~,ErrorStats]=absor(Bc,Ac); %note order

%The output regParam.q, is converted to a quaternion:

%(Note outputs: Regparams.s = 1, so no scaling required.
%and Regparams.t reveals translation required)

quat = quaternion(regParams.q');

%and the cube points converted to Nx3  list:
```

```
I2vq = reshape(I2,[],3);
TrV = regParams.t';%this is the translation vector
Trvec = cat(2, TrV(2), TrV(1), TrV(3));

Rres=rotatepoint(quat,I2vq);

I2v1q = Rres + Trvec;%translate

%pixel differences in z between two image overlaps
I2v1qf = round(I2v1q);
Olapq = ismembertol(I1v(:,1:2),I2v1qf(:,1:2),1/600,'ByRows',true);
Disparityq = I1v(Olapq,3)-I2v1qf(Olapq,3);
MnDispq = mean(abs(Disparityq));
SDDispq = std(abs(Disparityq));


I2v2q = reshape(I2v1q,500,600,3);

%hold on
Imi2q = figure;%remove % this line and remove hold on above to separate images,
%also the %{ %} 276 & 289 should be pressent to combine
%SLOpicMrNsize3 = ind2rgb8(SLOpicMrNsize2,copper);%changes color of Q (this for
merged- put in line below)
CubeHtmap2=surf(I2v2q(:,:,2),I2v2q(:,:,1),I2v2q(:,:,3),
SLOpicMrNsize2,'FaceColor','texturemap','EdgeColor','none','CDataMapping','direct',
'FaceAlpha',0.7,'FaceLighting','gouraud');
colormap(gray)%

hold on
CubeHtmap=surf(I1(:,:,2),I1(:,:,1),I1(:,:,3),SLOpicMrNsize1,'FaceColor','texturemap
','EdgeColor','none','CDataMapping','direct','FaceAlpha',0.7,'FaceLighting','gourau
d');
view(-64,14) %display image in 3D view
title('SSa 0102 Quaternion rotation, angles e+ d+');
set(gca,'XTick',[100 200 300 400 500 600 700] );
set(gca,'YTick',[100 200 300 400 500 600 700 800] );
set(gca,'zTick',[100 200 300] );
set(gca,'XTickLabel',[1.8 3.6 5.4 7.2 9 10.8 12.6] );
set(gca,'YTickLabel',[1.8 3.6 5.4 7.2 9 10.8 12.6 14.4] );
set(gca,'ZTickLabel',[1.8 3.6 5.4] );
xlabel('x mm');
ylabel('y mm');
zlabel('z mm');
```

Pupil Image Analysis

1. Pupilanalysis

```
%Get iris images from store, analyse pupil shape
%for SS OCT eyes
%CHANGE: open folder for eye data from store (complete raw IMG folders)
%CHANGE: saves Iristable once completed

%set variables
clear
Currfold = pwd;

%Eyesinfo=dir;
%Eyesinfo = Eyesinfo(~ismember({Eyesinfo.name},{'.','..','.DS_Store'}));
%Enames = {Eyesinfo.name};
%NumEyes = size(Enames,2);
load('/Users/stewartlake/Documents/MATLAB/SSOCT eyes.mat');
load('/Users/stewartlake/Documents/MATLAB/Iris table.mat');
SSDirstr = '/Users/stewartlake/Documents/SS OCT eyes/';
dimiris = [640 480];
roi = images.roi.Ellipse('Color','c','StripeColor','r', 'LineWidth',0.75,
'MarkerSize',4);
```

```
%for Eye = 1:NumEyes

    %enter eye folder
    %hostdir=cd(Enames{Eye});
    EyeID = Currfold(end-7:end);%Eye ID (eg 'SS1 0028')
    EyeIDs= Currfold(end-5:end);%Eye ID (eg '1 0028')
    EyeIDss = EyeIDs(~isspace(EyeIDs));%eye ID '10028'
    EyeIDn=str2double(EyeIDss);
    Match = find(strcmp(SSOCTeyes.ID,EyeID));%find table row to match current eye

    IMGinfoS = dir;
    IRISinfo = IMGinfoS(contains({IMGinfoS.name},'iris.bin'));%
    IRISnames = {IRISinfo.name};
    %IRISnames(1)=[];%CHECK need to remove first iris.bin all cases11
    %SStime =
cellfun(@(s)regexp(s,'\d*\S\d*\S\d*(?=iris)','all','match'),IRISnames,'UniformOutpu
t',false);
    numbiris = size(IRISnames,2);
    CCtime =
string(cellfun(@(s)regexp(s,'(?<=2020_)\d*\S\d*\S\d*','all','match'),IRISnames,'Uni
formOutput',false));%'11-4-42
    Tformat = datetime(CCtime,'InputFormat', 'HH-mm-ss');%
    [tsort(1,1:numbiris),Its(1,1:numbiris)] = sort(Tformat(1,1:numbiris));%ID time
sorted
    IRISnameS = IRISnames(Its(1,1:numbiris));%sort into time order
    CCtime = CCtime(Its(1,1:numbiris));%sort into time order

    irisDir = [SSDirstr EyeID '/' EyeID ' iris'];
       if (~exist(irisDir,'dir'))

           mkdir (irisDir)
       end

    %run through iris.bin images in an eye folder
    for Irisimg=1:length(IRISnameS)


        %iris tiff creation
        IRISnm = IRISnameS{Irisimg};
        IRISfileID = fopen(IRISnm);
        IRISfile = fread(IRISfileID);


        IRISfile1 = flipud(uint8(reshape(IRISfile,dimiris)));%orient R/L correctly
with flipud
        %CCtime = regexp(IRISnm,'(?<=2020_)\d*\S\d*\S\d*','all','match');%'11-4-42'

        TsaveNiris = [irisDir '/' EyeID ' ' CCtime{Irisimg} '.tif']; %tiff cube
name
        imwrite(IRISfile1',TsaveNiris);


        imshow(TsaveNiris)
        roi = images.roi.Ellipse('Color','c','StripeColor','r', 'LineWidth',0.75,
'MarkerSize',4);
        draw(roi)
        pause


        Iristable.Eye(end+1) = EyeIDn;
        Iristable.AspectRatio(end) = roi.AspectRatio;
        Iristable.Rotation(end) = roi.RotationAngle;
        Iristable.Center{end} = roi.Center;
        Iristable.SemiAxes{end} = roi.SemiAxes;
        %next line assumes sorted into time order to match location index
        Iristable.Direction{end} = SSOCTeyes.UHDSpot1{Match}(Irisimg);

        if Iristable.Direction{end} == 'M'
            AvAxM = (roi.SemiAxes(1)+roi.SemiAxes(2))/2;
            Iristable.AvAxM(end)=AvAxM;
```

```
        else
            cMiAxE = (AvAxM/max(roi.SemiAxes(:)))*min(roi.SemiAxes);

            Iristable.PitchAngle(end) = acosd(cMiAxE/AvAxM);
        end


    end

    %back up to eye directory
    %cd (hostdir)
%end

save('/Users/stewartlake/Documents/MATLAB/Iris table.mat','Iristable');
```

2. PupilanalysisSD2

```
% PupilanalysisSD2, to analyse SD pupil data, created by Pupilanalysis.m
% that was saved in MATLAB/Pupil analysis/IrisSD.mat. Rows in this array match rows
% in sALLIDt

%IrisSD/UseIris match col: 1=ID,2 =mac, 3 = sup, 4= Sup-temp
   %sheets 2+ 1=Aspectratio, 2=Rotation, 3&4=centrepoints, 5&6 = semiaxis
   %lengths, 7=pitchangle(=pupil angle, alpha)

%Aspect ratio corrrected from ht/wdith to max axis: min axis.
%rotation corrected from angle closest to x-axis to angle between major axis and
x=0.
clear
load('/Users/stewartlake/Documents/MATLAB/Pupil analysis/SD cube IDs m s st.mat');
load('/Users/stewartlake/Documents/MATLAB/Pupil analysis/IrisSD.mat');

UseID = sALLIDt;
UseIris2 = IrisSD;

Nomac = isnan(IrisSD(:,2,1));

UseID(Nomac,:)=[];%remove eyes NaN or no macula data
UseIris2(Nomac,:,:)=[];
UseIris = UseIris2;
LeftIs = UseIris2(:,1,1)>199;
NumIs = size(UseID,1);
%%
%use largest axis to determine angle. ellipse take semiaxis.1 as that
%closest to x. Add 90 degrees to these eyes rotation axis.
%step 1: if semaxis1 (UseIris2(:,2:4,5))< semiaxis2 (2:4,6) then angle=angle-90
Angchk=UseIris2(:,2:4,2);
RevAx = find(UseIris2(:,2:4,5) < UseIris2(:,2:4,6));

Angchk(RevAx) = Angchk(RevAx)-90;
%now angle -90 to 270, or 0-360

%step 2: IF Angle > 90, then Angle = Angle - 180
NumAng=numel(Angchk);

for CA=1:NumAng

    while Angchk(CA)>90
        Angchk(CA)=Angchk(CA)-180;%loops for each element individually
    end

end

%step 3: left eyes = - left eyes
Angchk(LeftIs,:)=-Angchk(LeftIs,:);
PupilRotn = Angchk;%this variable the corrected angles for analysis:col mac/S/st
%%
%determine scan axis displacement from centre of pupil
%note rho is in pixels
```

```
EllipseCenXY = UseIris(:,2:4,3:4);%Eyes x image (M/S/ST) x (x,y)
EllipseCenXY(:,:,2) = - EllipseCenXY(:,:,2);
Cen = [320 -240];% image centrepoint
EllX = EllipseCenXY(:,:,1) - 320;
EllY = EllipseCenXY(:,:,2) - (-240);
cEllCenXY = cat(3, EllX, EllY);%pupil centre displacment from centre of image
[ECtheta,ECrho] = cart2pol(EllX,EllY);
ECtheta = ECtheta - 90;
Newtheta = wrapTo180(ECtheta);%scan axis diplacement angle, 0 = vertical, +/-180
Newtheta(LeftIs,:) = -Newtheta(LeftIs,:);%mirror left eyes to right


CenDirVar = Newtheta - PupilRotn;%scan axis displacement relative to gaze direction
Mncdv = mean(CenDirVar,'omitnan');
SDcdv = std(CenDirVar,'omitnan');

figure %1
hold on
h(1) = scatter(ECrho(UseID.Diag==2,1),Newtheta(UseID.Diag==2,1),'o','b');
h(2) = scatter(ECrho(UseID.Diag==2,2),Newtheta(UseID.Diag==2,2),'o','b');
h(3) = scatter(ECrho(UseID.Diag==2,3),Newtheta(UseID.Diag==2,3),'o','b');

h(4) = scatter(ECrho(UseID.Diag==3,1),Newtheta(UseID.Diag==3,1),'x','r');
h(5) = scatter(ECrho(UseID.Diag==3,2),Newtheta(UseID.Diag==3,2),'x','r');
h(6) = scatter(ECrho(UseID.Diag==3,3),Newtheta(UseID.Diag==3,3),'x','r');

h(7) = scatter(ECrho(UseID.Diag==4,1),Newtheta(UseID.Diag==4,1),'+','m');
h(8) = scatter(ECrho(UseID.Diag==4,2),Newtheta(UseID.Diag==4,2),'+','m');
h(9) = scatter(ECrho(UseID.Diag==4,3),Newtheta(UseID.Diag==4,3),'+','m');

legend(h([1 4 7]),'PVD','RD','RT');
title('Scan axis displacement (from image centre), by diagnosis');
xlabel('Distance rho pixels (how far)');
ylabel('Angle theta (degrees) which way?');
hold off

figure %2
hold on
scatter(ECrho(:,1),abs(Newtheta(:,1)),'o','g');
scatter(ECrho(:,2),abs(Newtheta(:,2)),'s','r');
scatter(ECrho(:,3),abs(Newtheta(:,3)),'d','b');
legend('Macula','Superior','Supero-temporal');
title('Scan axis displacement (from image centre), by gaze direction');
xlabel('Distance rho pixels: how far)');
ylabel('Angle theta (degrees): which way?');
hold off

%Aspectratio2 = UseIris(:,2:4,1);
Aspectratio2 = max(UseIris(:,2:4,5:6),[],3)./min(UseIris(:,2:4,5:6),[],3);
figure %3
hold on
ha(1) = scatter(Aspectratio2(UseID.Diag==2,1),PupilRotn(UseID.Diag==2,1),'o','b');
ha(2) = scatter(Aspectratio2(UseID.Diag==2,2),PupilRotn(UseID.Diag==2,2),'o','b');
ha(3) = scatter(Aspectratio2(UseID.Diag==2,3),PupilRotn(UseID.Diag==2,3),'o','b');

ha(4) = scatter(Aspectratio2(UseID.Diag==3,1),PupilRotn(UseID.Diag==3,1),'x','r');
ha(5) = scatter(Aspectratio2(UseID.Diag==3,2),PupilRotn(UseID.Diag==3,2),'x','r');
ha(6) = scatter(Aspectratio2(UseID.Diag==3,3),PupilRotn(UseID.Diag==3,3),'x','r');

ha(7) = scatter(Aspectratio2(UseID.Diag==4,1),PupilRotn(UseID.Diag==4,1),'+','m');
ha(8) = scatter(Aspectratio2(UseID.Diag==4,2),PupilRotn(UseID.Diag==4,2),'+','m');
ha(9) = scatter(Aspectratio2(UseID.Diag==4,3),PupilRotn(UseID.Diag==4,3),'+','m');

legend(ha([1 4 7]),'PVD','RD','RT');
title('Aspect ratio v Pupil ellipse rotation, by diagnosis');
xlabel('Ellipse Aspect ratio');
ylabel('Pupil ellipse rotation (degrees)');
hold off

macmnaxisdim=mean(UseIris(:,2,5:6),'omitnan');
```

```
MnAspRdir = mean(Aspectratio2,'omitnan');
MnAspRall = mean(Aspectratio2(:),'omitnan');

MnNwthetadir = mean(Newtheta,'omitnan');%displacment direction from pupil centre
MnNwthetaall = mean(Newtheta(:),'omitnan');

MnNwthetaabsdir = mean(abs(Newtheta),'omitnan');%displacment direction from pupil
centre
MnNwthetaabsall = mean(abs(Newtheta(:)),'omitnan');

MnECrhodir = mean(ECrho,'omitnan');%distance from centre image
MnECrhoall = mean(ECrho(:),'omitnan');

MnProtdir = mean(PupilRotn,'omitnan');%gaze direction
MnProtall = mean(PupilRotn(:),'omitnan');

SDAspRdir = std(Aspectratio2,'omitnan');
SDAspRall = std(Aspectratio2(:),'omitnan');

SDNwthetadir = std(Newtheta,'omitnan');
SDNwthetaall = std(Newtheta(:),'omitnan');

SDECrhodir = std(ECrho,'omitnan');
SDECrhoall = std(ECrho(:),'omitnan');

SDProtdir = std(PupilRotn,'omitnan');%SD gaze direction
SDProtall = std(PupilRotn(:),'omitnan');

MnPitAngdir = mean(UseIris(:,3:4,7),'omitnan');%gaze excursion
SDPitAngdir = std(UseIris(:,3:4,7),'omitnan');
MnabsPitAngdir = mean(abs(UseIris(:,3:4,7)),'omitnan');

%%
%difference between individuals up gaze and upright gaze
diffS2ST = PupilRotn(:,3)-PupilRotn(:,2);%gaze direction diff
figure %4
alphadiff = abs(UseIris(:,3,7)-UseIris(:,4,7));
difftable = table(UseID{:,1}, alphadiff, diffS2ST);
scatter(abs(UseIris(:,3,7)-UseIris(:,4,7)),abs(diffS2ST),50,'o','m','filled')%sup

xlabel('ST - S Angle alpha (degrees)');
ylabel('ST - S gaze (degrees)');
title({'Difference between up & up/right gaze direction';'and pupil
eccentricity'});
%point close to the origin reflects overal s to ST? R289
%%
%non-mac (pitch angle) v ellipse rotation by diagnosis
figure %5
hold on
hb(1) = scatter(UseIris(UseID.Diag==2,3,7),PupilRotn(UseID.Diag==2,2),'o','b');
hb(2) = scatter(UseIris(UseID.Diag==2,4,7),PupilRotn(UseID.Diag==2,3),'o','b');

hb(3) = scatter(UseIris(UseID.Diag==3,3,7),PupilRotn(UseID.Diag==3,2),'x','r');
hb(4) = scatter(UseIris(UseID.Diag==3,4,7),PupilRotn(UseID.Diag==3,3),'x','r');

hb(5) = scatter(UseIris(UseID.Diag==4,3,7),PupilRotn(UseID.Diag==4,2),'+','m');
hb(6) = scatter(UseIris(UseID.Diag==4,4,7),PupilRotn(UseID.Diag==4,3),'+','m');

legend(hb([1 3 5]),'PVD','RD','RT');
title('Angle alpha v Pupil ellipse rotation, by diagnosis');
xlabel('Angle alpha (degrees)');
ylabel('Pupil ellipse rotation (degrees)');
hold off

%non-mac (pitch angle) v ellipse rotation by region (gaze direction)
figure %6
hold on
scatter(UseIris(:,3,7),abs(PupilRotn(:,2)),'s','r');%non macula (Pitch angle)
scatter(UseIris(:,4,7),abs(PupilRotn(:,3)),'d','b');
```

```
legend('Superior','Supero-temporal');
title('Angle alpha v Pupil ellipse rotation, by gaze direction');
xlabel('Angle alpha (degrees)');
ylabel('Pupil ellipse rotation (degrees)');
hold off

figure%fig7
GSu = PupilRotn(:,2);%gaze drn sup
%GSu(GSu>0)=GSu(GSu>0)-180;
GST = PupilRotn(:,3);
%GST(GST<0) = GST(GST<0)+180;
ax = polaraxes;
hold on
polarscatter (deg2rad(GSu+90), (UseIris(:,3,7)./90),'s','r');%sup
polarscatter (deg2rad(GST), (UseIris(:,4,7)./90),'d','b');%ST
title({'Polar plot, Angle alpha (rho) v Pupil ellipse rotation (theta),',' by gaze
direction'});
legend({'Superior','Supero-temporal'},'Location','best');
%xlabel('Gaze direction (degrees)');
%ylabel('Angle alpha (degrees)');
rticks([0.2 0.4 0.6])
rticklabels({'aa = 18','aa = 36','aa = 54'})
ax.RAxisLocation = 300;
hold off



%look at fovea angle and pitch/rotation
ODfovAngle = table2array(UseID(:,6));%optic disc-fovea angle
figure %8
hold on
scatter3(UseIris(:,3,7),abs(PupilRotn(:,2)),ODfovAngle,'s','r');%Superior,non
macula (Pitch angle)
scatter3(UseIris(:,4,7),abs(PupilRotn(:,3)),ODfovAngle,'d','b');%supero-temp
legend('Superior','Supero-temporal');
title('Angle alpha v Pupil ellipse rotation v Optic disc-fovea angle, by gaze
direction');
xlabel('Angle alpha (degrees)');
ylabel('Pupil ellipse rotation (+/- degrees from vertical)');
zlabel('Optic disc-fovea angle');
hold off


%non-mac (pitch angle) v ellipse rotation v OD fovea angle, by diagnosis
figure %9
hold on
hc(1) =
scatter3(UseIris(UseID.Diag==2,3,7),PupilRotn(UseID.Diag==2,2),ODfovAngle(UseID.Dia
g==2),'o','b');
hc(2) =
scatter3(UseIris(UseID.Diag==2,4,7),PupilRotn(UseID.Diag==2,3),ODfovAngle(UseID.Dia
g==2),'o','b');

hc(3) =
scatter3(UseIris(UseID.Diag==3,3,7),PupilRotn(UseID.Diag==3,2),ODfovAngle(UseID.Dia
g==3),'x','r');
hc(4) =
scatter3(UseIris(UseID.Diag==3,4,7),PupilRotn(UseID.Diag==3,3),ODfovAngle(UseID.Dia
g==3),'x','r');

hc(5) =
scatter3(UseIris(UseID.Diag==4,3,7),PupilRotn(UseID.Diag==4,2),ODfovAngle(UseID.Dia
g==4),'+','m');
hc(6) =
scatter3(UseIris(UseID.Diag==4,4,7),PupilRotn(UseID.Diag==4,3),ODfovAngle(UseID.Dia
g==4),'+','m');

legend(hc([1 3 5]),'PVD','RD','RT','best');
title('Angle alpha v Pupil ellipse rotation v OD-fovea angle, by diagnosis');
xlabel('Angle alpha (degrees)');
```

```
ylabel('Pupil ellipse rotation (degrees)');
zlabel('Optic disc-fovea angle');
hold off
%%
%ST eye images with angle <20 degrees
outSTrot = UseID(abs(PupilRotn(:,3))<20,:);

%Superior images with angle 25-55 degrees
outSurot = UseID((abs(PupilRotn(:,2))>25 & abs(PupilRotn(:,2))<55),:);

BigODf = UseID(ODfovAngle>13,:);
```

3. PupilanalysisSS

```
%Pupil analysis for SS OCT eyes
clear
load('/Users/stewartlake/Documents/MATLAB/Iris table.mat','Iristable');

EyeID = Iristable.Eye;
LeftIs = EyeID>19999;
RightIs = ~LeftIs;

Rotatangle = Iristable.Rotation;

%%
%get Gaze direction angle
%step 1: if semaxis1 (UseIris2(:,2:4,5))< semiaxis2 (2:4,6) then angle=angle-90
Angchk=Rotatangle;
smiaxes = cell2mat(table2array(Iristable(:,5)));

RevAx = find(smiaxes(:,1) < smiaxes(:,2));

Angchk(RevAx) = Angchk(RevAx)-90;
%now angle -90 to 270, or 0-360

%step 2: IF Angle > 90, then Angle = Angle - 180
NumAng=numel(Angchk);

for CA=1:NumAng

    while Angchk(CA)>90
        Angchk(CA)=Angchk(CA)-180;%loops for each element individually
    end

end

%step 3: left eyes = - left eyes
Angchk(LeftIs,:)=-Angchk(LeftIs,:);
GazeDrn = Angchk;%this variable the corrected angles for analysis

%%
%Get angle alpha
AngAlpha = Iristable.PitchAngle;


%%
%find macular rows
for Run=1:length(Iristable.Direction)

    if (ischar(Iristable.Direction{Run}))

        IdxM(Run) = contains(Iristable.Direction(Run),'M');
        IdxU(Run) = contains(Iristable.Direction(Run),'U');%indices of gaze
direction
        IdxD(Run) = contains(Iristable.Direction(Run),'D');
        IdxR(Run) = contains(Iristable.Direction(Run),'R');
        IdxL(Run) = contains(Iristable.Direction(Run),'L');
```

```
    end

end

TL = all([LeftIs IdxL'],2);%left eyes looking L = temp
NR = all([RightIs IdxL'],2);% RE looking L = Nasal
NL = all([LeftIs IdxR'],2);%left eyes looking right = nasal
TR = all([RightIs IdxR'],2);% RE looking L = nasal

IdxT = any([TL TR],2);
IdxN = any([NL NR],2);

macD = Iristable(IdxM,:);%macular rows. Can repeat for others

%%
%analyse AngAlpha and GazeDrn for each orientation
MnMAA = mean(AngAlpha(IdxM),'omitnan');
SDMAA = std(AngAlpha(IdxM),'omitnan');
MnMgd = mean(GazeDrn(IdxM),'omitnan');%ignore - see 138-145
SDMgd = std(GazeDrn(IdxM),'omitnan');%ignore - see 138-145

MnUAA = mean(AngAlpha(IdxU),'omitnan');
SDUAA = std(AngAlpha(IdxU),'omitnan');
MnUgd = mean(GazeDrn(IdxU),'omitnan');%ignore - see 138-145
SDUgd = std(GazeDrn(IdxU),'omitnan');%ignore - see 138-145

MnDAA = mean(AngAlpha(IdxD),'omitnan');
SDDAA = std(AngAlpha(IdxD),'omitnan');
MnDgd = mean(GazeDrn(IdxD),'omitnan');%ignore - see 138-145
SDDgd = std(GazeDrn(IdxD),'omitnan');%ignore - see 138-145

MnNAA = mean(AngAlpha(IdxN),'omitnan');
SDNAA = std(AngAlpha(IdxN),'omitnan');
MnNgd = mean(GazeDrn(IdxN),'omitnan');%ignore - see 138-145
SDNgd = std(GazeDrn(IdxN),'omitnan');%ignore - see 138-145

MnTAA = mean(AngAlpha(IdxT),'omitnan');
SDTAA = std(AngAlpha(IdxT),'omitnan');
MnTgd = mean(GazeDrn(IdxT),'omitnan');
SDTgd = std(GazeDrn(IdxT),'omitnan');

%%
figure
hold on
scatter (GazeDrn(IdxM), AngAlpha(IdxM),'o', 'k');
scatter (GazeDrn(IdxU), AngAlpha(IdxU),'^','r');
scatter (GazeDrn(IdxD), AngAlpha(IdxD),'v','b');
scatter (GazeDrn(IdxT), AngAlpha(IdxT),'<','m');
scatter (GazeDrn(IdxN), AngAlpha(IdxN),'>','c');
xlabel('Gaze direction (degrees)');
ylabel('Angle alpha (degrees)');
hold off

figure
hold on
scatter (abs(GazeDrn(IdxM)), AngAlpha(IdxM),'o', 'k');
scatter (abs(GazeDrn(IdxU)), AngAlpha(IdxU),'^','r');
scatter (abs(GazeDrn(IdxD)), AngAlpha(IdxD),'v','b');
scatter (abs(GazeDrn(IdxT)), AngAlpha(IdxT),'<','m');
scatter (abs(GazeDrn(IdxN)), AngAlpha(IdxN),'>','c');
xlabel('Gaze direction (degrees)');
ylabel('Angle alpha (degrees)');
hold off

figure
GN = GazeDrn(IdxN);
GN(GN>0)=GN(GN>0)-180;
GT = GazeDrn(IdxT);
GT(GT<0) = GT(GT<0)+180;
```

```
ax = polaraxes;
polarscatter (deg2rad(GazeDrn(IdxM)), (AngAlpha(IdxM)./90),'o', 'k');
hold on
polarscatter (deg2rad(GazeDrn(IdxU)+90), (AngAlpha(IdxU)./90),'^','r');
polarscatter (deg2rad(GazeDrn(IdxD)-90), (AngAlpha(IdxD)./90),'v','b');
polarscatter ((deg2rad(GT+90)), (AngAlpha(IdxT)./90),'<','m');
polarscatter ((deg2rad(GN+90)), (AngAlpha(IdxN)./90),'>','c');
%xlabel('Gaze direction (degrees)');
%ylabel('Angle alpha (degrees)');
rticks([0.2 0.4 0.6])
rticklabels({'aa = 18','aa = 36','aa = 54'})
ax.RAxisLocation = 300;
hold off

mGDU = mean(GazeDrn(IdxU),'omitnan');% mean gaze direction
sGDU = std(GazeDrn(IdxU),'omitnan');%sd gaze direction
mGDD = mean(GazeDrn(IdxD),'omitnan');
sGDD = std(GazeDrn(IdxD),'omitnan');
mGDT = mean(GT,'omitnan');
sGDT = std(GT,'omitnan');
mGDN = mean(GN,'omitnan');
sGDN = std(GN,'omitnan');
```

Irregularity distribution

1. XvalMYPVDbyALmm

```
%New cross validation - combined PVD and MY in each fold - mm data
%generate indices for combined MYPVD by axial length
%Normalised FFT moduli by length of retinal vector -
% FFTmm, saved in column 10 FFTconcat
%corrected for empty B scans
%loads FFTconcat,AllIKurv
%CHECK only one eye of bilateral data used: the shorter AL eye is removed
%CHECK correct number eyes without AL deleted line 31-32
%binvars treated like sumdiff - fold mean subtracted

load('/Users/stewartlake/Documents/MATLAB/FFTconcat');
load('/Users/stewartlake/Documents/MATLAB/AllIKurv');

PVDMYFb=cat (1,PVDFb,MYFb);%combined Fb
PVDMYFb(66,:)=[];%remove second eye from bilateral data participants
PVDMYFb(63,:)=[];
%get age and AL vector to match PVDMYFb
Agevec = zeros(size(PVDMYFb,1),1);
IDFblist = PVDMYFb(:,1);%eye ID
ALvec = zeros(size(PVDMYFb,1),1);
for findage=1:size(PVDMYFb,1)
    sIde = str2double(IDFblist{findage,1}(2));

    Agevec(findage) = PVDMYFb{findage,4}(3);
    ALvec(findage) = PVDMYFb{findage,4}(sIde);
end

%sort Fb by AL
[sALvec,ALorder]=sort(ALvec);% ascending order of AL
ALlFb=PVDMYFb(ALorder,:);
ALlFb(1:2,:)=[];%removes eyes with no AL
sALvec(1:2)=[];%removes head of sALvec to match ALlFb

NumPVD = size (PVDFb,1); % number of PVD eyes in array
NumMY = size (MYFb,1); % number of MY eyes
k = 5; %number of folds
Nrow = 12; %no rows must = Veye (max number eyes per subset)

Sumdiff10 = cell (Nrow,k);
absdiff10 = cell (Nrow,k);
Eyermsd10 = cell (Nrow,k);
maxeBs10 = cell (Nrow,k);
```

```
IndMeBs10 = cell (Nrow,k);
Kurv = cell (Nrow, k);

MaxCVar10 = cell (Nrow,k);
IndMCVar10 = cell (Nrow,k);
logMxvar10 = cell (Nrow,k);
sumbinvar10 = cell (Nrow,k);
SbVar10diff = cell (Nrow,k);
Eymsdf10 = zeros (Nrow,k);
Indmax10 = zeros (Nrow,k);
Eymsbv10 = zeros (Nrow,k);

dispPT = 0.1;
% generates a column vector to randomise Num? eyes into k=5 folds. Non AL
% stratified
%IndicesPVD = crossvalind('Kfold',NumPVD, k);%NumPVD - put back instead of 33 when
all eyes processed
%IndicesMY = crossvalind('Kfold',NumMY, k);

%generate random distribution into 5 folds
NumIpfold = floor(size(ALlFb,1)/k);%number of eyes per k folds
Rem=mod(size(ALlFb,1),k);%plus the remainder not divisible by k
Ransel = zeros(k,NumIpfold);
for Ranrun=1:NumIpfold

    Ransel(:,Ranrun) = randperm(k)';
end
Ranrem=randperm(Rem)';
Ransel = cat(1,Ransel(:),Ranrem);%these are the indices to divide into folds

%create five subsets for comparison
Grps10 = cell(k,1); %the '10'reflects the column where the data is stored
GrpAL = cell(k,1);
GrpIID10 = cell (k,1);
MnGrp10 = cell (k,1);
ColVec = cell (k,1);

for n = 1:k
  Grps10{n} = ALlFb(Ransel==n,10); % puts each fold of all eye cubes into a cell in
Grps
  GrpIID10 {n} = ALlFb(Ransel==n,1); %eye identifiers of each fold
  MnGrp10{n} = ALlFb(Ransel~=n,10); % selects not subset n: the training set for
Grps(n)
  GrpAL{n}=sALvec(Ransel==n);
  %create colour vector for plotting: not used here:not split into 2 groups
  %ColVec{n} = [repelem([0 0 1],nnz(IndicesPVD==n),1);repelem([0 1
0],nnz(IndicesMY==n),1)];

  TMnGrp10 = cat (3, MnGrp10{n}); %training set

  for Feyes = 1:length(TMnGrp10)
      FI= TMnGrp10 {Feyes};
      FI(FI==0) = NaN;
      TMnGrp10 {Feyes} = FI; %replaces all 0 with NaN to eliminate empty B scans in
training set
  end


  TMnGrp10 = cat (3, TMnGrp10{:}); %concatenates all cubes from all eyes in
MnGrp{n}

  FoldMnBV10 =  var(TMnGrp10,0,2,'omitnan');%30 x 1 x X array, x=number of cubes
  TFMnBV10 = mean (FoldMnBV10,3,'omitnan');%30 x 1 mean fold bin Var

  TMnGrp10 = TMnGrp10 (:,all(~isnan(TMnGrp10)));%removes Nan columns

  TSbmn10 = nanmean (TMnGrp10,2); %creates PVD/RD bin mean training set

  %The number of eyes in this subset Grps(n)
  SzC10 = size (Grps10{n},1); % SzC = number of eyes in this subset
```

```
  for Veye = 1:SzC10
      NowIFFT10 = Grps10{n}{Veye}; %call first eye in validation set
      NowIFFT10=NowIFFT10(:,any(NowIFFT10));%remove empty B scans
      NumBS=size(NowIFFT10,2);%number of non -zero B scans

      %generate the summary values, sumdiff, RMSD and max error, each row an eye,
each fold a %column
      % for 0 removed by Nan mean
      absdiff10 {Veye,n} = abs(NowIFFT10 - TSbmn10);
      Sumdiff10 {Veye, n} = sum(absdiff10{Veye,n});
      Sumdiff10 {Veye, n} = permute (Sumdiff10{Veye,n}, [3 2 1]); %sumabsdiff
moduli, cubes x Bs

      [Eymsdf10(Veye, n),Indmax10(Veye,n)] =max (Sumdiff10 {Veye,n}(:));%max
sumdiff for eye
      Isize=size(Sumdiff10{Veye,n});
      [cubemax,~] = ind2sub(Isize,Indmax10(Veye,n));%the cube index of max sumdiff

      Eyermsd10 {Veye, n} = sqrt ((sum (absdiff10{Veye,n}.*absdiff10{Veye,n}))/30);
      Eyermsd10 {Veye,n} = permute (Eyermsd10 {Veye,n}, [3 2 1]);


      [maxeBs10{Veye,n}, IndMeBs10{Veye,n}] = max(abs(NowIFFT10 - TSbmn10));

      maxeBs10 {Veye,n} = permute (maxeBs10 {Veye,n}, [3 2 1]);%can switch out for
cube bin var
      IndMeBs10{Veye,n} = permute (IndMeBs10{Veye,n}, [3 2 1]);

      %cube bin variance - (can put in scatter3 when desired), max and sum
      [MaxCVar10{Veye,n},IndMCVar10{Veye,n}] = max(var(NowIFFT10,0,2,'omitnan')-
TFMnBV10);
      %this is the SBV for the entire eye - ALL B scans ~=0
      SbVar10diff {Veye,n} = sum(var(NowIFFT10,0,2,'omitnan') - TFMnBV10);
      SbVar10diff {Veye,n} = permute (SbVar10diff {Veye,n},[3 2 1]);
      sumbinvar10 {Veye,n} = sum (var(NowIFFT10,0,2,'omitnan'));
      sumbinvar10 {Veye,n} = permute (sumbinvar10 {Veye,n},[3 2 1]);
      Eymsbv10 (Veye,n) = max (sumbinvar10{Veye,n}(:));%max sumbinvar10 for eye
      sumbinvar10 {Veye,n} = repmat(sumbinvar10 {Veye,n},1,21);
      SbVar10diff {Veye,n} = repmat(SbVar10diff {Veye,n},1,21);
      MaxCVar10{Veye,n} = permute (MaxCVar10{Veye,n}, [3 2 1]);
      MaxCVar10{Veye,n} = repmat (MaxCVar10{Veye,n},1,21); %repeat elements to plot
c sumdiff etc
      logMxvar10 {Veye,n} = log10 (MaxCVar10{Veye,n});
      IndMCVar10{Veye,n} = permute (IndMCVar10{Veye,n}, [3 2 1]);

      %match curvature array sheet with current eye
      Kurvmatch=find(strncmp(GrpIID10{n}{Veye},AllIEyenames2,4));
      Kurv{Veye,n} = AllIBsKurv(:,:,Kurvmatch);
      %Kurv{Veye,n} = Kurv{Veye,n}(any(Kurv{Veye,n},2),:);%removes empty rows
      %now vectorise to remove 0 to match SD etc for plotting
      vecKurv = Kurv{Veye,n}(:);
      vecKurv(vecKurv==0) = [];

      ClocoPt=(1:size(Sumdiff10{Veye,n}));
      ClocoPt = repmat(ClocoPt,1,21);%the cube sheet ID for each point (for
textlabel)
      %{
      %plot, with Eye title
      Fignamn0 = strcat (GrpIID10 {n} {Veye},GrpAL{n}(Veye),' MY&PVD Normalised mm
Sumdiff v BFCvK v max error');
      figure ('Name',Fignamn0);
      scatter3 (Sumdiff10 {Veye, n}(:), vecKurv(:), maxeBs10 {Veye,n}(:),24,'b')
      axis ([0 50 -1 3 0 15]);
      xlabel ('sumdiff');
      ylabel ('BFCvK');
      zlabel ('max error');
      savefig (strcat('Eye ',GrpIID10{n} {Veye}));
      %}
```

```
  end
end
save ('/Users/stewartlake/Documents/Retinalcontour/mm analyses/NfftXV AL
MYmm/XvalFTMYPVDbyAL4');
```

Chapter 4

1. MYPVDFrBsgtThr

```
%sd11cellvec in line 4 array holds the Total anomaly (sumdiff) for every B scan, by
%region.Generates fraction of B scans in each region > Thr
clear
cd ('/Users/stewartlake/Documents/Retinalcontour/Regional MY PVD by AL/')
BSreg = cell(1,17);

for Region = 2:18

Varfile = strcat(('XvalNfftMYPVDregionmm'),num2str(Region));

load (Varfile);

%SD11cellvec = Sumdiff11(:);%has been cleared of empty B scans

BSreg{Region-1}= [SD11cellvec{:}]';


end

for Thr = 1:10
   for Reg = 1:17


       %BSreg{Reg} = [BSreg{:,Reg}]';%all BS for each region
       rbs = BSreg{Reg};
       rbs(isnan(rbs)|rbs==0) = [];
       Numgt(Reg,Thr) = nnz(find(rbs>Thr));
       Frgt(Reg,Thr) = Numgt(Reg,Thr)/length(rbs);% fraction Bs with anomaly gt 5


   end
   allrBS = vertcat(BSreg{:});
   allrBS(isnan(allrBS)|allrBS==0) = [];
   allgt(Thr) = nnz(find(allrBS>Thr));
   frallgt(Thr) = allgt(Thr)/numel(allrBS);%fraction of all Bscans across all
regions

 end
```

2. MYPVDALregXvalmm

```
%%cross validation of cubes by region - myopic eyes plus PVD
%for correlation regions of MY+PVDFb by AL - mm data
%loads FFTconcat and AllIKurv
%takes cube by location (column) in column 11 of Fb
%IF plotting results open current folder to where figures are to be saved
%removes shortest eye data from bilaterally measured participants
load('/Users/stewartlake/Documents/MATLAB/FFTconcat');
load('/Users/stewartlake/Documents/MATLAB/AllIKurv');

PVDMYFb=cat (1,PVDFb,MYFb);%combined Fb
PVDMYFb(66,:)=[];%remove second eye from bilateral data participants
PVDMYFb(63,:)=[];
%get age and AL vector to match PVDMYFb
Agevec = zeros(size(PVDMYFb,1),1);
IDFblist = PVDMYFb(:,1);%eye ID
ALvec = zeros(size(PVDMYFb,1),1);
for findage=1:size(PVDMYFb,1)
```

```
    sIde = str2double(IDFblist{findage,1}(2));

    Agevec(findage) = PVDMYFb{findage,4}(3);
    ALvec(findage) = PVDMYFb{findage,4}(sIde);
end


k=5; %number of folds

Nrow = 12; %no rows must > Veye (max number eyes per subset)

for Region = 2:18 %one column (region) at a time)

%sort Fb by AL
[sALvec,ALorder]=sort(ALvec);% ascending order of AL
ALlFb=PVDMYFb(ALorder,:);
ALlFb(1:2,:)=[];%removes 2 eyes with no AL
sALvec(1:2)=[];%removes head of ALvec to match ALlFb

NumPVDMY = size (ALlFb,1);

KurvrowMP = cell(NumPVDMY,1);
PVDMYRegcubeID=cell(NumPVDMY,1);
PVDMYcols=cell(NumPVDMY,1);

Sumdiff11 = cell (Nrow,k);
absdiff11 = cell (Nrow,k);
Eyermsd11 = cell (Nrow,k);
maxeBs11 = cell (Nrow,k);
IndMeBs11 = cell (Nrow,k);
IKurv = cell (Nrow, k);%Kurv data for an entire eye
CKurv = cell (Nrow, k);%the Kurv data to match sumdiff etc

MaxCVar11 = cell (Nrow,k);
IndMCVar11 = cell (Nrow,k);
logMxvar11 = cell (Nrow,k);
sumbinvar11 = cell (Nrow,k);
SbVar11diff = cell (Nrow,k);
Eymsdf11 = zeros (Nrow,k);
Indmax11 = zeros (Nrow,k);
Eymsbv11 = zeros (Nrow,k);

%create five subsets for cross validation
Grps11 = cell(k,1); %the '9'reflects the column where the data is stored
GrpIID11 = cell (k,1);
TSGrp11 = cell (k,1);
FoldKurvrow = cell (k,1);
GrpAL11 = cell(k,1);

%This section gets the cubes for this region
for Iye= 1:size(ALlFb,1)

    PVDMYcols(Iye)=ALlFb{Iye,11}(Region);%this region cube FFT data - bins x Bs
    PVDMYRegcubeID{Iye} = ALlFb{Iye,6}{Region-1};%cube identifier
    if PVDMYRegcubeID{Iye}~=0
        KurvrowMP{Iye} =
find(contains(ALlFb{Iye,5}(:),num2str(PVDMYRegcubeID{Iye})));
    end
end

%remove empty values if region cube cell empty
PVDMYeyeID=ALlFb(:,1);
KurvrowMP(cellfun('isempty',PVDMYcols))=[];
PVDMYeyeID(cellfun('isempty',PVDMYcols))=[];
sALvec(cellfun('isempty',PVDMYcols))=[];
PVDMYcols(cellfun('isempty',PVDMYcols))=[];

NumPVDMY1 = length(PVDMYeyeID);

%generate random distribution into 5 folds
```

```
NumIpfold = floor(NumPVDMY1/k);%number of eyes per k folds
Rem=mod(NumPVDMY1,k);%plus the remainder not divisible by k
Ransel = zeros(k,NumIpfold);
for Ranrun=1:NumIpfold

    Ransel(:,Ranrun) = randperm(k)';
end
Ranrem=randperm(Rem)';
Ransel = cat(1,Ransel(:),Ranrem);%these are the indices to divide into folds



% generates a column vector to randomise ?Num? eyes into ?k?=5 subsets.
%IndicesPVD = crossvalind('Kfold',NumPVD1, k);
%IndicesMY = crossvalind('Kfold',NumMY1, k);

for n = 1:k % one fold at a time
  Grps11{n} = PVDMYcols(Ransel==n); % puts each subset into a cell in Grps
  GrpIID11 {n} = PVDMYeyeID(Ransel==n,1); %eye identifiers of the validation set
  TSGrp11{n} = PVDMYcols(Ransel~=n); % selects not subset n: the training set for
Grps(n)
  FoldKurvrow{n} = KurvrowMP(Ransel==n);%the row match in Kurv for current fold
cubes
  GrpAL11{n}=sALvec(Ransel==n);%AL for current fold cube
  %create colour vector to match GrpIID9
  %ColVec{n} = [repelem([0 0 1],nnz(IndicesPVD==n),1);repelem([0 1
0],nnz(IndicesMY==n),1)];

  TSMnGrp11 = cat (3, TSGrp11{n}); %training set

  for Feyes = 1:length(TSMnGrp11)
      FI= TSMnGrp11 {Feyes};
      FI(FI==0) = NaN;
      TSMnGrp11 {Feyes} = FI; %replaces all 0 with NaN to eliminate empty B scans
in training set
  end



  TSMnGrp11 = cat (3, TSMnGrp11{:}); %concatenates all cubes from all eyes in
MnGrp{n}

  FoldTSBV11 =  var(TSMnGrp11,0,2,'omitnan');%30 x 1 x X array, x=number of cubes
  TFMnBV11 = mean (FoldTSBV11,3,'omitnan');%30 x 1 mean fold bin Var

  TSMnGrp11 = TSMnGrp11 (:,all(~isnan(TSMnGrp11)));%removes Nan columns

  TSbmn11 = nanmean (TSMnGrp11,2); %creates PVD/MY bin mean training set

  %The number of cubes/eyes in this subset Grps(n)
  SzC11 = size (Grps11{n},1); % SzC = number of eyes in this subset

  for Veye = 1:SzC11
      NowIFFT11 = Grps11{n}{Veye}; %call first cube in validation set


      NowIFFT11=NowIFFT11(:,any(NowIFFT11));%added 22/9/18 to remove empty B scans
      NumBS=size(NowIFFT11,2);%number of non -zero B scans
      %generate the summary values, sumdiff, RMSD and max error, each row an eye,
each fold a %column
      % for 0 removed by Nan mean
      absdiff11 {Veye,n} = abs(NowIFFT11 - TSbmn11);%bins x B scans
      Sumdiff11 {Veye, n} = sum(absdiff11{Veye,n});%total all bins for each B scan
      Sumdiff11 {Veye, n} = permute (Sumdiff11{Veye,n}, [3 2 1]); %sumabsdiff
moduli, 1 cube x Bs

      Eymsdf11 (Veye, n) =max (Sumdiff11 {Veye,n}(:));%max sumdiff for eye

      Eyermsd11 {Veye, n} = sqrt ((sum (absdiff11{Veye,n}.*absdiff11{Veye,n}))/30);
      Eyermsd11 {Veye,n} = permute (Eyermsd11 {Veye,n}, [3 2 1]);
```

```
      [maxeBs11{Veye,n}, IndMeBs11{Veye,n}] = max(abs(NowIFFT11 - TSbmn11));

      maxeBs11 {Veye,n} = permute (maxeBs11 {Veye,n}, [3 2 1]);%can switch out for
cube bin var
      IndMeBs11{Veye,n} = permute (IndMeBs11{Veye,n}, [3 2 1]);

      %cube bin variance - (can put in scatter3 when desired), max and sum
      [MaxCVar11{Veye,n},IndMCVar11{Veye,n}] = max(var(NowIFFT11,0,2,'omitnan')-
TFMnBV11);
      SbVar11diff {Veye,n} = sum(var(NowIFFT11,0,2,'omitnan') - TFMnBV11);
      SbVar11diff {Veye,n} = permute (SbVar11diff {Veye,n},[3 2 1]);
      sumbinvar11 {Veye,n} = sum (var(NowIFFT11,0,2,'omitnan'));
      sumbinvar11 {Veye,n} = permute (sumbinvar11 {Veye,n},[3 2 1]);
      Eymsbv11 (Veye,n) = max (sumbinvar11{Veye,n}(:));%max sumbinvar3 for eye
      sumbinvar11 {Veye,n} = repmat(sumbinvar11 {Veye,n},1,NumBS);
      SbVar11diff {Veye,n} = repmat(SbVar11diff {Veye,n},1,NumBS);
      MaxCVar11{Veye,n} = permute (MaxCVar11{Veye,n}, [3 2 1]);
      MaxCVar11{Veye,n} = repmat (MaxCVar11{Veye,n},1,NumBS); %repeat elements to
plot c sumdiff etc
      logMxvar11 {Veye,n} = log10 (MaxCVar11{Veye,n});
      IndMCVar11{Veye,n} = permute (IndMCVar11{Veye,n}, [3 2 1]);

      %match curvature array sheet with current eye/cube
      Kurvmatch=find(strncmp(GrpIID11{n}{Veye},AllIEyenames2,4));
      IKurv{Veye,n} = AllIBsKurv(:,:,Kurvmatch);%Bs K for this eye
      IKurv{Veye,n} = IKurv{Veye,n}(any(IKurv{Veye,n},2),:);%removes empty rows
      CKurv{Veye,n} = IKurv{Veye,n}(FoldKurvrow{n}{Veye},:);
      CKurv{Veye,n}(CKurv{Veye,n}==0)=[];


    %{
       to plot select a single region
       %plot, with Eye title
      Fignamn0 = strcat (GrpIID9 {n} {Veye},' MY/PVD Normalised Sumdiff v Kurv v
max error: Region', num2str(Region));
      figure ('Name',Fignamn0);
      scatter3 (Sumdiff9 {Veye, n}(:), CKurv {Veye, n}(:), maxeBs9
{Veye,n}(:),24,'b');%
      axis ([0 50 -inf inf 0 12]); %for SD,CKurv,maxeBs
      xlabel ('sumdiff');
      ylabel ('BFC vertex K');
      zlabel ('max error');
      savefig (strcat('Eye ',GrpIID9{n} {Veye},'Region', num2str(Region)));

      %}

  end
end
save (['/Users/stewartlake/Documents/Retinalcontour/Regional MY PVD by
AL/XvalNfftMYPVDregionmm',num2str(Region)]);
end
```

3. MYPVDALstatsmm

```
%run from NfftXV AL MYmm/XvalFTMYPVDbyAL4
%generated by a XvalMYPVDbyALmm script (AL stratified MY and PVD)
%eg in mm analyses/NfftXV AL MYmm
%It is for whole eye analysis, and measures the volume of the scatter3
%plot for each eye
%saves in same folder
%determines ranges, med etc for all scans, and by eye
%calculates SRC for selected values
%includes corrected K vals for AL
%load XvalFTMYPVDbyAL....
SD10cellvec = Sumdiff10(:);
```

```
ID10cellvec = GrpIID10(:);
SBV10cellvec = SbVar10diff(:);
Me10cellvec = maxeBs10(:);
ALcellvec = vertcat(GrpAL{:});
ind10cellvec= reshape(IndMeBs10,[],1);
RM10cellvec = Eyermsd10(:);

SD10cellvec(cellfun('isempty', SD10cellvec)) = [];
SBV10cellvec(cellfun('isempty', SBV10cellvec)) = [];
ID10cellvec(cellfun('isempty', ID10cellvec)) = [];
Me10cellvec(cellfun('isempty', Me10cellvec)) = [];
RM10cellvec(cellfun('isempty', RM10cellvec)) = [];

ind10cellvec(cellfun('isempty',ind10cellvec)) = [];


Kay = cell(length(SD10cellvec),1);
Vol = zeros (length(SD10cellvec),1);
convKay = cell(length(SD10cellvec),1);
convVol = zeros (length(SD10cellvec),1);


%this converts Kurv into AKurv, a match for sumdiff10 etc
Kurvline=Kurv(:);

for clean=1:length(Kurvline)
    Kurvline{clean}= Kurvline{clean}(:);
    cleanspace=Kurvline{clean}';
    cleanspace(cleanspace==0)=[];
    Kurvline{clean}=cleanspace;

end

AKurv=reshape(Kurvline,size(Kurv,1),size(Kurv,2));

KVcellvec = AKurv(:);
KVcellvec(cellfun('isempty',KVcellvec)) = [];

Metr = zeros(length(SD10cellvec),3);
Metrc = zeros(length(SD10cellvec),3);
Metr2 = zeros(length(SD10cellvec),3);
Metr5 = zeros(length(SD10cellvec),3);
Metr6 = zeros(length(SD10cellvec),3);
Metr3 = zeros(length(SD10cellvec),3);
Metr4med = zeros(length(SD10cellvec),4);
Metr4iqr = zeros(length(SD10cellvec),4);
CorIval = zeros(length(SD10cellvec),3);

vectSD = cat(2,SD10cellvec{:});
vectMe = cat(2,Me10cellvec{:});
vectK = cat(2,KVcellvec{:});
vectRM= cat(2,RM10cellvec{:});

%corrected KVcellvec for AL
Alcorrcoeff = [0.0257,-2.1182,36.0516];
for Eye1 = 1:length(KVcellvec)

    Rcvec{Eye1} = KVcellvec{Eye1}.^(-1);

    corR = Alcorrcoeff(1).*ALcellvec(Eye1).^2 + ...
        Alcorrcoeff(2).*ALcellvec(Eye1) + Alcorrcoeff(3);

    Rcveccor{Eye1} = Rcvec{Eye1} - corR;

    KVcellveccor{Eye1} = Rcveccor{Eye1}.^(-1);


end

vectKc = cat(2,KVcellveccor{:});%AL corrected K
```

```
AllIMedSD = median(vectSD);%all eye values
AllIMedMe = median(vectMe);
AllIMedK = median(vectK);
AllIMedKc = median(vectKc);
AllIMedRM = median(vectRM);

AllIMinSD = min(vectSD);
AllIMinMe = min(vectMe);
AllIMinK = min(vectK);
AllIMinKc = min(vectKc);
AllIMinRM = min(vectRM);

AllIMaxSD = max(vectSD);
AllIMaxMe = max(vectMe);
AllIMaxK = max(vectK);
AllIMaxKc = max(vectKc);
AllIMaxRM = max(vectRM);

for RuN=1:length(SD10cellvec)

    [Kay{RuN},Vol(RuN)] = boundary(SD10cellvec{RuN}', KVcellvec{RuN}',
Me10cellvec{RuN}',1);
    %vol is the alpha shapes boundary volume
    [convKay{RuN},convVol(RuN)] = convhull(SD10cellvec{RuN}', KVcellvec{RuN}',
Me10cellvec{RuN}');

    MedSD = median(SD10cellvec{RuN});
    MedMe = median(Me10cellvec{RuN});
    MedK = median(KVcellvec{RuN});
    MedKc = median(KVcellveccor{RuN});
    MedRM = median(RM10cellvec{RuN});

    MinSD = min(SD10cellvec{RuN});
    MinMe = min(Me10cellvec{RuN});
    MinK = min(KVcellvec{RuN});
    MinKc = min(KVcellveccor{RuN});
    MinRM = min(RM10cellvec{RuN});

    MaxSD = max(SD10cellvec{RuN});
    MaxMe = max(Me10cellvec{RuN});
    MaxK = max(KVcellvec{RuN});
    MaxKc = max(KVcellveccor{RuN});
    MaxRM = max(RM10cellvec{RuN});

    iqrK = iqr(KVcellvec{RuN});
    iqrKc = iqr(KVcellveccor{RuN});
    iqrSD = iqr(SD10cellvec{RuN});
    iqrMe = iqr(Me10cellvec{RuN});
    iqrRM = iqr(RM10cellvec{RuN});

    %this is the first input matrix for corr
    %col1 = vol, col2 = medsd, c3=medMe, c4=medK
    %Metr(RuN,1) = Vol(RuN);
    Metr(RuN,1) = MedSD;
    Metr(RuN,2) = MedMe;
    Metr(RuN,3) = MedK;

    CorIval(RuN,1) = MedKc;%correct K by AL med, range
    CorIval(RuN,2) = MinKc;
    CorIval(RuN,3) = MaxKc;

    Metrc(RuN,1) = MedSD;
    Metrc(RuN,2) = MedMe;
    Metrc(RuN,3) = MedKc;

    Metr2(RuN,1) = MaxSD;
    Metr2(RuN,2) = MaxMe;
    Metr2(RuN,3) = MaxK;
```

```
    Metr3(RuN,1) = MinSD;
    Metr3(RuN,2) = MinMe;
    Metr3(RuN,3) = MinK;

    Metr4med(RuN,1) = MedSD;% the features for each eye
    Metr4med(RuN,2) = MedMe;
    Metr4med(RuN,3) = MedRM;
    Metr4med(RuN,4) = MedKc;


    Metr4iqr(RuN,1) = iqrSD;% the features for each eye
    Metr4iqr(RuN,2) = iqrMe;
    Metr4iqr(RuN,3) = iqrRM;
    Metr4iqr(RuN,4) = iqrKc;


    Metr5(RuN,1) = iqrSD;
    Metr5(RuN,2) = iqrMe;
    Metr5(RuN,3) = iqrK;

    Metr6(RuN,1) = iqrSD;
    Metr6(RuN,2) = iqrMe;
    Metr6(RuN,3) = iqrKc;
end

[rho,pval]=corr(Metr,ALcellvec,'Type','Spearman');
[rhoc,pvalc]=corr(Metrc,ALcellvec,'Type','Spearman');
[rho5,pval5]=corr(Metr5,ALcellvec,'Type','Spearman');
[rho6,pval6]=corr(Metr6,ALcellvec,'Type','Spearman');
[rho4m,pval4m]=corr(Metr4med,ALcellvec,'Type','Spearman');
[rho4i,pval4i]=corr(Metr4iqr,ALcellvec,'Type','Spearman');

 save ('/Users/stewartlake/Documents/Retinalcontour/mm analyses/NfftXV AL
MYmm/XVftMYPVDbyALstatsALKcor4a');
```

4. MYPVDallBSdatamm

```
%this gets summary values for each region
%
%runs through Xval files from MYPVDALregstatsmmKc
%and calculates average bin modulus for the B scans
%then median, max, iqr for all the B scan data each region

cd ('/Users/stewartlake/Documents/Retinalcontour/Regional MY PVD by AL/')

sumTSbin = zeros(18,1);
sumTSMedbin = zeros(18,1);

MEDK = zeros(18,1);
MEDMe = zeros(18,1);
MEDRM = zeros(18,1);
MEDSD = zeros(18,1);

MAXSD = zeros(18,1);
MAXMe = zeros(18,1);
MAXRM = zeros(18,1);
MAXK = zeros(18,1);

AvK = zeros(18,1);
AvMe = zeros(18,1);
AvRM = zeros(18,1);
AvSD= zeros(18,1);

IQRSD = zeros(18,1);
IQRMe = zeros(18,1);
IQRRM = zeros(18,1);
IQRK = zeros(18,1);
```

```
SDK = zeros(18,1);
SDMe = zeros(18,1);
SDRM = zeros(18,1);
SDSD = zeros(18,1);

for Region = 2:18

Varfile = strcat(('XvalNfftMYPVDregionmm'),num2str(Region));

load (Varfile);

AllBS=[PVDMYcols{:}];%PVDMYcols the raw FFT for 1-30 bins x number of B scans
AllBS = AllBS(:,any(AllBS));%this is all non empty B scans for a region

ALLBSMbn = nanmean(AllBS,2);
ALLBSMedbn = nanmedian (AllBS,2);

sumTSbin(Region,1) = sum (ALLBSMbn);%vector of mean total bin val for each region
sumTSMedbin(Region,1) = sum (ALLBSMedbn);%sum of median total bin value

MEDK(Region) = median([KVcellvec{:}]);%median K of entire region
MEDKc(Region) = median([KVcellveccor{:}]);
MEDMe(Region) = median([Me11cellvec{:}]);
MEDRM(Region) = median([RM11cellvec{:}]);
MEDSD(Region) = median([SD11cellvec{:}]);%median sumdiff
MAXSD(Region) = max(Metr2(:,2));
MAXMe(Region) = max(Metr2(:,3));
MAXRM(Region) = max(Metr2(:,4));
IQRK(Region) = iqr([KVcellvec{:}]);
IQRKc(Region) = iqr([KVcellveccor{:}]);

AvK(Region) = mean([KVcellvec{:}]);
AvKc(Region) = mean([KVcellveccor{:}]);
AvMe(Region) = mean([Me11cellvec{:}]);
AvRM(Region) = mean([RM11cellvec{:}]);
AvSD(Region) = mean([SD11cellvec{:}]);
IQRSD(Region) = iqr([SD11cellvec{:}]);
IQRMe(Region) = iqr([Me11cellvec{:}]);
IQRRM(Region) = iqr([RM11cellvec{:}]);
SDK(Region) = std([KVcellvec{:}]);
SDKc(Region) = std([KVcellveccor{:}]);
SDMe(Region) = std([Me11cellvec{:}]);
SDRM(Region) = std([RM11cellvec{:}]);
SDSD(Region) = std([SD11cellvec{:}]);

end

save('regionsumBsbin','sumTSbin','sumTSMedbin','MEDK','MEDMe','MEDSD','MAXSD','MAXM
e','IQRK',...
    'AvK', 'AvMe','AvSD','IQRSD','IQRMe',
'SDK','SDMe','SDSD','MEDRM','MAXRM','IQRRM','AvRM',...
    'SDRM','SDKc','AvKc','IQRKc','MEDKc');
```

5. MYPVDALregstatsmmKc

```
%this calculates from the SD,KV,ME,RM vectors for Regional
%plus median SD, K, ME,RM max SD, ME, RM and iqr K, mean and std
%then runs spearman's correlation
%generated by a MYPVDALregXvalmm script (AL stratified MY and PVD, mm)
%in /Regional MY PVD by AL
%It is for regional eye analysis,
%Metr4m/i do all 4 descriptors in Kc
%
%Can correct K for AL<28 only in Metr6 and Metrc for iqr and median,
%if lines in 170s are uncommented, and Metrc & 6 changed to use
%ALcellveclim.
cd ('/Users/stewartlake/Documents/Retinalcontour/Regional MY PVD by AL/')
```

```
for Region = 2:18

Varfile = strcat(('XvalNfftMYPVDregionmm'),num2str(Region));

load (Varfile);

SD11cellvec = Sumdiff11(:);
ID11cellvec = GrpIID11(:);
SBV11cellvec = SbVar11diff(:);
Me11cellvec = maxeBs11(:);
RM11cellvec = Eyermsd11(:);
ALcellvec = vertcat(GrpAL11{:});
ind11cellvec= reshape(IndMeBs11,[],1);

SD11cellvec(cellfun('isempty', SD11cellvec)) = [];
SBV11cellvec(cellfun('isempty', SBV11cellvec)) = [];
ID11cellvec(cellfun('isempty', ID11cellvec)) = [];
Me11cellvec(cellfun('isempty', Me11cellvec)) = [];
RM11cellvec(cellfun('isempty', RM11cellvec)) = [];
ind11cellvec(cellfun('isempty',ind11cellvec)) = [];


Kay = cell(length(SD11cellvec),1);
Vol = zeros (length(SD11cellvec),1);
Kay1 = cell(length(SD11cellvec),1);
Vol1 = zeros (length(SD11cellvec),1);
convKay = cell(length(SD11cellvec),1);
convVol = zeros (length(SD11cellvec),1);


%this converts Kurv into AKurv, a match for sumdiff11 etc
Kurvline=CKurv(:);

for clean=1:length(Kurvline)
    Kurvline{clean}= Kurvline{clean}(:);
    cleanspace=Kurvline{clean}';
    cleanspace(cleanspace==0)=[];
    Kurvline{clean}=cleanspace;

end

AKurv=reshape(Kurvline,size(CKurv,1),size(CKurv,2));

KVcellvec = AKurv(:);
KVcellvec(cellfun('isempty',KVcellvec)) = [];

%now correct KVcellvec for AL
ALcorrcoeff = [0.0257,-2.1182,36.0516];
for Eye1 = 1:length(KVcellvec)

    Rcvec{Eye1} = KVcellvec{Eye1}.^(-1);

    corR = ALcorrcoeff(1).*ALcellvec(Eye1).^2 + ALcorrcoeff(2).*ALcellvec(Eye1) +
...
        ALcorrcoeff(3);

    Rcveccor{Eye1} = Rcvec{Eye1} - corR;

    KVcellveccor{Eye1} = Rcveccor{Eye1}.^(-1);

    iqrKcorr(Eye1) = iqr(KVcellveccor{Eye1});

end


Metr = zeros(length(SD11cellvec),4);
Metrc = zeros(length(SD11cellvec),4);
Metr2 = zeros(length(SD11cellvec),4);
Metr3 = zeros(length(SD11cellvec),4);
```

```
Metr4 = zeros(length(SD11cellvec),4);
Metr4m = zeros(length(SD11cellvec),4);
Metr4i = zeros(length(SD11cellvec),4);
Metr5 = zeros(length(SD11cellvec),4);
Metr6 = zeros(length(SD11cellvec),4);

for RuN=1:length(SD11cellvec)

    [Kay{RuN},Vol(RuN)] = boundary(SD11cellvec{RuN}', KVcellvec{RuN}',
Me11cellvec{RuN}');
    [Kay1{RuN},Vol1(RuN)] = boundary(SD11cellvec{RuN}', KVcellvec{RuN}',
Me11cellvec{RuN}',1);
    %vol is the alpha shapes boundary volume. Vol1 is shrink val=1
    [convKay{RuN},convVol(RuN)] = convhull(SD11cellvec{RuN}', KVcellvec{RuN}',
Me11cellvec{RuN}');

    MedSD = median(SD11cellvec{RuN});
    MedMe = median(Me11cellvec{RuN});
    MedRM = median(RM11cellvec{RuN});

    MedK = median(KVcellvec{RuN});
    Rck = MedK.^(-1);
    corR = ALcorrcoeff(1).*ALcellvec(RuN).^2 + ALcorrcoeff(2).*ALcellvec(RuN) + ...
        ALcorrcoeff(3);
    Rccorr = Rck-corR;
    MedKcorr = Rccorr.^(-1);

    AvSD = mean(SD11cellvec{RuN});
    AvMe = mean(Me11cellvec{RuN});
    AvRM = mean(RM11cellvec{RuN});
    AvK = mean(KVcellvec{RuN});

    stdSD = std(SD11cellvec{RuN});
    stdMe = std(Me11cellvec{RuN});
    stdRM = std(RM11cellvec{RuN});
    stdK = std(KVcellvec{RuN});

    MaxSD = max(SD11cellvec{RuN});
    MaxMe = max(Me11cellvec{RuN});
    MaxRM = max(RM11cellvec{RuN});
    iqrKc = iqr(KVcellveccor{RuN});%this is corrected K
    iqrK = iqr(KVcellvec{RuN});

    iqrSD = iqr(SD11cellvec{RuN});
    iqrMe = iqr(Me11cellvec{RuN});
    iqrRM = iqr(RM11cellvec{RuN});

    %this is the first input matrix for correlation
    %
    %Metr(RuN,1) = Vol1(RuN);
    Metr(RuN,1) = MedSD;
    Metr(RuN,2) = MedMe;
    Metr(RuN,3) = MedK;

    Metrc(RuN,1) = MedSD;
    Metrc(RuN,2) = MedMe;
    Metrc(RuN,3) = MedKcorr;

    Metr4m(RuN,1) = MedSD;
    Metr4m(RuN,2) = MedMe;
    Metr4m(RuN,3) = MedRM;
    Metr4m(RuN,4) = MedKcorr;

    Metr4i(RuN,1) = iqrSD;
    Metr4i(RuN,2) = iqrMe;
    Metr4i(RuN,3) = iqrRM;
    Metr4i(RuN,4) = iqrKc;

    %second input matrix for corr
    Metr2(RuN,1) = Vol(RuN);
```

```
    Metr2(RuN,2) = MaxSD;
    Metr2(RuN,3) = MaxMe;
    Metr2(RuN,4) = MaxRM;

    Metr3(RuN,1) = Vol(RuN);
    Metr3(RuN,2) = stdSD;
    Metr3(RuN,3) = stdMe;
    Metr3(RuN,4) = stdK;

    Metr4(RuN,1) = Vol(RuN);
    Metr4(RuN,2) = AvSD;
    Metr4(RuN,3) = AvMe;
    Metr4(RuN,4) = AvK;

    Metr5(RuN,1) = iqrSD;
    Metr5(RuN,2) = iqrMe;
    Metr5(RuN,3) = iqrK;

    Metr6(RuN,1) = iqrSD;
    Metr6(RuN,2) = iqrMe;
    Metr6(RuN,3) = iqrKc;
end

%now remove AL > 28 mm eyes
ALcellveclim=ALcellvec;%use lim if avoiding AL > 28
ALcellveclim(ALcellveclim>28,:)=[];

%Metrc(ALcellvec>28,:)=[];

%Metr6(ALcellvec>28,:)=[];

[rho,pval]=corr(Metr,ALcellvec,'Type','Spearman');
[rhoC,pvalC]=corr(Metrc,ALcellvec,'Type','Spearman');%consider adding lim
[rho2,pval2]=corr(Metr2,ALcellvec,'Type','Spearman');
[rho3,pval3]=corr(Metr3,ALcellvec,'Type','Spearman');
[rho4,pval4]=corr(Metr4,ALcellvec,'Type','Spearman');
[rho4m,pval4m]=corr(Metr4m,ALcellvec,'Type','Spearman');
[rho4i,pval4i]=corr(Metr4i,ALcellvec,'Type','Spearman');
[rho5,pval5]=corr(Metr5,ALcellvec,'Type','Spearman');
[rho6,pval6]=corr(Metr6,ALcellvec,'Type','Spearman');%consider lim

save (Varfile);

end
```

6. BHcorrmmALK

```
%this collates all p values and rho from /Regional MY PVD by ALmm
%sorts and perform Bonferroni - Holm correction
%((result in 'where': col 1 sorted pval, col 2 alpha/(m-number)
%col3 index of unsorted p val, col4 corresponding rho
%first 6/8 rho/pvals are from all of eye stats. Then regional 2-18
%for AL corrected K values))
%whereALL is for all 4 descriptors, so first 8 rho/pvals are all of eye,
%then regions 2-18. 8 per region: med followed by iqr,in order SD Me rmse K
%CHANGE: have /regional MY PVD by AL open:
cd ('/Users/stewartlake/Documents/Retinalcontour/Regional MY PVD by AL/')

%this loads all of eye data from MYPVDALstatsmm
load ('/Users/stewartlake/Documents/Retinalcontour/mm analyses/NfftXV AL
MYmm/XVftMYPVDbyALstatsALKcor4a');

Allp = cat(1,pvalc(1:3,1), pval6(1:3,1));%starts p/rho vectors with all of eye...
Allrho = cat(1,rhoc(1:3,1),rho6(1:3,1));%...AL corrected med and iqr results

ALL4p = cat(1,pval4m(1:4,1), pval4i(1:4,1));%starts p/rho vectors with all of
eye...
```

```
ALL4rho = cat(1,rho4m(1:4,1),rho4i(1:4,1));%...AL corrected med and iqr results for
all 4 metrics


for Region = 2:18
    %from MYPVDALregstatsmmKc
    Varfile = strcat(('XvalNfftMYPVDregionmm'),num2str(Region));

    load (Varfile);

    Allp = cat(1, Allp, pvalC(1:4,1), pval6(1:4,1));%median and iqr p vals
    Allrho = cat(1, Allrho, rhoC(1:4,1), rho6(1:4,1));

    ALL4p = cat(1, ALL4p, pval4m(1:4,1), pval4i(1:4,1));%median and iqr p vals
    ALL4rho = cat(1, ALL4rho, rho4m(1:4,1), rho4i(1:4,1));


end


[sAllp,psort] = sort(Allp);
sAllrho = Allrho(psort);

[sALL4p,psort4] = sort(ALL4p);
sALL4rho = ALL4rho(psort4);


m=length(sAllrho);
mALL=length(sALL4rho);
alpha = 0.05;
BH=zeros(m,1);
BHALL=zeros(mALL,1);

for list=1:m
    BH(list) = alpha/(m-(list-1));
end

for list=1:mALL
    BHALL(list) = alpha/(mALL-(list-1));
end

where= cat(2,sAllp,BH,psort,sAllrho);

whereALL= cat(2,sALL4p,BHALL,psort4,sALL4rho);

save ('/Users/stewartlake/Documents/Retinalcontour/regional MY PVD by
AL/BHcorrectionmmALK4a');
```

Chapter 5.

1. MHFEPVxzcomp

```
%compare curvature for no PVD xz (or, see line 8) and PV xz files (radial HD 12)
%CHANGE: line 9 & 217, plus figure labels
%takes data from temp xz folder (line 8) and PV xz (line 216) and calculates FFT
and K
%plus median, var, and iqr sum bins
%plus median, iqr, and variance K
%signrank, cohens d and t test
%load 'MH' data = no PVD, PV data = PVD
clear
str1 = '/Users/stewartlake/Documents/MH contour/temp xz folder/';
cd (str1);

MHinfo = dir;
MHinfo = MHinfo(~ismember({MHinfo.name},{'.','..','.DS_Store'}));
MHnames = {MHinfo.name};
```

```
MHNum = size (MHnames,2);%number MH eyes
MHcubeFFTvec = cell(1,MHNum);%One eye per cell %each cell 30 bins x 12 B scans
MHbfccoeff = cell(1,MHNum);
MHK = cell(1,MHNum); % best fit curve vertex curvature.One eye per cell
MHID = cell(1,MHNum);
MHside = zeros(1,MHNum);
MedKMH = zeros(1,MHNum); %median MH K
IqrKMH = zeros(1,MHNum);%iqr MH K
VarKMH = zeros(1,MHNum);% variance MH K
MedFMH = zeros(1,MHNum);% median FFT bins 1-30
IqrFMH = zeros(1,MHNum);%iqr FFT bins
VarFMH = zeros(1,MHNum);%variance FFT bins


%generate data for MH maculae
for CurFol=1:MHNum

    MHnam = MHnames {1,CurFol}(1:5);%eye ID
    MHside = MHnames {1,CurFol}(2);%eye laterality
    MHprefix = MHnames {1,CurFol}(1:2);%first two characters for textfile str
    %open cube of data
    nowFolderMH=MHnames{1,CurFol};

    cd (nowFolderMH);%open cube xz data folder

    %get directory of textfile (B scan) names
    MHdinfo = dir;
    MHnames_cell = {MHdinfo.name};
%gives a matrix called names_cell where each column has a filename
%then:
    outMH=regexp(MHnames_cell,'\d+','match');
    outMH=str2double(cat(1,outMH{:}));
%gives a matrix called out in which each row has a number from an original filename
%these are in column 2 if text file header has a number, column 1 if it
%doesn't.

%script alpha. takes a cube of data and
%Puts x and z coordinate values into an array (myData), each cell a line of data.
%Then separates this into arrays for x, and z.
    numFiles = size(outMH, 1);%number of B scans in cube
    startRow = 1;
    endRow = inf;
    myData = cell(1,12);
    ximp = cell (1, 12);%this cubes x data
    zimp = cell (1, 12);%this cubes Z data
    cubeFFT = zeros (30, 12);
    Cubefreq = zeros (30, 12);
    MHKurv = zeros (12,1);

    fileName = cell(1);

    zedres = zeros(1024,numFiles);
    Quadcoeffs = zeros(3, 12);
    VecLen = zeros (1, numFiles);


     for fileNum = 1:numFiles %work through B scan xz txt files
            Bscanline = outMH(fileNum,end);
            %This loop is for a single cube
            fileName =[];
            fileName1 = sprintf('-%04d.txt',Bscanline);
            fileName = [MHprefix fileName1];
            myData{Bscanline} = importfile(fileName,startRow,endRow);

            ximp{Bscanline}=myData{Bscanline}(:,1);
            zimp{Bscanline}=myData{Bscanline}(:,2);

            %now reverse left to right eye orientation (reverse z)
            %and reposition scans in left to match right eyes
            if (MHside == 2)%if a left eye
```

```
    if (Bscanline == 1)
       zimp{Bscanline}=flipud(zimp{Bscanline});
    elseif (Bscanline == 2)
        zimp{12} = flipud(zimp{Bscanline});
        zimp{Bscanline}=[];
    elseif (Bscanline == 3)
        zimp{11} = flipud(zimp{Bscanline});
        zimp{Bscanline}=[];
    elseif (Bscanline == 4)
        zimp{10} = flipud(zimp{Bscanline});
        zimp{Bscanline}=[];
    elseif (Bscanline == 5)
        zimp{9} = flipud(zimp{Bscanline});
        zimp{Bscanline}=[];
    elseif (Bscanline == 6)
        zimp{8} = flipud(zimp{Bscanline});
        zimp{Bscanline}=[];
    elseif (Bscanline == 8)
        zimp{6} = flipud(zimp{Bscanline});
        zimp{Bscanline}=[];
    elseif (Bscanline == 9)
        zimp{5} = flipud(zimp{Bscanline});
        zimp{Bscanline}=[];
    elseif (Bscanline == 10)
        zimp{4} = flipud(zimp{Bscanline});
        zimp{Bscanline}=[];
    elseif (Bscanline == 11)
        zimp{3} = flipud(zimp{Bscanline});
        zimp{Bscanline}=[];
    elseif (Bscanline == 12)
        zimp{2} = flipud(zimp{Bscanline});
        zimp{Bscanline}=[];
    end
end



%now format x and z for FFT
x=table2cell(ximp{Bscanline});
z=table2cell(zimp{Bscanline});
x=cell2mat(x);
z=cell2mat(z);

L = length (z);

[FFTz,freq] = FFTforOCT_RMHmm(x,z);%mac hole FFT script
VecLen(fileNum) = length(z);%vector length(FFT already corrected)

%create matrix of residuals
zVlen = size (z);
zedres(1:zVlen,fileNum) = z;
%zedres = zedres(1:1024,fileNum);

%save quadratic coefficients
sf = 1024/6;% 6 mm scan length
xmm{Bscanline} = x/sf;%convert to mm
sfz = 1024/2;
ZMM{Bscanline} = z/sfz;
p{Bscanline} = polyfit(xmm{Bscanline},ZMM{Bscanline},2);%
Quadcoeffs (1,Bscanline) = p{Bscanline}(1);
Quadcoeffs (2,Bscanline) = p{Bscanline}(2);
Quadcoeffs (3,Bscanline) = p{Bscanline}(3);

%put FFTz, freq into matrix, one column per B scan
cubeFFT(1:30,Bscanline) = FFTz(1:30,1);
%cubeFFT(1:30,fileNum)=cubeFFT(1:30,fileNum)/VecLen(fileNuM);
Cubefreq(1:30,Bscanline) = freq(1:30)';

MHKurv(Bscanline) = 2* (Quadcoeffs(1,Bscanline));%unrotated K
```

```
 %{
            %this section (155 - 176)creates rotated BFCvK

%p1 is the best fit line to the curve, to determine rotation angle
MHp1{Bscanline} = polyfit(xmm{Bscanline},ZMM{Bscanline},1);%first element p1 is
gradient

%rotate that line to the horizontal
angleA(Bscanline) = -atan(MHp1{Bscanline}(1));%angle for rotation

%rotate the curve by the same angle

%rotation matrix
R = [cos(angleA(Bscanline)) -sin(angleA(Bscanline)); sin(angleA(Bscanline))
cos(angleA(Bscanline))];

MHRotCd{Bscanline} = (cat(2,xmm{Bscanline},ZMM{Bscanline}))';%combine x & z in one
array
MHOdisp{Bscanline}(1) = mean(nonzeros(MHRotCd{Bscanline}(1,:)));
MHOdisp{Bscanline}(2) = mean(nonzeros(MHRotCd{Bscanline}(2,:)));
MHRotCd{Bscanline} = MHRotCd{Bscanline} - MHOdisp{Bscanline}';%move to origin for
rotation

MHRotCd{Bscanline} = R*MHRotCd{Bscanline};%rotated coordinates
MHRotCd{Bscanline} = MHRotCd{Bscanline} + MHOdisp{Bscanline}';%translate to
original position
MHRotp2{Bscanline} = polyfit(MHRotCd{Bscanline}(1,:),MHRotCd{Bscanline}(2,:),2);
MHRotKurv(Bscanline) = 2* MHRotp2{Bscanline}(1);%rotated BFCvK
  %}

     end

        cubeFFT(cubeFFT==0) = NaN;%30 rows for bins, 12 columns for B scans
        MHcubeFFTvec{CurFol} = cubeFFT;%each cell 30 bins x 12 B scans
        MedFMH(CurFol) = median (sum(cubeFFT));
        IqrFMH(CurFol) = iqr (sum(cubeFFT));
        VarFMH(CurFol) = var (sum(cubeFFT));
        MeanFMH(CurFol) = mean (sum(cubeFFT));
        stdFMH(CurFol) = std (sum(cubeFFT));

        MHbfccoeff{CurFol} = Quadcoeffs;

        MedKMH(CurFol) = median (MHKurv);
        IqrKMH(CurFol) = iqr (MHKurv);
        VarKMH(CurFol) = var (MHKurv);
        MeanKMH(CurFol) = mean (MHKurv);
        stdKMH(CurFol) = std (MHKurv);
        MHK{CurFol} = MHKurv;
        %{
        MHRotK{CurFol} = MHRotKurv;
        MedKMHRot(CurFol) = median (MHRotKurv);
        IqrKMHRot(CurFol) = iqr (MHRotKurv);
        VarKMHRot(CurFol) = var (MHRotKurv);
        %}
        cd ../

        MHID{CurFol} = MHnam(4:5);
        %nowSide = MHIID(nowMHID,str2double(MHside)+1);
        MHside(CurFol) = MHnam(2);
end



%load PV data (PVD eyes)
str2 = '/Users/stewartlake/Documents/MH contour/PV xz/';
cd (str2);

PVinfo = dir;
PVinfo = PVinfo(~ismember({PVinfo.name},{'.','..','.DS_Store'}));
```

```
PVnames = {PVinfo.name};

PVNum = size (PVnames,2);%number PVD eyes
PVcubeFFTvec = cell(1,PVNum);%PVD FFT data
PVbfccoeff = cell(1,PVNum);
PVK = cell(1,PVNum);% best fit curve vertex curvature
PVID = cell(1,PVNum);
PVside = zeros(1,PVNum);
MedKPV = zeros(1,PVNum); %median MH K
IqrKPV = zeros(1,PVNum);%iqr MH K
VarKPV = zeros(1,PVNum);% variance MH K
MedFPV = zeros(1,PVNum);% median FFT bins 1-30
IqrFPV = zeros(1,PVNum);%iqr FFT bins
VarFPV = zeros(1,PVNum);%variance FFT bins

%generate data for PVD maculae
for CurFol=1:PVNum

    PVnam = PVnames {1,CurFol}(1:5);%eye ID
    PVside = PVnames {1,CurFol}(2);%eye laterality
    PVprefix = PVnames {1,CurFol}(1:2);%first two characters for textfile str
    %open cube of data
    nowFolderPV=PVnames{1,CurFol};

    cd (nowFolderPV);%open cube xz data folder

    %get directory of textfile (B scan) names
    PVdinfo = dir;
    PVnames_cell = {PVdinfo.name};
%gives a matrix called names_cell where each column has a filename
%then:
    outPV=regexp(PVnames_cell,'\d+','match');
    outPV=str2double(cat(1,outPV{:}));
%gives a matrix called out in which each row has a number from an original filename
%these are in column 2 if text file header has a number, column 1 if it
%doesn't.

%script alpha. takes a cube of data and
%Puts x and z coordinate values into an array (myData), each cell a line of data.
%Then separates this into arrays for x, and z.
    numFiles = size(outPV, 1);%number of B scans in cube
    startRow = 1;
    endRow = inf;
    myData = cell(1,12);
    ximp = cell (1, 12);%this cubes x data
    zimp = cell (1, 12);%this cubes Z data
    cubeFFT = zeros (30, 12);
    Cubefreq = zeros (30, 12);
    PVKurv = zeros (12,1);

    fileName = cell(1);

    zedres = zeros(1024,numFiles);
    Quadcoeffs = zeros(3, 12);
    VecLen = zeros (1, numFiles);


     for fileNum = 1:numFiles %work through B scan xz txt files
            Bscanline = outPV(fileNum,end);
            %This loop is for a single cube
            fileName =[];
            fileName1 = sprintf('-%04d.txt',Bscanline);
            fileName = [PVprefix fileName1];
            myData{Bscanline} = importfile(fileName,startRow,endRow);

            ximp{Bscanline}=myData{Bscanline}(:,1);
            zimp{Bscanline}=myData{Bscanline}(:,2);

            %now reverse left to right eye orientation (reverse z)
            %and reposition scans in left to match right eyes
```

```
if (PVside == 2)%if a left eye
    if (Bscanline == 1)
       zimp{Bscanline}=flipud(zimp{Bscanline});
    elseif (Bscanline == 2)
        zimp{12} = flipud(zimp{Bscanline});
        zimp{Bscanline}=[];
    elseif (Bscanline == 3)
        zimp{11} = flipud(zimp{Bscanline});
        zimp{Bscanline}=[];
    elseif (Bscanline == 4)
        zimp{10} = flipud(zimp{Bscanline});
        zimp{Bscanline}=[];
    elseif (Bscanline == 5)
        zimp{9} = flipud(zimp{Bscanline});
        zimp{Bscanline}=[];
    elseif (Bscanline == 6)
        zimp{8} = flipud(zimp{Bscanline});
        zimp{Bscanline}=[];
    elseif (Bscanline == 8)
        zimp{6} = flipud(zimp{Bscanline});
        zimp{Bscanline}=[];
    elseif (Bscanline == 9)
        zimp{5} = flipud(zimp{Bscanline});
        zimp{Bscanline}=[];
    elseif (Bscanline == 10)
        zimp{4} = flipud(zimp{Bscanline});
        zimp{Bscanline}=[];
    elseif (Bscanline == 11)
        zimp{3} = flipud(zimp{Bscanline});
        zimp{Bscanline}=[];
    elseif (Bscanline == 12)
        zimp{2} = flipud(zimp{Bscanline});
        zimp{Bscanline}=[];
    end
end



%now format x and z for FFT
x=table2cell(ximp{Bscanline});
z=table2cell(zimp{Bscanline});
x=cell2mat(x);
z=cell2mat(z);

L = length (z);

[FFTz,freq] = FFTforOCT_RMHmm(x,z);%mac hole FFT script
VecLen(fileNum) = length(z);%vector length(FFT already corrected)

%create matrix of residuals
zVlen = size (z);
zedres(1:zVlen,fileNum) = z;
%zedres = zedres(1:1024,fileNum);

%save quadratic coefficients
sf = 1024/6;% 6 mm scan length
xmm{Bscanline} = x/sf;
sfz = 1024/2;
ZMM{Bscanline} = z/sfz;
p{Bscanline} = polyfit(xmm{Bscanline},ZMM{Bscanline},2);%
Quadcoeffs (1,Bscanline) = p{Bscanline}(1);
Quadcoeffs (2,Bscanline) = p{Bscanline}(2);
Quadcoeffs (3,Bscanline) = p{Bscanline}(3);

%put FFTz, freq into matrix, one column per B scan
cubeFFT(1:30,Bscanline) = FFTz(1:30,1);
%cubeFFT(1:30,fileNum)=cubeFFT(1:30,fileNum)/VecLen(fileNuM);
Cubefreq(1:30,Bscanline) = freq(1:30)';

PVKurv(Bscanline) = 2* (Quadcoeffs(1,Bscanline));%unrotated K
```

```
%{
%this section (356 - 377)creates rotated BFCvK

%p1 is the best fit line to the curve
p1{Bscanline} = polyfit(xmm{Bscanline},ZMM{Bscanline},1);%first element p1 is
gradient

%rotate that line to the horizontal
angleA(Bscanline) = -atan(p1{Bscanline}(1));%angle for rotation

%rotate the curve by the same angle

%rotation matrix
R = [cos(angleA(Bscanline)) -sin(angleA(Bscanline)); sin(angleA(Bscanline))
cos(angleA(Bscanline))];

PVRotCd{Bscanline} = (cat(2,xmm{Bscanline},ZMM{Bscanline}))';%combine x & z in one
array
PVOdisp{Bscanline}(1) = mean(nonzeros(PVRotCd{Bscanline}(1,:)));
PVOdisp{Bscanline}(2) = mean(nonzeros(PVRotCd{Bscanline}(2,:)));
PVRotCd{Bscanline} = PVRotCd{Bscanline} - PVOdisp{Bscanline}';%move to origin for
rotation

PVRotCd{Bscanline} = R*PVRotCd{Bscanline};%rotated coordinates
PVRotCd{Bscanline} = PVRotCd{Bscanline} + PVOdisp{Bscanline}';%translate to
original position
PVRotp2{Bscanline} = polyfit(PVRotCd{Bscanline}(1,:),PVRotCd{Bscanline}(2,:),2);
PVRotKurv(Bscanline) = 2* PVRotp2{Bscanline}(1);%rotated BFCvK
 %}

     end
        cubeFFT(cubeFFT==0) = NaN;
        PVcubeFFTvec{CurFol} = cubeFFT;
        MedFPV(CurFol) = median (sum(cubeFFT));
        IqrFPV(CurFol) = iqr (sum(cubeFFT));
        MeanFPV(CurFol) = mean (sum(cubeFFT));
        stdFPV(CurFol) = std (sum(cubeFFT));
        VarFPV(CurFol) = var (sum(cubeFFT));
        PVbfccoeff{CurFol} = Quadcoeffs;
        PVK{CurFol} = PVKurv;
        MedKPV(CurFol) = median (PVKurv);
        IqrKPV(CurFol) = iqr (PVKurv);
        MeanKPV(CurFol) = mean (PVKurv);%mean K per eye PVD
        stdKPV(CurFol) = std (PVKurv);
        VarKPV(CurFol) = var (PVKurv);
        %{
        PVRotK{CurFol} = PVRotKurv;
        MedKPVRot(CurFol) = median (PVRotKurv);
        IqrKPVRot(CurFol) = iqr (PVRotKurv);
        VarKPVRot(CurFol) = var (PVRotKurv);
        %}

        cd ../

        PVID{CurFol} = PVnam(4:5);
        %nowSide = PVIID(nowPVID,str2double(PVside)+1);
        PVside(CurFol) = PVnam(2);
end


%stat tests for difference between groups: two tailed Mann Whitney
[pFI,hIF] = ranksum(IqrFPV,IqrFMH);
[pKI,hIK] = ranksum(IqrKPV,IqrKMH);
[pVF,hVF] = ranksum(VarFPV,VarFMH);
[pVK,hVK] = ranksum(VarKPV,VarKMH);
[pMF,hMF] = ranksum(MedFPV,MedFMH);
[pMK,hMK] = ranksum(MedKPV,MedKMH);

%parametric t test for CI (95%)
[hVKt,pVKt,ciVK,statsVK] = ttest2(VarKPV,VarKMH);
```

```
[hVFt,pVFt,ciVF,statsVF] = ttest2(VarFPV,VarFMH);
[hIKt,pIKt,ciIK,statsIK] = ttest2(IqrKPV,IqrKMH);
[hIFt,pIFt,ciIF,statsIF] = ttest2(IqrFPV,IqrFMH);
[hSKt,pSKt,ciSK,statsSK] = ttest2(stdKPV,stdKMH);
[hSFt,pSFt,ciSF,statsSF] = ttest2(stdFPV,stdFMH);
[hmKt,pmKt,cimK,statsmK] = ttest2(MeanKPV,MeanKMH);%compare mean K per eyes between
grps
[hmFt,pmFt,cimF,statsmF] = ttest2(MeanFPV,MeanFMH);%compare mean F

%Cohen's D effect size
dVK = (mean(VarKPV)-mean(VarKMH))/std(VarKPV);
dVF = (mean(VarFPV)-mean(VarFMH))/std(VarFPV);
dIK = (mean(IqrKPV)-mean(IqrKMH))/std(IqrKPV);
dIF = (mean(IqrFPV)-mean(IqrFMH))/std(IqrFPV);
dsK = (mean(stdKPV)-mean(stdKMH))/std(stdKPV);
dsF = (mean(stdFPV)-mean(stdFMH))/std(stdFPV);
dmK = (mean(MeanKPV)-mean(MeanKMH))/std(MeanKPV);
dmF = (mean(MeanFPV)-mean(MeanFMH))/std(MeanFPV);

%{
[pKrotI,hIKrot] = ranksum(IqrKPVRot,IqrKMHRot,'tail','right');%for rotated BFCvK
[pVKrot,hVKrot] = ranksum(VarKPVRot,VarKMHRot,'tail','right');
[pMKrot,hMKrot] = ranksum(MedKPVRot,MedKMHRot,'tail','right');
%}


%signrank all the FTR/K per group in a single vector
for EcPV=1:PVNum

    SUMFFTPV{EcPV} = sum(PVcubeFFTvec{EcPV});

    KallPV{EcPV} = 2*PVbfccoeff{EcPV}(1,:);

    %this section for range of variables
    SUMFFTPVbyeye{EcPV} = sum(PVcubeFFTvec{EcPV});%res by eye

    [~,locFmxPV(EcPV)] = max(SUMFFTPVbyeye{EcPV});

    [~,locFminPV(EcPV)] = min(SUMFFTPVbyeye{EcPV});

    MdiffresPV(EcPV) = range(SUMFFTPVbyeye{EcPV});%tange res by eye

    KallPVbyeye{EcPV} = 2*PVbfccoeff{EcPV}(1,:);% K by eye

    [~,locKmxPV(EcPV)] = max(KallPVbyeye{EcPV});

    [~,locKminPV(EcPV)] = min(KallPVbyeye{EcPV});

    MdiffKPV(EcPV) = range(KallPVbyeye{EcPV});%range K by eye


end

for EcMH=1:MHNum

    SUMFFTMH{EcMH} = sum(MHcubeFFTvec{EcMH});

    KallMH{EcMH} = 2*MHbfccoeff{EcMH}(1,:);

    %this section for range of variables
    SUMFFTMHbyeye{EcMH} = sum(MHcubeFFTvec{EcMH});% res by eye

    [~,locFmxMH(EcMH)] = max(SUMFFTMHbyeye{EcMH});

    [~,locFminMH(EcMH)] = min(SUMFFTMHbyeye{EcMH});

    MdiffresMH (EcMH) = range(SUMFFTMHbyeye{EcMH});

    KallMHbyeye{EcMH} = 2*MHbfccoeff{EcMH}(1,:);%k by eye
```

```
    [~,locKmxMH(EcMH)] = max(KallMHbyeye{EcMH});

    [~,locKminMH(EcMH)] = min(KallMHbyeye{EcMH});

    MdiffKMH(EcMH) = range(KallMHbyeye{EcMH});

end

SUMFFTMH = [SUMFFTMH{:}];%vector of all B scan FTR30
SUMFFTPV = [SUMFFTPV{:}];
KallMH = [KallMH{:}];%vector of all B scan Ks
KallPV = [KallPV{:}];

[pFsum,hFsum] = ranksum(SUMFFTMH,SUMFFTPV);
[pKall,hKall] = ranksum(KallMH,KallPV);

%{
%range of variables test (cf astigmatism)
[~,RangeKPVvnoTT, ciRangeK,~] = ttest2(MdiffKMH,MdiffKPV);
[~,RangeresPVvnoTT, ciRangeres,~] = ttest2(MdiffresMH, MdiffresPV);
%range cohens d
dRK = (mean(MdiffKPV)-mean(MdiffKMH))/sqrt((std(MdiffKPV).^2 +
std(MdiffKMH).^2)/2);
dRF = (mean(MdiffresPV)-mean(MdiffresMH))/sqrt((std(MdiffresPV).^2 +
std(MdiffresMH).^2)/2);
%}
%difference in location max and min axes (ie are they perpendicular to each
%other) pre to post PVD
KaxesMH = abs(locKmxMH- locKminMH);
FaxesMH = abs(locFmxMH - locFminMH);
KaxesPV = abs(locKmxPV - locKminPV);
FaxesPV = abs(locFmxPV - locFminPV);
num48PVK = find(KaxesPV>3 & KaxesPV<9);
num48MHK = find(KaxesMH>3 & KaxesMH<9);
num48K = length(num48PVK) + length(num48MHK);%number  4-8 scans apart K
num48PVF = find(FaxesPV>3 & FaxesPV<9);
num48MHF = find(FaxesMH>3 & FaxesMH<9);
num48F = length(num48PVF) + length(num48MHF);%number  4-8 scans apart F

num57PVK = find(KaxesPV>4 & KaxesPV<8);
num57MHK = find(KaxesMH>4 & KaxesMH<8);
num57K = length(num57PVK) + length(num57MHK);%number  5-7 scans apart K
num57PVF = find(FaxesPV>4 & FaxesPV<8);
num57MHF = find(FaxesMH>4 & FaxesMH<8);
num57F = length(num57PVF) + length(num57MHF);%number  5-7 scans apart F

[~,axKMxmnp, ciKMxmn,~] = ttest2(KaxesMH,KaxesPV);%diff in spread
[~,axresMxmnp, ciresMxMn,~] = ttest2(FaxesMH,FaxesPV);

[~,axKmxp,ciaxKmxp,~] = ttest2(locKmxMH, locKmxPV);%DIFF IN MAX LOCATION K
diffKmax = mean(locKmxMH,'omitnan') - mean(locKmxPV,'omitnan');
mnlocKmxMH = mean(locKmxMH,'omitnan');
mnlocKmxPV = mean(locKmxPV,'omitnan');
[~,axKminp,ciaxKminp,~] = ttest2(locKminMH, locKminPV);%min K

[~,axFmxp,ciaxFmxp,~] = ttest2(locFmxMH, locFmxPV);% diff in max loc F
[~,axFminp,ciaxFminp,~] = ttest2(locFminMH, locFminPV);%minF

%HERE!!!!!!!!!!!!!
%two sample t test range K and residual pre v post
[~,RangeKMHprpopaiTT, ciRangepK,~] = ttest2(MdiffKMH,MdiffKPV);
[~,RangeresprpopaiTT, ciRangepres,~] = ttest2(MdiffresMH, MdiffresPV);

%size of difference in ranges, PVD v noPVD
rangediffK = mean(MdiffKPV,'omitnan')-mean(MdiffKMH,'omitnan');%diff in mean range
K
rangediffF = mean(MdiffresPV,'omitnan')-mean(MdiffresMH,'omitnan');%diff in mean
range K

meanKPV = mean(KallPV);%mean K PVD eyes
```

```
meanKMH = mean(KallMH);%mean K no pVD eyes
meanFTR30PV = mean(SUMFFTPV);%mean  FTR30 PVD
meanFTR30MH = mean(SUMFFTMH);%mean FTR30 no PVD
diffKpvnPV = meanKPV-meanKMH;%diff between means to go with CI
diffFpvnPV= meanFTR30PV - meanFTR30MH;% diff means to go with CI
sdKPV = std(KallPV);
sdKMH = std(KallMH);
sdFPV = std(SUMFFTPV);
sdFMH = std(SUMFFTMH);
[~,pttKPVnPV,KallCI,~] = ttest2(KallPV,KallMH);%ttest compare K PVD v noPVD
[~,pttFPVnPV, FallCI] = ttest2(SUMFFTPV,SUMFFTMH);% tests compare F PVD v no
%Cohens d of effect of PVD on K and F
dK = (meanKPV-meanKMH)/sqrt((sdKMH.^2 + sdKPV.^2)/2);%effect size of PVD on K
dF = (meanFTR30PV-meanFTR30MH)/sqrt((sdFMH.^2 + sdFPV.^2)/2);%effect size of PVD on
F

pMWUKPVnPV = ranksum(KallPV,KallMH);%MWU compare K PVD v noPVD
pMWUFPVnPV = ranksum(SUMFFTPV,SUMFFTMH);% MWU tests compare F PVD v no
tablen = length(MeanKPV);
AL0pvd = zeros(tablen,1);
ALpvd = zeros (tablen,1);%(KMH to make it same length
PVDnames = cell(tablen,1);
PVDnames(1:length(PVnames)) = PVnames;

%match smaller group veclength to longer
ALpvd(end+1:tablen)=NaN;
MHnames{tablen}=[];
MdiffKMH(end+1:tablen)=NaN;
MdiffresMH(end+1:tablen)=NaN;
MeanKMH(end+1:tablen)=NaN;
MeanFMH(end+1:tablen)=NaN;

%create table, add AL vlues manually
PVDnoPVDsum = table(MHnames', AL0pvd, MdiffKMH', MdiffresMH', MeanKMH', MeanFMH',
...
    PVDnames, ALpvd, MdiffKPV', MdiffresPV', MeanKPV', MeanFPV',...
    'VariableNames',{'noPVDID','noPVDAL','noPVDrangeK','noPVDrangeres'...
    'noPVDmeanK', 'noPVDmeanres','PVDID','PVDAL','PVDrangeK','PVDrangeres'...
    'PVDmeanK', 'PVDmeanres'});

%HERE!!!!!!!!!!!!
%now compare mean K/res noPVD v PVD, paired t test
[~,meanKMHprpopaiTT, cimeanpK,~] = ttest2(PVDnoPVDsum.PVDmeanK,
PVDnoPVDsum.noPVDmeanK);
[~,meanresprpopaiTT, cimeanpres,~] = ttest2(PVDnoPVDsum.PVDmeanres,
PVDnoPVDsum.noPVDmeanres);
diffMK = mean(PVDnoPVDsum.PVDmeanK, 'omitnan') -
mean(PVDnoPVDsum.noPVDmeanK,'omitnan');%diffe pre v post K
diffMres = mean(PVDnoPVDsum.PVDmeanres,'omitnan')-
mean(PVDnoPVDsum.noPVDmeanres,'omitnan');


[~,pttALPVnPV,ALallCI,~] =
ttest2(PVDnoPVDsum.noPVDAL(9:end),PVDnoPVDsum.PVDAL);%ttest compare AL PVD v noPVD


%added summary values - mean & SD, pre & post range & mean K & res
%Here!!!!!!!!!!
mrngpreMHK=mean(PVDnoPVDsum.noPVDrangeK);
mrngpostMHK=mean(PVDnoPVDsum.PVDrangeK);
mrngpreMHres =mean(PVDnoPVDsum.noPVDrangeres);
mrngpostMHres =mean(PVDnoPVDsum.PVDrangeres);

meanpreMHK=mean(PVDnoPVDsum.noPVDmeanK);
meanpostMHK=mean(PVDnoPVDsum.PVDmeanK);
meanpreMHres =mean(PVDnoPVDsum.noPVDmeanres);
meanpostMHres =mean(PVDnoPVDsum.PVDmeanres);

sdrngpreMHK=std(PVDnoPVDsum.noPVDrangeK);
sdrngpostMHK=std(PVDnoPVDsum.PVDrangeK);
```

```
sdrngpreMHres =std(PVDnoPVDsum.noPVDrangeres);
sdrngpostMHres =std(PVDnoPVDsum.PVDrangeres);

sdmnpreMHK=std(PVDnoPVDsum.noPVDmeanK);
sdmnpostMHK=std(PVDnoPVDsum.PVDmeanK);
sdmnpreMHres =std(PVDnoPVDsum.noPVDmeanres);
sdmnpostMHres =std(PVDnoPVDsum.PVDmeanres);

figure
hold on
scatter(PVDnoPVDsum.noPVDrangeres,PVDnoPVDsum.PVDrangeres,[],'b')
scatter(PVDnoPVDsum.noPVDmeanres,PVDnoPVDsum.PVDmeanres,[],'c')
%text(MedKPV +dx2,MedFPV + dy2,PVID);
title('No PVD v PVD radial macula hole OCT mean and range irregularity');%FTI = FT
of irregularity
xlabel('No PVD');
ylabel('PVD');
refline(1,0);
legend('range res','mean res');

%check AL vector prior to this
%[ALH,ALP,ALCI,ALSTATS] = ttest2(PVDnoPVDsum.noPVDAL,PVDnoPVDsum.PVDAL);
%load other matrix for the next
%[ageH,ageP,ageCI,ageSTATS] =ttest2(NoPVDages.age,PVDages.age);
%meanAGEPVD = mean(PVDages.age);
%meanAGEnoPVD = mean(NoPVDages.age);
%stdAGEPVD = std(PVDages.age);
%stdAGEnoPVD = std(NoPVDages.age);
%meanALPVD = mean(PVDnoPVDsum.PVDAL,'omitnan');
%meanALnoPVD = mean(PVDnoPVDsum.noPVDAL,'omitnan');
%stdALPVD = std(PVDnoPVDsum.PVDAL,'omitnan');
%stdALnoPVD = std(PVDnoPVDsum.noPVDAL,'omitnan');
%{
%scatter plot variance of K and FFT,MH v PV, rotated K
dx=0.000001;%label displacement
dy=0.1;
figure
hold on
scatter(VarKMHRot,VarFMH,[],'r')
%text(VarKMH +dx,VarFMH + dy,MHID);
scatter(VarKPVRot, VarFPV,[],'b')
%text(VarKPV +dx,VarFPV + dy,PVID);
title('No PVD v PVD radial macula cube rotated K v FFT variance');
xlabel('Krot var');
ylabel('FFT var');
%}

%scatter plot variance of K and FFT,MH v PV
dx=0.000001;%label displacement
dy=0.1;
figure
hold on
scatter(VarKMH,VarFMH,[],'r')
%text(VarKMH +dx,VarFMH + dy,MHID);
scatter(VarKPV, VarFPV,[],'b')
%text(VarKPV +dx,VarFPV + dy,PVID);
title('No PVD v PVD radial macula cube K and FFT variance');
xlabel('K var');
ylabel('FFT var');

%scatter plot median K v FFT
figure
dx2=0.005;
dy2=0.1;
hold on
scatter(MedKMH,MedFMH,[],'r')
%text(MedKMH +dx2,MedFMH + dy2,MHID);
scatter(MedKPV, MedFPV,[],'b')
%text(MedKPV +dx2,MedFPV + dy2,PVID);
title('No PVD v PVD radial macula cube median K and FFT');
```

```
xlabel('K med');
ylabel('FFT med');

%scatter plot iqr K & FFT
figure
dx3=0.0001;
dy3=0.1;
hold on
scatter(IqrKMH,IqrFMH,[],'r')
%text(IqrKMH +dx3,IqrFMH + dy3,MHID);
scatter(IqrKPV, IqrFPV,[],'b')
%text(IqrKPV +dx3,IqrFPV + dy3,PVID);
title('No PVD v PVD radial macula cube iqr K and FFT');
xlabel('iqr K');
ylabel('iqr FFT');

%scatter plot K v FFT for all B scans
allBSfig = figure;
hold on
scatter(KallPV,SUMFFTPV,[],'r')
%text(MedKMH +dx2,MedFMH + dy2,MHID);
scatter(KallMH, SUMFFTMH,[],'b','+')
%text(MedKPV +dx2,MedFPV + dy2,PVID);
title('No PVD (blue) v PVD (red) radial macula B scan K and irregularity');
xlabel('K (/mm)');
ylabel('Irregularity (mm)');
%allBSfig.Visible = 'off';
```

2. prepostMHcomp

```
%compare curvature for pre (MH) xz (or, see line 8) to post (MH) xz files (radial
HD 12)
%CHANGE: line 8 & 213, plus figure labels, savename 620
%takes data from MH pre xz (or no PVD radial xz) (line 8) and MH post xz (or PV xz)
(line 213) and calculates FFT and K
%plus median, var, and iqr sum bins
%plus median, iqr, and variance K
clear
%load MH data
str1 = '/Users/stewartlake/Documents/MH contour/pre op for post op xz V eyes/';%MH
eyes in folder with MH suffix to this
cd (str1);

MHinfo = dir;
MHinfo = MHinfo(~ismember({MHinfo.name},{'.','..','.DS_Store'}));
MHnames = {MHinfo.name};

MHNum = size (MHnames,2);%number MH eyes
MHcubeFFTvec = cell(1,MHNum);%One eye per cell %each cell 30 bins x 12 B scans
MHbfccoeff = cell(1,MHNum);
MHK = cell(1,MHNum); % best fit curve vertex curvature.One eye per cell
MHID = cell(1,MHNum);
MHside = zeros(1,MHNum);
MedKMH = zeros(1,MHNum); %median MH K
IqrKMH = zeros(1,MHNum);%iqr MH K
VarKMH = zeros(1,MHNum);% variance MH K
MedFMH = zeros(1,MHNum);% median FFT bins 1-30
IqrFMH = zeros(1,MHNum);%iqr FFT bins
VarFMH = zeros(1,MHNum);%variance FFT bins


%generate data for MH maculae
for CurFol=1:MHNum

    MHnam = MHnames {1,CurFol}(1:5);%eye ID
    MHside = MHnames {1,CurFol}(2);%eye laterality
    MHprefix = MHnames {1,CurFol}(1:2);%first two characters for textfile str
```

```
    %open cube of data
    nowFolderMH=MHnames{1,CurFol};

    cd (nowFolderMH);%open cube xz data folder

    %get directory of textfile (B scan) names
    MHdinfo = dir;
    MHnames_cell = {MHdinfo.name};
%gives a matrix called names_cell where each column has a filename
%then:
    outMH=regexp(MHnames_cell,'\d+','match');
    outMH=str2double(cat(1,outMH{:}));
%gives a matrix called out in which each row has a number from an original filename
%these are in column 2 if text file header has a number, column 1 if it
%doesn't.

%script alpha. takes a cube of data and
%Puts x and z coordinate values into an array (myData), each cell a line of data.
%Then separates this into arrays for x, and z.
    numFiles = size(outMH, 1);%number of B scans in cube
    startRow = 1;
    endRow = inf;
    myData = cell(1,12);
    ximp = cell (1, 12);%this cubes x data
    zimp = cell (1, 12);%this cubes Z data
    cubeFFT = zeros (30, 12);
    Cubefreq = zeros (30, 12);
    MHKurv = zeros (12,1);

    fileName = cell(1);

    zedres = zeros(1024,numFiles);
    Quadcoeffs = zeros(3, 12);
    VecLen = zeros (1, numFiles);


     for fileNum = 1:numFiles %work through B scan xz txt files
            Bscanline = outMH(fileNum,end);
            %This loop is for a single cube
            fileName =[];
            fileName1 = sprintf('-%04d.txt',Bscanline);
            fileName = [MHprefix fileName1];
            myData{Bscanline} = importfile(fileName,startRow,endRow);

            ximp{Bscanline}=myData{Bscanline}(:,1);
            zimp{Bscanline}=myData{Bscanline}(:,2);

            %now reverse left to right eye orientation (reverse z)
            %and reposition scans in left to match right eyes
            if (MHside == 2)%if a left eye
                if (Bscanline == 1)
                   zimp{Bscanline}=flipud(zimp{Bscanline});
                elseif (Bscanline == 2)
                    zimp{12} = flipud(zimp{Bscanline});
                    zimp{Bscanline}=[];
                elseif (Bscanline == 3)
                    zimp{11} = flipud(zimp{Bscanline});
                    zimp{Bscanline}=[];
                elseif (Bscanline == 4)
                    zimp{10} = flipud(zimp{Bscanline});
                    zimp{Bscanline}=[];
                elseif (Bscanline == 5)
                    zimp{9} = flipud(zimp{Bscanline});
                    zimp{Bscanline}=[];
                elseif (Bscanline == 6)
                    zimp{8} = flipud(zimp{Bscanline});
                    zimp{Bscanline}=[];
                elseif (Bscanline == 8)
                    zimp{6} = flipud(zimp{Bscanline});
                    zimp{Bscanline}=[];
```

```
            elseif (Bscanline == 9)
                zimp{5} = flipud(zimp{Bscanline});
                zimp{Bscanline}=[];
            elseif (Bscanline == 10)
                zimp{4} = flipud(zimp{Bscanline});
                zimp{Bscanline}=[];
            elseif (Bscanline == 11)
                zimp{3} = flipud(zimp{Bscanline});
                zimp{Bscanline}=[];
            elseif (Bscanline == 12)
                zimp{2} = flipud(zimp{Bscanline});
                zimp{Bscanline}=[];
            end
        end



        %now format x and z for FFT
        x=table2cell(ximp{Bscanline});
        z=table2cell(zimp{Bscanline});
        x=cell2mat(x);
        z=cell2mat(z);

        L = length (z);

        [FFTz,freq] = FFTforOCT_RMHmm(x,z);%mac hole FFT script
        VecLen(fileNum) = length(z);%vector length(FFT already corrected)

        %create matrix of residuals
        zVlen = size (z);
        zedres(1:zVlen,fileNum) = z;
        %zedres = zedres(1:1024,fileNum);

        %save quadratic coefficients
        sf = 1024/6;% 6 mm scan length
        xmm{Bscanline} = x/sf;%convert to mm
        sfz = 1024/2;
        ZMM{Bscanline} = z/sfz;
        p{Bscanline} = polyfit(xmm{Bscanline},ZMM{Bscanline},2);%
        Quadcoeffs (1,Bscanline) = p{Bscanline}(1);
        Quadcoeffs (2,Bscanline) = p{Bscanline}(2);
        Quadcoeffs (3,Bscanline) = p{Bscanline}(3);

        %put FFTz, freq into matrix, one column per B scan
        cubeFFT(1:30,Bscanline) = FFTz(1:30,1);
        %cubeFFT(1:30,fileNum)=cubeFFT(1:30,fileNum)/VecLen(fileNuM);
        Cubefreq(1:30,Bscanline) = freq(1:30)';

        MHKurv(Bscanline) = 2* (Quadcoeffs(1,Bscanline));%unrotated K

 %{
        %this section (155 - 176)creates rotated BFCvK

%p1 is the best fit line to the curve, to determine rotation angle
MHp1{Bscanline} = polyfit(xmm{Bscanline},ZMM{Bscanline},1);%first element p1 is
gradient

%rotate that line to the horizontal
angleA(Bscanline) = -atan(MHp1{Bscanline}(1));%angle for rotation

%rotate the curve by the same angle

%rotation matrix
R = [cos(angleA(Bscanline)) -sin(angleA(Bscanline)); sin(angleA(Bscanline))
cos(angleA(Bscanline))];

MHRotCd{Bscanline} = (cat(2,xmm{Bscanline},ZMM{Bscanline}))';%combine x & z in one
array
MHOdisp{Bscanline}(1) = mean(nonzeros(MHRotCd{Bscanline}(1,:)));
MHOdisp{Bscanline}(2) = mean(nonzeros(MHRotCd{Bscanline}(2,:)));
```

```
MHRotCd{Bscanline} = MHRotCd{Bscanline} - MHOdisp{Bscanline}';%move to origin for
rotation

MHRotCd{Bscanline} = R*MHRotCd{Bscanline};%rotated coordinates
MHRotCd{Bscanline} = MHRotCd{Bscanline} + MHOdisp{Bscanline}';%translate to
original position
MHRotp2{Bscanline} = polyfit(MHRotCd{Bscanline}(1,:),MHRotCd{Bscanline}(2,:),2);
MHRotKurv(Bscanline) = 2* MHRotp2{Bscanline}(1);%rotated BFCvK
  %}

     end

        cubeFFT(cubeFFT==0) = NaN;%30 rows for bins, 12 columns for B scans
        MHcubeFFTvec{CurFol} = cubeFFT;%each cell 30 bins x 12 B scans
        MedFMH(CurFol) = median (sum(cubeFFT));
        IqrFMH(CurFol) = iqr (sum(cubeFFT));
        VarFMH(CurFol) = var (sum(cubeFFT));
        MeanFMH(CurFol) = mean (sum(cubeFFT));

        MHbfccoeff{CurFol} = Quadcoeffs;

        MedKMH(CurFol) = median (MHKurv);
        IqrKMH(CurFol) = iqr (MHKurv);
        VarKMH(CurFol) = var (MHKurv);
        MeanKMH(CurFol) = mean (MHKurv);
        MHK{CurFol} = MHKurv;
        %{
        MHRotK{CurFol} = MHRotKurv;
        MedKMHRot(CurFol) = median (MHRotKurv);
        IqrKMHRot(CurFol) = iqr (MHRotKurv);
        VarKMHRot(CurFol) = var (MHRotKurv);
        %}
        cd ../

        MHID{CurFol} = MHnam(4:5);
        %nowSide = MHIID(nowMHID,str2double(MHside)+1);
        MHside(CurFol) = MHnam(2);
end



%%
%load PV data (PVD eyes)
str1 = '/Users/stewartlake/Documents/MH contour/post op xz V eyes/';%end here for
MH
cd (str1);

PVinfo = dir;
PVinfo = PVinfo(~ismember({PVinfo.name},{'.','..','.DS_Store'}));
PVnames = {PVinfo.name};

PVNum = size (PVnames,2);%number PVD eyes
PVcubeFFTvec = cell(1,PVNum);%PVD FFT data
PVbfccoeff = cell(1,PVNum);
PVK = cell(1,PVNum);% best fit curve vertex curvature
PVID = cell(1,PVNum);
PVside = zeros(1,PVNum);
MedKPV = zeros(1,PVNum); %median MH K
IqrKPV = zeros(1,PVNum);%iqr MH K
VarKPV = zeros(1,PVNum);% variance MH K
MedFPV = zeros(1,PVNum);% median FFT bins 1-30
IqrFPV = zeros(1,PVNum);%iqr FFT bins
VarFPV = zeros(1,PVNum);%variance FFT bins

%generate data for PVD maculae
for CurFol=1:PVNum

    PVnam = PVnames {1,CurFol}(1:5);%eye ID
    PVside = PVnames {1,CurFol}(2);%eye laterality
    PVprefix = PVnames {1,CurFol}(1:2);%first two characters for textfile str
```

```
    %open cube of data
    nowFolderPV=PVnames{1,CurFol};

    cd (nowFolderPV);%open cube xz data folder

    %get directory of textfile (B scan) names
    PVdinfo = dir;
    PVnames_cell = {PVdinfo.name};
%gives a matrix called names_cell where each column has a filename
%then:
    outPV=regexp(PVnames_cell,'\d+','match');
    outPV=str2double(cat(1,outPV{:}));
%gives a matrix called out in which each row has a number from an original filename
%these are in column 2 if text file header has a number, column 1 if it
%doesn't.

%script alpha. takes a cube of data and
%Puts x and z coordinate values into an array (myData), each cell a line of data.
%Then separates this into arrays for x, and z.
    numFiles = size(outPV, 1);%number of B scans in cube
    startRow = 1;
    endRow = inf;
    myData = cell(1,12);
    ximp = cell (1, 12);%this cubes x data
    zimp = cell (1, 12);%this cubes Z data
    cubeFFT = zeros (30, 12);
    Cubefreq = zeros (30, 12);
    PVKurv = zeros (12,1);

    fileName = cell(1);

    zedres = zeros(1024,numFiles);
    Quadcoeffs = zeros(3, 12);
    VecLen = zeros (1, numFiles);


     for fileNum = 1:numFiles %work through B scan xz txt files
            Bscanline = outPV(fileNum,end);
            %This loop is for a single cube
            fileName =[];
            fileName1 = sprintf('-%04d.txt',Bscanline);
            fileName = [PVprefix fileName1];
            myData{Bscanline} = importfile(fileName,startRow,endRow);

            ximp{Bscanline}=myData{Bscanline}(:,1);
            zimp{Bscanline}=myData{Bscanline}(:,2);

            %now reverse left to right eye orientation (reverse z)
            %and reposition scans in left to match right eyes
            if (PVside == 2)%if a left eye
                if (Bscanline == 1)
                   zimp{Bscanline}=flipud(zimp{Bscanline});
                elseif (Bscanline == 2)
                    zimp{12} = flipud(zimp{Bscanline});
                    zimp{Bscanline}=[];
                elseif (Bscanline == 3)
                    zimp{11} = flipud(zimp{Bscanline});
                    zimp{Bscanline}=[];
                elseif (Bscanline == 4)
                    zimp{10} = flipud(zimp{Bscanline});
                    zimp{Bscanline}=[];
                elseif (Bscanline == 5)
                    zimp{9} = flipud(zimp{Bscanline});
                    zimp{Bscanline}=[];
                elseif (Bscanline == 6)
                    zimp{8} = flipud(zimp{Bscanline});
                    zimp{Bscanline}=[];
                elseif (Bscanline == 8)
                    zimp{6} = flipud(zimp{Bscanline});
                    zimp{Bscanline}=[];
```

```
                elseif (Bscanline == 9)
                    zimp{5} = flipud(zimp{Bscanline});
                    zimp{Bscanline}=[];
                elseif (Bscanline == 10)
                    zimp{4} = flipud(zimp{Bscanline});
                    zimp{Bscanline}=[];
                elseif (Bscanline == 11)
                    zimp{3} = flipud(zimp{Bscanline});
                    zimp{Bscanline}=[];
                elseif (Bscanline == 12)
                    zimp{2} = flipud(zimp{Bscanline});
                    zimp{Bscanline}=[];
                end
            end



            %now format x and z for FFT
            x=table2cell(ximp{Bscanline});
            z=table2cell(zimp{Bscanline});
            x=cell2mat(x);
            z=cell2mat(z);

            L = length (z);

            [FFTz,freq] = FFTforOCT_RMHmm(x,z);%mac hole FFT script
            VecLen(fileNum) = length(z);%vector length(FFT already corrected)

            %create matrix of residuals
            zVlen = size (z);
            zedres(1:zVlen,fileNum) = z;
            %zedres = zedres(1:1024,fileNum);

            %save quadratic coefficients
            sf = 1024/6;% 6 mm scan length
            xmm{Bscanline} = x/sf;
            sfz = 1024/2;
            ZMM{Bscanline} = z/sfz;
            p{Bscanline} = polyfit(xmm{Bscanline},ZMM{Bscanline},2);%
            Quadcoeffs (1,Bscanline) = p{Bscanline}(1);
            Quadcoeffs (2,Bscanline) = p{Bscanline}(2);
            Quadcoeffs (3,Bscanline) = p{Bscanline}(3);

            %put FFTz, freq into matrix, one column per B scan
            cubeFFT(1:30,Bscanline) = FFTz(1:30,1);
            %cubeFFT(1:30,fileNum)=cubeFFT(1:30,fileNum)/VecLen(fileNuM);
            Cubefreq(1:30,Bscanline) = freq(1:30)';

            PVKurv(Bscanline) = 2* (Quadcoeffs(1,Bscanline));%unrotated K
%{
%this section (356 - 377)creates rotated BFCvK

%p1 is the best fit line to the curve
p1{Bscanline} = polyfit(xmm{Bscanline},ZMM{Bscanline},1);%first element p1 is
gradient

%rotate that line to the horizontal
angleA(Bscanline) = -atan(p1{Bscanline}(1));%angle for rotation

%rotate the curve by the same angle

%rotation matrix
R = [cos(angleA(Bscanline)) -sin(angleA(Bscanline)); sin(angleA(Bscanline))
cos(angleA(Bscanline))];

PVRotCd{Bscanline} = (cat(2,xmm{Bscanline},ZMM{Bscanline}))';%combine x & z in one
array
PVOdisp{Bscanline}(1) = mean(nonzeros(PVRotCd{Bscanline}(1,:)));
PVOdisp{Bscanline}(2) = mean(nonzeros(PVRotCd{Bscanline}(2,:)));
```

```
PVRotCd{Bscanline} = PVRotCd{Bscanline} - PVOdisp{Bscanline}';%move to origin for
rotation

PVRotCd{Bscanline} = R*PVRotCd{Bscanline};%rotated coordinates
PVRotCd{Bscanline} = PVRotCd{Bscanline} + PVOdisp{Bscanline}';%translate to
original position
PVRotp2{Bscanline} = polyfit(PVRotCd{Bscanline}(1,:),PVRotCd{Bscanline}(2,:),2);
PVRotKurv(Bscanline) = 2* PVRotp2{Bscanline}(1);%rotated BFCvK
 %}

     end
        cubeFFT(cubeFFT==0) = NaN;
        PVcubeFFTvec{CurFol} = cubeFFT;
        MedFPV(CurFol) = median (sum(cubeFFT));
        IqrFPV(CurFol) = iqr (sum(cubeFFT));
        MeanFPV(CurFol) = mean (sum(cubeFFT));
        VarFPV(CurFol) = var (sum(cubeFFT));
        PVbfccoeff{CurFol} = Quadcoeffs;
        PVK{CurFol} = PVKurv;
        MedKPV(CurFol) = median (PVKurv);
        IqrKPV(CurFol) = iqr (PVKurv);
        MeanKPV(CurFol) = mean (PVKurv);%mean K per eye PVD
        VarKPV(CurFol) = var (PVKurv);
        %{
        PVRotK{CurFol} = PVRotKurv;
        MedKPVRot(CurFol) = median (PVRotKurv);
        IqrKPVRot(CurFol) = iqr (PVRotKurv);
        VarKPVRot(CurFol) = var (PVRotKurv);
        %}

        cd ../

        PVID{CurFol} = PVnam(4:5);
        %nowSide = PVIID(nowPVID,str2double(PVside)+1);
        PVside(CurFol) = PVnam(2);
end
%%

%stat tests for difference between groups: one tailed Mann Whitney
[pFI,hIF] = ranksum(IqrFPV,IqrFMH,'tail','right');
[pKI,hIK] = ranksum(IqrKPV,IqrKMH,'tail','right');
[pVF,hVF] = ranksum(VarFPV,VarFMH,'tail','right');
[pVK,hVK] = ranksum(VarKPV,VarKMH,'tail','right');
[pMF,hMF] = ranksum(MedFPV,MedFMH,'tail','right');
[pMK,hMK] = ranksum(MedKPV,MedKMH,'tail','right');

%{
[pKrotI,hIKrot] = ranksum(IqrKPVRot,IqrKMHRot,'tail','right');%for rotated BFCvK
[pVKrot,hVKrot] = ranksum(VarKPVRot,VarKMHRot,'tail','right');
[pMKrot,hMKrot] = ranksum(MedKPVRot,MedKMHRot,'tail','right');
%}


%signrank all the FTR/K per group in a single vector
for EcPV=1:PVNum

    SUMFFTPV{EcPV} = sum(PVcubeFFTvec{EcPV});%sum all FFT bins for each Bscan

    KallPV{EcPV} = 2*PVbfccoeff{EcPV}(1,:);% BFCvK for each eye

     %this section for range of variables
    SUMFFTPVbyeye{EcPV} = sum(PVcubeFFTvec{EcPV});%sum res by Bscan (1-12)

    [~,locFmxPV(EcPV)] = max(SUMFFTPVbyeye{EcPV});%loc max res

    [~,locFminPV(EcPV)] = min(SUMFFTPVbyeye{EcPV});%B scan loc min res

    MdiffresPV(EcPV) = range(SUMFFTPVbyeye{EcPV});%range res by eye

    KallPVbyeye{EcPV} = 2*PVbfccoeff{EcPV}(1,:);% K by eye
```

```
    [~,locKmxPV(EcPV)] = max(KallPVbyeye{EcPV});

    [~,locKminPV(EcPV)] = min(KallPVbyeye{EcPV});

    MdiffKPV(EcPV) = range(KallPVbyeye{EcPV});%range K by eye


end

for EcMH=1:MHNum

    SUMFFTMH{EcMH} = sum(MHcubeFFTvec{EcMH});

    KallMH{EcMH} = 2*MHbfccoeff{EcMH}(1,:);

    %this section for range of variables
    SUMFFTMHbyeye{EcMH} = sum(MHcubeFFTvec{EcMH});% res by eye

    [~,locFmxMH(EcMH)] = max(SUMFFTMHbyeye{EcMH});

    [~,locFminMH(EcMH)] = min(SUMFFTMHbyeye{EcMH});

    MdiffresMH (EcMH) = range(SUMFFTMHbyeye{EcMH});%range res pre-op

    KallMHbyeye{EcMH} = 2*MHbfccoeff{EcMH}(1,:);%k by eye

    [~,locKmxMH(EcMH)] = max(KallMHbyeye{EcMH});

    [~,locKminMH(EcMH)] = min(KallMHbyeye{EcMH});

    MdiffKMH(EcMH) = range(KallMHbyeye{EcMH});%range K pre-op

end

SUMFFTMH = [SUMFFTMH{:}];%vector of all B scan FTR30
SUMFFTPV = [SUMFFTPV{:}];
KallMH = [KallMH{:}];%vector of all B scan Ks
KallPV = [KallPV{:}];

[pFsum,hFsum] = ranksum(SUMFFTMH,SUMFFTPV);
[pKall,hKall] = ranksum(KallMH,KallPV);


%difference in location max and min axes (ie are they perpendicular to each
%other) pre and post OP

KaxesMH = abs(locKmxMH- locKminMH)';
FaxesMH = abs(locFmxMH - locFminMH)';
KaxesPV = abs(locKmxPV - locKminPV)';
FaxesPV = abs(locFmxPV - locFminPV)';
num48PVK = find(KaxesPV>3 & KaxesPV<9);
num48MHK = find(KaxesMH>3 & KaxesMH<9);
num48K = length(num48PVK) + length(num48MHK);%number  4-8 scans apart K
num48PVF = find(FaxesPV>3 & FaxesPV<9);
num48MHF = find(FaxesMH>3 & FaxesMH<9);
num48F = length(num48PVF) + length(num48MHF);%number  4-8 scans apart F

num57PVK = find(KaxesPV>4 & KaxesPV<8);
num57MHK = find(KaxesMH>4 & KaxesMH<8);
num57K = length(num57PVK) + length(num57MHK);%number  5-7 scans apart K
num57PVF = find(FaxesPV>4 & FaxesPV<8);
num57MHF = find(FaxesMH>4 & FaxesMH<8);
num57F = length(num57PVF) + length(num57MHF);%number  5-7 scans apart F

[~,axKMxmnp, ciKMxmn,~] = ttest(KaxesMH,KaxesPV);
[~,axresMxmnp, ciresMxMn,~] = ttest(FaxesMH,FaxesPV);

[~,axKmxp,ciaxKmxp,~] = ttest(locKmxMH, locKmxPV);%DIFF IN MAX LOCATION K
[~,axKminp,ciaxKminp,~] = ttest(locKminMH, locKminPV);%min K
```

```
[~,axFmxp,ciaxFmxp,~] = ttest(locFmxMH, locFmxPV);% diff in max loc F
[~,axFminp,ciaxFminp,~] = ttest(locFminMH, locFminPV);%minF

%HERE!!!!!!!!!!!!!
%paired t test range K and residual pre v post
[~,RangeKMHprpopaiTT, ciRangepK,~] = ttest(MdiffKMH,MdiffKPV);
[~,RangerespropaiTT, ciRangepres,~] = ttest(MdiffresMH, MdiffresPV);

%size of difference in ranges, pre v post
rangediffK = mean(MdiffKPV,'omitnan')-mean(MdiffKMH,'omitnan');%diff in mean range
K
rangediffF = mean(MdiffresPV,'omitnan')-mean(MdiffresMH,'omitnan');%diff in mean
range res

meanKPV = mean(KallPV);%mean K Post op eyes
meanKMH = mean(KallMH);%mean K MH eyes
meanFTR30PV = mean(SUMFFTPV);%mean  FTR30 PVD
meanFTR30MH = mean(SUMFFTMH);%mean FTR30 no PVD
diffKpvnPV = meanKPV-meanKMH;%diff between means to go with CI
diffFpvnPV= meanFTR30PV - meanFTR30MH;% diff means to go with CI
sdKPV = std(KallPV);
sdKMH = std(KallMH);
sdFPV = std(SUMFFTPV);
sdFMH = std(SUMFFTMH);
[~,pttKPVnPV,KallCI,~] = ttest(KallPV,KallMH);%paired ttest compare  meanK pre op v
post op all Bscans
[~,pttFPVnPV, FallCI] = ttest(SUMFFTPV,SUMFFTMH);% tests compare F pre v post
%Cohens d of effect of PVD on K and F
dK = (meanKPV-meanKMH)/sqrt((sdKMH.^2 + sdKPV.^2)/2);%effect size of PVD on K
dF = (meanFTR30PV-meanFTR30MH)/sqrt((sdFMH.^2 + sdFPV.^2)/2);%effect size of PVD on
F

pMWUKPVnPV = ranksum(KallPV,KallMH);%MWU compare K PVD v noPVD
pMWUFPVnPV = ranksum(SUMFFTPV,SUMFFTMH);% MWU tests compare F PVD v no
tablen = length(MeanKMH);
AL0pvd = zeros(tablen,1);
ALpvd = zeros (tablen,1);%(KMH to make it same length
PVDnames = cell(tablen,1);
PVDnames(1:length(PVnames)) = PVnames;


%create table, add AL values manually after
PrevPostMHsum = table(MHnames', AL0pvd, MdiffKMH', MdiffresMH', MeanKMH', MeanFMH',
...
    PVDnames, ALpvd, MdiffKPV', MdiffresPV', MeanKPV', MeanFPV',...
    'VariableNames',{'preID','preAL','prerangeK','prerangeres'...
    'premeanK', 'premeanres','PostID','PostAL','PostrangeK','Postrangeres'...
    'PostmeanK', 'Postmeanres'});

%HERE!!!!!!!!!!!!!
%now compare mean K/res pre-op v post-op, paired t test
[~,meanKMHprpopaiTT, cimeanpK,~] = ttest(PrevPostMHsum.premeanK,
PrevPostMHsum.PostmeanK);
[~,meanrespropaiTT, cimeanpres,~] = ttest(PrevPostMHsum.premeanres,
PrevPostMHsum.Postmeanres);
diffMK = mean(PrevPostMHsum.premeanK, 'omitnan') -
mean(PrevPostMHsum.PostmeanK,'omitnan');%diffe pre v post K
diffMres = mean(PrevPostMHsum.premeanres,'omitnan')-
mean(PrevPostMHsum.Postmeanres,'omitnan');

%load no PVD data
load('/Users/stewartlake/Documents/MH contour/CSEHDR19data2.mat', 'PVDnoPVDsum');
%Here!!!!!!!!!!!!!
noPVDmeanrngK = mean(PVDnoPVDsum.noPVDrangeK(9:end));%mean range K, excl MH eyes
noPVDmeanrngres = mean(PVDnoPVDsum.noPVDrangeres(9:end));%mean range res
noPVDmeanK = mean(PVDnoPVDsum.noPVDmeanK(9:end));%mean K, excl MH eyes
noPVDmeanres = mean(PVDnoPVDsum.noPVDmeanres(9:end));%mean res
%noPVDrangeK = range(PVDnoPVDsum.noPVDrangeK(9:end));
%noPVDrangeres = range(PVDnoPVDsum.noPVDrangeres(9:end));
```

```
preopMHmeanrngK = mean(PrevPostMHsum.prerangeK);
preopMHmeanrngres = mean(PrevPostMHsum.prerangeres);

%ttests 2 range K & res, meanK & res, (mean & range K excl myopic MH,)for noPVD v
%pre op MH HERE!!!!!!!!!!
[~,noPVvMHkp,noPVvMHkci,~]=
ttest2(PVDnoPVDsum.noPVDrangeK(9:end),PrevPostMHsum.prerangeK);%range K
[~,noPVvMHrep,noPVvMHreci,~]=
ttest2(PVDnoPVDsum.noPVDrangeres(9:end),PrevPostMHsum.prerangeres);%range res
[~,noPVvMHkmeanp,noPVvMHkmeanci,~]=
ttest2(PVDnoPVDsum.noPVDmeanK(9:end),PrevPostMHsum.premeanK);%mean K
[~,noPVvMHkno19p,noPVvMHkno19ci,~]=
ttest2(PVDnoPVDsum.noPVDrangeK(9:end),PrevPostMHsum.prerangeK([1:3,5:end],:));
[~,noPVvMHkmeanno19p,noPVvMHkmeanno19ci,~]=
ttest2(PVDnoPVDsum.noPVDmeanK(9:end),PrevPostMHsum.premeanK([1:3,5:end],:));
[~,noPVvMHmnresp,
noPVvMHmnresci,~]=ttest2(PVDnoPVDsum.noPVDmeanres(9:end),PrevPostMHsum.premeanres);
%mean res
[~,noPVvMHmnrespno19,
noPVvMHmnrescino19,~]=ttest2(PVDnoPVDsum.noPVDmeanres(9:end),PrevPostMHsum.premeanr
es([1:3,5:end],:));%mean res

%added summary values - mean & SD, pre & post range & mean K & res
%Here!!!!!!!!!!!
mrngpreMHK=mean(PrevPostMHsum.prerangeK);
mrngpostMHK=mean(PrevPostMHsum.PostrangeK);
mrngpreMHres =mean(PrevPostMHsum.prerangeres);
mrngpostMHres =mean(PrevPostMHsum.Postrangeres);

meanpreMHK=mean(PrevPostMHsum.premeanK);
meanpostMHK=mean(PrevPostMHsum.PostmeanK);
meanpreMHres =mean(PrevPostMHsum.premeanres);
meanpreMHresno19 =mean(PrevPostMHsum.premeanres([1:3,5:end],:));
meanpostMHres =mean(PrevPostMHsum.Postmeanres);

sdrngpreMHK=std(PrevPostMHsum.prerangeK);
sdrngpostMHK=std(PrevPostMHsum.PostrangeK);
sdrngpreMHres =std(PrevPostMHsum.prerangeres);
sdrngpostMHres =std(PrevPostMHsum.Postrangeres);

sdmnpreMHK=std(PrevPostMHsum.premeanK);
sdmnpostMHK=std(PrevPostMHsum.PostmeanK);
sdmnpreMHres =std(PrevPostMHsum.premeanres);
sdmnpostMHres =std(PrevPostMHsum.Postmeanres);



save('/Users/stewartlake/Documents/MH contour/PreVpostPVD');

figure
hold on
scatter(PrevPostMHsum.prerangeK,PrevPostMHsum.PostrangeK,[],'r')
scatter(PrevPostMHsum.premeanK,PrevPostMHsum.PostmeanK,[],'m')
title('Pre v post PVD radial OCT mean and range K');
xlabel('pre-op');
ylabel('post-op');
refline(1,0);
legend('range K','mean K');
%text(MedKMH +dx2,MedFMH + dy2,MHID);

figure
hold on
scatter(PrevPostMHsum.prerangeres,PrevPostMHsum.Postrangeres,[],'b')
scatter(PrevPostMHsum.premeanres,PrevPostMHsum.Postmeanres,[],'c')
%text(MedKPV +dx2,MedFPV + dy2,PVID);
title('Pre v post PVD radial OCT mean and range irregularity');%FTI = FT of
irregularity
xlabel('pre-op');
ylabel('post-op');
refline(1,0);
```

```
legend('range res','mean res');


%{
%scatter plot variance of K and FFT,MH v PV, rotated K
dx=0.000001;%label displacement
dy=0.1;
figure
hold on
scatter(VarKMHRot,VarFMH,[],'r')
%text(VarKMH +dx,VarFMH + dy,MHID);
scatter(VarKPVRot, VarFPV,[],'b')
%text(VarKPV +dx,VarFPV + dy,PVID);
title('No PVD v PVD radial macula cube rotated K v FFT variance');
xlabel('Krot var');
ylabel('FFT var');
%}

%scatter plot variance of K and FFT,MH v PV
dx=0.000001;%label displacement
dy=0.1;
figure
hold on
scatter(VarKMH,VarFMH,[],'r')
%text(VarKMH +dx,VarFMH + dy,MHID);
scatter(VarKPV, VarFPV,[],'b')
%text(VarKPV +dx,VarFPV + dy,PVID);
title('Pre v post PVD radial macula K & FFT variance');
xlabel('K var');
ylabel('FFT var');

%scatter plot median K v FFT
figure
dx2=0.005;
dy2=0.1;
hold on
scatter(MedKMH,MedFMH,[],'r')
%text(MedKMH +dx2,MedFMH + dy2,MHID);
scatter(MedKPV, MedFPV,[],'b')
%text(MedKPV +dx2,MedFPV + dy2,PVID);
title('Pre v post PVD radial macula hole median K & FFT');
xlabel('K med');
ylabel('FFT med');

%scatter plot iqr K & FFT
figure
dx3=0.0001;
dy3=0.1;
hold on
scatter(IqrKMH,IqrFMH,[],'r')
%text(IqrKMH +dx3,IqrFMH + dy3,MHID);
scatter(IqrKPV, IqrFPV,[],'b')
%text(IqrKPV +dx3,IqrFPV + dy3,PVID);
title('Pre v post PVD radial macula iqr K & FFT');
xlabel('iqr K');
ylabel('iqr FFT');

%scatter plot K v FFT for all B scans
allBSfig = figure;
hold on
scatter(KallPV,SUMFFTPV,[],'r')
%text(MedKMH +dx2,MedFMH + dy2,MHID);
scatter(KallMH, SUMFFTMH,[],'b','+')
%text(MedKPV +dx2,MedFPV + dy2,PVID);
title('Pre- (blue) v post- PVD (red) radial macula B scan K and irregularity');
xlabel('K (/mm)');
ylabel('Irregularity (mm)');
%allBSfig.Visible = 'off';

%loads summary mn/rng/me/sd for PVD v NoPVD, prevpost PVD and Pre v post MH
```

```
load('/Users/stewartlake/Documents/MH contour/radial kImr table mnsd.mat');
Xid(7)={'.'};
Yk = cat(2,ymK,yrK);%mean K and range K
YI = cat(2,ymI,yrI);%mean I and range I
ERRk = cat(2,smK,srK);%?sd average K and SD range K
ERRI = cat(2,smI,srI);%?sd average I and range I
%above rows in order pvd v no pvd, pre v post pvd and pre v post mh
CoVK = ERRk./Yk;
CoVI = ERRI./YI;

%xK=[1:2:11;1.2:2:11.2]';
%xI=[0.5:2:10.5;0.7:2:10.7]';

xK=[1:6;8:13]';
xI=[15:20;22:27]';

EBcolor6=[0 0.4470 0.7410;0.3010 0.7450 0.9330;0.8500 0.3250 0.0980;...
0.9290 0.6940 0.1250;0.4940 0.1840 0.5560;0.6350 0.0780 0.1840];
Summns=figure;
for sm=1:6
yyaxis left
ee(1)=errorbar(xK(sm,1),Yk(sm,1),ERRk(sm,1),'vertical','s');%average K

hold on
ee(2)=errorbar(xK(sm,2),Yk(sm,2),ERRk(sm,2),'vertical','d');%range K
ylabel('Curvature');
yyaxis right
ee(3)=errorbar(xI(sm,1),YI(sm,1),ERRI(sm,1),'vertical','+');% average I
hold on
ee(4)=errorbar(xI(sm,2),YI(sm,2),ERRI(sm,2),'vertical','x');%range I
set(ee,'Color',EBcolor6(sm,:));
ylabel('Irregularity');
end



xticks([3.5 10.5 17.5 24.5]);
xticklabels({'average K','range K','average I','range I'});
title('Average (SD) and range (SD) of curvature and irregularity');
text(1.4,-0.075,'PVD','Color',[0 0.4470 0.7410]);
text(3.5,-0.075,'no PVD','Color',[0.3010 0.7450 0.9330]);
text(6.5,-0.075,'pre PVD','Color',[0.8500 0.3250 0.0980]);
text(10,-0.075,'post PVD','Color',[0.9290 0.6940 0.1250]);
text(1.4,-0.4,'pre MH','Color',[0.4940 0.1840 0.5560]);
text(4.5,-0.4,'post MH','Color',[0.6350 0.0780 0.1840]);

xline(7,':')
xline(14,'-')
xline(21,':')

%%
%plot error bars with 95% CI
%where x is the data vector
%CIFcn = @(xx,pp)prctile(xx,abs([0,100]-(100-pp)/2));% p = 95 for 95%
%see shape - macula hole & PVD v no PVD.doc
Yk = cat(2,ymK,yrK);%mean K and range K
YI = cat(2,ymI,yrI);%mean I and range I

%all above rows in order pvd v no pvd, pre v post pvd and pre v post mh

xK=[1:6;8:13]';
xI=[15:20;22:27]';

EBcolor6=[0 0.4470 0.7410;0.3010 0.7450 0.9330;0.8500 0.3250 0.0980;...
0.9290 0.6940 0.1250;0.4940 0.1840 0.5560;0.6350 0.0780 0.1840];
Summns=figure;
for sm=1:6
yyaxis left
ee(1)=errorbar(xK(sm,1),Yk(sm,1),Yk(sm,1)-meanK(sm,1),meanK(sm,2)-
Yk(sm,1),'vertical','s');%average K
```

```
hold on
ee(2)=errorbar(xK(sm,2),Yk(sm,2),Yk(sm,2)-rangeK(sm,1),rangeK(sm,2)-
Yk(sm,2),'vertical','d');%range K
ylabel('Curvature');
yyaxis right
ee(3)=errorbar(xI(sm,1),YI(sm,1),YI(sm,1)-meanI(sm,1),meanI(sm,2)-
YI(sm,1),'vertical','+');% average I
hold on
ee(4)=errorbar(xI(sm,2),YI(sm,2),YI(sm,2)-rangeI(sm,1),rangeI(sm,2)-
YI(sm,2),'vertical','x');%range I
set(ee,'Color',EBcolor6(sm,:));
ylabel('Irregularity');
end



xticks([3.5 10.5 17.5 24.5]);
xticklabels({'average K','range K','average I','range I'});
title('Average and range of curvature and irregularity (95% CI)');
text(26,14,'PVD','Color',[0 0.4470 0.7410]);
text(26,13,'no PVD','Color',[0.3010 0.7450 0.9330]);
text(26,12,'pre PVD','Color',[0.8500 0.3250 0.0980]);
text(26,11,'post PVD','Color',[0.9290 0.6940 0.1250]);
text(26,10,'pre MH','Color',[0.4940 0.1840 0.5560]);
text(26,9,'post MH','Color',[0.6350 0.0780 0.1840]);

xline(7,':')
xline(14,':')
xline(21,':')
```

3. Regdescr

```
%cross validate RD,PVD balanced in each fold, mm data
%equally distributed by AL. Plus FE
%
%Col 11 data to identify index of max/min for location
%for regional analysis of MaxE and its indices
%Normalised FFT moduli by length of retinal vector -
% FFTmm, saved in column 11 FFTconcat
%
%corrected for empty B scans
%FFTconcat, and AllIKurv loaded
%
%see RD compared to PVD 2.doc in /notes
%
%

%key indices are    RDID,RDSD,RDMx11,RDIndM,PVDID,PVDSD,PVDMx11,PVDIndM
%SD11 hols all anomaly values: n per fold x region x 21
% K values are not from column 11 so absent!!
%these are numbered 1-17 for the region of the eye (column in column 11)

load('/Users/stewartlake/Documents/MATLAB/FFTconcat');
load('/Users/stewartlake/Documents/MATLAB/AllIKurv');

NumPVD = size (PVDFb,1); % number of PVD eyes in array
NumRD = size (RDFb,1); % number of RD eyes

k = 5; %number of folds
%Nrow = 30; %no rows must = Veye (max number eyes per subset)
%Sumdiff11 = cell (Nrow,k);
%absdiff11 = cell (Nrow,k);
  SD11 = cell(k,1); %sumdiff by fold
  abs11 = cell(k,1);
  Grpdata = cell(k,1);
  Mxe11 = cell(k,1);
  IndMe11 = cell(k,1);
```

```
        RDID = cell(1,1);
        RDSD = cell(1,17);
        RDMx11 = cell(1,17);
        RDabs11 = cell(1,17);
        RDIndM = cell(1,17);
        PVDID = cell(1,1);
        PVDSD = cell(1,17);
        PVDMx11 = cell(1,17);
        PVDIndM = cell(1,17);
        PVDabs11 = cell(1,17);
        FEID = cell(1,1);
        FESD = cell(1,17);
        FEMx11 = cell(1,17);
        FEIndM = cell(1,17);
        FEabs11 = cell(1,17);
        nALPVD(1,:) = zeros(1,1);%new AL/age to match folded shaped data
        nAgePVD(1,:) =zeros(1,1);
        nALRD(1,:) = zeros(1,1);
        nAgeRD(1,:) = zeros(1,1);
        nALFE(1,:) = zeros(1,1);
        nAgeFE(1,:) = zeros(1,1);

meanBS = cell(5,1); %average b scan bin values for each fold

%get age and AL vector to match RDFb
AgevecRD = zeros(size(RDFb,1),1);
IDFblistRD = RDFb(:,1);%eye ID
ALvecRD = zeros(size(RDFb,1),1);
for findage=1:size(RDFb,1)
    sIde = str2double(IDFblistRD{findage,1}(2));

    AgevecRD(findage) = RDFb{findage,4}(3);
    ALvecRD(findage) = RDFb{findage,4}(sIde);

    RDcurrI11 = RDFb{findage,11};%replace empty regions with 30 x 21 NaN array
    for cellregionRD=2:18

    if isempty(RDcurrI11{1,cellregionRD})
        RDcurrI11{1,cellregionRD} = NaN(30,21);%replace empty regions with NaN
    end

    end
    RDFb{findage,11} = RDcurrI11(2:18);%and removes eye ID from array
end

%get age and AL vector to match PVDFb
AgevecPVD = zeros(size(PVDFb,1),1);
IDFblistPVD = PVDFb(:,1);%eye ID
ALvecPVD = zeros(size(PVDFb,1),1);
for findage=1:size(PVDFb,1)
    sIde = str2double(IDFblistPVD{findage,1}(2));

    AgevecPVD(findage) = PVDFb{findage,4}(3);
    ALvecPVD(findage) = PVDFb{findage,4}(sIde);

    PVDcurrI11 = PVDFb{findage,11};%replace empty regions with 30 x 21 NaN array
    for cellregionPVD=2:18

    if isempty(PVDcurrI11{1,cellregionPVD})
        PVDcurrI11{1,cellregionPVD} = NaN(30,21);
    end
    end
    PVDFb{findage,11} = PVDcurrI11(2:18);

end


%age and AL vec for FEFb
AgevecFE = zeros(size(FEFb,1),1);
```

```
IDFblistFE = FEFb(:,1);%eye ID
ALvecFE = zeros(size(FEFb,1),1);
for findage=1:size(FEFb,1)
    sIde = str2double(IDFblistFE{findage,1}(2));

    AgevecFE(findage) = FEFb{findage,4}(3);
    ALvecFE(findage) = FEFb{findage,4}(sIde);

    FEcurrI11 = FEFb{findage,11};%replace empty regions with 30 x 21 NaN array
    for cellregionFE=2:18

    if isempty(FEcurrI11{1,cellregionFE})
        FEcurrI11{1,cellregionFE} = NaN(30,21);
    end
    end
    FEFb{findage,11} = FEcurrI11(2:18);



end

%sort FEFb by AL
[sALvecFE,ALorderFE]=sort(ALvecFE);% ascending order of AL
sFEFb=FEFb(ALorderFE,:);
sAgevecFE = AgevecFE(ALorderFE,:);

sALvecFE(sALvecFE==0,:) = NaN;


%randomly distribute FE eyes
NumIpfoldFE = floor(size(sFEFb,1)/k);%number of eyes per k folds
RemFE=mod(size(sFEFb,1),k);%plus the remainder not divisible by k
RanselFE = zeros(k,NumIpfoldFE);
for Ranrun=1:NumIpfoldFE

    RanselFE(:,Ranrun) = randperm(k)';
end
RanremFE=randperm(RemFE)';
RanselFE = cat(1,RanselFE(:),RanremFE);%these are the indices to divide into folds



%sort RDFb by AL
[sALvecRD,ALorderRD]=sort(ALvecRD);% ascending order of AL
sRDFb=RDFb(ALorderRD,:);
sAgevecRD = AgevecRD(ALorderRD,:);
%sRDFb(sALvecRD==0,:) = [];%remove all eyes with no AL
%sAgevecRD(sALvecRD==0,:) = [];
sALvecRD(sALvecRD==0,:) = NaN;%keep "no AL" eyes

%sort PVDFb by AL
[sALvecPVD,ALorderPVD]=sort(ALvecPVD);% ascending order of AL
sPVDFb=PVDFb(ALorderPVD,:);
sAgevecPVD = AgevecPVD(ALorderPVD,:);
%sPVDFb(sALvecPVD==0,:) = [];%remove all eyes with no AL
%sAgevecPVD(sALvecPVD==0,:) = [];
sALvecPVD(sALvecPVD==0,:) = NaN;

%generate random distribution into 5 folds for RD
NumIpfoldRD = floor(size(sRDFb,1)/k);%number of eyes per k folds
RemRD=mod(size(sRDFb,1),k);%plus the remainder not divisible by k
RanselRD = zeros(k,NumIpfoldRD);
for Ranrun=1:NumIpfoldRD

    RanselRD(:,Ranrun) = randperm(k)';
end
RanremRD=randperm(RemRD)';
RanselRD = cat(1,RanselRD(:),RanremRD);%these are the indices to divide into folds

%generate random distribution into 5 folds for PVD
```

```
NumIpfoldPVD = floor(size(sPVDFb,1)/k);%number of eyes per k folds
RemPVD=mod(size(sPVDFb,1),k);%plus the remainder not divisible by k
RanselPVD = zeros(k,NumIpfoldPVD);
for Ranrun=1:NumIpfoldPVD

    RanselPVD(:,Ranrun) = randperm(k)';
end
RanremPVD=randperm(RemPVD)';
RanselPVD = cat(1,RanselPVD(:),RanremPVD);%these are the indices to divide into
folds


%create five subsets for cross validation
Grps11 = cell(k,1); %the '11'reflects the column where the data is stored
GrpIID11 = cell (k,1);
MnGrp11 = cell (k,1);
ColVec = cell (k,1);
ALvec = cell (k,1);
Agevec = cell (k,1);
Diag = cell (k,1);


for n = 1:k %data in 5 folds to calculate anomaly cf to 80% sample
  Grps11{n} =
[sPVDFb(RanselPVD==n,11);sRDFb(RanselRD==n,11);sFEFb(RanselFE==n,11)]; % puts each
subset coll 11 into a cell in Grps
  GrpIID11 {n} =
[sPVDFb(RanselPVD==n,1);sRDFb(RanselRD==n,1);sFEFb(RanselFE==n,1)]; %eye
identifiers of the validation set
  MnGrp11{n} = [sPVDFb(RanselPVD~=n,11);
sRDFb(RanselRD~=n,11);sFEFb(RanselFE~=n,11)]; % selects not subset n: the training
set for Grps(n)
  ALvec{n} = [sALvecPVD(RanselPVD==n);sALvecRD(RanselRD==n);sALvecFE(RanselFE==n)];
  Agevec{n} =
[sAgevecPVD(RanselPVD==n);sAgevecRD(RanselRD==n);sAgevecFE(RanselFE==n)];
  Diag{n} =
[repelem(1,nnz(RanselPVD==n),1);repelem(2,nnz(RanselRD==n),1);repelem(3,nnz(RanselF
E==n),1)];
  %create colour vector to match GrpIID8
  ColVec{n} = [repelem([0 0 1],nnz(RanselPVD==n),1);repelem([1 0
0],nnz(RanselRD==n),1)];


  %set for average scan creation (4/5 folds)
  TMnGrp11 = cat(2,MnGrp11{n}{:}); %note multiples by 4 (each eye counted 4 times)

  for Feyes = 1:length(TMnGrp11)

        Indcube = TMnGrp11{Feyes};
        Indcube(Indcube==0)=NaN;%replaces all 0 with NaN in FFT data
        TMnGrp11{Feyes} = Indcube;

  end

  TMnGrp11 = cat (2, TMnGrp11{:}); %concatenates all cubes from all eyes from
MnGrp{n}

  FoldMnBV11 =  var(TMnGrp11,0,2,'omitnan');%30 x 1 x X array, x=number of cubes
  TFMnBV11 = mean (FoldMnBV11,3,'omitnan');%30 x 1 mean fold bin Var

  TSbmn11 = nanmean (TMnGrp11,2); %creates bin mean B scan (all regional data)

  meanBS{n} = TSbmn11;%save average B scan bins

  %The number of eyes in this subset Grps(n)
  SzC11 = size (Grps11{n},1); % SzC = number of eyes in this subset
  Grpcubes = cell(SzC11,17);%recreate blank to avoid retaining longer array in
shorter fold

  for Grprun = 1:SzC11
```

```
    %collect fold region cubes in an array, one col per region, row per eye
    Grpcubes(Grprun,1:17) = Grps11{n}{Grprun};

  end

  absdiff11 = cell(SzC11,17);
  Sumdiff11 = cell(SzC11,17);
  MaxE11 = cell(SzC11,17);
  IndMaxe11 = cell(SzC11,17);


  for Metcal = 1:(SzC11*17)%work through entire array

      nowcube = Grpcubes {Metcal};%single region cube
      nowcube(nowcube==0) = NaN;
      Grpcubes{Metcal} = nowcube;

      absdiff11{Metcal} = abs(nowcube - TSbmn11);%each cell bins x B scans
      Sumdiff11 {Metcal} = sum(absdiff11{Metcal});% each cell 1 x 21
      [MaxE11{Metcal},IndMaxe11{Metcal}] = max(absdiff11{Metcal});%1 x 21

  end


  SD11{n} = Sumdiff11;%record data from each fold this holds all anomaly
  abs11{n} = absdiff11;
  Grpdata{n} = Grpcubes;
  Mxe11{n} = MaxE11;
  IndMe11{n} = IndMaxe11;


end

  for revert = 1:k %put data back to diagnosis arrays


      RDPVDeyes = cell2mat(Diag(revert));
      RDID = cat(1,RDID, GrpIID11{revert}(RDPVDeyes==2));
      RDSD = cat(1,RDSD, SD11{revert}(RDPVDeyes==2,:));
      RDMx11 = cat(1,RDMx11, Mxe11{revert}(RDPVDeyes==2,:));
      RDIndM = cat(1,RDIndM, IndMe11{revert}(RDPVDeyes==2,:));
      RDabs11 = cat(1,RDabs11,abs11{revert}(RDPVDeyes==2,:));
      nALRD = cat(1,nALRD,ALvec{revert}(RDPVDeyes==2,:));
      nAgeRD = cat(1,nAgeRD,Agevec{revert}(RDPVDeyes==2,:));

      PVDID = cat(1,PVDID, GrpIID11{revert}(RDPVDeyes==1));
      PVDSD = cat(1,PVDSD, SD11{revert}(RDPVDeyes==1,:));
      PVDMx11 = cat(1,PVDMx11, Mxe11{revert}(RDPVDeyes==1,:));
      PVDIndM = cat(1,PVDIndM, IndMe11{revert}(RDPVDeyes==1,:));
      PVDabs11 = cat(1,PVDabs11,abs11{revert}(RDPVDeyes==1,:));%eachbin by Bs by
cube
      nALPVD = cat(1,nALPVD,ALvec{revert}(RDPVDeyes==1,:));
      nAgePVD = cat(1,nAgePVD,Agevec{revert}(RDPVDeyes==1,:));

      FEID = cat(1,FEID, GrpIID11{revert}(RDPVDeyes==3));
      FESD = cat(1,FESD, SD11{revert}(RDPVDeyes==3,:));
      FEMx11 = cat(1,FEMx11, Mxe11{revert}(RDPVDeyes==3,:));
      FEIndM = cat(1,FEIndM, IndMe11{revert}(RDPVDeyes==3,:));
      FEabs11 = cat(1,FEabs11,abs11{revert}(RDPVDeyes==3,:));
      nALFE = cat(1,nALFE,ALvec{revert}(RDPVDeyes==3,:));
      nAgeFE = cat(1,nAgeFE,Agevec{revert}(RDPVDeyes==3,:));

  end

      RDID(1) = [];%remove (empty) initiating cells of arrays
      RDSD(1,:) = [];
      RDMx11(1,:) = [];
      RDIndM(1,:) = [];
      RDabs11(1,:) = [];
      PVDID(1) = [];
```

```
      PVDSD(1,:) = [];
      PVDMx11(1,:) = [];
      PVDIndM(1,:) = [];
      PVDabs11(1,:) = [];
      FEID(1) = [];
      FESD(1,:) = [];
      FEMx11(1,:) = [];
      FEIndM(1,:) = [];
      FEabs11(1,:) = [];
      nALPVD(1,:) = [];
      nAgePVD(1,:) = [];
      nALRD(1,:) = [];
      nAgeRD(1,:) = [];
      nALFE(1,:) = [];
      nAgeFE(1,:) = [];


 for Thr = 1:10
   for Reg = 1:17


       Rbsall{Reg} = [BSreg{:,Reg}]';%all BS for each region
       rbs = Rbsall{Reg};
       rbs(isnan(rbs)|rbs==0) = [];
       Numgt(Reg,Thr) = nnz(find(rbs>Thr));
       Frgt(Reg,Thr) = Numgt(Reg,Thr)/length(rbs);% fraction Bs with anomaly gt 5


   end
   allrBS = [Rbsall{:}];
   allrBS(isnan(allrBS)|allrBS==0) = [];
   allgt(Thr) = nnz(find(allrBS>Thr));
   frallgt(Thr) = allgt(Thr)/numel(allrBS);%fraction all

 end



%histogram of MaxE indices, RD v PVD
h1 = histogram([RDIndM{:}],'FaceColor','r');
hold on
h2 = histogram([PVDIndM{:}],'FaceColor','b');
h1.Normalization = 'probability';
h2.Normalization = 'probability';
legend('RD','PVD')
title('Bin location MaxE');


 %subplot of maxE indices by region
 figure
for regions = 1:17
    h(regions) = subplot (6,3,regions);
    RDreg = RDIndM(:,regions);
    allRDinds = [RDreg{:}];
    PVDreg = PVDIndM(:,regions);
    allPVDinds = [PVDreg{:}];
    h1 = histogram(allRDinds,'FaceColor','r');
    hold on
    h2 = histogram(allPVDinds,'FaceColor','b');
    h1.Normalization = 'probability';
    h2.Normalization = 'probability';
    str  = ['Region',num2str(regions)];
    text(6,0.6,str);

end

linkaxes(h(:),'xy');
 h(2).XLim = [0,8];
```

```
%histogram for Indices Maxe including only B scans with SD >= 5
figure
RDsdv = [RDSD{:}]';
RDindV = [RDIndM{:}]';
RDindV(RDsdv<5)=NaN;
numRDbs = sum(~isnan(RDindV));

PVDsdv = [PVDSD{:}]';
PVDindV = [PVDIndM{:}]';
PVDindV(PVDsdv<5)=NaN;
numPVDbs = sum(~isnan(PVDindV));

h1 = histogram(RDindV,'FaceColor','r');
hold on
h2 = histogram(PVDindV,'FaceColor','b');
h1.Normalization = 'probability';
h2.Normalization = 'probability';
legend(sprintf('RD sd >= 5, n = %d',numRDbs),sprintf('PVD sd >= 5, n = %d',
numPVDbs))

%total no real B scans, RD & PVD
numrealRDbs = sum(~isnan(RDsdv));
numrealPVDbs = sum(~isnan(PVDsdv));


%histogram for Indices Maxe including only B scans with maxe > 0.55
figure
RDmxev = [RDMx11{:}]';%vector of MaxE table
RDindmxV = [RDIndM{:}]';%vector INdices of MaxE
RDindmxV(RDmxev<0.55)=NaN;%make all indices of MaxE < 0.55 NaN
numRDbsmx = sum(~isnan(RDindmxV));%count number B scans left

PVDmxev = [PVDMx11{:}]';
PVDindmxV = [PVDIndM{:}]';
PVDindmxV(PVDmxev<0.55)=NaN;
numPVDbsmx = sum(~isnan(PVDindmxV));

%histogram([RDmxev',PVDmxev']);%used to identify MaxE distribution

h1 = histogram(RDindmxV,'FaceColor','r');
hold on
h2 = histogram(PVDindmxV,'FaceColor','b');
h1.Normalization = 'probability';
h2.Normalization = 'probability';
legend(sprintf('RD mxE >= 0.55, n = %d', numRDbsmx),sprintf('PVD mxE >= 0.55, n =
%d', numPVDbsmx))
```

4. Regdescre3D

```
%create 3D double of metric arrays. Uses data created by Regdescr and converts
%arrays to doubles: row = eyes, columns = regions (17), z = B scans (21)
%for each region

%set limits for filtering variables
Sdlim = 5;
Mxlim = 0.55;

%RD
for yy=1:(size(RDSD,1))

    for xx = 1:17
```

```
    RD3dSD(yy,xx,1:21) = RDSD{yy,xx};
    RD3dMxe(yy,xx,1:21) = RDMx11{yy,xx};
    RD3dInd(yy,xx,1:21) = RDIndM{yy,xx};

    end
end

%PVD
for yyp=1:(size(PVDSD,1))

    for xxp = 1:17

    PVD3dSD(yyp,xxp,1:21) = PVDSD{yyp,xxp};%eye x region x B scan
    PVD3dMxe(yyp,xxp,1:21) = PVDMx11{yyp,xxp};
    PVD3dInd(yyp,xxp,1:21) = PVDIndM{yyp,xxp};

    end
end

%%
%data metrics
%find number retinal B scans in each double.
numRDBscan = sum(~isnan(RD3dInd),3);
numPVDBscan = sum(~isnan(PVD3dInd),3);

numRDBSreg = sum(~isnan(RD3dInd),[1 3]);%no Bscans by region, RD
numPVDBSreg = sum(~isnan(PVD3dInd),[1 3]);
numRDPVDBSreg = numRDBSreg + numPVDBSreg;
%%
%find elements with larger values of SD AND MaxE
IndRDsd5mx55 = RD3dInd;
IndPVDsd5mx55 = PVD3dInd;
IndRDsd5mx55(RD3dSD<Sdlim | RD3dMxe<Mxlim)=NaN;%indices double for large SD/MxE
IndPVDsd5mx55(PVD3dSD<Sdlim | PVD3dMxe<Mxlim)=NaN;

IndRDsd5 = RD3dInd;
IndPVDsd5 = PVD3dInd;
IndRDsd5(RD3dSD<Sdlim)=NaN;%indices double for large SD
IndPVDsd5(PVD3dSD<Sdlim)=NaN;

RDlargeMxe = RD3dMxe;
PVDlargeMxe = PVD3dMxe;
RDlargeMxe(RD3dSD<Sdlim | RD3dMxe<Mxlim)=NaN;%Larger MxE/SD MaxE elements
PVDlargeMxe(PVD3dSD<Sdlim | PVD3dMxe<Mxlim)=NaN;

%numbers of large sd/MxE by region and by eye
EyesumRD = sum(~isnan(IndRDsd5mx55),[2 3],'omitnan');%number largeSD/MxE by eye
EyesumPVD = sum(~isnan(IndPVDsd5mx55),[2 3],'omitnan');
regionsumRD = sum(~isnan(IndRDsd5mx55),[1 3],'omitnan');%number largeSD/MxE by
region
regionsumPVD = sum(~isnan(IndPVDsd5mx55),[1 3],'omitnan');%

regionsumRD5 = sum(~isnan(IndRDsd5),[1 3],'omitnan');%number Bscans largeSD by
region
regionsumPVD5 = sum(~isnan(IndPVDsd5),[1 3],'omitnan');%

regionsumPVDRD5 = regionsumPVD5 + regionsumRD5;
PCPBDRDbs5reg = (regionsumPVDRD5*100)./numRDPVDBSreg; % %bscan each region gtr
Sdlim

PVDpcBsGT5 = regionsumPVD5/numPVDBSreg;%PVD Bs > sdlim
RDpcBsGT5 = regionsumRD5/numRDBSreg; %RD Bs > sdlim

EyeregsumRD = sum(~isnan(IndRDsd5mx55), 3,'omitnan');%table eye x region outliers
EyeregsumPVD = sum(~isnan(IndPVDsd5mx55), 3,'omitnan');%total numbers not indices

%need to account 4 denominator (no B Sc) - numRDBscan, numPVDBscan
propRDlarge = EyeregsumRD ./ numRDBscan;% must all be 0-1
propPVDlarge = EyeregsumPVD ./ numPVDBscan;%
```

```
propRDlarge(propRDlarge==0) = NaN;
propPVDlarge(propPVDlarge==0) = NaN;
rangeRDlgeprop  = range(propRDlarge); %range proportion large for each region
rangePVDlgeprop = range(propPVDlarge);


%rest of this is cardinal point (+ and X regions) analysis
xvec = [1:17];%scatter plot range of proportion of high MxE/SD by region by
diagnosis
scatter(xvec, rangeRDlgeprop, [], 'r');
hold on
scatter((xvec+0.1), rangePVDlgeprop, [], 'b');
legend('RD','PVD','Location', 'east')
text(14,0.7,['SD > ',num2str(Sdlim), ', MaxE > ',num2str(Mxlim)]);
xlabel('Region')

%%
%Use the above to plot in 3D: MaxE and its index, by region

EyeCRD = zeros(8,3,length(RDID));%sheet = eye, row = region, col = axis coordinate
x,y,z
EyeCPVD = zeros(8,3,length(PVDID));
Iird = zeros(length(RDID),17);
Iipvd = zeros(length(PVDID),17);

for nRD=1:length(RDID)

    %see tables in RD compared to PVD 2, each sheet matches those
    %RD, upright cross
    [EyeCRD(1,3,nRD),Iird(nRD,3)] = max(RDlargeMxe(nRD,3,:));%region col 3
    EyeCRD(1,2,nRD) = IndRDsd5mx55(nRD,3,Iird(nRD,3));

    [EyeCRD(3,3,nRD),Iird(nRD,7)] = max(RDlargeMxe(nRD,7,:));%region col 7
    EyeCRD(3,1,nRD) = -IndRDsd5mx55(nRD,7,Iird(nRD,7));

    [EyeCRD(5,3,nRD),Iird(nRD,11)] = max(RDlargeMxe(nRD,11,:));%region col 11
    EyeCRD(5,2,nRD) = -IndRDsd5mx55(nRD,11,Iird(nRD,11));

    [EyeCRD(7,3,nRD),Iird(nRD,15)] = max(RDlargeMxe(nRD,15,:));%region col 15
    EyeCRD(7,1,nRD) = IndRDsd5mx55(nRD,15,Iird(nRD,15));


    %RD, diagonal crosses/regions
    [EyeCRD(2,3,nRD),Iird(nRD,5)] = max(RDlargeMxe(nRD,5,:));%region col 5
    EyeCRD(2,2,nRD) = IndRDsd5mx55(nRD,5,Iird(nRD,5))*sqrt(2);
    EyeCRD(2,1,nRD) = -IndRDsd5mx55(nRD,5,Iird(nRD,5))*sqrt(2);

    [EyeCRD(4,3,nRD),Iird(nRD,9)] = max(RDlargeMxe(nRD,9,:));%region col 9
    EyeCRD(4,1,nRD) = -IndRDsd5mx55(nRD,9,Iird(nRD,9))*sqrt(2);
    EyeCRD(4,2,nRD) = -IndRDsd5mx55(nRD,9,Iird(nRD,9))*sqrt(2);

    [EyeCRD(6,3,nRD),Iird(nRD,13)] = max(RDlargeMxe(nRD,13,:));%region col 13
    EyeCRD(6,2,nRD) = -IndRDsd5mx55(nRD,13,Iird(nRD,13))*sqrt(2);
    EyeCRD(6,1,nRD) = IndRDsd5mx55(nRD,13,Iird(nRD,13))*sqrt(2);

    [EyeCRD(8,3,nRD),Iird(nRD,17)] = max(RDlargeMxe(nRD,17,:));%region col 17
    EyeCRD(8,1,nRD) = IndRDsd5mx55(nRD,17,Iird(nRD,17))*sqrt(2);
    EyeCRD(8,2,nRD) = IndRDsd5mx55(nRD,17,Iird(nRD,17))*sqrt(2);


end



for nPV=1:length(PVDID)

    %see tables in RD compared to PVD 2
    %PVD, upright cross
    [EyeCPVD(1,3,nPV),Iipvd(nPV,3)] = max(PVDlargeMxe(nPV,3,:));%region col 3
```

```
    EyeCPVD(1,2,nPV) = IndPVDsd5mx55(nPV,3,Iipvd(nPV,3));

    [EyeCPVD(3,3,nPV),Iipvd(nPV,7)] = max(PVDlargeMxe(nPV,7,:));%region col 7
    EyeCPVD(3,1,nPV) = -IndPVDsd5mx55(nPV,7,Iipvd(nPV,7));

    [EyeCPVD(5,3,nPV),Iipvd(nPV,11)] = max(PVDlargeMxe(nPV,11,:));%region col 11
    EyeCPVD(5,2,nPV) = -IndPVDsd5mx55(nPV,11,Iipvd(nPV,11));

    [EyeCPVD(7,3,nPV),Iipvd(nPV,15)] = max(PVDlargeMxe(nPV,15,:));%region col 15
    EyeCPVD(7,1,nPV) = IndPVDsd5mx55(nPV,15,Iipvd(nPV,15));



    %PVD, diagonal crosses/regions
    [EyeCPVD(2,3,nPV),Iipvd(nPV,5)] = max(PVDlargeMxe(nPV,5,:));%region col 5
    EyeCPVD(2,2,nPV) = IndPVDsd5mx55(nPV,5,Iipvd(nPV,5))*sqrt(2);
    EyeCPVD(2,1,nPV) = -IndPVDsd5mx55(nPV,5,Iipvd(nPV,5))*sqrt(2);

    [EyeCPVD(4,3,nPV),Iipvd(nPV,9)] = max(PVDlargeMxe(nPV,9,:));%region col 9
    EyeCPVD(4,1,nPV) = -IndPVDsd5mx55(nPV,9,Iipvd(nPV,9))*sqrt(2);
    EyeCPVD(4,2,nPV) = -IndPVDsd5mx55(nPV,9,Iipvd(nPV,9))*sqrt(2);

    [EyeCPVD(6,3,nPV),Iipvd(nPV,13)] = max(PVDlargeMxe(nPV,13,:));%region col 13
    EyeCPVD(6,2,nPV) = -IndPVDsd5mx55(nPV,13,Iipvd(nPV,13))*sqrt(2);
    EyeCPVD(6,1,nPV) = IndPVDsd5mx55(nPV,13,Iipvd(nPV,13))*sqrt(2);

    [EyeCPVD(8,3,nPV),Iipvd(nPV,17)] = max(PVDlargeMxe(nPV,17,:));%region col 17
    EyeCPVD(8,1,nPV) = IndPVDsd5mx55(nPV,17,Iipvd(nPV,17));
    EyeCPVD(8,2,nPV) = IndPVDsd5mx55(nPV,17,Iipvd(nPV,17));


end


%%
%{
%Use the doubles of ALL data (not just the larger values) to plot in 3D:
%MaxE and its index, by region

EyeCRDa = zeros(8,3,length(RDID));%sheet = eye, row = region, col = axis coordinate
x,y,z
EyeCPVDa = zeros(8,3,length(PVDID));
Iirda = zeros(length(RDID),17);
Iipvda = zeros(length(PVDID),17);
PVDk3 = cell(length(PVDID),1);
PVDvol3 = zeros(length(PVDID),1);
RDk3 = cell(length(RDID),1);
RDvol3 = zeros(length(RDID),1);

for nRD=1:length(RDID)

    %see tables in RD compared to PVD 2, each sheet matches those
    %RD, upright cross
    [EyeCRDa(1,3,nRD),Iirda(nRD,3)] = max(RD3dMxe(nRD,3,:));%region col 3
    EyeCRDa(1,2,nRD) = RD3dInd(nRD,3,Iirda(nRD,3));

    [EyeCRDa(3,3,nRD),Iirda(nRD,7)] = max(RD3dMxe(nRD,7,:));%region col 7
    EyeCRDa(3,1,nRD) = -RD3dInd(nRD,7,Iirda(nRD,7));

    [EyeCRDa(5,3,nRD),Iirda(nRD,11)] = max(RD3dMxe(nRD,11,:));%region col 11
    EyeCRDa(5,2,nRD) = -RD3dInd(nRD,11,Iirda(nRD,11));

    [EyeCRDa(7,3,nRD),Iirda(nRD,15)] = max(RD3dMxe(nRD,15,:));%region col 15
    EyeCRDa(7,1,nRD) = RD3dInd(nRD,15,Iirda(nRD,15));


    %RD, diagonal crosses/regions
    [EyeCRDa(2,3,nRD),Iirda(nRD,5)] = max(RD3dMxe(nRD,5,:));%region col 5
    EyeCRDa(2,2,nRD) = RD3dInd(nRD,5,Iirda(nRD,5))*sqrt(2);
    EyeCRDa(2,1,nRD) = -RD3dInd(nRD,5,Iirda(nRD,5))*sqrt(2);
```

```
    [EyeCRDa(4,3,nRD),Iirda(nRD,9)] = max(RD3dMxe(nRD,9,:));%region col 9
    EyeCRDa(4,1,nRD) = -RD3dInd(nRD,9,Iirda(nRD,9))*sqrt(2);
    EyeCRDa(4,2,nRD) = -RD3dInd(nRD,9,Iirda(nRD,9))*sqrt(2);

    [EyeCRDa(6,3,nRD),Iirda(nRD,13)] = max(RD3dMxe(nRD,13,:));%region col 13
    EyeCRDa(6,2,nRD) = -RD3dInd(nRD,13,Iirda(nRD,13))*sqrt(2);
    EyeCRDa(6,1,nRD) = RD3dInd(nRD,13,Iirda(nRD,13))*sqrt(2);

    [EyeCRDa(8,3,nRD),Iirda(nRD,17)] = max(RD3dMxe(nRD,17,:));%region col 17
    EyeCRDa(8,1,nRD) = RD3dInd(nRD,17,Iirda(nRD,17))*sqrt(2);
    EyeCRDa(8,2,nRD) = RD3dInd(nRD,17,Iirda(nRD,17))*sqrt(2);

    if ~any(isnan(EyeCRDa(:,:,nRD)))
    [RDk3{nRD},RDvol3(nRD)]=
convhull(EyeCRDa(:,1,nRD),EyeCRDa(:,2,nRD),EyeCRDa(:,3,nRD));
    %RDvol3 is the convex hull volume enclosed by the coordinates for eye nRD
    [RDk2xv{nRD},RDvol2xv(nRD)]= convhull(abs(EyeCRDa([1 3 5 7],1,nRD)+EyeCRDa([1 3
5 7],2,nRD)),EyeCRDa([1 3 5 7],3,nRD));
    %RDvol2xv area enclosed by vertical cross regions
    [RDk2xd{nRD},RDvol2xd(nRD)]= convhull(abs(EyeCRDa([2 4 6 8],1,nRD)),EyeCRDa([2
4 6 8],3,nRD));
    %RDvol2xd area enclosed by diagonal cross regions
    end


end



for nPV=1:length(PVDID)

    %see tables in RD compared to PVD 2
    %PVD, upright cross
    [EyeCPVDa(1,3,nPV),Iipvda(nPV,3)] = max(PVD3dMxe(nPV,3,:));%region col 3
    EyeCPVDa(1,2,nPV) = PVD3dInd(nPV,3,Iipvda(nPV,3));

    [EyeCPVDa(3,3,nPV),Iipvda(nPV,7)] = max(PVD3dMxe(nPV,7,:));%region col 7
    EyeCPVDa(3,1,nPV) = -PVD3dInd(nPV,7,Iipvda(nPV,7));

    [EyeCPVDa(5,3,nPV),Iipvda(nPV,11)] = max(PVD3dMxe(nPV,11,:));%region col 11
    EyeCPVDa(5,2,nPV) = -PVD3dInd(nPV,11,Iipvda(nPV,11));

    [EyeCPVDa(7,3,nPV),Iipvda(nPV,15)] = max(PVD3dMxe(nPV,15,:));%region col 15
    EyeCPVDa(7,1,nPV) = PVD3dInd(nPV,15,Iipvda(nPV,15));



    %PVD, diagonal crosses/regions
    [EyeCPVDa(2,3,nPV),Iipvda(nPV,5)] = max(PVD3dMxe(nPV,5,:));%region col 5
    EyeCPVDa(2,2,nPV) = PVD3dInd(nPV,5,Iipvda(nPV,5))*sqrt(2);
    EyeCPVDa(2,1,nPV) = -PVD3dInd(nPV,5,Iipvda(nPV,5))*sqrt(2);

    [EyeCPVDa(4,3,nPV),Iipvda(nPV,9)] = max(PVD3dMxe(nPV,9,:));%region col 9
    EyeCPVDa(4,1,nPV) = -PVD3dInd(nPV,9,Iipvda(nPV,9))*sqrt(2);
    EyeCPVDa(4,2,nPV) = -PVD3dInd(nPV,9,Iipvda(nPV,9))*sqrt(2);

    [EyeCPVDa(6,3,nPV),Iipvda(nPV,13)] = max(PVD3dMxe(nPV,13,:));%region col 13
    EyeCPVDa(6,2,nPV) = -PVD3dInd(nPV,13,Iipvda(nPV,13))*sqrt(2);
    EyeCPVDa(6,1,nPV) = PVD3dInd(nPV,13,Iipvda(nPV,13))*sqrt(2);

    [EyeCPVDa(8,3,nPV),Iipvda(nPV,17)] = max(PVD3dMxe(nPV,17,:));%region col 17
    EyeCPVDa(8,1,nPV) = PVD3dInd(nPV,17,Iipvda(nPV,17));
    EyeCPVDa(8,2,nPV) = PVD3dInd(nPV,17,Iipvda(nPV,17));


    if ~any(isnan(EyeCPVDa(:,:,nPV)))
    [PVDk3{nPV},PVDvol3(nPV)]=
convhull(EyeCPVDa(:,1,nPV),EyeCPVDa(:,2,nPV),EyeCPVDa(:,3,nPV));
    %PVDvol3 is the convex hull enclosed by the coordinates for eye nPV
```

```
    [PVDk2xv{nPV},PVDvol2xv(nPV)]= convhull(abs(EyeCPVDa([1 3 5
7],1,nPV)+EyeCPVDa([1 3 5 7],2,nPV)),EyeCPVDa([1 3 5 7],3,nPV));
    %PVDvol2xv area enclosed by vertical cross regions
    [PVDk2xd{nPV},PVDvol2xd(nPV)]= convhull(abs(EyeCPVDa([2 4 6
8],1,nPV)),EyeCPVDa([2 4 6 8],3,nPV));
    %PVDvol2xd area enclosed by diagonal cross regions
    end



end



%plot distribution of these values by eye
for showIp = 1:16

    subplot(4,4,showIp)
    scatter(EyeCPVDa([2 4 6 8],1,showIp),EyeCPVDa([2 4 6 8],3,showIp).*EyeCPVDa([2
4 6 8],2,showIp)./abs(EyeCPVDa([2 4 6 8],2,showIp)),'b')
    view(0,0)
    %xlim([-20 10])
    %ylim([-10 20])
    %zlim([0 5])
end

figure
for showIr = 1:16

    subplot(4,4,showIr)
    scatter(EyeCRDa([2 4 6 8],1,showIr),EyeCRDa([2 4 6 8],3,showIr).*EyeCRDa([2 4 6
8],2,showIr)./EyeCRDa([2 4 6 8],2,showIr),'r')
    view(0,0)
    %xlim([-20 10])
    %ylim([-10 20])
    %zlim([0 5])
end


%plot RDvol/PVDvol (the volume enclosed by these 3D points convex hull)
xRD = 1:length(RDID);
xPV = 1:length(PVDID);

figure
scatter(RDvol2xv,RDvol2xd,'r');
hold on
scatter(PVDvol2xv,PVDvol2xd,'b');
%}
%%
%new method to
%determine values of vertical and diagonal regions (maxE & Index)
%for a simple four quandrant distribution of metrics
xVc = [3 7 11 15];%columns for vertical cross
xDc = [5 9 13 17];%diagonal cross

for regcol = 1:4

for nRD = 1:length(RDID)
    %MaxE value, RD, vertical cross, row per eye, col = region
[IRDcMvalV(nRD,regcol), IndIRDcV(nRD,regcol)] = max(RD3dMxe(nRD,xVc(regcol),:));
% index for maxE value
IRDcMindV(nRD,regcol) = RD3dInd(nRD,xVc(regcol),IndIRDcV(nRD,regcol));

[IRDcMvalD(nRD,regcol), IndIRDcD(nRD,regcol)] = max(RD3dMxe(nRD,xDc(regcol),:));
IRDcMindD(nRD,regcol) = RD3dInd(nRD,xDc(regcol),IndIRDcD(nRD,regcol));
end

%
for nPV = 1:length(PVDID)
```

```
[IPVDcMvalV(nPV,regcol), IndIPVDcV(nPV,regcol)] = max(PVD3dMxe(nPV,xVc(regcol),:));
IPVDcMindV(nPV,regcol) = PVD3dInd(nPV,xVc(regcol),IndIPVDcV(nPV,regcol));

[IPVDcMvalD(nPV,regcol), IndIPVDcD(nPV,regcol)] = max(PVD3dMxe(nPV,xDc(regcol),:));
IPVDcMindD(nPV,regcol) = PVD3dInd(nPV,xDc(regcol),IndIPVDcD(nPV,regcol));
end

end


%distribute to quadrants:
%vertical cross
IRDcMvalV(:,1:2) = - IRDcMvalV(:,1:2);%MaxE value
IRDcMindV(:,2:3) = - IRDcMindV(:,2:3);%MaxE index
IPVDcMvalV(:,1:2) = - IPVDcMvalV(:,1:2);
IPVDcMindV(:,2:3) = - IPVDcMindV(:,2:3);

%polar coords, vertical cross
[thRDV, RhoRDV] = cart2pol(IRDcMvalV,IRDcMindV);%polar coords RD vert cross
[thPVDV,RhoPVDV] = cart2pol(IPVDcMvalV,IPVDcMindV);

polRD = complex(RhoRDV, thRDV);%polar coords as complex number
polPVD = complex(RhoPVDV, thPVDV);%still row = eye, col = region



%diagonal cross
IRDcMvalD(:,1:2) = - IRDcMvalD(:,1:2);
IRDcMindD(:,2:3) = - IRDcMindD(:,2:3);
IPVDcMvalD(:,1:2) = - IPVDcMvalD(:,1:2);
IPVDcMindD(:,2:3) = - IPVDcMindD(:,2:3);


figure

for showIr = 1:16

    subplot(4,4,showIr)
    scatter(IRDcMvalV(showIr+16,:),IRDcMindV(showIr+16,:),'r')

    xlim([-4 4])
    ylim([-10 10])
    %zlim([0 5])
end

figure
for showIp = 1:16

    subplot(4,4,showIp)
    scatter(IPVDcMvalV(showIp+16,:),IPVDcMindV(showIp+16,:),'b')

    xlim([-4 4])
    ylim([-10 10])
    %zlim([0 5])
end


%create DA models from polar coordinates - vertical cross
DiagRD = ones(length(polRD),1);%RD = 1
DiagPVD = zeros(length(polPVD),1);%PVD = 0
Diagall = cat(1, DiagRD, DiagPVD);
allpol = cat(1, polRD, polPVD);
%NEED MATCHING AL:
AllAL = cat(1,nALRD,nALPVD);

%create random selection: 75/25
Split = cvpartition(size(allpol,1),'HoldOut', 0.25);
SplitID = Split.test;

Trainset = allpol(~SplitID,:);
```

```
Testset = allpol(SplitID,:);
TrsetD = Diagall(~SplitID,:);%training set label
TesetD = Diagall(SplitID,:);%test set label
TrsetAL = AllAL(~SplitID,:);
TesetAL = AllAL(SplitID,:);

Trainset = cat(2, Trainset,TrsetAL);%makes col5 = AL
Testset = cat(2, Testset, TesetAL);

for Ln = 1:size(Trainset,2) %single variable models to find best results
    %this examines use of 4 quadrant MaxE/Ind utility, and AL

    sinquadmod{Ln} = fitcdiscr(Trainset(:,Ln),TrsetD,'DiscrimType','quadratic');
    %determine single variable (quadrant) ability

    Trsetdistr{Ln} = confusionmat(sinquadmod{Ln}.Y,resubPredict(sinquadmod{Ln}));

    SCSTrset{Ln} = (Trsetdistr{Ln}(1)+Trsetdistr{Ln}(4))/sum(Trsetdistr{Ln}(1:4));
    %success rate of training set allocation:

    valres{Ln} = predict(sinquadmod{Ln},Testset(:,Ln));
    %test set prediction

    RDscs{Ln} = nnz(valres{Ln}==1 & TesetD==1);%RD labels correct
    PVDfl{Ln} = nnz(valres{Ln}==1 & TesetD==0);%PVD incorrect

end

%try 5 variable model
quad5mdl = fitcdiscr(Trainset,TrsetD,'DiscrimType','quadratic');
quad5mdldistr = confusionmat(quad5mdl.Y,resubPredict(quad5mdl));
val5res = predict(quad5mdl,Testset);
RDscs5 = nnz(val5res==1 & TesetD==1);%RD labels correct
PVDfl5 = nnz(val5res==1 & TesetD==0);%PVD incorrect

%then 5 variables with adjusted known prior
quad5mdl.Prior = [50 1];
val5resP50 = predict(quad5mdl,Testset);
RDscs5P50 = nnz(val5resP50==1 & TesetD==1);%RD labels correct
PVDfl5P50 = nnz(val5resP50==1 & TesetD==0);%PVD incorrect

quad5mdl.Prior = [20 1];
val5resP20 = predict(quad5mdl,Testset);
RDscs5P20 = nnz(val5resP20==1 & TesetD==1);%RD labels correct
PVDfl5P20 = nnz(val5resP20==1 & TesetD==0);%PVD incorrect

quad5mdl.Prior = [6 1];
val5resP6 = predict(quad5mdl,Testset);
RDscs5P6 = nnz(val5resP6==1 & TesetD==1);%RD labels correct
PVDfl5P6 = nnz(val5resP6==1 & TesetD==0);%PVD incorrect


%%
%combine the most successful single regions from both vertical and diagonal
%crosses: SN, S, IN, I.

%vert cols 1 & 3

%Diag cols 3 & 4

NasregsVRD = cat(2,IRDcMvalV(:,[1 3]),IRDcMvalD(:,[3 4]));
NasregsIRD = cat(2,IRDcMindV(:,[1 3]),IRDcMindD(:,[3 4]));

NasregsVPVD = cat(2,IPVDcMvalV(:,[1 3]),IPVDcMvalD(:,[3 4]));
NasregsIPVD = cat(2,IPVDcMindV(:,[1 3]),IPVDcMindD(:,[3 4]));

[thRDn, RhoRDn] = cart2pol(NasregsVRD,NasregsIRD);%polar coords RD vert cross
[thPVDn,RhoPVDn] = cart2pol(NasregsVPVD,NasregsIPVD);

polRDn = complex(RhoRDn, thRDn);%polar coords as complex number
```

```
polPVDn = complex(RhoPVDn, thPVDn);%still row = eye, col = region

%create DA models from polar coordinates - vertical cross
DiagRDn = ones(length(polRDn),1);%RD = 1
DiagPVDn = zeros(length(polPVDn),1);%PVD = 0
Diagalln = cat(1, DiagRDn, DiagPVDn);
allpoln = cat(1, polRDn, polPVDn);
%NEED MATCHING AL:
AllALn = cat(1,nALRD,nALPVD);

%create random selection: 75/25
Splitn = cvpartition(size(allpoln,1),'HoldOut', 0.25);
SplitIDn = Splitn.test;

Trainsetn = allpoln(~SplitIDn,:);
Testsetn = allpoln(SplitIDn,:);
TrsetDn = Diagalln(~SplitIDn,:);%training set label
TesetDn = Diagalln(SplitIDn,:);%test set label
TrsetALn = AllALn(~SplitIDn,:);
TesetALn = AllALn(SplitIDn,:);

Trainsetn = cat(2, Trainsetn,TrsetALn);%makes col5 = AL
Testsetn = cat(2, Testsetn, TesetALn);

for Lnn = 1:size(Trainsetn,2) %single variable models to find best results
    %this examines use of 4 quadrant MaxE/Ind utility, and AL

    sinquadmodn{Lnn} =
fitcdiscr(Trainsetn(:,Lnn),TrsetDn,'DiscrimType','quadratic');
    %determine single variable (quadrant) ability

    Trsetdistrn{Lnn} =
confusionmat(sinquadmodn{Lnn}.Y,resubPredict(sinquadmodn{Lnn}));

    SCSTrsetn{Lnn} =
(Trsetdistrn{Lnn}(1)+Trsetdistrn{Lnn}(4))/sum(Trsetdistrn{Lnn}(1:4));
    %success rate of training set allocation:

    valresn{Lnn} = predict(sinquadmodn{Lnn},Testsetn(:,Lnn));
    %test set prediction

    RDscsn{Lnn} = nnz(valresn{Lnn}==1 & TesetDn==1);%RD labels correct
    PVDfln{Lnn} = nnz(valresn{Lnn}==1 & TesetDn==0);%PVD incorrect

end

%try 5 variable model
quad5mdln = fitcdiscr(Trainsetn,TrsetDn,'DiscrimType','quadratic');
quad5mdldistrn = confusionmat(quad5mdln.Y,resubPredict(quad5mdln));
val5resn = predict(quad5mdln,Testsetn);
RDscs5n = nnz(val5resn==1 & TesetDn==1);%RD labels correct
PVDfl5n = nnz(val5resn==1 & TesetDn==0);%PVD incorrect

%then 5 variables with adjusted known prior
quad5mdln.Prior = [50 1];
val5resP50n = predict(quad5mdln,Testsetn);
RDscs5P50n = nnz(val5resP50n==1 & TesetDn==1);%RD labels correct
PVDfl5P50n = nnz(val5resP50n==1 & TesetDn==0);%PVD incorrect

quad5mdln.Prior = [20 1];
val5resP20n = predict(quad5mdln,Testsetn);
RDscs5P20n = nnz(val5resP20n==1 & TesetDn==1);%RD labels correct
PVDfl5P20n = nnz(val5resP20n==1 & TesetDn==0);%PVD incorrect

quad5mdln.Prior = [6 1];
val5resP6n = predict(quad5mdln,Testsetn);
RDscs5P6n = nnz(val5resP6n==1 & TesetDn==1);%RD labels correct
PVDfl5P6n = nnz(val5resP6n==1 & TesetDn==0);%PVD incorrect
```

5. ClsXval

```
%cross validate a model - RD eyes
%CHANGE save file name to reflect modelled data (line 14) in final line
%CHANGE data in 14 and vectors in 17 to match 14
% Use data from XvalRDPVDbyALmm eg LDA/qdaRDPVDmetrV, with Diagv (diagnosis),
% to create a classifier.
% Randomly (AL stratified) split the data (and diagv) into 5 five folds.
% Run new model on 4 folds, predict on 5th fold.
% Compare predict results to the folds Diagv to score result.
% Calculate success rate for each fold.
% Standard deviation of success rates.
%runs validation set on whole classifier
%now runs 100 x to get multiple SDs etc

Clsdata = cat(2, ALvecv, RDPVDvars5noK(:,3:6));% the modelled data/observations
Clsdiag = Diagv;% labels for each eye/row
%final validation data
Valset = cat(2,valsetALvecv, valsetrms10maxv, valsetrms10minv,...
    valsetMaxe10maxv, valsetMaxe10minv);%concat matching features for line 12

FEset = cat(2,FEALvecv, FErms10maxv, FErms10minv,...
    FEMaxe10maxv, FEMaxe10minv);

k = 5; %number of folds
NumR=100; %number of iterations
SDCls = zeros(NumR,1);
rSDCls= zeros(NumR,1);
SDCls50 = zeros(NumR,1);
rSDCls50 = zeros(NumR,1);
SDCls20 = zeros(NumR,1);
rSDCls20= zeros(NumR,1);
SDCls6 = zeros(NumR,1);
rSDCls6= zeros(NumR,1);
SDCls75 = zeros(NumR,1);
rSDCls75= zeros(NumR,1);
SDClsC = zeros(20,NumR);
rSDClsC = zeros(20,NumR);
TSclassall = cell (NumR,1);
valsetlbls20 = cell (NumR,1);
valsetlbls6 = cell (NumR,1);
valsetlbls50 = cell (NumR,1);
valsetlbls75 = cell (NumR,1);
FElbls20 = cell (NumR,1);
FElbls6 = cell (NumR,1);
FElbls50 = cell (NumR,1);
FElbls75 = cell (NumR,1);
TSconmat = cell (NumR,1);
NumIpfold = zeros(NumR,1);
ValIfeat = cell (k,NumR);
ValIdiag = cell (k,NumR);
TSfeat = cell (k,NumR);
TSdiag = cell (k,NumR);
TSclass = cell(k,NumR);
VSdiag = cell(k,NumR);
Rtlbl = cell(k,NumR);
Wrglbl = cell(k,NumR);
PVDrt = cell(k,NumR);
RDrt = cell(k,NumR);
PVDwrg = cell(k,NumR);
RDwrg = cell(k,NumR);
Scsrate=zeros(k,NumR);
VSdiag50 = cell(k,NumR);
Rtlbl50 = cell(k,NumR);
Wrglbl50 = cell(k,NumR);
PVDrt50 = cell(k,NumR);
RDrt50 = cell(k,NumR);
PVDwrg50 = cell(k,NumR);
RDwrg50 = cell(k,NumR);
Scsrate50 = zeros(k,NumR);
```

```
VSdiag6 = cell(k,NumR);
Rtlbl6 = cell(k,NumR);
Wrglbl6 = cell(k,NumR);
PVDrt6 = cell(k,NumR);
RDrt6 = cell(k,NumR);
PVDwrg6 = cell(k,NumR);
RDwrg6 = cell(k,NumR);
Scsrate6 = zeros(k,NumR);
VSdiag20 = cell(k,NumR);
Rtlbl20 = cell(k,NumR);
Wrglbl20 = cell(k,NumR);
PVDrt20 = cell(k,NumR);
RDrt20 = cell(k,NumR);
PVDwrg20 = cell(k,NumR);
RDwrg20 = cell(k,NumR);
Scsrate20 = zeros(k,NumR);
VSdiag75 = cell(k,NumR);
Rtlbl75  = cell(k,NumR);
Wrglbl75 = cell(k,NumR);
PVDrt75 = cell(k,NumR);
RDrt75 = cell(k,NumR);
RDwrg75 = cell(k,NumR);
PVDwrg75 = cell(k,NumR);
Scsrate75 = zeros(k,NumR);
VSdiagC = cell (k,20,NumR);
RtlblC = cell (k,20,NumR);
WrglblC = cell (k,20,NumR);
PVDrtC = cell (k,20,NumR);
RDrtC = cell (k,20,NumR);
PVDwrgC = cell (k,20,NumR);
RDwrgC = cell (k,20,NumR);
ScsrateC = zeros (k,20,NumR);


%run 100 times
for Rpt=1:NumR

%the full classifier to run the validation set on
TSclassall{Rpt} = fitcdiscr(Clsdata,Clsdiag,'DiscrimType','quadratic');
TSconmat{Rpt}=confusionmat(TSclassall{Rpt}.Y, resubPredict(TSclassall{Rpt}));

%validation sets and FE predictions
valsetlblsvanilla{Rpt} = predict(TSclassall{Rpt},Valset);
FElblsvanilla{Rpt} = predict(TSclassall{Rpt},FEset);

TSclassall{Rpt}.Prior = [6 1];
valsetlbls6{Rpt} = predict(TSclassall{Rpt},Valset);
FElbls6{Rpt} = predict(TSclassall{Rpt},FEset);

TSclassall{Rpt}.Prior = [20 1];
valsetlbls20{Rpt} = predict(TSclassall{Rpt},Valset);
FElbls20{Rpt} = predict(TSclassall{Rpt},FEset);

TSclassall{Rpt}.Prior = [50 1];
valsetlbls50{Rpt} = predict(TSclassall{Rpt},Valset);
FElbls50{Rpt} = predict(TSclassall{Rpt},FEset);

TSclassall{Rpt}.Prior = [75 1];
valsetlbls75{Rpt} = predict(TSclassall{Rpt},Valset);
FElbls75{Rpt} = predict(TSclassall{Rpt},FEset);

TSclassall{Rpt}.Prior = [0.64 0.36];
valsetlblsOpti{Rpt} = predict(TSclassall{Rpt},Valset);
FElblsOpti{Rpt} = predict(TSclassall{Rpt},FEset);
%randomly allocate to 5 folds
%generate random distribution into 5 folds for RD SD etc

NumIpfold(Rpt) = floor(size(Clsdata,1)/k);%number of eyes per k folds
RemI=mod(size(Clsdata,1),k);%plus the remainder not divisible by k
RanselI = zeros(k,NumIpfold(Rpt));
```

```
for Ranrun=1:NumIpfold(Rpt)

    RanselI(:,Ranrun) = randperm(k)';
end
RanremI=randperm(RemI)';
RanselI = cat(1,RanselI(:),RanremI);%these are the indices to divide into folds

%now divide into k folds
%validating sets here are a fold of the training set
for n =1:k
    ValIfeat{n,Rpt} = Clsdata(RanselI==n,:);%validation set
    ValIdiag{n,Rpt} = Clsdiag(RanselI==n,:);
    TSfeat {n,Rpt} = Clsdata(RanselI~=n,:);%training set
    TSdiag {n,Rpt} = Clsdiag(RanselI~=n,:);

    %create classifier
    TSclass{n,Rpt} =
fitcdiscr(TSfeat{n,Rpt},TSdiag{n,Rpt},'DiscrimType','quadratic');

    %test classifier with validation set (= SINGLE FOLD)
    VSdiag{n,Rpt} = predict(TSclass{n,Rpt},ValIfeat{n,Rpt});

    %number right/wrong in validation set
    Rtlbl{n,Rpt} = nnz(VSdiag{n,Rpt}==ValIdiag{n,Rpt});
    Wrglbl{n,Rpt} = nnz(VSdiag{n,Rpt}~=ValIdiag{n,Rpt});

    %correct label by diagnosis
    PVDrt{n,Rpt}=nnz((ValIdiag{n,Rpt}==1)&(VSdiag{n,Rpt}==ValIdiag{n,Rpt}));
    RDrt{n,Rpt}=nnz((ValIdiag{n,Rpt}==2)&(VSdiag{n,Rpt}==ValIdiag{n,Rpt}));

    %incorrect label by diagnosis
    PVDwrg{n,Rpt}=nnz((ValIdiag{n,Rpt}==1)&(VSdiag{n,Rpt}~=ValIdiag{n,Rpt}));
    RDwrg{n,Rpt}=nnz((ValIdiag{n,Rpt}==2)&(VSdiag{n,Rpt}~=ValIdiag{n,Rpt}));

    Scsrate(n,Rpt) = Rtlbl{n,Rpt}/(Rtlbl{n,Rpt}+Wrglbl{n,Rpt});


    %next section NOT NEEDED (to line 264)
    %change prior probability
    TSclass{n,Rpt}.Prior = [50 1];

    %test classifier with validation set
    VSdiag50{n,Rpt} = predict(TSclass{n,Rpt},ValIfeat{n,Rpt});

    %number right/wrong in validation set
    Rtlbl50{n,Rpt} = nnz(VSdiag50{n,Rpt}==ValIdiag{n,Rpt});
    Wrglbl50{n,Rpt} = nnz(VSdiag50{n,Rpt}~=ValIdiag{n,Rpt});

    %correct label by diagnosis
    PVDrt50{n,Rpt}=nnz((ValIdiag{n,Rpt}==1)&(VSdiag50{n,Rpt}==ValIdiag{n,Rpt}));
    RDrt50{n,Rpt}=nnz((ValIdiag{n,Rpt}==2)&(VSdiag50{n,Rpt}==ValIdiag{n,Rpt}));

    %incorrect label by diagnosis
    PVDwrg50{n,Rpt}=nnz((ValIdiag{n,Rpt}==1)&(VSdiag50{n,Rpt}~=ValIdiag{n,Rpt}));
    RDwrg50{n,Rpt}=nnz((ValIdiag{n,Rpt}==2)&(VSdiag50{n,Rpt}~=ValIdiag{n,Rpt}));

    Scsrate50(n,Rpt) = Rtlbl50{n,Rpt}/(Rtlbl50{n,Rpt}+Wrglbl50{n,Rpt});


    %change prior probability
    TSclass{n,Rpt}.Prior = [6 1];

    %test classifier with validation set
    VSdiag6{n,Rpt} = predict(TSclass{n,Rpt},ValIfeat{n,Rpt});

    %number right/wrong in validation set
    Rtlbl6{n,Rpt} = nnz(VSdiag6{n,Rpt}==ValIdiag{n,Rpt});
    Wrglbl6{n,Rpt} = nnz(VSdiag6{n,Rpt}~=ValIdiag{n,Rpt});

    %correct label by diagnosis
```

```
    PVDrt6{n,Rpt}=nnz((ValIdiag{n,Rpt}==1)&(VSdiag6{n,Rpt}==ValIdiag{n,Rpt}));
    RDrt6{n,Rpt}=nnz((ValIdiag{n,Rpt}==2)&(VSdiag6{n,Rpt}==ValIdiag{n,Rpt}));

    %incorrect label by diagnosis
    PVDwrg6{n,Rpt}=nnz((ValIdiag{n,Rpt}==1)&(VSdiag6{n,Rpt}~=ValIdiag{n,Rpt}));
    RDwrg6{n,Rpt}=nnz((ValIdiag{n,Rpt}==2)&(VSdiag6{n,Rpt}~=ValIdiag{n,Rpt}));

    Scsrate6(n,Rpt) = Rtlbl6{n,Rpt}/(Rtlbl6{n,Rpt}+Wrglbl6{n,Rpt});



    %change prior probability
    TSclass{n,Rpt}.Prior = [20 1];

    %test classifier with validation set
    VSdiag20{n,Rpt} = predict(TSclass{n,Rpt},ValIfeat{n,Rpt});

    %number right/wrong in validation set
    Rtlbl20{n,Rpt} = nnz(VSdiag20{n,Rpt}==ValIdiag{n,Rpt});
    Wrglbl20{n,Rpt} = nnz(VSdiag20{n,Rpt}~=ValIdiag{n,Rpt});

    %correct label by diagnosis
    PVDrt20{n,Rpt}=nnz((ValIdiag{n,Rpt}==1)&(VSdiag20{n,Rpt}==ValIdiag{n,Rpt}));
    RDrt20{n,Rpt}=nnz((ValIdiag{n,Rpt}==2)&(VSdiag20{n,Rpt}==ValIdiag{n,Rpt}));

    %incorrect label by diagnosis
    PVDwrg20{n,Rpt}=nnz((ValIdiag{n,Rpt}==1)&(VSdiag20{n,Rpt}~=ValIdiag{n,Rpt}));
    RDwrg20{n,Rpt}=nnz((ValIdiag{n,Rpt}==2)&(VSdiag20{n,Rpt}~=ValIdiag{n,Rpt}));

    Scsrate20(n,Rpt) = Rtlbl20{n,Rpt}/(Rtlbl20{n,Rpt}+Wrglbl20{n,Rpt});


    %change prior probability to 75
    TSclass{n,Rpt}.Prior = [75 1];

    %test classifier with validation set
    VSdiag75{n,Rpt} = predict(TSclass{n,Rpt},ValIfeat{n,Rpt});

    %number right/wrong in validation set
    Rtlbl75{n,Rpt} = nnz(VSdiag75{n,Rpt}==ValIdiag{n,Rpt});
    Wrglbl75{n,Rpt} = nnz(VSdiag75{n,Rpt}~=ValIdiag{n,Rpt});

    %correct label by diagnosis
    PVDrt75{n,Rpt}=nnz((ValIdiag{n,Rpt}==1)&(VSdiag75{n,Rpt}==ValIdiag{n,Rpt}));
    RDrt75{n,Rpt}=nnz((ValIdiag{n,Rpt}==2)&(VSdiag75{n,Rpt}==ValIdiag{n,Rpt}));

    %incorrect label by diagnosis
    PVDwrg75{n,Rpt}=nnz((ValIdiag{n,Rpt}==1)&(VSdiag75{n,Rpt}~=ValIdiag{n,Rpt}));
    RDwrg75{n,Rpt}=nnz((ValIdiag{n,Rpt}==2)&(VSdiag75{n,Rpt}~=ValIdiag{n,Rpt}));

    Scsrate75(n,Rpt) = Rtlbl75{n,Rpt}/(Rtlbl75{n,Rpt}+Wrglbl75{n,Rpt});



    for cOst = 1:10
        %vary cost to create points for an ROC

        TSclassall{Rpt}.Cost(1,2) = cOst*2;%increase cost of misclassifying PVD

        %change prior
        TSclassall{Rpt}.Prior = [50 1];
        valsetlbls50roc{Rpt,cOst} = predict(TSclassall{Rpt},Valset);
        RDTP50(Rpt,cOst)=nnz(valsetlbls50roc{Rpt,cOst}==2 & valsetDiagv==2);
        PVDFP50(Rpt,cOst)=nnz(valsetlbls50roc{Rpt,cOst}==2 & valsetDiagv==1);
        RDFN50(Rpt,cOst)=nnz(valsetlbls50roc{Rpt,cOst}==1 & valsetDiagv==2);
        PVDTN50(Rpt,cOst)=nnz(valsetlbls50roc{Rpt,cOst}==1 & valsetDiagv==1);

        falposx50(Rpt,cOst) =
PVDFP50(Rpt,cOst)/(PVDFP50(Rpt,cOst)+PVDTN50(Rpt,cOst));
        truposy50(Rpt,cOst) = RDTP50(Rpt,cOst)/(RDTP50(Rpt,cOst)+RDFN50(Rpt,cOst));
```

```
        %change prior
        TSclassall{Rpt}.Prior = [6 1];
        valsetlbls6roc{Rpt,cOst} = predict(TSclassall{Rpt},Valset);
        RDTP6(Rpt,cOst)=nnz(valsetlbls6roc{Rpt,cOst}==2 & valsetDiagv==2);
        PVDFP6(Rpt,cOst)=nnz(valsetlbls6roc{Rpt,cOst}==2 & valsetDiagv==1);
        RDFN6(Rpt,cOst)=nnz(valsetlbls6roc{Rpt,cOst}==1 & valsetDiagv==2);
        PVDTN6(Rpt,cOst)=nnz(valsetlbls6roc{Rpt,cOst}==1 & valsetDiagv==1);

        falposx6(Rpt,cOst) = PVDFP6(Rpt,cOst)/(PVDFP6(Rpt,cOst)+PVDTN6(Rpt,cOst));
        truposy50(Rpt,cOst) = RDTP50(Rpt,cOst)/(RDTP50(Rpt,cOst)+RDFN50(Rpt,cOst));


    end

end


%standard deviation of success rate of the folds
SDCls(Rpt) = std (Scsrate(:,Rpt));
rSDCls(Rpt)= SDCls(Rpt)/(mean(Scsrate(:,Rpt)));%relative SD = coefficient of
variation

SDCls50(Rpt) = std (Scsrate50(:,Rpt));
rSDCls50(Rpt) = SDCls50(Rpt)/(mean(Scsrate50(:,Rpt)));

SDCls20(Rpt) = std (Scsrate20(:,Rpt));
rSDCls20(Rpt)= SDCls20(Rpt)/(mean(Scsrate20(:,Rpt)));

SDCls6(Rpt) = std (Scsrate6(:,Rpt));
rSDCls6(Rpt)= SDCls6(Rpt)/(mean(Scsrate6(:,Rpt)));

SDCls75(Rpt) = std (Scsrate75(:,Rpt));
rSDCls75(Rpt)= SDCls75(Rpt)/(mean(Scsrate75(:,Rpt)));

for cOst = 1:10
    SDClsC(cOst,Rpt) = std (ScsrateC(:,cOst,Rpt));
    rSDClsC(cOst,Rpt)= SDClsC(cOst)/(mean(ScsrateC(:,cOst,Rpt)));
end

end

%average entries of classifier confusion matrix
vecPVDwrg=cell2mat(PVDwrg);
vecPVDrt=cell2mat(PVDrt);
vecRDwrg=cell2mat(RDwrg);
vecRDrt=cell2mat(RDrt);

sumFvecPVDwrg=sum(vecPVDwrg);
sumFvecPVDrt=sum(vecPVDrt);
sumFvecRDwrg=sum(vecRDwrg);
sumFvecRDrt=sum(vecRDrt);

MeanPVDwrg = mean(sumFvecPVDwrg);
MeanRDwrg = mean(sumFvecRDwrg);
MeanPVDrt = mean(sumFvecPVDrt);
MeanRDrt = mean(sumFvecRDrt);

%mean SD of X validated classifiers
SDClsMn = mean(SDCls(:));
SDCls6Mn = mean(SDCls6(:));
SDCls20Mn = mean(SDCls20(:));
SDCls50Mn = mean(SDCls50(:));
SDCls75Mn = mean(SDCls75(:));

%validation set results
CMres=1;
%number correctly labelled RD
```

```
    RDscs6(CMres)=nnz(valsetlbls6{CMres}==2 & valsetDiagv==2);
    RDscs20(CMres)=nnz(valsetlbls20{CMres}==2 & valsetDiagv==2);
    RDscs50(CMres)=nnz(valsetlbls50{CMres}==2 & valsetDiagv==2);
    RDscs75(CMres)=nnz(valsetlbls75{CMres}==2 & valsetDiagv==2);
    RDscsVanilla(CMres)=nnz(valsetlblsvanilla{CMres}==2 & valsetDiagv==2);
    RDscsOpti(CMres)=nnz(valsetlblsOpti{CMres}==2 & valsetDiagv==2);

    %Number of PVDs incorrectly labelled (same each) (FP)
    PVDfl6(CMres)=nnz(valsetlbls6{CMres}==2 & valsetDiagv==1);
    PVDfl20(CMres)=nnz(valsetlbls20{CMres}==2 & valsetDiagv==1);
    PVDfl50(CMres)=nnz(valsetlbls50{CMres}==2 & valsetDiagv==1);
    PVDfl75(CMres)=nnz(valsetlbls75{CMres}==2 & valsetDiagv==1);
    PVDflvanilla(CMres)=nnz(valsetlblsvanilla{CMres}==2 & valsetDiagv==1);
    PVDflOpti(CMres)=nnz(valsetlblsOpti{CMres}==2 & valsetDiagv==1);

%incorrect RD
    RDflVanilla(CMres)=nnz(valsetlblsvanilla{CMres}==1 & valsetDiagv==2);
    RDflOpti(CMres)=nnz(valsetlblsOpti{CMres}==1 & valsetDiagv==2);
%correct PVD
    PVDscsvanilla(CMres)=nnz(valsetlblsvanilla{CMres}==1 & valsetDiagv==1);
    PVDscsOpti(CMres)=nnz(valsetlblsOpti{CMres}==1 & valsetDiagv==1);

%table lists the predictions by prior probability
FErestable = table(FEGrpIID10v,FElbls6{1}, FElbls20{1}, FElbls50{1},FElbls75{1},...
    'VariableNames',{'ID','prior6','prior20', 'prior50', 'prior75'});
%RD success ID
RDscsID6 = valsetGrpIID10v(valsetlbls6{CMres}==2 & valsetDiagv==2);
RDscsID20 = valsetGrpIID10v(valsetlbls20{CMres}==2 & valsetDiagv==2);
RDscsID50 = valsetGrpIID10v(valsetlbls50{CMres}==2 & valsetDiagv==2);
RDscsID75 = valsetGrpIID10v(valsetlbls75{CMres}==2 & valsetDiagv==2);
%PVD fail ID
PVDflID6 = valsetGrpIID10v(valsetlbls6{CMres}==2 & valsetDiagv==1);
PVDflID20 = valsetGrpIID10v(valsetlbls20{CMres}==2 & valsetDiagv==1);
PVDflID50 = valsetGrpIID10v(valsetlbls50{CMres}==2 & valsetDiagv==1);
PVDflID75 = valsetGrpIID10v(valsetlbls75{CMres}==2 & valsetDiagv==1);

%save ('/Users/stewartlake/Documents/Retinalcontour/LDA/Rpt
S107/DAXvalRD5MmS107FEkb');
```

6. BSspec

```
%BSspec - explore the difference in B scan spectra difference from the
%normal, comparing RD & PVD. Uses Regdescr data
%Uses data determined by Regdescr, which calculate RDabs11 and PVDabs11, FE
%create mean FT distribution for larger values sumdiff
%sets sumdiff == 1 to look at relative distribution (RD/PVDspecnormI)
%non normalised data for magnitude analysis is RD/PVDmeanspecI
%the aim is to look for areas of difference between RD & PVD
%ADJUST: RUN TO LINE 169 AND ADJUST Sdlim, ie feature selection and
%training different
%ADJUST:then run single var mdl, then multi variable model from that
Sdlim = 0.001;%SD threshold below which B scans are ignored (low for training,
higher for feature selection
%CHANGE Feats (line 285) to select model predictors from possible (R,I)
%variable
%This creates models with only B scans > Sdlim. To include all B scans run
%once to line 169 to find regions,bin colmns, set these in mdldata, and run
%again from beginning with Sdlim set very low (0.001?)
%classifier saved - classifiers/reg bin QDA/ Fs5Trs3v.mat
%full data saved in classifiers/reg bin QDA/BSspec110520
%RD
for yy=1:(size(RDSD,1))

    for xx = 1:17

    RD3dSD(yy,xx,1:21) = RDSD{yy,xx};
    RD3dMxe(yy,xx,1:21) = RDMx11{yy,xx};
```

```
    RD3dInd(yy,xx,1:21) = RDIndM{yy,xx};
    for absr = 1:21
    RD3dabs11(yy,xx,absr,1:30) = RDabs11{yy,xx}(:,absr);%4D double contains B scan
30 bins
    end
    end
end

%PVD
for yyp=1:(size(PVDSD,1))

    for xxp = 1:17

    PVD3dSD(yyp,xxp,1:21) = PVDSD{yyp,xxp};%eye x region x B scan
    PVD3dMxe(yyp,xxp,1:21) = PVDMx11{yyp,xxp};
    PVD3dInd(yyp,xxp,1:21) = PVDIndM{yyp,xxp};
    for absp = 1:21
    PVD3dabs11(yyp,xxp,absp,1:30) = PVDabs11{yyp,xxp}(:,absp);
    end
    end
end


%FE
for yyf=1:(size(FESD,1))

    for xxf = 1:17

    FE3dSD(yyf,xxf,1:21) = FESD{yyf,xxf};
    FE3dMxe(yyf,xxf,1:21) = FEMx11{yyf,xxf};
    FE3dInd(yyf,xxf,1:21) = FEIndM{yyf,xxf};
    for absf = 1:21
    FE3dabs11(yyf,xxf,absf,1:30) = FEabs11{yyf,xxf}(:,absf);%4D double contains B
scan 30 bins
    end
    end
end

%%
%data metrics
%{
%to get training set numbers:
RDsplit = SplitID(1:53);
PVDSplit = SplitID(54:end);

RD3dSD(RDsplit==1,:,:)=[];
PVD3dSD(PVDSplit==1,:,:)=[];
%}

%find number retinal B scans in each double.
numRDBscan = sum(~isnan(RD3dInd),3);
numPVDBscan = sum(~isnan(PVD3dInd),3);

numRDBSreg = sum(~isnan(RD3dInd),[1 3]);%no Bscans by region, RD
numPVDBSreg = sum(~isnan(PVD3dInd),[1 3]);
numRDPVDBSreg = numRDBSreg + numPVDBSreg;

IndRDsd5 = RD3dInd;
IndPVDsd5 = PVD3dInd;
IndRDsd5(RD3dSD<Sdlim)=NaN;%indices double for large SD
IndPVDsd5(PVD3dSD<Sdlim)=NaN;

regionsumRD5 = sum(~isnan(IndRDsd5),[1 3],'omitnan');%number Bscans largeSD by
region
regionsumPVD5 = sum(~isnan(IndPVDsd5),[1 3],'omitnan');%

regionsumPVDRD5 = regionsumPVD5 + regionsumRD5;
PCPBDRDbs5reg = (regionsumPVDRD5*100)./numRDPVDBSreg; % %bscan each region gtr
Sdlim
```

```
PVDpcBsGT5 = regionsumPVD5/numPVDBSreg;%PVD Bs > sdlim
RDpcBsGT5 = regionsumRD5/numRDBSreg; %RD Bs > sdlim


%number B scans over threshold, per eye
numRDOT = sum(RD3dSD>Sdlim,[2 3]);
numPVDOT = sum(PVD3dSD>Sdlim,[2 3]);
numFEOT = sum(FE3dSD>Sdlim,[2 3]);
%get location of SD<Sdlim
%[RDr,RDc,RDp] = ind2sub(size(RD3dSD),find(RD3dSD<Sdlim));
%[PVDr,PVDc,PVDp] = ind2sub(size(PVD3dSD),find(PVD3dSD<Sdlim));
totRDOT = sum(numRDOT(:));
totPVDOT = sum(numPVDOT(:));

%%
RD4dabs11 = reshape(RD3dabs11,[],30);
RD3dSDv = reshape(RD3dSD,[],1);
IndRDlo = find(RD3dSDv<Sdlim);
RD4dabs11(IndRDlo,:) = NaN;
RD5abs = reshape(RD4dabs11,size(RDID,1),17,21,30);%only B scans greater than Sdlim

PVD4dabs11 = reshape(PVD3dabs11,[],30);
PVD3dSDv = reshape(PVD3dSD,[],1);
IndPVDlo = find(PVD3dSDv<Sdlim);
PVD4dabs11(IndPVDlo,:) = NaN;
PVD5abs = reshape(PVD4dabs11,size(PVDID,1),17,21,30);

FE4dabs11 = reshape(FE3dabs11,[],30);
FE3dSDv = reshape(FE3dSD,[],1);
IndFElo = find(FE3dSDv<Sdlim);
FE4dabs11(IndFElo,:) = NaN;
FE5abs = reshape(FE4dabs11,size(FEID,1),17,21,30);

DiagRD = ones(size(RD5abs,1),1);%RD = 1
DiagPVD = zeros(size(PVD5abs,1),1);%PVD = 0
Diagall = cat(1, DiagRD, DiagPVD);


%create random selection: 70/30
Split = cvpartition(size(Diagall,1),'HoldOut', 0.30);
SplitID = Split.test;%test set

%how many Bscans SD>5: sizes of IndSD5/allSD
allSD = cat(1, RD3dSDv, PVD3dSDv,FE3dSDv);%? include FE
allSDsorted = sort(allSD);
IndSD5 = find(allSDsorted>5);
IndSD2 = find(allSDsorted>2);

figure
HistRDPVD = histogram(allSD);
%HistRDPVD.BinLimits = [0 10];%if required to illustrate lower bins
figure%distribution of sd by diagnosis
HistRD = histogram(RD3dSDv,'FaceColor','r');
hold on
HistPVD = histogram(PVD3dSDv,'FaceColor','b');
HistRD.Normalization = 'probability';
HistPVD.Normalization = 'probability';

RDmeanspecI=mean(RD5abs,[1 3], 'omitnan');%so mean B scan value per cube
RDmeanspecI= reshape(RDmeanspecI,[17,30]);%17 x 30 array mean region x bin

PVDmeanspecI=mean(PVD5abs,[1 3],'omitnan');%mean bin value
PVDmeanspecI= reshape(PVDmeanspecI,[17,30]);%row per region, column = bin

FEmeanspecI=mean(FE5abs,[1 3],'omitnan');
FEmeanspecI= reshape(FEmeanspecI,[17,30]);%17 x 30 array mean region x bin


RDspecnormI = RDmeanspecI./sum(RDmeanspecI,2);%normalise to sum=1
PVDspecnormI = PVDmeanspecI./sum(PVDmeanspecI,2);%
```

```
FEspecnormI = FEmeanspecI./sum(FEmeanspecI,2);%normalise to sum=1

%find indices of maximum differences of regional bins
diffRDPVDn = abs(RDspecnormI-PVDspecnormI);%normalised diff
[Mdiffn,IndMdiffn] = maxk(diffRDPVDn(:),6);%4 largest differences
[Rdiffn,Cdiffn] = ind2sub([17 30],IndMdiffn);

diffRDPVD = abs(RDmeanspecI-PVDmeanspecI);%absolute diff
[Mdiff,IndMdiff] = maxk(diffRDPVD(:),6);%4 largest differences
[Rdiff,Cdiff] = ind2sub([17 30],IndMdiff);



%%
%here the data is split to use only the training set data for feature
%selection. e.g., for Sdlim=2, with differences in the
%regions, if not the bin indices:
%region (all I) 4 1 2 1 2 14
%region (feature/trining set) 4 5 1 4 14 3
%norm region (all I) 2 3 14 9 1 13
%norm region (feat/Tr set) 3 5 9 14 10 1
%so end up with 1 region different: 5 instead of 1

FeatIDsetRD = RD5abs(~SplitID(1:length(RD5abs)),:,:,:);%not test set = training
FeatIDsetPVD = PVD5abs(~SplitID(length(RD5abs)+1:end),:,:,:);


RDmeanspecIf=mean(FeatIDsetRD,[1 3],'omitnan');
RDmeanspecIf= reshape(RDmeanspecIf,[17,30]);%17 x 30 array mean region x bin

PVDmeanspecIf=mean(FeatIDsetPVD,[1 3],'omitnan');%mean bin value
PVDmeanspecIf= reshape(PVDmeanspecIf,[17,30]);%row per region, column = bin

RDspecnormIf = RDmeanspecIf./sum(RDmeanspecIf,2);%normalise to sum=1
PVDspecnormIf = PVDmeanspecIf./sum(PVDmeanspecIf,2);


%find indices of maximum differences of regional bins
diffRDPVDnf = abs(RDspecnormIf-PVDspecnormIf);%normalised diff
[Mdiffnf,IndMdiffnf] = maxk(diffRDPVDnf(:),6);%6 largest differences
[Rdiffnf,Cdiffnf] = ind2sub([17 30],IndMdiffnf);

diffRDPVDf = abs(RDmeanspecIf-PVDmeanspecIf);%absolute diff
[Mdifff,IndMdifff] = maxk(diffRDPVDf(:),6);%6 largest differences
[Rdifff,Cdifff] = ind2sub([17 30],IndMdifff);

%STOP HERE TO SELECT COLUMNS/STRINGS FROM R/CDIFFF(N) FOR BELOW
%%
%now construct DA models from the (region,bins) with the largest difference
%between PVD and RD eyes (feature selection Sdliminted, above)
%arrays with large value SD are RD5abs and PVD5abs. If not enough elements
%in these include all values SD using RD/PVD3dabs11 (ie training set from
%all data)
%these arrays are eyes x regions x B scans x bins
%((cols and pages selected from lines 76 & 80 Cdiff(n) & Rdiff(n)))
%BETTER to select features from training set only: R/Cdifff(n)
%where R = region, C = bin (vector 2 & 4 in RD5abs respectively)
%model data, MAX single value for each eye from any B scan in region/bin
RDmdldata(1:size(RD5abs,1),1) = max(squeeze(RD5abs(:,8,:,3)),[],2,'omitnan');%eyes
in rows, first region
RDmdldata(1:size(RD5abs,1),2) = max(squeeze(RD5abs(:,3,:,2)),[],2,'omitnan');
RDmdldata(1:size(RD5abs,1),3) = max(squeeze(RD5abs(:,5,:,3)),[],2,'omitnan');
RDmdldata(1:size(RD5abs,1),4) = max(squeeze(RD5abs(:,3,:,3)),[],2,'omitnan');
RDmdldata(1:size(RD5abs,1),5) = max(squeeze(RD5abs(:,16,:,3)),[],2,'omitnan');
RDmdldata(1:size(RD5abs,1),6) = max(squeeze(RD5abs(:,6,:,2)),[],2,'omitnan');
%RDmdldata(1:size(RD5abs,1),7) = max(squeeze(RD5abs(:,3,:,2)),[],2,'omitnan');

PVDmdldata(1:size(PVD5abs,1),1) =
max(squeeze(PVD5abs(:,8,:,3)),[],2,'omitnan');%eyes x b scans, first region
```

```
PVDmdldata(1:size(PVD5abs,1),2) = max(squeeze(PVD5abs(:,3,:,2)),[],2,'omitnan');
PVDmdldata(1:size(PVD5abs,1),3) = max(squeeze(PVD5abs(:,5,:,3)),[],2,'omitnan');
PVDmdldata(1:size(PVD5abs,1),4) = max(squeeze(PVD5abs(:,3,:,3)),[],2,'omitnan');
PVDmdldata(1:size(PVD5abs,1),5) = max(squeeze(PVD5abs(:,16,:,3)),[],2,'omitnan');
PVDmdldata(1:size(PVD5abs,1),6) = max(squeeze(PVD5abs(:,6,:,2)),[],2,'omitnan');
%PVDmdldata(1:size(PVD5abs,1),7) = max(squeeze(PVD5abs(:,3,:,2)),[],2,'omitnan');


FEmdldata(1:size(FE5abs,1),1) = max(squeeze(FE5abs(:,8,:,3)),[],2,'omitnan');%eyes
in rows, first region
FEmdldata(1:size(FE5abs,1),2) = max(squeeze(FE5abs(:,3,:,2)),[],2,'omitnan');
FEmdldata(1:size(FE5abs,1),3) = max(squeeze(FE5abs(:,5,:,3)),[],2,'omitnan');
FEmdldata(1:size(FE5abs,1),4) = max(squeeze(FE5abs(:,3,:,3)),[],2,'omitnan');
FEmdldata(1:size(FE5abs,1),5) = max(squeeze(FE5abs(:,16,:,3)),[],2,'omitnan');
FEmdldata(1:size(FE5abs,1),6) = max(squeeze(FE5abs(:,6,:,2)),[],2,'omitnan');
%FEmdldata(1:size(FE5abs,1),7) = max(squeeze(FE5abs(:,3,:,2)),[],2,'omitnan');

%training set
alldata = cat(1, RDmdldata, PVDmdldata);%Dont need FE as FE is an additional
testing set
%NEED MATCHING AL:
AllAL = cat(1,nALRD,nALPVD);%the n prefix ensures correct alignment AL with data
allID = cat(1, RDID, PVDID);
Allage = cat(1,nAgeRD,nAgePVD);

Trainset = alldata(~SplitID,:);%the training set
Testset = alldata(SplitID,:);
TrsetD = Diagall(~SplitID,:);%training set group diagnostic category
TesetD = Diagall(SplitID,:);%test set group
TrsetAL = AllAL(~SplitID,:);
TesetAL = AllAL(SplitID,:);
TesetID = allID(SplitID,:);
Trainset = cat(2, Trainset,TrsetAL);%makes col7 = AL
Testset = cat(2, Testset, TesetAL);
Feset = cat(2,FEmdldata,nALFE);
TrsetID = allID(~SplitID,:);
TrsetAge = Allage(~SplitID,:);
TesetAge = Allage(SplitID,:);
for Ln1 = 1:size(Trainset,2) %single variable models to find best results
    %((this examined use of 4 quadrant MaxE/Ind utility, and AL (from
    %Regdescr3D)))
    sinquadmod1{Ln1} = fitcdiscr(Trainset(:,Ln1),TrsetD,'DiscrimType','quadratic');
    %determine single variable (quadrant) ability

    Trsetdistr1{Ln1} =
confusionmat(sinquadmod1{Ln1}.Y,resubPredict(sinquadmod1{Ln1}));

    SCSTrset1{Ln1} =
(Trsetdistr1{Ln1}(1)+Trsetdistr1{Ln1}(4))/sum(Trsetdistr1{Ln1}(1:4));
    %success rate of training set allocation:

    valres1{Ln1} = predict(sinquadmod1{Ln1},Testset(:,Ln1));
    %test set prediction, single variable models

    RDscs1{Ln1} = nnz(valres1{Ln1}==1 & TesetD==1);%RD labels correct
    PVDfl1{Ln1} = nnz(valres1{Ln1}==1 & TesetD==0);%PVD incorrect

end
%Feats = [2 3 7] is [3,2], [5,3], AL (see RDmdldata lines 221-226)
Feats = [3 7];%variables to use as features (from Trainset/Teset)
%try n variable model. n= number of vars(columns) taken from Trainset)
quad4mdl1 = fitcdiscr(Trainset(:,Feats),TrsetD,'DiscrimType','quadratic');
quad4mdldistr1 = confusionmat(quad4mdl1.Y,resubPredict(quad4mdl1));
%added predict FE here
val4res1 = predict(quad4mdl1,Testset(:,Feats));%vanilla
FE4pre1 = predict(quad4mdl1,Feset(:,Feats));
RDscs41 = nnz(val4res1==1 & TesetD==1);%RD labels correct
PVDfl41 = nnz(val4res1==1 & TesetD==0);%PVD incorrect
```

```
%added predict FE after each valres
%then 4 variables with adjusted known prior
quad4mdl1.Prior = [50 1];
val4resP501 = predict(quad4mdl1,Testset(:,Feats));%test sets
FepreP501 = predict(quad4mdl1,Feset(:,Feats));
RDscs4P501 = nnz(val4resP501==1 & TesetD==1);%RD labels correct
PVDfl4P501 = nnz(val4resP501==1 & TesetD==0);%PVD incorrect

quad4mdl1.Prior = [20 1];
val4resP201 = predict(quad4mdl1,Testset(:,Feats));
FepreP201 = predict(quad4mdl1,Feset(:,Feats));
RDscs4P201 = nnz(val4resP201==1 & TesetD==1);%RD labels correct
PVDfl4P201 = nnz(val4resP201==1 & TesetD==0);%PVD incorrect

quad4mdl1.Prior = [6 1];
val4resP61 = predict(quad4mdl1,Testset(:,Feats));
FepreP61 = predict(quad4mdl1,Feset(:,Feats));
RDscs4P61 = nnz(val4resP61==1 & TesetD==1);%RD labels correct
PVDfl4P61 = nnz(val4resP61==1 & TesetD==0);%PVD incorrect

quad4mdl1.Prior = [0.64 0.36];
val4resPopti = predict(quad4mdl1,Testset(:,Feats));%wt optimised test set results
FeprePopti = predict(quad4mdl1,Feset(:,Feats));
RDscs4Popti = nnz(val4resPopti==1 & TesetD==1);%RD labels correct
PVDfl4Popti = nnz(val4resPopti==1 & TesetD==0);%PVD incorrect
RDfl4Popti = nnz(val4resPopti==0 & TesetD==1);%RD labels incorrect
PVDscs4Popti = nnz(val4resPopti==0 & TesetD==0);%PVD correct
Tesetlble1 = TesetID(val4resPopti==1);%ID of test set labelled '1'


RDvset = Testset(TesetD==1,Feats);%RD variables
%develop sens/spec for different weighting - see CreROCTS
%{
for Wtp = 1:50
quad4mdl1.Prior = [Wtp 1];
val4resPWt{Wtp} = predict(quad4mdl1,Testset(:,Feats));
nowresvec = [];
nowresvec = val4resPWt{Wtp};
FeprePWt{Wtp} = predict(quad4mdl1,Feset(:,Feats));
RDscs1Wt(Wtp) = nnz(nowresvec==1 & TesetD==1);%RD labels correct
PVDfl1Wt(Wtp) = nnz(nowresvec==1 & TesetD==0);%PVD incorrect
PVDsc1Wt(Wtp) = nnz(nowresvec==0 & TesetD==0);%PVD correct

Wtscs(Wtp) = (RDscs1Wt(Wtp)+PVDsc1Wt(Wtp))/size(TesetD,1);%success rate
Wtsens(Wtp) = RDscs1Wt(Wtp)/nnz(TesetD==1);%sensitivity
Wtspec(Wtp) = PVDsc1Wt(Wtp)/nnz(TesetD==0);%specificity

end

for WtR = 1:50
quad4mdl1.Prior = [1 WtR];
val4resRWt{WtR} = predict(quad4mdl1,Testset(:,Feats));
nowresvec = [];
nowresvec = val4resRWt{WtR};
FepreRWt{WtR} = predict(quad4mdl1,Feset(:,Feats));
RDscs1WtR(WtR) = nnz(nowresvec==1 & TesetD==1);%RD labels correct
PVDfl1WtR(WtR) = nnz(nowresvec==1 & TesetD==0);%PVD incorrect
PVDsc1WtR(WtR) = nnz(nowresvec==0 & TesetD==0);%PVD correct

WtscsR(WtR) = (RDscs1WtR(WtR)+PVDsc1WtR(WtR))/size(TesetD,1);%success rate
WtsensR(WtR) = RDscs1WtR(WtR)/nnz(TesetD==1);%sensitivity
WtspecR(WtR) = PVDsc1WtR(WtR)/nnz(TesetD==0);%specificity

end
%}
%%
spsz=18;%figure spot size
figure%mean bin distribution difference across all of eyes
scatter(1:30,mean(RDspecnormI,'omitnan'),spsz,'r','x');
hold on
```

```
scatter(1:30,mean(PVDspecnormI,'omitnan'),spsz,'b','+');
title('Mean value all regions');
ylabel('Normalised bin magnitude');
xlabel('Bin (0.11 cycles/mm per bin)');
legend('RD','PVD');



figure %tiled plot of regional bin distribution
regfig = tiledlayout(5,5,'TileSpacing','none','Padding', 'none');

Rfig(1) = nexttile(1);
scatter(1:30,RDspecnormI(5,:),spsz,'r','x');
hold on
scatter(1:30,PVDspecnormI(5,:),spsz,'b','+');

Rfig(2) = nexttile(3);
scatter(1:30,RDspecnormI(3,:),spsz,'r','x');
hold on
scatter(1:30,PVDspecnormI(3,:),spsz,'b','+');

Rfig(3) = nexttile(5);
scatter(1:30,RDspecnormI(17,:),spsz,'r','x');
hold on
scatter(1:30,PVDspecnormI(17,:),spsz,'b','+');

Rfig(4) = nexttile(7);
scatter(1:30,RDspecnormI(4,:),spsz,'r','x');
hold on
scatter(1:30,PVDspecnormI(4,:),spsz,'b','+');

Rfig(5) = nexttile(8);
scatter(1:30,RDspecnormI(2,:),spsz,'r','x');
hold on
scatter(1:30,PVDspecnormI(2,:),spsz,'b','+');

Rfig(6) = nexttile(9);
scatter(1:30,RDspecnormI(16,:),spsz,'r','x');
hold on
scatter(1:30,PVDspecnormI(16,:),spsz,'b','+');

Rfig(7) = nexttile(11);
scatter(1:30,RDspecnormI(6,:),spsz,'r','x');
hold on
scatter(1:30,PVDspecnormI(6,:),spsz,'b','+');

Rfig(8) = nexttile(12);
scatter(1:30,RDspecnormI(6,:),spsz,'r','x');
hold on
scatter(1:30,PVDspecnormI(6,:),spsz,'b','+');

Rfig(9) = nexttile(13);
scatter(1:30,RDspecnormI(1,:),spsz,'r','x');
hold on
scatter(1:30,PVDspecnormI(1,:),spsz,'b','+');

Rfig(10) = nexttile(14);
scatter(1:30,RDspecnormI(14,:),spsz,'r','x');
hold on
scatter(1:30,PVDspecnormI(14,:),spsz,'b','+');

Rfig(11) = nexttile(15);
scatter(1:30,RDspecnormI(15,:),spsz,'r','x');
hold on
scatter(1:30,PVDspecnormI(15,:),spsz,'b','+');

Rfig(12) = nexttile(17);
scatter(1:30,RDspecnormI(8,:),spsz,'r','x');
hold on
scatter(1:30,PVDspecnormI(8,:),spsz,'b','+');
```

```
Rfig(13) = nexttile(18);
scatter(1:30,RDspecnormI(10,:),spsz,'r','x');
hold on
scatter(1:30,PVDspecnormI(10,:),spsz,'b','+');

Rfig(14) = nexttile(19);
scatter(1:30,RDspecnormI(12,:),spsz,'r','x');
hold on
scatter(1:30,PVDspecnormI(12,:),spsz,'b','+');

Rfig(15) = nexttile(21);
scatter(1:30,RDspecnormI(9,:),spsz,'r','x');
hold on
scatter(1:30,PVDspecnormI(9,:),spsz,'b','+');

Rfig(16) = nexttile(23);
scatter(1:30,RDspecnormI(11,:),spsz,'r','x');
hold on
scatter(1:30,PVDspecnormI(11,:),spsz,'b','+');

Rfig(17) = nexttile(25);
scatter(1:30,RDspecnormI(13,:),spsz,'r','x');
hold on
scatter(1:30,PVDspecnormI(13,:),spsz,'b','+');

linkaxes(Rfig(:),'xy');%link axes limits
Rfig(1).XLim = [0 10];%remove bins 11-30

title(regfig,['Region bin variation, RD & PVD, for B scans SD>' num2str(Sdlim)]);
ylabel(regfig,'Mean (normalised) bin, difference from average');
xlabel(regfig,'Bin number (0.11 cycles/mm)');


%%
%demographic stats of groups - better to see RTDPVDdem as combines sets
PVDalmean = mean(nALPVD,'omitnan');
PVDagemean = mean(nAgePVD,'omitnan');
PVDalsd = std(nALPVD, 'omitnan');
PVDagesd = std(nAgePVD, 'omitnan');

RDalmean = mean(nALRD,'omitnan');
RDagemean = mean(nAgeRD,'omitnan');
RDalsd = std(nALRD, 'omitnan');
RDagesd = std(nAgeRD, 'omitnan');

TeRDalmean = mean(TesetAL(TesetD==1),'omitnan');
TeRDagemean = mean(TesetAge(TesetD==1),'omitnan');
TeRDalsd = std(TesetAL(TesetD==1), 'omitnan');
TeRDagesd = std(TesetAge(TesetD==1), 'omitnan');

TrRDalmean = mean(TrsetAL(TrsetD==1),'omitnan');
TrRDagemean = mean(TrsetAge(TrsetD==1),'omitnan');
TrRDalsd = std(TrsetAL(TrsetD==1), 'omitnan');
TrRDagesd = std(TrsetAge(TrsetD==1), 'omitnan');

TrPVDalmean = mean(TrsetAL(TrsetD==0),'omitnan');
TrPVDagemean = mean(TrsetAge(TrsetD==0),'omitnan');
TrPVDalsd = std(TrsetAL(TrsetD==0), 'omitnan');
TrPVDagesd = std(TrsetAge(TrsetD==0), 'omitnan');

TePVDalmean = mean(TesetAL(TesetD==0),'omitnan');
TePVDagemean = mean(TesetAge(TesetD==0),'omitnan');
TePVDalsd = std(TesetAL(TesetD==0), 'omitnan');
TePVDagesd = std(TesetAge(TesetD==0), 'omitnan');

[hAL,pAL,ciAL,stAL] = ttest2(nALRD,nALPVD);%are RD/PVD the same AL?

[hAge,pAge,ciAge,stAge] = ttest2(nAgeRD,nAgePVD);%are RD/PVD the same Age?
```

```
%Identify eyes incorreclty labelled as PVD
TesetRDfl1 = TesetID;%validation set IDs
TesetRDfl1(TesetD==0) = {NaN};%remove IDs of PVD eyes
TesetRDfl1(val4res1==1) = {NaN}; %remove IDS of successfully labelled

%%
spsz=18;
figure %tiled plot of regional bin distribution training set
regfigts = tiledlayout(5,5,'TileSpacing','none','Padding', 'none');

Rfigts(1) = nexttile(1);
scatter(1:30,RDspecnormIf(5,:),spsz,'r','x');
hold on
scatter(1:30,PVDspecnormIf(5,:),spsz,'b','+');

Rfigts(2) = nexttile(3);
scatter(1:30,RDspecnormIf(3,:),spsz,'r','x');
hold on
scatter(1:30,PVDspecnormIf(3,:),spsz,'b','+');

Rfigts(3) = nexttile(5);
scatter(1:30,RDspecnormIf(17,:),spsz,'r','x');
hold on
scatter(1:30,PVDspecnormIf(17,:),spsz,'b','+');

Rfigts(4) = nexttile(7);
scatter(1:30,RDspecnormIf(4,:),spsz,'r','x');
hold on
scatter(1:30,PVDspecnormIf(4,:),spsz,'b','+');

Rfigts(5) = nexttile(8);
scatter(1:30,RDspecnormIf(2,:),spsz,'r','x');
hold on
scatter(1:30,PVDspecnormIf(2,:),spsz,'b','+');

Rfigts(6) = nexttile(9);
scatter(1:30,RDspecnormIf(16,:),spsz,'r','x');
hold on
scatter(1:30,PVDspecnormIf(16,:),spsz,'b','+');

Rfigts(7) = nexttile(11);
scatter(1:30,RDspecnormIf(6,:),spsz,'r','x');
hold on
scatter(1:30,PVDspecnormIf(6,:),spsz,'b','+');

Rfigts(8) = nexttile(12);
scatter(1:30,RDspecnormIf(6,:),spsz,'r','x');
hold on
scatter(1:30,PVDspecnormIf(6,:),spsz,'b','+');

Rfigts(9) = nexttile(13);
scatter(1:30,RDspecnormIf(1,:),spsz,'r','x');
hold on
scatter(1:30,PVDspecnormIf(1,:),spsz,'b','+');

Rfigts(10) = nexttile(14);
scatter(1:30,RDspecnormIf(14,:),spsz,'r','x');
hold on
scatter(1:30,PVDspecnormIf(14,:),spsz,'b','+');

Rfigts(11) = nexttile(15);
scatter(1:30,RDspecnormIf(15,:),spsz,'r','x');
hold on
scatter(1:30,PVDspecnormIf(15,:),spsz,'b','+');

Rfigts(12) = nexttile(17);
scatter(1:30,RDspecnormIf(8,:),spsz,'r','x');
hold on
scatter(1:30,PVDspecnormIf(8,:),spsz,'b','+');
```

```
Rfigts(13) = nexttile(18);
scatter(1:30,RDspecnormIf(10,:),spsz,'r','x');
hold on
scatter(1:30,PVDspecnormIf(10,:),spsz,'b','+');

Rfigts(14) = nexttile(19);
scatter(1:30,RDspecnormIf(12,:),spsz,'r','x');
hold on
scatter(1:30,PVDspecnormIf(12,:),spsz,'b','+');

Rfigts(15) = nexttile(21);
scatter(1:30,RDspecnormIf(9,:),spsz,'r','x');
hold on
scatter(1:30,PVDspecnormIf(9,:),spsz,'b','+');

Rfigts(16) = nexttile(23);
scatter(1:30,RDspecnormIf(11,:),spsz,'r','x');
hold on
scatter(1:30,PVDspecnormIf(11,:),spsz,'b','+');

Rfigts(17) = nexttile(25);
scatter(1:30,RDspecnormIf(13,:),spsz,'r','x');
hold on
scatter(1:30,PVDspecnormIf(13,:),spsz,'b','+');

linkaxes(Rfigts(:),'xy');%link axes limits
Rfigts(1).XLim = [0 10];%remove bins 11-30

title(regfigts,['Region bin variation, RD & PVD, for B scans SD>' num2str(Sdlim)]);
ylabel(regfigts,'Mean (normalised) bin, difference from average');
xlabel(regfigts,'Bin number (0.11 cycles/mm)');
set(gca, 'LineWidth', 1, 'FontWeight', 'bold', 'FontSize', 10);

%surf plots of bin/region anomaly differences between diagnosis
xG=1:30;
yG = 1:17;
[Xgrid,Ygrid] = meshgrid(xG,yG);
figure
surf(Xgrid,Ygrid,abs(RDspecnormI-PVDspecnormI));%normalised
xlabel('frequency bin');
ylabel('region');
zlabel('anomaly');

figure
surf(Xgrid,Ygrid,abs(RDmeanspecI-PVDmeanspecI));%real values
xlabel('frequency bin');
ylabel('region');
zlabel('anomaly');

PVDmnbin = mean(PVDmeanspecI);
RDmnbin = mean(RDmeanspecI);
bindiff = RDmnbin-PVDmnbin;

%ttests of signififcant bin differences between groups
[hA2, pA2, ciA2, ~] = ttest2(PVDmeanspecI(:,2), RDmeanspecI(:,2));
[hA3, pA3, ciA3, ~] = ttest2(PVDmeanspecI(:,3), RDmeanspecI(:,3));
PVDbins23 = cat(1, PVDmeanspecI(:,2),PVDmeanspecI(:,3));
RDbins23 = cat(1, RDmeanspecI(:,2),RDmeanspecI(:,3));
[hA23, pA23, ciA23, ~] = ttest2(PVDbins23,RDbins23);

%%
%{
%settings used for tech paper figure:
spsz=32;
scatter(1:30,RDspecnormIf(3,:),spsz,[0.6350 0.0780 0.1840],'d','LineWidth', 1.5);
hold on
scatter(1:30,PVDspecnormIf(3,:),spsz,[0 0.4470 0.7410],'x','LineWidth', 1.5);
ylabel('Mean (normalised) anomaly (mm)');
xlabel('Bin number (0.11 cycles/mm per bin)');
set(gca, 'LineWidth', 1, 'FontWeight', 'bold', 'FontSize', 12);
```

```
%}
```

7. CreROCTS

```
%ROC curve generation, from training set RD c PVD c/RD53PVD61xt2.mat data
%weights the classifier training set results from BSspec data
%vectors go from RD 50 x PVD incidence, to 1:1, to PVD 50x RD, so all vectors
%99 elements long
%training set to get the optimum weighting for the validation set

load('/Users/stewartlake/Documents/Retinalcontour/RD c PVD 2/RD53PVD61xt2.mat');

Feats=[2 3 7];
%TrsetD is the training set diagnosis, RD = 1, PVD = 0
nRDts = nnz(TrsetD==1);%number Tr set RD eyes
nPVDts = nnz(TrsetD==0);%number PVD eyes in Tr set
for WtR = 1:99
    Wt= (0.01*WtR);
quad4mdl1 =
fitcdiscr(Trainset(:,Feats),TrsetD,'DiscrimType','quadratic','Prior',[1-Wt Wt]);
quad4mdldistr1 = confusionmat(quad4mdl1.Y,resubPredict(quad4mdl1));
CmatR{WtR,1} = quad4mdldistr1;

SensR(WtR,1) = CmatR{WtR,1}(4)/(CmatR{WtR,1}(2) + CmatR{WtR,1}(4));%training set
SpecR(WtR,1) = CmatR{WtR,1}(1)/(CmatR{WtR,1}(1) + CmatR{WtR,1}(3));

scsR(WtR) = (quad4mdldistr1(1) + quad4mdldistr1(4))/sum(quad4mdldistr1(1:4));% =
accuracy
RDsR(WtR) = CmatR{WtR,1}(4);
PVDfR(WtR) = CmatR{WtR,1}(3);
RDsrate(WtR) = RDsR(WtR)/nRDts;%fratcion success rate RD
PVDfrate(WtR) = PVDfR(WtR)/nPVDts;%fraction failure rate PVD
end

AUC = trapz(1-SpecR,SensR);% AUC of ROC

%Total sensitivity/specificity range:
x=fliplr(0.01:0.01:0.99);

figure
plot(1-SpecR,SensR,'r');
refline(1,0)
title('ROC curve, 3 variable model training set');
xlabel('1-Specificity');
ylabel('Sensitivity');


%plot RD success  and PVD fail on same graph
%represents RDs and PVDfl as fractions against their denominator = no of
%each group in the training set
figure
yyaxis left
%plot(x,RDsrate,'m:');%same as sensitivity
hold on
%plot(x,PVDfrate,'-.k','LineWidth', 1);
%plot(x, RDsrate-PVDfrate,'k');
plot(x, SensR, 'r-.','LineWidth', 1);
plot(x, SpecR, 'b-.','LineWidth', 1);
set(gca, 'XDir','reverse')
set(gca, 'LineWidth', 1, 'FontWeight', 'bold', 'FontSize', 10);
xlabel({'Class weighting';'<--PVD weight increased RD weight-->'});
ylabel('proportion of eyes');

yyaxis right
plot(x, scsR,'Color',[0.8500 0.3250 0.0980]);
ylabel('Accuracy');
legend('Sensitivity', 'Specificity', 'Accuracy', 'Location'...
    ,'southoutside','Orientation', 'horizontal');
```

```
title('Training set performance by class weighting')

%{
%this version uses absolute number of eyes for RDs/PVDf. the above uses
rate
%plot RD success and PVD fail on same graph
figure
yyaxis left
plot(x,RDsR,'m');
hold on
plot(x,PVDfR,'b');
plot(x, RDsR-PVDfR,'k');
set(gca, 'XDir','reverse')
xlabel({'PVD weighting';'<--PVD weighted RD weighted-->'});
ylabel('No. of eyes');

yyaxis right
plot(x, scsR,'Color',[0.8500 0.3250 0.0980]);
ylabel('success rate');
legend('RD success', 'PVD fail', 'difference', 'success rate');
title('Classifier RD success and PVD failure rate')

%}
```

8. CreClsImg

```
%create 3D image of classifier results.

%Variable max/mins from AL and the alldata arrays from BSspec
%can load in from Retinalcontour/classifiers/reg bin QDA

%this creates a 3 var classifier image:
%load('/Users/stewartlake/Documents/Retinalcontour/classifiers/reg bin
QDA/Fs5Trs3v.mat');

%this creates the 2 variable classifier image:
%load('/Users/stewartlake/Documents/Retinalcontour/classifiers/reg bin
QDA/BSspec110520.mat');

Alax = linspace(21.11, 28.09, 50);
R3ax = linspace(0.2, 2.88, 50);
R5ax = linspace(0.39, 4.45, 50);

[R3v, R5v, Alv] = meshgrid(R3ax, R5ax, Alax);

Mdlcoord = cat(2, R3v(:), R5v(:), Alv(:));%three col array to match mdl data


quad4mdl1.Prior = [1 1];%in case it needs changing
Mdlspace = predict(quad4mdl1, Mdlcoord);% 0s and 1s

RDvol = Mdlcoord;%the region occupied by RD label
RDvol(Mdlspace==1,:) = [];%this is removing RD region as its larger than PVD!

%{
figure% this figure marks out the PVD group
scatter3(RDvol(:,1), RDvol(:,2), RDvol(:,3),750, '.');
xlabel('Region 3');
ylabel('Region 5');
zlabel('Axial length');
xlim([0.20 2.88]);
ylim([0.39 4.45]);
zlim([21.11 28.09]);
title('Volume of classifier space occupied by PVD')


figure - does not work
```

```
TD=delaunay(RDvol(:,1), RDvol(:,2), RDvol(:,3));
trisurf(TD,RDvol(:,1), RDvol(:,2), RDvol(:,3), 'EdgeColor','none',
'FaceColor','b');
xlabel('Region 3');
ylabel('Region 5');
zlabel('Axial length');
xlim([0.20 2.88]);
ylim([0.39 4.45]);
zlim([21.11 28.09]);
title('Volume of classifier space occupied by PVD')
%}

SurfC = Mdlcoord;

SurfC(~ischange(Mdlspace),:) = [];%remove all points in mdlspace not the surface
%between 0 (PVD) and 1 (RD) space


[xq,yq] =
meshgrid(min(SurfC(:,1)):range(SurfC(:,1))/75:max(SurfC(:,1)),min(SurfC(:,2)):range
(SurfC(:,2))/75:max(SurfC(:,2)));
Surfres = griddata(SurfC(:,1),SurfC(:,2),SurfC(:,3),xq,yq);

mesh(xq(1,:), yq(:,1), Surfres);
xlabel('Region 3');
ylabel('Region 5');
zlabel('Axial length');
xlim([0.20 2.88]);%max and min of each variable
ylim([0.39 4.45]);
zlim([21.11 28.09]);
title('Region of classifier space occupied by PVD')

%{
% alternative image - point cloud
ptC = pointCloud([xq(:) yq(:) Surfres(:)]);
pcshow(ptC);
xlabel('Retinal region 3');
ylabel('Retinal region 5');
zlabel('Axial length');
%xticks(0.20:0.2:2.88);
xlim([0.20 2.88]);%max and min of each variable
ylim([0.39 4.45]);
zlim([21.11 28.09]);
title('Region of classifier space occupied by PVD')
%pbaspect([8 2 1]);
%}
%%
%this creates a 2 D classifier image, as an example
%Variable max/mins from AL and the alldata arrays from BSspec

Alax2 = linspace(21.11, 28.09, 50);
R3ax2 = linspace(0.2, 2.88, 50);


[R3v2, Alv2] = meshgrid(R3ax2, Alax2);

Mdlcoord2 = cat(2, R3v2(:), Alv2(:));%two col array to match mdl data

quad2mdl = fitcdiscr(Trainset(:,[2 7]),TrsetD,'DiscrimType','quadratic');
%quad4mdl1.Prior = [1 1];%in case it needs changing
[Mdlspace2,scoreMdl2,~] = predict(quad2mdl, Mdlcoord2);% 0s and 1s

figure
scatter3(Mdlcoord2(:,2), Mdlcoord2(:,1), scoreMdl2(:,1),'b');
hold on
scatter3(Mdlcoord2(:,2), Mdlcoord2(:,1), scoreMdl2(:,2),'r');
xlabel('Axial length');
ylabel('Region 3');
zlabel('Probability');
view(40,43);
```

```
%title('Disciminant analysis surfaces, 2 variable model')
```

9. A2FFT. Lines 78-191 were written by Tyra Lange

```
%IMG to test result, (3,2) (5,3) AL QDA classifier function
%save xz data from tyra lange's graph theory shape identification A2;
%now works if img files are in Current folder, will ask for axial length, region3
cube
%name, then region 5 cube name. reports result in Command window.
%Works on Zeiss Cirrus HD 21 9 mm x 0.4 mm cubes, from superior and supero-temporal
retina
%CHANGE: have img folder on current folder
%CHANGE str2 line 24 (if not T data folder)
%ONCE cube x,z saved, edited length by accuracy on IMGs. Then FFT
%Typical run takes 9 minutes
%For each B scan mark the start (left hand side) and end (RHS) of
%accurately identified contour.
%If B scan is empty/no data/not wanted, enter start to the Right of the end
%Locates points by A scan, so only x index needed (z position does not need
%to be accurate)
%Graph theory & Dijkstra'a algorithm
%% Determine Number of Bscans in Cube
clear
prompt0 = 'Enter Eye ID: ';
EyeID = input(prompt0,'s');
prompt1 = 'Enter axial length: ';
AL1 = input(prompt1);
prompt2{1} = 'Enter name superior region cube IMG (eg T2 038 13-59-47.img: ';
prompt2{2} = 'Enter name superotemporal region cube IMG (eg T2 038 13-59-47.img: ';
str2 = '/Users/stewartlake/Documents/OCT RT T data/';
Ncubes = 2;
McubeFFT = cell(Ncubes,1);
%mkdir ([EyeID ' tiff']);

for Rc = 1:Ncubes

NowC{Rc} = input(prompt2{Rc},'s');

%%
%This section converts input IMG file to tiff for next section
IMGnm = [NowC{Rc} '.img'];
IMGfileID = fopen(IMGnm);
IMGfile = fread(IMGfileID);
%next line HD21 = [1024 1024 21], mac cube  = [512 1024 128],MChidef = [1024 1024
2]
IMGfile1 = uint8(reshape(IMGfile,[1024 1024 21]));
TsaveN = [EyeID ' ' IMGnm(30:end-27) '.tif']; %cube ID
%{
if (~exist([EyeID ' tiff/' ],'dir'))
       mkdir ([EyeID ' tiff/' ]);%creates tiff folder if not present
end

oldFolder = cd([EyeID ' tiff/' ]);
%}
for mt = 1:21

if mt==1
    imwrite(IMGfile1(:,:,mt)',TsaveN);%mac cube change mt to mt*6
else
    imwrite(IMGfile1(:,:,mt)',TsaveN,'WriteMode','append');

end
%cd (oldFolder)

end

%%
```

```
%FileTif = 'T2 028 13-59-47.tif'; %Insert cube tiff name here
FileTif = TsaveN;
InfoImage=imfinfo(FileTif);
NumberImages=length(InfoImage);
Xc1 = cell(NumberImages,1);
Zc1 = cell(NumberImages,1);
cubeFFT = NaN(30, NumberImages);
Cubefreq = NaN(30, NumberImages);
nowI = FileTif(1:6);%eye ID
startXY = NaN(NumberImages, 2);
finXY = NaN(NumberImages, 2);
DirChk = [str2 nowI '/FFTA2'];
if (~exist(DirChk,'dir'))
       mkdir (DirChk);%creates FFTA2 folder if not present
end

for i1=1:NumberImages
I = imread(FileTif, 'Index', i1);

%% Preprocessing

img = imfilter(I,fspecial('gaussian',[15 15],11));            % Blur Image
img = img > 0.75*max(img);                                    %

% Insert Vertical Column of Zeros (Both Sides)
size1 = size(img);                                            % Determine Size
(1024 x 1024)
img1 = zeros([size1(1) size1(2)+2]);                          % Matrix of Zeros
(Rows by Columns +2) (1024 x 1026)
img1(:,2:1+size1(2)) = img;                                   % Insert image from
2nd column to 2nd last column which is 1 more than img columns
                                                              % size is size of new
img with two extra columns (308 x 310)
sizeNew = size(img1);
%% Determine Graph Gradients (Graph Weights)

% get  vertical gradient image
G = nan(sizeNew);                                        % Matrix of NaN values of 308 x
310

for i3 = 1:sizeNew(2)                                     % For columns
    G(:,i3) = -1*gradient(img1(:,i3),2);                   % Positive vertical gradient
between 2 pixels
end

G = (G-min(G(:)))/(max(G(:))-min(G(:)));

G2 = G*-1+1;                                             % Get the "invert" of the
gradient image

%% Generate Adjacency Matrix

minWeight = 1E-5;                                        % Minimum weight

MW_pos = nan([numel(img1(:)) 8]);                        % Array to store positive
weights
MW_neg = nan([numel(img1(:)) 8]);                        % Array to store negative
weights
MX = nan([numel(img1(:)) 8]);                            % Array to store point A
locations
MY = nan([numel(img1(:)) 8]);                            % Array to store point B
locations

%Each node is associated with only its eight nearest neighbors

n = [1 1  1 0  0 -1 -1 -1; 1 0 -1 1 -1  1  0 -1];

%fill in the above arrays

szMW_pos = size(MW_pos);
```

```
ind = 1;


while ind ~= szMW_pos(1)*szMW_pos(2) %While ind not = col * row (not = 8404992)

    [i2, j] = ind2sub(szMW_pos,ind);  % i = 1050624x8, j = 1
    [iX,iY] = ind2sub(sizeNew,i2);

    jX = iX + n(1,j);
    jY  = iY + n(2,j);

     if jX >=1 && jX <= sizeNew(1) && jY >=1 && jY <= sizeNew(2) % 1024 , 1026
         %save weight

         % set to minimum if on the sides
         if jY == 1 || jY == sizeNew(2)
            MW_pos(i2,j) = minWeight;
            MW_neg(i2,j) = minWeight;

         % else, calculate the actual weights
         else
            MW_pos(i2,j) = 2 - G(iX,iY) - G(jX,jY) + minWeight;
            MW_neg(i2,j) = 2 - G2(iX,iY) - G2(jX,jY) + minWeight;
         end

        %save the subscript of the corresponding nodes
        MX(i2,j) = sub2ind(sizeNew,iX,iY);
        MY(i2,j) = sub2ind(sizeNew,jX,jY);
    end
    ind = ind+1;

end

%assemble the adjacency matrix
keepInd = ~isnan(MW_pos(:)) & ~isnan(MX(:)) & ~isnan(MY(:)) & ~isnan(MW_neg(:));
MW_pos = MW_pos(keepInd);
MW_neg = MW_neg(keepInd);
MX = MX(keepInd);
MY = MY(keepInd);

%sparse matrices, based on eq 1 with the gradient,
adjMatrixW = sparse(MX(:),MY(:),MW_pos(:),numel(img1(:)),numel(img1(:)));
                    % and the invert of gradient.
adjMatrixMW = sparse(MX(:),MY(:),MW_neg(:),numel(img1(:)),numel(img1(:)));

%% Shortest Path

% get layer going from light to dark
[ dist,path{1} ] = graphshortestpath( adjMatrixW, 1, numel(img1(:)) );
[pathX,pathY] = ind2sub(sizeNew,path{1});

% get rid of first and last few points that is by the image borders
pathX =pathX(gradient(pathY)~=0);
pathY =pathY(gradient(pathY)~=0);

Xc1{i1} = pathY;
Zc1{i1} = pathX;

%% Succesful RPE Delineation

BSfig = figure;
%BSfig.WindowState = 'maximized';
imagesc(I); axis image; colormap('gray'); hold on;
plot(pathY,pathX,'g-','linewidth',1.5); hold on;
legend({'rpe'});


[startXY(i1,1),startXY(i1,2)] = ginput(1);%start X,Y and finish X,Y from image
[finXY(i1,1),finXY(i1,2)] = ginput(1);
```

```
end

close all

%%
%set(startfinXY,'WindowStyle','normal');%attempt to undock and show
%variable

%edit above results with startXY and finXY

%data in Xc, Zc corrected by manually completed matrices startfinXY using
%ginput

%
startXY = fix(startXY);
finXY = fix(finXY);
%to remove a Bscan data,
%make startfinXY (Bs,1) one greater then startfin(BS,3), eg 513 and 512
%complete then run A2FFTa
Xc = cell(NumberImages,1);
Zc = cell(NumberImages,1);

for Tr = 1:NumberImages

    BsX = Xc1{Tr};
    BsZ = Zc1{Tr};

    StrtX = find(BsX == startXY(Tr,1));
    Fin1X = find(BsX == finXY(Tr,1));


   if StrtX(end)>Fin1X(1)

       Xc{Tr} = NaN(size(Xc1{Tr}'));%empty B scan vector if not wanted
       Zc{Tr} = NaN(size(Zc1{Tr}'));

   else

       BsX(Fin1X(1)+1:end) = [];
       BsZ(Fin1X(1)+1:end) = [];

       BsX(1:StrtX(end)-1) = [];
       BsZ(1:StrtX(end)-1) = [];

       Xc{Tr} = BsX';
       Zc{Tr} = BsZ';

   end

end


%%
%A2FFTPt2 follows on from A2FFT & A2FFTa. From Tyra's A2 function
%Performs FFT on Xc, Zc,
%one cube a time, with length Xc/Zc curated by accuracy in images from
%A2FFT second section
%this is from FFT4Eye to process FFT for OCT_R3 data
VecLen = NaN(NumberImages);
for Bs = 1:NumberImages

    if (~isnan(Zc{Bs}))
            L = length (Zc{Bs});

            [FFTz,freq] = FFTforOCT_R3mm(Xc{Bs},Zc{Bs});
            VecLen(Bs) = length(Zc{Bs});%vector length(FFT already corrected)

            %create matrix of residuals
            zVlen = size (Zc{Bs},1);
            zedres(1:zVlen,Bs) = Zc{Bs};
```

```
            %zedres = zedres(1:1024,fileNum);

            %save quadratic coefficients
            sf = 1024/9;
            xmm = Xc{Bs}/sf;
            sfz = 1024/2;
            ZMM = Zc{Bs}/sfz;
            p = polyfit(xmm,ZMM,2);%
            Quadcoeffs (1,Bs) = p(1);
            Quadcoeffs (2,Bs) = p(2);
            Quadcoeffs (3,Bs) = p(3);

            %put FFTz, freq into matrix, one column per B scan, bins by
            %rows
            cubeFFT(1:30,Bs) = FFTz(1:30);
            %cubeFFT(1:30,fileNum)=cubeFFT(1:30,fileNum)/VecLen(fileNuM);
            Cubefreq(1:30,Bs) = freq(1:30)';

            %now determine the relative proportion of each frequency bin to the
signal
            TSig(1,Bs) = sum (cubeFFT(:,Bs));
            CubeSigPror(1:30,Bs) = FFTz(1:30)'/TSig(1,Bs);

            %find number of bins to make 50% signal
            binprorV = CubeSigPror (1:30,Bs);
            BScusu (1:30) = cumsum (binprorV);
            NumBin50(1,Bs) = find (BScusu > 0.5, 1);

    else
        cubeFFT(1:30,Bs) = NaN(30,1);
%}
    end


end
%look like x vector = pathY, z-vector is pathX
%so save these two columns for use in new FFT processing above
%cubeFFT is for one cube
McubeFFT{Rc} = cubeFFT;%bins x B scans

        %now save each cube's data
        str4 = FileTif(1:end-4);% cube ID
        str6 = [DirChk '/' str4];
        save (str6, '-
regexp','^(?!(adjMatrixMW|adjMatrixW|G|G2|img|img1|MW_neg|MW_pos|MX|MY)$).');

end

load('/Users/stewartlake/Documents/Retinalcontour/classifiers/reg bin
QDA/Fs5Trs3v.mat');

%generate mean BS from average of 5 folds of RD/PVD eyes
for bl =1:5
    bsM(1:30,bl) = meanBS{bl};
end
bsMmean = mean(bsM,2);%average bin value from classifier data
bsMsd = std(bsM,0,2);
bsmsdall = mean(bsMsd);
bsMcoev = bsMsd./bsMmean;
bsMmncov = mean(bsMcoev);

%variables for model data
%if (3,2) and (5,3)
%(3,2) is first input cube bin 2: max(McubeFFT{1}(2,:))
%assuming r/c = bins/B scans
%(5,3) is second cube input bin 3: max(McubeFFT{2}(3,:))
%model data = cat((3,2),(5,3) Axl,)


numTeyes = 1;
```

```
Dcat = cell(numTeyes,2);%col 1 category labels, col 2 number of each category
Tvalvars = NaN(numTeyes,3);%variables for classifier

    %get bin diff by subtracting max val from
    Tvalvars(numTeyes,1) = max(abs(McubeFFT{1}(2,:) -
bsMmean(2)),[],'omitnan');%(3,2)
    Tvalvars(numTeyes,2) = max(abs(McubeFFT{2}(3,:) -
bsMmean(3)),[],'omitnan');%(5,3)

    Tvalvars(numTeyes,3) = AL1;%AxL



%then
quad4mdl1.Prior = [1 1];% change prior here as required
[Ttestlabels1,Tscore1] = predict (quad4mdl1,Tvalvars);
Rep = ['0 = not RD, 1 = RD, Eye ' EyeID];
Unwtrep = 'prior 1:1 test result';
Wtrep = 'prior 6:1 test result';
OWtrep = 'optimised prior, test result';

disp(Rep);
disp(Unwtrep);
disp(Ttestlabels1);

quad4mdl1.Prior = [6 1];% change prior here as required
[Ttestlabels6,Tscore6] = predict (quad4mdl1,Tvalvars);
disp(Wtrep);
disp(Ttestlabels6);

quad4mdl1.Prior = [0.64 0.36];% change prior here as required
[TtestlabelsO,TscoreO] = predict (quad4mdl1,Tvalvars);
disp(OWtrep);
disp(TtestlabelsO);
```

10. AnnotSLO

```
%AnnotSLO marks up the SLO images, changing the green/blue B scan marker
%lines to red where retinal signal is present in the B scan

%it assumes the pdfs have been merged into a single tiff file in the host
%eye folder named e.g., 'Q2 03 pdftif' (the 17 region identified cubes)

%a directory named 'png pdfs' is created in the eye folder
%THIS works, but do an eye at a time (set EyE manually)
%CHANGE
%CHANGE directory line 17, Eye line 28
locVec = [13 8 3 7 1 12 11 17 21 18 23 19 25 14 15 9 5];
%loc vec is the positions in a tiledlayout(5,5) corresponding to the index of
%FFT(:,6). So macula = cube 1 region = position 13 in (5,5)
load ('/Users/stewartlake/Documents/MATLAB/FFTconcat');
AllIconcat = cat(1,PVDFb,RDFb,RTFb,RepFb,MYFb,MHFb,GRTFb);

str1 = '/Users/stewartlake/Documents/OCT RT S data/';
cd (str1);
Einfo = dir;
Einfo = Einfo(~ismember({Einfo.name},{'.','..','.DS_Store'}));
Enames = {Einfo.name};%list of eye names
%{
Enames(47:end) = [];% left sided eyes remove first
Enames(1:36) = [];% RH eyes. these 2 line remove uncompleted eyes
%}
ENum = size (Enames,2);

for EyE = 26%:ENum %runs through the eye folders, or select individual
    Cprefix2 = Enames{EyE}(~isspace(Enames{EyE}));
    Cprefix=Cprefix2(1:2);%eye letter and laterality
```

```
    nowI = [str1, Enames{EyE},'/'];
    cd (nowI);%opens an eye folder
    %the merged tiff file of all the pdfs should be here

    if (~exist('png pdfs','dir'))
       mkdir ('png pdfs');%creates dir to place image files
    end

    %open the tiff and take each tiff sheet separately
    %import a tiff file
    Filetifnamestr= [Enames{EyE} ' pdftif.tiff'];

    if (exist(Filetifnamestr,'file')==2)%check pdftif created. If not, skip

    FileTif = Filetifnamestr; %puts eye pdf tiff file here
    %[~,cubenamestr,~]=fileparts(FileTif);%get cube name NOPE!
    InfoImage=imfinfo(FileTif);
    mImage=InfoImage(1).Width;
    nImage=InfoImage(1).Height;
    NumberImages=length(InfoImage);
    %FinalImage=zeros(nImage,mImage,NumberImages,'uint32');
    %FinalImage=cell(NumberImages,1);
    TifLink = Tiff(FileTif, 'r');
    cd ('png pdfs');
    for imi=1:NumberImages
        TifLink.setDirectory(imi);
        savename=['image', num2str(imi), '.png'];
        IMG1=TifLink.read();
        imwrite(IMG1(:,:,1:3), savename);%the set of tiff images from the
        %cube, saved in /png pdfs,
    end
    TifLink.close();
    mkdir ('Annot');%save folder for annotated pngs

    for cubescans=1:NumberImages%working through each tiff sheet

        savename=['image', num2str(cubescans), '.png'];
       Curimg=imread(savename);
       %Input file Curimg is current tiff sheet of pdfs

       SLOpart=imcrop(Curimg,[849 1355 1855 1543]);%copy SLO image: [205 333 483
400]

      %[imi,
j]=find((SLOpart(:,:,1)~=SLOpart(:,:,2))&(SLOpart(:,:,1)~=SLOpart(:,:,3)));
      %grey pixels have (approx)= sheet values in 1,2,3, so not equal is a colour

      [imi,
j]=find(((SLOpart(:,:,1)+9)<SLOpart(:,:,2))|((SLOpart(:,:,1)+9)<SLOpart(:,:,3)));
      %G or B greater than R by 10 is a line.

      %first and last of j are the start and end column of the SLO line
      BSfirst = j(1);
      BSlast = j(end);

      [uniI,iaI,icI]=unique(imi);
      Icounts=accumarray(icI,1);
      valcountsI=[uniI,Icounts];%col2 > 400 has horizontal line y coordinate in
col1
      LongI=uniI(Icounts>400);%y coords of the coloured lines

      SLOpicnew=SLOpart;%copy of image

      %now find distinct lines
      GaP=find(diff(LongI)>3);%20 break points for 21 lines

      xzstr=[nowI, Enames{EyE},' xz'];
      xzdir=dir(xzstr);%list of xz data files
      xzdir = xzdir(~ismember({xzdir.name},{'.','..','.DS_Store'}));
```

```
        xznames={xzdir.name};
        xzcubestr=[xzstr,'/', xznames{cubescans}];

        %{
        Finfo=dir;
        Finfo = Finfo(~ismember({Finfo.name},{'.','..','.DS_Store'}));
        Fnames={Finfo.name};
        FoldNum=size(Fnames,2);%number of cubes
        %}

        oldfolder = cd (xzcubestr);
        dinfo = dir(xzcubestr);
        names_cell = {dinfo.name};

        out=regexp(names_cell,'\d+','match');
        out=str2double(cat(1,out{:}));
        numFiles = size(out, 1);%number of Bscan data files
        outR = flipud(out);%reversed as top B scan is number 21


        startRow = 1;
        endRow = inf;

for fileNum = 1:numFiles
            Bscanline = outR(fileNum,end);
            %This loop is for a single cube xz data
            %outR is the line to highlight, Bscanline the data to match
            fileNamea = sprintf('-%04d.txt',Bscanline);
            fileName = [Cprefix fileNamea];
            myData{Bscanline} = importfile(fileName,startRow,endRow);

            ximp{Bscanline}=myData{Bscanline}(:,1);
            zimp{Bscanline}=myData{Bscanline}(:,2);

            %now format x and z for FFT
            x=table2cell(ximp{Bscanline});
            z=table2cell(zimp{Bscanline});
            x=cell2mat(x);
            z=cell2mat(z);

            x1=x(1);%first element coordinate from livewire;
            xn=x(end);%last element from Livewire

    %startL:GaP(Bscanline) is current Bscan rows in image

    %SLO green line length
    %livewire vector is x1 to xn out of 1-1024
    %so xz is (x*BSlength/1024)-38 in this image (which is j values)
    %reverse with f(x)=(max+min)-x as B scans are inverted
    %image is 484 columns (line 70)
    BSlength = BSlast - BSfirst;
    imgwidth=size(SLOpicnew,2);
    BSbegin = imgwidth-BSlast;
    xend=floor(imgwidth - (x1*BSlength/1024)-BSbegin);
    xstart=floor(imgwidth - (xn*BSlength/1024)-BSbegin);

    if Bscanline==21
        if LongI(1) == 1
            LongI(1) = 2;
        end
       SLOpicnew(LongI(1)-1:LongI(GaP(1))+1,xstart:xend,1)=255;
       SLOpicnew(LongI(1)-1:LongI(GaP(1))+1,xstart:xend,2)=0;
       SLOpicnew(LongI(1)-1:LongI(GaP(1))+1,xstart:xend,3)=0;

    elseif Bscanline==1
       SLOpicnew(LongI(GaP(end)+1)-1:LongI(end)+1,xstart:xend,1)=255;
       SLOpicnew(LongI(GaP(end)+1)-1:LongI(end)+1,xstart:xend,2)=0;
       SLOpicnew(LongI(GaP(end)+1)-1:LongI(end)+1,xstart:xend,3)=0;

    else
```

```
        SLOpicnew(LongI(GaP(21-Bscanline)+1)-1:LongI(GaP(22-
Bscanline))+1,xstart:xend,1)=255;
        SLOpicnew(LongI(GaP(21-Bscanline)+1)-1:LongI(GaP(22-
Bscanline))+1,xstart:xend,2)=0;
        SLOpicnew(LongI(GaP(21-Bscanline)+1)-1:LongI(GaP(22-
Bscanline))+1,xstart:xend,3)=0;
        %-1/+1 at end of SLOpicnew row range is to thicken the lines
    end

end

savestr= [nowI, 'png pdfs/Annot/', xznames{cubescans}, '.png'];
cd(oldfolder);%go back to png pdfs folder
imwrite(SLOpicnew, savestr);


    end
    %{
    %block out here if not matching
    cd('Annot');
    picinfo=dir;
    picinfo = picinfo(~ismember({picinfo.name},{'.','..','.DS_Store'}));
    picnames = {picinfo.name};%list of eye names
    picNum = size (picnames,2);

    for pic = 1:picNum
        Cprefix3 = picnames{pic}(1:5);
        Cprefix3 = Cprefix3(~isspace(Cprefix3));

        Irow = find(strcmp(Cprefix3,AllIconcat(:,1)));%the concat row of current
eye
        SplNm=strsplit(picnames{pic});
        CubeNum=SplNm(3);%the number of the cube image

        Pe = locVec(find(isequal(CubeNum{1}, AllIconcat{Irow,6}(:))));
       %Pe is subplot location of this cube
       if ~isempty(Pe)
           subplot(5,5,Pe)
           imshow(SLOpicnew)
       end
    end

    savefigstr=[Enames{EyE}, 'SLOmosaic'];
    savefig(savefigstr);%saves mosaic in png pdfs folder
    %end block out here if not matching
    %}
    end
end

%create SLOmap
cd([str1 Cprefix2(1:2) ' ' Cprefix2(3:4) '/png pdfs/Annot/']);
colSLO = dir;
colSLO = colSLO(~ismember({colSLO.name},{'.','..','.DS_Store'}));
SLOnames = {colSLO.name};%list of eye names
SLOmap = tiledlayout(5,5);
SLOmap.TileSpacing = 'none';
SLOmap.Padding = 'none';
nexttile
imshow(SLOnames{5});

nexttile(3)
imshow(SLOnames{3});

nexttile(5)
imshow(SLOnames{17});

nexttile(7)
imshow(SLOnames{4});

nexttile(8)
```

```
imshow(SLOnames{2});

nexttile(9)
imshow(SLOnames{16});

nexttile(11)
imshow(SLOnames{7});

nexttile(12)
imshow(SLOnames{6});

nexttile(13)
imshow(SLOnames{1});

nexttile(14)
imshow(SLOnames{14});

nexttile(15)
imshow(SLOnames{15});

nexttile(17)
imshow(SLOnames{8});

nexttile(18)
imshow(SLOnames{10});

nexttile(19)
imshow(SLOnames{12});

nexttile(21)
imshow(SLOnames{9});

nexttile(23)
imshow(SLOnames{11});

nexttile(25)
imshow(SLOnames{13});

namefig = [str1 Cprefix2(1:2) ' ' Cprefix2(3:4) '/' Cprefix2 ' SLOmap'];
savefig(namefig);
```

11. Comprep

```
%to compare RepFb eyes by cube region
%compared to a "training set" of the PVD eyes
%Have MATLAB as current folder: FFTconcat and AllIKurv are loaded
%
clear
load('/Users/stewartlake/Documents/MATLAB/FFTconcat');
load('/Users/stewartlake/Documents/MATLAB/AllIKurv');

NumRep = size (RepFb, 1);
NumPVD = size (PVDFb, 1);

RepeyeID=repmat(RepFb(:,1),[1,18]);%vector of Rep eye names
PVDeyeID = repmat(PVDFb(:,1),[1,18]);%

Repcols = cell(NumRep,18);
RepRegcubeID = cell(NumRep,18);
KurvrowRep = cell(NumRep,18);
PVDcols = cell(NumPVD,18);
PVDRegcubeID = cell(NumPVD,18);
KurvrowPVD = cell(NumPVD,18);

absdiffRep = cell(NumRep,18);
maxabsd = cell(NumRep,18);
SumdiffRep = cell(NumRep,18);
maxeBsRep = cell(NumRep,18);
```

```
IndMeBsRep = cell(NumRep,18);
rmsdRep = cell(NumRep,18);
IKurv = cell(NumRep,18);%whole eye Kurv data
CKurv = cell(NumRep,18);%cube curve data to match sumdiff etc
MedCkurv = zeros(NumRep,18);%features, row per eye...
MedMaxe = zeros(NumRep,18);%column per cube region...
MedSD = zeros(NumRep,18);%first column will be empty
Medrmsd = zeros(NumRep,18);
MaxCkurv = zeros(NumRep,18);
MaxMaxe = zeros(NumRep,18);
MaxSD = zeros(NumRep,18);
Maxrmsd = zeros(NumRep,18);
MinCkurv = zeros(NumRep,18);
MinMaxe = zeros(NumRep,18);
MinSD = zeros(NumRep,18);
Minrmsd = zeros(NumRep,18);
iqrCkurv = zeros(NumRep,18);
iqrMaxe = zeros(NumRep,18);
iqrSD = zeros(NumRep,18);
iqrrmsd = zeros(NumRep,18);

for Region = 2:18 %Region should be 2-18 - columns of locFFT/column 11 of Fb


%This section gets the cubes for this region
for Iye = 1:NumRep %size(RepFb,1)

    Repcols(Iye,Region)=RepFb{Iye,11}(Region);%vector of Repcube FFT data for
region
    Repcols{Iye,Region}=Repcols{Iye,Region}(:,any(Repcols{Iye,Region}));%removes
empty Bscan columns
    RepRegcubeID(Iye,Region) = RepFb{Iye,6}(Region-1);
    if RepRegcubeID{Iye,Region}~=0
        KurvrowRep{Iye,Region} =
find(contains(RepFb{Iye,5}(:),num2str(RepRegcubeID{Iye,Region})));
    end
end

for Iye=1:NumPVD %size(PVDFb,1)

    PVDcols(Iye,Region)=PVDFb{Iye,11}(Region);%vector of all PVD cube FFTs this
region
    PVDRegcubeID(Iye,Region) = PVDFb{Iye,6}(Region-1);
    if PVDRegcubeID{Iye,Region}~=0
        KurvrowPVD{Iye,Region} =
find(contains(PVDFb{Iye,5}(:),num2str(PVDRegcubeID{Iye,Region})));
    end
end

%remove empty values
Tempcurv=KurvrowRep(:,Region);
Tempcurv(cellfun('isempty',Repcols(:,Region)))={NaN};
KurvrowRep(:,Region)=Tempcurv;

TemprepID=RepeyeID(:,Region);
TemprepID(cellfun('isempty',Repcols(:,Region)))={NaN};
RepeyeID(:,Region)=TemprepID;

Temprepcols=Repcols(:,Region);
Temprepcols(cellfun('isempty',Repcols(:,Region)))={NaN(30,1)};
Repcols(:,Region)=Temprepcols;

%remove empty values
TempKPVD=KurvrowPVD(:,Region);
TempKPVD(cellfun('isempty', PVDcols(:,Region)))={NaN};
KurvrowPVD(:,Region)=TempKPVD;

TempPVDID=PVDeyeID(:,Region);
TempPVDID(cellfun('isempty', PVDcols(:,Region)))={NaN};
PVDeyeID(:,Region)=TempPVDID;
```

```
TempPVDcols=PVDcols(:,Region);
TempPVDcols(cellfun('isempty', PVDcols(:,Region)))={NaN(30,21)};
PVDcols(:,Region)=TempPVDcols;

PVDset = cat (2,PVDcols{:,Region});%all PVD cubes in a strip
PVDset(PVDset==0) = NaN;
TSbmn = mean(PVDset,2,'omitnan');%mean bin value for PVD cubes


for n=1:NumRep

    %the objective is to compare matched values for rescanned eyes
    %matched values should be pairs of n(1&2, 3&4, 5&6, 7&8)
    absdiffRep {n,Region} = abs(Repcols{n,Region} - TSbmn);%30 bin x 21 Bscans
    maxabsd{n,Region} = max(absdiffRep {n,Region},[],2,'omitnan');%vector max each
bin in cube
    SumdiffRep {n,Region} = sum(absdiffRep{n,Region}); %total value per B scan
    %SumdiffRep {n,Region} = permute (SumdiffRep{n,Region}, [3 2 1]); %sumabsdiff
moduli, 1 cube x Bs

    [maxeBsRep{n,Region}, IndMeBsRep{n,Region}] = max(abs(Repcols{n,Region} -
TSbmn));

    %maxeBsRep {n,Region} = permute (maxeBsRep {n,Region}, [3 2 1]);%
    %IndMeBsRep{n,Region} = permute (IndMeBsRep{n,Region}, [3 2 1]);

    rmsdRep {n,Region} = sqrt ((sum
(absdiffRep{n,Region}.*absdiffRep{n,Region}))/30);

    %match curvature array sheet with current eye/cube sumdiff
    Kurvmatch=find(strncmp(RepeyeID{n},AllIEyenames2,4));
    IKurv{n,Region} = AllIBsKurv(:,:,Kurvmatch);
    IKurv{n,Region} = IKurv{n,Region}(any(IKurv{n,Region},2),:);%removes empty rows
    if ~isnan(KurvrowRep{n,Region})
    CKurv{n,Region} = IKurv{n,Region}(KurvrowRep{n,Region},:);
    else
    CKurv{n,Region} = NaN;
    end

    MedCkurv(n,Region) = median(CKurv{n,Region}(:),'omitnan');
    MedMaxe(n,Region) = median(maxeBsRep{n,Region}(:),'omitnan');
    MedSD(n,Region) = median(SumdiffRep{n,Region}(:),'omitnan');
    Medrmsd(n,Region) = median(rmsdRep{n,Region}(:),'omitnan');

    MaxCkurv(n,Region) = max(CKurv{n,Region}(:),[],'omitnan');
    MaxMaxe(n,Region) = max(maxeBsRep{n,Region}(:),[],'omitnan');
    MaxSD(n,Region) = max(SumdiffRep{n,Region}(:),[],'omitnan');
    Maxrmsd(n,Region) = max(rmsdRep{n,Region}(:),[],'omitnan');

    MinCkurv(n,Region) = min(CKurv{n,Region}(:),[],'omitnan');
    MinMaxe(n,Region) = min(maxeBsRep{n,Region}(:),[],'omitnan');
    MinSD(n,Region) = min(SumdiffRep{n,Region}(:),[],'omitnan');
    Minrmsd(n,Region) = min(rmsdRep{n,Region}(:),[],'omitnan');

    iqrCkurv(n,Region) = iqr(CKurv{n,Region}(:));
    iqrMaxe(n,Region) = iqr(maxeBsRep{n,Region}(:));
    iqrSD(n,Region) = iqr(SumdiffRep{n,Region}(:));
    iqrrmsd(n,Region) = iqr(rmsdRep{n,Region}(:));

end


end

save ('/Users/stewartlake/Documents/Retinalcontour/Retest eyes/Region retest
summary 2');


%{
```

```
%1. to compare eye retests by ICC
colfirst = cell(NumRep/2,1);
col2d = cell(NumRep/2,1);
for Rowrun = 1:2:NumRep-1

colfirst{(Rowrun+1)/2} = [MedSD(Rowrun,2:end) MaxSD(Rowrun,2:end)
MinSD(Rowrun,2:end)...
 iqrSD(Rowrun,2:end) MedMaxe(Rowrun,2:end) MaxMaxe(Rowrun,2:end)...
 MinMaxe(Rowrun,2:end) iqrMaxe(Rowrun,2:end)...
 Medrmsd(Rowrun,2:end) Maxrmsd(Rowrun,2:end) Minrmsd(Rowrun,2:end)...
 iqrrmsd(Rowrun,2:end) MedCkurv(Rowrun,2:end) MaxCkurv(Rowrun,2:end)...
 MinCkurv(Rowrun,2:end) iqrCkurv(Rowrun,2:end)]';

end

for Reprun = 2:2:NumRep

%creates arrays for each eye

col2d{Reprun/2} = [MedSD(Reprun,2:end) MaxSD(Reprun,2:end) MinSD(Reprun,2:end)...
 iqrSD(Reprun,2:end) MedMaxe(Reprun,2:end) MaxMaxe(Reprun,2:end)...
 MinMaxe(Reprun,2:end) iqrMaxe(Reprun,2:end) Medrmsd(Reprun,2:end)...
 Maxrmsd(Reprun,2:end) Minrmsd(Reprun,2:end) iqrrmsd(Reprun,2:end)...
 MedCkurv(Reprun,2:end) MaxCkurv(Reprun,2:end) MinCkurv(Reprun,2:end)
iqrCkurv(Reprun,2:end)]';

%for ICC need to compare columns, so colfirst/2d contents in single column



end

for runICC = 1:length(col2d)

    for Others = 1:length(col2d)
    CurI = cat(2,colfirst{runICC},col2d{Others});
    origsize(runICC) = size(CurI,1);
    CurI(any(isnan(CurI), 2), :) = [];%remove any metrics where no matching data
(NaN)
    corsize(runICC) = size(CurI,1);

    Numdleted(runICC) = origsize(runICC) - corsize(runICC);

    ICCres(runICC,Others) = icc21(CurI);

   end
end
%}




%{
2. to compare eye retests by signrank
for Rowrun = 1:2:NumRep-1

Eyerun1st = Rowrun;% the row no first eye run

for Reprun = 2:2:NumRep

Eyerun2d = Reprun;%row number 2d eye run
%creates
colfirst = [MedSD(Eyerun1st,2:18) MaxSD(Eyerun1st,2:18) MinSD(Eyerun1st,2:18)...
 iqrSD(Eyerun1st,2:18) MedMaxe(Eyerun1st,2:18) MaxMaxe(Eyerun1st,2:18)...
 MinMaxe(Eyerun1st,2:18) iqrMaxe(Eyerun1st,2:18)...
 Medrmsd(Eyerun1st,2:18) Maxrmsd(Eyerun1st,2:18) Minrmsd(Eyerun1st,2:18)...
 iqrrmsd(Eyerun1st,2:18) MedCkurv(Eyerun1st,2:18) MaxCkurv(Eyerun1st,2:18)...
 MinCkurv(Eyerun1st,2:18) iqrCkurv(Eyerun1st,2:18)];
```

```
col2d = [MedSD(Eyerun2d,2:18) MaxSD(Eyerun2d,2:18) MinSD(Eyerun2d,2:18)...
 iqrSD(Eyerun2d,2:18) MedMaxe(Eyerun2d,2:18) MaxMaxe(Eyerun2d,2:18)...
 MinMaxe(Eyerun2d,2:18) iqrMaxe(Eyerun2d,2:18) Medrmsd(Eyerun2d,2:18)...
 Maxrmsd(Eyerun2d,2:18) Minrmsd(Eyerun2d,2:18) iqrrmsd(Eyerun2d,2:18)...
 MedCkurv(Eyerun2d,2:18) MaxCkurv(Eyerun2d,2:18) MinCkurv(Eyerun2d,2:18)
iqrCkurv(Eyerun2d,2:18)];

p(Rowrun,Reprun)=signrank(colfirst,col2d);

storeI2{Reprun/2} = col2d;
storeI1{Reprun/2} = colfirst;

end


end
%}
```

12. ComprepBA

```
%analyse rep eye data from CompRep,using Bland Altman plots. Saved in BA plots
folder
% stored in Retest eyes/Region retest summary 2
%CHANGE LoAhi, LoAlo for upper and lower LoA found after running once lines
%CHANGE 101-102. then re-run final outlyer analysis plot,
%CHANGE eye/symbols 200-203, 278-279
%see Does PVD or RD change all of eye metrics.doc for guide
%needed for BA function. Not sure
Gnames = {'test1', 'test2', 'test3', 'test4', 'test5', 'test6', 'test7', 'test8',
'test9','test10'};
%black(k) = control eyes, blue (c/b) = PVD, red (r/m) = RD
%%
%organise data
for Rowrun = 1:2:NumRep-1

Eyerun1st = Rowrun;% the row no first eye run

for Reprun = 2:2:NumRep

Eyerun2d = Reprun;%row number 2d eye run
%creates
colfirst = [MedSD(Eyerun1st,2:18) MaxSD(Eyerun1st,2:18) MinSD(Eyerun1st,2:18)...
 iqrSD(Eyerun1st,2:18) MedMaxe(Eyerun1st,2:18) MaxMaxe(Eyerun1st,2:18)...
 MinMaxe(Eyerun1st,2:18) iqrMaxe(Eyerun1st,2:18)...
 Medrmsd(Eyerun1st,2:18) Maxrmsd(Eyerun1st,2:18) Minrmsd(Eyerun1st,2:18)...
 iqrrmsd(Eyerun1st,2:18) MedCkurv(Eyerun1st,2:18) MaxCkurv(Eyerun1st,2:18)...
 MinCkurv(Eyerun1st,2:18) iqrCkurv(Eyerun1st,2:18)];

col2d = [MedSD(Eyerun2d,2:18) MaxSD(Eyerun2d,2:18) MinSD(Eyerun2d,2:18)...
 iqrSD(Eyerun2d,2:18) MedMaxe(Eyerun2d,2:18) MaxMaxe(Eyerun2d,2:18)...
 MinMaxe(Eyerun2d,2:18) iqrMaxe(Eyerun2d,2:18) Medrmsd(Eyerun2d,2:18)...
 Maxrmsd(Eyerun2d,2:18) Minrmsd(Eyerun2d,2:18) iqrrmsd(Eyerun2d,2:18)...
 MedCkurv(Eyerun2d,2:18) MaxCkurv(Eyerun2d,2:18) MinCkurv(Eyerun2d,2:18)
iqrCkurv(Eyerun2d,2:18)];

p(Rowrun,Reprun)=signrank(colfirst,col2d);



storeI2{Reprun/2} = col2d;
storeI1{Reprun/2} = colfirst;
end


end

%below values are row number for pairs of eyes in RepFb
```

```
bincol1= maxabsd([1 3 5 7 9 11 13 15 17 19 21 23 25],2:end);%bin maxima for each
region and eye image 1
bincol2= maxabsd([2 4 6 8 10 12 14 16 18 20 22 24 26],2:end);%second image set of
eye. Increase as more eyes added
binrangemin =2;%max & min bins to be used in BA plot
binrangemax = 20;
for obin = 1:13%eye pairs - increase as eyes added to RepFb
    for obinc = 1:17%regions

    Ibin3d1(1:(binrangemax-binrangemin)+1,obinc,obin) =
bincol1{obin,obinc}(binrangemin:binrangemax);%array for BA plot
    Ibin3d2(1:(binrangemax-binrangemin)+1,obinc,obin) =
bincol2{obin,obinc}(binrangemin:binrangemax);%bins x regions x eye
    end
end
%%

for Drw = 1:NumRep/2

    %BlandAltman(storeI1{Drw}',storeI2{Drw}','baStatsMode','Non-parametric',
'diffValueMode','percent');
    %namsav = RepeyeID{Drw*2,1};
    %plots and saves each eye BA individually
    %savefig(namsav)

    %data for single BA for all eyes/data
    sqI1a(1:17,1:16,Drw) = reshape(storeI1{Drw},[17,16]);%raw data arrays, eye
test1
    sqI2a(1:17,1:16,Drw) = reshape(storeI2{Drw},[17,16]);% and eye test 2 (med/mean
SD etc)
    %region x vars (1-16 - colfirst & 2d) x eye

    Xmeanval{Drw}=(storeI1{Drw}'+storeI2{Drw}')/2;%X coord BA (mean)
    Ydiffval{Drw} = (storeI1{Drw}-storeI2{Drw})';%y coords for BA (diff)


end

sqI1 = permute(sqI1a,[2 1 3]);%convert to vars x regions x eye

sqI2 = permute(sqI2a,[2 1 3]);

%%
%First BA method
%all eye data BA plot: difference (not ratio) to value
%{
BlandAltman(sqI1, sqI2,Gnames, 'baStatsMode','Non-parametric',...
    'symbols','Num','colors','rbgmckyw','markerSize',7);
%this for colfirst/2d data ie stat sumar variables


set(gca, 'color', [0.6 0.6 0.6]); %set background colour to grey (to see white)
%}
%%
Ydiffs= sqI2 - sqI1;%the y coordinates of the BA plot

%tables give variable/region/eye of outlying values
[Yhi{1},Yhi{2},Yhi{3}] = ind2sub(size(Ydiffs),find(Ydiffs>1.3));%row/col =
variable/region of outliers
Yhitab = table(Yhi{1},Yhi{2},Yhi{3}, 'Variablenames',{'variable','region','eye'});

[Ylow{1},Ylow{2},Ylow{3}] = ind2sub(size(Ydiffs),find(Ydiffs<-1.2));
Ylowtab = table(Ylow{1},Ylow{2},Ylow{3},
'Variablenames',{'variable','region','eye'});

LoAhi = 0.97;
LoAlo = -0.92;
```

```
%%
%creates arrays of the X, Y data (mean/diff) for the eyes
Nm = repelem(17,16);
tabrownm = {'MedSD'; 'MaxSD'; 'MinSD';...
 'iqrSD'; 'MedMaxe'; 'MaxMaxe';...
 'MinMaxe'; 'iqrMaxe';...
 'Medrmsd'; 'Maxrmsd'; 'Minrmsd';...
 'iqrrmsd'; 'MedCkurv'; 'MaxCkurv';...
 'MinCkurv'; 'iqrCkurv'};
Tabroenames = repelem(tabrownm,Nm);

%convert variable number to name in outlier tables Yhi Ylow
for Getname=1:length(Yhitab.eye)
    outliersourcehi{Getname} = tabrownm(Yhitab.variable(Getname));
end
Yhitab.varname=outliersourcehi';

for Getnamelow=1:length(Ylowtab.eye)
    outliersourcelow{Getnamelow} = tabrownm(Ylowtab.variable(Getnamelow));
end
Ylowtab.varname=outliersourcelow';

%{
%hist plot of BA outliers by region
figure
outlyreg = histogram ([Yhitab.region; Ylowtab.region]);
xticks(1:17);

%hist plot BA variable (number corr to name in tabrownm)
figure
outlyvar = histogram ([Yhitab.variable; Ylowtab.variable]);
xticks([1 2 3 4 5 6 7 8]);
xticklabels({'MedSD', 'MaxSD', 'MinSD',...
 'iqrSD', 'MedMaxe', 'MaxMaxe','MinMaxe', 'iqrMaxe'});

%}
%%
%Second BA method: analysis of log 2 BA plot, stats variables (col1st/2d)
%uncommment 150-151, 174-189 to use
indi1 = find(sqI1<0);
indi2 = find(sqI2<0);

logsq1 = log2(abs(sqI1));
logsq2 = log2(abs(sqI2));
logsq1(:,:,10:12)=[];%this removed second last eye (PVD =9, or 10 for first RD, or
11 for 2d RD, 12 2d PVD) eye)
logsq2(:,:,10:12)=[];% 13 is S2/4 10 - PVD
%BlandAltman(logsq1, logsq2,Gnames, 'baStatsMode','Non-parametric',...
%    'symbols','Num','colors','kkkkkkkkbrmc','markerSize',7);


logYdiffs= logsq2 - logsq1;%the log2 y coordinates of the BA plot

%tables give variable/region/eye of outlying values (log2)
[YhiL{1},YhiL{2},YhiL{3}] = ind2sub(size(logYdiffs),find(logYdiffs>2));%row/col =
variable/region of outliers
YhiLtab = table(YhiL{1},YhiL{2},YhiL{3},
'Variablenames',{'variable','region','eye'});

[YlowL{1},YlowL{2},YlowL{3}] = ind2sub(size(logYdiffs),find(logYdiffs<-2.1));
YlowLtab = table(YlowL{1},YlowL{2},YlowL{3},
'Variablenames',{'variable','region','eye'});

%convert variable number to name in outlier tables Yhi Ylow (log 2)
for GetnameL=1:length(YhiLtab.eye)
    outliersourcehiL{GetnameL} = tabrownm(YhiLtab.variable(GetnameL));
end
YhiLtab.varname=outliersourcehiL';

for GetnamelowL=1:length(YlowLtab.eye)
```

```
    outliersourcelowL{GetnamelowL} = tabrownm(YlowLtab.variable(GetnamelowL));
end
YlowLtab.varname=outliersourcelowL';

%{
%hist plot of BA log outliers by region
figure
outlyregL = histogram ([YhiLtab.region; YlowLtab.region]);
xticks(1:17);

%hist plot BA log variable (number corr to name in tabrownm)
figure
outlyvarL = histogram ([YhiLtab.variable; YlowLtab.variable]);
xticks(1:16);
xticklabels({'MedSD', 'MaxSD', 'MinSD',...
 'iqrSD', 'MedMaxe', 'MaxMaxe','MinMaxe', 'iqrMaxe',...
 'Medrmsd', 'Maxrmsd', 'Minrmsd','iqrrmsd', 'MedCkurv', 'MaxCkurv',...
 'MinCkurv', 'iqrCkurv'});
title('LoA outliers of summary metrics');
%}

%%
%Second BA method: analysis of log 2 BA plot of bin maxima each cube
indi1bin = find(Ibin3d1<0);%this from maxabsd (from compRep), the cube max diff
indi2bin = find(Ibin3d2<0);% from average Bscan for each bin

logbin1 = log2(abs(Ibin3d1));
logbin2 = log2(abs(Ibin3d2));
logbin1(:,:,[9:12])=[];%this removes eyes (PVD =9/12, or 10/11 for RD) eye)
logbin2(:,:,[9:12])=[];%13 is S2/4 10 = PVD
BlandAltman(logbin1, logbin2,Gnames, 'Pre/post PVD','Non-parametric',...
    'symbols','.................','colors','kkkkkkkkrbmcr','markerSize',7);
%BlandAltman(logbin1, logbin2,Gnames, 'Pre/post PVD S113/125','Non-parametric',...
%    'symbols','Num','colors','kkkkkkkkbrmc','markerSize',7);
%with 199-200 used, the colour of studied eye is the ninth letter in colors


logYdiffsbn= logbin2 - logbin1;%the log2 y coordinates of the BA plot

%tables give variable/region/eye of outlying values (log2)
%the numbers after > & < taken from viewing the range values in BA plot
[YhiLb{1},YhiLb{2},YhiLb{3}] =
ind2sub(size(logYdiffsbn),find(logYdiffsbn>LoAhi));%row/col = variable/region of
outliers
YhiLtabbn = table(YhiLb{1},YhiLb{2},YhiLb{3},
'Variablenames',{'bin','region','eye'});


[YlowLb{1},YlowLb{2},YlowLb{3}] =
ind2sub(size(logYdiffsbn),find(logYdiffsbn<LoAlo));
YlowLtabbn = table(YlowLb{1},YlowLb{2},YlowLb{3},
'Variablenames',{'bin','region','eye'});


%hist plot of BA log outliers by region
figure
outlyregLb = histogram ([YhiLtabbn.region; YlowLtabbn.region]);
xticks(1:17);
title('LoA anomaly outliers by frequency region');

%hist plot BA log variable (number corr to name in tabrownm)by bin???
figure
outlyvarLb = histogram ([YhiLtabbn.bin; YlowLtabbn.bin]);
xticks(1:30);
title('LoA anomaly outliers by frequency bin');
%xticklabels();
%%
 BAXvals =
table(Tabroenames,Xmeanval{1},Xmeanval{2},Xmeanval{3},Xmeanval{4},Xmeanval{5},Xmean
val{6},...
```

```
     Xmeanval{7},Xmeanval{8});

 BAXarray =
cat(2,Xmeanval{1},Xmeanval{2},Xmeanval{3},Xmeanval{4},Xmeanval{5},Xmeanval{6},...
     Xmeanval{7},Xmeanval{8});%the mean of each value across the 2 tests

  BAYarray =
cat(2,Ydiffval{1},Ydiffval{2},Ydiffval{3},Ydiffval{4},Ydiffval{5},Ydiffval{6},...
     Ydiffval{7},Ydiffval{8});%the mean of each value across the 2 tests



 for flipX=1:16

     lreg=17*flipX;
     freg=lreg-16;

     BAXcube(flipX,:,1:17)=permute(BAXarray(freg:lreg,1:8),[3 2 1]);
     BAYcube(flipX,:,1:17)=permute(BAYarray(freg:lreg,1:8),[3 2 1]);
     %variable(med/max etc) x eye x region



 end

 %%
 %plot outliers from LoA
 figure
 Eye = 9; %eye indexm usually 9
 Hival = (YhiLtabbn.eye==Eye);
 Loval = (YlowLtabbn.eye==Eye);
 scatter (YhiLtabbn.region(Hival), YhiLtabbn.bin(Hival)+1,50,'+m');%+1 for 2-20
from 1-19
 hold on
 scatter (YlowLtabbn.region(Loval), YlowLtabbn.bin(Loval)+1,50,'xr');
 ylim([0 21]);
 xlim([0 18]);
 legend({'Above LoA','Below LoA'},'Location','best');
 xlabel('Region');
 ylabel('Bin');
 title('Anomaly values for study eye outside LoA');

 %identify outliying LoA anomaly values. MATCH Ibin3d1/2 to lines199-200
hivals = find(logYdiffsbn>LoAhi);
hivals(hivals<2584) = [];%19 x 17 x 8 = 2584, remove rep eyes
anomsused1 = Ibin3d1(:,:,[1:8,13]);%1:8 plus the eye used in 200-202
anomsused2 = Ibin3d2(:,:,[1:8,13]);
hianom1 = anomsused1(hivals);
hianom2 = anomsused2(hivals);

lovals = find(logYdiffsbn<LoAlo);
lovals(lovals<2584) = [];
loanom1 = anomsused1(lovals);
loanom2 = anomsused2(lovals);

figure
His1 = histogram([hianom1; loanom1]);
hold on
His2 = histogram([hianom2; loanom2]);
xlabel('Anomaly value');
ylabel('No. of variables');
title('Histogram of anomaly moduli outside limits of agreement');
legend({'First exam','Second exam'});
His1.BinWidth=His2.BinWidth;
```

Chapter 6.

1. CretiffSS

```
%convert IMG to tiff - for a directory of IMG files (SS OCT, UHD spot)
%Part 1 gets directory current folder, and its IMG names
%Part 2 converts IMG to tiff stack (use in SSA2FFT). Creates eye folder
%OPEN Eye IMG directory (named after eye ID) in Current folder
%CHANGE dims line 39 (if not UHD spot), CCtime 2021 to current year line 42
%also saves SLO images and IRIS image. Creates host eye folder itself
%%
clear
Currfold = pwd;
IMGinfoR = dir;
IMGinfo = IMGinfoR(contains({IMGinfoR.name},'.img'));%add z to .img for cubes
LSOinfo = IMGinfoR(contains({IMGinfoR.name},'lslo.bin'));%add z to .img for cubes
IRISinfo = IMGinfoR(contains({IMGinfoR.name},'iris.bin'));%add z to .img for cubes
LSOnames = {LSOinfo.name};
IMGnames = {IMGinfo.name};
IRISnames = {IRISinfo.name};
%IRISnames(1)=[];%CHECK need to remove first iris.bin all cases11
NumIMG = size(IMGnames,2);
Dirstr = '/Users/stewartlake/Documents/SS OCT eyes/';
EyeID = Currfold(end-7:end);%Eye ID (eg 'SS1 0028')
nDir = [Dirstr EyeID '/' EyeID ' tiff'];
sloDir = [Dirstr EyeID '/' EyeID ' lslo'];
irisDir = [Dirstr EyeID '/' EyeID ' iris'];
if (~exist(nDir,'dir'))
    mkdir ([Dirstr EyeID]);
    mkdir (nDir);
    mkdir (sloDir);
    mkdir (irisDir)
end


for NxIMG = 1:NumIMG
%%
IMGnm = IMGnames{NxIMG};
IMGfileID = fopen(IMGnm);
IMGfile = fread(IMGfileID);
%dims: UHDspotlight = [2047 3072 1], cube512  = [512 1536 512],
%angio15x9 = [500 1536 834], cubes 800 = [800 1536 800]
dims = [2047 3072 1];
IMGfile1 = uint8(reshape(IMGfile,dims));
%IMGnm time stamp created below
CCtime = regexp(IMGnm,'(?<=2021_)\d*\S\d*\S\d*','all','match');%'11-4-42'
TsaveN = [nDir '/' EyeID ' ' CCtime{1} '.tif']; %tiff cube name

%slo tiff creation
SLOnm = LSOnames{NxIMG};
SLOfileID = fopen(SLOnm);
SLOfile = fread(SLOfileID);

dimslo = [664 512];
SLOfile1 = uint8(reshape(SLOfile,dimslo));%

%iris tiff creation
IRISnm = IRISnames{NxIMG};
IRISfileID = fopen(IRISnm);
IRISfile = fread(IRISfileID);

dimiris = [640 480];
IRISfile1 = flipud(uint8(reshape(IRISfile,dimiris)));%orient R/L correctly with
flipud

%IMGnm selction 48:55 12x12 cube
TsaveNslo = [sloDir '/' EyeID ' ' CCtime{1} '.tif']; %tiff cube name
TsaveNiris = [irisDir '/' EyeID ' ' CCtime{1} '.tif']; %tiff cube name

for mt = 1:dims(3)
```

```
if mt==1
    imwrite(IMGfile1(:,:,mt)',TsaveN);%
    imwrite(SLOfile1',TsaveNslo);
    imwrite(IRISfile1',TsaveNiris);
else
    imwrite(IMGfile1(:,:,mt)',TsaveN,'WriteMode','append');

end

end

end
```

2. SSA2FFT

Lines 95-204 are function A2.m, written by Tyra Lange, Flinders University

Lines 274-457 are function FFTforOCT.m, written by Associate Professor Murk Bottema, Flinders University

```
%SS OCT tiff contour extraction
%saves xz data from tyra lange's graph theory shape identification A2;
%works on tiff files in Current folder, will ask for axial length, B scan
%width and depth (mm & pixels) - *16 6 2047 3072 for UHD spotlight*
%Works on Zeiss SS OCT cube tiffs from CretiffSS or similar,
%CHANGE: have tiff folder open in current folder
%CHANGE str2 line 31 if required if not SS OCT
%ONCE cube x,z saved, edited length by accuracy on tiffs. Then FFT
%Typical run takes 3:30 for 4 UHD, 10:30 for 2 x 25 Bs cubes
%For each B scan mark the start (left hand side) and end (RHS) of
%accurately identified contour.
%If B scan is empty/no data/not wanted, enter start to the Right of the end
%Locates points by A scan, so only x index needed (z position does not need
%to be accurate)  *12 3 512 1536 for 12 x 12 cube*
%Graph theory & Dijkstra's algorithm
%FFTforOCT is included in this script to allow adjustment of B scan size
%% Determine Number of Bscans in Cube
clear
%prompt0 = 'Enter Eye ID: ';
%EyeID = input(prompt0,'s');
prompt1 = 'Enter axial length: ';
AL1 = input(prompt1);
prompt2{1} = 'Enter B scan width (mm):';
prompt2{2} = 'Enter B scan depth (mm):';
BSw = input(prompt2{1});
BSd = input(prompt2{2});
prompt2{3} = 'Enter B scan width (pixels):';
prompt2{4} = 'Enter B scan depth (pixels):';
BSpw = input(prompt2{3});
BSpd = input(prompt2{4});
str2 = '/Users/stewartlake/Documents/SS OCT eyes/';

Currfold = pwd;
tiffinfo = dir;
tiffinfo = tiffinfo(~ismember({tiffinfo.name},{'.','..','.DS_Store'}));
tiffnames = {tiffinfo.name};
Numtiff = size(tiffnames,2);

McubeFFT = cell(Numtiff,1);
%mkdir ([EyeID ' tiff']);

for Rc = 1:Numtiff

%NowC{Rc} = tiffnames{Rc};

%%
%{
```

```
%This section converts input IMG file to tiff for next section
IMGnm = [NowC{Rc} '.img'];
IMGfileID = fopen(IMGnm);
IMGfile = fread(IMGfileID);
%next line HD21 = [1024 1024 21], mac cube  = [512 1024 128],MChidef = [1024 1024
2]
IMGfile1 = uint8(reshape(IMGfile,[1024 1024 21]));
TsaveN = [EyeID ' ' IMGnm(30:end-27) '.tif']; %cube ID
%{
if (~exist([EyeID ' tiff/' ],'dir'))
       mkdir ([EyeID ' tiff/' ]);%creates tiff folder if not present
end

oldFolder = cd([EyeID ' tiff/' ]);
%}
for mt = 1:21

if mt==1
    imwrite(IMGfile1(:,:,mt)',TsaveN);%mac cube change mt to mt*6
else
    imwrite(IMGfile1(:,:,mt)',TsaveN,'WriteMode','append');

end
%cd (oldFolder)

end
%}
%%

%FileTif = 'T2 028 13-59-47.tif'; %Insert cube tiff name here
FileTif = tiffnames{Rc};
InfoImage=imfinfo(FileTif);
NumberImages=length(InfoImage);
Xc1 = cell(NumberImages,1);
Zc1 = cell(NumberImages,1);
cubeFFT = NaN(30, NumberImages);
Cubefreq = NaN(30, NumberImages);
nowI = FileTif(1:8);%eye ID
startXY = NaN(NumberImages, 2);
finXY = NaN(NumberImages, 2);
DirChk = [str2 nowI '/FFTA2'];
if (~exist(DirChk,'dir'))
       mkdir (DirChk);%creates FFTA2 folder if not present
end

for i1=1:NumberImages
I = imread(FileTif, 'Index', i1);

%% Preprocessing

img = imfilter(I,fspecial('gaussian',[15 15],11));            % Blur Image
img = img > 0.75*max(img);                                    %

% Insert Vertical Column of Zeros (Both Sides)
size1 = size(img);                                            % Determine Size
(1024 x 1024)
img1 = zeros([size1(1) size1(2)+2]);                          % Matrix of Zeros
(Rows by Columns +2) (1024 x 1026)
img1(:,2:1+size1(2)) = img;                                   % Insert image from
2nd column to 2nd last column which is 1 more than img columns
                                                              % size is size of new
img with two extra columns (308 x 310)
sizeNew = size(img1);
%% Determine Graph Gradients (Graph Weights)

% get  vertical gradient image
G = nan(sizeNew);                                  % Matrix of NaN values of 308 x
310

for i3 = 1:sizeNew(2)                               % For columns
```

```
    G(:,i3) = -1*gradient(img1(:,i3),2);              % Positive vertical gradient
between 2 pixels
end

G = (G-min(G(:)))/(max(G(:))-min(G(:)));

G2 = G*-1+1;                                        % Get the "invert" of the
gradient image

%% Generate Adjacency Matrix

minWeight = 1E-5;                                   % Minimum weight

MW_pos = nan([numel(img1(:)) 8]);                   % Array to store positive
weights
MW_neg = nan([numel(img1(:)) 8]);                   % Array to store negative
weights
MX = nan([numel(img1(:)) 8]);                       % Array to store point A
locations
MY = nan([numel(img1(:)) 8]);                       % Array to store point B
locations

%Each node is associated with only its eight nearest neighbors

n = [1 1  1 0  0 -1 -1 -1; 1 0 -1 1 -1  1  0 -1];

%fill in the above arrays

szMW_pos = size(MW_pos);
ind = 1;


while ind ~= szMW_pos(1)*szMW_pos(2) %While ind not = col * row (not = 8404992)

    [i2, j] = ind2sub(szMW_pos,ind);  % i = 1050624x8, j = 1
    [iX,iY] = ind2sub(sizeNew,i2);

    jX = iX + n(1,j);
    jY  = iY + n(2,j);

     if jX >=1 && jX <= sizeNew(1) && jY >=1 && jY <= sizeNew(2) % 1024 , 1026
         %save weight

         % set to minimum if on the sides
         if jY == 1 || jY == sizeNew(2)
            MW_pos(i2,j) = minWeight;
            MW_neg(i2,j) = minWeight;

         % else, calculate the actual weights
         else
            MW_pos(i2,j) = 2 - G(iX,iY) - G(jX,jY) + minWeight;
            MW_neg(i2,j) = 2 - G2(iX,iY) - G2(jX,jY) + minWeight;
         end

        %save the subscript of the corresponding nodes
        MX(i2,j) = sub2ind(sizeNew,iX,iY);
        MY(i2,j) = sub2ind(sizeNew,jX,jY);
    end
    ind = ind+1;

end

%assemble the adjacency matrix
keepInd = ~isnan(MW_pos(:)) & ~isnan(MX(:)) & ~isnan(MY(:)) & ~isnan(MW_neg(:));
MW_pos = MW_pos(keepInd);
MW_neg = MW_neg(keepInd);
MX = MX(keepInd);
MY = MY(keepInd);

%sparse matrices, based on eq 1 with the gradient,
```

```
adjMatrixW = sparse(MX(:),MY(:),MW_pos(:),numel(img1(:)),numel(img1(:)));
                    % and the invert of gradient.
adjMatrixMW = sparse(MX(:),MY(:),MW_neg(:),numel(img1(:)),numel(img1(:)));

%% Shortest Path

% get layer going from light to dark
[ dist,path{1} ] = graphshortestpath( adjMatrixW, 1, numel(img1(:)) );
[pathX,pathY] = ind2sub(sizeNew,path{1});

% get rid of first and last few points that is by the image borders
pathX =pathX(gradient(pathY)~=0);
pathY =pathY(gradient(pathY)~=0);

Xc1{i1} = pathY;
Zc1{i1} = pathX;

%% Succesful RPE Delineation

BSfig = figure;
%BSfig.WindowState = 'maximized';
imagesc(I); axis image; colormap('gray'); hold on;
plot(pathY,pathX,'g-','linewidth',1.5); hold on;
legend({'rpe'});


[startXY(i1,1),startXY(i1,2)] = ginput(1);%start X,Y and finish X,Y from image
[finXY(i1,1),finXY(i1,2)] = ginput(1);

end

close all

%%
%set(startfinXY,'WindowStyle','normal');%attempt to undock and show
%variable

%edit above results with startXY and finXY

%data in Xc, Zc corrected by manually completed matrices startfinXY using
%ginput

%
startXY = fix(startXY);
finXY = fix(finXY);
%to remove a Bscan data,
%make startfinXY (Bs,1) one greater then startfin(BS,3), eg 513 and 512
%complete then run A2FFTa
Xc = cell(NumberImages,1);
Zc = cell(NumberImages,1);

for Tr = 1:NumberImages

    BsX = Xc1{Tr};
    BsZ = Zc1{Tr};

    StrtX = find(BsX == startXY(Tr,1));
    Fin1X = find(BsX == finXY(Tr,1));


   if StrtX(end)>Fin1X(1)

       Xc{Tr} = NaN(size(Xc1{Tr}'));%empty B scan vector if not wanted
       Zc{Tr} = NaN(size(Zc1{Tr}'));

   else

       BsX(Fin1X(1)+1:end) = [];
       BsZ(Fin1X(1)+1:end) = [];
```

```
        BsX(1:StrtX(end)-1) = [];
        BsZ(1:StrtX(end)-1) = [];

        Xc{Tr} = BsX';
        Zc{Tr} = BsZ';

    end

end


%%
%Pt2 follows on from Tyra's A2 function
%Performs FFT on Xc, Zc,
%one cube a time, with length Xc/Zc curated by accuracy in images from
%A2FFT second section
%this is from FFT4Eye to process FFT for OCT_R3 data
VecLen = NaN(NumberImages);
Quadcoeffs = zeros(3,NumberImages);
TSig = zeros(1,NumberImages);
CubeSigPror = zeros(30,NumberImages);
NumBin50 = zeros(1,NumberImages);

for Bs = 1:NumberImages

    if (~isnan(Zc{Bs}))
            %L = length (Zc{Bs});
            %Written by A/Prof Murk Bottema

            %[FFTz,freq] = FFTforOCT_R3mm(Xc{Bs},Zc{Bs});
            %FFTforOCT inserted here instead of calling function
            %to allow for varying B scan size
            %FFTforR3 convert x and z to mm for consistency and results
            %R2 is normalised FFT bins by Veclen
            % allows adjustment B scan size
            %
            % Further revision to normalise data by vector length Veclen line 186 &
222
            % February 23, 2018
%
            % Compute FFT so that the output is comparable regardless of the length
of
            % the retinal data. Adjust for possible missing or repeated measurement
locations
            % (x-values). Express the results as spacial frequency in terms of
cycles
            % per mm.
%
            % The spacing in x is width pixels/width mm,
            % which determines sampling frequency (sf).
%
            % Step 1. If there are duplicated values of x, then a single z value is
            % attached to this x value equal to the mean of the z values recorded
for
            % the duplicate x values.
%
            % Step 2. If there are gaps in the sequence of x values, these are
filled
            % by interpolation.
%
            % Step 3. The best quadratic fit to the signal is removed to avoid
            % contamination of the FT by mismatches at the endpoints of the signal.
%
            % Step 4. If the signal is less than 1024(BSwp) points long, then the
signal is
            % padded by zeros to attain length 1024. If the signal si more than
1024
            % points long, the ends are cut to attain a length of 1024.
%
```

```
            % Step 5. The Fourier transform is computed. The values of the modulus
or
            % the transformed signal are recorded for frequencies 1 to Ny (Nyquist
            % frequency) at pixel width/2 points. These values constitute the
output vector FFTz.
%
%
            % FFTz is the Fourier transform of z. freq is the vector of spatial
            % frequency values.
            % This is now normalised by Veclen final line
%
            % retain the original values of x and z for display purposes
            %xold = x;
            %zold = z;

            % %%%%%%%%%%%%%%%%%%%%%%%%%%%%%%%%%%%%%%%%%%%%%%%%%%%
            % Step 0.5. Sort the data according to the first column. This step is
new
            % to this version and is meant to fix the fault in FFTforOCT.m in the
            % header for this version.
            % %%%%%%%%%%%%%%%%%%%%%%%%%%%%%%%%%%%%%%%%%%%%%%%%%%%

            [sortx,sortind] = sort(Xc{Bs});
            sortz = Zc{Bs}(sortind);
            x = sortx;
            z = sortz;


            % %%%%%%%%%%%%%%%%%%%%%%%%%%%%%%%%%%%%%%%%%%%%%%%%%%%
            % Step 1. Replace multiple z values for a single x by the mean
            % %%%%%%%%%%%%%%%%%%%%%%%%%%%%%%%%%%%%%%%%%%%%%%%%%%%


            Dflag = 1;
            while Dflag == 1
                L = length(x);
                Dx = x(2:L) - x(1:L-1);    % differences of consecutive x values
                zeroDx = find(Dx == 0);    % find places where x does not change
                 if isempty(zeroDx) == 0    % if repeated values are found:
                   indxr = zeroDx(1);     % index of first repeated value
                    xr = x(zeroDx(1));     % the first repeated value
                    vecr = find(x == xr);  % find all x's with this value
                    Lxr = length(vecr);    % the number of these repeats
                    meanz = mean(z(vecr)); % the mean of the z values

                    % construct the new x and z vectors
                 if indxr > 1
                    x = [x(1:indxr) ; x(indxr+Lxr:L)];
                    z = [z(1:indxr-1) ; meanz ; z(indxr+Lxr:L)];
                 else
                    x = [x(1)  ; x(1+Lxr:L)];
                    z = [meanz ; z(1+Lxr:L)];
                 end

                 else
                    Dflag = 0;          % if no repeats are found end the process
                 end
            end

            % %%%%%%%%%%%%%%%%%%%%%%%%%%%%%%%%%%%%%%%%%%%%%%%%%%%%%%%%%%%%%%%%%%%
            % %%%%%%%%%%%%%%%%%%%%%%%%%%%%%%%%%%%%%%%%%%%%%%%%%%%%%%%%%%%%%%%%%%%

            % Diagnostic steps
            %sizex = size(x)
            %roundz = round(z);
            %disp([x roundz])

            % %%%%%%%%%%%%%%%%%%%%%%%%%%%%%%%%%%%%%%%%%%%%%%%%%%%
            % Step 3. Remove the quadratic approximation of the background
            % %%%%%%%%%%%%%%%%%%%%%%%%%%%%%%%%%%%%%%%%%%%%%%%%%%%
```

```
        sf = BSpw/BSw;
        sfz = BSpd/BSd;
        xmm = x/sf;
        ZMM = z/sfz;
        p = polyfit(xmm,ZMM,2);
        B = p(1)*(xmm.^2) + p(2)*xmm + p(3);

        z = ZMM - B;


        %pixel BFC
        Bspz = p(1)*(x.^2) + p(2)*x + p(3);

        % %%%%%%%%%%%%%%%%%%%%%%%%%%%%%%%%%%%%%%%%%%%%%%%%
        % Step 2. Fill any gaps in the data
        % %%%%%%%%%%%%%%%%%%%%%%%%%%%%%%%%%%%%%%%%%%%%%%%%

        L = length(x);
        x1 = x(1);
        xL = x(L);
        runvec = (x1:1:xL)';  % this works because the values of x are integers
        LENRUNVEC = length(runvec);

for kL = 1:L-1
    D = x(kL+1) - x(kL);
    if D ~= 1
        disp(['Here is a problem'])
        disp([x(kL) x(kL+1)])
    end


end

if L ~= length(runvec)
    z = interp1(x,z,runvec);
end
x = runvec;

% retain the adjusted x vector, z vector and quadratic background B for
% display
zmm = z;
Bmm = B;

% %%%%%%%%%%%%%%%%%%%%%%%%%%%%%%%%%%%%%%%%%%%%%%%%
% Step 4. Adjust the length of the signal to be B scan width points long
% %%%%%%%%%%%%%%%%%%%%%%%%%%%%%%%%%%%%%%%%%%%%%%%%
Veclen = length (z);
L = length(z);
if L < BSpw   % If too short, pad by zeros at each end
    D = BSpw - L;
    w = floor(D/2);
    v = D - w;
    newz = [zeros(w,1); z ; zeros(v,1)];
    z = newz;
end

if L > BSpw  % if too long, remove points at each end
    D = L - BSpw;
    w = floor(D/2);
    %v = D - w;
    newz = z(w+1:w+BSpw);
    z = newz;
end


% %%%%%%%%%%%%%%%%%%%%%%%%%%%%%%%%%%%%%%%%%%%%%%%%
% Step 5. Compute the fast Fourier transform
% %%%%%%%%%%%%%%%%%%%%%%%%%%%%%%%%%%%%%%%%%%%%%%%%
```

```
    % Set the sampling frequency
    L = length(z);
    Ny = sf/2;                          % Nyquist frequency
    freqvec = linspace(-Ny,Ny,L+1);
    freqvec = freqvec(1:L);             % frequency vector

    % Compute the Fourier transform
    Fz = fft(z);                        % Fourier transform (FFT)
    AFz = abs(Fz);                      % modulus of FFT

    % Retain only frequencies 0 to Nyquist
    L2 = floor(L/2);
    FFTz = AFz(1:L2);
    freq = freqvec(L2+1:L);
    FFTz = FFTz*(sf/Veclen);%correct FFTz for length - sf to keep veclen in mm


            VecLen(Bs) = length(Zc{Bs});%vector length(FFT already corrected)
            %note VecLen uncorrected length and Veclen for FFT correction
            %create matrix of residuals
            zVlen = size (Zc{Bs},1);
            zedres(1:zVlen,Bs) = Zc{Bs};
            %zedres = zedres(1:1024,fileNum);

            %save quadratic coefficients
            %sf = 1024/BSw;%already used, above
            %xmm = Xc{Bs}/sf;
            %sfz = 1024/BSd;
            %ZMM = Zc{Bs}/sfz;
            %p = polyfit(xmm,ZMM,2);%
            Quadcoeffs (1,Bs) = p(1);
            Quadcoeffs (2,Bs) = p(2);
            Quadcoeffs (3,Bs) = p(3);

            %put FFTz, freq into matrix, one column per B scan, bins by
            %rows
            cubeFFT(1:30,Bs) = FFTz(1:30);
            %cubeFFT(1:30,fileNum)=cubeFFT(1:30,fileNum)/VecLen(fileNuM);
            Cubefreq(1:30,Bs) = freq(1:30)';

            %now determine the relative proportion of each frequency bin to the
signal
            TSig(1,Bs) = sum (cubeFFT(:,Bs));
            CubeSigPror(1:30,Bs) = FFTz(1:30)'/TSig(1,Bs);

            %find number of bins to make 50% signal
            binprorV = CubeSigPror (1:30,Bs);
            BScusu (1:30) = cumsum (binprorV);
            NumBin50(1,Bs) = find (BScusu > 0.5, 1);

    else
        cubeFFT(1:30,Bs) = NaN(30,1);
%}
    end


end
%look like x vector = pathY, z-vector is pathX
%so save these two columns for use in new FFT processing above
%cubeFFT is for one cube
McubeFFT{Rc} = cubeFFT;%bins x B scans

        %now save each cube's data
        str4 = FileTif(1:end-4);% cube ID
        str6 = [DirChk '/' str4];
        save (str6, '-
regexp','^(?!(adjMatrixMW|adjMatrixW|G|G2|img|img1|MW_neg|MW_pos|MX|MY)$).');

end
```

```
%%
%{
%classifier
load('/Users/stewartlake/Documents/Retinalcontour/classifiers/reg bin
QDA/Fs5Trs3v.mat');

%generate mean BS from average of 5 folds of RD/PVD eyes
for bl =1:5
    bsM(1:30,bl) = meanBS{bl};
end
bsMmean = mean(bsM,2);%average bin value from classifier data
bsMsd = std(bsM,0,2);
bsmsdall = mean(bsMsd);
bsMcoev = bsMsd./bsMmean;
bsMmncov = mean(bsMcoev);

%variables for model data
%if (3,2) and (5,3)
%(3,2) is first input cube bin 2: max(McubeFFT{1}(2,:))
%assuming r/c = bins/B scans
%(5,3) is second cube input bin 3: max(McubeFFT{2}(3,:))
%model data = cat((3,2),(5,3) Axl,)


numTeyes = 1;
Dcat = cell(numTeyes,2);%col 1 category labels, col 2 number of each category
Tvalvars = NaN(numTeyes,3);%variables for classifier

    %get bin diff by subtracting max val from
    Tvalvars(numTeyes,1) = max(abs(McubeFFT{1}(2,:) -
bsMmean(2)),[],'omitnan');%(3,2)
    Tvalvars(numTeyes,2) = max(abs(McubeFFT{2}(3,:) -
bsMmean(3)),[],'omitnan');%(5,3)

    Tvalvars(numTeyes,3) = AL1;%AxL



%then
quad4mdl1.Prior = [1 1];% change prior here as required
[Ttestlabels1,Tscore1] = predict (quad4mdl1,Tvalvars);
Rep = ['0 = not RD, 1 = RD, Eye ' EyeID];
Unwtrep = 'prior 1:1 test result';
Wtrep = 'prior 6:1 test result';

disp(Rep);
disp(Unwtrep);
disp(Ttestlabels1);

quad4mdl1.Prior = [6 1];% change prior here as required
[Ttestlabels6,Tscore6] = predict (quad4mdl1,Tvalvars);
disp(Wtrep);
disp(Ttestlabels6);

%}
```

3. SStabFFT

```
%populate SSOCTeyes.mat table with FFT data from FFTA2 in eye folders
%individual variables/columns for M U D R L, (can also add NSWE)
%also BFCvC,
%START: Use import data to import SS OCT eyes.xlsx to a table with the useful
columns.
%ID, diagnostic category, AAL, Age, UHDspot1
%For the UHDspot key column ('MUDRL') import as text, so it is a string (if
%imported as a category need another step % below).
%Gets FFT data from /FFTA2, so this (SSA2FFT) needs completion.
```

```
SSOCTeyes3=[];%change this to the table to be used
clear
load('/Users/stewartlake/Documents/MATLAB/SSOCT eyes.mat');
a1={'M';'U';'D';'R';'L'};
NumpGrp = groupcounts(SSOCTeyes3,'category');%No. per category
str2 = '/Users/stewartlake/Documents/SS OCT eyes/';
cd (str2)
SSIR = dir;
%SSIR([149:150,289:290],:)=[];%change rows to remove incomplete eyes
SSI = SSIR(contains({SSIR.name},{'SS1', 'SS2'}));
SSInm = {SSI.name};
numI = size(SSInm,2);
sIdeI = cellfun(@(x)x(3),SSInm);%laterality
SSOCTeyes3.timeID(:) = {[]};
SSOCTeyes3.BFCvC(:) = {[]};
SSOCTeyes3.up(:) = {[]};
SSOCTeyes3.down(:) = {[]};
SSOCTeyes3.nasal(:) = {[]};
SSOCTeyes3.temp(:) = {[]};
SSOCTeyes3.mac(:) = {[]};
SSOCTeyes3.BFCup(:) = {[]};
SSOCTeyes3.BFCdown(:) = {[]};
SSOCTeyes3.BFCnasal(:) = {[]};
SSOCTeyes3.BFCtemp(:) = {[]};
SSOCTeyes3.BFCmac(:) = {[]};


for Eyes = 1:numI
       eyedir = cd ([SSInm{Eyes} '/FFTA2']);
    Row = find(strcmp(SSOCTeyes3.ID,SSInm{Eyes}));%find table row to match current
eye
    %Row (in SSOCTeyes table) matches Eyes (in SSInm)
    UHDkey=SSOCTeyes3.UHDSpot1(Row);
    BSloc=num2cell(UHDkey{:});% array of UHDkey

    %indices for columns in table
    Out = cellfun(@(s)find(~cellfun('isempty',strfind(BSloc,s))),a1,'uni',0);


    BSinfoR = dir;
    BSinfo = BSinfoR(contains({BSinfoR.name},'.mat'));%get .mat files
    nms = {BSinfo.name};
    SStime =
string(cellfun(@(s)regexp(s,'\d*\S\d*\S\d*(?=.mat)','all','match'),nms));
    numbs = size(nms,2);
    Tformat(Eyes,1:numbs) = datetime(SStime,'InputFormat', 'HH-mm-ss');%



        for BS = 1:numbs
              load(nms{BS}, 'cubeFFT','Quadcoeffs');

                 Ibsfft{Eyes,BS} = cubeFFT;%rows = eyes, cols = Bscans
           QC(Eyes,BS) = 2*Quadcoeffs(1);

        end

       cd (eyedir)

    [tsort(Eyes,1:numbs),Its(Eyes,1:numbs)] = sort(Tformat(Eyes,1:numbs));%ID time
sorted
    allcubeFFTs = Ibsfft(Eyes,1:numbs);%this is cubeFFTs sorted into time order for
allocation with Out
    allcubeFFTs = allcubeFFTs(Its(Eyes,1:numbs));
    QC1(Eyes,1:numbs) = QC(Eyes,Its(Eyes,1:numbs));%sorted BFCvC
```

```
    SSOCTeyes3.timeID{Row} = tsort(Eyes,:);%time ID sorted in time order
    SSOCTeyes3.BFCvC{Row} = QC1(Eyes,:);%BFCvC
    % So macular B scans data
        if ~isempty(Out{1})
    SSOCTeyes3.mac{Row} = allcubeFFTs(Out{1});%number Out from M U D R L
    SSOCTeyes3.BFCmac{Row}=QC1(Out{1});% Best fit curve vertex curvature
        end

        if ~isempty(Out{2})
    SSOCTeyes3.up{Row} = allcubeFFTs(Out{2});
    SSOCTeyes3.BFCup{Row}=QC1(Out{2});%
        end

        if ~isempty(Out{3})
    SSOCTeyes3.down{Row} = allcubeFFTs(Out{3});
    SSOCTeyes3.BFCdown{Row}=QC1(Out{3});
        end

    if sIdeI(Eyes) == 2 %left eyes
        if ~isempty(Out{4})
    SSOCTeyes3.nasal{Row} = allcubeFFTs(Out{4});
    SSOCTeyes3.BFCnasal{Row}=QC1(Out{4});
        end
        if ~isempty(Out{5})
    SSOCTeyes3.temp{Row} = allcubeFFTs(Out{5});
    SSOCTeyes3.BFCtemp{Row}=QC1(Out{5});
        end


    else  % right eye

        if ~isempty(Out{5})
    SSOCTeyes3.nasal{Row} = allcubeFFTs(Out{5});
    SSOCTeyes3.BFCnasal{Row}=QC1(Out{5});
        end

        if ~isempty(Out{4})
    SSOCTeyes3.temp{Row} = allcubeFFTs(Out{4});
    SSOCTeyes3.BFCtemp{Row}=QC1(Out{4});
        end

    end

end

%Summary data
Meanage = mean(SSOCTeyes3.age,'omitnan');
MeanAL = mean(SSOCTeyes3.AAL,'omitnan');
SDage = std(SSOCTeyes3.age,'omitnan');
SDAL = std(SSOCTeyes3.AAL,'omitnan');
%meanBFCr = mean(SSOCTeyes2{:,13:17},'omitnan');%incs multiple B scans in a region
%SDBFCr = std(SSOCTeyes2(:,13:17),'omitnan');

%for anomaly determination
% see SStabana
```

4. SStabana

```
%analyse SStabfft output - save in MATLAB/SSOCT eyes.mat
%identifies eyes by category
%calculates anomaly from an average B scan of 80% sample (mBs) AL stratified
%selects highest irregularity B scan if multiple present in any region
%irregularity = Allis
%anomaly = Anom
%plots anomaly/irregularity by region and diagnosis
```

```
%histograms of RD PVD anom/irreg distribution by region and
%total irreg/anom for all eyes
%%
%collate all scans
SSOCTeyes2=[];%the table to use
clear
load('/Users/stewartlake/Documents/MATLAB/SSOCT eyes.mat');
SSOCTeyes2(139,:)=[];%remove any empty rows
NumpGrp = groupcounts(SSOCTeyes2,'category');%No. per category
Allis=SSOCTeyes2{:,8:11};%this is FFT bins
BFCs = table2array(SSOCTeyes2(:,13:16));%this is bfc
BFCsize = size(BFCs);
BFC = NaN(BFCsize);%Best fit curve numerical array
AxL = SSOCTeyes2.AAL;
iel=0;%this just keeps track of regions with multiple B scans
for Ai = 1:numel(Allis)

    if numel(Allis{Ai})==1
        AllBs(Ai,1:30)=Allis{Ai}{1};
        Allis{Ai} = cell2mat(Allis{Ai});
        BFC(Ai) = BFCs{Ai};

    elseif numel(Allis{Ai})>1
        %clean multiple-B scan regions to hold max irreg B scan data
        iel = iel+1;
        iMel(iel)=Ai;%indices of multiple B scan regions
        Regsel = cell2mat(Allis{Ai});
        Regselt=sum(Regsel);
        [~,iMc]=max(Regselt);
        AllBs(Ai,1:30)=Regsel(:,iMc);%max irregularity B scan from region
        Allis{Ai}=Regsel(:,iMc);
        BFC(Ai) = BFCs{Ai}(iMc);

    else
        AllBs(Ai,1:30)=NaN(1,30);%empty (0) region
    end

end


RDis = ismember(SSOCTeyes2.category,{'RD'});
RTis = ismember(SSOCTeyes2.category,{'RT'});
PVDis = ismember(SSOCTeyes2.category,{'PVD'});
FEis = ismember(SSOCTeyes2.category,{'FE'});
FPVDis = ismember(SSOCTeyes2.category,{'FPVD'});
notPVDis = ismember(SSOCTeyes2.category,{'no PVD'});
Stis = ismember(SSOCTeyes2.category,{'St'});

PVDirreg=Allis(PVDis,:);
PVDAxL = AxL(PVDis,:);
%meanBs = mean(AllBs,'omitnan');%do not use: use 5 fold averages, below
%%
%create anomaly values by 5 fold averages, create mean Bscan from PVD eyes
[sALvec,ALorder]=sort(SSOCTeyes2.AAL);% ascending order of AL
%{
%original mean Bscan from all eyes
%AL sorted
%sort eyes by AL

sAllis=Allis(ALorder,:);
sAgevec = SSOCTeyes1.age(ALorder);
sALvec(sALvec==0) = NaN;%keep "no AL" eyes

%generate random distribution into 5 folds
k=5;
NumIpfold = floor(size(sAllis,1)/k);%number of eyes per k folds
```

```
Remis=mod(size(sAllis,1),k);%plus the remainder not divisible by k
Ranselis = zeros(k,NumIpfold);
for Ranrun=1:NumIpfold

    Ranselis(:,Ranrun) = randperm(k)';
end
Ranremis=randperm(Remis)';
Ranselis = cat(1,Ranselis(:),Ranremis);%these are the row indices to divide ALLis
into 1-5 folds

for n=1:k

    Fis{n} = sAllis(Ranselis==n,:);
    notFis{n} = sAllis(Ranselis~=n,:);
    ALvec{n} = sALvec(Ranselis==n);

    notFisX = notFis{n};%only works if each consists only of one cell
    notFisd=horzcat(notFisX{:})';%Bs x 30 double
    mBs(n,1:30)=mean(notFisd,'omitnan');%mean B scan irregularity

end

uRanselis(ALorder)=Ranselis;%'unsort' the randomisation to match Anom/Allis
Anom=Allis;

for rr=1:size(Allis,1)%
    %aim to subtract the correct means Bs from each row Allis
   Anom(rr,:)=cellfun(@(x) abs(x-mBs(uRanselis(rr),:)'), Anom(rr,:), 'un', 0);

end
%}

%create anomaly values by 5 fold averages, create mean Bscan from PVD eyes
%AL sorted
%sort PVD eyes by AL
PVDgrp = SSOCTeyes2(PVDis,:);

[sALvecP,ALorderP]=sort(PVDgrp.AAL);% ascending order of AL
sAllpvdis=PVDirreg(ALorderP,:);
sAgevecP = PVDgrp.age(ALorderP);
sALvecP(sALvecP==0) = NaN;%keep "no AL" eyes

%generate random distribution into 5 folds
k=5;

%PVD
NumIpfoldp = floor(size(sAllpvdis,1)/k);%number of eyes per k folds
Remisp=mod(size(sAllpvdis,1),k);%plus the remainder not divisible by k
RanselisP = zeros(k,NumIpfoldp);
for RanrunP=1:NumIpfoldp

    RanselisP(:,RanrunP) = randperm(k)';
end
Ranremisp=randperm(Remisp)';
RanselisP = cat(1,RanselisP(:),Ranremisp);%these are the row indices to divide
ALLis into 1-5 folds

%All eyes
NumIpfold = floor(size(Allis,1)/k);%number of eyes per k folds
Remis=mod(size(Allis,1),k);%plus the remainder not divisible by k
Ranselis = zeros(k,NumIpfold);
for Ranrun=1:NumIpfold

    Ranselis(:,Ranrun) = randperm(k)';
end
Ranremis=randperm(Remis)';
```

```
Ranselis = cat(1,Ranselis(:),Ranremis);%these are the row indices to divide ALLis
into 1-5 folds

%calculate 5 average irregularity scans
for n=1:k

    FisP{n} = sAllpvdis(RanselisP==n,:);
    notFisP{n} = sAllpvdis(RanselisP~=n,:);
    ALvecP{n} = sALvecP(RanselisP==n);

    notFisXP = notFisP{n};%only works if each consists only of one cell
    notFisdP=horzcat(notFisXP{:})';%Bs x 30 double
    mBs(n,1:30)=mean(notFisdP,'omitnan');%Average B scan irregularity from PVD eyes

end
sdmBs = std(mBs);
MnmBs = mean(mBs);
mBsCoV = sdmBs./MnmBs;%Coefficients of variation of average b scan  bins
MnCoVmBs = mean(mBsCoV); %average CoV of average b scan bins

uRanselis(ALorder)=Ranselis;%'unsort' the randomisation to match Anom/Allis (not
necessary)
%uRanselisP(ALorderP)=RanselisP;%'unsort' the randomisation to match Anom/Allis
Anom=Allis;

for rr=1:size(Allis,1)%
    %aim to subtract the correct means Bs from each row Allis
   Anom(rr,:)=cellfun(@(x) abs(x-mBs(uRanselis(rr),:)'), Anom(rr,:), 'un', 0);
    %creates the anomaly values for all eyes & scans
end

%%
%Anomaly, irregularity, axial length, age and BFC collection for each group
RDirreg=Allis(RDis,:);
RDanom = Anom(RDis,:);
RDAxL = AxL(RDis,:);
RDage = SSOCTeyes2.age(RDis);
RDbfc = BFC(RDis,:);
RDID = SSOCTeyes2.ID(RDis);
for RDi = 1:length(RDirreg)

   RDupi(RDi,1:30) = RDirreg{RDi,1};
   RDupa(RDi,1:30) = RDanom{RDi,1};
   RDdowni(RDi,1:30) = RDirreg{RDi,2};
   RDdowna(RDi,1:30) = RDanom{RDi,2};
   RDnasali(RDi,1:30) = RDirreg{RDi,3};
   RDnasala(RDi,1:30) = RDanom{RDi,3};
   RDtempi(RDi,1:30) = RDirreg{RDi,4};
   RDtempa(RDi,1:30) = RDanom{RDi,4};

end

mRDui = mean(RDupi,'omitnan');
mRDdi = mean(RDdowni,'omitnan');
mRDni = mean(RDnasali,'omitnan');
mRDti = mean(RDtempi,'omitnan');

mRDua = mean(RDupa,'omitnan');
mRDda = mean(RDdowna,'omitnan');
mRDna = mean(RDnasala,'omitnan');
mRDta = mean(RDtempa,'omitnan');

allRDBsanom = [RDanom{:}];
avRDanom = mean(allRDBsanom,2,'omitnan');%mean of all RD B scans

RTirreg=Allis(RTis,:);
```

```
RTanom = Anom(RTis,:);
RTAxL = AxL(RTis,:);
RTage = SSOCTeyes2.age(RTis);
RTbfc = BFC(RTis,:);
RTID = SSOCTeyes2.ID(RTis);
for RTi = 1:length(RTirreg)

   RTupi(RTi,1:30) = RTirreg{RTi,1};
   RTupa(RTi,1:30) = RTanom{RTi,1};
   RTdowni(RTi,1:30) = RTirreg{RTi,2};
   RTdowna(RTi,1:30) = RTanom{RTi,2};
   RTnasali(RTi,1:30) = RTirreg{RTi,3};
   RTnasala(RTi,1:30) = RTanom{RTi,3};
   RTtempi(RTi,1:30) = RTirreg{RTi,4};
   RTtempa(RTi,1:30) = RTanom{RTi,4};

end

mRTui = mean(RTupi,'omitnan');
mRTdi = mean(RTdowni,'omitnan');
mRTni = mean(RTnasali,'omitnan');
mRTti = mean(RTtempi,'omitnan');

mRTua = mean(RTupa,'omitnan');
mRTda = mean(RTdowna,'omitnan');
mRTna = mean(RTnasala,'omitnan');
mRTta = mean(RTtempa,'omitnan');

%PVDirreg=Allis(PVDis,:);%moved up for Mean B scan calculation
PVDanom = Anom(PVDis,:);
allPVDBsanom = [PVDanom{:}];
avPVDanom = mean(allPVDBsanom,2,'omitnan');%mean of all RD B scans
PVDAxL = AxL(PVDis,:);
PVDage = SSOCTeyes2.age(PVDis);
PVDbfc = BFC(PVDis,:);
PVDID = SSOCTeyes2.ID(PVDis);

for PVDi = 1:length(PVDirreg)

   PVDupi(PVDi,1:30) = PVDirreg{PVDi,1};
   PVDupa(PVDi,1:30) = PVDanom{PVDi,1};
   PVDdowni(PVDi,1:30) = PVDirreg{PVDi,2};
   PVDdowna(PVDi,1:30) = PVDanom{PVDi,2};
   PVDnasali(PVDi,1:30) = PVDirreg{PVDi,3};
   PVDnasala(PVDi,1:30) = PVDanom{PVDi,3};
   PVDtempi(PVDi,1:30) = PVDirreg{PVDi,4};
   PVDtempa(PVDi,1:30) = PVDanom{PVDi,4};

end

mPVDui = mean(PVDupi,'omitnan');
mPVDdi = mean(PVDdowni,'omitnan');
mPVDni = mean(PVDnasali,'omitnan');
mPVDti = mean(PVDtempi,'omitnan');

mPVDua = mean(PVDupa,'omitnan');
mPVDda = mean(PVDdowna,'omitnan');
mPVDna = mean(PVDnasala,'omitnan');
mPVDta = mean(PVDtempa,'omitnan');

FEirreg=Allis(FEis,:);
FEanom = Anom(FEis,:);
FEAxL = AxL(FEis,:);
FEage = SSOCTeyes2.age(FEis);
FEbfc = BFC(FEis,:);
for FEi = 1:length(FEirreg)
```

```
    FEupi(FEi,1:30) = FEirreg{FEi,1};
    FEupa(FEi,1:30) = FEanom{FEi,1};
    FEdowni(FEi,1:30) = FEirreg{FEi,2};
    FEdowna(FEi,1:30) = FEanom{FEi,2};
    FEnasali(FEi,1:30) = FEirreg{FEi,3};
    FEnasala(FEi,1:30) = FEanom{FEi,3};
    FEtempi(FEi,1:30) = FEirreg{FEi,4};
    FEtempa(FEi,1:30) = FEanom{FEi,4};

end

mFEui = mean(FEupi,'omitnan');
mFEdi = mean(FEdowni,'omitnan');
mFEni = mean(FEnasali,'omitnan');
mFEti = mean(FEtempi,'omitnan');

mFEua = mean(FEupa,'omitnan');
mFEda = mean(FEdowna,'omitnan');
mFEna = mean(FEnasala,'omitnan');
mFEta = mean(FEtempa,'omitnan');


FPVDirreg=Allis(FPVDis,:);
FPVDanom = Anom(FPVDis,:);
FPVDAxL = AxL(FPVDis,:);
FPVDage = SSOCTeyes2.age(FPVDis);
FPVDbfc = BFC(FPVDis,:);
for FPVDi = 1:length(FPVDirreg)

    FPVDupi(FPVDi,1:30) = FPVDirreg{FPVDi,1};
    FPVDupa(FPVDi,1:30) = FPVDanom{FPVDi,1};
    FPVDdowni(FPVDi,1:30) = FPVDirreg{FPVDi,2};
    FPVDdowna(FPVDi,1:30) = FPVDanom{FPVDi,2};
    FPVDnasali(FPVDi,1:30) = FPVDirreg{FPVDi,3};
    FPVDnasala(FPVDi,1:30) = FPVDanom{FPVDi,3};
    FPVDtempi(FPVDi,1:30) = FPVDirreg{FPVDi,4};
    FPVDtempa(FPVDi,1:30) = FPVDanom{FPVDi,4};

end

mFPVDui = mean(FPVDupi,'omitnan');
mFPVDdi = mean(FPVDdowni,'omitnan');
mFPVDni = mean(FPVDnasali,'omitnan');
mFPVDti = mean(FPVDtempi,'omitnan');

mFPVDua = mean(FPVDupa,'omitnan');
mFPVDda = mean(FPVDdowna,'omitnan');
mFPVDna = mean(FPVDnasala,'omitnan');
mFPVDta = mean(FPVDtempa,'omitnan');

notPVDirreg=Allis(notPVDis,:);
notPVDanom = Anom(notPVDis,:);
notPVDAxL = AxL(notPVDis,:);
notPVDage = SSOCTeyes2.age(notPVDis);
notPVDbfc = BFC(notPVDis,:);
for notPVDi = 1:length(notPVDirreg)

    notPVDupi(notPVDi,1:30) = notPVDirreg{notPVDi,1};
    notPVDupa(notPVDi,1:30) = notPVDanom{notPVDi,1};
    notPVDdowni(notPVDi,1:30) = notPVDirreg{notPVDi,2};
    notPVDdowna(notPVDi,1:30) = notPVDanom{notPVDi,2};
    notPVDnasali(notPVDi,1:30) = notPVDirreg{notPVDi,3};
    notPVDnasala(notPVDi,1:30) = notPVDanom{notPVDi,3};
    notPVDtempi(notPVDi,1:30) = notPVDirreg{notPVDi,4};
    notPVDtempa(notPVDi,1:30) = notPVDanom{notPVDi,4};
```

```
end

mnotPVDui = mean(notPVDupi,'omitnan');
mnotPVDdi = mean(notPVDdowni,'omitnan');
mnotPVDni = mean(notPVDnasali,'omitnan');
mnotPVDti = mean(notPVDtempi,'omitnan');

mnotPVDua = mean(notPVDupa,'omitnan');
mnotPVDda = mean(notPVDdowna,'omitnan');
mnotPVDna = mean(notPVDnasala,'omitnan');
mnotPVDta = mean(notPVDtempa,'omitnan');

Stirreg=Allis(Stis,:);
Stanom = Anom(Stis,:);
StAxL = AxL(Stis,:);
Stage = SSOCTeyes2.age(Stis);
Stbfc = BFC(Stis,:);
for Sti = 1:length(Stirreg)

   Stupi(Sti,1:30) = Stirreg{Sti,1};
   Stupa(Sti,1:30) = Stanom{Sti,1};
   Stdowni(Sti,1:30) = Stirreg{Sti,2};
   Stdowna(Sti,1:30) = Stanom{Sti,2};
   Stnasali(Sti,1:30) = Stirreg{Sti,3};
   Stnasala(Sti,1:30) = Stanom{Sti,3};
   Sttempi(Sti,1:30) = Stirreg{Sti,4};
   Sttempa(Sti,1:30) = Stanom{Sti,4};

end

mStui = mean(Stupi,'omitnan');
mStdi = mean(Stdowni,'omitnan');
mStni = mean(Stnasali,'omitnan');
mStti = mean(Sttempi,'omitnan');

mStua = mean(Stupa,'omitnan');
mStda = mean(Stdowna,'omitnan');
mStna = mean(Stnasala,'omitnan');
mStta = mean(Sttempa,'omitnan');

%all PVD (aPVD), combined PVD and FPVD
aPVDirreg=Allis(PVDis|FPVDis,:);%moved up for Mean B scan calculation
aPVDanom = Anom(PVDis|FPVDis,:);
aallPVDBsanom = [aPVDanom{:}];
aavPVDanom = mean(aallPVDBsanom,2,'omitnan');%mean of all RD B scans
aPVDAxL = AxL(PVDis|FPVDis,:);
aPVDage = SSOCTeyes2.age(PVDis|FPVDis);
aPVDbfc = BFC(PVDis|FPVDis,:);

for aPVDi = 1:length(aPVDirreg)

   aPVDupi(aPVDi,1:30) = aPVDirreg{aPVDi,1};
   aPVDupa(aPVDi,1:30) = aPVDanom{aPVDi,1};
   aPVDdowni(aPVDi,1:30) = aPVDirreg{aPVDi,2};
   aPVDdowna(aPVDi,1:30) = aPVDanom{aPVDi,2};
   aPVDnasali(aPVDi,1:30) = aPVDirreg{aPVDi,3};
   aPVDnasala(aPVDi,1:30) = aPVDanom{aPVDi,3};
   aPVDtempi(aPVDi,1:30) = aPVDirreg{aPVDi,4};
   aPVDtempa(aPVDi,1:30) = aPVDanom{aPVDi,4};

end

maPVDui = mean(aPVDupi,'omitnan');
maPVDdi = mean(aPVDdowni,'omitnan');
maPVDni = mean(aPVDnasali,'omitnan');
```

```
maPVDti = mean(aPVDtempi,'omitnan');

maPVDua = mean(aPVDupa,'omitnan');
maPVDda = mean(aPVDdowna,'omitnan');
maPVDna = mean(aPVDnasala,'omitnan');
maPVDta = mean(aPVDtempa,'omitnan');

%%
%
% PVD eyes (aPVD), Use this section to check if results differ when not including
FPVD
% revertd to PVD only: no FPVD
aPVDirreg = PVDirreg;%moved up for Mean B scan calculation
aPVDanom = PVDanom;
aallPVDBsanom = [aPVDanom{:}];
aavPVDanom = mean(aallPVDBsanom,2,'omitnan');%mean of all RD B scans
aPVDAxL = PVDAxL;
aPVDage = PVDage;
aPVDbfc = PVDbfc;


   aPVDupi = PVDupi;
   aPVDupa = PVDupa;
   aPVDdowni = PVDdowni;
   aPVDdowna = PVDdowna;
   aPVDnasali = PVDnasali;
   aPVDnasala = PVDnasala;
   aPVDtempi = PVDtempi;
   aPVDtempa = PVDtempa;


maPVDui = mean(aPVDupi,'omitnan');
maPVDdi = mean(aPVDdowni,'omitnan');
maPVDni = mean(aPVDnasali,'omitnan');
maPVDti = mean(aPVDtempi,'omitnan');

maPVDua = mean(aPVDupa,'omitnan');
maPVDda = mean(aPVDdowna,'omitnan');
maPVDna = mean(aPVDnasala,'omitnan');
maPVDta = mean(aPVDtempa,'omitnan');
%

%%

Tirr = sum(AllBs,2);%total scan irrregularity
figure
histogram(Tirr)
title('All eyes, total irregularity distribution');

TAnom = cell2mat(cellfun(@(x1) sum(x1), Anom, 'un', 0));%total scan anomaly
figure
histogram(TAnom);
title('All eyes, total anomaly distribution');

figure
[tAn,edges] = histcounts(TAnom(:,3));
tAd=histcounts(TAnom(:,2),edges);
tAu=histcounts(TAnom(:,1),edges);
tAt=histcounts(TAnom(:,4),edges);
ctrs = (edges(1:end-1)+edges(2:end))/2; % Calculate the bin centers
bar(ctrs, [tAu' tAd' tAn' tAt'],1,'stacked','FaceAlpha',0.6);
title('All scans total anomaly by region');
legend('Up','Down','Nasal','Temporal');
xlabel('anomaly, mm');
ylabel('No. of scans');
%%
```

```
%irregularity plot
figure
ti=tiledlayout(2,2,'TileSpacing','none','Padding','none');

ti(1) = nexttile(1);
hold on
plot(1:30,mFEui,'g');
plot(1:30,mRDui,'r');
plot(1:30,mRTui,'m');
plot(1:30,mPVDui,'b');
plot(1:30,mFPVDui,'c');
plot(1:30,mnotPVDui,'k');
plot(1:30,mStui,'y');
%legend('FE','RD','RT','PVD');
title('Up');

ti(4) = nexttile(4);
hold on
plot(1:30,mFEdi,'g');
plot(1:30,mRDdi,'r');
plot(1:30,mRTdi,'m');
plot(1:30,mPVDdi,'b');
plot(1:30,mFPVDui,'c');
plot(1:30,mnotPVDui,'k');
plot(1:30,mStui,'y');
legend('FE','RD','RT','PVD', 'FE PVD', 'not PVD', 'Stickler');
title('Down');

ti(3) = nexttile(3);
hold on
plot(1:30,mFEni,'g');
plot(1:30,mRDni,'r');
plot(1:30,mRTni,'m');
plot(1:30,mPVDni,'b');
plot(1:30,mFPVDui,'c');
plot(1:30,mnotPVDui,'k');
plot(1:30,mStui,'y');
%legend('FE','RD','RT','PVD');
title('Nasal');

ti(2) = nexttile(2);
hold on
plot(1:30,mFEti,'g');
plot(1:30,mRDti,'r');
plot(1:30,mRTti,'m');
plot(1:30,mPVDti,'b');
plot(1:30,mFPVDui,'c');
plot(1:30,mnotPVDui,'k');
plot(1:30,mStui,'y');
%legend('FE','RD','RT','PVD');
title('Temporal');
%ti.Title.String = 'Irregularity by region';

xlabel(ti,'Bin number','FontWeight','bold');
ylabel(ti,'Irregularity modulus, mm','FontWeight','bold');

linkaxes(ti,'xy');

%%
%irregularity plot, RD RT and PVD only for thesis
figure
ti=tiledlayout(2,2,'TileSpacing','tight','Padding','tight');

ti(1) = nexttile(1);
hold on
%plot(1:30,mFEui,'g');
```

```
plot(1:30,mRDui,'r');
plot(1:30,mRTui,'m');
plot(1:30,mPVDui,'b');
%plot(1:30,mFPVDui,'c');
%plot(1:30,mnotPVDui,'k');
%plot(1:30,mStui,'y');
%legend('FE','RD','RT','PVD');
title('Up');

ti(4) = nexttile(4);
hold on
%plot(1:30,mFEdi,'g');
plot(1:30,mRDdi,'r');
plot(1:30,mRTdi,'m');
plot(1:30,mPVDdi,'b');
%plot(1:30,mFPVDui,'c');
%plot(1:30,mnotPVDui,'k');
%plot(1:30,mStui,'y');
legend('RD','RT','PVD');
title('Down');

ti(3) = nexttile(3);
hold on
%plot(1:30,mFEni,'g');
plot(1:30,mRDni,'r');
plot(1:30,mRTni,'m');
plot(1:30,mPVDni,'b');
%plot(1:30,mFPVDui,'c');
%plot(1:30,mnotPVDui,'k');
%plot(1:30,mStui,'y');
%legend('FE','RD','RT','PVD');
title('Nasal');

ti(2) = nexttile(2);
hold on
%plot(1:30,mFEti,'g');
plot(1:30,mRDti,'r');
plot(1:30,mRTti,'m');
plot(1:30,mPVDti,'b');
%plot(1:30,mFPVDui,'c');
%plot(1:30,mnotPVDui,'k');
%plot(1:30,mStui,'y');
%legend('FE','RD','RT','PVD');
title('Temporal');
%ti.Title.String = 'Irregularity by region';

xlabel(ti,'Bin number','FontWeight','bold');
ylabel(ti,'Irregularity modulus, mm','FontWeight','bold');

linkaxes(ti,'xy');
%%
%anomaly plot
figure
ta=tiledlayout(2,2,'TileSpacing','none','Padding','none');

ta(1) = nexttile(1);
hold on
plot(1:30,mFEua,'g');
plot(1:30,mRDua,'r');
plot(1:30,mRTua,'m');
plot(1:30,mPVDua,'b');
plot(1:30,mFPVDua,'c');
plot(1:30,mnotPVDua,'k');
plot(1:30,mStua,'y');
%legend('FE','RD','RT','PVD');
title('Up');
```

```
ta(4) = nexttile(4);
hold on
plot(1:30,mFEda,'g');
plot(1:30,mRDda,'r');
plot(1:30,mRTda,'m');
plot(1:30,mPVDda,'b');
plot(1:30,mFPVDda,'c');
plot(1:30,mnotPVDda,'k');
plot(1:30,mStda,'y');
legend('FE','RD','RT','PVD', 'FE PVD', 'not PVD', 'Stickler');
title('Down');

ta(3) = nexttile(3);
hold on
plot(1:30,mFEna,'g');
plot(1:30,mRDna,'r');
plot(1:30,mRTna,'m');
plot(1:30,mPVDna,'b');
plot(1:30,mFPVDna,'c');
plot(1:30,mnotPVDna,'k');
plot(1:30,mStna,'y');
%legend('FE','RD','RT','PVD');
title('Nasal');

ta(2) = nexttile(2);
hold on
plot(1:30,mFEta,'g');
plot(1:30,mRDta,'r');
plot(1:30,mRTta,'m');
plot(1:30,mPVDta,'b');
plot(1:30,mFPVDta,'c');
plot(1:30,mnotPVDta,'k');
plot(1:30,mStta,'y');
%legend('FE','RD','RT','PVD');
title('Temporal');
%title(ta,'Anomaly by region','FontWeight','bold');
xlabel(ta,'Bin number','FontWeight','bold');
ylabel(ta,'Anomaly, mm','FontWeight','bold');

linkaxes(ta,'xy');
%%
%anomaly plot, RD/PVD only
figure
ta=tiledlayout(2,2,'TileSpacing','none','Padding','none');

ta(1) = nexttile(1);
hold on
plot(1:30,mRDua,'r');
plot(1:30,mPVDua,'b');
%legend('FE','RD','RT','PVD');
title('Up');

ta(4) = nexttile(4);
hold on
plot(1:30,mRDda,'r');
plot(1:30,mPVDda,'b');
legend('RD','PVD');
title('Down');

ta(3) = nexttile(3);
hold on
plot(1:30,mRDna,'r');
plot(1:30,mPVDna,'b');
title('Nasal');
```

```
ta(2) = nexttile(2);
hold on
plot(1:30,mRDta,'r');
plot(1:30,mPVDta,'b');
title('Temporal');

xlabel(ta,'Bin number','FontWeight','bold');
ylabel(ta,'Anomaly, mm','FontWeight','bold');

linkaxes(ta,'xy');

figure%average RD and PVD anomaly, all B scans
hold on
plot(1:30,avRDanom,'r');
plot(1:30,avPVDanom,'b');
xlabel('Bin number','FontWeight','bold');
ylabel('Anomaly, mm','FontWeight','bold');
legend('RD anomaly','PVD anomaly');
%%

%now look at total irregulrity
%start by looking at total irregularity = sum of rows
tRDu = sum(RDupi,2);
tRDd = sum(RDdowni,2);
tRDn = sum(RDnasali,2);
tRDt = sum(RDtempi,2);

tRTu = sum(RTupi,2);
tRTd = sum(RTdowni,2);
tRTn = sum(RTnasali,2);
tRTt = sum(RTtempi,2);

tPVDu = sum(PVDupi,2);
tPVDd = sum(PVDdowni,2);
tPVDn = sum(PVDnasali,2);
tPVDt = sum(PVDtempi,2);

tFEu = sum(FEupi,2);
tFEd = sum(FEdowni,2);
tFEn = sum(FEnasali,2);
tFEt = sum(FEtempi,2);

tFPVDu = sum(FPVDupi,2);
tFPVDd = sum(FPVDdowni,2);
tFPVDn = sum(FPVDnasali,2);
tFPVDt = sum(FPVDtempi,2);

tnotPVDu = sum(notPVDupi,2);
tnotPVDd = sum(notPVDdowni,2);
tnotPVDn = sum(notPVDnasali,2);
tnotPVDt = sum(notPVDtempi,2);

tStu = sum(Stupi,2);
tStd = sum(Stdowni,2);
tStn = sum(Stnasali,2);
tStt = sum(Sttempi,2);
%{
tiledlayout(1,2,'TileSpacing','none','Padding','none')
h=nexttile;
h(1)=histogram(tRDu);
hold on
h(2)=histogram(tRDd);
h(3)=histogram(tRDn);
h(4)=histogram(tRDt);
h(2).BinWidth=5;
title('RD eyes total irregularity');
```

```
h1=nexttile;
h1(1)=histogram(tPVDu);
hold on
h1(2)=histogram(tPVDd);
h1(3)=histogram(tPVDn);
h1(4)=histogram(tPVDt);
h1(1).BinWidth=5;
h1(2).BinWidth=5;
h1(3).BinWidth=5;
h1(4).BinWidth=5;
title('PVD eyes total irregularity');
linkaxes([h(1:4), h1(1:4)],'xy');
%}
figure
HiT=tiledlayout(1,2,'TileSpacing','none','Padding','none');

H1=nexttile;
[tDd,edges] = histcounts(tRDd);
tDu=histcounts(tRDu,edges);
tDn=histcounts(tRDn,edges);
tDt=histcounts(tRDt,edges);
ctrs = (edges(1:end-1)+edges(2:end))/2; % Calculate the bin centers
bar(ctrs, [tDu' tDd' tDn' tDt'],1,'stacked','FaceAlpha',0.6);
xticks([5 15 25 35 45 55]);
title('RD eyes total irregularity');
legend('Up','Down','Nasal','Temporal');

H2=nexttile;
[tPDd,edgesP] = histcounts(tPVDd);
tPDu=histcounts(tPVDu,edgesP);
tPDn=histcounts(tPVDn,edgesP);
tPDt=histcounts(tPVDt,edgesP);
ctrsP = (edgesP(1:end-1)+edgesP(2:end))/2; % Calculate the bin centers
bar(ctrsP, [tPDu' tPDd' tPDn' tPDt'],1,'stacked','FaceAlpha',0.6);
title('PVD eyes total irregularity');
title(HiT,'Irregularity by diagnosis and region','FontWeight','bold');
xlabel(HiT,'Irregularity, mm','FontWeight','bold');
ylabel(HiT,'Number of scans','FontWeight','bold');
linkaxes([H1 H2],'xy');
%bler =cat(2,tPVDu, tPVDd, tPVDn, tPVDt);
%%
%now look at total anomaly
%start by looking at total anomaly = sum of rows
tRDua = sum(RDupa,2);
tRDda = sum(RDdowna,2);
tRDna = sum(RDnasala,2);
tRDta = sum(RDtempa,2);

tRTua = sum(RTupa,2);
tRTda = sum(RTdowna,2);
tRTna = sum(RTnasala,2);
tRTta = sum(RTtempa,2);

tPVDua = sum(PVDupa,2);
tPVDda = sum(PVDdowna,2);
tPVDna = sum(PVDnasala,2);
tPVDta = sum(PVDtempa,2);

tFEua = sum(FEupa,2);
tFEda = sum(FEdowna,2);
tFEna = sum(FEnasala,2);
tFEta = sum(FEtempa,2);

figure
HiA=tiledlayout(1,2,'TileSpacing','none','Padding','none');
```

```
H3=nexttile;
[tDda,edgesa] = histcounts(tRDda);
tDua=histcounts(tRDua,edgesa);
tDna=histcounts(tRDna,edgesa);
tDta=histcounts(tRDta,edgesa);
ctrsa = (edgesa(1:end-1)+edgesa(2:end))/2; % Calculate the bin centers
bar(ctrsa, [tDua' tDda' tDna' tDta'],1,'stacked','FaceAlpha',0.6);
title('RD eyes total anomaly');
legend('Up','Down','Nasal','Temporal');

%{
H4=nexttile;
[tPDda,edgesPa] = histcounts(tPVDda);
tPDua=histcounts(tPVDua,edgesPa);
tPDna=histcounts(tPVDna,edgesPa);
tPDta=histcounts(tPVDta,edgesPa);
ctrsPa = (edgesPa(1:end-1)+edgesPa(2:end))/2; % Calculate the bin centers
bar(ctrsPa, [tPDua' tPDda' tPDna' tPDta'],1,'stacked','FaceAlpha',0.6);
title('PVD eyes total anomaly');
xticks([0 10 20 30 40]);
%}

H4=nexttile;
[tPDda,edgesPa] = histcounts(tPVDda,edgesa);%makes hist bars same as RD group
tPDua=histcounts(tPVDua,edgesPa);
tPDna=histcounts(tPVDna,edgesPa);
tPDta=histcounts(tPVDta,edgesPa);
ctrsPa = (edgesPa(1:end-1)+edgesPa(2:end))/2; % Calculate the bin centers
bar(ctrsPa, [tPDua' tPDda' tPDna' tPDta'],1,'stacked','FaceAlpha',0.6);
title('PVD eyes total anomaly');
%xticks([0 10 20 30 40]);

title(HiA,'Scan total Anomaly by diagnosis and region','FontWeight','bold');
xlabel(HiA,'Anomaly, mm','FontWeight','bold');
ylabel(HiA,'Number of scans','FontWeight','bold');
linkaxes([H3 H4],'xy');

%%



%%
%Part 2

%create array with each eye in a row (all 4 scans in row)
%matching Response vector
%1 = no PVD
%2 = PVD
%3 = RD
%4 = RT
%5 = FE

RDallBsBn=cat(2,RDupa, RDdowna, RDtempa, RDnasala);
aPVDallBsBn=cat(2,aPVDupa, aPVDdowna, aPVDtempa, aPVDnasala);
RTallBsBn=cat(2,RTupa, RTdowna, RTtempa, RTnasala);

RDfts = cat(2, RDallBsBn,RDbfc, RDAxL, RDage);
aPVDfts = cat(2, aPVDallBsBn, aPVDbfc, aPVDAxL, aPVDage);
RTfts = cat(2, RTallBsBn, RTbfc, RTAxL, RTage);

RDlbl=ones(size(RDallBsBn,1),1)*3;
aPVDlbl=ones(size(aPVDallBsBn,1),1)*2;
RTlbl=ones(size(RTallBsBn,1),1)*4;

Allfeats = cat(1, aPVDfts, RDfts);% features (bins, AxL, Age, BFC)
```

```
Alllbls = cat(1, aPVDlbl, RDlbl);%response labels
AllID = cat(1,PVDID, RDID);

%Part 2a: split into training and testing
%create random selection: 70/30
Split = cvpartition(size(Alllbls,1),'HoldOut', 0.30);
Splittest = test(Split);%test set indices
Splittrain = training(Split);%training indices

Avbins = mean(Allfeats, 'omitnan');%mean anomaly
AvbinsTr = mean(Allfeats(Splittrain,:), 'omitnan');%mean anomaly, training

AvbinsRD = mean(Allfeats(Alllbls==3,:), 'omitnan');%mean anomaly, RD
AvbinsPVD = mean(Allfeats(Alllbls==2,:), 'omitnan');%mean anomaly, RD

%Do age, AXLm differ between groups (all eyes)
[~,pAge] = ttest2(RDage, aPVDage);
[~,pAxL] = ttest2(RDAxL, aPVDAxL);
% Axl and age difference between training set groups
[~,pAgAlTr] = ttest2(Allfeats(Alllbls==3 & Splittrain==1,end-
1:end),Allfeats(Alllbls==2 & Splittrain==1,end-1:end));
MnRDage = mean(RDage, 'omitnan');% for all eyes
MnPVDage = mean(aPVDage, 'omitnan');
MnRDAxL = mean(RDAxL, 'omitnan');
MnPVDAxL = mean(aPVDAxL, 'omitnan');
sdRDage = std(RDage, 'omitnan');
sdPVDage = std(aPVDage, 'omitnan');
sdRDAxL = std(RDAxL, 'omitnan');
sdPVDAxL = std(aPVDAxL, 'omitnan');

MnRTfts = mean(RTfts, 'omitnan');
sdRTfts = std(RTfts, 'omitnan');

[~,pAgeTR] = ttest2(RDage, RTfts(:,126));
[~,pAxLTR] = ttest2(RDAxL, RTfts(:,125));%RT to RD

[~,pAgePT] = ttest2(aPVDage,RTfts(:,126));
[~,pAxLPT] = ttest2(aPVDAxL,RTfts(:,125));%PVD to RT

%Feature selection methods
% performed on all eyes:
allRDiA = cat(1, mRDua', mRDda', mRDta', mRDna');%mean anomaly
allPVDiA = cat(1,maPVDua', maPVDda', maPVDta', maPVDna');
RDa = cell2mat(RDanom(:));
aPVDa = cell2mat(aPVDanom(:));
RDat = reshape(RDa,30,[]);
aPVDat = reshape(aPVDa, 30, []);
[~,prAnomall] = ttest2(RDat',aPVDat');%sig diff between anom all region? ALL
eyes.Ignore
diffRDPVD = allRDiA - allPVDiA;%difference between av anomaly RD & PVD
[sdiffRDPVD, IdxRDPVDdiff] = sort(abs(diffRDPVD), 'descend');%indices of greatest
difference in anomaly

%training set eyes
mRDTra = mean(Allfeats(Alllbls==3 & Splittrain==1,:),'omitnan');%mean training set
features
maPVDTra = mean(Allfeats(Alllbls==2 & Splittrain==1,:),'omitnan');%126 columns
sdRDTra = std(Allfeats(Alllbls==3 & Splittrain==1,:),'omitnan');%STD training set
features
sdaPVDTra = std(Allfeats(Alllbls==2 & Splittrain==1,:),'omitnan');%126 columns
[~,prAnTr] = ttest2(Allfeats(Alllbls==3 & Splittrain==1,:),Allfeats(Alllbls==2 &
Splittrain==1,:));
diffRDPVDTrS = abs(mRDTra - maPVDTra)./maPVDTra;%difference between av anomaly RD &
PVD, training set
[sdiffRDPVDTrS, IdxRDPVDdiffTrS] = sort(abs(diffRDPVDTrS), 'descend');%indices of
greatest difference in anomaly
```

```
%Use MRMR to select best features - training set
%[Featidxmrmr, scFeatsmrmr] = fscmrmr(Allfeats, Alllbls);%this is all eyes
[Featidxmrmr, scFeatsmrmr] = fscmrmr(Allfeats(Splittrain,:),
Alllbls(Splittrain));%this is training set eyes
%Featidxmrmr lists in order the best features for prediction

figure
Brcht = bar(scFeatsmrmr(Featidxmrmr(1:10)));%show top 10 features
xlabel('Predictor rank')
ylabel('Predictor importance score')
title('Best features for prediction, MRMR - training set')
xtips1 = Brcht.XEndPoints;
ytips1 = Brcht.YEndPoints;
labelsBar = string(Brcht.YData);
%text(xtips1,ytips1,num2str(Featidx(1:10)))


%Use chi2 to select best features
[Featidxchi2, scFeatschi2] = fscchi2(Allfeats(Splittrain,:), Alllbls(Splittrain));
%Featidxchi2 lists in order the best features for prediction
figure
Brcht2 = bar(scFeatschi2(Featidxchi2));%show top 10 features
xlabel('Predictor rank')
ylabel('Predictor importance score')
title('Best features for prediction, Chi2 - training set')

%Use relieff to select best features
[Featidxrlf, scFeatscrlf] = relieff(Allfeats(Splittrain,:), Alllbls(Splittrain),
10, 'method', 'classification');
%Featidxrlf lists in order the best features for prediction
figure
Brcht3 = bar(scFeatscrlf(Featidxrlf));%show top 10 features
xlabel('Predictor rank')
ylabel('Predictor importance score')
title('Best features for prediction, relieff, training set')

%use fscnca (neighborhood component analysis) for classification
NCAmdl = fscnca(Allfeats(Splittrain,:), Alllbls(Splittrain));
figure
plot(NCAmdl.FeatureWeights,'ro')
grid on
xlabel('Feature index')
ylabel('Feature weight')
[BestNCAfeats, IdxNCAb] = sort(NCAmdl.FeatureWeights, 'descend');
%IdxNCAb lists in order the best features for prediction


%maximum variance
VarTrfts = var(Allfeats(Splittrain,:),'omitnan');
[BestVarTr,IdxBVar] = sort(VarTrfts,'descend');

%Kendall's rank coefficient for predictor ranks
rhoKen = corr(Allfeats(Splittrain,:),Alllbls(Splittrain),'type','Kendall');
[BestKenrho, IdxBKr] = sort(rhoKen,'ascend');%want least correlated?

%Univariate feature ranking with F-tests
idxFtest = fsrftest(Allfeats(Splittrain,:), Alllbls(Splittrain));

%LASSO regularisation
[Blasso fitinfoB] = lasso(Allfeats(Splittrain,:), Alllbls(Splittrain),
'Lambda',linspace(0,1),'CV',10);
[Alasso fitinfoA] = lasso(Allfeats(Splittrain,:), Alllbls(Splittrain),
'Lambda',linspace(0,1),'Alpha',0.5,'CV',10);
%Best features the indices of columns with most zeros.Row indices = vars
VaridxA = cell(100,1);
```

```
VaridxB = cell(100,1);
LCol0A=NaN(100,1);
LCol0B=NaN(100,1);
for La0=1:100
   LCol0A(La0)=nnz(Alasso(:,La0));
   VaridxA{La0}=find(Alasso(:,La0)~=0);
   LCol0B(La0)=nnz(Blasso(:,La0));
   VaridxB{La0}=find(Blasso(:,La0)~=0);
end
[~,IdxLA]=sort(LCol0A,'ascend');
[~,IdxLB]=sort(LCol0B,'ascend');%top indices here = look at non zero rows for vars
sVaridxA=VaridxA(IdxLA);
sVaridxB=VaridxB(IdxLB);%check this

%ANOVA
[pANOVA,tblAn, statsAN] = anova1(Allfeats(Splittrain,:));
Canova = multcompare(statsAN);
[BestpAN, IdxBAn] = sort(Canova(:,6),'ascend');
AnovMD(:,1:2)=Canova(IdxBAn,1:2);%list variables most dissimlar by ANOVA (low p
value)

%as ANOVA has 1765 var combinations with p<0.05
SelAnovVar= AnovMD(1:1765,:);
[selVAn,NSelAn] = groupcounts(SelAnovVar(:));
[~,IdxselAn] = sort(selVAn,'descend');
BselVAn = NSelAn(IdxselAn);%the most commonly seen Vars in ANOVA
```

5. SSTrTst

```
%from SStabana candidate feature reduction, explore to select features from
%training set to progress to classifier development
%Allfeats/Alllbls is all anomaly, BFC, age & Axl in an array arranged:
%(eyes in rows, 30 bins in columns x 4)
%  PVDupa, PVDdowna, PVDtempa, PVDnasala, BFC(up,d,t,n), axl, Age
%  RDupa, RDdowna, RDtempa, RDnasala, , BFC(up,d,t,n), axl, Age
%Part 0
ALLiAxL = cat(1,PVDAxL,RDAxL);
AxLTrS = ALLiAxL(Splittrain==1);
IdXCfeats = [2      3      4      8      12     15     16     28     32     33     34
       35     36     44     56     63     71     72     79     82     83     85     90
       92     93     96     97     100    102    111    118    119    121    123    124
       125    126];
%candidate features indices (column numbers of Allfeats)
Candfeats = Allfeats(Splittrain==1,IdXCfeats);%training set variables
CandFlbls = Alllbls(Splittrain==1);

%
%Use training set only

%%Use this section to reduce number of candidate features
%determine coefficient of variation of each candidate feature
RDmns = mean(Candfeats(CandFlbls==3,:),'omitnan');%column vector
PVDmns = mean(Candfeats(CandFlbls==2,:),'omitnan');
RDsds = std(Candfeats(CandFlbls==3,:),'omitnan');
PVDsds = std(Candfeats(CandFlbls==2,:),'omitnan');
RDcv = RDsds./RDmns;%coefficient of variation, RD anomalies
PVDcv = PVDsds./RDmns;
%what Cv is acceptable? (certainly) not >1

%how about 1 or 2 x sd > average difference between groups
dfeatRDPVD = mRDTra-maPVDTra;
dfeatRDPVDCF = dfeatRDPVD(IdXCfeats);
featDiffSD=cat(1,dfeatRDPVDCF,RDsds, PVDsds);%displays RD,PVD average difference v
SD
```

```
%or just two sample ttest the variables from PVD & RD?
[~, pRP, ciRP,~]=ttest2(Candfeats(CandFlbls==3,:),Candfeats(CandFlbls==2,:));

%A further method of feature selection is from an independent set. This could be
%the SD OCT eye information

%%
%Part 1.1.a Section: featarray
%Featredx is the final selcted variables. there are 12
Featredx = [2 4 8 16 79 82 83 85 90 125 ];
CFperm = cell(12,1);
for Vc = 1:12
   %CFperm holds all the possible combinations of variables
   CFperm{Vc} = nchoosek(Featredx,Vc);

end
Mdl12p = cell(12,924);
RDPVD12v = cell(12,924);
RDPVD12vsens = NaN(12,924);
RDPVD12vspec = NaN(12,924);
RDPVD12caccu = NaN(12,924);
for CFc = 1:12
   for CFr = 1:size(CFperm{CFc},1)
       MdlfeatsIdx = CFperm{CFc}(CFr,:);
       Mdlfeats = Allfeats(Splittrain,MdlfeatsIdx);
       Mdl12p{CFc,CFr} = fitcdiscr(Mdlfeats,CandFlbls,'DiscrimType','quadratic');

       RDPVD12v{CFc,CFr} =
confusionmat(Mdl12p{CFc,CFr}.Y,resubPredict(Mdl12p{CFc,CFr}));
       RDPVD12vsens(CFc,CFr) =
RDPVD12v{CFc,CFr}(2,2)/(RDPVD12v{CFc,CFr}(2,1)+RDPVD12v{CFc,CFr}(2,2));
       RDPVD12vspec(CFc,CFr) =
RDPVD12v{CFc,CFr}(1,1)/(RDPVD12v{CFc,CFr}(1,1)+RDPVD12v{CFc,CFr}(1,2));
       RDPVD12caccu(CFc,CFr) = sum(RDPVD12v{CFc,CFr}([1
4]))/sum(RDPVD12v{CFc,CFr}(:));%accuracy


   end

end

RDPVD12avsens = mean(RDPVD12vsens(:), 'omitnan');
RDPVD12avspec = mean(RDPVD12vspec(:), 'omitnan');
RDPVD12avacc = mean(RDPVD12caccu(:), 'omitnan');

figure
mesh(RDPVD12vsens,'FaceAlpha','0.5','LineStyle','none');
hold on
mesh(RDPVD12vspec,'FaceAlpha','0.5');
mesh(RDPVD12caccu,'FaceAlpha','0.5','LineStyle','none');

figure
surf(RDPVD12vsens,'FaceAlpha','0.3','LineStyle','none', 'FaceColor','g',
'FaceLighting', 'gouraud');
hold on
surf(RDPVD12vspec,'FaceAlpha','0.3', 'FaceColor','b', 'FaceLighting', 'flat');
surf(RDPVD12caccu,'FaceAlpha','0.3','LineStyle','none', 'FaceColor','m',
'FaceLighting', 'gouraud');

SPec90Idx=find(RDPVD12vspec>0.9);%specificity > .9 models
[SeSp90R,SeSp90C] = ind2sub([12 924],SPec90Idx);
L4featsIdx = find(SeSp90R<4);%models with 3 or fewer variable and spec> 0.9
CmR = SeSp90R(L4featsIdx);%CFperm cell number
CmC = SeSp90C(L4featsIdx);%CFperm row number in Cell CmR
SS90Idx=sub2ind([12 924],CmR,CmC);
SensSpec90 = cat(2,RDPVD12vspec(SS90Idx),RDPVD12vsens(SS90Idx));
```

```
feat90 = cell(length(CmR),1);%the best feaure combins for SensSpec90
for getVars=1:length(CmR)
   feat90{getVars} = CFperm{CmR(getVars)}(CmC(getVars),:);
end

%%
%Part 1.1.b Section: featarray for larger bins 2-4 (4 quads) + AxL
%Featredx is the final selected variables. there are 13
Featredx13 = [2 3 4 32 33 34 62 63 64 92 93 94 125];
CFperm13 = cell(13,1);
for Vc13 = 1:13
   %CFperm holds all the possible combinations of variables
   CFperm13{Vc13} = nchoosek(Featredx13,Vc13);

end
Mdl13p = cell(13,1716);
RDPVD13v = cell(13,1716);
RDPVD13vsens = NaN(13,1716);
RDPVD13vspec = NaN(13,1716);
RDPVD13caccu = NaN(13,1716);
for CFc13 = 1:13
   for CFr13 = 1:size(CFperm13{CFc13},1)
       MdlfeatsIdx13 = CFperm13{CFc13}(CFr13,:);
       Mdlfeats13 = Allfeats(Splittrain,MdlfeatsIdx13);
       Mdl13p{CFc13,CFr13} =
fitcdiscr(Mdlfeats13,CandFlbls,'DiscrimType','quadratic');

       RDPVD13v{CFc13,CFr13} =
confusionmat(Mdl13p{CFc13,CFr13}.Y,resubPredict(Mdl13p{CFc13,CFr13}));
       RDPVD13vsens(CFc13,CFr13) =
RDPVD13v{CFc13,CFr13}(2,2)/(RDPVD13v{CFc13,CFr13}(2,1)+RDPVD13v{CFc13,CFr13}(2,2));
       RDPVD13vspec(CFc13,CFr13) =
RDPVD13v{CFc13,CFr13}(1,1)/(RDPVD13v{CFc13,CFr13}(1,1)+RDPVD13v{CFc13,CFr13}(1,2));
       RDPVD13caccu(CFc13,CFr13) = sum(RDPVD13v{CFc13,CFr13}([1
4]))/sum(RDPVD13v{CFc13,CFr13}(:));%accuracy


   end

end

RDPVD13avsens = mean(RDPVD13vsens(:), 'omitnan');
RDPVD13avspec = mean(RDPVD13vspec(:), 'omitnan');
RDPVD13avacc = mean(RDPVD13caccu(:), 'omitnan');

figure
mesh(RDPVD13vsens,'FaceAlpha','0.5','LineStyle','--');
hold on
mesh(RDPVD13vspec,'FaceAlpha','0.5');
mesh(RDPVD13caccu,'FaceAlpha','0.5','LineStyle',':');

figure
surf(RDPVD13vsens,'FaceAlpha','0.3','LineStyle','--', 'FaceColor','g');
hold on
surf(RDPVD13vspec,'FaceAlpha','0.3', 'FaceColor','b');
surf(RDPVD13caccu,'FaceAlpha','0.3','LineStyle',':', 'FaceColor','m');

SPec90Idx13=find(RDPVD13vspec>0.90);%specificity > .95 models
[SeSp90R13,SeSp90C13] = ind2sub([13 1716],SPec90Idx13);
L4featsIdx13 = find(SeSp90R13<4);%models with 3 or fewer variable and spec> 0.9
CmR13 = SeSp90R13(L4featsIdx13);%CFperm cell number
CmC13 = SeSp90C13(L4featsIdx13);%CFperm row number in Cell CmR
SS90Idx13=sub2ind([13 1716],CmR13,CmC13);
SensSpec9013 = cat(2,RDPVD13vspec(SS90Idx13),RDPVD13vsens(SS90Idx13));
feat90b = cell(length(CmR13),1);
for getVars=1:length(CmR13)
```

```
   feat90b{getVars} = CFperm13{CmR13(getVars)}(CmC13(getVars),:);
end


%%
%%
%Part 1.1. c Lasso Section: (featarray for larger bins 2-4 (4 quads) + AxL)
%Featredx is the final selected variables. there are 6
Featredx6 = [4 36 79 83 86 125];
CFperm6 = cell(6,1);
for Vc6 = 1:6
   %CFperm holds all the possible combinations of variables
   CFperm6{Vc6} = nchoosek(Featredx6,Vc6);

end

Mdl6p = cell(6,58);
RDPVD6v = cell(6,58);
RDPVD6vsens = NaN(6,58);
RDPVD6vspec = NaN(6,58);
RDPVD6caccu = NaN(6,58);
for CFc6 = 1:6
   for CFr6 = 1:size(CFperm6{CFc6},1)
       MdlfeatsIdx6 = CFperm6{CFc6}(CFr6,:);
       Mdlfeats6 = Allfeats(Splittrain,MdlfeatsIdx6);
       Mdl6p{CFc6,CFr6} = fitcdiscr(Mdlfeats6,CandFlbls,'DiscrimType','quadratic');

       RDPVD6v{CFc6,CFr6} =
confusionmat(Mdl6p{CFc6,CFr6}.Y,resubPredict(Mdl6p{CFc6,CFr6}));
       RDPVD6vsens(CFc6,CFr6) =
RDPVD6v{CFc6,CFr6}(2,2)/(RDPVD6v{CFc6,CFr6}(2,1)+RDPVD6v{CFc6,CFr6}(2,2));
       RDPVD6vspec(CFc6,CFr6) =
RDPVD6v{CFc6,CFr6}(1,1)/(RDPVD6v{CFc6,CFr6}(1,1)+RDPVD6v{CFc6,CFr6}(1,2));
       RDPVD6caccu(CFc6,CFr6) = sum(RDPVD6v{CFc6,CFr6}([1
4]))/sum(RDPVD6v{CFc6,CFr6}(:));%accuracy


   end

end

RDPVD6avsens = mean(RDPVD6vsens(:), 'omitnan');
RDPVD6avspec = mean(RDPVD6vspec(:), 'omitnan');
RDPVD6avacc = mean(RDPVD6caccu(:), 'omitnan');

figure
mesh(RDPVD6vsens,'FaceAlpha','0.5','LineStyle','--');
hold on
mesh(RDPVD6vspec,'FaceAlpha','0.5');
mesh(RDPVD6caccu,'FaceAlpha','0.5','LineStyle',':');

figure
surf(RDPVD6vsens,'FaceAlpha','0.3','LineStyle','--', 'FaceColor','g');
hold on
surf(RDPVD6vspec,'FaceAlpha','0.3', 'FaceColor','b');
surf(RDPVD6caccu,'FaceAlpha','0.3','LineStyle',':', 'FaceColor','m');


SPec90Idx6=find(RDPVD6vspec>0.90);%specificity > .90 models
[SeSp90R6,SeSp90C6] = ind2sub([6 58],SPec90Idx6);
L4featsIdx6 = find(SeSp90R6<4);%models with 3 or fewer variable and spec> 0.9
CmR6 = SeSp90R6(L4featsIdx6);%CFperm cell number
CmC6 = SeSp90C6(L4featsIdx6);%CFperm row number in Cell CmR
SS90Idx6=sub2ind([6 58],CmR6,CmC6);
SensSpec906 = cat(2,RDPVD6vspec(SS90Idx6),RDPVD6vsens(SS90Idx6));
feat90bL = cell(length(CmR6),1);
```

```
for getVars=1:length(CmR6)
   feat90bL{getVars} = CFperm6{CmR6(getVars)}(CmC6(getVars),:);
end

%%
%Part 1.1.c Section: featarray from Table 3 (CoV candidate features)
%Featredx14 is the final selected variables. there are 14
Featredx14 = [2 3 4 32 33 62 63 93 121 122 123 124 125 126 ];
CFperm14 = cell(14,1);
for Vc14 = 1:14
   %CFperm holds all the possible combinations of variables
   CFperm14{Vc14} = nchoosek(Featredx14,Vc14);

end
Mdl14p = cell(14,3432);
RDPVD14v = cell(14,3432);
RDPVD14vsens = NaN(14,3432);
RDPVD14vspec = NaN(14,3432);
RDPVD14caccu = NaN(14,3432);
for CFc14 = 1:14
   for CFr14 = 1:size(CFperm14{CFc14},1)
       MdlfeatsIdx14 = CFperm14{CFc14}(CFr14,:);
       Mdlfeats14 = Allfeats(Splittrain,MdlfeatsIdx14);
       Mdl14p{CFc14,CFr14} =
fitcdiscr(Mdlfeats14,CandFlbls,'DiscrimType','quadratic');

       RDPVD14v{CFc14,CFr14} =
confusionmat(Mdl14p{CFc14,CFr14}.Y,resubPredict(Mdl14p{CFc14,CFr14}));
       RDPVD14vsens(CFc14,CFr14) =
RDPVD14v{CFc14,CFr14}(2,2)/(RDPVD14v{CFc14,CFr14}(2,1)+RDPVD14v{CFc14,CFr14}(2,2));
       RDPVD14vspec(CFc14,CFr14) =
RDPVD14v{CFc14,CFr14}(1,1)/(RDPVD14v{CFc14,CFr14}(1,1)+RDPVD14v{CFc14,CFr14}(1,2));
       RDPVD14caccu(CFc14,CFr14) = sum(RDPVD14v{CFc14,CFr14}([1
4]))/sum(RDPVD14v{CFc14,CFr14}(:));%accuracy


   end

end

RDPVD14avsens = mean(RDPVD14vsens(:), 'omitnan');
RDPVD14avspec = mean(RDPVD14vspec(:), 'omitnan');
RDPVD14avacc = mean(RDPVD14caccu(:), 'omitnan');

figure
mesh(RDPVD14vsens,'FaceAlpha','0.5','LineStyle','--');
hold on
mesh(RDPVD14vspec,'FaceAlpha','0.5');
mesh(RDPVD14caccu,'FaceAlpha','0.5','LineStyle',':');

figure
surf(RDPVD14vsens,'FaceAlpha','0.3','LineStyle','--', 'FaceColor','g');
hold on
surf(RDPVD14vspec,'FaceAlpha','0.3', 'FaceColor','b');
surf(RDPVD14caccu,'FaceAlpha','0.3','LineStyle',':', 'FaceColor','m');

SPec90Idx14=find(RDPVD14vspec>0.90);%specificity > .95 models
[SeSp90R14,SeSp90C14] = ind2sub([14,3432],SPec90Idx14);
L4featsIdx14 = find(SeSp90R14<4);%models with 3 or fewer variable and spec> 0.9
CmR14 = SeSp90R14(L4featsIdx14);%CFperm cell number
CmC14 = SeSp90C14(L4featsIdx14);%CFperm row number in Cell CmR
SS90Idx14=sub2ind([14,3432],CmR14,CmC14);
SensSpec9014 = cat(2,RDPVD14vspec(SS90Idx14),RDPVD14vsens(SS90Idx14));
feat90c = cell(length(CmR14),1);
for getVars=1:length(CmR14)
   feat90c{getVars} = CFperm14{CmR14(getVars)}(CmC14(getVars),:);
```

```
end

%%
%{
%Part 1.2. Feature reduction.

%7 variable model

DaTavarsmaxK7a = Candfeats;

MdlRDPVDmaxK7 = fitcdiscr(DaTavarsmaxK7a,CandFlbls,'DiscrimType','quadratic');

 RDPVD7v = confusionmat(MdlRDPVDmaxK7.Y,resubPredict(MdlRDPVDmaxK7));
 RDPVD7vsens = RDPVD7v(2,2)/(RDPVD7v(2,1)+RDPVD7v(2,2));
 RDPVD7vspec = RDPVD7v(1,1)/(RDPVD7v(1,1)+RDPVD7v(1,2));
 RDPVD7caccu = sum(RDPVD7v([1 4]))/sum(RDPVD7v(:));%accuracy



%6 var model
RDPVD6v = cell (7,1);%array of confusion matrices
MdlRDPVDmaxK6 = cell(7,1);%models array
RDPVD6vsens = NaN(7,1);
RDPVD6vspec = NaN(7,1);
RDPVDvarsmaxK6 = Candfeats;

%6 variable model
for CoLs = 1:7
        DaTavarsmaxK6a = RDPVDvarsmaxK6;
        DaTavarsmaxK6a(:,CoLs)=[];%removes one variable

        MdlRDPVDmaxK6{CoLs} =
fitcdiscr(DaTavarsmaxK6a,CandFlbls,'DiscrimType','quadratic');

        RDPVD6v{CoLs} =
confusionmat(MdlRDPVDmaxK6{CoLs}.Y,resubPredict(MdlRDPVDmaxK6{CoLs}));
        RDPVD6vsens(CoLs) =
RDPVD6v{CoLs}(2,2)/(RDPVD6v{CoLs}(2,1)+RDPVD6v{CoLs}(2,2));
        RDPVD6vspec(CoLs) =
RDPVD6v{CoLs}(1,1)/(RDPVD6v{CoLs}(1,1)+RDPVD6v{CoLs}(1,2));
        RDPVD6caccu(CoLs) = sum(RDPVD6v{CoLs}([1
4]))/sum(RDPVD6v{CoLs}(:));%accuracy

end

RDPVD6avsens = mean(RDPVD6vsens(:), 'omitnan');
RDPVD6avspec = mean(RDPVD6vspec(:), 'omitnan');
RDPVD6avacc = mean(RDPVD6caccu(:), 'omitnan');

%5 var model
RDPVD5v = cell (7,6);%array of confusion matrices
MdlRDPVDmaxK5 = cell(7,6);%models array
RDPVD5vsens = NaN(7,6);
RDPVD5vspec = NaN(7,6);
RDPVDvarsmaxK5 = Candfeats;

%5 variable model
for CoLs = 1:7
        DaTavarsmaxK5a = RDPVDvarsmaxK5;
        DaTavarsmaxK5a(:,CoLs)=[];%removes one variable

     for C2 = 1:6

         DaTavarsmaxK5a1 = DaTavarsmaxK5a;
         DaTavarsmaxK5a1(:,C2)=[];
```

```
        MdlRDPVDmaxK5{CoLs,C2} =
fitcdiscr(DaTavarsmaxK5a1,CandFlbls,'DiscrimType','quadratic');

        RDPVD5v{CoLs,C2} =
confusionmat(MdlRDPVDmaxK5{CoLs,C2}.Y,resubPredict(MdlRDPVDmaxK5{CoLs,C2}));
        RDPVD5vsens(CoLs,C2) =
RDPVD5v{CoLs,C2}(2,2)/(RDPVD5v{CoLs,C2}(2,1)+RDPVD5v{CoLs,C2}(2,2));
        RDPVD5vspec(CoLs,C2) =
RDPVD5v{CoLs,C2}(1,1)/(RDPVD5v{CoLs,C2}(1,1)+RDPVD5v{CoLs,C2}(1,2));
        RDPVD5caccu(CoLs,C2) = sum(RDPVD5v{CoLs,C2}([1
4]))/sum(RDPVD5v{CoLs,C2}(:));%accuracy

     end
end

RDPVD5avsens = mean(RDPVD5vsens(:), 'omitnan');
RDPVD5avspec = mean(RDPVD5vspec(:), 'omitnan');
RDPVD5avacc = mean(RDPVD5caccu(:), 'omitnan');


%4 var model
RDPVD4v = cell (7,6,5);%array of confusion matrices
MdlRDPVDmaxK4 = cell(7,6,5);%models array
RDPVD4vsens = NaN(7,6,5);
RDPVD4vspec = NaN(7,6,5);
RDPVDvarsmaxK4 = Candfeats;

%4 variable model
for CoLs = 1:7
        DaTavarsmaxK4a = RDPVDvarsmaxK4;
        DaTavarsmaxK4a(:,CoLs)=[];%removes one variable

     for C2 = 1:6

         DaTavarsmaxK4a1 = DaTavarsmaxK4a;
         DaTavarsmaxK4a1(:,C2)=[];

         for C3 = 1:5

         DaTavarsmaxK4a2 = DaTavarsmaxK4a1;
         DaTavarsmaxK4a2(:,C3)=[];

        MdlRDPVDmaxK4{CoLs,C2,C3} =
fitcdiscr(DaTavarsmaxK4a2,CandFlbls,'DiscrimType','quadratic');

        RDPVD4v{CoLs,C2,C3} =
confusionmat(MdlRDPVDmaxK4{CoLs,C2,C3}.Y,resubPredict(MdlRDPVDmaxK4{CoLs,C2,C3}));
        RDPVD4vsens(CoLs,C2,C3) =
RDPVD4v{CoLs,C2,C3}(2,2)/(RDPVD4v{CoLs,C2,C3}(2,1)+RDPVD4v{CoLs,C2,C3}(2,2));
        RDPVD4vspec(CoLs,C2,C3) =
RDPVD4v{CoLs,C2,C3}(1,1)/(RDPVD4v{CoLs,C2,C3}(1,1)+RDPVD4v{CoLs,C2,C3}(1,2));
        RDPVD4caccu(CoLs,C2,C3) = sum(RDPVD4v{CoLs,C2,C3}([1
4]))/sum(RDPVD4v{CoLs,C2,C3}(:));%accuracy

         end
     end
end

RDPVD4avsens = mean(RDPVD4vsens(:), 'omitnan');
RDPVD4avspec = mean(RDPVD4vspec(:), 'omitnan');
RDPVD4avacc = mean(RDPVD4caccu(:), 'omitnan');


%3 var model
RDPVD3v = cell (7,6,5,4);%array of confusion matrices
MdlRDPVDmaxK3 = cell(7,6,5,4);%models array
```

```
RDPVD3vsens = NaN(7,6,5,4);
RDPVD3vspec = NaN(7,6,5,4);
RDPVDvarsmaxK3 = Candfeats;

%3 variable model
for CoLs = 1:7
        DaTavarsmaxK3a = RDPVDvarsmaxK3;
        DaTavarsmaxK3a(:,CoLs)=[];%removes one variable

     for C2 = 1:6

         DaTavarsmaxK3a1 = DaTavarsmaxK3a;
         DaTavarsmaxK3a1(:,C2)=[];

         for C3 = 1:5

         DaTavarsmaxK3a2 = DaTavarsmaxK3a1;
         DaTavarsmaxK3a2(:,C3)=[];

         for C4 = 1:4

         DaTavarsmaxK3a3 = DaTavarsmaxK3a2;
         DaTavarsmaxK3a3(:,C4)=[];

        MdlRDPVDmaxK3{CoLs,C2,C3,C4} =
fitcdiscr(DaTavarsmaxK3a3,CandFlbls,'DiscrimType','quadratic');

        RDPVD3v{CoLs,C2,C3,C4} =
confusionmat(MdlRDPVDmaxK3{CoLs,C2,C3,C4}.Y,resubPredict(MdlRDPVDmaxK3{CoLs,C2,C3,C
4}));
        RDPVD3vsens(CoLs,C2,C3,C4) =
RDPVD3v{CoLs,C2,C3,C4}(2,2)/(RDPVD3v{CoLs,C2,C3,C4}(2,1)+RDPVD3v{CoLs,C2,C3,C4}(2,2
));
        RDPVD3vspec(CoLs,C2,C3,C4) =
RDPVD3v{CoLs,C2,C3,C4}(1,1)/(RDPVD3v{CoLs,C2,C3,C4}(1,1)+RDPVD3v{CoLs,C2,C3,C4}(1,2
));
        RDPVD3caccu(CoLs,C2,C3,C4) = sum(RDPVD3v{CoLs,C2,C3,C4}([1
4]))/sum(RDPVD3v{CoLs,C2,C3,C4}(:));%accuracy

         end
         end
     end
end

%see results: array 7*5, 6*4 (r x sheets, cols X 4D)
%v3sens=NaN(35,24);
v3sens = reshape(RDPVD3vsens,[35,24]);
v3spec = reshape(RDPVD3vspec,[35,24]);

MxAcc3 = max(RDPVD3caccu(:));%max accuracy
IMxAcc3 = find(RDPVD3caccu==MxAcc3);%index max accuracy
SeSpmxAc3=NaN(length(IMxAcc3),3);
SeSpmxAc3(:,1) = RDPVD3vsens(IMxAcc3);
SeSpmxAc3(:,2) = RDPVD3vspec(IMxAcc3);
SeSpmxAc3(:,3) = RDPVD3caccu(IMxAcc3);%Max acc sens spe accuracy array

Mxspec3 = max(RDPVD3vspec(:));
MxIspec3 = find(RDPVD3vspec==Mxspec3);%indices of max spec 3 vars
sensMxspec = RDPVD3vsens(MxIspec3);%sens of maximal spec
[r3,c3,s,d3]= ind2sub([7 6 5 4],MxIspec3);
v3subs=cat(2,r3,c3,s,d3);%row col sheet dim4 location of max spec 3 var model

 Afeats=1:7;
 RegBin3 = cell(length(MxIspec3),1);
 %determine which [region,bin] are indexed by v3subs
 %Regbin3 numbers refer to which Trainset columns are retained.
```

```
for subs3 = 1:length(MxIspec3)
   nowfeat=Afeats;
    for Swr=1:4

        nowfeat(v3subs(subs3,Swr))=[];

    end
    RegBin3{subs3}=nowfeat;
end

Mxsens3 = max(RDPVD3vsens(:));
MxIsens3 = find(RDPVD3vsens==Mxsens3);

%bler = 1:35*24;
%bler4d = reshape(bler, [7,6,5,4]);
%bler2d= reshape(bler4d,[35,24]);

RDPVD3avsens = mean(RDPVD3vsens(:), 'omitnan');
RDPVD3avspec = mean(RDPVD3vspec(:), 'omitnan');
RDPVD3avacc = mean(RDPVD3caccu(:), 'omitnan');


%2 var model

RDPVD2v = cell (7,1);%array of confusion matrices
MdlRDPVDmaxK2 = cell(7,1);%models array
RDPVD2vsens = NaN(7,1);
RDPVD2vspec = NaN(7,1);
RDPVDvarsmaxK2 = Candfeats;

%2 variable model
for CoLs = 1:7
        DaTavarsmaxK2a = RDPVDvarsmaxK2(:,CoLs);%adds one var
        nDaTavarsmaxK2a = RDPVDvarsmaxK2;
        nDaTavarsmaxK2a(:,CoLs)=[];

     for C2 = 1:6

         DaTavarsmaxK2a1 = [];
         DaTavarsmaxK2a1 = cat(2,DaTavarsmaxK2a,nDaTavarsmaxK2a(:,C2));


        MdlRDPVDmaxK2{CoLs,C2} =
fitcdiscr(DaTavarsmaxK2a1,CandFlbls,'DiscrimType','quadratic');

        RDPVD2v{CoLs,C2} =
confusionmat(MdlRDPVDmaxK2{CoLs,C2}.Y,resubPredict(MdlRDPVDmaxK2{CoLs,C2}));
        RDPVD2vsens(CoLs,C2) =
RDPVD2v{CoLs,C2}(2,2)/(RDPVD2v{CoLs,C2}(2,1)+RDPVD2v{CoLs,C2}(2,2));
        RDPVD2vspec(CoLs,C2) =
RDPVD2v{CoLs,C2}(1,1)/(RDPVD2v{CoLs,C2}(1,1)+RDPVD2v{CoLs,C2}(1,2));
        RDPVD2caccu(CoLs,C2) = sum(RDPVD2v{CoLs,C2}([1
4]))/sum(RDPVD2v{CoLs,C2}(:));%accuracy

     end
end

RDPVD2avsens = mean(RDPVD2vsens(:), 'omitnan');
RDPVD2avspec = mean(RDPVD2vspec(:), 'omitnan');
RDPVD2avacc = mean(RDPVD2caccu(:), 'omitnan');


[F2msens,F2mIsens] = max(RDPVD2vsens(:),[],'omitnan');% max sensitivity, for
[F3msens,F3mIsens] = max(RDPVD3vsens(:),[],'omitnan');% each number of vars
[F4msens,F4mIsens] = max(RDPVD4vsens(:),[],'omitnan');
[F5msens,F5mIsens] = max(RDPVD5vsens(:),[],'omitnan');
```

```
[F6msens,F6mIsens] = max(RDPVD6vsens(:),[],'omitnan');

[F2mspec,F2mIspec] = max(RDPVD2vspec(:),[],'omitnan');
[F3mspec,F3mIspec] = max(RDPVD3vspec(:),[],'omitnan');
[F4mspec,F4mIspec] = max(RDPVD4vspec(:),[],'omitnan');
[F5mspec,F5mIspec] = max(RDPVD5vspec(:),[],'omitnan');
[F6mspec,F6mIspec] = max(RDPVD6vspec(:),[],'omitnan');

%table of average sens/spec, 7 to 2
senspecAc = NaN(6,3);
senspecAc(1,1) = RDPVD7vsens;
senspecAc(1,2) = RDPVD7vspec;
senspecAc(2,1) = RDPVD6avsens;
senspecAc(2,2) = RDPVD6avspec;
senspecAc(3,1) = RDPVD5avsens;
senspecAc(3,2) = RDPVD5avspec;
senspecAc(4,1) = RDPVD4avsens;
senspecAc(4,2) = RDPVD4avspec;
senspecAc(5,1) = RDPVD3avsens;
senspecAc(5,2) = RDPVD3avspec;
senspecAc(6,1) = RDPVD2avsens;
senspecAc(6,2) = RDPVD2avspec;
senspecAc(1,3) = RDPVD7caccu;
senspecAc(2,3) = RDPVD6avacc;
senspecAc(3,3) = RDPVD5avacc;
senspecAc(4,3) = RDPVD4avacc;
senspecAc(5,3) = RDPVD3avacc;
senspecAc(6,3) = RDPVD2avacc;
%}
%%
%{
%Part 1.2b
Xinds = repmat(1:7,7,1);
Yinds = repmat(1:7,7,1)';

figure
%classifier sensitivity by number of variable
hold on
plot3 ([1:7],[1:7], RDPVD7vsens,'go')
plot3 (Xinds(1:7,1:7),[2], RDPVD6vsens,'go')
plot3 (Xinds(1:7,1:6),Yinds(1:6, 1:7), RDPVD5vsens,'go')
plot3 (Xinds(1:7,1:6),Yinds(1:6, 1:5), RDPVD4vsens,'go')
plot3 (Xinds(1:7,1:6),Yinds(1:5, 1:4), RDPVD3vsens,'go')
plot3 (Xinds(1:7,1:7),Yinds(1:6, 1:6), RDPVD2vsens,'go')
title('sensitivity')
hold off

figure
%classifier specificity by number of variable
hold on
plot3 ([1:7],[1:7], RDPVD7vspec,'go')
plot3 (Xinds(1:7,1:7),[2], RDPVD6vspec,'go')
plot3 (Xinds(1:7,1:6),Yinds(1:6, 1:7), RDPVD5vspec,'go')
plot3 (Xinds(1:7,1:6),Yinds(1:6, 1:5), RDPVD4vspec,'go')
plot3 (Xinds(1:7,1:6),Yinds(1:5, 1:4), RDPVD3vspec,'go')
plot3 (Xinds(1:7,1:7),Yinds(1:6, 1:6), RDPVD2vspec,'go')
title('specificity')
hold off


figure
hold on
plot(RDPVD7vsens,RDPVD7vspec,'go')
plot(RDPVD6vsens,RDPVD6vspec,'g+')
plot(RDPVD5vsens,RDPVD5vspec,'bo')
plot(RDPVD4vsens,RDPVD4vspec,'b+')
```

```
plot(RDPVD3vsens,RDPVD3vspec,'mo')
plot(RDPVD2vsens,RDPVD2vspec,'m+')
xlabel('sensitivity')
ylabel('specificity')
%}
%%
%Part 2
%This section is for optimisation selection of class weighting from
%training set data
%Selectedfeatures = the selected features for training and testing from
%Candfeats not Allfeats
%CandFlbls is the training set diagnosis, RD = 3, PVD = 2
nRDts = nnz(CandFlbls==3);%number Tr set RD eyes
nPVDts = nnz(CandFlbls==2);%number PVD eyes in Tr set
Selectedfeatures = [4,83,86];%feat90c{41};%Indices from Allfeats NOT Candfeats:
final variables chosen
for WtR = 1:99
    Wt= (0.01*WtR);
quad4mdl1 =
fitcdiscr(Allfeats(Splittrain,Selectedfeatures),CandFlbls,'DiscrimType','quadratic'
,'Prior',[1-Wt Wt]);
quad4mdldistr1 = confusionmat(quad4mdl1.Y,resubPredict(quad4mdl1));
CmatR{WtR,1} = quad4mdldistr1;

SensR(WtR,1) = CmatR{WtR,1}(4)/(CmatR{WtR,1}(2) + CmatR{WtR,1}(4));%training set
SpecR(WtR,1) = CmatR{WtR,1}(1)/(CmatR{WtR,1}(1) + CmatR{WtR,1}(3));

scsR(WtR) = (quad4mdldistr1(1) + quad4mdldistr1(4))/sum(quad4mdldistr1(1:4));% =
accuracy
RDsR(WtR) = CmatR{WtR,1}(4);
PVDfR(WtR) = CmatR{WtR,1}(3);
RDsrate(WtR) = RDsR(WtR)/nRDts;%fratcion success rate RD
PVDfrate(WtR) = PVDfR(WtR)/nPVDts;%fraction failure rate PVD
end

AUC = trapz(1-SpecR,SensR);% AUC of ROC

%Total sensitivity/specificity range:
x=fliplr(0.01:0.01:0.99);

figure
plot(1-SpecR,SensR,'r');
refline(1,0)
title('ROC curve, 3 variable model training set');
xlabel('1-Specificity');
ylabel('Sensitivity');


%plot RD success  and PVD fail on same graph
%represents RDs and PVDfl as fractions against their denominator = no of
%each group in the training set
figure
yyaxis left
%plot(x,RDsrate,'m:');%same as sensitivity
hold on
%plot(x,PVDfrate,'-.k','LineWidth', 1);
%plot(x, RDsrate-PVDfrate,'k');
plot(x, SensR, 'r-.','LineWidth', 1);
plot(x, SpecR, 'b-.','LineWidth', 1);
set(gca, 'XDir','reverse')
set(gca, 'LineWidth', 1, 'FontWeight', 'bold', 'FontSize', 10);
xlabel({'Class weighting';'<--PVD weight increased RD weight-->'});
ylabel('proportion of eyes');

yyaxis right
plot(x, scsR,'Color',[0.8500 0.3250 0.0980]);
```

```
ylabel('Accuracy');
legend('Sensitivity', 'Specificity', 'Accuracy', 'Location'...
    ,'southoutside','Orientation', 'horizontal');
title('Training set performance by class weighting')

%%
%Part 3
%Now test the classifier
OptiWt = [0.58 0.42];% optimised classifier weighting
Valset = Allfeats(Splittest==1,Selectedfeatures);
Vallbls = Alllbls(Splittest==1,:);%sample class

%Candfeats/Allfeats is training set. Use only final selected features
SSOCTmdl =
fitcdiscr(Allfeats(Splittrain,Selectedfeatures),CandFlbls,'DiscrimType','quadratic'
,'Prior',OptiWt);

Valsetlbls = predict(SSOCTmdl,Valset);
VSsens= (nnz(Valsetlbls==3 & Vallbls==3))/nnz(Vallbls==3);
VSspec= (nnz(Valsetlbls==2 & Vallbls==2))/nnz(Vallbls==2);

VSTP = nnz(Valsetlbls==3 & Vallbls==3);%true positive, D in conf matrix
VDTN = nnz(Valsetlbls==2 & Vallbls==2);%true negatives, A in conf matrix
VStpfn = nnz(Vallbls==3);%TP + FN, D+C in conf matrix
VStnfp = nnz(Vallbls==2);%TN+FP, A+B on conf matrix

MdlperfRD= classperf(Vallbls,Valsetlbls);
VSID = AllID(Splittest==1); %test set eyes
VSTPID = VSID(Valsetlbls==3 & Vallbls==3);%TP ID
VSTNID = VSID(Valsetlbls==2 & Vallbls==2);%TN ID

%retinal tear eyes
%RTvalset = RTfts(:,Selectedfeatures);%RT candidate features
RTvalfts = RTfts(:,Selectedfeatures);%RT features for classifier
RTtestlbls = ones(size(RTvalfts,1))*3;%labelling RT as 3 for test results

RTtesting = predict(SSOCTmdl,RTvalfts);
RTsens=(nnz(RTtesting==3))/length(RTtesting);
%MdlperfRT = classperf(RTtestlbls,RTtesting);%performance with RT eyes



%%
%Part 4
%correlation betweeen values - Axl & anomaly

%PVD vars corr c AxL
[rhocPVD,pcPVD] = corr(aPVDfts(:,1:end-2),aPVDfts(:,end-1),'Type',
'Spearman','rows','pairwise');
%RD vars corr c AxL
[rhocRD,pcRD] = corr(RDfts(:,1:end-2),RDfts(:,end-1),'Type',
'Spearman','rows','pairwise');
%RT vars corr c AxL
[rhocRT,pcRT] = corr(RTfts(:,1:end-2),RTfts(:,end-1),'Type',
'Spearman','rows','pairwise');
%PVD + RD vars corr c AxL
[rhocPR,pcPR] = corr(Allfeats(:,1:end-2),Allfeats(:,end-1),'Type',
'Spearman','rows','pairwise');
%PVD, RT & RD corr c AxL
PRTfeats = cat(1,Allfeats,RTfts);
[rhocPRR,pcPRR] = corr(PRTfeats(:,1:end-2),PRTfeats(:,end-1),'Type',
'Spearman','rows','pairwise');


%Total anomaly
tAnRD = cellfun(@sum,RDanom);
```

```
tAnRT = cellfun(@sum,RTanom);
tAnPVD = cellfun(@sum,aPVDanom);

tAnPR = cat(1,tAnPVD,tAnRD);
tAnbAAPR = cat(2,tAnPR,Allfeats(:,121:126));%T anom, BFC, AxL, Age PVD & RD
tAnbAAPRR = cat(1,tAnbAAPR,cat(2,tAnRT,RTfts(:,121:126)));%PVD, RD, RT
%all eyes - these look at each region
[rhoctAPRR,pctAPRR] = corr(tAnbAAPRR(:,[1:end-2,end]),tAnbAAPRR(:,end-1),'Type',
'Spearman','rows','pairwise');
%PVD
[rhoctAP,pctAP] = corr(tAnPVD,aPVDAxL,'Type', 'Spearman','rows','pairwise');
%RD
[rhoctARD,pctARD] = corr(tAnRD,RDAxL,'Type', 'Spearman','rows','pairwise');
%RT
[rhoctART,pctART] = corr(tAnRT,RTAxL,'Type', 'Spearman','rows','pairwise');

%all eyes - these look at average of each bin - all regions
[rhoctMnAPRR,pctMnAPRR] = corr(mean(tAnbAAPRR(:,1:4),2,'omitnan'),tAnbAAPRR(:,end-
1),'Type', 'Spearman','rows','pairwise');
%PVD
[rhoctMnAP,pctMnAP] = corr(mean(tAnPVD,2,'omitnan'),aPVDAxL,'Type',
'Spearman','rows','pairwise');
%RD
[rhoctMnARD,pctMnARD] = corr(mean(tAnRD,2,'omitnan'),RDAxL,'Type',
'Spearman','rows','pairwise');
%RT
[rhoctMnART,pctMnART] = corr(mean(tAnRT,2,'omitnan'),RTAxL,'Type',
'Spearman','rows','pairwise');


%BH correction for SS OCT correlation

AllrhoSS = cat(1,
rhoctMnAPRR,rhoctMnAP,rhoctMnARD,rhoctMnART,rhoctAPRR(1:4),rhoctAP(1:4),rhoctARD(1:
4),rhoctART(1:4));
AllpvSS = cat(1,
pctMnAPRR,pctMnAP,pctMnARD,pctMnART,pctAPRR(1:4),pctAP(1:4),pctARD(1:4),pctART(1:4)
);


%BH correction
[sAllpvSS,psortSS] = sort(AllpvSS);
sAllrhoSS = AllrhoSS(psortSS);

m=length(sAllrhoSS);
alpha = 0.05;
BH=zeros(m,1);
for list=1:m
    BH(list) = alpha/(m-(list-1));
end

SummT= cat(2,sAllpvSS,BH,psortSS,sAllrhoSS);


figure
scatter(repmat(aPVDAxL,4,1),tAnPVD(:));
```

6. SSneweyetest

```
%test all new eyes and create array of labels/features, plus ROC
clear
SSOCTeyes3=[];%the table to use

%average B scan, classifier, feature indices
```

```
load('/Users/stewartlake/Documents/retinalcontour/SS OCT
notes/SSOCT2mdls3var0FLasso.mat'...
    ,'MnmBs','SSOCTmdl','Selectedfeatures', 'Vallbls', 'Valset','VSID','VSTPID',
'VSTNID');
%Valset = predictors fr each sample - original test set
%Vallbls = class for each sample - original test set
%SSOCTmdl  = model

%load eye data
load('/Users/stewartlake/Documents/MATLAB/SSOCT eyes.mat');

%Identify new eyes
nSSi = ismember(SSOCTeyes3.ID,SSOCTeyes2.ID,'rows');
newSS = SSOCTeyes3(~nSSi,:);

ftiBs = NaN(4,30);
%%
%Test new eyes (irrespective of diagnosis)
for Ai = 1:size(newSS,1)

   EyeId= table2array(newSS(Ai,1));
   AxI = table2array(newSS(Ai,4)); %axial length
   AgeI = table2array(newSS(Ai,3)); %age

   %get irregularity and BFC
   for Regs=8:11
      if numel(newSS{Ai,Regs})==1
           ftiBs(Regs-7,1:30)=cell2mat(newSS{Ai,Regs}{1});%region irreg FFT in rows

           BFCt(Regs-7) = newSS{Ai,Regs+5};

       elseif numel(newSS{Ai,Regs})>1

           Regsel = cell2mat(newSS{Ai,Regs});
           Regselt=sum(Regsel);
           [~,iMc]=max(Regselt);
           ftiBs(Regs-7,1:30)=Regsel(:,iMc);%max irregularity B scan from region

           BFCt(Regs-7) = newSS{Ai,Regs+5}(iMc);

       else
           ftiBs(Regs-7,1:30)=NaN(1,30);%empty (0) region
           BFCt(Regs-7) = NaN;
      end


   end

   Tianom(1:4,1:30) = abs(ftiBs(:,1:30) - MnmBs);%anomaly of this eye, rows =
region x 1:30 cols

   %in vector, order up down temp nasal (SSOCT table order U D N T)
   Teyev(Ai,1:126) = cat(2, Tianom(1,:), Tianom(2,:),Tianom(4,:),Tianom(3,:),...
       BFCt{1:2}, BFCt{4}, BFCt{3},AxI,AgeI);


end

%%
   nSScllbl= predict(SSOCTmdl,Teyev(:,Selectedfeatures));


nnRdPvdI = find(newSS.category=='PVD'|newSS.category=='RD');%new RD/PVD
nnGrpRDPVD = newSS(nnRdPvdI,:);%new RD PVD table data

nnSSfeats = Teyev(nnRdPvdI,:);%new RD PVD features
```

```
nnD = NaN(size(nnRdPvdI,1),1);%new RD PVD eyes diagnostic labels
nnD(nnGrpRDPVD.category=='PVD')=2;
nnD(nnGrpRDPVD.category=='RD')=3;

%%
%create ROC for entre test set

allSSdiag = cat(1,Vallbls, nnD);%observation diagnoses, RD & PVD test set
allSSfeats = cat(1, Valset,nnSSfeats(:,Selectedfeatures));%observation features
allSSID = cat(1, VSID, nnGrpRDPVD.ID);

[SSLbl, SSscore,~] = predict(SSOCTmdl,allSSfeats);

[ROCXSS, ROCYSS, TSS,AUCSS, OptptSS] =
perfcurve(allSSdiag,SSscore(:,2),'3','NBoot',5000,'XVals',[0:0.05:1]);

figure
hold on
ssROC = errorbar(ROCXSS(:,1),ROCYSS(:,1),ROCYSS(:,1)-ROCYSS(:,2),ROCYSS(:,3)-
ROCYSS(:,1), 'LineWidth',1.5);
ssROC.Color = [0.8500 0.3250 0.0980];
%plot(Optpttr(1),Optpttr(2),'ro')
xlabel('False positive rate')
ylabel('True positive rate')

hold off

%%
%ROC v2.0 now ROC corrected by median (see Ho 2017)
CoSSscor2 = (SSscore(:,2) - median(SSscore(:,2),'omitnan')).^2;

[cROCXSS, cROCYSS, cTSS,cAUCSS, cOptptSS] =
perfcurve(allSSdiag,CoSSscor2,'3','NBoot',5000,'XVals',[0:0.05:1]);

figure
hold on
cssROC = errorbar(cROCXSS(:,1),cROCYSS(:,1),cROCYSS(:,1)-cROCYSS(:,2),cROCYSS(:,3)-
cROCYSS(:,1), 'LineWidth',1.5);
cssROC.Color = [0.8500 0.3250 0.0980];
%plot(Optpttr(1),Optpttr(2),'ro')
xlabel('False positive rate')
ylabel('True positive rate')

hold off

%%
save('/Users/stewartlake/Documents/retinalcontour/SS OCT notes/Newtesteyesets',...
    'ssROC',"nSScllbl", 'allSSdiag','allSSfeats','allSSID','SSLbl','SSscore',...
    'ROCXSS', 'ROCYSS', 'AUCSS','nnD','nnRdPvdI', 'nnGrpRDPVD','nnSSfeats',...
    'Teyev','newSS');
```

Bibliography

1. Sonka, M. & Abràmoff, M. D. Quantitative analysis of retinal OCT. *Med. Image Anal.* **33**, 165–169 (2016) DOI: 10.1016/j.media.2016.06.001.
2. Kuo, A. N., Liu, A., Wong, C. W., McNabb, R. P., Lee, S. Y., Cheung, G. C. M., Saw, S.-M. & Hoang, Q. V. Curvature differences in myopic eyes with and without staphyloma using OCT. *Invest. Ophthalmol. Vis. Sci.* **60**, 4356 (2019).
3. Holden, B. A., Fricke, T. R., Wilson, D. A., Jong, M., Naidoo, K. S., Sankaridurg, P., Wong, T. Y., Naduvilath, T. J. & Resnikoff, S. Global prevalence of myopia and high myopia and temporal trends from 2000 through 2050. *Ophthalmology* **123**, 1036–1042 (2016) DOI: https://dx.doi.org/10.1016/j.ophtha.2016.01.006.
4. Moriyama, M., Ohno-Matsui, K., Hayashi, K., Shimada, N., Yoshida, T., Tokoro, T. & Morita, I. Topographic analyses of shape of eyes with pathologic myopia by high-resolution three-dimensional magnetic resonance imaging. *Ophthalmology* **118**, 1626–1637 (2011) DOI: 10.1016/j.ophtha.2011.01.018.
5. Jonas, J. B., Ohno-Matsui, K. & Panda-Jonas, S. Myopia: anatomic changes and consequences for its etiology. *Asia-Pacific J. Ophthalmol.* **8**, 355–359 (2019) DOI: 10.1097/01.APO.0000578944.25956.8b.
6. Wakazono, T., Yamashiro, K., Miyake, M., Nakanishi, H., Oishi, A., Ooto, S., Tsujikawa, A. & Yoshimura, N. Association between eye shape and myopic traction maculopathy in high myopia. *Ophthalmology* **123**, 919–921 (2016) DOI: 10.1016/j.ophtha.2015.10.031.
7. Ohno-Matsui, K., Akiba, M., Modegi, T., Tomita, M., Ishibashi, T., Tokoro, T. & Moriyama, M. Association between shape of sclera and myopic retinochoroidal lesions in patients with pathologic myopia. *Invest. Ophthalmol. Vis. Sci.* **53**, 6046–6061 (2012) DOI: 10.1167/iovs.12-10161.
8. Shinohara, K., Tanaka, N., Jonas, J. B., Shimada, N., Moriyama, M., Yoshida, T. & Ohno-Matsui, K. Ultrawide-field OCT to investigate relationships between myopic macular retinoschisis and posterior staphyloma. *Ophthalmology* **125**, 1575–1586 (2018) DOI: 10.1016/j.ophtha.2018.03.053.
9. Gaucher, D., Erginay, A., Lecleire-Collet, A., Haouchine, B., Puech, M., Cohen, S. Y., Massin, P. & Gaudric, A. Dome-shaped macula in eyes with myopic posterior staphyloma. *Am J Ophthalmol* **145**, 909–914 (2008) DOI: 10.1016/j.ajo.2008.01.012.

10. Choudhry, N., Golding, J., Manry, M. W. & Rao, R. C. Ultra-widefield steering-based spectral-domain optical coherence tomography imaging of the retinal periphery. *Ophthalmology* **123**, 1368–1374 (2016).
11. Stehouwer, M., Verbraak, F. D., de Vries, H. R. & van Leeuwen, T. G. Scanning beyond the limits of standard OCT with a Fourier domain optical coherence tomography integrated into a slit lamp: the SL SCAN-1. *Eye* **25**, 97–104 (2011).
12. Mori, K., Kanno, J., Gehlbach, P. L. & Yoneya, S. Montage images of spectral-domain optical coherence tomography in eyes with idiopathic macular holes. *Ophthalmology* **119**, 2600–2608 (2012) DOI: http://dx.doi.org/10.1016/j.ophtha.2012.06.027.
13. Han, X., Ong, J.-S., An, J., Craig, J. E., Gharahkhani, P., Hewitt, A. W. & MacGregor, S. Association of myopia and intraocular pressure with retinal detachment in european descent participants of the uk biobank cohort: a mendelian randomization study. *JAMA Ophthalmol.* **138**, 671–678 (2020) DOI: 10.1001/jamaophthalmol.2020.1231.
14. Wilkinson, C. P. & Rice, T. A. *Michels's Retinal Detachment*. (Mosby, 1997).
15. Quintyn, J. C. & Brasseur, G. Subretinal fluid in primary rhegmatogenous retinal detachment: physiopathology and composition. *Surv. Ophthalmol.* **49**, 96–108 (2016) DOI: 10.1016/j.survophthal.2003.10.003.
16. Kita, M. & Marmor, M. F. Retinal adhesive force in living rabbit, cat, and monkey eyes. Normative data and enhancement by mannitol and acetazolamide. *Invest. Ophthalmol. Vis. Sci.* **33**, 1879–1882 (1992).
17. Boulton, M. & Dayhaw-Barker, P. The role of the retinal pigment epithelium: topographical variation and ageing changes. *Eye* **15**, 384–389 (2001).
18. Kolb, H. http://webvision.med.utah.edu/book/part-xiii-facts-and-figures-concerning-the-human-retina/. *Date accessed 30 November 2016*.
19. Karampelas, M., Sim, D. A., Keane, P. A., Papastefanou, V. P., Sadda, S. R., Tufail, A. & Dowler, J. Evaluation of retinal pigment epithelium-Bruch's membrane complex thickness in dry age-related macular degeneration using optical coherence tomography. *Br J Ophthalmol* **97**, 1256–1261 (2013) DOI: 10.1136/bjophthalmol-2013-303219.
20. Sebag, J. Anatomy and pathology of the vitreo-retinal interface. *Eye* **6**, 541–552 (1992).
21. de Smet, M. D., Gad Elkareem, A. M. & Zwinderman, A. H. The vitreous, the retinal

interface in ocular health and disease. *Ophthalmologica* **230**, 165–178 (2013).

22. Schepens, C. L. & Neetens, A. *The vitreous and vitreoretinal interface*. (Springer Science & Business Media, 1987).
23. Le Goff, M. M. & Bishop, P. N. Adult vitreous structure and postnatal changes. *Eye* **22**, 1214–1222 (2008).
24. Wang, J., McLeod, D., Henson, D. B. & Bishop, P. N. Age-dependent changes in the basal retinovitreous adhesion. *Invest. Ophthalmol. Vis. Sci.* **44**, 1793–1800 (2003) DOI: 10.1167/iovs.02-0802.
25. Syed, Z. & Stewart, M. W. Age-dependent vitreous separation from the macula in a clinic population. *Clin. Ophthalmol.* **10**, 1237–1243 (2016) DOI: 10.2147/OPTH.S99635.
26. Itakura, H. & Kishi, S. Evolution of vitreomacular detachment in healthy subjects. *JAMA Ophthalmol.* **131**, 1348–1352 (2013) DOI: 10.1001/jamaophthalmol.2013.4578.
27. Uchino, E., Uemura, A. & Ohba, N. Initial stages of posterior vitreous detachment in healthy eyes of older persons evaluated by optical coherence tomography. *Arch. Ophthalmol.* **119**, 1475–1479 (2001).
28. Yonemoto, J., Ideta, H., Sasaki, K., Tanaka, S., Hirose, A. & Oka, C. The age of onset of posterior vitreous detachment. *Graefes Arch Clin Exp Ophthalmol* **232**, 67–70 (1994).
29. Akiba, J. Prevalence of posterior vitreous detachment in high myopia. *Ophthalmology* **100**, 1384–1388 (1993) DOI: 10.1016/S0161-6420(93)31471-5.
30. Sebag, J. Vitreoschisis. *Graefes Arch Clin Exp Ophthalmol* **246**, 329–332 (2008) DOI: 10.1007/s00417-007-0743-x.
31. Shao, L., Xu, L., You, Q. S., Wang, Y. X., Chen, C. X., Yang, H., Zhou, J. Q., Jonas, J. B. & Wei, W. Bin. Prevalence and associations of incomplete posterior vitreous detachment in adult chinese: The Beijing Eye Study. *PLoS One* **8**, e58498 (2013) DOI: 10.1371/journal.pone.0058498.
32. Tsukahara, M., Mori, K., Gehlbach, P. L. & Mori, K. Posterior vitreous detachment as observed by wide-angle OCT imaging. *Ophthalmology* **125**, 1372–1383 (2018).
33. Hwang, E. S., Kraker, J. A., Griffin, K. J., Sebag, J., Weinberg, D. V & Kim, J. E. Accuracy of spectral-domain OCT of the macula for detection of complete posterior vitreous detachment. *Ophthalmol. Retin.* **4**, 148–153 (2020).
34. Pang, C. E., Freund, K. B. & Engelbert, M. Enhanced vitreous imaging technique with

spectral-domain optical coherence tomography for evaluation of posterior vitreous detachment. *JAMA Ophthalmol.* **132**, 1148–1150 (2014) DOI: 10.1001/jamaophthalmol.2014.1037.

35. Coffee, R. E., Westfall, A. C., Davis, G. H., Mieler, W. F. & Holz, E. R. Symptomatic Posterior vitreous detachment and the incidence of delayed retinal breaks: case series and meta-analysis. *Am. J. Ophthalmol.* **144**, 409-413.e1 (2016) DOI: 10.1016/j.ajo.2007.05.002.
36. Brown, G. C., Brown, M. M. & Fischer, D. H. Photopsias: a key to diagnosis. *Ophthalmology* **122**, 2084–2094 (2015) DOI: http://dx.doi.org/10.1016/j.ophtha.2015.06.025.
37. Steel, D. H. W. & Lotery, A. J. Idiopathic vitreomacular traction and macular hole: a comprehensive review of pathophysiology, diagnosis, and treatment. *Eye* **27**, S1–S21 (2013) DOI: 10.1038/eye.2013.212.
38. Smiddy, W. E. & Flynn Jr, H. W. Pathogenesis of macular holes and therapeutic implications. *Am. J. Ophthalmol.* **137**, 525–537 (2004).
39. Kim, J. W., Freeman, W. R., Azen, S. P., El-Haig, W., Klein, D. J. & Bailey, I. L. Prospective randomized trial of vitrectomy or observation for stage 2 macular holes. *Am. J. Ophthalmol.* **121**, 605–614 (1996) DOI: 10.1016/S0002-9394(14)70625-7.
40. Lewis, M. Lou, Cohen, S. M., Smiddy, W. E. & Gass, J. D. M. Bilaterality of idiopathic macular holes. *Graefe's Arch. Clin. Exp. Ophthalmol.* **234**, 241–245 (1996) DOI: 10.1007/BF00430416.
41. Smiddy, W. E., Feuer, W. & Cordahi, G. Internal limiting membrane peeling in macular hole surgery. *Ophthalmology* **108**, 1471–1476 (2001) DOI: https://doi.org/10.1016/S0161-6420(00)00645-X.
42. Zhao, P.-P., Wang, S., Liu, N., Shu, Z.-M. & Zhao, J.-S. A review of surgical outcomes and advances for macular holes. *J. Ophthalmol.* **2018**, 7389412 (2018) DOI: 10.1155/2018/7389412.
43. Lochhead, J., Jones, E., Chui, D., Lake, S., Karia, N., Patel, C. K. & Rosen, P. Outcome of ICG-assisted ILM peel in macular hole surgery. *Eye* **18**, 804–808 (2004) DOI: 10.1038/sj.eye.6701328.
44. Ghazi, N. G. & Green, W. R. Pathology and pathogenesis of retinal detachment. *Eye* **16**, 411 (2002) DOI: 10.1038/sj.eye.6700197.

45. Byer, N. E. Clinical study of retinal breaks. *Trans. Acad. Ophthalmol. Otolaryngol. Am. Acad. Ophthalmol. Otolaryngol.* **71**, 461–473 (1967).
46. Mitry, D., Fleck, B. W., Wright, A. F., Campbell, H. & Charteris, D. G. Pathogenesis of rhegmatogenous retinal detachment: predisposing anatomy and cell biology. *Retina* **30**, 1561–1572 (2010) DOI: 10.1097/IAE.0b013e3181f669e6.
47. Straatsma, B. R. Peripheral retinal tears: classification, prevalence and principles of management. *Aust. J. Opthalmology* **8**, 275–279 (1980) DOI: 10.1111/j.1442-9071.1980.tb00283.x.
48. Foos, R. Y. Tears of the peripheral retina; pathogenesis, incidence and classification in autopsy eyes. *Mod. Probl. Ophthalmol.* **15**, 68–81 (1975).
49. Martín Sánchez, M. D. & Roldán Pallarés, M. [Myopia: prevalence of retinal tears and throphic holes]. *Arch. Soc. Esp. Oftalmol.* **75**, 81–84 (2000).
50. Westfall, A. C., Maa, A., Mieler, W. & Holz, E. Incidence of retinal tears and late–onset retinal breaks in eyes with a symptomatic posterior vitreous detachment . *Invest. Ophthalmol. Vis. Sci.* **45**, 2066 (2004).
51. Hollands, H., Johnson, D., Brox, A. C., Almeida, D., Simel, D. L. & Sharma, S. Acute-onset floaters and flashes: Is this patient at risk for retinal detachment? *JAMA* **302**, 2243–2249 (2009) DOI: 10.1001/jama.2009.1714.
52. Howie, A. R., Darian-Smith, E., Allen, P. L. & Vote, B. J. Whole population incidences of patients presenting with rhegmatogenous retinal detachments within Tasmania, Australia. *Clin. Experiment. Ophthalmol.* **44**, 144–146 (2016) DOI: 10.1111/ceo.12640.
53. Van de Put, M. A. J., Hooymans, J. M. M. & Los, L. I. The incidence of rhegmatogenous retinal detachment in The Netherlands. *Ophthalmology* **120**, 616–622 (2013) DOI: https://doi.org/10.1016/j.ophtha.2012.09.001.
54. Wong, T. Y., Tielsch, J. M. & Schein, O. D. Racial difference in the incidence of retinal detachment in Singapore. *Arch. Ophthalmol.* **117**, 379–383 (1999) DOI: 10.1001/archopht.117.3.379.
55. Hisatomi, T., Sakamoto, T., Goto, Y., Yamanaka, I., Oshima, Y., Hata, Y., Ishibashi, T., Inomata, H., Susin, S. A. & Kroemer, G. Critical role of photoreceptor apoptosis in functional damage after retinal detachment. *Curr. Eye Res.* **24**, 161–172 (2002) DOI: 10.1076/ceyr.24.3.161.8305.
56. Geiger, M., Smith, J. M., Lynch, A., Patnaik, J. L., Oliver, S. C. N., Dixon, J. A., Mandava,

N., Palestine, A. G. & Group, U. of C. R. R. Predictors for recovery of macular function after surgery for primary macula-off rhegmatogenous retinal detachment. *Int. Ophthalmol.* **40**, 609–616 (2020).

57. Polkinghorne, P. J. & Craig, J. P. Northern New Zealand Rhegmatogenous Retinal Detachment Study: epidemiology and risk factors. *Clin. Experiment. Ophthalmol.* **32**, 159–163 (2004) DOI: 10.1111/j.1442-9071.2004.00003.x.
58. Törnquist, R., Stenkula, S. & Törnquist, P. Retinal detachment. *Acta Ophthalmol.* **65**, 213–222 (1987) DOI: 10.1111/j.1755-3768.1987.tb07003.x.
59. Mitry, D., Charteris, D. G., Yorston, D., Siddiqui, M. A. R., Campbell, H., Murphy, A.-L., Fleck, B. W., Wright, A. F. & Singh, J. The epidemiology and socioeconomic associations of retinal detachment in Scotland: a two-year prospective population-based study. *Invest. Ophthalmol. Vis. Sci.* **51**, 4963–4968 (2010) DOI: 10.1167/iovs.10-5400.
60. Mitry, D., Singh, J., Yorston, D., Siddiqui, M. A. R., Murphy, A. L., Wright, A. F., Fleck, B. W., Campbell, H. & Charteris, D. G. The fellow eye in retinal detachment: findings from the Scottish Retinal Detachment Study. *Br. J. Ophthalmol.* **96**, 110–113 (2012) DOI: 10.1136/bjo.2010.194852.
61. Gupta, O. P. & Benson, W. E. The risk of fellow eyes in patients with rhegmatogenous retinal detachment. *Curr. Opin. Ophthalmol.* **16**, (2005).
62. Group, T. E. D. C.-C. S. Risk factors for idiopathic rhegmatogenous retinal detachment. *Am. J. Epidemiol.* **137**, 749–757 (1993) DOI: 10.1093/oxfordjournals.aje.a116735.
63. Meyer-Schwickerath, G. & Gerke, E. Biometric studies of the eyeball and retinal detachment. *Br. J. Ophthalmol.* **68**, 29–31 (1984).
64. Byer, N. E. Long-term natural history of lattice degeneration of the retina. *Ophthalmology* **96**, 1396–1402 (1989).
65. Pollack, A., Milstein, A., Oliver, M. & Zalish, M. Circumferential argon laser photocoagulation for prevention of retinal detachment. *Eye* **8 (Pt 4)**, 419–422 (1994) DOI: 10.1038/eye.1994.99.
66. RANZCO. https://ranzco.edu/media-and-advocacy/blog/ranzco-choosing-wisely-messages. *Date accessed 30 December 2015*.
67. Fincham, G. S., Pasea, L., Carroll, C., McNinch, A. M., Poulson, A. V, Richards, A. J., Scott, J. D. & Snead, M. P. Prevention of retinal detachment in Stickler syndrome: the

Cambridge prophylactic cryotherapy protocol. *Ophthalmology* **121**, 1588–1597 (2014).

68. Verhoekx, J. S. N., van Etten, P. G., Wubbels, R. J., van Meurs, J. C. & van Overdam, K. A. Prophylactic laser treatment to decrease the incidence of retinal detachment in fellow eyes of idiopathic giant retinal tears. *Retina* **40**, 1094–1097 (2020).
69. Ang, A., Poulson, A. V, Goodburn, S. F., Richards, A. J., Scott, J. D. & Snead, M. P. Retinal detachment and prophylaxis in type 1 Stickler syndrome. *Ophthalmology* **115**, 164–168 (2008) DOI: 10.1016/j.ophtha.2007.03.059.
70. Bond-Taylor, M., Jakobsson, G. & Zetterberg, M. Posterior vitreous detachment - prevalence of and risk factors for retinal tears. *Clin. Ophthalmol.* **11**, 1689–1695 (2017) DOI: 10.2147/OPTH.S143898.
71. Gishti, O., van den Nieuwenhof, R., Verhoekx, J. & van Overdam, K. Symptoms related to posterior vitreous detachment and the risk of developing retinal tears: a systematic review. *Acta Ophthalmol.* **0**, (2019) DOI: 10.1111/aos.14012.
72. Snead, M. P., Snead, D. R. J., Mahmood, A. S. & Scott, J. D. Vitreous detachment and the posterior hyaloid membrane: A clinicopathological study. *Eye* **8**, 204 (1994) DOI: 10.1038/eye.1994.47.
73. Saw, S. M., Katz, J., Schien, O. D., Chew, S. J. & Chan, T. K. Epidemiology of myopia. *Epidem Rev* **18**, (1996) DOI: 10.1093/oxfordjournals.epirev.a017924 LB - Saw1996.
74. Saka, N., Moriyama, M., Shimada, N., Nagaoka, N., Fukuda, K., Hayashi, K., Yoshida, T., Tokoro, T. & Ohno-Matsui, K. Changes of axial length measured by IOL master during 2 years in eyes of adults with pathologic myopia. *Graefe's Arch. Clin. Exp. Ophthalmol.* **251**, 495–499 (2012) DOI: 10.1007/s00417-012-2066-9.
75. Ho, M., Liu, D. T., Chan, V. C. & Lam, D. S. Choroidal thickness measurement in myopic eyes by enhanced depth optical coherence tomography. *Ophthalmology* **120**, 1909–1914 (2013) DOI: 10.1016/j.ophtha.2013.02.005.
76. Verkicharla, P. K., Ohno-Matsui, K. & Saw, S. M. Current and predicted demographics of high myopia and an update of its associated pathological changes. *Ophthalmic Physiol Opt* **35**, 465–475 (2015) DOI: 10.1111/opo.12238.
77. Frisina, R., Baldi, A., Cesana, B. M., Semeraro, F. & Parolini, B. Morphological and clinical characteristics of myopic posterior staphyloma in Caucasians. *Graefes Arch Clin Exp Ophthalmol* **11**, 2119–2129 (2016) DOI: 10.1007/s00417-016-3359-1.

78. Jonas, J. B. & Xu, L. Histological changes of high axial myopia. *Eye* **28**, 113–117 (2014) DOI: 10.1038/eye.2013.223.

79. Ohno-Matsui, K. What is the fundamental nature of pathologic myopia? *Retina* **37**, 1042–1048 (2017) DOI: 10.1097/iae.0000000000001348.

80. Dziubek, A., Guidoboni, G., Harris, A., Hirani, A. N., Rusjan, E. & Thistleton, W. Effect of ocular shape and vascular geometry on retinal hemodynamics: a computational model. *Biomech Model Mechanobiol* **14**, 893–907 (2016) DOI: 10.1007/s10237-015-0731-8.

81. Xu, L., Wang, Y., Wang, S., Wang, Y. & Jonas, J. B. High myopia and glaucoma susceptibility: the Beijing Eye Study. *Ophthalmology* **114**, 216–220 (2007).

82. Dolgin, E. The myopia boom. *Nature* **519**, 276–278 (2015).

83. Vongphanit, J., Mitchell, P. & Wang, J. J. Prevalence and progression of myopic retinopathy in an older population. *Ophthalmology* **109**, 704–711 (2002).

84. Liu, H. H., Xu, L., Wang, Y. X., Wang, S., You, Q. S. & Jonas, J. B. Prevalence and progression of myopic retinopathy in Chinese adults: the Beijing Eye Study. *Ophthalmology* **117**, 1763–1768 (2010).

85. Lin, L. L. K., Shih, Y. F., Hsiao, C. K. & Chen, C. J. L. B.-L. Prevalence of myopia in Taiwanese schoolchildren: 1983 to 2000. *Ann Acad Med* **33**, 27–33 (2004).

86. Eye Health in Australia. *Date accessed 15 August 2016* https://www.health.gov.au/health-topics/eye-health?utm_source=health.gov.au&utm_medium=callout-auto-custom&utm_campaign=digital_transformation (2005).

87. Foster, P. J. & Jiang, Y. Epidemiology of myopia. *Eye* **28**, 202–208 (2014) DOI: 10.1038/eye.2013.280.

88. Junghans, B. M. & Crewther, S. G. Little evidence for an epidemic of myopia in Australian primary school children over the last 30 years. *BMC Ophthalmol.* **5**, 1–10 (2005) DOI: 10.1186/1471-2415-5-1.

89. Khor, C. C., Miyake, M., Chen, L. J., Shi, Y., Barathi, V. A., Qiao, F., Nakata, I., Yamashiro, K., Zhou, X., Tam, P. O. S., Cheng, C.-Y., Tai, E. S., Vithana, E. N., Aung, T., Teo, Y.-Y., Wong, T.-Y., Moriyama, M., Ohno-Matsui, K., Mochizuki, M., *et al.* Genome-wide association study identifies ZFHX1B as a susceptibility locus for severe myopia. *Hum. Mol. Genet.* **22**, 5288–5294 (2013) DOI: 10.1093/hmg/ddt385.

90. Harper, A. R. & Summers, J. A. The dynamic sclera: extracellular matrix remodeling in normal ocular growth and myopia development. *Exp. Eye Res.* **133**, 100–111 (2015) DOI: 10.1016/j.exer.2014.07.015.

91. Stone, R. A. & Flitcroft, D. I. Ocular shape and myopia. *Ann. Med. Singapore* **33**, 7–15 (2004).

92. Raviola, E. & Wiesel, T. N. An animal model of myopia. *N. Engl. J. Med.* **312**, 1609–1615 (1985) DOI: doi:10.1056/NEJM198506203122505.

93. Troilo, D., Gottlieb, M. D. & Wallman, J. Visual deprivation causes myopia in chicks with optic nerve section. *Curr. Eye Res.* **6**, 993–999 (1987) DOI: 10.3109/02713688709034870.

94. Weakley, D. R., Birch, E., McClatchey, S. K., Felius, J., Parks, M. M. & Stager, D. The association between myopic shift and visual acuity outcome in pediatric aphakia. *J. Am. Assoc. Pediatr. Ophthalmol. Strabismus* **7**, 86–90 (2003) DOI: 10.1016/S1091-8531(03)00009-0.

95. Benavente-Pérez, A., Nour, A. & Troilo, D. Axial eye growth and refractive error development can be modified by exposing the peripheral retina to relative myopic or hyperopic defocus. *Invest. Ophthalmol. Vis. Sci.* **55**, 6765–6773 (2014).

96. Clark, C. A., Elsner, A. E. & Konynenbelt, B. J. Eye shape using partial coherence interferometry, autorefraction, and SD-OCT. *Optom Vis Sci* **92**, 115–122 (2015) DOI: 10.1097/opx.0000000000000453.

97. Schaeffel, F. & Feldkaemper, M. Animal models in myopia research. *Clin Exp Optom* **98**, 507–517 (2015) DOI: 10.1111/cxo.12312.

98. Ramamurthy, D., Lin Chua, S. Y. & Saw, S. M. A review of environmental risk factors for myopia during early life, childhood and adolescence. *Clin Exp Optom* **98**, 497–506 (2015) DOI: 10.1111/cxo.12346.

99. Zhang, Y. & Wildsoet, C. F. The RPE in myopia development. in *Retinal Pigment Epithelium in Health and Disease* 117–138 (Springer, 2020).

100. Meng, W., Butterworth, J., Malecaze, F. & Calvas, P. Axial length of myopia: a review of current research. *Ophthalmologica* **225**, 127–134 (2011) DOI: 10.1159/000317072.

101. Heitz, R. F. The earliest visualizations of the living eye's fundus by immersion in water. *Arch. Hist. Philos. Med. Hist. i Filoz. Med.* **75**, (2012).

102. Pearlman, J. T., Pearlman, S. J. & Engreen, F. E. Early efforts to view the human

fundus. *Doc Ophthalmol* **34**, 317–325 (1973).

103. Ehinger, B. & Grzybowski, A. Allvar Gullstrand (1862–1930)–the Gentleman with the lamp. *Acta Ophthalmol.* **89**, 701–708 (2011).
104. Choe, T. E., Cohen, I., Medioni, G., Walsh, A. C. & Sadda, S. R. Evaluation of 3-D shape reconstruction of retinal fundus. *Med Image Comput Comput Assist Interv* **9**, 134–141 (2006).
105. Abràmoff, M. D., Garvin, M. K. & Sonka, M. Retinal imaging and image analysis. *Biomed. Eng. IEEE Rev.* **3**, 169–208 (2010).
106. Malhotra, A., Minja, F. J., Crum, A. & Burrowes, D. Ocular anatomy and cross-sectional imaging of the eye. in *Seminars in Ultrasound, CT and MRI* vol. 32 2–13 (Elsevier, 2011).
107. Fujimoto, J. G., Pitris, C., Boppart, S. A. & Brezinski, M. E. Optical coherence tomography: an emerging technology for biomedical imaging and optical biopsy. *Neoplasia* **2**, 9–25 (2000).
108. Bedi, D. G., Gombos, D. S., Ng, C. S. & Singh, S. Sonography of the eye. *Am. J. Roentgenol.* **187**, 1061–1072 (2006) DOI: 10.2214/AJR.04.1842.
109. McNicholas, M. M., Brophy, D. P., Power, W. J. & Griffin, J. F. Ocular sonography. *AJR. Am. J. Roentgenol.* **163**, 921–926 (1994).
110. Kuo, A. N., Verkicharla, P. K., McNabb, R. P., Cheung, C. Y., Hilal, S., Farsiu, S., Chen, C., Wong, T. Y., Ikram, M. K., Cheng, C. Y., Young, T. L., Saw, S. M. & Izatt, J. A. Posterior eye shape measurement with retinal OCT Compared to MRI. *Invest. Ophthalmol. Vis. Sci.* **57**, 196–203 (2016) DOI: 10.1167/iovs.15-18886.
111. Nayak, B., Desai, S. & Maheshwari, S. Interpretation of magnetic resonance imaging of orbit: Simplified for ophthalmologists (Part I). *J. Clin. Ophthalmol. Res.* **1**, 29–35 (2013).
112. Beenakker, J.-W. M., Shamonin, D. P., Webb, A. G., Luyten, G. P. M. & Stoel, B. C. Automated retinal topographic maps measured with magnetic resonance imaging. *Invest. Ophthalmol. Vis. Sci.* **56**, 1033–1039 (2015) DOI: 10.1167/iovs.14-15161.
113. McNabb, R. P., Polans, J., Keller, B., Jackson-Atogi, M., James, C. L., Vann, R. R., Izatt, J. A. & Kuo, A. N. Wide-field whole eye OCT system with demonstration of quantitative retinal curvature estimation. *Biomed. Opt. Express* **10**, 338–355 (2019).
114. Yu, C., Apuzzo, M. L. J., Zee, C.-S. & Petrovich, Z. A phantom study of the geometric

accuracy of computed tomographic and magnetic resonance imaging stereotactic localization with the Leksell stereotactic system. *Neurosurgery* **48**, 1092–1099 (2001).

115. Kernt, M. & Kampik, A. Imaging of the peripheral retina. *Oman J. Ophthalmol.* **6**, S32–S35 (2013) DOI: 10.4103/0974-620X.122292.
116. Witmer, M. T. & Kiss, S. Wide-field imaging of the retina. *Surv. Ophthalmol.* **58**, 143–154 (2013) DOI: http://dx.doi.org/10.1016/j.survophthal.2012.07.003.
117. Borodkin, M. J. & Thompson, J. T. Retinal cartography. An analysis of two-dimensional and three-dimensional mapping of the retina. *Retina* **12**, 273–280 (1992).
118. Spaide, R. F. Peripheral areas of nonperfusion in treated central retinal vein occlusion as imaged by wide-field fluorescein angiography. *Retina* **31**, 829–837 (2011).
119. Choudhry, N., Duker, J. S., Freund, K. B., Kiss, S., Querques, G., Rosen, R., Sarraf, D., Souied, E. H., Stanga, P. E., Staurenghi, G. & Sadda, S. R. Classification and guidelines for widefield imaging. *Ophthalmol. Retin.* **3**, 843–849 (2019) DOI: 10.1016/j.oret.2019.05.007.
120. Baghaie, A., Yu, Z. & D'Souza, R. M. State-of-the-art in retinal optical coherence tomography image analysis. *Quant. Imaging Med. Surg.* **5**, 603–617 (2015).
121. Fercher, A. F., Drexler, W., Hitzenberger, C. K. & Lasser, T. Optical coherence tomography - principles and applications. *Reports Prog. Phys.* **66**, 239 (2003).
122. Huang, D., Swanson, E. A., Lin, C. P., Schuman, J. S., Stinson, W. G., Chang, W., Hee, M. R., Flotte, T., Gregory, K. & Puliafito, C. A. Optical coherence tomography. *Sci. (New York, NY)* **254**, 1178–1181 (1991).
123. Schuman, J. S. Spectral domain optical coherence tomography for glaucoma (an AOS Thesis). *Trans. Am. Ophthalmol. Soc.* **106**, 426–458 (2008).
124. Schmitt, J. M. Optical coherence tomography (OCT): a review. *IEEE J. Sel. Top. quantum Electron.* **5**, 1205–1215 (1999).
125. Gabriele, M. L., Wollstein, G., Ishikawa, H., Kagemann, L., Xu, J., Folio, L. S. & Schuman, J. S. Optical coherence tomography: history, current status, and laboratory work. *Invest. Ophthalmol. Vis. Sci.* **52**, 2425–2436 (2011).
126. Drexler, W., Morgner, U., Ghanta, R. K., Kärtner, F. X., Schuman, J. S. & Fujimoto, J. G. Ultrahigh-resolution ophthalmic optical coherence tomography. *Nat. Med.* **7**, 502–507 (2001).
127. Mansouri, K., Medeiros, F. A., Tatham, A. J., Marchase, N. & Weinreb, R. N. Evaluation

of retinal and choroidal thickness by swept-source optical coherence tomography: repeatability and assessment of artifacts. *Am. J. Ophthalmol.* **157**, 1022-1032. e3 (2014).

128. van Velthoven, M. E. J., Faber, D. J., Verbraak, F. D., van Leeuwen, T. G. & de Smet, M. D. Recent developments in optical coherence tomography for imaging the retina. *Prog. Retin. Eye Res.* **26**, 57–77 (2007) DOI: http://dx.doi.org/10.1016/j.preteyeres.2006.10.002.
129. Lang, A., Carass, A., Hauser, M., Sotirchos, E. S., Calabresi, P. A., Ying, H. S. & Prince, J. L. Retinal layer segmentation of macular OCT images using boundary classification. *Biomed. Opt. Express* **4**, 1133–1152 (2013).
130. Chen, M., Lang, A., Sotirchos, E., Ying, H. S., Calabresi, P. A., Prince, J. L. & Carass, A. Deformable registration of macular OCT using A-mode scan similarity. in *2013 IEEE 10th International Symposium on Biomedical Imaging* 476–479 (IEEE, 2013).
131. Antony, B. J., Abràmoff, M. D., Lee, K., Sonkova, P., Gupta, P., Kwon, Y., Niemeijer, M., Hu, Z. & Garvin, M. K. Automated 3D segmentation of intraretinal layers from optic nerve head optical coherence tomography images. in *SPIE Medical Imaging* 76260U-76260U–12 (International Society for Optics and Photonics, 2010).
132. Garvin, M. K., Abràmoff, M. D., Kardon, R., Russell, S. R., Wu, X. & Sonka, M. Intraretinal layer segmentation of macular optical coherence tomography images using optimal 3-D graph search. *IEEE Trans. Med. Imaging* **27**, 1495–1505 (2008).
133. Koprowski, R., Teper, S., Wróbel, Z. & Wylegala, E. Automatic analysis of selected choroidal diseases in OCT images of the eye fundus. *Biomed. Eng. Online* **12**, 1 (2013).
134. Spaide, R. F. & Curcio, C. A. Anatomical correlates to the bands seen in the outer retina by optical coherence tomography: literature review and model. *Retina* **31**, 1609 (2011).
135. Steidle, M. A. J. & Straub, J. Estimating the shape of the human eye using widefield optical coherence tomography (OCT). in *Biophotonics: Photonic Solutions for Better Health Care VI* vol. 10685 106851V (International Society for Optics and Photonics, 2018).
136. McNabb, R. P., Liu, A. S., Gospe, S. M. I. I. I., El-Dairi, M., Meekins, L. C., James, C., Vann, R. R., Izatt, J. A. & Kuo, A. N. Quantitative topographic curvature maps of the posterior eye utilizing optical coherence tomography. *Retina* **41**, 804–811 (2021).

137. Kuo, A. N., McNabb, R. P., Chiu, S. J., El-Dairi, M. A., Farsiu, S., Toth, C. A. & Izatt, J. A. Correction of ocular shape in retinal optical coherence tomography and effect on current clinical measures. *Am. J. Ophthalmol.* **156**, 304–311 (2013).
138. Bumstead, J., Steidle, M., Leahy, C. & Straub, J. Repeatability of retinal curvature estimation on wide field OCT systems. *Invest. Ophthalmol. Vis. Sci.* **60**, PB034–PB034 (2019).
139. Zawadzki, R. J., Fuller, A. R., Choi, S. S., Wiley, D. F., Hamann, B. & Werner, J. S. Correction of motion artifacts and scanning beam distortions in 3D ophthalmic optical coherence tomography imaging. in *Biomedical Optics (BiOS) 2007* 642607–642611 (International Society for Optics and Photonics, 2007).
140. Zawadzki, R. J., Choi, S. S., Fuller, A. R., Evans, J. W., Hamann, B. & Werner, J. S. Cellular resolution volumetric in vivo retinal imaging with adaptive optics–optical coherence tomography. *Opt. Express* **17**, 4084–4094 (2009).
141. Zhang, L., Lee, K., Niemeijer, M., Mullins, R. F., Sonka, M. & Abramoff, M. D. Automated segmentation of the choroid from clinical SD-OCT. *Invest. Ophthalmol. Vis. Sci.* **53**, 7510–7519 (2012).
142. Lujan, B. J., Roorda, A., Knighton, R. W. & Carroll, J. Revealing Henle's fiber layer using spectral domain optical coherence tomography. *Invest. Ophthalmol. Vis. Sci.* **52**, 1486–1492 (2011).
143. Podoleanu, A., Charalambous, I., Plesea, L., Dogariu, A. & Rosen, R. Correction of distortions in optical coherence tomography imaging of the eye. *Phys. Med. Biol.* **49**, 1277 (2004).
144. Uji, A. & Yoshimura, N. The application of extended field imaging to optical coherence tomography. *Invest. Ophthalmol. Vis. Sci.* **56**, 594 (2015).
145. Pichi, F., Carrai, P., Bonsignore, F., Villani, E., Ciardella, A. P. & Nucci, P. Wide-field spectral domain optical coherence tomography. *Retina* **35**, 2584–2592 (2015).
146. McNabb, R. P., Grewal, D. S., Mehta, R., Schuman, S. G., Izatt, J. A., Mahmoud, T. H., Jaffe, G. J., Mruthyunjaya, P. & Kuo, A. N. Wide field of view swept-source optical coherence tomography for peripheral retinal disease. *Br. J. Ophthalmol.* **100**, 1377–1382 (2016) DOI: 10.1136/bjophthalmol-2015-307480 NV - 10.
147. Kolb, J. P., Klein, T., Kufner, C. L., Wieser, W., Neubauer, A. S. & Huber, R. Ultra-widefield retinal MHz-OCT imaging with up to 100 degrees viewing angle. *Biomed.*

Opt. Express **6**, 1534–1552 (2015).

148. Kothari, A., Narendran, V. & Saravanan, V. R. In vivo sectional imaging of the retinal periphery using conventional optical coherence tomography systems. *Indian J. Ophthalmol.* **60**, 235–239 (2012) DOI: 10.4103/0301-4738.95885.

149. Carrai, P., Pichi, F., Bonsignore, F., Ciardella, A. P. & Nucci, P. Wide-field spectral domain-optical coherence tomography in central serous chorioretinopathy. *Int. Ophthalmol.* **35**, 167–171 (2015).

150. Mori, K., Kanno, J. & Gehlbach, P. L. Retinochoroidal morphology described by wide-field montage imaging of spectral domain optical coherence tomography. *Retina* **36**, 375–384 (2016) DOI: 10.1097/iae.0000000000000703.

151. Sawada, O., Mori, T., Ichiyama, Y., Obata, S., Kakinoki, M., Sawada, T., Saishin, Y. & Ohji, M. An attachment including a+ 20-D lens to gain extended field images in wide-angle optical coherence tomography angiography. *J. Vitreoretin. Dis.* **4**, 210–213 (2020).

152. Polans, J., Jaeken, B., McNabb, R. P., Artal, P. & Izatt, J. A. Wide-field optical model of the human eye with asymmetrically tilted and decentered lens that reproduces measured ocular aberrations. *Optica* **2**, 124–134 (2015) DOI: 10.1364/OPTICA.2.000124.

153. De Pretto, L. R., Moult, E. M., Alibhai, A. Y., Carrasco-Zevallos, O. M., Chen, S., Lee, B., Witkin, A. J., Baumal, C. R., Reichel, E., de Freitas, A. Z., Duker, J. S., Waheed, N. K. & Fujimoto, J. G. Controlling for artifacts in widefield optical coherence tomography angiography measurements of non-perfusion area. *Sci. Rep.* **9**, 9096 (2019) DOI: 10.1038/s41598-019-43958-1.

154. Atchison, D. A., Jones, C. E., Schmid, K. L., Pritchard, N., Pope, J. M., Strugnell, W. E. & Riley, R. A. Eye shape in emmetropia and myopia. *Invest. Ophthalmol. Vis. Sci.* **45**, 3380–3386 (2004) DOI: 10.1167/iovs.04-0292.

155. Atchison, D. A., Pritchard, N., Schmid, K. L., Scott, D. H., Jones, C. E. & Pope, J. M. Shape of the retinal surface in emmetropia and myopia. *Invest Ophthalmol Vis Sci* **46**, 2698–2707 (2005) DOI: 10.1167/iovs.04-1506.

156. Singh, K. D., Logan, N. S. & Gilmartin, B. Three-dimensional modeling of the human eye based on magnetic resonance imaging. *Invest. Ophthalmol. Vis. Sci.* **47**, 2272–2279 (2006) DOI: 10.1167/iovs.05-0856.

157. Shimada, Y., Sakurai, R., Mizuguchi, T., Nomura, R., Tanikawa, A. & Horiguchi, M. Wide-angle B-mode evaluation of the shape of eyeballs in rhegmatogenous retinal detachment. *Invest. Ophthalmol. Vis. Sci.* **60**, 6572 (2019).
158. Miyake, M., Yamashiro, K., Akagi-Kurashige, Y., Oishi, A., Tsujikawa, A., Hangai, M. & Yoshimura, N. Analysis of fundus shape in highly myopic eyes by using curvature maps constructed from optical coherence tomography. *PLoS One* **9**, e107923 (2014) DOI: 10.1371/journal.pone.0107923.
159. Ohno-Matsui, K., Fang, Y., Shinohara, K., Takahashi, H., Uramoto, K. & Yokoi, T. Imaging of pathologic myopia. *Asia-Pacific J. Ophthalmol.* **8**, 172–177 (2019) DOI: 10.22608/apo.2018494.
160. Guo, X., Xiao, O., Chen, Y., Wu, H., Chen, L., Morgan, I. G. & He, M. Three-dimensional eye shape, myopic maculopathy, and visual acuity: The Zhongshan Ophthalmic Center–Brien Holden Vision Institute High Myopia Cohort Study. *Ophthalmology* **124**, 679–687 (2017) DOI: 10.1016/j.ophtha.2017.01.009.
161. Shinohara, K., Shimada, N., Moriyama, M., Yoshida, T., Jonas, J. B., Yoshimura, N. & Ohno-Matsui, K. Posterior staphylomas in pathologic myopia imaged by widefield optical coherence tomography. *Invest Ophthalmol Vis Sci* **58**, 3750–3758 (2017) DOI: 10.1167/iovs.17-22319.
162. Caillaux, V., Gaucher, D., Gualino, V., Massin, P., Tadayoni, R. & Gaudric, A. Morphologic characterization of dome-shaped macula in myopic eyes with serous macular detachment. *Am. J. Ophthalmol.* **156**, 958-967. e1 (2013).
163. Fernández-Vega Sanz, Á., Rangel, C. M., Villota Deleu, E., Fernández-Vega Sanz, B. & Sánchez-Ávila, R. M. Serous retinal detachment associated with dome-shaped macula and staphyloma edge in myopic patients before and after treatment with spironolactone. *J. Ophthalmol.* **2016**, 1–6 (2016) DOI: 10.1155/2016/8491320.
164. Imamura, Y., Iida, T., Maruko, I., Zweifel, S. A. & Spaide, R. F. Enhanced depth imaging optical coherence tomography of the sclera in dome-shaped macula. *Am. J. Ophthalmol.* **151**, 297–302 (2011).
165. Scheibe, P., Lazareva, A., Braumann, U. D., Reichenbach, A., Wiedemann, P., Francke, M. & Rauscher, F. G. Parametric model for the 3D reconstruction of individual fovea shape from OCT data. *Exp Eye Res* **119**, 19–26 (2014) DOI: 10.1016/j.exer.2013.11.008.

166. Ruiz-Medrano, J., Flores-Moreno, I., Montero, J. A., Duker, J. S. & Ruiz-Moreno, J. M. Morphologic features of the choroidoscleral interface in a healthy population using swept-source optical coherence tomography. *Am J Ophthalmol* **160**, 596-601.e1 (2015) DOI: 10.1016/j.ajo.2015.05.027.

167. Guimarães, P., Rodrigues, P., Celorico, D., Serranho, P. & Bernardes, R. Three-dimensional segmentation and reconstruction of the retinal vasculature from spectral-domain optical coherence tomography. *J. Biomed. Opt.* **20**, 016006 (2015) DOI: 10.1117/1.JBO.20.1.016006.

168. Numa, S., Yamashiro, K., Wakazono, T., Yoshikawa, M., Miyake, M., Nakanishi, H., Oishi, A., Kawaguchi, T., Setoh, K., Takahashi, Y., Kosugi, S., Nakayama, T., Tabara, Y., Matsuda, F., Yoshimura, N., Tsujikawa, A. & Group, T. N. S. Prevalence of posterior staphyloma and factors associated with its shape in the Japanese population. *Sci. Rep.* **8**, 4594 (2018) DOI: 10.1038/s41598-018-22759-y.

169. McNabb, R. P., Liu, A., Gospe, S., El-Dairi, M., James, C., Vann, R., Izatt, J. A. & Kuo, A. N. True retinal topography: quantitative curvature maps of the retina using OCT. *Invest. Ophthalmol. Vis. Sci.* **60**, 1548 (2019).

170. Breher, K., Calabuig, A., Kühlewein, L., Ziemssen, F., Ohlendorf, A. & Wahl, S. Comparison of methods for estimating retinal shape: peripheral refraction vs. optical coherence tomography. *J. Clin. Med.* **10**, 174 (2021) DOI: 10.3390/jcm10020174.

171. Tabernero, J. & Schaeffel, F. More irregular eye shape in low myopia than in emmetropia. *Invest. Ophthalmol. Vis. Sci.* **50**, 4516–4522 (2009) DOI: 10.1167/iovs.09-3441.

172. Minami, S., Ito, Y., Ueno, S., Kataoka, K., Takeuchi, J., Ito, H., Nakano, Y., Kitagawa, M., Leahy, C., Straub, J. & Terasaki, H. Analysis of macular curvature in normal eyes using swept-source optical coherence tomography. *Jpn. J. Ophthalmol.* **64**, 180–186 (2020) DOI: 10.1007/s10384-020-00721-8.

173. Thomas, A., Sunija, A. P., Manoj, R., Ramachandran, R., Ramachandran, S., Varun, P. G. & Palanisamy, P. RPE layer detection and baseline estimation using statistical methods and randomization for classification of AMD from retinal OCT. *Comput. Methods Programs Biomed.* **200**, 105822 (2021) DOI: https://doi.org/10.1016/j.cmpb.2020.105822.

174. Naz, S., Ahmed, A., Akram, M. U. & Khan, S. A. Automated segmentation of RPE layer

for the detection of age macular degeneration using OCT images. in *2016 Sixth International Conference on Image Processing Theory, Tools and Applications (IPTA)* 1–4 (IEEE, 2016). DOI: 10.1109/IPTA.2016.7821033.

175. Khalid, S., Akram, M. U., Jameel, A. & Khalil, T. Automated detection of drusens to diagnose age related macular degeneration using OCT images. *Int. J. Comput. Sci. Inf. Secur.* **14**, 1 (2016).
176. Srinivasan, P. P., Kim, L. A., Mettu, P. S., Cousins, S. W., Comer, G. M., Izatt, J. A. & Farsiu, S. Fully automated detection of diabetic macular edema and dry age-related macular degeneration from optical coherence tomography images. *Biomed. Opt. Express* **5**, 3568–3577 (2014).
177. Kafieh, R., Rabbani, H., Abramoff, M. D. & Sonka, M. Curvature correction of retinal OCTs using graph-based geometry detection. *Phys. Med. Biol.* **58**, 2925–2938 (2013) DOI: 10.1088/0031-9155/58/9/2925.
178. Xu, H., Zeng, F., Shi, D., Sun, X., Chen, X. & Bai, Y. Focal choroidal excavation complicated by choroidal neovascularization. *Ophthalmology* **121**, 246–250 (2014) DOI: 10.1016/j.ophtha.2013.08.014.
179. Margolis, R., Mukkamala, S. K., Jampol, L. M., Spaide, R. F., Ober, M. D., Sorenson, J. A., Gentile, R. C., Miller, J. A., Sherman, J. & Freund, K. B. The expanded spectrum of focal choroidal excavation. *Arch. Ophthalmol.* **129**, 1320–1325 (2011).
180. Matsubara, H., Uchiyama, E., Suzuki, K., Matsuda, Y. & Kondo, M. A case of focal choroidal excavation development associated with multiple evanescent white dot syndrome. *Case Rep. Ophthalmol.* **9**, 388–394 (2018).
181. Shah, R. C., Gopalakrishnan, M., Goyal, A., Anantharaman, G. & Sethia, A. Focal choroidal excavation: Cause or effect? *Indian J. Ophthalmol.* **67**, 696 (2019).
182. Shah, V. S., Manayath, G. & Narendran, V. Focal choroidal excavation associated with choroidal neovascular membrane. *Kerala J. Ophthalmol.* **28**, 213 (2016).
183. Kuroda, Y., Tsujikawa, A., Ooto, S., Yamashiro, K., Oishi, A., Nakanishi, H., Kumagai, K., Hata, M., Arichika, S. & Ellabban, A. A. Association of focal choroidal excavation with age-related macular degeneration. *Invest. Ophthalmol. Vis. Sci.* **55**, 6046–6054 (2014).
184. Kupersmith, M. J., Sibony, P., Mandel, G., Durbin, M. & Kardon, R. H. Optical coherence tomography of the swollen optic nerve head: deformation of the peripapillary retinal pigment epithelium layer in papilledema. *Invest. Ophthalmol. Vis.*

Sci. **52**, 6558–6564 (2011) DOI: 10.1167/iovs.10-6782.

185. Chen, J. J. & Costello, F. The role of optical coherence tomography in neuro-ophthalmology. *Ann. Eye Sci. Vol 3, No 6 (June 2018) Ann. Eye Sci.* (2018).
186. M.D., N. B., Wang, M., Wang, H., Jin, Q. & Elze, T. Ametropia, retinal anatomy, and OCT abnormality patterns in glaucoma. 2. Impacts of optic nerve head parameters. *J. Biomed. Opt.* **22**, 1–9 (2017) DOI: 10.1117/1.JBO.22.12.121714.
187. Abe, O. & Oi, D. The look input system using the sclera reflection method by image analysis. *Inst. Image Inf. Telev. Eng.* **57**, 1354–1360 (2003).
188. Arai, K. & Mardiyanto, R. Improvement of gaze estimation robustness using pupil knowledge BT - computational science and its applications – ICCSA 2010. in (eds. Taniar, D., Gervasi, O., Murgante, B., Pardede, E. & Apduhan, B. O.) 336–350 (Springer Berlin Heidelberg, 2010).
189. ETL-600 Eye & Head tracking laboratory. *Date accessed 26 March 2021* https://www.creact.co.jp/wp-content/uploads/2017/10/ETL-600-Instructional-Manual.pdf.
190. Brown, M., Marmor, M., Vaegan, Zrenner, E., Brigell, M. & Bach, M. ISCEV standard for clinical electro-oculography (EOG) 2006. *Doc. Ophthalmol.* **113**, 205–212 (2006) DOI: 10.1007/s10633-006-9030-0.
191. Fuhl, W., Kübler, T., Sippel, K., Rosenstiel, W. & Kasneci, E. ExCuSe: Robust pupil detection in real-world scenarios BT - computer analysis of images and patterns. in (eds. Azzopardi, G. & Petkov, N.) 39–51 (Springer International Publishing, 2015).
192. Peréz, A., Córdoba, M. L., García, A., Méndez, R., Muñoz, M. L., Pedraza, J. L., Sánchez, F. A precise eye-gaze detection and tracking system. in *The 11-th International Conference in Central Europe on Computer Graphics, Visualization and Computer Vision* 105–108 (2003).
193. Ballard, D. H. Generalizing the Hough transform to detect arbitrary shapes. *Pattern Recognit.* **13**, 111–122 (1981).
194. Bozomitu, R. G., Pasarica, A., Cehan, V., Rotariu, C. & Barabasa, C. Pupil centre coordinates detection using the circular Hough transform technique. in *2015 38th International Spring Seminar on Electronics Technology (ISSE)* 462–465 (IEEE, 2015). DOI: 10.1109/ISSE.2015.7248041.
195. Gwon, S. Y., Cho, C. W., Lee, H. C., Lee, W. O. & Park, K. R. Robust eye and pupil

detection method for gaze tracking. *Int. J. Adv. Robot. Syst.* **10**, 98 (2013) DOI: 10.5772/55520.

196. Han, S. Y. & Cho, N. I. User-independent gaze estimation by extracting pupil parameter and its mapping to the gaze angle. in *2020 25th International Conference on Pattern Recognition (ICPR)* 1993–2000 (IEEE, 2021). DOI: 10.1109/ICPR48806.2021.9412709.
197. George, A. & Routray, A. Real-time eye gaze direction classification using convolutional neural network. in *2016 International Conference on Signal Processing and Communications (SPCOM)* 1–5 (IEEE, 2016).
198. Roig, A. B., Morales, M., Espinosa, J., Perez, J., Mas, D. & Illueca, C. Pupil detection and tracking for analysis of fixational eye micromovements. *Optik (Stuttg).* **123**, 11–15 (2012) DOI: https://doi.org/10.1016/j.ijleo.2010.10.049.
199. Kotsiantis, S. B., Zaharakis, I. & Pintelas, P. Supervised machine learning: A review of classification techniques. *Emerg. Artif. Intell. Appl. Comput. Eng.* **160**, 3–24 (2007).
200. Wainberg, M., Merico, D., Delong, A. & Frey, B. J. Deep learning in biomedicine. *Nat. Biotechnol.* **36**, 829 (2018) DOI: 10.1038/nbt.4233.
201. Riley, P. Three pitfalls to avoid in machine learning. *Nature* **572**, 27–29 (2019) DOI: https://doi.org/10.1038/d41586-019-02307-y.
202. Foster, K. R., Koprowski, R. & Skufca, J. D. Machine learning, medical diagnosis, and biomedical engineering research-commentary. *Biomed. Eng. Online* **13**, 94 (2014).
203. Somorjai, R. L., Dolenko, B. & Baumgartner, R. Class prediction and discovery using gene microarray and proteomics mass spectroscopy data: curses, caveats, cautions. *Bioinformatics* **19**, 1484–1491 (2003) DOI: 10.1093/bioinformatics/btg182.
204. Peduzzi, P., Concato, J., Kemper, E., Holford, T. R. & Feinstein, A. R. A simulation study of the number of events per variable in logistic regression analysis. *J. Clin. Epidemiol.* **49**, 1373–1379 (1996) DOI: https://doi.org/10.1016/S0895-4356(96)00236-3.
205. Lu, R.-S., Dennison, E., Denison, H., Cooper, C., Taylor, M. & Bottema, M. J. Texture analysis based on Gabor filters improves the estimate of bone fracture risk from DXA images. *Comput. Methods Biomech. Biomed. Eng. Imaging Vis.* **6**, 453–464 (2018) DOI: 10.1080/21681163.2016.1271726.
206. Lemm, S., Blankertz, B., Dickhaus, T. & Müller, K.-R. Introduction to machine learning for brain imaging. *Neuroimage* **56**, 387–399 (2011).

207. Kohavi, R. A study of cross-validation and bootstrap for accuracy estimation and model selection. in *Inljcai* vol. 14 1137–1145 (Montreal, Canada, 1995).
208. Koppen, M., Wolpert, D. H. & Macready, W. G. Remarks on a recent paper on the 'no free lunch' theorems. *IEEE Trans. Evol. Comput.* **5**, 295–296 (2001) DOI: 10.1109/4235.930318.
209. Friedman, J., Hastie, T. & Tibshirani, R. *The elements of statistical learning*. vol. 1 (Springer series in statistics New York, 2001).
210. Fisher, R. A. The use of multiple measurements in taxonomic problems. *Ann. Eugen.* **7**, 179–188 (1936) DOI: https://doi.org/10.1111/j.1469-1809.1936.tb02137.x.
211. Bose, S., Pal, A., SahaRay, R. & Nayak, J. Generalized quadratic discriminant analysis. *Pattern Recognit.* **48**, 2676–2684 (2015) DOI: 10.1016/j.patcog.2015.02.016.
212. Hogarty, D. T., Mackey, D. A. & Hewitt, A. W. Current state and future prospects of artificial intelligence in ophthalmology: a review. *Clin. Experiment. Ophthalmol.* **47**, 128–139 (2019).
213. Armstrong, G. W. & Lorch, A. C. A(eye): A review of current applications of artificial intelligence and machine learning in ophthalmology. *Int. Ophthalmol. Clin.* **60**, (2020).
214. Poplin, R., Varadarajan, A. V, Blumer, K., Liu, Y., McConnell, M. V, Corrado, G. S., Peng, L. & Webster, D. R. Prediction of cardiovascular risk factors from retinal fundus photographs via deep learning. *Nat. Biomed. Eng.* **2**, 158–164 (2018).
215. Faes, L., Liu, X., Wagner, S. K., Fu, D. J., Balaskas, K., Sim, D. A., Bachmann, L. M., Keane, P. A. & Denniston, A. K. A clinician's guide to artificial intelligence: how to critically appraise machine learning studies. *Transl. Vis. Sci. Technol.* **9**, 7 (2020) DOI: 10.1167/tvst.9.2.7.
216. Wang, Y., Zhang, Y., Yao, Z., Zhao, R. & Zhou, F. Machine learning based detection of age-related macular degeneration (AMD) and diabetic macular edema (DME) from optical coherence tomography (OCT) images. *Biomed. Opt. Express* **7**, 4928–4940 (2016).
217. Hussain, M. A., Bhuiyan, A., Luu, C. D., Smith, R. T., Guymer, R. H., Ishikawa, H., Schuman, J. S. & Ramamohanarao, K. Classification of healthy and diseased retina using SD-OCT imaging and Random Forest algorithm. *PLoS One* **13**, e0198281 (2018).
218. Kuwayama, S., Ayatsuka, Y., Yanagisono, D., Uta, T., Usui, H., Kato, A., Takase, N., Ogura, Y. & Yasukawa, T. Automated detection of macular diseases by optical

coherence tomography and artificial intelligence machine learning of optical coherence tomography images. *J. Ophthalmol.* **2019**, 6319581 (2019) DOI: 10.1155/2019/6319581.

219. Yim, J., Chopra, R., Spitz, T., Winkens, J., Obika, A., Kelly, C., Askham, H., Lukic, M., Huemer, J., Fasler, K., Moraes, G., Meyer, C., Wilson, M., Dixon, J., Hughes, C., Rees, G., Khaw, P. T., Karthikesalingam, A., King, D., *et al.* Predicting conversion to wet age-related macular degeneration using deep learning. *Nat. Med.* **26**, 892–899 (2020) DOI: 10.1038/s41591-020-0867-7.
220. Burgansky-Eliash, Z., Wollstein, G., Chu, T., Ramsey, J. D., Glymour, C., Noecker, R. J., Ishikawa, H. & Schuman, J. S. Optical coherence tomography machine learning classifiers for glaucoma detection: a preliminary study. *Invest. Ophthalmol. Vis. Sci.* **46**, 4147–4152 (2005).
221. Goldbaum, M. H., Sample, P. A., Chan, K., Williams, J., Lee, T.-W., Blumenthal, E., Girkin, C. A., Zangwill, L. M., Bowd, C. & Sejnowski, T. Comparing machine learning classifiers for diagnosing glaucoma from standard automated perimetry. *Invest. Ophthalmol. Vis. Sci.* **43**, 162–169 (2002).
222. Bambo, M. P., Fuentemilla, E., Cameo, B., Fuertes, I., Ferrandez, B., Güerri, N., Polo, V., Larrosa, J. M., Pablo, L. E. & Garcia-Martin, E. Diagnostic capability of a linear discriminant function applied to a novel Spectralis OCT glaucoma-detection protocol. *BMC Ophthalmol.* **20**, 1–8 (2020).
223. Essock, E. A., Sinai, M. J., Bowd, C., Zangwill, L. M. & Weinreb, R. N. Fourier analysis of optical coherence tomography and scanning laser polarimetry retinal nerve fiber layer measurements in the diagnosis of glaucoma. *Arch. Ophthalmol.* **121**, 1238–1245 (2003) DOI: 10.1001/archopht.121.9.1238.
224. Harrison, D. A 'brief' introduction to the Fourier Transform. *Date accessed 14 May 2020.* https://faraday.physics.utoronto.ca/PVB/Harrison/FourierTransform.pdf.
225. Pappuru, R. R., Briceno, C., Ouyang, Y., Walsh, A. C. & Sadda, S. R. Clinical significance of B-scan averaging with SD-OCT. *Ophthalmic Surgery, Lasers Imaging Retin.* **43**, 63–68 (2012).
226. Baggio, D. LiveWire plugin. *Date accessed 23 February 2017.* http://imagejdocu.tudor.lu/doku.php?id=plugin:segmentation:livewire_plugin:start (2008).

227. Schindelin, J., Arganda-Carreras, I., Frise, E., Kaynig, V., Longair, M., Pietzsch, T., Preibisch, S., Rueden, C., Saalfeld, S., Schmid, B., Tinevez, J.-Y. Y., White, D. J., Hartenstein, V., Eliceiri, K., Tomancak, P. & Cardona, A. Fiji: an open-source platform for biological-image analysis. *Nat Methods* **9**, 676–682 (2012) DOI: http://www.nature.com/nmeth/journal/v9/n7/abs/nmeth.2019.html#supplementary-information.

228. Caruso, J. C. & Cliff, N. Empirical size, coverage, and power of confidence intervals for spearman's rho. *Educ. Psychol. Meas.* **57**, 637–654 (1997) DOI: 10.1177/0013164497057004009.

229. Medical Devices Essential Principles Checklist. *Date accessed 12 June 2020.* https://www.tga.gov.au/sites/default/files/essential-principles-checklist-medical-devices.pdf.

230. Hoseini-Yazdi, H., Vincent, S. J., Collins, M. J., Read, S. A. & Alonso-Caneiro, D. Repeatability of wide-field choroidal thickness measurements using enhanced-depth imaging optical coherence tomography. *Clin. Exp. Optom.* **102**, 327–334 (2019) DOI: 10.1111/cxo.12893.

231. Shrout, P. E. & Fleiss, J. L. Intraclass correlations: uses in assessing rater reliability. *Psychol. Bull.* **86**, 420 (1979).

232. Zoeller, T. Intraclass correlation coefficient with confidence intervals. *Accessed 12 November 2019* https://au.mathworks.com/matlabcentral/fileexchange/26885-intraclass-correlation-coefficient-with-confidence-intervals (2007).

233. Salarian, A. Intraclass correlation coefficient. *Accessed 7 November 2019* https://au.mathworks.com/matlabcentral/fileexchange/22099-intraclass-correlation-coefficient-icc (2008).

234. Koo, T. K. & Li, M. Y. A guideline of selecting and reporting intraclass correlation coefficients for reliability research. *J. Chiropr. Med.* **15**, 155–163 (2016) DOI: 10.1016/j.jcm.2016.02.012.

235. Jacobson, M. Absolute Orientation - Horn's method. *Date accessed 12 September 2020.* https://www.mathworks.com/matlabcentral/fileexchange/26186-absolute-orientation-horn-s-method (2015).

236. Fagerland, M. W. t-tests, non-parametric tests, and large studies—a paradox of statistical practice? *BMC Med. Res. Methodol.* **12**, 78 (2012) DOI: 10.1186/1471-2288-

12-78.

237. Ross, R. G., Olincy, A., Harris, J. G., Radant, A., Adler, L. E., Compagnon, N. & Freedman, R. The effects of age on a smooth pursuit tracking task in adults with schizophrenia and normal subjects. *Biol. Psychiatry* **46**, 383–391 (1999) DOI: https://doi.org/10.1016/S0006-3223(98)00369-2.

238. Hayes, T. R. & Petrov, A. A. Mapping and correcting the influence of gaze position on pupil size measurements. *Behav. Res. Methods* **48**, 510–527 (2016) DOI: 10.3758/s13428-015-0588-x.

239. Ohno-Matsui, K., Kawasaki, R., Jonas, J. B., Cheung, C. M. G., Saw, S.-M., Verhoeven, V. J. M., Klaver, C. C. W., Moriyama, M., Shinohara, K., Kawasaki, Y., Yamazaki, M., Meuer, S., Ishibashi, T., Yasuda, M., Yamashita, H., Sugano, A., Wang, J. J., Mitchell, P., Wong, T. Y., *et al.* International photographic classification and grading system for myopic maculopathy. *Am. J. Ophthalmol.* **159**, 877-883.e7 (2015) DOI: https://doi.org/10.1016/j.ajo.2015.01.022.

240. Bargary, G., Bosten, J. M., Goodbourn, P. T., Lawrance-Owen, A. J., Hogg, R. E. & Mollon, J. D. Individual differences in human eye movements: An oculomotor signature? *Vision Res.* **141**, 157–169 (2017) DOI: https://doi.org/10.1016/j.visres.2017.03.001.

241. Dowiasch, S., Marx, S., Einhäuser, W. & Bremmer, F. Effects of aging on eye movements in the real world. *Front. Hum. Neurosci.* **9**, 46 (2015) DOI: 10.3389/fnhum.2015.00046.

242. Lee, W. J., Kim, J. H., Shin, Y. U., Hwang, S. & Lim, H. W. Differences in eye movement range based on age and gaze direction. *Eye* **33**, 1145–1151 (2019) DOI: 10.1038/s41433-019-0376-4.

243. Ghazizadeh Hashemi, S. A. H., Jafarzadeh, S., Haddadi Aval, M. & Hosseinabadi, R. Ocular motor function in patients with bilateral vestibular weakness. *Iran. J. Otorhinolaryngol.* **28**, 177–181 (2016).

244. Marx, S., Respondek, G., Stamelou, M., Dowiasch, S., Stoll, J., Bremmer, F., Oertel, W. H., Höglinger, G. U. & Einhäuser, W. Validation of mobile eye-tracking as novel and efficient means for differentiating progressive supranuclear palsy from Parkinson's disease. *Front. Behav. Neurosci.* **6**, 88 (2012) DOI: 10.3389/fnbeh.2012.00088.

245. Dowiasch, S., Backasch, B., Einhäuser, W., Leube, D., Kircher, T. & Bremmer, F. Eye

movements of patients with schizophrenia in a natural environment. *Eur. Arch. Psychiatry Clin. Neurosci.* **266**, 43–54 (2016) DOI: 10.1007/s00406-014-0567-8.

246. Aguirre, G. K. A model of the entrance pupil of the human eye. *Sci. Rep.* **9**, 9360 (2019) DOI: 10.1038/s41598-019-45827-3.
247. Wyatt, H. J. The human pupil and the use of video-based eyetrackers. *Vision Res.* **50**, 1982–1988 (2010).
248. Haarman, A. E. G., Enthoven, C. A., Tideman, J. W. L., Tedja, M. S., Verhoeven, V. J. M. & Klaver, C. C. W. The complications of myopia: a review and meta-analysis. *Invest. Ophthalmol. Vis. Sci.* **61**, 49 (2020) DOI: 10.1167/iovs.61.4.49.
249. Sharma, I. P., Lepcha, N. T., Lhamo, T., Ellwein, L. B., Pokharel, G. P., Das, T., Sapkota, Y. D., Dorji, T. & Peldon, S. Visual impairment and refractive error in school children in Bhutan: The findings from the Bhutan School Sight Survey (BSSS 2019). *PLoS One* **15**, e0239117 (2020).
250. Gogate, P. M., Chottopadhyay, T., Kaur, H., Narayandas, S., Phadke, S., Kharat, M., Dhangar, A., Inamdar, M., Badkere, A. & Khanna, R. C. Making blind children see: impact of correcting moderate and severe visual impairment in schools for the blind. *Middle East Afr. J. Ophthalmol.* **26**, 216–222 (2020) DOI: 10.4103/meajo.MEAJO_111_19.
251. Moriyama, M., Ohno-Matsui, K., Modegi, T., Kondo, J., Takahashi, Y., Tomita, M., Tokoro, T. & Morita, I. Quantitative analyses of high-resolution 3D MR images of highly myopic eyes to determine their shapes. *Invest. Ophthalmol. Vis. Sci.* **53**, 4510–4518 (2012) DOI: 10.1167/iovs.12-9426.
252. Ellabban, A. A., Tsujikawa, A., Matsumoto, A., Yamashiro, K., Oishi, A., Ooto, S., Nakata, I., Akagi-Kurashige, Y., Miyake, M. & Elnahas, H. S. Three-dimensional tomographic features of dome-shaped macula by swept-source optical coherence tomography. *Am. J. Ophthalmol.* **155**, 320-328. e2 (2013).
253. Dowding, I. & Haufe, S. Powerful statistical inference for nested data using sufficient summary statistics. *Front. Hum. Neurosci.* **12**, 103 (2018) DOI: 10.3389/fnhum.2018.00103.
254. Picquelle, S. J. & Mier, K. L. A practical guide to statistical methods for comparing means from two-stage sampling. *Fish. Res.* **107**, 1–13 (2011).
255. Tekin, K., Sonmez, K., Inanc, M., Ozdemir, K., Goker, Y. S. & Yilmazbas, P. Evaluation of

corneal topographic changes and surgically induced astigmatism after transconjunctival 27-gauge microincision vitrectomy surgery. *Int. Ophthalmol.* **38**, 635–643 (2018) DOI: 10.1007/s10792-017-0507-5.

256. Mohamed, A. A. A. & Abdrabbo, M. Corneal topographic changes following trans-conjunctival 20 gauge sutureless vitrectomy (TC20V). *Clin. Ophthalmol.* **6**, 565–569 (2012) DOI: 10.2147/OPTH.S29758.
257. Button, K. S., Ioannidis, J. P. A., Mokrysz, C., Nosek, B. A., Flint, J., Robinson, E. S. J. & Munafò, M. R. Power failure: why small sample size undermines the reliability of neuroscience. *Nat. Rev. Neurosci.* **14**, 365–376 (2013) DOI: 10.1038/nrn3475.
258. Bossuyt, P. M. & Reitsma, J. B. The STARD initiative. *Lancet* **361**, 71 (2003) DOI: 10.1016/S0140-6736(03)12122-8.
259. Bossuyt, P. M., Irwig, L., Craig, J. & Glasziou, P. Comparative accuracy: assessing new tests against existing diagnostic pathways. *BMJ* **332**, 1089–1092 (2006).
260. Shunmugam, M., Shah, A. N., Hysi, P. G. & Williamson, T. H. The Pattern and Distribution of retinal breaks in eyes with rhegmatogenous retinal detachment. *Am. J. Ophthalmol.* **157**, 221–226 (2014) DOI: 10.1016/j.ajo.2013.09.011.
261. Emergency declaration. *SA Health. Date accessed 18 April 2020.* https://www.covid-19.sa.gov.au/emergency-declarations/emergency-declaration (2020).
262. Clinical trials in the context of COVID-19. *Date accessed 19 April 2020.* https://www.nhmrc.gov.au/research-policy/COVID-19-impacts.
263. Lange, T. OCT automated image analysis. (Flinders University, 2019).
264. Wilkinson, C. P. Interventions for asymptomatic retinal breaks and lattice degeneration for preventing retinal detachment. *Cochrane Database Syst. Rev.* (2014) DOI: 10.1002/14651858.CD003170.pub4 doi:10.1002/14651858.CD003170.pub4.
265. Mitry, D., Charteris, D. G., Fleck, B. W., Campbell, H. & Singh, J. The epidemiology of rhegmatogenous retinal detachment: geographical variation and clinical associations. *Br. J. Ophthalmol.* **94**, 678–684 (2010) DOI: 10.1136/bjo.2009.157727.
266. Bland, J. M. & Altman, D. G. Measuring agreement in method comparison studies. *Stat. Methods Med. Res.* **8**, 135–160 (1999).
267. More, S., Kubach, S., Gregori, G., Shen, M., Wang, L., Jiang, X., Laiginhas, R., shi, yingying, De Sisternes, L. & Rosenfeld, P. J. Comparison of retinal pigment epithelium elevation between scans acquired at 200 kHz and 100 kHz rates. *Invest. Ophthalmol.*

Vis. Sci. **62**, 2529 (2021).

268. Akman, A. Optical coherence tomography: manufacturers and current systems. in *Optical Coherence Tomography in Glaucoma* (eds. Akman, A., Bayer, A. & Nouri-Mahdavi, K.) 27–37 (Springer International Publishing, 2018). DOI: 10.1007/978-3-319-94905-5_4.
269. Adhi, M., Liu, J. J., Qavi, A. H., Grulkowski, I., Lu, C. D., Mohler, K. J., Ferrara, D., Kraus, M. F., Baumal, C. R., Witkin, A. J., Waheed, N. K., Hornegger, J., Fujimoto, J. G. & Duker, J. S. Choroidal analysis in healthy eyes using swept-source optical coherence tomography compared to spectral domain optical coherence tomography. *Am. J. Ophthalmol.* **157**, 1272-1281.e1 (2014) DOI: https://doi.org/10.1016/j.ajo.2014.02.034.
270. Zheng, F., Zhang, Q., Shi, Y., Russell, J. F., Motulsky, E. H., Banta, J. T., Chu, Z., Zhou, H., Patel, N. A., de Sisternes, L., Durbin, M. K., Feuer, W., Gregori, G., Wang, R. & Rosenfeld, P. J. Age-dependent changes in the macular choriocapillaris of normal eyes imaged with swept-source optical coherence tomography angiography. *Am. J. Ophthalmol.* **200**, 110–122 (2019) DOI: https://doi.org/10.1016/j.ajo.2018.12.025.
271. Ohayon, A., Sacconi, R., Semoun, O., Corbelli, E., Souied, E. H. & Querques, G. Choroidal neovascular area and vessel density comparison between two swept-source optical coherence tomography angiography devices. *Retina* **40**, 521–528 (2020).
272. Cicinelli, M. V., Cavalleri, M., Consorte, A. C., Rabiolo, A., Sacconi, R., Bandello, F. & Querques, G. Swept-source and spectral domain optical coherence tomography angiography versus dye angiography in the measurement of type 1 neovascularization. *Retina* **40**, 499–506 (2020) DOI: 10.1097/IAE.0000000000002452.
273. Choi, W., Moult, E. M., Waheed, N. K., Adhi, M., Lee, B., Lu, C. D., de Carlo, T. E., Jayaraman, V., Rosenfeld, P. J., Duker, J. S. & Fujimoto, J. G. Ultrahigh-speed, swept-source optical coherence tomography angiography in nonexudative age-related macular degeneration with geographic atrophy. *Ophthalmology* **122**, 2532–2544 (2015) DOI: https://doi.org/10.1016/j.ophtha.2015.08.029.
274. Choma, M. A., Sarunic, M. V, Yang, C. & Izatt, J. A. Sensitivity advantage of swept source and Fourier domain optical coherence tomography. *Opt. Express* **11**, 2183–2189 (2003) DOI: 10.1364/OE.11.002183.

275. Klein, T., Wieser, W., Eigenwillig, C. M., Biedermann, B. R. & Huber, R. Megahertz OCT for ultrawide-field retinal imaging with a 1050nm Fourier domain mode-locked laser. *Opt. Express* **19**, 3044–3062 (2011) DOI: 10.1364/OE.19.003044.

276. Zou, H., Hastie, T. & Tibshirani, R. On the “degrees of freedom” of the lasso. *Ann. Stat.* **35**, 2173–2192 (2007).

277. Ding, C. & Peng, H. Minimum redundancy feature selection from microarray gene expression data. *J. Bioinform. Comput. Biol.* **3**, 185–205 (2005).

278. Ho, K. M. Effect of non-linearity of a predictor on the shape and magnitude of its receiver-operating-characteristic curve in predicting a binary outcome. *Sci. Rep.* **7**, 10155 (2017) DOI: 10.1038/s41598-017-10408-9.

279. Hoang, Q. V, Chang, S., Yu, D. J. G., Yannuzzi, L. A., Freund, K. B. & Grinband, J. 3-D assessment of gaze-induced eye shape deformations and downgaze-induced vitreous chamber volume increase in highly myopic eyes with staphyloma. *Br. J. Ophthalmol.* **105**, 1149 LP – 1154 (2021) DOI: 10.1136/bjophthalmol-2020-316084.

280. Stehouwer, M., Tan, S. H., van Leeuwen, T. G. & Verbraak, F. D. Senile retinoschisis versus retinal detachment, the additional value of peripheral retinal OCT scans (SL SCAN-1, Topcon). *Acta Ophthalmol.* **92**, 221–227 (2014).

281. Burlina, P., Paul, W., Mathew, P., Joshi, N., Pacheco, K. D. & Bressler, N. M. Low-shot deep learning of diabetic retinopathy with potential applications to address artificial intelligence bias in retinal diagnostics and rare ophthalmic diseases. *JAMA Ophthalmol.* **138**, 1070–1077 (2020) DOI: 10.1001/jamaophthalmol.2020.3269.

282. Rudin, C. Stop explaining black box machine learning models for high stakes decisions and use interpretable models instead. *Nat. Mach. Intell.* **1**, 206–215 (2019) DOI: 10.1038/s42256-019-0048-x.

283. Price, W. N. Artificial intelligence in health care: applications and legal issues. *TheSciTech Lawyer* **14**, (2017).

284. Ghosh, A., Collins, M. J., Read, S. A. & Davis, B. A. Axial length changes with shifts of gaze direction in myopes and emmetropes. *Invest. Ophthalmol. Vis. Sci.* **53**, 6465–6471 (2012) DOI: 10.1167/iovs.12-9973.

285. Sakamoto, M., Matsumoto, Y., Mori, S., Ueda, K., Inoue, Y., Kurimoto, T., Kanamori, A., Yamada, Y. & Nakamura, M. Excessive scleral shrinkage, rather than choroidal thickening, is a major contributor to the development of hypotony maculopathy after

trabeculectomy. *PLoS One* **13**, e0191862–e0191862 (2018) DOI: 10.1371/journal.pone.0191862.

286. Chebil, A., Achour, B., Chaker, N., Jedidi, L., Mghaieth, F. & El Matri, L. Choroidal thickness assessment with SD-OCT in high myopia with dome-shaped macula. *J. Fr. Ophtalmol.* **37**, 237–241 (2014).
287. Ohsugi, H., Ikuno, Y., Oshima, K., Yamauchi, T. & Tabuchi, H. Morphologic characteristics of macular complications of a dome-shaped macula determined by swept-source optical coherence tomography. *Am. J. Ophthalmol.* **158**, 162-170. e1 (2014).
288. Mehdizadeh, M. & Nowroozzadeh, M. H. Dome-shaped macula in eyes with myopic posterior staphyloma. *Am. J. Ophthalmol.* **146**, 478 (2008).
289. Iyer, S. S. R., Regan, K. A., Burnham, J. M. & Chen, C. J. Surgical management of diabetic tractional retinal detachments. *Surv. Ophthalmol.* **64**, 780–809 (2019) DOI: https://doi.org/10.1016/j.survophthal.2019.04.008.
290. Fujimoto, M., Hangai, M., Suda, K. & Yoshimura, N. Features associated with foveal retinal detachment in myopic macular retinoschisis. *Am. J. Ophthalmol.* **150**, 863-870.e1 (2010) DOI: https://doi.org/10.1016/j.ajo.2010.06.023.
291. Huang, R. A kinetics approach to surface wrinkling of elastic thin films. in *Mechanical Self-Assembly* (ed. Chen, X.) 69–109 (Springer New York, 2013). DOI: 10.1007/978-1-4614-4562-3_5.
292. Nikravesh, S., Ryu, D. & Shen, Y.-L. Direct numerical simulations of three-dimensional surface instability patterns in thin film-compliant substrate structures. *Sci. Rep.* **11**, 16449 (2021) DOI: 10.1038/s41598-021-95414-8.
293. Jonas, J. B., Ohno-Matsui, K., Jiang, W. J. & Panda-Jonas, S. Bruch membrane and the mechanism of myopization: a new theory. *Retina* **37**, 1428–1440 (2017).
294. Boutin, T. S., Charteris, D. G., Chandra, A., Campbell, S., Hayward, C., Campbell, A., Consortium, U. K. B. E. & V., Nandakumar, P., Hinds, D., Mitry, D. & Vitart, V. Insights into the genetic basis of retinal detachment. *Hum. Mol. Genet.* **29**, 689–702 (2020) DOI: 10.1093/hmg/ddz294.
295. Johnston, T., Chandra, A. & Hewitt, A. W. Current understanding of the genetic architecture of rhegmatogenous retinal detachment. *Ophthalmic Genet.* **37**, 121–129 (2016) DOI: 10.3109/13816810.2015.1033557.

296. Wolfensberger, T. J., Aylward, G. W. & Leaver, P. K. Prophylactic 360° cryotherapy in fellow eyes of patients with spontaneous giant retinal tears. *Ophthalmology* **110**, 1175–1177 (2003) DOI: https://doi.org/10.1016/S0161-6420(03)00256-2.

297. Ripandelli, G., Rossi, T., Cacciamani, A., Scarinci, F., Piaggi, P. & Stirpe, M. Laser prophylactic treatment of the fellow eye in giant retinal tears: Long-Term Follow-up. *Retina* **36**, 962–966 (2016) DOI: 10.1097/iae.0000000000000805.

298. Ang, G. S., Townend, J. & Lois, N. Interventions for prevention of giant retinal tear in the fellow eye. *Cochrane Database Syst. Rev.* (2012) DOI: 10.1002/14651858.CD006909.pub3.

299. Kozak, I. & Luttrull, J. K. Modern retinal laser therapy. *Saudi J. Ophthalmol. Off. J. Saudi Ophthalmol. Soc.* **29**, 137–146 (2015) DOI: 10.1016/j.sjopt.2014.09.001.

300. Deschler, E. K., Sun, J. K. & Silva, P. S. Side-effects and complications of laser treatment in diabetic retinal disease. *Semin. Ophthalmol.* **29**, 290–300 (2014) DOI: 10.3109/08820538.2014.959198.

301. Gross, J. G., Glassman, A. R., Liu, D., Sun, J. K., Antoszyk, A. N., Baker, C. W., Bressler, N. M., Elman, M. J., Ferris III, F. L., Gardner, T. W., Jampol, L. M., Martin, D. F., Melia, M., Stockdale, C. R., Beck, R. W. & Network, for the D. R. C. R. Five-year outcomes of panretinal photocoagulation vs intravitreous ranibizumab for proliferative diabetic retinopathy: a randomized clinical trial. *JAMA Ophthalmol.* **136**, 1138–1148 (2018) DOI: 10.1001/jamaophthalmol.2018.3255.

302. A randomized clinical trial of early panretinal photocoagulation for ischermic central vein occlusion: The Central Vein Occlusion Study Group N Report. *Ophthalmology* **102**, 1434–1444 (1995) DOI: https://doi.org/10.1016/S0161-6420(95)30848-2.

303. Graham, E. M., Stanford, M. R., Shilling, J. S. & Sanders, M. D. Neovascularisation associated with posterior uveitis. *Br. J. Ophthalmol.* **71**, 826 LP – 833 (1987) DOI: 10.1136/bjo.71.11.826.

304. Ng, E. Y. J., Connolly, B. P., McNamara, J. A., Regillo, C. D., Vander, J. F. & Tasman, W. A comparison of laser photocoagulation with cryotherapy for threshold retinopathy of prematurity at 10 years: part 1. Visual function and structural outcome1 1None of the authors has any financial or proprietary interest in any of the techniques or equipm. *Ophthalmology* **109**, 928–934 (2002) DOI: https://doi.org/10.1016/S0161-6420(01)01017-X.

305. DeJonge, M. H., Ferrone, P. J. & Trese, M. T. Diode laser ablation for threshold retinopathy of prematurity: short-term structural outcome. *Arch. Ophthalmol.* **118**, 365–367 (2000) DOI: 10.1001/archopht.118.3.365.

306. Ling, C. S., Fleck, B. W., Wright, E., Anderson, C. & Laing, I. Diode laser treatment for retinopathy of prematurity: structural and functional outcome. *Br. J. Ophthalmol.* **79**, 637–641 (1995).

307. Stahl, A., Lepore, D., Fielder, A., Fleck, B., Reynolds, J. D., Chiang, M. F., Li, J., Liew, M., Maier, R. & Zhu, Q. Ranibizumab versus laser therapy for the treatment of very low birthweight infants with retinopathy of prematurity (RAINBOW): an open-label randomised controlled trial. *Lancet* **394**, 1551–1559 (2019).

308. Pendergast, S. D. & Trese, M. T. Familial exudative vitreoretinopathy: Results of surgical management. *Ophthalmology* **105**, 1015–1023 (1998) DOI: https://doi.org/10.1016/S0161-6420(98)96002-X.

309. Nguyen, J. K. & Brady-McCreery, K. M. Laser photocoagulation in preproliferative retinopathy of incontinentia pigmenti. *J. Am. Assoc. Pediatr. Ophthalmol. Strabismus* **5**, 258–259 (2001) DOI: https://doi.org/10.1067/mpa.2001.117098.

310. Schefler, A. C., Berrocal, A. M. & Murray, T. G. Advanced Coats' Disease. *Retina* **28**, S38–S41 (2008) DOI: 10.1097/IAE.0b013e318163cd7c.

311. Kraushar, M. F. & Morse, P. H. The relationship between retina surgery and preretinal macular fibrosis. *Ophthalmic Surgery, Lasers Imaging Retin.* **19**, 843–848 (1988) DOI: https://doi.org/10.3928/1542-8877-19881201-05.

312. Morse, P. H. & Scheie, H. G. Prophylactic cryoretinopexy of retinal breaks. *Arch. Ophthalmol.* **92**, 204–207 (1974).

313. Saran, B. R. & Brucker, A. J. Macular epiretinal membrane formation and treated retinal breaks. *Am J Ophthalmol* **120**, 480–485 (1995) DOI: 10.1016/s0002-9394(14)72662-5.

314. Mester, U., Volker, B., Kroll, P. & Berg, P. Complications of prophylactic argon laser treatment of retinal breaks and degenerations in 2,000 eyes. *Ophthalmic Surg* **19**, 482–484 (1988).

315. Blackorby, B. L., Jeroudi, A. M., Blinder, K. J. & Shah, G. K. Epiretinal membrane formation after treatment of retinal breaks: cryoretinopexy versus laser retinopexy. *Ophthalmol. Retin.* **3**, 1087–1090 (2019) DOI: 10.1016/j.oret.2019.06.015.

316. Govan, J. A. Prophylactic circumferential cryopexy: a retrospective study of 106 eyes. *Br. J. Ophthalmol.* **65**, 364–370 (1981).

317. Al-Khairi, A. M., Al-Kahtani, E., Kangave, D. & Abu El-Asrar, A. M. Prognostic factors associated with outcomes after giant retinal tear management using perfluorocarbon liquids. *Eur. J. Ophthalmol.* **18**, 270–277 (2008) DOI: 10.1177/112067210801800216.

318. Ghosh, Y. K., Banerjee, S., Savant, V., Kotamarthi, V., Benson, M. T., Scott, R. A. H. & Tyagi, A. K. Surgical treatment and outcome of patients with giant retinal tears. *Eye* **18**, 996–1000 (2004).

319. Glasspool, M. G. & Kanski, J. J. Prophylaxis in giant tears. *Trans. Ophthalmol. Soc. U. K.* **93**, 363–371 (1973).

320. Snead, D. R. J., James, S. & Snead, M. P. Pathological changes in the vitreoretinal junction 1: epiretinal membrane formation. *Eye* **22**, 1310–1317 (2008) DOI: 10.1038/eye.2008.36.

321. Idrees, S., Kuriyan, A. E., Schwartz, S. G., Parel, J.-M. & Flynn, H. W. Recent developments in vitreo-retinal surgery. in *Current Concepts in Ophthalmology* (ed. Grzybowski, A.) 165–199 (Springer International Publishing, 2020). DOI: 10.1007/978-3-030-25389-9_7.

322. Markan, A., Kumar, A., Vira, J., Gupta, V. & Agarwal, A. Advances in the tools and techniques of vitreoretinal surgery. *Expert Rev. Ophthalmol.* **15**, 331–345 (2020) DOI: 10.1080/17469899.2020.1810018.

323. McCloud, C. H. People's experience of vitreo-retinal day surgery: a Gadamerian guided study embedded within an evidence based nursing practice framework. (Thesis (Ph.D.) - Flinders University of South Australia, School of Nursing and Midwifery, 2013).